Proceedings of the 5th International Workshop on Functional-Structural Plant Models

Napier, New Zealand
November 4-9, 2007

Abstracts of Papers and Posters

Edited by
Przemyslaw Prusinkiewicz, Jim Hanan,
and Brendan Lane

HortResearch

Proceedings of the 5th International Workshop on Functional-Structural Plant Models

Napier, New Zealand
November 4-9, 2007

Abstracts of Papers and Posters

Edited by
Przemyslaw Prusinkiewicz, Jim Hanan,
and Brendan Lane

Abstracts in these Proceedings have been accepted by the scientific committee. The editors are not responsible for the material contents of the abstracts.

Abstracts are paginated by abstract number and page number within that abstract, rather than cumulatively from the start of the abstracts.

Printed by Print Solutions Hawke's Bay Limited
Napier, New Zealand, October 2007

Table of Contents

Invited Presentations

Oral Presentations

Session 1: Resource allocation

Session 2: Signals and development

Session 3: Photosynthesis

Session 4: Nitrogen in plants / Plant measurement techniques

Session 5: Modeling software

Session 6: Plants, pathogens, and sprays

Session 7: Biophysics and biomechanics

Session 8: Crop plants

Session 9: Tree models

Session 10: Leaves to canopies

Session 11: Mathematical methods

Session 12: Patterns and tissue

Session 13: Light environment

Posters

Introduction

> *Computer models that treat plants as consisting of elementary units have become increasingly popular. The core of such a model is the description of what happens in a single element.... A computer program takes care of all the elements and integrates their activities to the functioning of the whole plant. Both the 3-D architecture and the metabolic processes can be treated in the same model at the same time in a natural way. Increasing speed of computers, developing programming tools and available mathematical techniques have made the construction of such models increasingly feasible.*
>
> Risto Sievänen, Annikki Mäkelä and Eero Nikinmaa, organizers of the first FSPM workshop (preface of Silva Fennica, Vol 31(3), 1997).

This short text outlines the spirit of the series of workshops on functional-structural plant modeling, initiated in 1996. The goal is to provide a forum for researchers and students from all over the world, who work on theory and practical applications of integrative plant models, combining plant architecture, molecular genetics, plant physiology, and environmental influences with computer science and mathematics. The general aim is to better understand the complex biological processes that are involved in plant functioning and growth, by designing and making use of advanced computer simulation techniques, and to put these models into practical use.

The first workshop took place in Helsinki, Finland, in December, 1996. It focused on the modeling of the distribution of growth within an individual tree, and the mathematical description and measurement of three-dimensional tree structure. See the special issue of Silva Fennica, vol 31, number 3.

The second workshop, with the same scientific profile, was held in Clermont-Ferrand, France, in October, 1998. See the special issue of Annals of Forest Science, vol. 57, number 5/6.

The third workshop was held in Montreal, Canada, in September, 2001. It broadened the scope of the series to include models of tree stand structure and function.

The fourth workshop took place in Montpellier, France, in June, 2004. Its scope was further broadened to include all types of plants (woody and herbaceous), and functional-structural plant models operating at the molecular level. The workshop attracted over 170 participants from all over the world. For a record of this meeting, including full proceedings, see http://amap.cirad.fr/workshop/FSPM04/index.html, as well as the special issue of New Phytologist, vol 166, number 3.

The 2007 meeting is the fifth edition in the FSPM series.

Committees

FSPM Advisory Board

Bruno Andrieu
INRA, France

Christophe Godin
INRIA, France

Jim Hanan
University of Queensland, Australia

Philip Lewis
University College London, U.K.

Przemyslaw Prusinkiewicz
University of Calgary, Canada

Risto Sievänen
Finnish Forest Research Institute, Finland

Jan Vos
Wageningen University and Research Centre, The Netherlands

Theodore DeJong
University of California, Davis, U.S.A.

Yan Guo
China Agricultural University, China

Winfried Kurth
Brandenburg University of Technology at Cottbus, Germany

Eero Nikinmaa
University of Helsinki, Finland

Alla Seleznyova
HortResearch, New Zealand

Hervé Sinoquet
INRA, France

Organization

Conference Chair

Alla Seleznyova
HortResearch, New Zealand

Brendan Lane
University of Calgary, Canada

Karen McLean
Encore Events

Stuart Tustin
HortResearch, New Zealand

Andrea Leonard-Jones
HortResearch, New Zealand

Sue Page
Encore Events

Program Committee

Program Chairs

Przemyslaw Prusinkiewicz
University of Calgary, Canada

Jim Hanan
University of Queensland, Australia

Bruno Andrieu
INRA, France

Christine Beveridge
University of Queensland, Australia

Gerhard Buck-Sorlin
Leibniz Institute for Plant Genetics and Crop Plant Research, Germany

Michael Chelle
INRA, France

Theodore DeJong
University of California, Davis, U.S.A.

Thierry Fourcaud
CIRAD, France

Christophe Godin
INRIA, France

Yann Guédon
CIRAD, France

Yan Guo
China Agricultural University, China

Henrik Jönsson
Lund University, Sweden

Winfried Kurth
Brandenburg University of Technology at Cottbus, Germany

André Lacointe
INRA, France

Philip Lewis
University College London, U.K.

Minami Matsui
RIKEN Yokohama Institute, Japan

Peter Minchin
HortResearch, New Zealand

Eero Nikinmaa
University of Helsinki, Finland

Loïc Pagès
INRA, France

Alla Seleznyova
HortResearch, New Zealand

Risto Sievänen
Finnish Forest Research Institute, Finland

Wendy Silk
University of California, Davis, U.S.A.

Hervé Sinoquet
INRA, France

Suchada Siripant
Chulalongkorn University, Thailand

Dave Skirvin
University of Warwick, U.K.

Kiyoshi Umeki
Chiba University, Japan

Jan Vos
Wageningen University and Research Centre, The Netherlands

Support

The following organizations supported this workshop:

The Horticulture and Food Research Institute of New Zealand Ltd. (HortResearch)

New Zealand Institute of Agriculture and Horticultural Science

Special Presentations

Looking back: Ten years of FSPM

Risto Sievänen
Finnish Forest Research Institute, PB 18, 01301 Vantaa, Finland

Keywords: functional-structural plant model, plant architecture, plant growth

Functional Structural Plant Models (FSPMs) can be defined as models that combine descriptions of metabolic (physiological) processes with a presentation of the 3D structure of a plant. The architectural structure of the model plant is usually presented on the basis of a small number of elementary units. The structural dynamics of the plant is based on the production, death and growth of the elementary units, and is affected by the metabolic processes. Under this definition four workshops have been arranged since 1996. The workshops have covered many aspects of plant modeling from measurement and representation of plant architecture, models of resource use and internal processes to mathematical and computer science methods. It seems that the focus of the meetings, interaction of function and structure in plants, has turned out to be fruitful, being open to scientists from any scientific discipline to contribute to the topic to better understand the complex biological processes that are involved in plant development.

This presentation will give an overview of functional structural plant modeling. First, a historical look is made on development of FSPMs and the basis on which they have been built. A short examination of different approaches to FSPMs will be made. Finally, the major challenges and avenues of development for FSPMs are discussed.

Experiment-based models of phyllotaxis

Cris Kuhlemeier
Institute of Plant Sciences, University of Berne

Phyllotaxis, the regular arrangement of leaves or flowers around a plant stem, is an example of developmental pattern formation and organogenesis. Phyllotaxis is characterized by the divergence angles between the organs, the most common angle being 137.5°, the golden angle. Models of phyllotaxis must explain its de novo establishment in the radially symmetric embryo, the stable maintenance of the different arrangements and the observed transitions between phyllotactic patterns. Most importantly, they must explain the specific divergence angles of 180°, 90°, 137.5° and in rarer cases other angles as well [1].

This quantitative aspect makes phyllotaxis an unusual developmental problem. It has traditionally attracted the interest of mathematicians and computer scientists, who have constructed a wide variety of simulation models. To the biologist it is surprising that only minimal assumptions about the underlying molecular mechanisms are sufficient to arrive at mathematical models that correctly and robustly recreate phyllotactic patterns. In this presentation I will give an overview of the experimental work on phyllotaxis and how these experiments form the basis for a new generation of simulation models. The interplay between modeling and experiment will be discussed.

Early experimental work [2] showed that phyllotactic patterns can be disrupted by experimental interference, but that they will quickly recover and reestablish the original arrangement. Apparently, aberrant positioning can be somehow corrected. On the other hand, transitions between patterns, for instance from decussate to spiral, occur frequently during the life of a single plant, indicating that developmental switches can override the self-correction mechanism. In our own work we showed that inhibition of polar auxin transport specifically inhibits organ formation but not stem growth or meristem maintenance. Local application of a microdroplet of auxin to the flank of the naked meristem could rescue the defect [3]. The subcellular localization of the auxin transporters was consistent with auxin accumulation at the site of organ initiation. The ensuing model postulates that auxin is an inducer of lateral organ formation, that preexisting organs serveas auxin sinks and that the position of a new organ is determined by active transport of auxin [4].

This conceptual model formed the basis for a new generation of computer simulations that were constructed in collaboration with our colleagues at the University of Calgary [5]. The three key assumptions of the model are that patterning occurs in the L1 surface layer of the meristem, that auxin is readily available within the patterning tissue but is redistributed by a combination of diffusion and active transport, and that auxin transport proteins are positioning towards the neighboring cell with the highest auxin concentration (“up-the-gradient” polarization). Such a model can be tested by experiment, guide further experiments and lead to further development of the model.

1. Kuhlemeier, C., *Phyllotaxis.* Trends Plant Sci., 2007. **12**: p. 143-150.
2. Snow, M.S., R., *Experiments on Phyllotaxis.* Philos Trans R Soc Lond B Biol Sci, 1931. **221**: p. 1-43.
3. Reinhardt, D., T. Mandel, and C. Kuhlemeier, *Auxin regulates the initiation and radial position of plant lateral organs.* Plant Cell, 2000. **12**(4): p. 507-518.
4. Reinhardt, D., et al., *Regulation of phyllotaxis by polar auxin transport.* Nature, 2003. **426**(6964): p. 255-260.
5. Smith, R.S., et al., *A plausible model of phyllotaxis.* Proceedings of the National Academy of Sciences of the United States of America, 2006. **103**(5): p. 1301-1306.

Oral Presentations

Mechanistic modelling of carbon allocation among sinks
A generalised Münch model for branched architectures

André Lacointe[(1)] and Peter Minchin[(2)]
[(1)]UMR (INRA - Université B. Pascal) PIAF, INRA, Site de Crouel,
234 avenue du Brézet, F-63039 Clermont-Ferrand Cedex 2, France
[(2)] The Horticultural and Food Research Institute of New Zealand Ltd., 412 No. 1 Rd., RD2
Te Puke, New Zealand
lacointe@clermont.inra.fr , pminchin@hortresearch.co.nz

Keywords: xylem, phloem, water, fluxes, loading, unloading, sink priority, modularity

Introduction

Partitioning of carbohydrate between competing sites is fundamental to all plant development, growth, and eventually yield. Carbohydrate is synthesised in the mature leaves and distributed by the phloem vasculature to sites of utilisation. The mechanism currently believed to drive phloem transport was proposed by Münch in 1928 and only recently generally accepted. However, the processes determining how much goes to each competing sink are still unknown. Models of plant growth that integrate knowledge of the individual processes still rely upon empirical algorithms to describe carbon (C) partitioning, which is a major bottleneck to allow truly predictive modelling, especially in changing conditions (Lacointe 2000, Minchin and Lacointe 2005), and can only be solved through mechanistic understanding.

Mechanistic models: phloem transport v. C allocation

To date, all mechanistic modelling of phloem transport, i.e. pressure-driven mass flow, has involved simple flow geometries (Thompson and Holbrook 2003, and references therein; Hölttä et al. 2006), as realistic geometries make the mathematics intractable. As a result, these attempts could not address spatial allocation among sinks, although they successfully simulated a number of quantitative properties of phloem transport. On the other hand, Minchin et al. (1993) developed a mechanistic model, based upon a simplified version of Münch's hypothesis, which successfully mimicked C flows to two competing sinks, suggesting that sink priority is an emergent property of osmotically driven mass flow. That is, sink priority is a property of the entire system, not any single component. Recently, the same minimal Münch model of osmotically generated pressure driven phloem flow through a resistive non-leaky transport pathway, has been incorporated into the functional-structural tree model L-PEACH (Allen et al., 2005) which can handle a realistic complex branched architecture. However, this minimal model ignores most of the known physiology of conduction tissues, including ubiquitous lateral transfers between both sap systems. As a result, the importance of these to the overall function and partitioning of phloem flow is still unclear.

A generalised Münch model for realistic architectures

A few years ago, Daudet et al. (2002) introduced the modular approach to handle realistic geometries in an extended Münch model that quantitatively described the coupled water/C fluxes through the double xylem/phloem pathway. Beside its ability to represent any branched architecture, the modular concept allowed explicit descriptions of local C and water exchange properties as well as C metabolism at an arbitrary level of detail (i.e. the size of elemental modules), thus allowing a realistic description of the local source/sink functions throughout the architecture and eventually a mechanistic description of C allocation among organs. However,

because of its implementation based on the electronic circuit simulation software SPICE, the original version was hardly user-friendly, and above all could not be easily interfaced with other process modules in an integrated structural-functional model. To overcome these limitations, the generalised Münch model has recently been transcribed into the C++ computer language.

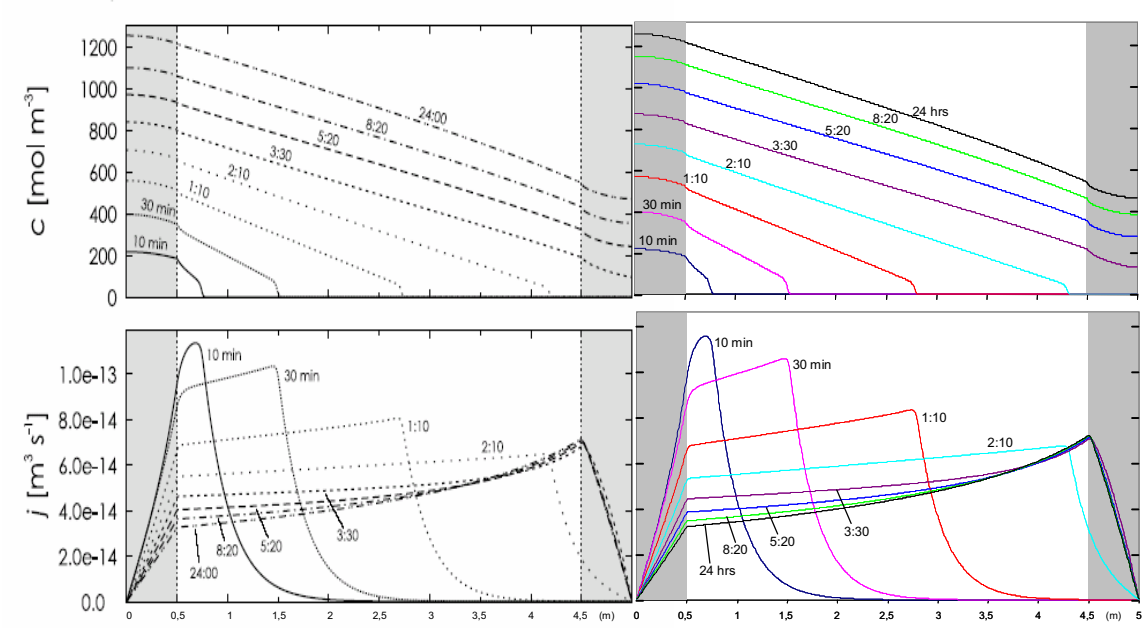

Fig. 1. Münch model: standard continuous approach (Thompson and Holbrook 2003, to the left) v. modular approach (to the right) : simulation of dynamic profiles of concentration and axial water fluxes along an ideal 5-metre-long sieve tube with a 50-cm-long uniform loading area and a 50-cm-long uniform unloading area at either end. On this simple, unbranched architecture, both approaches yield quasi-identical results; however, contrary to the continuous approach, the modular approach can handle realistic, branched architectures and complex loading/unloading patterns.

Current version of the model

Beside its ability to interact with other processes, the generalised Münch model has been significantly improved in 2 aspects: (1) entering the architecture configuration and source-sink properties is much more straightforward, by just editing a few lines in the code; (2) the mathematical solving capacities, now allowing a significantly larger number of elemental (branched or not) modules to be included in the architecture (N > 1000). It has been validated by comparison with the current reference for the Münch model (Thompson and Holbrook 2003), in the simple, unbranched configuration that the continuous approach can handle (Fig. 1). This comparison further demonstrated the flexibility and extensibility of our modular approach, as a few refined biophysical details (e.g. viscosity changes with concentration, or non-zero specific sugar volume) that were not originally present in the SPICE version (Daudet et al. 2002) had to be included in the model.

At the current stage of development this model describes a static (non-growing) architecture, but the same approach is easily extended to a developing architecture by inclusion into any modular FSPM that allows deriving parameters and state variables of the new modular elements from those of pre-existing elements. Accordingly, it will be implemented into the model PIAF-1 (Lacointe and Donès, 2007) as a mechanistic module for water and C fluxes.

This presentation will further show how the generalised Münch model can account for sink priority in a simple branched configuration: 1 source / 2 sinks, i.e. the original configuration of Minchin et al. (1993) but including more relevant physiological processes, especially xylem/phloem interactions in relation to loading/unloading properties.

References

Allen MT, Prusinkiewicz P, DeJong TM 2005. Using L-systems for modelling source-sink interactions, architecture and physiology of growing trees: the L-PEACH model. New Phytologist 166(3): 869-880.

Daudet F.A, Lacointe A., Gaudillère J.P., Cruiziat P. 2002. Generalized Münch coupling between sugar and water fluxes for modelling carbon allocation as affected by water status. Journal of Theoretical Biology 21: 481–498.

Hölttä T., Vesala T., Sevanto S., Perämäki M., Nikinmaa E., 2006. Modeling xylem and phloem water flows in trees according to cohesion theory and Munch hypothesis. Trees 20: 67-78.

Lacointe A., 2000. Carbon allocation among tree organs: A review of basic processes and representations in functional-structural tree models. Annals of Forest Science 57, 521-533.

Lacointe A., Donès N., 2007. Functional –structural modelling using the generic tool PIAF-1 : a simulation example on young walnut. This workshop, oral presentation.

Minchin PEH, Thorpe MR, Farrar JF., 1993. A simple mechanistic model of phloem transport which explains sink priority. Journal of Experimental Botany 44: 947–955.

Minchin P.E.H., Lacointe A., 2005. New understanding on phloem physiology and possible consequences for modelling long-distance carbon transport. New Phytologist 166: 771–779.

Münch E, 1928. Versuche über den Saftkreislauf. Deutsche botanische Gesellschaft 45, 340-356.

Thompson MV, Holbrook NM., 2003. Application of a single-solute non-steady-state phloem model to the study of long-distance assimilate transport. Journal of Theoretical Biology 220: 419–455.

A dynamic 3D model of rape (*Brassica napus* L.) computing yield components under variable nitrogen fertilisation regimes

Christian Groer[1], Ole Kniemeyer[2], Reinhard Hemmerling[2], Winfried Kurth[2], Heiko Becker[3] and Gerhard Buck-Sorlin[4,*]
[1]SALT Solutions GmbH, Charlottenstraße 34, D-01099 Dresden, Germany
[2]Dept. of Computer Science, Chair for Practical Computer Science / Graphics Systems, Brandenburg Technical University Cottbus, Ewald-Haase-Str. 12/13, D-03044 Cottbus, Germany
[3]Dept. of Crop Sciences, Plant Breeding Unit, University of Göttingen,Von-Siebold-Str. 8, D-37075 Göttingen, Germany
[4]Dept. Crop and Weed Ecology, Wageningen UR, Haarweg 333, 6709 RZ Wageningen, The Netherlands; gerhard.buck-sorlin@wur.nl; [*]corresponding author

Keywords: L-Systems, GroIMP, optimal yield, oilseed rape, *Brassica napus* L., nitrogen fertilisation

Introduction

Oilseed rape (*Brassica napus* L.) is a crop which is grown mainly for its high quality oil and protein. Rapeseed provides a versatile oil, being used not only for cooking and frying but also as a fuel and a raw material for the chemical industry. In the face of global climate change, rapeseed could play a much more important role in the future as source of renewable energy. There is thus a considerable interest in an optimisation of seed yields. One factor determining yield of rapeseed in the field is the amount and timing of nitrogen (N) fertilisation. The major downside of this crop management measure is the easy overfertilisation and subsequent infiltration of nitrate into the groundwater. The experimental determination of optimal fertilisation timing and dosage scenarios is notoriously difficult under variable soil and climate conditions and thus justifies the use of a functional-structural rapeseed model.

We will here present such an FSPM of rapeseed, which has been implemented in the modelling language XL (Kniemeyer 2004), an extension of the rule-based L-system formalism. This FSPM constitutes a set of morphogenetic rules describing the dynamics of organ formation and extension, as well as the topology of organs to form the next higher scale, that of the plant individual. The model is coupled with a Java implementation of a leaf photosynthesis model, allowing the computation of CO_2-assimilation for each leaf, based on climatic input parameters. Furthermore, assimilates are transported according to a sink-source model based on credit points, explained below.

Materials and Methods

The FSPM of rapeseed presented here includes, besides detailed morphogenetic rules, a set of rules and functions that describe certain important metabolic processes (mainly concerning carbon (C) and N budget). Associated processes that have an influence on both morphological and physiological aspects of the plant have also been considered in the model, such as: leaf senescence, respiration and interdependencies between N and C metabolism, especially during photosynthesis.

Composition of the rapeseed FSPM: Scope of morphology and phenology: The model has been constructed from published morphological and phenological descriptions (e.g., Sylvester-Bradley and Makepeace, 1984) and parameterised using several data sets captured during field trials conducted at the University of Göttingen over several years. The mature virtual rapeseed individual is made up of the following organ categories: shoot (shoot apical meristem, leaf, stem internode), inflorescence (inflorescence internode, flower petiole, flower (sepal, petal, stamen, carpel → silique)). The time frame considered for the model is March 1 (vernal regrowth of the hibernated leaf rosette) to July 15 (harvest of the mature plant in Germany). The time from sowing (end of

August) to the rosette stage (end of February) is neglected as no yield-relevant processes are taking place during this period and therefore no usable biometrical and developmental information were available about this period. The developmental phases covered in the model are thus: 1) late rosette growth, 2) bolting (i.e. rapid elongation of upper internodes with a terminal inflorescence), 3) flowering, 4) maturity (including formation of siliques and seeds).

C- and N budget: In our model, we only closely consider assimilation of C and N. All other mineral nutrients are regarded as non-limiting, to simplify matters. Sources of C-assimilates in rapeseed are the leaves and the walls of the siliques. C-assimilates are transported from the sources to sinks via internodes. Every part of the plant is a sink, thus C-assimilates are also consumed in source organs. However, flowers, seed forming siliques and meristems, including all young extending organs, are much stronger sinks. Part of the assimilates is also allocated to root growth although roots are not explicitly included in the structural model. C-assimilation depends on a set of environmental (temperature, humidity, radiation) and biometric variables (leaf area). Finally, the onset of senescence decreases the assimilative power of leaves. Further factors that determine consumption of assimilated C are growth respiration and maintenance respiration, which are computed as losses of about 30% of assimilated C, and 2 % per day per g biomass, respectively. A big percentage of assimilates is stored in seeds, and maximisation of this amount is an important breeding target.
To model C assimilation, a Java implementation of the model LEAFC3 (Nikolov et al. 1995) was used and its extension LEAFC3-N (for photosynthesis at different N-regimes in winter wheat, Müller et al. 2005) consulted. Leaf senescence was simulated as a linear function of leaf age.
N-assimilation in rapeseed takes place via the roots only and as nitrate. As roots are not modelled here, N-assimilation is achieved via a set of parameters linked to a virtual root node. The parameter-set is an XML-formatted file containing an array of daily input values for nitrogen. Missing daily values are interpolated. Shortage of nitrogen induces early bolting and flowering, ensuing a short stature and reduced yield. Vice versa, additional doses of N during the right developmental phases can lead to considerable increments in yield, but this easily ensues overfertilisation. Assimilated N is used in the first place in C-assimilating plant organs and seeds. N thus plays an important role for C-assimilation.
Shading of leaves was simply computed as a function of the topological rank of a shaded organ relative to the maximum rank, assuming that lower leaves are more shaded than higher ones. Light distribution within the canopy was therefore not computed in this simplified shading model.

Sink-source method and transport system: Sink strengths were determined according to a system of credit points where each organ category (root, leaves, internodes, petioles, flowers, siliques, and seeds) was allocated a fixed number of basic credit points for C and N (e.g., 1000 for internodes, 500 for seeds, 400 for leaves). These basic points were derived from field observations of dry matter courses of these organ classes during development. The sink strength for C or N of a single organ instance is then computed as the ratio of the basic points for that organ category and the number of instances of that organ currently present on the plant.
The transport system is intrinsically related to the system of sinks and sources in the plant (e.g., cf. GREENLAB, de Reffye et al. 2004). We tested four different approaches to modelling transport: distribution based on requirement analysis, transport based on sink strength, direct transport with fixed rates, and transport based on diffusion. Of these, only the first proved to be practical; the features and disadvantages of the other three solutions will be discussed in the extended paper.

Simulations

Fig. 1 gives some screenshots of simulated oilseed rape individuals at three different developmental stages (bolting, flowering, full maturity). Model development and all simulations were done using our modelling language XL within the GroIMP environment (Kniemeyer 2004). The model is

capable of reproducing the overall dynamic appearance realistically, given an input weather file. Simulated time courses of dry masses of all organs, C-assimilation rates, C and N contents largely corresponded to observations and measurements, with simulated C- and N-assimilation rates typically showing ranges between 0.1 - 0.95, and 0.001- 0.009 g plant^{-1} d^{-1}, respectively, within the simulated time span of 122 days. However, simulated leaf dry mass decreased by only 50%, whereas in reality it drops to 10% of the maximum dry mass. This was due to the fact that the model just included leaf shedding but did not consider enough remobilisation of biomass from dying leaves. A comparative survey of simulated mobile and fixed C and N contents yielded that in the simulated days 30 to 60 there were hardly any mobile N reserves available: This can be explained by the fact that during this time mobile C reserves are built up which are later used to form flowers, siliques and seeds.

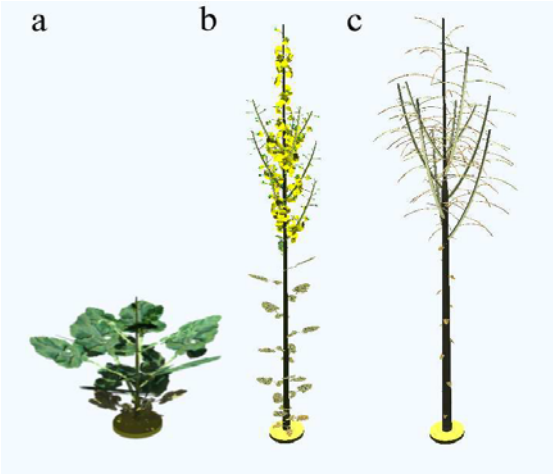

Fig. 1: Developmental stages of the virtual rapeseed: a) bolting, b) flowering, c) harvest maturity

Outlook

Future work will concentrate on the recalibration of parameters with new field data as well as on the application of optimisation algorithms (e.g., Hill Climbing, Threshold Accepting, Simulated Annealing) for the optimisation of seed oil content at reduced nitrogen fertiliser input. Also, the simple light model will be replaced with a raytracer-based radiation model in GroIMP in order to make proper use of the capabilities of the LEAFC3 photosynthesis model.

References

de Reffye, P., Yan, H., Kang, M.Z. and Dingkuhn, M. 2004. A dynamic, architectural plant model simulating resource-dependent growth. *Annals of Botany* **93**, 591-502.

Kniemeyer, O. 2004. Rule-based modelling with the XL/GroIMP software. In: Schaub, H., Detje, F. and Brüggemann, U. (eds.), The Logic of Artificial Life. Proceedings of 6th GWAL, Bamberg April 14-16, 2004, AKA Akademische Verlagsgesellschaft Berlin (2004), 56-65.

Müller, J., Wernecke, P. and Diepenbrock, W. 2005. LEAFC3-N: A nitrogen-sensitive extension of the CO_2 and H_2O gas exchange model LEAFC3 parameterised and tested for winter wheat (*Triticum aestivum* L.). *Ecological Modelling* **183**, 183-210.

Nikolov, N.T., Massman, W.J. and Schoettle, A.W. 1995. Coupling biochemical and biophysical processes at the leaf level: an equilibrium photosynthesis model for leaves of C3 plants. *Ecological Modelling* **80**, 205-235.

Sylvester-Bradley, R. and Makepeace, R.J. 1984. A code for stages of development of oilseed rape (*Brassica napus* L.). *Aspects of Applied Biology* **6**, 399-419.

Calibration of fruit cyclic patterns in cucumber plants as a function of source-sink ratio with the GreenLab model

A.Mathieu[1], B.G. Zhang[2], E. Heuvelink[3], S.J. Liu[2], P.H. Cournède[1], P. de Reffye[4]
[1] Ecole Centrale de Paris, Laboratoire MAS, Châtenay-Malabry, France
[2] China Agricultural University, College of resource environment, Beijing 100094 China
[3] Wageningen University, Horticultural Production Chains Group, Wageningen, The Netherlands
[4] INRIA Futurs, Digiplante, 91893 Orsay, France
Keywords: cucumber, *Cucumis sativus,* cyclic pattern, GreenLab, Functional-structural model

Introduction

The cyclic pattern in cucumber fruit production has been studied by several authors (Heuvelink and Marcelis, 1989; Marcelis, 1992) and it has been linked with the distribution of dry matter in the plant. We intend to test the influence of the biomass (assimilate) partitioning on these cycles (Marcelis, 1994; Bertin, 1995). To do so, the cucumber plant growth is reproduced with the functional structural plant model GreenLab, a generic model based on carbon production and allocation to control the plant architecture (Cournède et al, 2006). A new version of the model has been developed in which interactions between growth and development are taken into account through the introduction of a variable representing the source-sink ratio of the plant (Mathieu, 2006). For some set of parameters, the dynamic evolution of this variable generates rhythms in fruit set, and theoretical studies were presented in (Mathieu et al, 2006). As GreenLab is a mathematical model, its parameters can easily be estimated by inverse methods. Here, the growth of a cultivated cucumber plant is calibrated. Functional parameters are first estimated. As we suppose that fruit apparition depends on the source-sink ratio through parametric functions, we can compute in a second step the parameters controlling the interactions between growth and development.

Materials and Methods

The GreenLab model

In the GreenLab FSM (Yan et al, 2004), the plant growth is discretized by a time step based on the plant phyllochron. At each time step called a growth cycle (GC), the terminal apex builds a new metamer (one internode one flower, one leaf and one or more axillary buds). The model can run based on dry matter as well as fresh matter. For cucumber, fruits contain more than 95% water and are the main part of biomass produced, so it seems reasonable to take fresh mass instead of dry mass. In the model, we assume that assimilates produced by the plant fill a common pool that feed all the organs. At GC t, the amount of biomass Q^t is computed with a photosynthetic equation at the level of a single plant (g/plant).

$$Q^t = \frac{E.S_p}{R}(1 - e^{-\frac{S_f^t}{S_p}}) \qquad (1)$$

It depends on the total leaf surfaces S_f^t, an empirical coefficient S_p characteristic of the competition for light in the canopy, E the product of potential evapotranspiration (PET) and transpiration efficiency and R an empirical resistance. Then, this fresh matter is shared between all organs with a proportional allocation model: the distribution to each sink is proportional to its sink strength relative to the total sink strength called the demand D^t. Each organ has a fixed life span and a sink variation function determines the variations of the organ sink strength during its life. It is a flexible mathematical function based on the beta law and its parameters are estimated by inverse methods. A fruit grows during an expansion time of T_e^f GC. After a delay of t_0 growth cycles after its appearance, the fruit can develop if the ratio of biomass to demand at this cycles exceeds the threshold θ_0.

Parameter identification

To fit the growth of a given plant, we estimate hidden parameters of the model: S_p ,R for the biomass production, the organ sink variation functions for the allocation model, t_0 and θ_0. The error to minimize is based on the differences of organ weights and dimensions of simulated and measured plants (Guo et al, 2006). The calibration of the model is made by iterations of two successive steps. Firstly, the position of the fruit abortion on the stem are given as input parameters to estimate the functional parameters. Then, the delay t_0 and the corresponding threshold θ_0 are identified with a heuristic method as the error is a non continuous function of parameters.

Plant observations and measures

Cucumber plants (*Cucumis sativus* cv. mini2) were grown in a greenhouse of Beijing academy of agricultural sciences (BAAS) from 20 March to 15 June 2006. Plants received no supplementary light. Air temperature inside the greenhouse varying from 15 to 30 degrees and GDD (growing degree day) were calculated with a base temperature of 12 degrees. The plants were grown in containers with row spacing of 1 m and 0.5 m within a row. Cucumber plants were pruned with all axillary buds removed immediately after appearance. At each of the harvest dates, 4 plants were taken randomly and separated into root system and shoot, the later further divided into metamers. Length and diameter of internodes, leaves and petioles were measured with a digital vernier caliper, surface of individual leaves was analyzed by a software developed in BAAS.

Results

Three plants harvested at 10 May, 17 May and 13 June were fitted with the *Digiplante* software (Cournède et al, 2006). The growth cycle (GC) expressed in thermal time is equal to 30 GDD. The estimated seed values are similar for all the plants (0.34 g). The specific leaf weight of blades is set to an average value of 0.02 g.cm^{-2} and leaves are photosynthetically active during 20 GC. Blades, petioles are growing during 20 GC, internodes during 10 GC and fruits during 25 GC. In equation (1), E is set to 1 and the parameters are estimated $\boldsymbol{R} = 29.28, \boldsymbol{Sp} = 0.78$ m². The sink of an organ is the product of a maximum value that is estimated to 1 for blades, 0.51 for internodes, 0.62 for petioles and 68.5 for fruits and of a function of its age controlled by two empirical parameters *a, b* (see on figure 1a). Figure 2 shows the comparison between simulations and measures for the three measured plants.

When we fix the fruit position, the identification of the functional parameters gives the evolution of the ratio of biomass to demand (see figure 3). Then, we use inverse methods to compute the delay t_0 of 7 GC and the threshold $\theta_0 = 0.67$.

a)

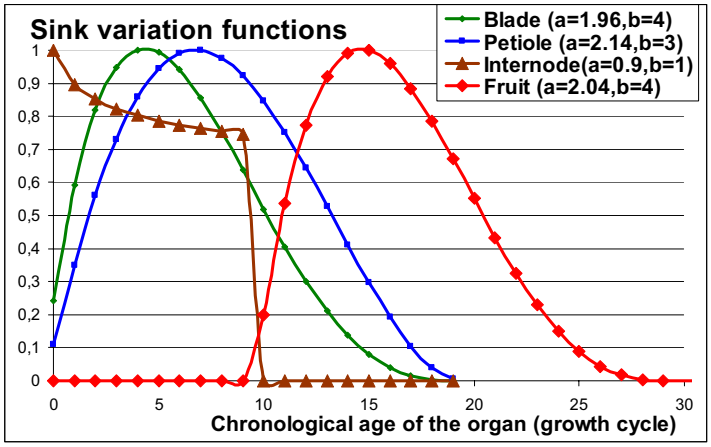

b)

Fig.1 a. Sink variation functions of the different organs of the plant. b. Visualization of the simulated plant.

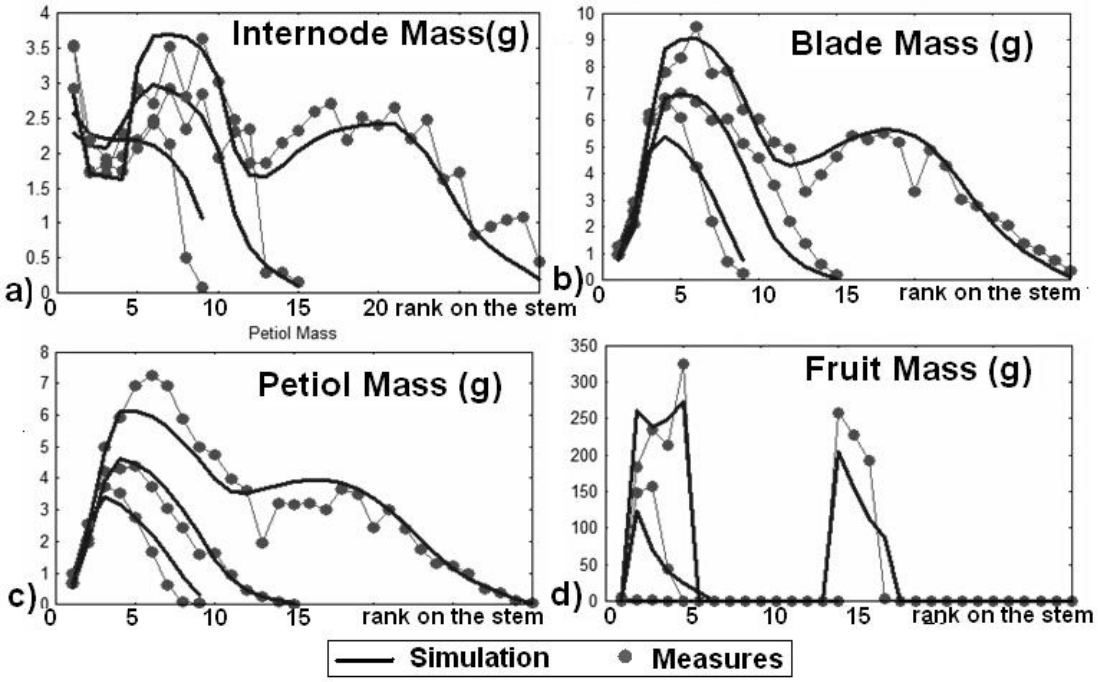

Fig 2.Simulated (lines) and measured (dots) fresh mass of a) internode, b) blade, c) petiol, d) fruit.

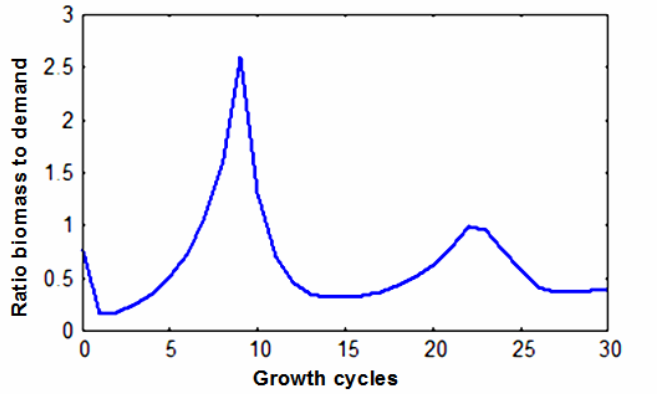

Fig. 3: Evolution of the ratio biomass to demand during growth. It shows the strong action of the fruits sinks that induces waves.

Discussion and conclusion

In the studied cucumber cultivar, every node bore flowers at emergence, and all flowers became fruits but some of them aborted sometimes later. We used our model to test a hypothesis proposed in (Marcelis, 1994) that the low assimilate availability was a cause of fruit abortion. In the model, the feedback of biomass partitioning on topology is set at the level of fruit apparition. The parallel between the rapid growth of fruits at some nodes and abortion of those on the following nodes did suggest a competition of assimilate and inhibition of early established fruits on the younger ones (and also on leaves and corresponding phytomers as their final sizes and biomass were smaller than the one of phytomers bearing the fruits).

The results we obtained are encouraging as we could fit the growth of the cucumber (sizes of organs) and the positions of the fruits with a small number of parameters. Although the model still

needs further validation and some phenomena that could have a great influence on plant growth and biomass partitioning should be implemented (energetic cost of the structure, storage compartment), it simulates with success the assimilate competition among organs and confirms the hypothesis that the growth and abortion of fruits depend on assimilate availability.

Acknowledgments

Xu S.Y. is kindly acknowledged for taking part in the measurement and Dr. Guo X.Y. for providing experimental facility. This work was supported by the High-Tech Research and Development Programme Ministry of Science and Technology of China project (2003AA209020)

References

Bertin, N. 1995. Competition fot assimilates and fruit position affect fruit set in indeterminate greenhouse tomato. *Annals of Botany* 75, 55-62.

Counède P, Kang M, Mathieu A, Yan H, Hu B, de Reffye P. 2006. Structural factorization of plants to compute their functional and architectural growth. *Simulation.* 82(7): 427-438.

Guo Y, Ma Y, Zhan Z, Li B, Dingkuhn M, Luquet D, de Reffye P. 2006. Parameter optimization and field validation for the functional-structural model GreenLab for maize. *Ann. Bot,* 97: 217-230.

Heuvelink E, Marcelis L. 1989. Dry Matter distribution in tomato and cucumber. Acta Hort. 260: 149-180.

Marcelis L. 1992. The dynamics of growth and dry matter distribution in cucumber. *Ann. Bot.*69: 487-492.

Marcelis L. 1994. A simulation model for dry matter partitioning in cucumber. *Annals of Botany*, 74: 43-52.

Mathieu A. 2006 *Essai sur la modélisation des interactions entre la croissance et le développement d'une plante: cas du modèle GreenLab*. PhD thesis, Ecole Centrale de Paris.

Mathieu A, Cournède P, Barthélémy D, de Reffye P. 2006. Generation of rhythms in plant development controlled by their functioning: theoretical and numerical study. In *IEEE International Conference on Plant Models and Applications, Chine.*

Yan HP, Kang MZ, de Reffye P, Dingkuhn M. 2004. A dynamic, architectural plant model simulating resource-dependent growth**.** *Ann. Bot.* 93: 591 – 602.

Self-organized resource allocation and growth partitioning at the whole plant level: a modeling study

Zongjian Yang[a] and David J. Midmore[b]

[a]Agricultural Production Systems Research Unit, School of Land, Crop and Food Sciences
The University of Queensland, Brisbane, Qld 4072, Australia
[b]Centre for Plant and Water Science, School of Biological and Environmental Sciences
Central Queensland University, Rockhampton, Qld 4702, Australia
z.yang1@uq.edu.au

Keywords: auxin, self-organization, light foraging, apical control, resource allocation

Introduction

The development of different parts of a plant is highly coordinated, which enables them to capture and use resources efficiently in spatially and temporally heterogeneous environments (Sachs, 2006). The underlying physiological mechanisms that coordinate the growth of distantly located plant tissues/organs are still not fully understood. It is well known that the phytohormone auxin plays a pivotal role in integrating development throughout a plant (Leyser, 2003). But how auxin acts to integrate activities at the whole plant level remains to be elucidated.

Recent advances in complexity science have suggested that, based on distributed-control mechanisms, complicated structures and functions can emerge from the collective behavior of aggregates of smaller-scale subunits (Camazine et al., 2003). Because of their distributed-control character, self-organized systems tend to be robust and flexible in the face of varying environmental conditions. Plants are modular organisms. They consist of morphological and physiological subunits that act semi-autonomously (Orians et al., 2005). The morphological development of a plant largely relies on distributed-control mechanisms. The concept of self-organization based on distributed-control mechanisms holds great promise for an in-depth understanding of the organizational laws that generate overall plant structure and functions (Colasanti and Hunt, 1997; Sachs, 2004).

Based on a self-organization mechanism for resource allocation mediated by auxin, a mathematical model is proposed in this study to explain the origin of coordination among shoot branches.

The model

According to the hypothesis of pipe model and the theory of branch autonomy, the shoot canopy of an individual plant is represented as an assemblage of relatively independent modular subunits (branches) competing for root-derived resources (water, nutrients and/or hormonal factors). The allocation of root-derived resources to different parts of the shoot canopy is determined by their relative vascular contacts with the root system. For simplicity, in this study, the shoot canopy of an individual plant is divided into n macro-branches arranged in parallel. These macro-branches can be divided into more detailed subunits in a nested hierarchical way and included in the model following the same rules. Subunits of a macro-branch compete for resources allocated to this macro-branch, but they join force to compete with other macro-branches.

It is well known that the basipetal flow of auxin plays a pivotal role in the regulation of primary and secondary growth of vascular tissues. Auxin moves in a basipetal polar manner in defined pathways, which leads to oriented vascular differentiation (Aloni, 2004; Berleth et al., 2000). In the model, development of vascular network is specified by the polar transport of auxin produced by various parts of the shoot canopy in response to their immediate internal and external environments. Conductivity of vascular elements is modeled as a power function of their cross-sectional area.

The site and mechanism of auxin synthesis and activation are still not well known. High levels of IAA are found in regions of active cell division. Young leaves, especially the fast growing regions, are generally considered to be the primary locations of auxin biosynthesis. In the model presented here, rates of bioactive auxin production are determined by rates of branch growth and are modified by local light conditions.

Simulation results

Model behaviors were studied by running the model under various light conditions. In response to within canopy light heterogeneity, proportionally more root-derived resources were allocated to branches growing under better light conditions so the growth of this branch was enhanced. The performance of shaded branches declined gradually and, when the maintenance requirement exceeded their nitrogen capture rate, senescence occurred (Fig. 1). These simulation results are consistent with general observations in realistic plants that, in response to light heterogeneity within a single canopy, plant tends to partition proportionally more growth to branches in more favorable positions whereas shaded branches gradually cease growing and are eventually shed.

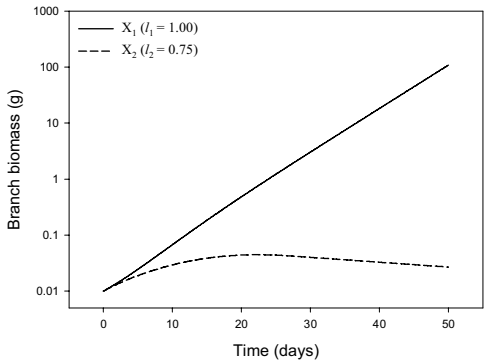

Figure 1. Simulated branch growth in response to a spatially heterogeneous light environment within the shoot canopy. Branch X_1 was growing under saturating light while X_2 on the same plant was shaded.

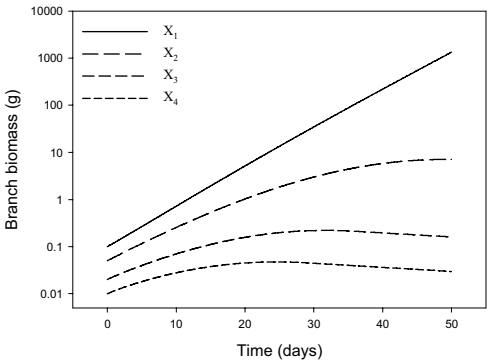

Figure 2. Simulations including four branches with different initial sizes. Showing the inhibition effects of X_1, the largest dominant branch, on the development of smaller branches (X_2, X_3 and X_4).

It has generally been assumed that morphological adjustment in response to light heterogeneity within a shoot canopy will lead to an advantage to the plant in terms of resource acquisition and whole plant performance. In order to assess the cost and benefit of the optimal partitioning function, the performance of the whole plant was simulated under heterogeneous light conditions. This simulation result was compared with the performance of the plant under the same light profile but without morphological adjustment ability. The simulation results suggest that, in a spatially heterogeneous light environment, the performance of the whole plant can be greatly improved by selective placement of shoot canopy under better light conditions.

Asymmetric competition also occurs when changing the relative initial size of competing branches. Fig. 2 shows the simulated correlative interactions among four branches with different initial sizes. In the presence of the largest branch (X_1), the development of other smaller branches (X_2, X_3 and X_4) was greatly inhibited (Fig. 2). If X_1 was removed or shaded, the second largest branch (X_2) was released from inhibitory control and became the dominant branch which exerted inhibitory effects over the growth of other two smaller branches (X_3 and X_4). This inhibitory effect might be able to explain the origin of apical dominance and apical control in which the primary shoot apex exerts inhibitory control over the growth of smaller lateral buds and branches.

Discussion

The model was constructed on the basis of minimal requirement, but it displays rich and realistic behaviors with respect to light foraging and correlative control. In the model, subunits of a plant

follow only simple local rules regarding growth and auxin production. By altering the amount of auxin they release individually in response to the local environment and modifying their relative vascular contact with the root system, subunits of a shoot canopy are able to coordinate without a central controller and self-organize into functional and structural patterns. The results of this modeling study indicate that morphological dynamics at the whole plant level can be understood as the sum of all modular responses to their local environments.

Oriented vascular differentiation specified by polar auxin transport plays a central role in the model. The auxin production by growing branches creates a self-reinforcing feedback loop. Branches with greater sizes and/or developing under better light conditions release more auxin, which enhances their vascular contact with the root system and further increases their competitive ability. This self-reinforcing mechanism might have adaptive significance, as it enables the plant to invest proportionally more and more biomass in the most promising branches with greater developmental potential and higher photosynthetic activity (Sachs, 2006). Nutrient diversion hypotheses have long been proposed to explain the phenomena of light foraging and correlative dominance, but how allocation of resource to different parts of a plant is controlled remains unclear. The success of this simple abstract model in reproducing realistic correlative effects suggests that oriented-vascular-differentiation specified by polar auxin transport could be the invisible 'guiding hand' that controls the proportion of resource going to each sink. Growing shoot parts, including vegetative and reproductive organs, continuously release auxin to maintain adequate vascular links for resource supply.

Similar to the architecture of shoot canopies, root systems are modular and plastic. Different parts of the root system of an individual plant compete for auxin and photoassimilates from the shoot canopy. An extension of the model including root development and function may well be able to account for the root morphological response to the patchy distribution of nutrient resources in the soil. This model does not consider reproductive growth. Similar to the competition between vegetative modules, reproductive organs compete with one another. Early-formed fruits and seeds inhibit later-established fruits and seeds. It is possible that the self-organizing control for resource allocation is a basic mechanism for all developing sinks including both vegetative and reproductive organs.

Acknowledgements

We thank Professor Tsvi Sachs, Professor Graeme Hammer and Dr Jim Hanan for valuable comments. Financial support was provided by Central Queensland University and Australian Research Council.

References

Aloni, R., 2004. The induction of vascular tissues by auxin, in: Davies, P. J. (Eds.), Plant hormones: biosynthesis, signal transduction, action. Kluwer Academic Publishers, Dordrecht, The Netherlands, pp. 471-492.

Berleth, T., Mattsson, J., Hardtke, C. S., 2000. Vascular continuity and auxin signals. Trends Plant Sci. 5(9), 387-393.

Camazine, S., Deneubourg, J.-L., Franks, N. R., Sneyd, J., Theraula, G., Bonabeau, E., 2003. Self-organization in biological systems. Princeton University Press, Princeton, USA.

Colasanti, R. L., Hunt, R., 1997. Resource dynamics and plant growth - a self-assembling model for individuals, populations and communities. Funct. Ecol. 11(2), 133-145.

Leyser, O., 2003. Regulation of shoot branching by auxin. Trends Plant Sci. 8(11), 541-545.

Orians, C. M., Babst, B., Zanne, A. E., 2005. Vascular constraints and long distance transport in dicots, in: Holbrook, N. M., Zwieniechi, M. A. (Eds.), Vascular transport in plants. Elsevier Academic Press, Boston, USA, pp. 355-371.

Sachs, T., 2004. Self-organization of tree form: a model for complex social systems. J. Theor. Biol. 230(2), 197-202.

Sachs, T., 2006. How plants choose the most promising organs?, in: Baluska, F., Manusco, S., Volkmann, D. (Eds.), Communication in plants: neuronal aspects of plant life. Springer-Verlag, Berlin, pp. 53-63.

Evaluation and Calibration of the Carbohydrate Assimilation, Partitioning, and Transport Processes in the L-PEACH Model

Romeo Favreau, Gerardo Lopez, Colin Smith and Theodore DeJong
Department of Plant Sciences University of California Davis, CA 95616 USA
rrfavreau@ucdavis.edu, gerlopez@ucdavis.edu, smithco@gmail.com,
tmdejong@ucdavis.edu

Keywords: tree modeling, carbohydrate partitioning, source-sink relationships, L-systems, plant growth simulation, functional structural plant modeling

Introduction

The goal of the L-PEACH functional-structural plant model (Allen *et al*., 2005) is to simulate the development of a plant's architecture, track its functional elements during growth, exchange carbon and other resources between all the plant's elements and make the individual components sensitive to local availability of carbon and external environmental signals. L-systems (Lindenmayer, 1968) with subsequent extensions (Karwowski & Prusinkiewicz, 2003; Mech & Prusinkiewicz, 1996; Prusinkiewicz & Lindemayer, 1990) were used to integrate these elements. The carbon source-sink interactions and carbohydrate transport within the plant were modeled using an analogy of electric circuits (Minchin *et al*., 1993). The underlying method was proposed by Federl and Prusinkiewicz (2004) for linear circuits, and was extended in L-PEACH for non-linear circuits. While the original model provided a prototype for how to integrate plant architectural growth and carbon economy, much calibration and quantitative evaluation work on the functionality of the proposed electrical circuit network analogy for distributing carbohydrate within the modeled tree structure remained. The goal of this presentation is to document this calibration and quantitative evaluation and present recent upgrades to the L-PEACH model.

General improvements to the L-PEACH model

The original model (Allen *et al*., 2005) was not calibrated to specific units of carbon and did not address plant respiration. The model is now calibrated to a basic "currency" of grams of carbohydrate. Organ maintenance respiration has been included as a component in the electrical circuit of each module and is estimated during each daily time step. Growth respiration is accounted for in the carbohydrate cost of adding dry matter to each organ. Real time weather data can be included to account for changes in temperature and light.

The original model contained more than thirty–two functions describing theoretical responses of each module type to various parameters. Many of these functions were similar; so, the model was simplified by replacing the similarly shaped functions with a single function that is scaled for the particular relationships of other various components. Architectural components were also improved; but, these will be reported in a separate paper. An important new practical feature is that the model outputs can be saved at the end of several years of the simulation and then the model can be repeatedly restarted from the same point. This allows *in silico* management experiments (*eg.,.*tree pruning and fruit thinning).

Calibration and evaluation of the electrical circuit analogy for distributing carbohydrate

Due to the extreme complexity of the interactions of the components of the model, the most difficult aspect of calibration and quantitative evaluation has been the development of meaningful tools for systematically displaying quantitative outputs and tracking the behavior of individual modules in connection with other components of the model. Subroutines to automatically transfer

model generated data files to MatLab and MatLab programs were developed to graphically display data. With each simulation, hundreds of data files can be generated in MatLab and the quantitative behavior of each electrical component of every module can be displayed and analyzed, if desired. This has allowed systematic analysis and debugging of many aspects of the model and increased confidence that the source-sink/carbon partitioning components of the model are actually functioning in the manner that was originally anticipated. Using these techniques, the sensitivity of the model to resistance functions in several parts of the electronic circuitry has been tested and functional ranges for many resistances have been identified. The model is highly sensitive to some specific resistances in the electrical circuit and the complexity of interactions in the model can lead to unanticipated consequences, similar to real biological experiments. It is intriguing to anticipate specific carbohydrate transport resistance values within various parts of the plants may eventually be developed as emergent properties from this type of modeling effort when they have been virtually impossible to measure *in vivo*.

For demonstration purposes two figures are presented to illustrate the types of outputs that can be generated during simulation runs of L-PEACH. Figure 1 provides output data on the behavior of various organ types and some general data over two years of simulation. Stem weight declined between years because of stem loss during pruning. Stem and root storage declined early in the second year due to mobilization of stored carbon. The net source-sink balance is an error term indicating that virtually all the CHO that was fixed was distributed somewhere in the plant. Figure 2 provides the detailed behavior of the CHO balance in a single leaf over one year. The photosynthetic rate was quite sensitive to cloudy days but oscillations in the leaf CHO export rate were dampened over the same period. The leaf maintenance respiration rate was strongly influenced by fluctuations in temperature.

Conclusion

The basic approach for simultaneously modeling plant architectural growth and carbohydrate source-sink relationships and transport in plants appears to be functioning well in L-PEACH. More work remains in quantitatively calibrating and validating the model but it already has been used for integrating, simulating and understanding interactions between CHO source-sink relationships, architectural growth in trees and crop yield characteristics.

References

Allen, M., Prusinkiewicz, P., & DeJong, T. (2005). Using L-systems for modeling source-sink interactions, architecture and physiology of growing trees: the L-PEACH model. *New Phytologist,* 166, 869-880.

Federl, P., & Prusiniewicz, P. (2004). Solving differential equations in developmental models of multicellular structures expressed using L-systems. *Lecture Notes in Computer Science, 3037,* 65-72.

Karwowski, R., & Prusinkiewicz, P. (2003). Design and implementation of the L+C modeling language. *Electronic Notes in Theoretical Computer Science, 86(2)*. 19p.

Lindenmayer, A. (1968). Mathematical models of cellular interaction in development, Parts I and II. *Journal of Theoretical Biology., 18,* 280-315.

Mech, R., & Prusinkiewicz, P. (1996). Visual models of plants interacting with their environment. *Proceedings of SIGGRAPH 1996,* pp. 397-410.

Minchin, P., Thorpe, M., & Farrar, J. (1993). A simple mechanistic model of phloem transport which explains sink priority. *Journal of. Experimental. Botany*., *44,* 947-955.

Prusinkiewicz, P, & Lindenmayer, A. (1990). *The Algorithmic Beauty of Plants*, Springer-Verlag. New York. 228p.

Hypothesis-driven computational modelling of branching control in pea

Elizabeth A. Dun[a,b], Jim Hanan[a,c] and Christine A. Beveridge[a,b]
[a] Australian Research Council Centre of Excellence for Integrative Legume Research, The University of Queensland, St. Lucia, Queensland, 4072, Australia
[b] School of Integrative Biology, The University of Queensland, St. Lucia, Queensland, 4072, Australia
[c] Australian Research Council Centre for Complex Systems, The University of Queensland, St. Lucia, Queensland, 4072, Australia

Keywords: genetic network, branching regulation, signalling

Background

The control of shoot architecture is a multi-factorial process, involving long-distance signalling and coordination between distinct and spatially separated plant tissues. Multiple plant hormones appear to be involved in the regulation of axillary bud outgrowth. For example, auxin is widely recognised as a repressor of bud outgrowth, while cytokinin is acknowledged as an inducer of bud outgrowth. Auxin, however, may not directly regulate bud outgrowth, but may require an alternative messenger (reviewed in Dun *et al*., 2006). Candidates for auxin's secondary messenger include cytokinin (Bangerth, 1994; Li *et al*., 1995), in addition to a novel signal (Foo *et al*., 2005; reviewed in Leyser, 2005) named SMS, for Shoot Multiplication Signal (Beveridge, 2006). Cytokinin is thought to promote bud outgrowth, though its exact role remains unknown. The application of cytokinin directly to axillary buds, and the over-expression of cytokinin biosynthesis genes sometimes, but not always, induces bud outgrowth (King and Van Staden, 1984; Medford *et al*., 1989).

A number of genes involved in the control of shoot branching have been identified in pea (*Pisum sativum*). These include five *Ramosus* (*RMS*) genes, *RMS1* through *RMS5* (reviewed in Beveridge, 2006). Grafting studies have demonstrated a role for these genes in shoot and rootstock tissues. The inability of exogenous auxin applications to rescue the increased branching phenotypes of the *rms* mutants (Beveridge *et al*., 2000), and the auxin-inducible *RMS1* and *RMS5* gene expression (Foo *et al*., 2005; Johnson *et al*., 2006), suggests these genes are involved in the synthesis of auxin's secondary messenger.

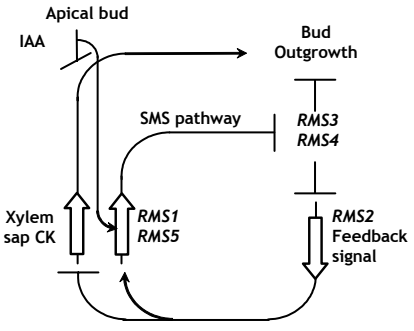

Fig. 1. Model for branching regulation in pea. Flat ended lines indicate repression; arrowhead lines indicate promotion. Adapted from Beveridge (2006)

Auxin and cytokinin analyses, together with grafting studies and putative enzymatic functions, suggest novel hormone-like signals, other than auxin and cytokinin, are involved in the regulation of shoot branching, and that their synthesis and/or level is regulated by the *RMS* genes. At least two novel signals are thought to exist, SMS moving from rootstock to shoot, and a *RMS2*-mediated feedback signal, moving from shoot to rootstock (Fig. 1). Evidence for the existence and regulation of the novel signals, both SMS and feedback signal, will be presented and explored using computational modelling techniques.

Research methodology

The research strategy employed essentially consists of two parts: computational modelling of the *RMS* branching regulatory network and biological experiments aimed to test features and/or predictions of the computational models. In the computational models, gene action was spatially separated into rootstock(s) and shoot(s), with directional flow of long-distance signals between the compartments. Genotypes were represented with a value of 1 if wild type, and 0 if mutant. The computational models were created in L-Studio using algebraic equations and simple mass action and conservation principles to represent the hypotheses about the relationships and interactions between model components. Only three parameters were utilized in the models, representing the proportion of signal made in the rootstock that is transported to the shoot, the proportion of signal made in the shoot that is transported to the rootstock, and the proportion of functional RMS2 product made in the *rms2* mutant. Many parameter value combinations were tested, and if a broad range of sensible parameters produced acceptable output, this was taken as support that the network interactions were responsible for the emergent behavior rather than the specific parameter values. In order to assess whether model output was acceptable, biological data were categorized, and the model output compared to the biological categories. If the computational model output did not correspond with the biological datasets, then the hypotheses were further adjusted. However, if the model output corresponded with the biological results, then predictions could be made for new biological plant-based experiments, and the experiments conducted. These new biological results could then be utilized to further refine hypotheses, making the approach iterative.

Directions

Computational models have been created that explain all the published experimental datasets. The models have been utilised to aid experimental design and result prediction. For example, based on a new proposed function for the gene *RMS4* in the rootstock, the model predicted that an *rms4* rootstock would be more inhibitory of branching in a wild-type scion than a wild-type rootstock. This was confirmed experimentally (Johnson *et al*., 2006). New plant-based experimental results testing aspects of the *RMS2*-mediated feedback signal's regulation and action will be presented, in addition to the implications to the regulation of branching in pea.

The results of this study indicate that systems with many unknowns can be modelled computationally based on hypotheses, and the effort is worthwhile, yielding both an improved understanding of the system and experimental predictions that can be tested. The strength of the approach is that it highlights data that are not explained by the hypotheses, triggering much thought to create alternate hypotheses that can be tested against the entire dataset computationally. The computational models can also be utilised to predict the results of new experiments, so it can be determined whether the experiment is worthwhile and indeed tests the hypothesis.

Acknowledgements

This research has been funded by the Australian Research Council, and by Australian Postgraduate Awards (scholarship to E.A.D.).

References

Bangerth, F. (1994). Response of cytokinin concentration in the xylem exudate of bean (*Phaseolus vulgaris* L.) plants to decapitation and auxin treatment, and relationship to apical dominance. Planta. 194, 439-442.

Beveridge, C.A. (2000). Long-distance signalling and a mutational analysis of branching in pea. Plant Growth Regul. 32, 193-203.

Beveridge, C.A. (2006). Axillary bud outgrowth: sending a message. Curr. Opin. Plant Biol. 9, 35-40.

Dun, E.A., Ferguson, B.J., and Beveridge, C.A. (2006). Apical dominance and shoot branching. Divergent opinions or divergent mechanisms? Plant Physiol. 142, 812-819.

Foo, E., Bullier, E., Goussot, M., Foucher, F., Rameau, C., and Beveridge, C.A. (2005). The branching gene *RAMOSUS1* mediates interactions among two novel signals and auxin in pea. Plant Cell. 17, 464-474.

Johnson, X., Brcich, T., Dun, E.A., Goussot, M., Haurogné, K., Beveridge, C.A., and Rameau, C. (2006). Branching genes are conserved across species: genes controlling a novel signal in pea are co-regulated by other long-distance signals. Plant Physiol. 142, 1014-1026.

King, R.A., and Van Staden, J. (1988). Differential responses of buds along the shoots of *Pisum sativum* to isopentyladenine and zeatin application. Plant Physiol. Biochem. 26, 253-259.

Leyser, O. (2005) The fall and rise of apical dominance. Curr. Opin. Genet. Dev. 15, 468-471.

Li, C.J., Guevara, E., Gerrera, J., and Bangerth, F. (1995). Effect of apex excision and replacement by 1-naphthylacetic acid on cytokinin concentration and apical dominance in pea plants. Plant Physiol. 94, 465-469.

Medford, J.I., Horgan, R., El-Sawi, Z., and Klee, H.J. (1989). Alterations of endogenous cytokinins in transgenic plants using a chimeric isopentyl transferase gene. Plant Cell. 1, 403-413.

Integrative Hybrid Modelling of Plant Shoot Branching

Philip Garnett, Susan Stepney, Ottoline Leyser.
Department of Biology, University of York,
Heslington, York, UK, YO10 5DD.

Keywords: Integrative Modelling, Auxin, Shoot Branching, Arabidopsis.

Introduction

The regulation of shoot branching in Arabidopsis involves a complex network of interacting genes, proteins, hormones, and environmental influences (Leyser, O. 2005). As our knowledge of the molecular biology of the individual processes increases, it becomes increasingly difficult to understand and visualise the system as a whole. We propose that techniques used in computer science for the development of complex software systems can be combined or integrated with existing computational biology techniques to produce new computer models of the shoot branching processes.

Shoot Branching

Shoot branching in Arabidopsis is thought to be controlled by two semi-discret regulatory systems. The first to be identified was the repression of branching by the hormone auxin which is produced by the primary shoot apex and transported down through the shoot stem. Auxin acts to down-regulate cytokinin which is a direct promoter of bud outgrowth (Nordstrom, A. 2004).

The second proposed regulatory system, known as the MAX pathway, is concerned with the control of the transport capacity for auxin in the stem, and consequently the number of branches (Bennett, T. et al 2006). The MAX pathway consists of 3 closely operating MAX genes, *MAX4*, *MAX3*, and *MAX1*, which are thought to be involved in the production of a yet be fully characterized hormone mds (max-derived-signal). The presence of mds is detected by MAX2 which then goes on to negatively regulate PIN1. PIN1 is a polar membrane bound auxin transport protein. The levels of PIN1 expressed in the membrane of vascular-associated cells determines the capacity of that cell to export auxin (PIN1 accumulates on the lower membrane of the vascular cell). Experiments have shown that the capacity of the shoot to transport auxin is positively associated with the number of branches on the shoot (Bennett, T., et al 2006). The production of PIN1 within the cell is regulated by the presence of auxin in a positive feedback loop, kept in check by *MAX2* down regulating PIN1. Therefore the removal of the *MAX2* activity by interruption of the MAX pathway causes a phenotype of runaway branching.

Taken alone, these systems are not trivial, but they should be considered even less so when thought of in in the larger context of a plant where phenotype must also be taken into account. Consequently it would be highly beneficial for any model of this system to capture not only the subtleties of the interacting genes, proteins, and hormones, but also their effect on the larger plant. We believe that combined modeling techniques from computer science and computational biology will assist in the production of models that are up to the challenge of answering such questions.

Software Engineering Plant Models

The Unified Modelling Language (UML, Object Management Group) is a mature visual modelling tool for the development of complex object oriented software systems, and is based on a series of diagrams. We use a UML based software engineering process to produce UML models of plants. The abstract concept of programming objects (from object oriented programming languages) within UML maps neatly onto the real physical objects that define plants and their cells. For example, programming objects can be used to describe the parts of the plant, such as cells, proteins, and genes. These objects can be modelled in UML and the different interactions captured. The UML model can then form the basis of an executable simulation. If later, after further research and experiments, the plant model needs to be modified, these changes can be made to the high level UML diagrams, which can then automatically update the simulation code structure appropriately. Fig 1 shows a high level UML diagram capturing some components of a plant cell. Other groups have started to apply UML to developing models of biological systems (Webb, K. White, T. 2005).

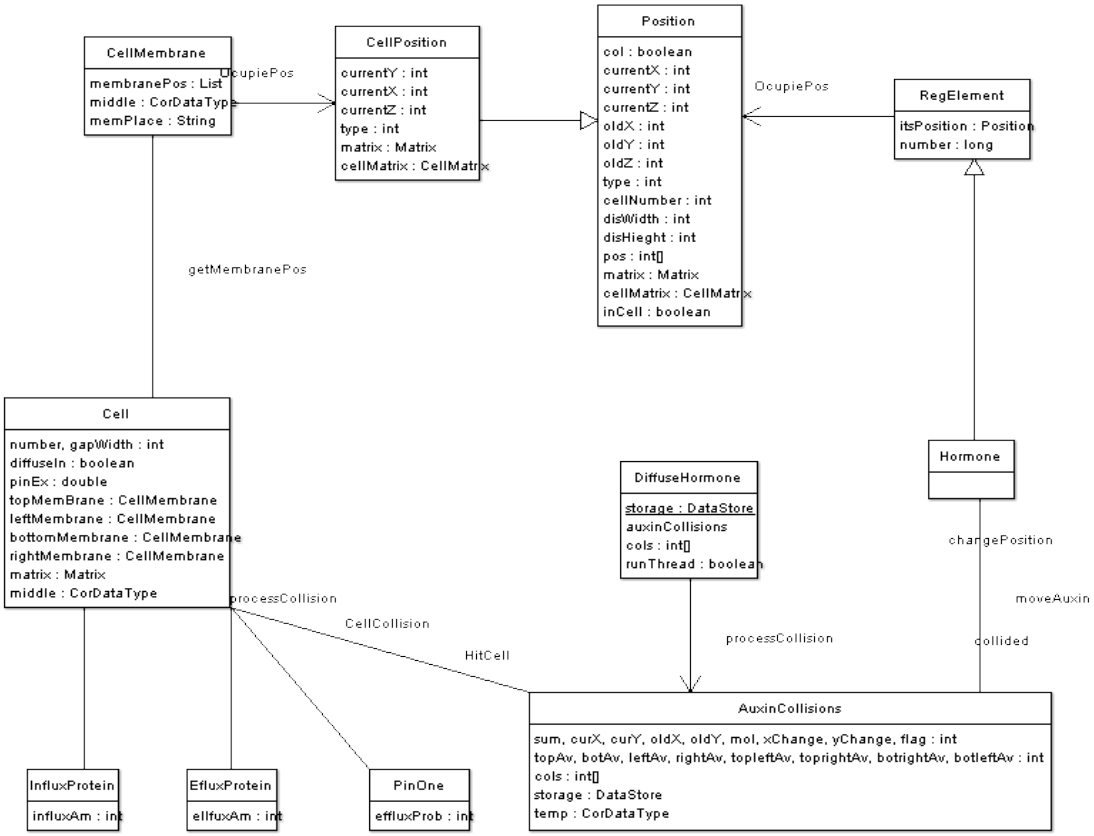

Fig1. The UML class diagram showing the interactions of the programming objects within the program. The boxes represent different classes within a program, each class defines the attributes of an object. The different classes represent parts of a real plant. The arrows show how the program interacts and is modelled on how those interactions are thought to be in real life. Objects are designed to be discrete and therefore it should be relatively easy to alter the interactions between them to alter the behaviour of the program (OMG).

We have applied this modelling approach to the problem of auxin transport canalisation, which is a small part of the greater question of shoot branching. The process of canalisation occurs during vascular tissue specification, and is thought to be an auxin regulated positive feedback loop, in which auxin increases its own transport by up-regulating proteins like PIN1. The differentiation of vascular tissue and the formation of canals of auxin flow has been hypothesised from a number of experiments by Tvsi Sachs (Sachs, T. 1981).

The formation of canals can easily be seen but the exact mechanism controlling this is not fully understood. There is a question mark over the mechanisms at work: are the canals produced at a higher or lower local auxin concentration relative to the surrounding tissue? Models developed to investigate canalisation originally suggested that the canals would be at a lower concentration relative to the surrounding tissue (Mitchison, G. 1980) but, experimental evidence now suggests otherwise. Newer models have been produced which agree with the experimental data, however they rely on the existence of transport proteins that have not yet been found by experimentation (Kramer, E. 2004).

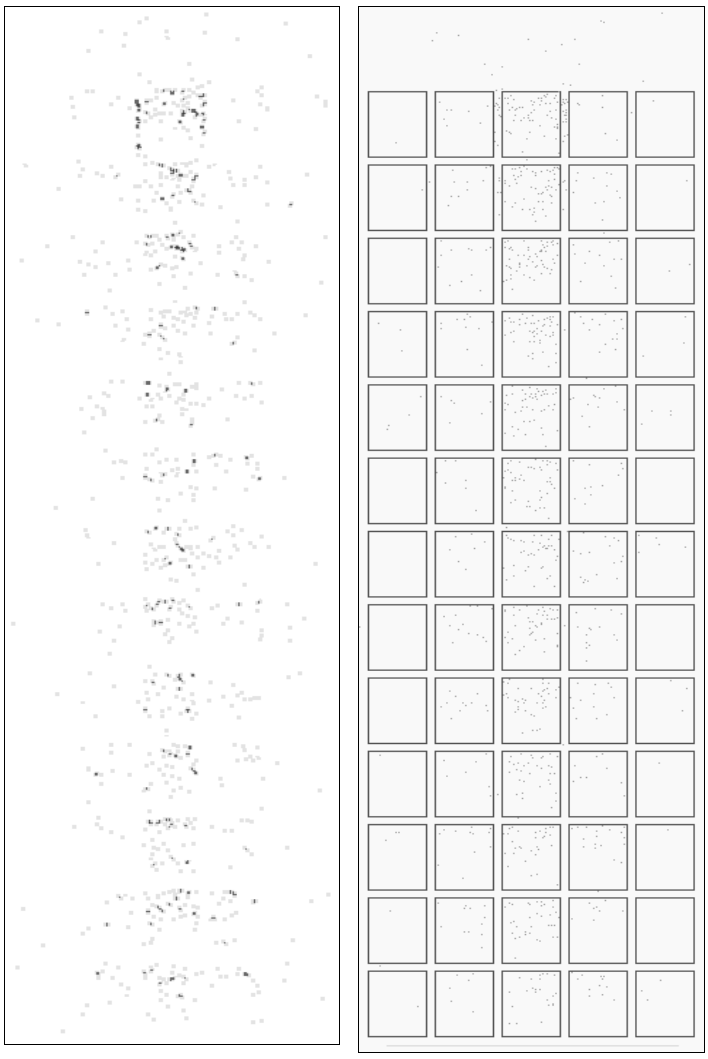

Fig 2: (A) Heatmap showing areas of high auxin concentration following the path of the canal. (B) The visual output of the 2D model, auxin enters the model in cell marked X and leaves via the sink at the bottom. The canal is formed by the diffusion of auxin into cells and the transport by proteins out of cells between an area of high concentration, the source X and an area of low concentration, the sink.

There are currently two models in development, one of which is 3D and the other 2D. Early data from both models indicate that the canals represent a local maximum in auxin concentration. The 2D model, shown in Fig. 2(A), shows the layout of the model and consists of a grid of cells with the auxin moving around, shown as dots. Auxin enters the model in the middle cell of the first row, a unit of auxin arrives here for every one lost at the sink (grey line at the bottom) so the system is closed. Currently when the model is started a set amount of auxin is released on top of the cells. The auxin moves around in the model by diffusion and transport. Diffusion into cells by auxin is permitted but diffusion out is not, as in reality the auxin would become deprotonated and thus unable to cross the membrane[Blakeslee, J. 2005].

The auxin can only leave the cells via an efflux protein. Efflux proteins are currently split into two types. Firstly, there are a set of efflux proteins which are randomly distributed around the cell membrane. Secondly, there are efflux proteins that represent the PIN1 family of proteins. These currently bind to the bottom membrane only and the amount in a cell at any one time is positively linked to the amount of auxin in the cell. This relationship can be altered within the program via a slidebar.

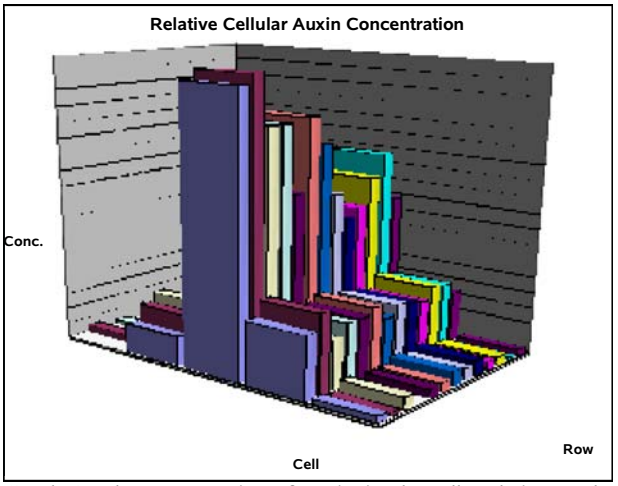

Graph 1: The concentration of auxin in the cells relative to the average across all cells. The cells forming part of the canal have a much higher relative concentration.

Graph 1 shows the relative concentration of auxin in the different cells in the model, and Fig 2(B) shows an auxin heatmap. Both show that a canal has formed between the cell that the auxin enters the model (as if it were coming from further up the plant) and the sink at the bottom where it leaves the plant. It is also clear that this canal is a local maxima of auxin concentration. The models are still undergoing testing and there are a few areas which require improvement. We would like to make the shape and layout of the cells more natural. This will be important for modelling how canals join up as seen in plants. Also, rather than releasing a set amount of auxin into the model, it would be better to have auxin producing cells that maintained a set cellular auxin concentration. Finally we would like to develop rules where the localisation and amount of all efflux proteins in the cells is influenced by the amount and position of auxin within them.

Future work: L-systems

L-systems are a well established method of computationally modelling the development of plants. They already have a facility whereby some of the modelling is captured in the form of and external computer program, and not as part of the L-system description itsself. Environmental models are a good example (Karwowski & Prusinkiewicz. 2003) as these models feed parameters into the L-system which affect is outcome. We are planning to produce more tightly linked models where an L-system that models branching and UML based models of auxin flow work closely together to model more of the developing plant.

Acknowledgements

I would like to thank Przemyslaw Prusinkiewicz and Leo Caves for their help and input, a long with the other members of the Leyser Lab. This research is funded by a BBSRC Case award in conjunction with Microsoft Research Europe.

References

Leyser, O. 2005. The fall and rise of apical dominance**.** Current Opinion in Genetics and Development, 15, pp. 468-471.

Nordstrom, A. 2004. Auxin regulation of cytokinin biosynthesis in Arabidopis thaliana: A factor of potential importance for auxin-cytokinin-regulated development.

Bennett, T. Sieberer, T. Willet, T. Booker, J. Luschnig, C. Leyser, O. 2006. The Arabidopsis Max Pathway Controls Shoot Branching by Regulating Auxin Transport. Current Biology, 16, pp. 553-563.

Webb, K. White, T. 2005. UML as a cell and biochemistry modeling language. BioSystems, 80, pp. 283-302.
Kramer, E. 2004. PIN and AUX/LAX proteins: their role in auxin accumulation. TRENDS in Plant Science, 9, pp. 578-582.
Sachs, T. 1981. The Control of the Patterned Differentiation of Vascular Tissues. Advances in Botanical Research Incorporating Advances in Plant Pathology, 9, pp. 151-262.
Karwowski, R. Prusinkiewicz, P. 2003. Design and Implementation of the L+C Modeling Language. Electronic Notes in Theoretical Computer Science, 86(2), pp. 19-38.
Mitchison, G. J. 1980. A Model for vein formation in higher plants. Proc. Soc. Lond., pp 79-109.
Object Management Group (OMG), Maintainer of UML Standard. www.uml.org.
Blakeslee, J. Peer, W. and Murphy, A. 2005. Auxin transport. Current Opinion in Plant Biology, 8, pp. 1-7. (review)

Apical dominance models can generate basipetal patterns of bud activation

Przemyslaw Prusinkiewicz[1], Richard S. Smith[1] and Ottoline Leyser[2]
[1]Department of Computer Science, University of Calgary
[2]Department of Biology, University of York

Keywords: activation sequence, auxin, canalization, L-system, traffic intersection model

An important aspect of plant development is the order in which lateral buds are activated to produce branches. This order may manifest itself, for example, in the gradient of branch lengths, or in the flowering sequence. One progression type is acropetal, with the lateral buds activated from the bottom up. Other plants exhibit a basipetal sequence of bud activation, with a downward progression of branch development. More complex, mixed sequences also occur, with the activation sequence converging towards or diverging away from the central part of the shoot axis. The acropetal progression can be simply explained by postulating that lateral buds are activated in the same order in which they were created (possibly with some delay). However, basipetal progression eludes such a simple explanation, raising the question of what mechanisms may be responsible. As details of the underlying signaling processes, and their interplay with development, are difficult to observe directly, simulation models are helpful in integrating diverse experimental data, in highlighting the dynamic relations between local processes and the resulting emergent structures, and in assessing plausibility of alternative hypotheses.

Basipetal activation progression is likely related to apical dominance. The hypothesis is that the shoot apical meristem in the vegetative state has a strong inhibitory influence on the lateral buds below, which is lifted upon the transition of the apex to the flowering state. This information propagates down the stem, causing gradual activation of the lateral buds. The inhibitory signal may be auxin, produced by the shoot apex and actively transported down the plant [Thimann and Skoog 1933]. The timing of activation of each successive bud might then reflect the speed with which the wave of auxin depletion propagates down the stem after the transition to flowering.

Although this "depletion-wave" model is capable of generating branching sequences of some plants found in nature [Lindenmayer 1984, Janssen and Lindenmayer 1987, Prusinkiewicz and Lindenmayer 1990], two questions can be raised. First, it is not clear how this model could account for the activation sequences of buds within rosettes. Here extremely short internodes should lead to almost simultaneous activation of lateral buds, yet in Arabidopsis, for example, a basipetal sequence is observed in the rosette in spite of the short internodes [Stirnberg et al. 1999, Figure 1A]. Second, the depletion-wave model does not take into consideration contributions of the lateral branches to the auxin flow in the stem, contrary to experimental data [Morris 1977].

To address these problems, we propose an alternative conceptual model of bud activation. Lifting of apical dominance due to floral transition of the main apex activates the topmost lateral bud, as in the wave model. At this point, the active lateral bud becomes a source of auxin that inhibits more basal buds, until its own switch to flowering. This in turn activates the next lateral bud, resulting in a mechanism in which the inhibitory influence is relayed from one active bud to the next.

To test the plausibility of this conceptual model, we developed a sequence of simulation models. Model 1 captures the essence of the relay process. A sequence of metamers, each

associated with an axillary bud, is created by the apex with a constant plastochron. Auxin produced in the apex is transported basipetally through these metamers, and is drained from the basal metamer by the root. Furthermore, the auxin is subject to decay in each metamer. Transition to flowering takes place after a user-defined number of metamers have been produced, and decreases the production of auxin. Activation of the lateral bud is controlled locally within each metamer, by the level of auxin falling below a specified threshold. Upon activation, a lateral apex produces auxin, which is transported into the main stem. As for the main apex, the lateral apex switches to the flowering state after a delay. As expected, a basipetal sequence of lateral bud activation and flowering emerges due to the relay effect. Interestingly, if the transition to flowering in the main apex is delayed, resulting in a larger number of metamers, the model produces a convergent activation sequence. This is due to the gradual decrease of auxin concentration in the basal direction due to auxin decay. As the distance between the apex and the basal metamers increases due to growth, auxin concentration in the basal metamers falls below the threshold for bud inhibition. This relation between metamer number and the pattern of bud activation is a robust emergent property of the model, and coincides with the change in the progression of activation in Arabidopsis plants grown in long-day (15 metamers) vs. short-day conditions (>30 metamers) [Stirnberg et al. 1999]. Furthermore, due to the residual production of auxin by the floral apices, a zone in which buds are never activated may emerge in the central part of the stem, as it does in Arabidopsis plants grown under short-day conditions.

Model 1 confirms the plausibility of the relay concept in regulation of bud activation. However, experimental data with radiolabelled auxin show that auxin transported from the main apex through the stem does not pass in the vicinity of the dormant buds, and does not enter them [Morris 1977]. This raises the question of how the auxin signal is conveyed to the bud. A widely held view is that auxin acts on the lateral bud indirectly, through the intermediacy of another hormone, cytokinin, which can move freely between the stem and the bud [Cline 1991]. It is known that cytokinin is synthesized in the root and in the stem, at rates negatively regulated by auxin [Li et al. 1995, Nordstrom et al. 2004, Tanaka et al. 2006], and directly promotes bud growth [Cline 1991]. We tested the plausibility of this intermediate-signal hypothesis by constructing Model 2, which incorporates the acropetal flow of cytokinin and the regulation of cytokinin synthesis by auxin. Bud activation is now triggered by the level of cytokinin in the bud exceeding a predefined threshold. Simulation results confirm that the relay mechanism can produce the observed activation patterns under these conditions as well.

The intermediacy of a second hormone, however, is not the only possible explanation for the action of basipetally transported auxin on lateral buds. Another possibility is based on two assumptions: that lateral buds remain dormant until they can export locally produced auxin, and that the main stem has a limited capacity for auxin transport. Thus, lateral buds compete with the main apex for limited auxin transport capacity of the main stem. As long as the main apex is active, the auxin it produces appropriates the entire transport capacity of the stem. After the switch to flowering, the auxin depletion wave relinquishes transport capacity, allowing for auxin transport from the most apical lateral bud. This triggers its activation and restores auxin flow in the stem. By the same mechanism, the subsequent switch to flowering of this bud triggers activation of the next one, and the relay progresses. We call this model the “traffic intersection model”, since it resembles the situation on a highway, where vehicles from the subsidiaries can only join the traffic if the carrying capacity of the highway is not fully utilized.

We tested the plausibility of this concept using Model 3. To account for the interplay between different streams of auxin flow (from the main apex vs. from the lateral buds), we used a more detailed model of auxin transport than in Models 1 and 2. Similar to the canalization model [Sachs 1981], we assume that auxin flux between adjacent metamers is a combination of diffusion and polar transport. Polar transport is related to auxin flux in a feedback loop, such that increased flux promotes more efficient polar transport in the direction of the flux. However, polar transport is capped, thus limiting the maximum auxin transport capacity. With

properly chosen parameters, diffusive transport of auxin from the apex towards the root rapidly triggers a saturated polar transport stream in the main stem. The resulting relatively high concentration of auxin in the stem limits diffusion from the lateral buds, thus inhibiting polar transport form the buds. The situation changes when the main apex switches from the vegetative to the floral state. This reduces auxin concentration in the stem. The diffusive flux from the lateral buds increases, triggering the establishment of polar transport into the stem. The resulting auxin outflux activates the buds. As in previous relay-based models, this process begins with the topmost lateral bud and proceeds downwards, with consecutive lateral buds using, then relinquishing, the carrying capacity of the stem in succession (Figure 1).

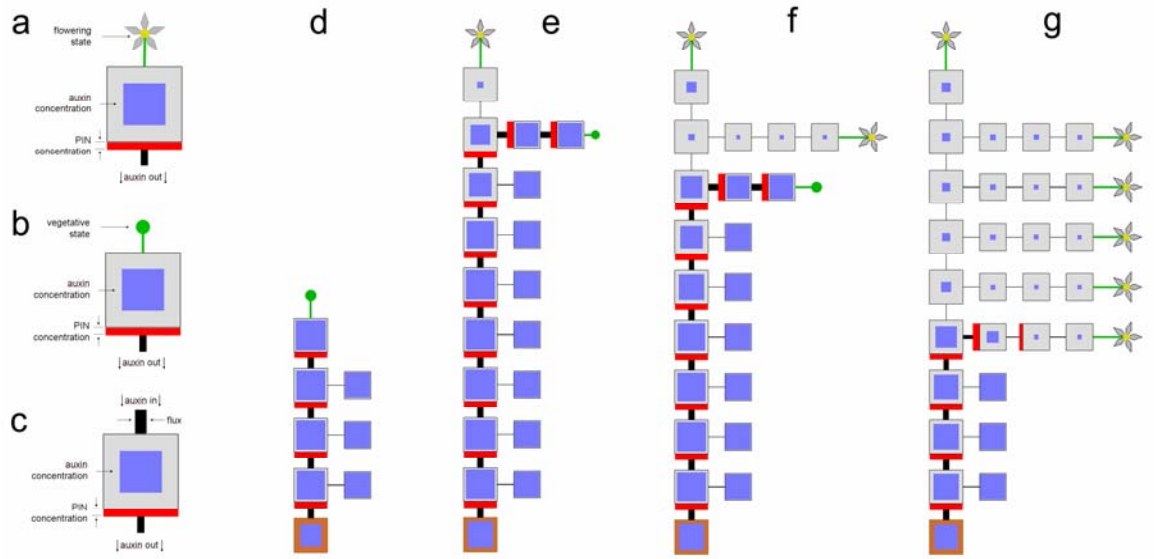

Figure 1. Illustration of Model 3. a-c) Schematic representations of an apex in the flowering and vegetative state. b) Schematic representation of a metamer. d-g) Selected stages of the simulation. The simulation begins with the main apex creating a sequence of metamers with the associated lateral buds. The flow of auxin from the apex saturates auxin transport capacity in the shoot (d). Upon transition to flowering, production of auxin in the main apex decreases. The resulting excess transport capacity in the stem enables auxin efflux from the topmost lateral bud, which results in its activation. Auxin produced by this bud re-saturates the stem (e). After transition of the topmost bud to the flowering state, the next lateral bud becomes activated (f). The resulting relay process continues (g) until all buds become activated.

There are several conceptually attractive features of this model. First, it explains the basipetal activation sequence of lateral buds without invoking additional signals. Next, the model can explain the phenotype of the Arabidopsis *max* mutants, where increased branching is associated with increased auxin transport capacity in the stem [Bennett et al. 2006]. Finally, the model integrates several aspects of auxin biology; in particular, in relates apical dominance and activation progression to canalization mechanisms.

An important aspect of canalization, however, is not only the feedback between auxin flow and cell or module polarization, but also the convergence of auxin flow into focused streams: canals, precursors of vascular differentiation. In the case of lateral buds, vascular connections may be formed concurrently with, and indeed as an integral part of, increased auxin outflow from the buds [Grbic and Bleeker 2000, Figure 2]. To test whether Model 3 is compatible with such behavior, we constructed a schematic model of canalization at tissue level, modified from [Rolland-Lagan and Prusinkiewicz 2005]. The resulting Model 4 expresses cell polarization in terms of the allocation of efflux carriers (PIN proteins) from a given pool to specific faces of the cell according to net auxin efflux [Feugier et al. 2005]. A polarization exceeding a predefined threshold is locked, simulating vascular differentiation. In the sample simulation illustrated in

Figure 2, the cellular grid is constrained to a shape representing a longitudinal section of the stem with two buds (b). Following the placement of an auxin source at the top of the main segment, a vascular strand running through the segment emerges (c). Subsequent placement of auxin sources in the two buds (d) does not trigger formation of lateral vasculature until the auxin source at the top of the main stem is removed. The resulting decrease of auxin concentration in the main vasculature then triggers the formation of a vein connecting the higher bud to the central vasculature (e). When the source of auxin associated with this bud is removed, a similar process occurs in the lower bud (f). This confirms that the "traffic intersection" model of bud activation (Model 3) is consistent with processes that take place at the tissue level according to the canalization paradigm (Model 4).

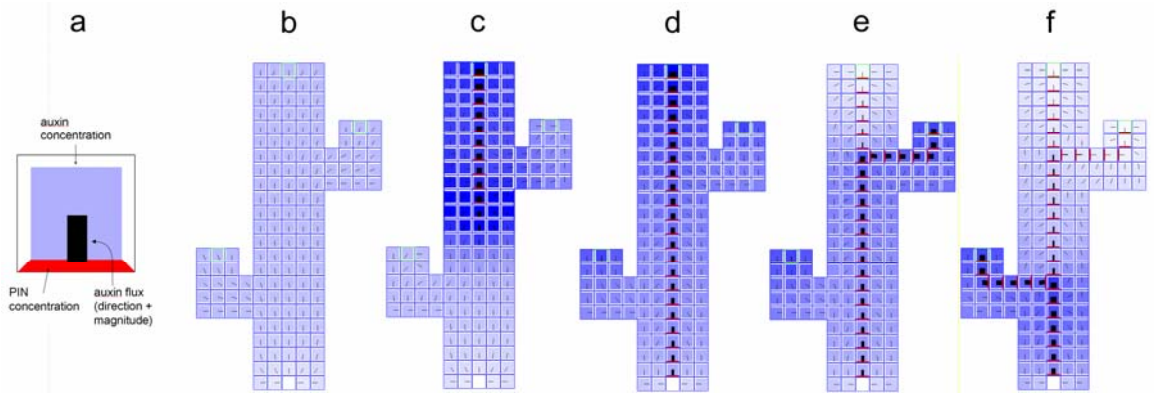

Figure 2. Illustration of Model 4. a) Iconic representation of a cell. b-f) Selected stages of the simulation. Detailed explanation in the text.

In conclusion, we have shown that relay models are capable of forming basipetal and convergent activation patterns in a manner qualitatively consistent with experimental data. Variations of the basic model (Model 1) confirm the plausibility of postulated molecular-level mechanisms: mediation of auxin action by cytokinin (Model 2), and competition for the limited auxin-carrying capacity of the stem (Models 3 and 4). These mechanisms are not mutually exclusive, and can operate in concert. Our models provide a basis for further simulation studies of processes controlling activation patterns, such as the effect of mutations and manipulations of auxin distribution and transport on the activation patterns. Another open problem, challenging from both a conceptual and modeling perspectives, is the interplay between hormones and resources in bud activation.

Materials and methods. Architectural-level models (1-3) were specified in the L-system-based L+C language [Karwowski and Prusinkiewicz 2003]. The tissue-level Model 4 was specified in the vv modeling language [Smith et al. 2004]. All models were implemented in the L-studio/vlab environment [Prusinkiewicz 2004].

References:

Bennett, T., Sieberer, T., Willett, B., Booker, J., Luschnig, C. and Leyser, O. [2006]: The Arabidopsis MAX pathway controls shoot branching by regulating auxin transport. *Current Biology* 16: 553-563

Cline, M.G. [1991]: Apical dominance. *Bot Rev.* 57, 318-358.

Feugier, F. G., Mochizuki, A. and Iwasa, Y. [2005]: Self-organization of the vascular system in plant leaves: inter-dependent dynamics of auxin flux and carrier proteins. *J Theor Biol* 236: 366-375.

Grbic, V. and Bleeker, A. B. [2000]: Axillary meristem development in *Arabidopsis thaliana*. *Plant J.* 21: 215-223

Janssen, J. M. and Lindenmayer, A. [1987]: Models for the control of branch positions and flowering sequences of capitula in *Mycelis muralis* (L.) Dumont (Compositae). *New Phytol.* 105: 191-220.

Karwowski. R. and Prusinkiewicz. P. [2003] Design and implementation of the L+C modeling language. *Electronic Notes in Theoretical Computer Science* 86 (2), 19 pp.

Li, C-J., Guevara, E., Herrera, J. and Bangerth, F. [1995]: Effect of apex excision and replacement by 1-naphthylacetic acid on cytokinin concentration and apical dominance in peas. *Plant Physiol*. 94: 465-469.

Lindenmayer, A. [1984]: Positional and temporal control mechanisms in inflorescence development. In P. W. Barlow and D. J. Carr (Eds.), *Positional Controls in Plant Development*, Cambridge University Press, Cambridge, pp. 461-486.

Morris, D. A. [1977]: Transport of exogenous auxin in two-branched dwarf pea seedlings (*Pisum sativum* L.). *Planta* 136(1): 91-96.

Nordstrom, A., Tarkowski, P., Tarkowska, D., Norbaek, R., Astot, C., Dolezal, K. and Sandberg G. [2004]: Auxin regulation of cytokinin biosynthesis in Arabidopsis thaliana: a factor of potential importance for auxin-cytokinin-regulated development. *Proc Natl Acad Sci U S A.* 10: 8039-8044.

Prusinkiewicz, P. and Lindenmayer, A. [1990]: *The Algorithmic Beauty of Plants*. Springer, New York. With J. S. Hanan, F. D. Fracchia, D. R. Fowler, M. J. M. de Boer and L. Mercer.

Prusinkiewicz. P. [2004]: Art and science for life: Designing and growing virtual plants with L-systems. *Acta Horticulturae* 630, pp. 15-28.

Rolland-Lagan, A.-G. and Prusinkiewicz, P. [2005] Reviewing models of auxin canalization in the context of leaf vein pattern formation in Arabidopsis. *The Plant Journal* 44: 854-865.

Sachs, T. [1981]: The control of patterned differentiation of vascular tissues. *Ad Bot Res*. 9: 151-162.

Smith, C., Prusinkiewicz, P. and Samavati, F. [2004] Local specification of surface subdivision algorithms. *Lecture Notes in Computer Science* 3062: 313-327.

Stirnberg, P., Chatfield, S. P. and Leyser, H. M. O. [1999]: AXR1 acts after lateral bud formation to inhibit lateral bud growth in Arabidopsis. *Plant Physiology* 121: 839-847.

Stirnberg, P., Karin van de Sande, K., and Leyser, H. M. O. [2002]: MAX1and MAX2 control shoot lateral branching in *Arabidopsis*. *Developmen*t 129: 1131-1141.

Tanaka, M., Takei, K., Kojima, M., Sakakibara, H. and Mori, H. [2006]: Auxin controls local cytokinin biosynthesis in the nodal stem in apical dominance. *Plant J.* 45: 1028-1036.

Thimann, K. V. and Skoog, F, [1933]: Studies on the growth hormone of plants III. The inhibitory action of the growth substance on bud development. *Proc. Natl Acad Sci USA* 19: 714-716.

Modeling auxin fluxes and *Arabidopsis* root ramification at different scales

Mikaël LUCAS[1,2], Laurent LAPLAZE[1], Christian JAY-ALLEMAND[1], Christophe GODIN[2]

[1] Equipe Rhizogènese, UMR DIA-PC (Agro.M/INRA/IRD/UMII), Institut de Recherche pour le Développement (IRD), 911 Avenue Agropolis, 34394 Montpellier Cedex 5, France
[2] Equipe VirtualPlants (INRIA/CIRAD/INRA), UMR DAP - Développement et Amélioration des Plantes, TA40/02, Cirad, Avenue Agropolis, 34398 MONTPELLIER CEDEX 5, France

Keywords: *Arabidopsis*, auxin transport, root development, lateral root initiation

Introduction

Plant primary growth occurs in two opposite directions, stems and roots both generating branched patterns during their development. However, where stem development appears extremely regular, based on phyllotactic patterns, root architecture appears somewhat random, controlled essentially by external clues such as nutrients concentration (Malamy et al. 2005).

The regularity of stem development has been ground to a large panel of pure mathematical and physical modeling (Adler et al. 1997). By contrast, the apparent chaos of root development has essentially directed the modeling effort toward ecophysiological and environmentally constrained models (Doussan et al. 2003).

Yet, as the biological knowledge of development and the available microscopy tools evolves, mathematicians and computer scientists are now able to glimpse at the cellular level of development. They can create new models taking into account previously ignored mechanisms and giving rise to new perception on ancient problems, as described by Barbier de Reuille et al. (2006), Jönsson et al. (2006), and Smith et al. (2006) on the topic of phyllotaxis.

Until recently, root systems development was considered too chaotic to be modelled on the same basis as shoot development. However, recent biological results suggest that lateral root initiation (LRI), main determinant of root architecture, may itself be more regular than first supposed (Dubrovsky et al. 2000; Dubrovsky et al. 2006; De Smet et al. 2007; Lucas et al. 2007). Global root architecture now appears as the superposition of regular LRI and irregular emergence, the latter phenomenon being more strongly subjected to environmental conditions.

As LRI and root development both depend on complex auxin fluxes and genetic interactions, we used a modeling approach to integrate the large biological knowledge available on root development and the complexity of flux dynamics. The models we choose to develop address the control of LRI by auxin fluxes. Our aim was to test various hypotheses concerning LRI regularity and the positioning of root primordia.

Modeling root development and auxin fluxes

Auxin fluxes occurring during root development can be considered at the macroscopic (tissue level) or microscopic (cellular level) scales. We will here distinguish between two kinds of models we developed, each aiming to reproduce the fluxes at one of those two levels.

The first kind of model is centered on the whole root. It is geared toward a representation of the whole developmental sequence, and well adapted to treat the problem of the regularity and distribution of LRI. The spatial representation of the root in this model can be considered as almost linear. The main computational topic of this model is one of competition and transport within a dynamic system based upon a dynamic structure, also known as $(DS)^2$. The principal advantage of this model is the ultimate possibility to generate LRI distribution to be compared with LRI distribution observed *in vivo*. We addressed the inherent lack of precision on the positioning of LRI at the microscopic scale by developing our second model.

Based on the cellular structure of a single root slice, the second model is geared towards the simulation of cellular auxin fluxes dynamics. This approach is similar to the one currently applied to stem apical meristem modeling (Barbier de Reuille et al. 2006). The cellular structure of the root slice is here represented as a static graph taking into account each cell and its cell wall. The main

computational topic associated with this kind of model is the complex flux dynamics and the study of its stability. This model has the advantage to allow us to test various hypotheses concerning the precise positioning of root primordia, and to experiment *in silico* on the consequences of auxin fluxes perturbation on initiation. It is however static, and as such can only be used to simulate a snapshot of the auxin accumulation points during root development.

Results

The large scale model was developed based on L-System. Biological studies indicates that LRI is caused by basipetal auxin fluxes, flowing back from the apical root meristem along the lateral root cap, and that primordia development and lateral root emergence are caused by acropetal auxin fluxes coming from the aerial parts (Casimiro et al. 2001; Bhalerao et al. 2002). We introduced those two fluxes in our model as well as auxin production in the aerial parts and at the apex. We were able to generate auxin accumulation at the root apex under certain conditions, and to test which parameters influence this accumulation, as well as other characteristics of the fluxes (fig. 1).

Introducing LRI in the model proved to be problematic, as little was known of the precise dynamic of auxin fluxes which take place above the root apical meristem and are responsible for initiation. We proceeded to a thorough structural analysis of LRI. We showed that LRI appears tightly co-regulated with gravitropism in *Arabidopsis*, as the mechanisms controlling those two phenomena involve a common auxin transport route (Lucas et al. 2007). We suggested that observed LRI regularities may in fact be linked to the periodical nature of gravitropic and thigmotropic responses.

We integrated those results in the fine scale model, as well as known dynamics of auxin fluxes in root tissue whenever such data was available (Friml et al. 2002; Blilou et al. 2005; Swarup et al. 2005; Sauer et al. 2006; Fukaki et al. 2007) (see fig. 2 for an example of flux dynamics). To palliate for the lack or imprecision of data concerning some tissues, we implemented in our model rules for PIN dynamics such as those described in Feugier et al. (2005, 2006), Jönsson et al. (2006) and Smith et al. (2006).

We will insist in our talk on the cellular modeling approach and on the associated problems. One of the main topics we will address is how to account for the observed inconsistency between the positions of the gravitropic responsive tissues and the lateral root primodium. Indeed, the auxin maximum causing the gravitropic response in the epidermis appears on the inside of root turns, whereas LRI always takes place on the outside of root turns, where one would expect the lowest auxin level. We will present one hypothesis to explain this paradox and the results of its implementation in our model. We will also discuss of the potential evolution of the cellular model toward a $(DS)^2$ model.

References

Adler I, Barabe D, Jean RV. 1997. A History of the Study of Phyllotaxis. *Annals of Botany* **80**, 231-244

Bhalerao RP, Eklöf J, Ljung K, Marchant A, Bennett MJ, Sandberg G. 2002. Shoot-derived auxin is essential for early lateral root emergence in Arabidopsis seedlings. *The Plant Journal* **29,** 325-332

Blilou I, Xu J, Wildwater M, Willemsen V, Paponov I, Friml J, Heidstra R, Aida M, Palme K, Scheres B. 2005. The PIN auxin efflux facilitator network controls growth and patterning in Arabidopsis roots. *Nature* **433,** 39-44

Casimiro I, Marchant A, Bhalerao RP, Beeckman T, Dhooge S, Swarup R, Graham N, Inzé D, Sandberg G, et al.. 2001. Auxin transport promotes Arabidopsis lateral root initiation. *The Plant Cell* **13,** 843-852

Barbier de Reuille P, Bohn-Courseau I, Ljung K, Morin H, Carraro N, Godin C, Traas J. 2006. Computer simulations reveal novel properties of the cell-cell signaling network at the shoot apex in *Arabidopsis*. *PNAS* **103**, 1627-1632.

De Smet I, Tetsumura T, De Rybel B, Frei Dit Frey N, Laplaze L, Casimiro I, Swarup R, Naudts M, Vanneste S, et al.. 2007. Auxin-dependent regulation of lateral root positioning in the basal meristem of Arabidopsis. *Development* **134,** 681-690

Dubrovsky JG, Doerner PW, Colón-Carmona A, Rost TL. 2000. Pericycle cell proliferation and lateral root initiation in Arabidopsis. *Plant Physiology* **124,** 1648-1657

Dubrovsky JG, Gambetta GA, Hernández-Barrera A, Shishkova S, González I. 2006. Lateral Root Initiation in Arabidopsis: Developmental Window, Spatial Patterning, Density and Predictability. *Annals of Botany (Lond)* **97,** 903-915

Feugier FG, Mochizuki A, Iwasa Y. 2005. Self-organization of the vascular system in plant leaves: inter-dependent dynamics of auxin flux and carrier proteins. *J Theor Biol.* **236**, 366-75

Feugier FG, Iwasa Y. 2006. How canalization can make loops: A new model of reticulated leaf vascular pattern formation. *J Theor Biol.* **243**, 235-244

Friml J, Wiśniewska J, Benková E, Mendgen K, Palme K. 2002. Lateral relocation of auxin efflux regulator PIN3 mediates tropism in Arabidopsis. *Nature* **415,** 806-809

Fukaki H, Okushima Y, and Tasaka M. 2007. Auxin-Mediated Lateral Root Formation in Higher Plants. *International Review of Cytology* **256,** 113-137

Jönsson H, Heisler MG, Shapiro BE, Meyerowitz EM, Mjolsness E. 2006. An auxin-driven polarized transport model for phyllotaxis. *PNAS* **103**, 1633-1638

Lucas M, Godin C, Jay-Allemand C, Laplaze L. 2007. Auxin fluxes in the root apex co-regulate gravitropism and lateral root initiation. Submitted to Journal of Experimental botany.

Malamy JE. 2005. Intrinsic and environmental response pathways that regulate root system architecture. *Plant Cell Environment* **28,** 67-77

Doussan C, Pages L, Pierret A. 2003. Soil exploration and resource acquisition by plant roots: an architectural and modelling point of view. *Agronomie* **23,** 419-431

Sauer M, Balla J, Luschnig C, Wisniewska J, Reinöhl V, Friml J, Benková E. 2006. Canalization of auxin flow by Aux/IAA-ARF-dependent feedback regulation of PIN polarity. *Genes & Develpment* **20,** 2902-2911

Smith RS, Guyomarc'h S, Mandel T, Reinhardt D, Kuhlemeier C, Prusinkiewicz P. 2006. A plausible model of phyllotaxis. *PNAS* **103,** 1301-1306

Swarup R, Kramer EM, Perry P, Knox K, Leyser HM, Haseloff J, Beemster GT, Bhalerao R, Bennett MJ. 2005. Root gravitropism requires lateral root cap and epidermal cells for transport and response to a mobile auxin signal. *Nature Cell Biology* **7,** 1057-1065

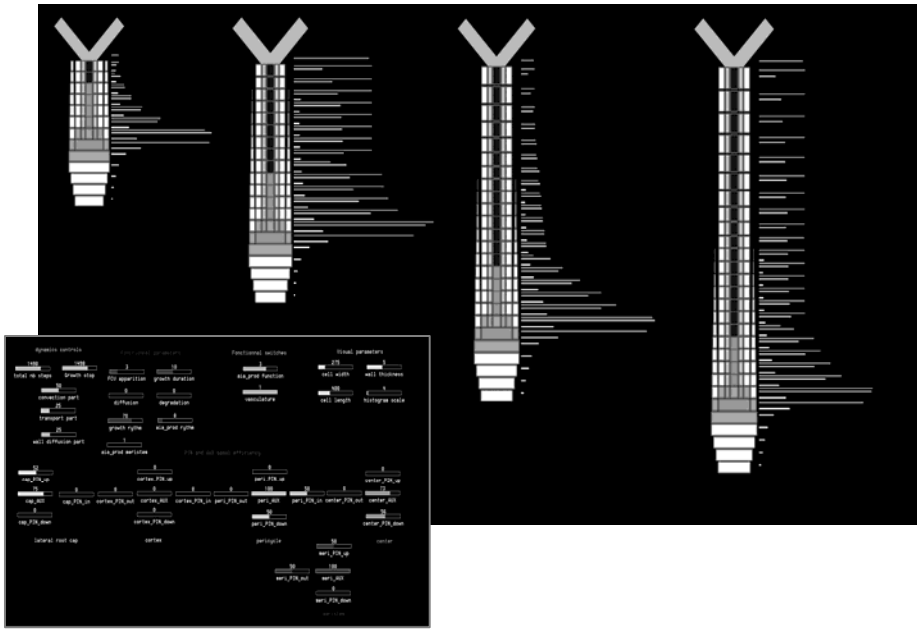

Figure 1.
L-System based model of auxin fluxes in a growing root

Global auxin fluxes are the synthesis between cell wall diffusion, cell/cell diffusion, active transport and convection of auxin.

Auxin production takes place in the aerial part and at the root apex.

The control panel on the bottom left show the various parameters that can be changed to challenge the stability of the model.

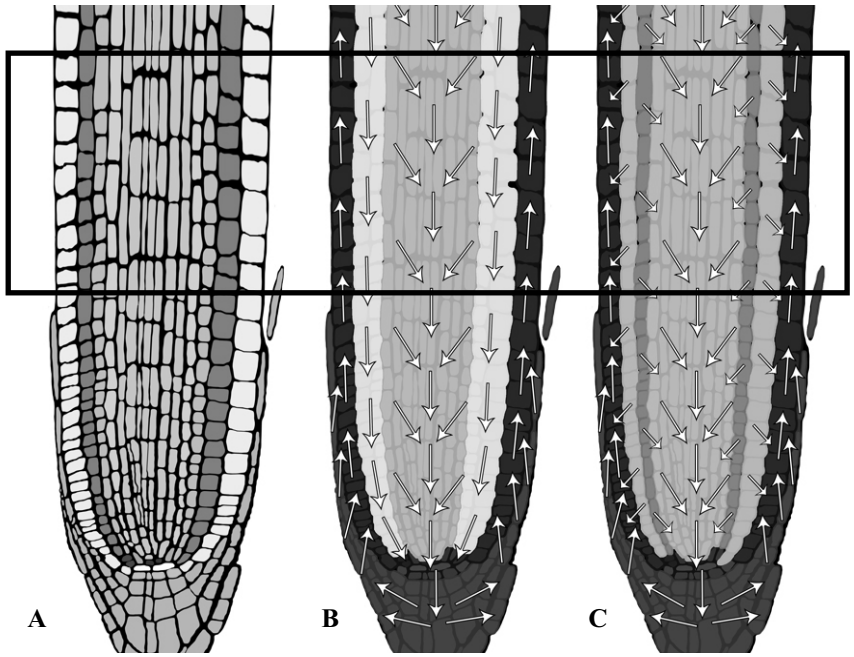

Figure 2.
Dynamic of auxin fluxes in root tissues

A. Root superstructure. Each colour identifies a specific tissue.

B. Global auxin fluxes. Tissues are grouped under a new common colour when they direct the flux along a common path.

C. Changes in auxin fluxes patterns during an exogenous auxin application. Tissues react according different rules, creating divergent auxin paths and isolating inner tissues from auxin present in outer tissues.

The black border define the size and position of the root slice considered in the fine scale model.

Virtual soybean—a computational model for studying autoregulation of nodulation

Liqi Han[1,2,3], Peter M. Gresshoff[1], Jim Hanan[1,2,4]
[1]ARC Centre of Excellence for Integrative Legume Research
[2]ARC Centre for Complex Systems
[3]School of Information Technology and Electrical Engineering
[4]Advanced Computational Modelling Centre
The University of Queensland
Brisbane, Queensland, Australia 4072
l.han@uq.edu.au

Keywords: bioinformatics, virtual plant, soybean, autoregulation of nodulation

Introduction

Nitrogen fixation by legumes is the product of a symbiosis of legume plants and a group of bacteria known as rhizobia (Carroll, et al., 1985; Kinkema, et al., 2006). It has been hypothesised that when rhizobia receive flavonoid signals from the host plants, production of a chemical nodulation factor is induced. The perception of nodulation factor by legume roots then activates a signal cascade leading to division of cortical cells for nodule formation. The activated cells produce a translocatable signal (Q), sent through a root-shoot pathway to the leaves and then detected by a leucine-rich repeat receptor kinase encoded by the *NARK* gene (Searle, et al., 2003). The detection of this root-shoot signal further induces the production of a shoot-derived signal (SDI) transported to the root, which inhibits development of new nodules. These signals, operating in a growing structure of root and shoot, compose a regulatory network known as autoregulation of nodulation (AON). The overall purpose of this study is to develop a greater understanding of this system through multi-scale modelling of processes including intra- and inter-cellular signalling, long-distance signalling and phenotypic development regulated by internal control mechanisms. The first step is to build a structural framework capable of simulating soybean growth driven by empirical results and hypothetical patterns, incorporating control mechanisms modelling Q and SDI.

Materials and Methods

Two soybean (*Glycine max* L. Merrill) genotypes—wild-type Bragg and supernodulating mutant *nts1007* (Carroll, et al., 1985)—were grown in a glasshouse with controlled temperature of 28 °C during day and 23 °C at night. The irradiance inside the glasshouse was approximately 80% of that outdoors. Experiments were carried out from November 14th to December 21st 2006, during which the sun hours in Brisbane were approximately 10 per day on average. Inoculation was conducted 5 days after planting with 75 ml of a late-log phase culture of *Bradyrhizobium japonicum* CB1809 for each pot. All plants were watered with 500 ml B&D solution (Broughton and Dilworth, 1971) supplemented with 2 mmolL^{-1} KNO_3 twice a week and were irrigated 1-2 times a week with tap water only. This low level of nitrate stimulates plant growth but has a minimal effect on nodule number per plant, though marginal delay in nodule initiation. Positions and orientations of the pots were randomised every week to diminish the distorting influence of phototaxis.

In this study, shoot structure was mapped as sequences of symbol strings (Hanan and Room, 1996) where each symbol represents a particular type of plant component (Fig.1.a). A Model GP12-XL sonic digitizer (Freepoint 3D, Scientific Accessories Corporation / GTCO CalComp) and Floradig

software (Hanan and Wang, 2004) were used to identify topological positions and collect 3D coordinates of significant points of shoot components (Hanan and Room, 1996).

Since root development is much more irregular than in the shoot, different methods were required. A root mapping method (Fig.1.b) was used to characterize the first-order lateral roots according to their starting points on the primary root. Lateral and nodule numbers were counted for a series of 50 mm regions along the primary root (Fig.1.c). Each region was composed of a number of segments, and each segment consists of four potential branching sites for which probabilities of generating lateral roots on the right (R), down (D), left (L) and up (U) were determined. Heading behaviours of root growth were simulated using the methods from the ROOTMAP model (Diggle, 1988). Second-order laterals were not taken into account in this work. The L-system-based software L-studio (Karwowski and Prusinkiewicz, 2004) was used for simulating plant growth.

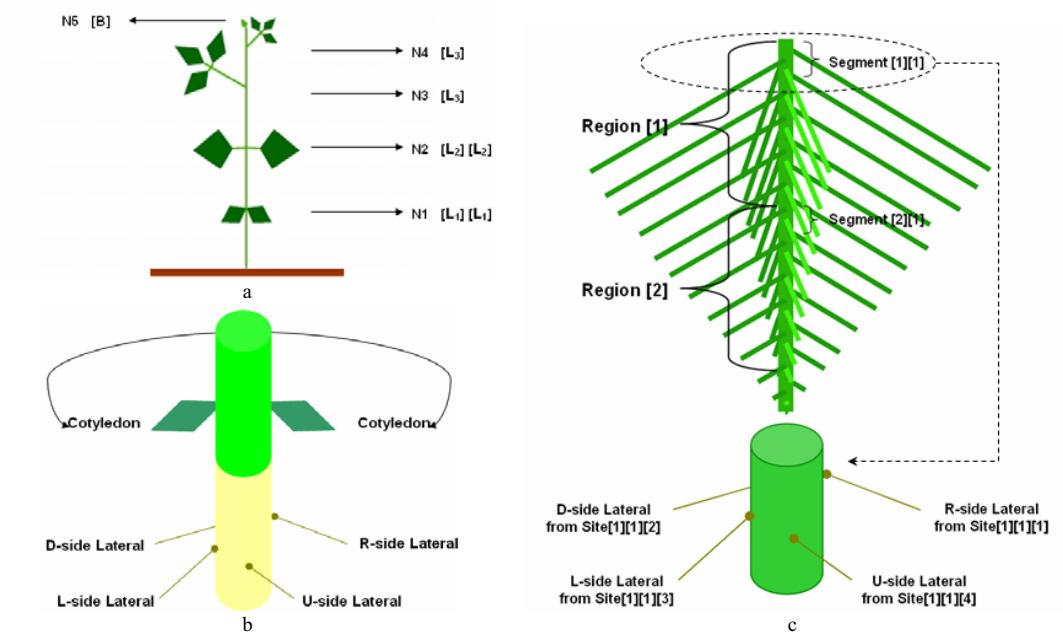

Fig. 1. Shoot and Root Mapping Methods. (a) Example of the shoot mapping method in which N means node; L_1 means cotyledon; L_2 means unifoliate leaf; L_3 means trifoliate leaf and B means bud. (b) The root mapping method characterizes the first-order lateral roots according to their starting points from the primary root. (c) Lateral root classification by "region", "segment" and "site".

Results

Shoot growth is modelled by L-system production rules capturing production of opposite cotyledons and unifoliate leaves at nodes 1 and 2 and subsequent production of trifoliates at higher nodes. Leaf blade, petiole and internode expansion are modelled by positional growth functions derived from the empirical data. Internodes and petioles are represented by a user-controlled number of segments in order to allow synchronization of growth rates and signal transport rates.

Primary root elongation is simulated by adding a standard increment at each step. Increments make up segments composed of four sites of potential lateral root development. Once four sites have been created, the current segment will be finished and a new segment started. Number of segments, lengths of sites and their probability of creating a lateral are determined positionally according to region. Lateral elongation is modelled in the same manner. Nodulation can be modelled either empirically using a similar probabilistic distribution, or under control of the auto-regulation model.

Simulation results for plant structure were verified against empirical data for cumulative statistics such as shoot height, root lengths and number of laterals, with no significant differences for either Bragg or *nts1007* (Fig.2.a, b). For the empirical model of nodulation, spatial and temporal distributions of nodules are as appropriate for these two genotypes. For example, aside from agreement on the overall number itself, nodules of Bragg (Fig.2.c) concentrated more in lateral segments closer to the primary root while nodules of *nts1007* (Fig.2.d) are more well distributed, in accordance with the observed results from real plants.

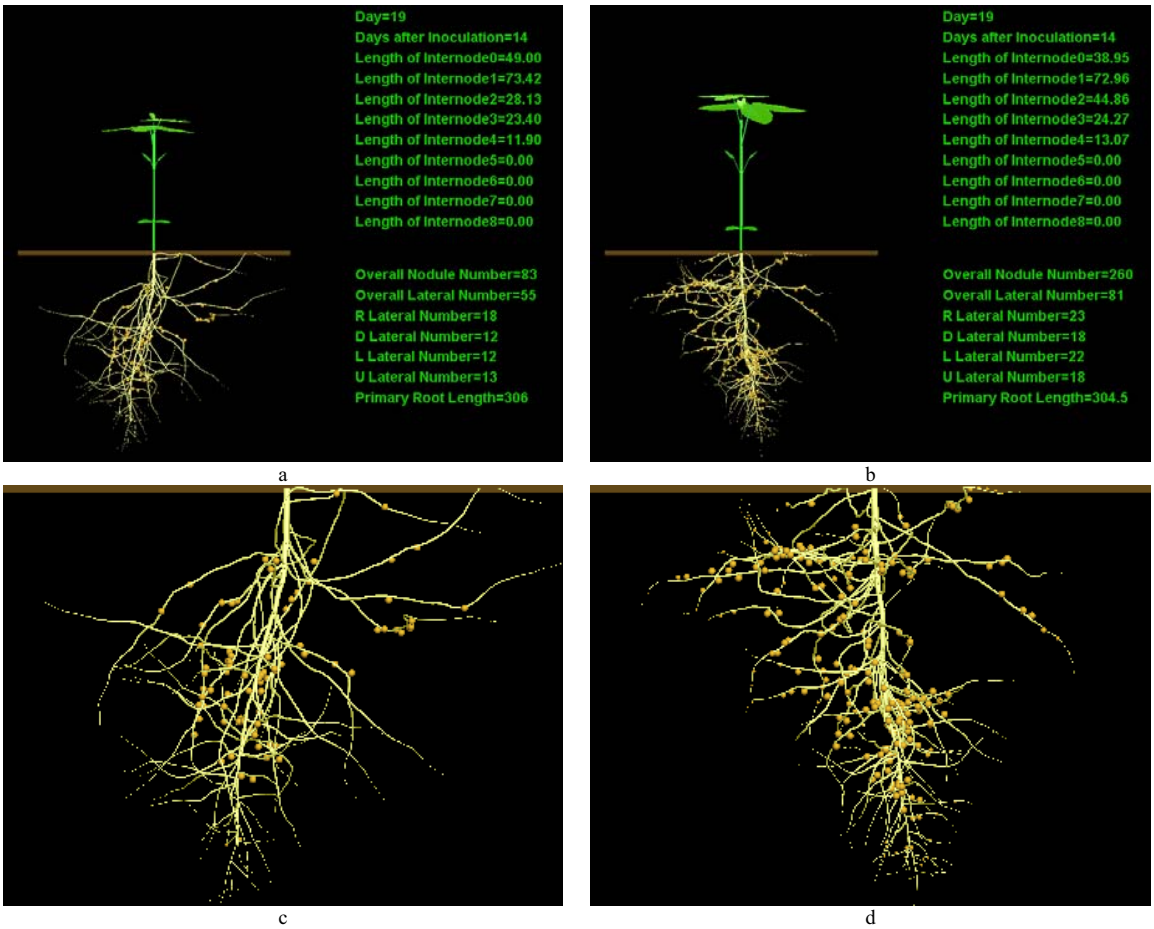

Fig. 2. Simulation of Shoot and Root Development. The results shown in (a) and (c) are from simulation of Bragg development, while those shown in (b) and (d) are from *nts1007*.

The flow of signals Q and SDI in the growing structure (Fig. 3) are modelled using context-sensitive production rules (Prusinkiewicz and Lindenmayer, 1990). The presence of rhizobia is modelled abstractly by inoculation date and concentration, probabilistically initiating nodulation and the consequent induction of the signal Q near the root tip at the appropriate time. Since the root and shoot systems are represented by L-system sub-strings that grow towards their respective growing tips, right context-sensitive productions in the root zone and left context-sensitive productions in the shoot zone move the signal "up" towards the leaves. Productions applicable to the hypocotyl transfer the signal between the root and shoot systems. If NARK is present and the Q signal is detected in the leaves, the SDI signal is generated and transmitted “down” by right and left context-sensitive rules in the shoot and root respectively. Once the level of SDI reaching the root tip is above the appropriate threshold, further nodulation is suppressed. Though currently restricted to modelling the primary

root, this model captures observed phenomena such as supernodulation in *nts1007* and autoregulation of nodulation in Bragg. Nodulation patterns as described in the literature for different inoculation dates can also be simulated appropriately.

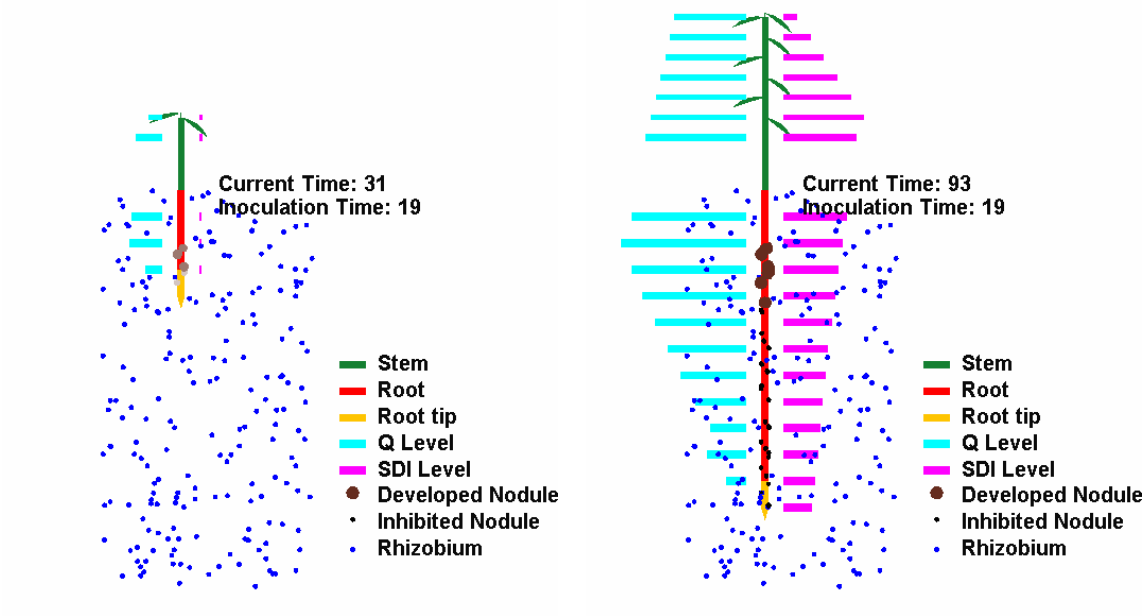

a b

Fig. 3. Model for Predicting Nodulation Behaviours. (a) Nodulation was initiated at time 19, and the Q signal represented by the bars to the left of the plant has travelled up to the leaves, initiating the SDI signal represented by the bars to the right, but levels are not high enough to inhibit nodulation. (b) Nodulation has been suppressed.

Discussion

The empirical architectural models of Bragg and *nts1007* successfully simulate the growth process for both shoot and root. The resulting realistic visualization integrates the different architectural attributes, allowing a holistic phenotypic representation of the differences between a wild type plant and its mutant. Since our focus is to develop computational approaches for studying the control mechanisms underlying autoregulation of nodulation, such a structural model represents target phenotypes for our mechanistic modelling. In the next step, the prototype root-shoot signalling model, will be extended to handle branching architecture and for modelling of the differing rates of hormone flow and organ growth. The integration of models of structural development with hypothesised models of long distance signalling and gene regulation will contribute to a better understanding of the complexity involved in autoregulation of nodulation.

Acknowledgements

This research has been supported by the ARC Centre of Excellence for Integrative Legume Research, the ARC Centre for Complex Systems, and the School of Information Technology and Electrical Engineering based at the University of Queensland.

References

Broughton, W.J. and Dilworth, M.J. 1971. Control of leghaemoglobin synthesis in snake beans, Biochemical Journal **125**, 1075-1080.

Carroll, B.J., McNeil, D.L. and Gresshoff, P.M. 1985. A supernodulation and nitrate-tolerant symbiotic (nts) soybean mutant, Plant Physiology **78**, 34-40.

Diggle, A.J. 1988. ROOTMAP—a model in three-dimensional coordinates of the growth and structure of fibrous root systems, Plant and Soil **105**, 169-178.

Hanan, J. and Wang, Y. 2004. Floradig: a configurable program for capturing plant architecture. The 4th International Workshop on Functional-Structural Plant Models, Montpellier, France, 407-411.

Hanan, J.S. and Room, P.M. 1996. Practical aspects of virtual plant research. In Michalewicz, M.T. (ed), Advances in Computational Life Sciences, Kevin Jeans, Collingwood, 28-44.

Karwowski, R. and Prusinkiewicz, P. 2004. The L-system-based plant-modeling environment L-studio 4.0. The 4th International Workshop on Functional-Structural Plant Models, Montpellier, France, 403-405.

Kinkema, M., Scott, P.T. and Gresshoff, P.M. 2006. Legume nodulation: successful symbiosis through short- and long-distance signalling, Functional Plant Biology **33**, 707-721.

Prusinkiewicz, P. and Lindenmayer, A. 1990. The Algorithmic Beauty of Plants, Springer-Verlag New York, Inc, New York.

Searle, I.R., Men, A.E., Laniya, T.S., Buzas, D.M., Iturbe-Ormaetxe, I., Carroll, B.J. and Gresshoff, P.M. 2003. Long-distance signaling in nodulation directed by a CLAVATA1-like receptor kinase, Science **299**, 109-112.

Towards universality and modularity: a generic photosynthesis and transpiration module for functional structural plant models

Johannes Müller, Henning Braune, Peter Wernecke and Wulf Diepenbrock
Group Plant Systems Modelling and Ecophysiology
Institute of Agricultural and Nutritional Sciences
Martin-Luther-University of Halle-Wittenberg
Ludwig-Wucherer-Str. 2, D-06108 Halle (Saale), Germany
johannes.mueller@landw.uni-halle.de

Keywords: Photosynthesis, transpiration, model, parameterization, leaves, awns, pods

Introduction

Functional Structural Plant Models (FSPMs) that combine functional and architectural submodels within the framework of an organ-based plant model are typically rather complex. To successfully overcome this problem, FSPM development requires establishing strictly modular model structures. In particular, physiological submodels should be generic and universal for different plant species, solidly tested and parameterized, provide clearly defined input-output interfaces, and facilitate the exchange between different research groups. To this end, here we present a generalized version of the nitrogen-sensitive LEAFC3-N model of the coupled CO_2, H_2O and radiation fluxes (Müller et al., 2005, 2006) that was designed to meet this requirements. The model combines and extends recent developments in ecophysiological leaf gas exchange modelling (for review, see Müller et al., 2005). It was tested and calibrated for leaves of wheat (*Triticum aestivum* L.), leaves and pods of oilseed rape (*Brassica napus* L.), and leaves and awns of barley (*Hordeum vulgare* L.). Adaptation to further plant species and organs is planned in future. The barley LEAFC3-N version was integrated into an FSPM of this crop (Wernecke et al., 2007). Here we discuss aspects of the universal formulation and parameterization of the LEAFC3-N model for different plant species and organs and its integration into FSPMs.

Model

LEAFC3-N is a nitrogen-sensitive extension of the generic steady-state flux model LEAFC3 (Nikolov et al., 1995) that couples major processes of CO_2 and H_2O gas exchange with stomatal function and the energy and mass transfer in the leaf-boundary layer. Because of the model complexity, we only outline main aspects related to the present study. A survey on combined photosynthesis-stomatal models as described in literature and further details on LEAFC3 and LEAFC3-N are given by Nikolov et al. (1995) and Müller et al. (2005).

In LEAFC3-N, biochemical processes determining net assimilation rate A_n (µmol m^{-2} s^{-1}) are modeled according to Farquhar et al. (1980). Main parameters of this submodel are: maximum carboxylation rate $V_{c,max}$ (µmol m^{-2} s^{-1}), Michaelis-Menten constants of Rubisco for carboxylation and oxygenation of RuBP, K_c and K_o (µmol mol^{-1}), CO_2 compensation concentration in the absence of mitochondrial respiration Γ^* (µmol mol^{-1}), light saturated rate of electron transport J_{max} (µ$mol_{(e-)}$ m^{-2} s^{-1}), quantum yield for electron transport φ ($mol_{(e-)}$ $mol_{(quanta)}^{-1}$), and the rate of mitochondrial respiration in the dark R_{dark} (µmol m^{-2} s^{-1}). The parameters $V_{c,max}$, J_{max}, K_c, K_o, Γ^*, and R_{dark} are functions of temperature. Stomatal function in LEAFC3-N is modeled following Ball et al. (1987). The modified version of their model used here relates stomatal conductance g_s (mol m^{-2} s^{-1}) by a dimensionless scaling factor m to gross photosynthesis rate A_g and to the ratio of air humidity

and CO_2 concentration in the leaf boundary layer. Further, a minimum value $g_{s,min}$ of g_s is considered.

Farquhar et al. (1980) gave a mechanistic explanation of the relationship between $V_{c,max}$ and nitrogen content N. A dependency of V_{cmax} and other photosynthetic or stomatal characteristics on N was incorporated into several gas exchange models (for review, see Müller et al., 2005). In developing LEAFC3-N, parameter-nitrogen relationships were subjected to special analysis and included in the model for $V_{c,max}$, J_{max}, φ, θ, R_{dark}, m, and $g_{s,min}$. For leaves, N per unit of one-sided leaf area N_a (g m^{-2}) is used. For other organs like pods of rapeseed or awns of barley ears, N must be defined in organ-specific way. Alternatively, N dependency of J_{max}, φ, and R_{dark} may be considered indirectly based on correlations between these parameters and V_{cmax}, which are stable under many conditions. Introducing N sensitivity into LEAFC3-N allows accounting for effects of organ development, mineral nutrition, and adaptation to growth conditions on gas exchange (cf. Müller et al., 2005, 2006).

Universality of parameter-nitrogen relationships

The parameter-nitrogen functions were derived from comprehensive measurements of the response of A_n and g_s to environmental factors on leaves or other organs during the course of organ and plant development. The relationships were analysed for different growth conditions and validated on the basis of field measurements of diurnal time courses of A_n and g_s. As expected, the function type of the considered parameter-nitrogen relationships differs between model parameters, but as a rule it was universal for different organs and plant species under study.

Basic parameter-nitrogen relationships mainly determining the response of the model to the effects listed above are those for V_{cmax}, J_{max}, φ, and m. Typically, the relationships between $V_{c,max}$ or J_{max} and N_a may be expressed by the linear function:

$$p_{max} = \begin{cases} s_{Na}\left(N_a - N_{a,min}\right), & \text{if } N_a > N_{a,min} \\ 0, & \text{if } N_a \le N_{a,min}, \end{cases} \quad (1)$$

where p_{max} stands for $V_{c,max}$ or J_{max}, s_{Na} (μmol g^{-1} s^{-1}) is the slope of the relationship, and $N_{a,min}$ is a minimum value of N_a at which p_{max} approaches zero. Alternatively, the nitrogen dependency of J_{max} may be accounted for indirectly using a correlation between J_{max} and $V_{c,max}$ (Leuning et al., 1997). The relationship between φ and N_a typically shows a saturation pattern as described by:

$$\varphi = \gamma_{Na1}\left(1 - \exp\left(-\gamma_{Na2}\, N_a\right)\right), \quad (2)$$

where γ_{Na1} (mol mol^{-1}) is the value of φ at high N_a, and γ_{Na2} (m^2 g^{-1}) defines the saturation pattern. Alternatively, nitrogen dependency of φ was accounted for indirectly based on the correlation between φ and $V_{c,max}$, where the same type of function applies. To compare φ for different organs and species, the characteristic φ_{ref} calculated for a reference concentration $N_{a,ref}$ (e.g, 3.5 g m^{-2}) may be derived from eq. (2).

The parameter m typically drops with increasing N_a according to the relationship:

$$m = \delta_1 N_a^{-\delta_2}, \quad (3)$$

where δ_1 (m^2 g^{-1}) and δ_2 (dimensionless) are empirical coefficients. However, in rapeseed leaves the m-N_a dependency tended to a linear one, whereas none dependency was found for pods. Again, most appropriate for comparisons is the characteristic m_{ref} calculated for $N_{a,ref}$.

For different plant species and organs, the values of key characteristics of the parameter-N_a relationships except of m_{ref} for awns and pods generally are in close range (Table 1). The values of s_{Na} for $V_{c,max}$ and J_{max} as well as those for φ_{ref} correspond well to those theoretically expected. The range of values given for several parameters of wheat and rapeseed is related to the method of its deter-

mination (for further detail, see the literature cited in Table 1). The upper values of these ranges were derived from parameter optimization based on adapting the complete model to data from diurnal time courses of gas exchange rates measured in the field. Therefore, these parameter values may be recommended for applying the model under comparable conditions. Nevertheless, it should be pointed out that further information is needed on the effects of growth conditions and genetic factors on the stability of parameter values.

Table 1. Characteristics of parameter-N_a relationships.

Object		$V_{c,max}$ vs. N_a		J_{max} vs. N_a or $V_{c,max}$			φ vs. N_a	m vs. N_a
Species	**Organ**	s_{Na}	$N_{a,min}$	s_{Na}	$N_{a,min}$	$J_{max}/V_{c,max}$	φ_{ref}	m_{ref}
Wheat	leaves	58-76[a]	0.1-0.3[a]	116-152[ac]	0.1-0.3[ac]	2[c]	0.43[a]	6.2[a]
Barley	leaves	63	0.2	151	0.2	2.2	0.44	7.4
	awns	52	0	108	0.1	1.9	0.41	2.6
Rapeseed	leaves	54-67[b]	0.3-0.4[b]	108-134[bc]	0.3-0.4[bc]	2[c]	0.32[b]	6.0-8.7[b]
	pods	49[b]	0.1[b]	98[bc]	0.1[bc]	2[c]	0.25[b]	11[b]

[a] from Müller et al., 2005; [b] from Müller et al., 2006; [c] value re-calculated or adopted based on Leuning, 1997.

Universality of temperature dependencies

The applicability of the parameter values of temperature dependencies of photosynthetic characteristics given for C_3-plants in literature was confirmed for the wheat, barley and rapeseed model versions by analysis of diurnal time courses of A_n and for the barley model version additionally by measurements of temperature response curves of temperature-sensitive parameters.

Model application

LEAFC3-N can be integrated into plant models via an interface providing local environmental characteristics and organ-based state variables (N, chlorophyll content, characteristic dimension of area elements, specific area). It was tested successfully with an FSPM for barley (cf. Müller et al., 2007, Wernecke et al., 2007) and with 1D multi-layer models for rapeseed (Müller et al., 2005) and wheat (Müller, unpublished). In principle, the LEAFC3-N model can be used with FSPMs of different level of discretization of the 3D structure, depending on the discretization of absorbed radiation provided by the light model used as well as on the discretization of organ-based state variables provided by the FSPM. However, in simulation studies covering the entire growth period, assembling individual polygons according to a 1D multi-layer scheme may be useful to reduce computational time. Concerning the choice of the time step for using LEAFC3-N as submodel of an FSPM, it must be noted that model calibration was derived from steady-state response curves of gas exchange rates and validated against diurnal time course data given with a measuring time interval of 10 s for the barley data and a time interval resulting from averaging of the measurement data in order of 2 or 6 minutes for the rapeseed and wheat data, respectively. Thus, by using LEAFC3-N with other time steps, the resulting biases must be analyzed and, if required, corrected.

Acknowledgments

The present study was funded by the German Research Association (Deutsche Forschungsgemeinschaft, DFG). The support of the state of Saxony-Anhalt is highly appreciated.

References

Ball, J.T., Woodrow, I.E. and Berry, J.A., 1987. A model predicting stomatal conductance and its contribution to the control of photosynthesis under different environmental conditions. In: Biggins, J. (Editor),

Progress in Photosynthesis Research. Proceedings of the VII. International Congress on Photosynthesis. Martinus Nijhoff Publishers, Dordrecht-Boston-Lancaster, 4: 221-224.

Farquhar G.D., von Caemmerer S. and Berry J.A., 1980. A biochemical model of photosynthetic CO_2 assimilation in leaves of C_3 species. Planta 149: 78-90.

Leuning, R., 1997. Scaling to a common temperature improves the correlation between the photosynthesis parameters J_{max} and V_{cmax}. J. Exp. Bot. 48: 345-347.

Müller, J., Behrens, T., Diepenbrock, W. 2005. Measurement and modelling of canopy gas exchange of winter oilseed rape (*Brassica napus* L.). Agric. For. Meteor. 132: 181-200.

Müller, J., Wernecke, P., Diepenbrock, W., 2005. LEAFC3–N: a nitrogen-sensitive extension of the CO_2 and H_2O gas exchange model LEAFC3 parameterised and tested for winter wheat (*Triticum aestivum* L.). Ecol. Model. 183: 183-210.

Müller, J., Diepenbrock W. , 2006. Measurement and modelling of canopy gas exchange of leaves and pods of oilseed rape. Agric. For. Met. 139: 307-322.

Müller, J., Wernecke, P., Braune, H., Diepenbrock, W., 2007. Photosynthesis and carbon balance. In: Vos, J., Marcelis, L.F.M., de Visser, P.H.B., Struik, P.C., Evers, J.B. (Eds.): Functional-Structural Plant Modelling in Crop Production. Wageningen UR Frontis Series v. 22, Springer, Dordrecht, The Netherlands, 91-101.

Nikolov, N.T., Massman, W.J. and Schoettle, A.W., 1995. Coupling biochemical and biophysical processes at the leaf level: An equilibrium photosynthesis model for leaves of C-3 plants. Ecol. Model. 80: 205-235.

Wernecke, P.; J. Müller, T. Dornbusch, Diepenbrock, W., 2007. The Virtual Crop Modelling System 'VICA' Specified for Barley. In: Vos, J., Marcelis, L.F.M., de Visser, P.H.B., Struik, P.C., Evers, J.B. (Eds.): Functional-Structural Plant Modelling in Crop Production. Wageningen UR Frontis Series v. 22, Springer, Dordrecht, The Netherlands, 53-64.

Dissecting maize matter production variability using a structural model – An original approach to drive maize breeding for cold tolerance

G. LOUARN[1], K. CHENU[1], C. FOURNIER[2], B. ANDRIEU[2] and C. GIAUFFRET[1]

[1]UMR 1281 SADV, INRA-USTL, Estrées-Mons, BP 136, F80203 Péronne, France
[2]UMR1091 Environnement et Grandes Cultures, INRA, AgroParisTech, F78850 Thiverval – Grignon

Backgrounds and Aims –

Plant response to temperature is one of the most important factors governing the yield of crops. Many crops are however cultivated well outside their original zones of natural selection, and hence are bound to experience temperatures out of their optimal range, with potentially detrimental effects on matter production and yield elaboration. In maize, a cold sensitive species of subtropical origin, breeders have so far extended cultivation areas by using predominantly shunting strategies (selection of early-maturing photoperiod-insensitive hybrids). In northern Europe, this leads to growing cycles taking place during a climatic window reasonably favourable in terms of temperatures but presenting frequent water shortage from the critical flowering stage on, and decreasing light availability during grain filling. Because earlier sowing would allow a better fit between crop cycle and overall resource availability, breeders are now seeking for original adaptation strategies enabling plants to grow more efficiently under cool temperature conditions (Greaves, 1996).

Suboptimal temperatures have a major impact on radiation interception through modification of foliage development (Chenu *et al*., 2007) and on radiation use efficiency (RUE) through the reduction of leaf photosynthetic activity (Dolstra *et al*., 1994). However, our limited understanding of how these processes interact in the course of canopy development and our knowledge of their genetic variability still hamper our ability to define relevant selection criteria to improve productivity in a realistic range of climatic scenarios. A modelling approach able to sort out the processes involved in different climatic scenarios would help making sensible decisions according to breeders' objectives. Such a tool has to rely on an organ scale description of plant structure in order to deal with the heterogeneous canopy structure when cold stresses usually occurs (early growth stages).

This study quantifies, for four contrasted inbred lines grown in climatic sequences including periods of suboptimal temperatures, the impact of architectural traits involved in light interception and of RUE on biomass production. It implied the calibration and assessment of the 3D model, ADEL-maize (Fournier and Andrieu, 1998) for each of the studied genotypes and its use, together with a radiosity model (Chelle and Andrieu, 1998), to calculate light absorption by plants.

Materials and Methods –

Field experiments were carried out at Estrées-Mons (49°N, 3°E, 85m), France, in 2005 and 2006 with four cold-tolerant inbred lines (F2 and F286 from temperate origin; F331 and F334 from tropical-highland origin). In both experiments, two sowing dates (early: first week of April; normal: first week of May) were used to generate contrasted temperature regimes during seedling establishment. In addition, the two years differed in the temperature conditions during this period (Fig. 1): in 2005 cold stress occurred only for the early sown plants before the stage "emergence of the 3rd leaf", while in 2006 it affected early sown plants during short periods at the stage "emergence of the 2nd leaf" and at the beginning of their autotrophic phase (6 unfolded leaves), and normally sown seedlings in their very first stage of development.

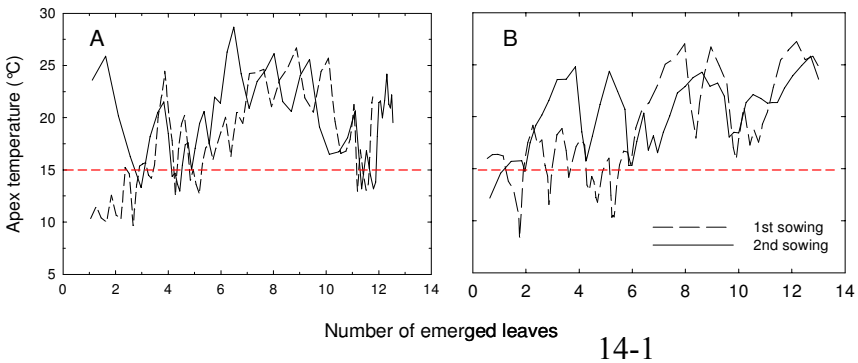

Figure 1: Apex temperatures over plant development expressed in number of emerged leaves for the inbred line F2, in the 2005 (A) and 2006 (B) experiments. Red dashes represent the temperature below which cold stress occurs in maize.

For each situation, plant phenology, leaf senescence and plant architecture were characterised over time. These records enabled the analysis of the plant architecture modifications in response to low temperatures and to parameterise the 3D model (i.e. define plant phyllochrone, organ dimensions and leaf shapes in each situation). Measurements of ground cover were performed to assess the quality of the generated virtual plants (comparison of real and computer-generated pictures). Destructive biomass measurements were made to determined RUE (ratio between above ground biomass and cumulated intercepted PAR) from simulation of radiative transfer within the virtual stands. Finally, we carried out a sensitivity analysis to evaluate the relative importance of architectural traits (leaf length, leaf width, shape of the vertical profile of leaf area, leaf angles, internode length) and of the photosynthetic activity with respects to dry matter production and available genotypic variability.

Main results –

Low temperatures modified plant development during and after the cold period. Inbred lines exhibited a range of phyllochron sensitivity (F334 systematically increased its phyllochron for early sowing while F286 remained unaffected; F2 and F331 were affected in 2005 but unaffected in 2006). Leaf lifespan also showed a strong response to cold stress, senescence being hastened for early sowings (Fig. 2). Interestingly, this response was more pronounced in 2006, when the cold period extended in June concomitantly with high incoming PAR radiation. It suggests possible interactions between plant functioning (i.e. photoinhibition induced by the imbalance between intercepted energy and the reduction capacity of leaves at low temperature, Fig. 3) and the dynamic evolution of its structure that are potentially important during seedling establishment.

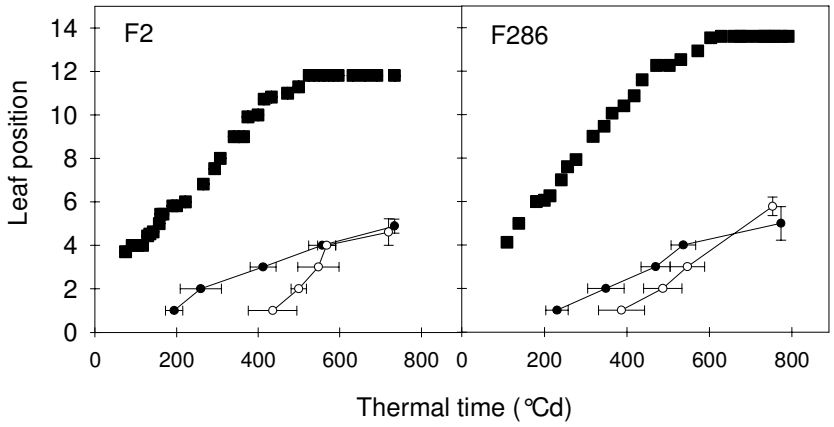

Figure 2: Thermal time of leaf emergence (squares) and of leaf senescence (circles) for early (plain symbols) and normal (open symbols) sowings in the 2006 experiment (F2 and F286 inbred lines).

.

Figure 3: Efficiency of the photosystem II (Fv/Fm) as a function of plant development for early (A) and normal (B) sowings in the 2006 experiment (F2 and F286 inbred lines).

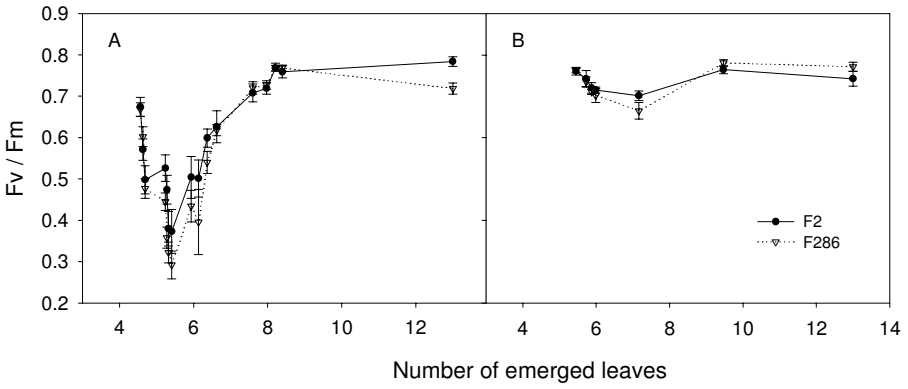

Whatever the genotype considered, length and width of mature leaves were severely reduced for early sowings (Fig. 4), some inbred lines being more prone to this effect of suboptimal temperatures on leaf expansion (F2 being the most and F331 the less sensitive lines). Modification of the leaf area profiles seemed to initiate only after the first occurrence of a significant thermal stress (later in 2006

than in 2005), then propagating until the topmost leaves for all lines but F331 (delayed tassel initiation in this genotype resulting in a significant increase of the final number of leaves).

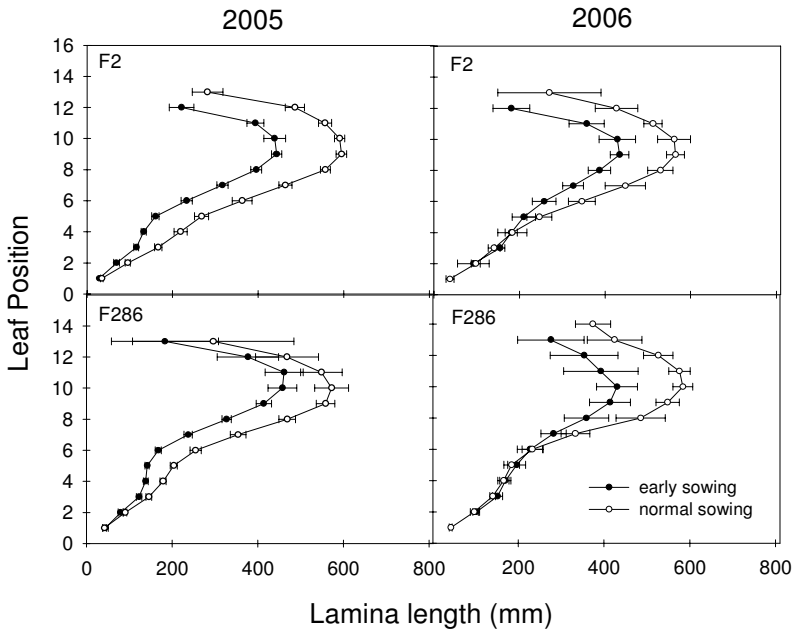

Figure 4: Final lamina length of successive leaves along the shoot for early and normal sowings in the 2006 experiment (F2 and F286 inbred lines).

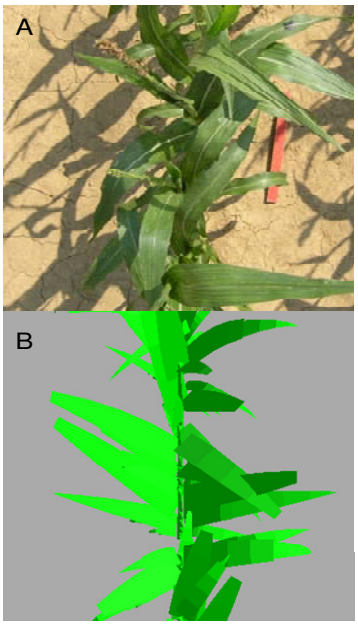

Figure 5: Examples of real (A) and generated (B) images used for virtual plants assessment (F2 inbred line at flowering)

Biomass production was also reduced for early sowing in both years. Relative reduction was lower in 2006 and ranking of inbred lines also changed (F2 exhibited the strongest response in 2005 but the slightest in 2006).

Collected developmental and architectural data were used to fit the simulation model ADEL-maize. Generated 3D virtual stands were successfully assessed against ground cover measurements at various developmental stages (Fig. 5). Special attention was paid to the period of seedling establishment as it corresponds to the period during which cold stress and photoinhibition most likely occur (and thus to the most relevant period to identify potential reductions of RUE). Computation of light interception on these validated mock-ups revealed that the contribution of RUE to the reduction of biomass accumulated at flowering was marginal as compared to the impact of cumulative radiation captured in 2005. It also highlighted potentially important transient effects of RUE during early stages for climatic scenarios leading to photoinhibition.

The sensitivity analysis allowed us to identify that stability of final leaf number, final leaf area and RUE are the traits affecting most directly the stability of matter production under cold conditions. Among them, organ size-related traits displayed the most interesting genotypic variability.

Conclusion –

In this study virtual plants coupled with a biophysical model of radiative transfer helped to better characterise plant response to contrasted cold stresses through accurate quantification of light interception. These results constitute a first step toward a tool for phenotyping plant response to low temperature, considering both plant structure and functioning.

Key Words: maize, low temperature, light interception, RUE, genetic variability, virtual plants

References –

Chelle C., Andrieu B. 1998. The nested radiosity model for the distribution of light within plant canopies. *Ecological Modelling* **111**: 75-91.

Chenu K., Fournier C., Andrieu B., Giauffret C., 2007. An architectural approach to investigate maize response to low temperature. *Scale and Complexity in Plant Systems Research: Gene-Plant-Crop Relations. J.H.J. Spiertz, P.C. Struick and H.H. van Laar (eds.), 2007 Springer, The Netherlands*, pp 201-210.

Dolstra O., Haalstra S.R., Van der Putten P.E.L., Schapendonk AHCM., 1994. Genetic variation for resistance to low temperature photoinhibition of photosynthesis in maize. *Euphytica*, 80: 85-93.

Fournier C, Andrieu B. 1998. A 3D architectural and process-based model of maize development. *Annals of Botany* **81**: 233-250.

Greaves J.A., 1996. Improving suboptimal temperature tolerance in maize – the search for variation. *J. Exp. Bot*., 47:307-323.

Models of photosynthesis need to and can be upgraded to include the effects of drought, phenological changes, sink activity and carbohydrate accumulation on the light exposure/photosynthetic capacity relationship

Gaëlle Damour
CIRAD-PERSYST, Station de Bassin Plat
BP 180, 97455 Saint Pierre cedex
La Réunion, France

Laurent Urban
INRA-UR 1103
Déterminismes Génétiques et Environnementaux de la Qualité des Agrumes
20230 San Giuliano
Corse, France
urban@corse.inra.fr

Keywords: carbohydrate, drought, modelling, photosynthesis, source-sink relationship, starch

Introduction

Biochemical models of leaf photosynthesis, based on the seminal work of Farquhar et al. (1980), have been widely used to compare photosynthetic performance among plant species and to analyse photosynthetic acclimation to high CO_2 concentrations or growth irradiance. Such functional models may also be coupled to radiation transfer models, which are structural models, to simulate photosynthesis at the canopy level. FSPM based on coupled models of leaf photosynthesis and radiation transfer are also used in global change modelling. Such coupled models are based on two key relationships, the first between the amount of leaf nitrogen per unit leaf area (N_a) and light exposure or leaf age, and the second between leaf photosynthetic capacity (essentially the light saturated rate of electron transport, J_{max}, and the maximal rate of carboxylation, V_{cmax}) and N_a. These fundamental relationhips are implicitly assumed to be constants. Moreover it is generally assumed that V_{cmax}/J_{max} is stable.

Although there is an increasingly large body of evidence that drought impacts negatively photosynthetic capacity, these models do not include such effects, impairing our capacity to model photosynthesis in conditions of limiting water supply. Similarly, such models do not satisfy the specific needs of fruit production, mainly because they don't integrate the effects of phenology and cultural practices, with the exception of nitrogen fertilisation. In fruit production, the effects of flowering and fruiting, which modify source-sink relationships, cannot be overlooked. This is even more true in tropical fruit production, where the flowering and fruiting phases exceed six months at the individual tree scale, depending on climatic conditions. More specifically, little is known about the effects of source/sink balance, and the associated changes in carbon export rate from leaves and leaf carbohydrate concentration, like the ones resulting from the presence of developing fruits, on leaf nitrogen and photosynthetic capacity within the crown of field-growing trees. This can restrict our ability to accurately predict the spatial distribution of carbon gains and fruit growth within the canopy of fruit trees.

The objectives of this paper are: 1) to provide an overview of the effects of long-term drought, phenological changes and the associated variations in sink activity and carbohydrate accumulation on the key relationships of the coupled model of photosynthesis, and 2) to evaluate the prospects of improving these models. Data presented here were collected over more than seven years on two tropical trees, mango and lychee.

Effects of climatic changes, long-term drought, the proximity of inflorescences, low fruit load and starch accumulation in the presence or absence of sink activity

Observations on adult mango trees suggest that in the absence of drought, and provided that there are no phenological changes, mild climatic variations, like the ones occurring in tropical conditions, do not affect the fundamental relationships between leaf nitrogen concentration and light exposure, and between photosynthetic capacity and leaf nitrogen concentration (Urban et al. 2006).

Long-term drought in two-year old lychee trees results in a decrease in leaf starch concentration expressed on an area basis $[starch]_a$, an increase in N_a, and a decrease in both J_{max} and J_{max}/N_a (Damour et al. 2007).

The proximity of inflorescences does not affect $[starch]_a$ but results in a decrease in N_a, and a decrease in J_{max} and J_{max}/N_a (Urban et al. 2004a and 2007b). The proximity of inflorescences is moreover associated with a reversible decrease in mesophyll conductance and increase in photosynthetic electron fluxes towards alternative sinks (Urban et al. 2007b).

Starch accumulates while N_a decreases as a consequence of low fruit load. Photosynthetic capacity decreases although it may be argued that V_{cmax} and J_{max} are underestimated in the presence of starch accumulation. Consequently, the decreases in V_{cmax}/N_a and J_{max}/N_a which were observed as a consequence of low fruit load may be considered with caution (Urban et al. 2004b, Urban and Léchaudel 2005). The V_{cmax}/J_{max} ratio was found to be unaffected by starch accumulation.

Starch accumulation in the presence of sink activity results in a decrease in N_a like when fruit load is low (Urban et al. 2007a). However, in the absence of sink activity, N_a is not significantly affected. But then the absence of sink activity results in an increase in photoinhibition and a decrease in the apparent efficiency of light energy conversion (α), more pronounced than in the presence of sink activity.

Data basically show that the fundamental relationships between leaf nitrogen concentration and light exposure, and between photosynthetic capacity and leaf nitrogen concentrations cannot be considered as constants in the presence of long-term drought or phenological events, when sink activity is modified or carbohydrates accumulate. Our observations also show that the effect of starch accumulation on leaf nitrogen concentration depends on sink activity (Urban et al. 2007a), which seems to put an additional layer of complexity. Now the question is whether modelling is possible.

Prospects for modelling

As far as long-term drought is concerned, we are confident about our capacity to design very simple empirical models expressing N_a as a monomolecular and J_{max}/N_a as an exponential function of the predawn water potential (Damour et al. 2007). The complexity of the processes involved during the development of inflorescences leaves us with very little hope about the prospects for modelling (Urban et al. 2007b). The effect of starch accumulation, on

the contrary, lends itself to modelling. Modelling the effect of starch accumulation on N_a may be achieved using a negative linear relationship (Fig. 1).

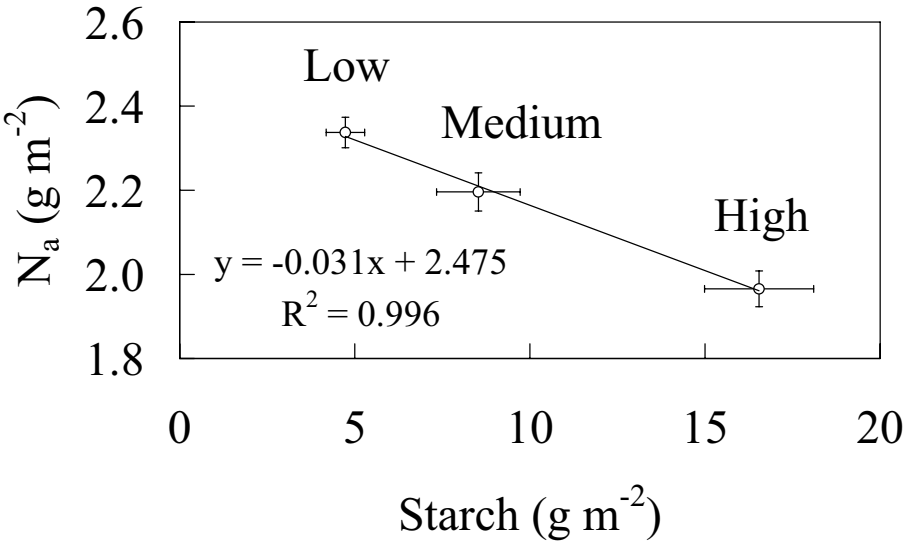

Fig. 1. The relationship between the amount of leaf nitrogen and the amount of starch per unit leaf area in mango leaves (redrawn from Urban and Léchaudel 2005). Low, medium and high refer to leaf-to-fruit ratios.

However, such relationships apply only in the presence of sink activity. In the absence of sink activity, N_a may simply be considered as a constant (Urban et al. 2007a). The most tricky part consists in modelling the effect of starch accumulation on J_{max}/N_a and V_{cmax}/N_a. Considering that J_{max} may be underestimated in the presence of starch accumulation and that α is negatively correlated to leaf starch concentration, we decided to consider J_{max}/N_a as a constant (as well as V_{cmax}/N_a and V_{cmax}/J_{max}) and to integrate the effect of starch in the biochemical model of leaf photosynthesis in the form of a global corrective factor C_{starch} applied to the rate of electron flow, J (Urban et al. 2007a):

$J = C_{starch}\alpha\theta Q(1 + (\alpha\theta Q/J_{max})^2)^{-0.5}$
where θ represents leaf absorptance and Q the photosynthetically active flux density.

$C_{starch} = e^{-0.0412[starch]a}$ (in the absence of sink activity)
or $C_{starch}' = e^{-0.0398[starch]a}$ (in the presence of sink activity)

Differences between C_{starch} and C_{starch}' are due to the fact that the absence of sink activity results in an increase in photoinhibition and a decrease in α. The model of the effect of starch accumulation on A_{net} in the presence of sink activity was tested on an independent set of data obtained from gas exchange measurements made on leaves from girdled branches with 10 and 100 leaves per fruit. The modified model of leaf photosynthesis of Urban et al. (2003) that incorporated the corrective factor C_{starch}' performed much better than the uncorrected model (Fig. 2).

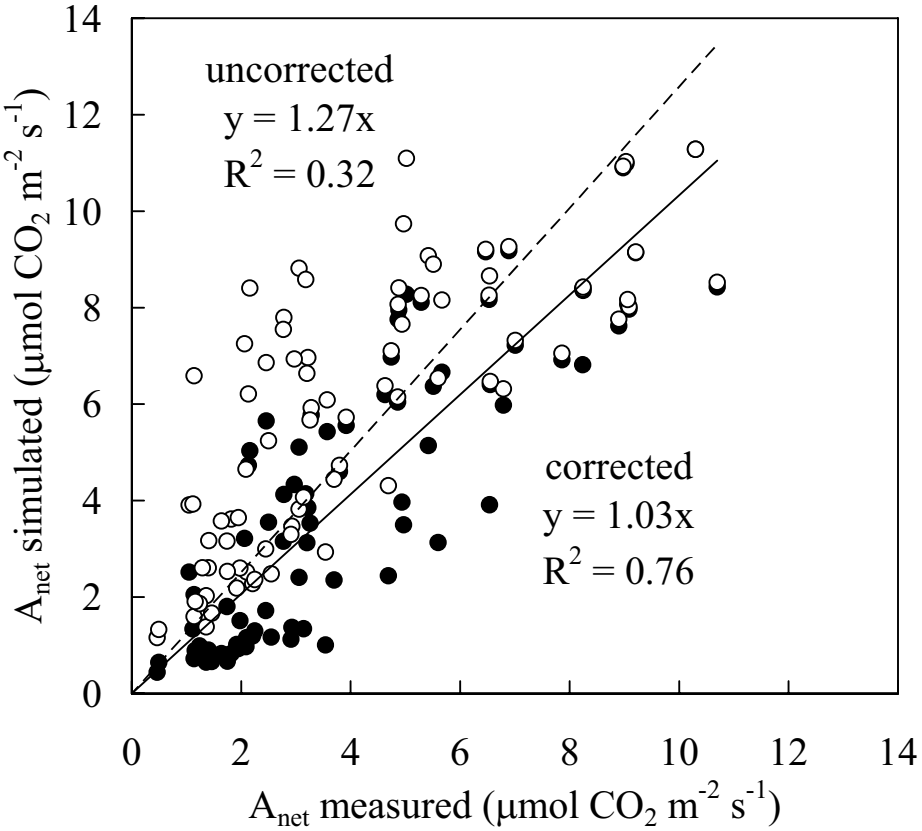

Fig. 2. Effect of the corrective factor C_{starch}' on simulation of A_{net} (redrawn from Urban and Alphonsout, 2007a).

Conclusion

With the exception of the proximity of inflorescences, the effects of seasonal changes, including long-term drought, starch accumulation and variations in sink activity resulting from such phenological changes like fruiting can be easily handled to correct and adapt the biochemical model of Farquhar et al. (1980). One of the major challenge for the future will consist in coupling models of water relationships and models of starch accumulation, on one side, with models of photosynthesis, on the other side.

References

Damour, G., Vandame, M. and Urban, L. 2007. Long-term drought modifies the fundamental relationships between light exposure, leaf nitrogen content and photosynthetic capacity in leaves of lychee tree (*Lychee chinensis* Sonn.). Journal of Plant Physiology. Submitted.

Farquhar, G.D., von Caemmerer, S. and Berry, J.A. 1980. A biochemical model of photosynthetic CO_2 assimilation in leaves of C_3 species. Planta, 149, 78-90.

Urban, L., Le Roux, X., Sinoquet, H., Jaffuel, S. and Jannoyer, M. 2003. A biochemical model of photosynthesis for mango leaves: evidence for an effect of the local source/sink balance on photosynthetic capacity. Tree Physiology, 23, 289-300.

Urban, L ., Lu, P. and Thibaud, R. 2004a. Inhibitory effect of flowering on leaf photosynthesis in mango. Tree Physiology, 24, 387-399.

Urban, L., Léchaudel, M. and Lu, P. 2004b. Effect of fruit load and girdling on leaf net photosynthesis in *Mangifera indica* L. Journal of Experimental Botany, 405, 2075-2085.

Urban, L. and Léchaudel, M. 2005. Effect of leaf-to-fruit ratio on leaf nitrogen content and net photosynthesis in girdled branches of *Mangifera indica* L. Trees, 19, 564-571.

Urban, L., Montpied, P. and Normand, F. 2006. Season effects on leaf nitrogen partitioning and photosynthetic water use efficiency in mango. Journal of Plant Physiology, 163, 48-57 .

Urban, L. and Alphonsout, L. 2007a. Girdling decreases photosynthetic electron fluxes and induces sustained photoprotection in mango leaves. Tree Physiology, 27, 345-352.

Urban, L. Jégouzo, L., Damour, G., Vandame, M. and François, C. 2007b. The effect of flowering on some parameters of the mango leaf photosynthesis model. Tree Physiology, submitted.

Extending a functional-structural plant model of spring wheat with sub-models for photosynthesis and carbon distribution

J.B. Evers[1], J. Vos[1], P. Romero[2], X. Yin[1], P.E.L. van der Putten[1], M.Z. Kang[3,4], P.C. Struik[1]

[1]Crop and Weed Ecology, Plant Sciences Group, Wageningen University, Haarweg 333, 6709 RZ Wageningen, the Netherlands
[2]Department of Viticulture, IMIDA, 30150, La Alberca, Spain
[3]Capital Normal University, 100037, Beijing, China
[4]Institute of Automation, LIAMA, Chinese Academy of Sciences, 100080, Beijing, China
jochem.evers@wur.nl

Keywords: spring wheat, architecture, tillering, photosynthesis, sink-source, nitrogen

Introduction

Members of the Poaceae family have been rewarding subjects of research in the field of functional-structural plant modelling (FSPM) (Fournier *et al.*, 2007). Poaceae comprise important cereal crop species such as rice, wheat, and maize, and the plants usually exhibit a regular and co-ordinated development making them particularly suitable for FSPM. The models that have been reported up to now range from descriptive (e.g. Watanabe *et al.*, 2005) to (partially) mechanistic (e.g. Guo *et al.*, 2006; Wernecke *et al.*, 2007).

Here we report on our ongoing work on an FSPM of spring wheat (*Triticum aestivum* L.), of which simulation of growth and development, until recently, have been mainly descriptive. The outgrowth of tiller buds into tillers (branches in Poaceae) has been made dependent on the local ratio between red and far-red light (Evers *et al.*, 2007a). Once the 'decision' is taken to develop a particular bud into a tiller, the emergent organs attain more or less predefined properties (*e.g.* dimensions, shape, etc.). The limitations to this (provisional) approach are (I) source activity is not included and (II) organ outgrowth and dimensions of organs are not subjected to modulation due to sink-source interactions.

The general objective of the current work is to add 'functionality', *i.e.* carbon gain and partitioning, to the architectural model in order to obtain a complete FSPM of a canopy of spring wheat plants. Operational objectives of the work include the extension of the current architectural model of spring wheat with provisions that convert radiation absorbed by each element of the 3D structure into photosynthates, and distribute carbon over individual, growing organs.

Approach

The model used in this study is based on the concepts of Fournier *et al.* (2003), and has been calibrated and validated for spring wheat (Evers *et al.*, 2005, 2007b), see Fig. 1 for a visualisation. Details can be found in the papers cited. This model provides a solid basis for extension with sub-models for photosynthesis and carbon distribution.

Fig. 1: Visualisation of a small simulated wheat plot

Data collection

Data to realize the objectives stated, were gathered in two experiments conducted in Wageningen, the Netherlands: one outdoor experiment, and one in a growth chamber. In the outdoor experiment plants were grown at three plant population densities and exposed to two nitrogen treatments (limiting and non-limiting),

and two light treatments (75% shading and full light). In this experiment data were gathered on the distribution of chlorophyll meter values (SPAD) in the canopy, and on plant growth and organ weight by harvesting plants at five stages of development. In the growth chamber experiment, two nitrogen treatments (limiting and non-limiting) were applied. In this experiment a diversity of photosynthesis parameters were assessed (both through gas exchange and chlorophyll fluorescence) and calculated. A calibration curve was created for leaf nitrogen content versus SPAD value. Details on the experimental setups and measurement protocols will follow in later communications.

Source activity

For a given hemispherical distribution of daily incoming solar radiation, the illumination of each plant organ of the canopy structure (leaves, internodes) can be simulated using the wheat architectural model in combination with the nested radiosity model for crop canopies (Chelle and Andrieu, 1998). Using organ-specific reflection and transmission coefficients, PAR absorption by the plant organs was calculated from this illumination on an hourly basis. Subsequently, rate of photosynthesis of each individual organ was modelled by applying an updated biochemical model for C_3 photosynthesis (Yin *et al.*, submitted), based on Farquhar *et al.* (1980), and extended by Yin *et al.* (2004). A (photosynthesis rate), C_i (intercellular CO_2 concentration), and g_s (stomatal conductance) were calculated using an analytical solution to a coupled photosynthesis - stomatal conductance model.

The biochemical photosynthesis model was parameterized by fitting the photosynthesis (gas exchange and chlorophyll fluorescence) data derived from the growth chamber experiment, measured for the two nitrogen treatments, two leaf insertion levels and three leaf age categories (Yin *et al.*, submitted). The estimated parameters were maximum carboxylation rate of Rubisco ($V_{c,max}$), maximum rate of linear electron transport (J_{max}), Rubisco CO_2/O_2 specificity factor ($S_{c/o}$), mesophyll conductance (g_m), 'dark' respiration rate in the light (R_d), residual g_s at the light compensation point (g_0), minimum leaf nitrogen content for photosynthesis (N_b), and a parameter for maximum efficiency of light conversion into linear electron flux on incident light basis ($\kappa_{2(LL)}$). Remaining parameter values required by the model of Farquhar *et al.* (1980) are considered to be conservative among C3 species, and taken from Von Caemmerer *et al.* (1994) and Bernacchi *et al.* (2002).

Sink strength

Sink strength is defined as the potential capacity of sink tissues to accumulate assimilates (Marcelis and Heuvelink, 2007). Experimentally, the sink strength can be derived from the growth curve under conditions ensuring abundant source supply, either by removing competing sinks or by enhancing photosynthesis (high radiation and/or CO_2). For the current work, sink strength values were derived using the GreenLab plant modelling approach (Yan *et al.*, 2004). Based on several growth chamber experiments using the same wheat cultivar as in the present study, sink strength values for various organ types (blades, sheaths, internodes, spikes, root system) have been calculated by a non-linear least squares root fitting procedure (Kang *et al.*, in press). These values were used in the present study.

Sink-source relations

To simulate the distribution of assimilates from the sources to the sinks, the semi-mechanistic concept of carbon allocation being determined by the relative sink strengths of competing sinks can be implemented (Heuvelink, 1996; Marcelis, 1996). However, bud break and the appearance of tillers is not straightforward: whether or not particular tillers will appear will not 'automatically' emerge as a result of the simulation. Here extra rules might be needed, *e.g.* specifying that the local assimilate production of the parent leaf has to be taken into account (Bos, 1999).

It is possible to efficiently implement carbon fluxes between plant components, based on gradients in driving forces (*i.e.* Ohm's law analogy) (Allen *et al.*, 2005; Prusinkiewicz *et al.*, 2007). The virtue of that approach is that local effects and sink priorities become an emergent property. Sink activity is represented by Michaelis-Menten kinetics, the parameters of which

(V_{max} and k_m) are being deduced from the sink strength functions, while resistance is proportional to distance. In the FSPM distance is deduced from organ dimensions and topology that are kept track of. However, it will be examined first whether the semi-mechanistic approach can be used satisfactorily.

Nitrogen distribution
Instead of modelling the entire nitrogen economy of a wheat plant, an empirical function was developed that describes the distribution of SPAD values of the individual leaf blades throughout the development of a wheat plant. The function is a cubic polynomial relation between SPAD value and thermal time, of which the four parameters are themselves linear functions of the cumulative phytomer number of the leaf blade (which is the total number of phytomers from the bottom of the plant until the leaf blade in question):

$$S = (p_a C + p_b) \cdot t^3 + (q_a C + q_b) \cdot t^2 + (r_a C + r_b) \cdot t + s_a C + s_b \quad \text{(Eq. 1)}$$

where S is SPAD value (dimensionless), C is cumulative phytomer number of the leaf blade, t is thermal time (ºCd), p_a, q_a, r_a, s_a, are slope parameters and p_b, q_b, r_b, s_b are intercept parameters fitted to the *S*-*C*-*t* data, for each of the treatments. Subsequently, the calculated SPAD values were converted into nitrogen content per surface area, using the calibration curve obtained from the growth chamber experimental data.

Outlook
The combination of an architectural plant model and sub-models for carbon assimilation and distribution throughout the plant is promising. The added value of taking plant geometry into account will show its strength when phenomena that rely on local processes are simulated (*e.g.* bud break). This is what the current work is aiming at.

Acknowledgements
We thank the staff of the experimental facilities UNIFARM of Wageningen University, Fleur Sterk, and Guillaume Castel for their contributions to the experiments; Dr. A. Schapendonk, Mr. S. Pot (Plant Dynamics B.V.), Dr. T. Pons and Mr. R. Welschen (Utrecht University) for their support. The C.T. de Wit Graduate School for Production Ecology and Resource Conservation (PE&RC) and the Instituto Nacional de Investigación Agraria y Alimentaria (INIA) funded this work.

References

Allen MT, Prusinkiewicz P, DeJong TM. 2005. Using L-systems for modeling source-sink interactions, architecture and physiology of growing trees: the L-PEACH model. *New Phytologist* 166: 869-880.

Bernacchi CJ, Portis AR, Nakano H, Von Caemmerer S, Long SP. 2002. Temperature response of mesophyll conductance. Implications for the determination of Rubisco enzyme kinetics and for limitations to photosynthesis in vivo. *Plant Physiology* 130: 1992-1998.

Bos HJ. 1999. *Plant morphology, environment, and leaf area growth in wheat and maize.* PhD thesis, Wageningen UR. 149 pp.

Chelle M, Andrieu B. 1998. The nested radiosity model for the distribution of light within plant canopies. *Ecological Modelling* 111: 75-91.

Evers JB, Vos J, Fournier C, Andrieu B, Chelle M, Struik PC. 2005. Towards a generic architectural model of tillering in Gramineae, as exemplified by spring wheat (*Triticum aestivum*). *New Phytologist* 166: 801-812.

Evers JB, Vos J, Chelle M, Andrieu B, Fournier C, Struik PC. 2007a. Simulating the effects of localized red : far-red ratio on tillering in spring wheat (*Triticum aestivum*) using a three-dimensional virtual plant model. *New Phytologist*: doi: 10.1111/j.1469-8137.2007.2168.x.

Evers JB, Vos J, Fournier C, Andrieu B, Chelle M, Struik PC. 2007b. An architectural model of spring wheat: evaluation of the effects of population density and shading on model parameterization and performance. *Ecological Modelling* 200: 308-320.

Farquhar GD, von Caemmerer S, Berry JA. 1980. A biochemical model of photosynthetic CO_2 assimilation in leaves of C3 species. *Planta* 149: 78-90.

Fournier C, Andrieu B, Ljutovac S, Saint-Jean S. 2003. "ADEL-wheat: a 3D architectural model of wheat development". In Hu BG and Jaeger M, eds. *2003' International Symposium on Plant Growth Modeling, Simulation, Visualization, and their Applications*. Beijing, China PR: Tsinghua University Press / Springer, 54-63.

Fournier C, Andrieu B, Buck-Sorlin G, Evers JB, Drouet J-L, Escobar-Gutiérrez A, Vos J. 2007. Functional-structural modelling of Gramineae. In: Vos J, Marcelis LFM, de Visser PHB, Struik PC and Evers JB, eds. *Functional-Structural Plant Modelling in Crop Production*. Dordrecht, the Netherlands: Springer, 175-186.

Guo Y, Ma Y, Zhan Z, Li B, Dingkuhn M, Luquet D, De Reffye P. 2006. Parameter optimization and field validation of the functional-structural model GREENLAB for maize. *Annals of Botany* 97: 217-230.

Heuvelink E. 1996. Dry matter partitioning in tomato: validation of a dynamic simulation model. *Annals of Botany* 77: 71-80.

Kang MZ, Evers JB, Vos J, de Reffye P. in press. Fitting weight of individual organs in spring wheat using the GreenLab model. *Annals of Botany*.

Marcelis LFM. 1996. Sink strength as a determinant of dry matter partitioning in the whole plant. *Journal of Experimental Botany* 47: 1281-1291.

Marcelis LFM, Heuvelink E. 2007. Concepts of modelling carbon allocation among plant organs. In: Vos J, Marcelis LFM, de Visser PHB, Struik PC and Evers JB, eds. *Functional-Structural Plant Modelling in Crop Production*. Dordrecht, the Netherlands: Springer, 103-111.

Prusinkiewicz P, Allen M, Escobar-Gutiérrez A, DeJong T. 2007. Numerical methods for transport-resistance source-sink allocation models. In: Vos J, Marcelis LFM, de Visser PHB, Struik PC and Evers JB, eds. *Functional-Structural Plant Modelling in Crop Production*. Dordrecht, the Netherlands: Springer, 127-137.

von Caemmerer S, Evans JR, Hudson GS, Andrews TJ. 1994. The kinetics of ribulose-1,5-bisphosphate carboxylase/oxygenase in vivo inferred from measurements of photosynthesis in leaves of transgenic tobacco. *Planta* 195: 88-97.

Watanabe T, Hanan JS, Room PM, Hasegawa T, Nakagawa H, Takahashi W. 2005. Rice morphogenesis and plant architecture: measurement, specification and the reconstruction of structural development by 3D architectural modelling. *Annals of Botany* 95: 1131-1143.

Wernecke P, Müller J, Dornbusch T, Wernecke A, Diepenbrock W. 2007. The virtual crop-modelling system "VICA" specified for barley. In: Vos J, Marcelis LFM, de Visser PHB, Struik PC and Evers JB, eds. *Functional-Structural Plant Modelling in Crop Production*. Dordrecht, the Netherlands: Springer, 53-64.

Yan H-P, Kang MZ, de Reffye P, Dingkuhn M. 2004. A dynamic, architectural plant model simulating resource-dependent growth. *Annals of Botany* 93: 591-602.

Yin X, Van Oijen M, Schapendonk AHCM. 2004. Extension of a biochemical model for the generalized stoichiometry of electron transport limited C3 photosynthesis. *Plant, Cell and Environment* 27: 1211-1222.

Yin X, Struik PC, Romero P, Harbinson J, Evers JB, van der Putten PEL, Vos J. submitted. Model analysis of combined measurements of gas exchange and chlorophyll fluorescence to quantify variation in photosynthesis parameters of leaves in a wheat (*Triticum aestivum*) canopy.

Modelling N nutrition impact on plant functioning and root architecture in various genotypes of *Arabidopsis thaliana*

Céline Richard-Molard[1], François Brun[1], Anne Laperche[1], Michaël Chelle[1], Loïc Pagès[2] and Bertrand Ney[1]

[1]INRA, AgroParisTech, UMR1091 Environnement et Grandes Cultures, F-78850 Thiverval-Grignon, France.
[2] INRA, UR1115 Plantes et Systèmes Horticoles, Site Agroparc, F-84900 Avignon, France
richardm@grignon.inra.fr

Keywords: assimilate partitioning, root morphogenesis, genetic variability, nitrogen uptake efficiency, whole-plant modelling

Introduction

Breeding new varieties adapted to low-input agricultural practices, mainly for nitrogen and pesticides, is of particular interest when considering economic and environmental concerns. However, screening pertinent traits for crop adaptation to low N supply remains difficult because plant response to N availability is a set of closely interacting processes, and because this response displays a wide genetic and environmental variability. Thus, Loudet et al. (2003) showed that most of the variables involved in N use efficiency exhibit wide variations in response to varying N supplies in a population of *Arabidopsis thaliana* recombinant inbred line (RILs). Therefore, a quantitative modelling of whole-plant C/N functioning should be a suitable tool to identify the key-parameters determining plant efficiency under low or high N nutrition, that will be pertinent for phenotype screening. Such an approach has been successfully employed to identify QTLs (Quilot et al., 2004; Yin et al., 2000) and to simulate phenotypes with allelic composition (Reymond et al., 2004).

A whole-plant structure-function model was developed for that purpose on one genotype (WS) of *A. thaliana*. The model is based on interactions between N and C fluxes and offers an explicit and dynamic description of root system and leaf area growths (Fig. 1). The model was then simplified (root system output was merely considered as biomass) to interpret the behaviour of several RILs of *Arabidopsis* and wheat, and of one *Arabidopsis* mutant impaired on high affinity nitrate uptake.

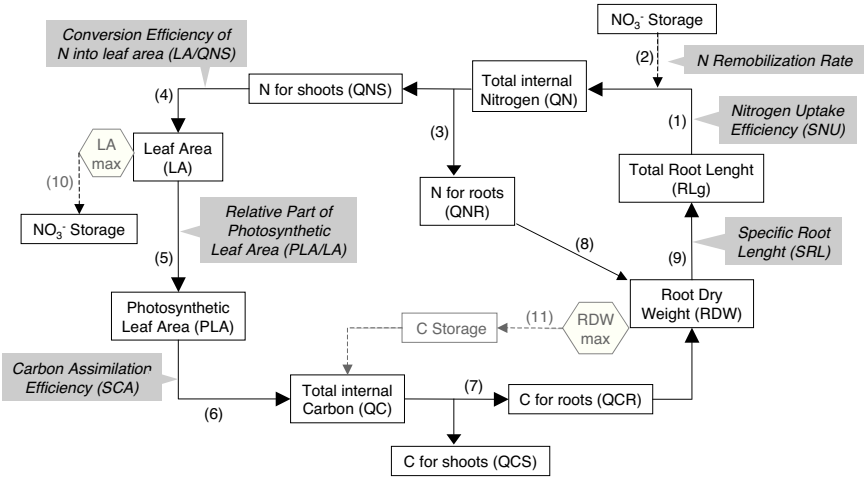

Fig. 1: Schematic diagram of the model. The model was constituted of a shoot and a root compartment, exchanging C and N fluxes. Priority was given to shoots for C and to roots for N. Leaf expansion and root growth were limited by relative maximum growth rates obtained in our culture conditions. Total internal N quantity resulted from root uptake (1) and reserve remobilization (2) and determined the increment of total leaf area (4), after satisfaction of root N demand (3). Total internal C quantity was produced by photosynthetic leaf area (6), obtained from total leaf area using the Beer-Lambert's law (5). Effective root growth resulted from the growth allowed by internal N quantity (8) and by the C quantity remaining after satisfaction of shoot C demand (7). Root dry mass was then partitioned in root length (9). N and C storage pools emerged (10, 11) when N and C internal quantities were not fully depleted by growth.

Root architecture modelling for *Arabidopsis thaliana*

One of the aims of this work was to estimate to what extent the impact of an homogeneous N limiting nutrition on root architecture can be explained the decrease of endogenous carbon availability arising from leaf area reduction in response to low N supply. To answer this question, *A. thaliana* plants (WS) were grown in rhizotrons (Devienne-Barret et al., 2006) in growth chamber with two levels of N supply (2 and 10 mM NO_3^-) and a combination of CO_2 or radiation levels (3 treatments). Root architecture was recorded daily and plants were harvested four times between 10 and 29 days after sowing to measure shoot and root dry weights and N metabolite contents.

A model was implemented in Python language, on the same basis and rules as other object-oriented models for root system architecture (Thaler and Pagès 1998, Drouet and Pagès 2003) and was designed to account for the effect of C availability on root system architecture. The model compares supply and demand for C within the root system described as a network of roots. The C supply was defined here from the flux of accumulated root dry weight. It was calculated from data as an input variable and corresponded to the flux of C provided by shoots (arrow (7) in Fig. 1). Thus, the effect of N supply was taken into account only through the modulation of this shoot-originating C flux, in accordance with our working hypothesis. Indeed, the quantity of nitrogen taken up by the roots was shown to be related to leaf area through a linear relationship (arrow (4) in Fig. 1). The "C demand" was calculated for each root according to its diameter (Farrar 1993) and summed for the whole root system. C availability was defined as the C Supply/Demand ratio and was used as a "satisfaction" coefficient of the demand. When C supply matched or exceeded C demand (*i.e.* C availability ≥ 1), effective elongation of each apex reached the potential elongation rate, calculated for each apex from its current diameter *via* a close relationship found between both variables. When C supply was lower than C demand (*i.e.* C availability < 1), effective elongation was reduced, from the potential elongation rate, proportionally to the satisfaction coefficient. Apex size was also driven by C availability, the relative variation rate of apex diameter varying linearly with C availability, between a minimum (reached when C availability was null) and a maximum (reached when C availability was superior or equal to 1).

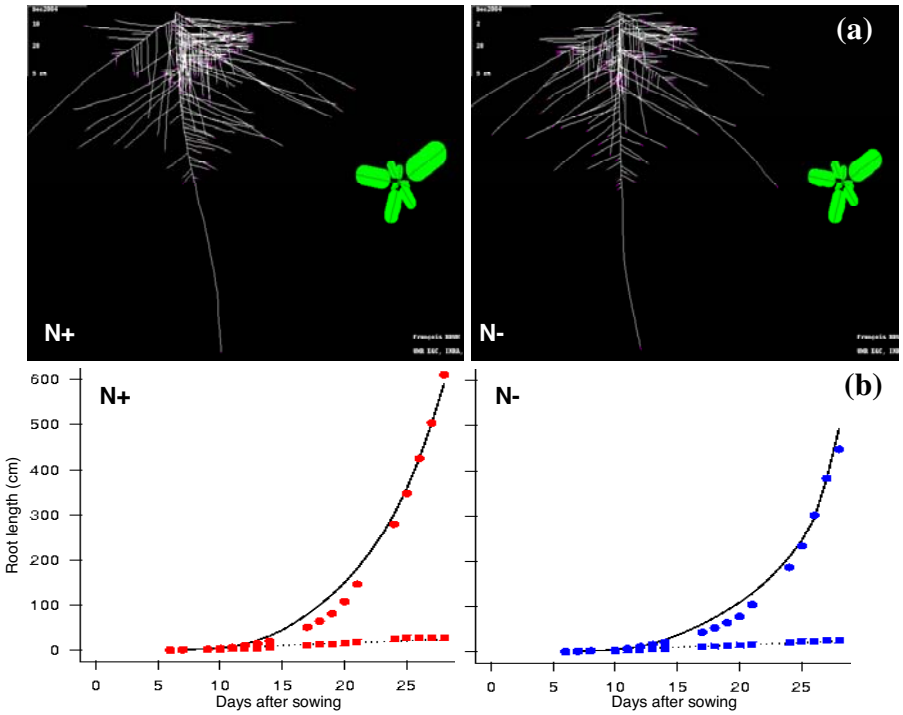

Fig. 2: Simulations of *Arabidopsis thaliana* root morphogenesis during vegetative growth under two levels of N nutrition. Plants (ecotype WS) were grown on soil with plethoric (left panel) or limited (right panel) N supply. (a) Graphical outputs generated by the model showing shoot and root architecture at 29 days after sowing. (b) Dynamics of root length during vegetative growth, measured (points) or simulated (lines) for taproot (squares, solid line) and for the whole root system (circles, dotted line).

Parameters were estimated under the high C x high N treatment and then the model was used with the same parameterization for the other CxN datasets. Only 12 model parameters were needed to simulated contrasted responses of root system architecture under our various C conditions when N supply was not limiting. Root length (Fig. 2) was well predicted as well as root branching, and root emergence in a lesser extent. Time of emergence of lateral root showed the expected distribution. Even if our model was not able to simulate local effect of nitrogen availability and presented limited conditions of validity, our modelling approach showed that major effect of global N availability on root system architecture was mediated by modifications of C fluxes. However, these modifications were not sufficient to fully predict root apical diameter or specific root length when N supply was low. A specific effect of N on root elongation had to be introduced to improved simulation in low N supply, and explained a part of root system adaptation to N limitation. C x N levels did not affect the other parameters. In particular, branching parameters were not affected even if branching adaptation was observed in our culture conditions.

Toward a more functional model dedicated to genotype analysis and QTL detection

High-throughput phenotype analysis using simulation tools require the use of models with few and easily measurable parameters. With the aim to identify the key parameters determining genetic and environmental variability of plant response to N availability, we present a simple compartmental model of C and N absorption and partitioning for *A. thaliana* during the vegetative growth simplified from the above-presented one (Fig. 1). This model combines integrative variables (biomasses, N or nitrate accumulated), exchange surfaces for shoots (*i.e.* leaf area) but not for roots (in contrast with the above-model), and efficiencies (grey areas in Fig. 1) such as carbon assimilation efficiency, N uptake efficiency or N remobilization rate.

As the first step, the model was used to quantitatively interpret the behaviour of five contrasted genotypes of *A. thaliana* grown in soil (rhizotrons) with 3 levels of nitrate supply. Parameters were estimated on one genotype and one N level and then they were checked under the other genotype x nutrition conditions (Fig. 3). We found that nitrogen uptake efficiency (*snu*) and carbon assimilation efficiency (*sca*) were the key variables explaining the responses of the five genotypes to nitrogen nutrition under steady state conditions.

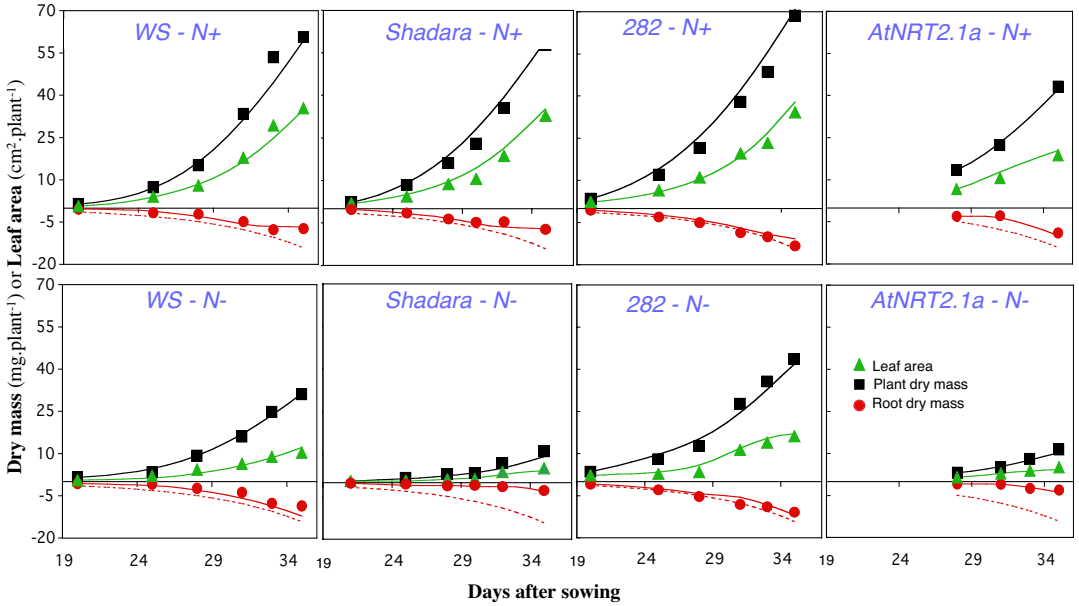

Fig. 3: Dynamics of leaf area (triangles), root dry mass (circles) and whole plant dry mass (squares) during vegetative growth in plethoric (upper part) or limited (lower part) N conditions for four genotypes of *A. thaliana.* Solid lines correspond to the simulations performed by the model. Values of root biomass were mirrored to increase legibility.

In the second step, the model was tested using the *atnrt2.1a* mutant. Due to the mutation of *AtNRT2.1* and *AtNRT2.2* genes, this mutant is impaired in high affinity nitrate uptake (Filleur et al. 2003). The model simulated satisfyingly the behaviour of the mutant (Fig. 3). This allowed us to validate the determining role of nitrogen uptake efficiency in plant response to N supply and to point out the main role of the *AtNRT2.1* gene in plant response efficiency to N limited nutrition.

In the last step, the model was used on a population of 120 doubled haploid lines of wheat, to characterize the genotypic variability of each parameter and to investigate QTLs involved in plant tolerance to a N deficiency. The lines were obtained from a cross between a N stress tolerant variety and a N stress sensitive one and were grown hydroponically under N limited conditions. We found that, as for *Arabidopsis*, the main source of variation relied on *snu*, indicating that this parameter was the major determinant of the variability of plant response to N supply. In addition, eight QTLs related to model parameters were detected in wheat.

Conclusion

An *Arabidopsis* FSPM was built to study plant response to steady-state N nutrition with a focus to root system architecture. It was used as a reference to develop a simpler model, more suited to high-throughput analysis, which highlighted the determinant role of nitrogen uptake efficiency in plant response to N supply. The next step will be to study and model variations of nitrogen use efficiency within the root system, especially in case of heterogeneous N supply.

References

Devienne-Barrret F., Richard-Molard C., Chelle M., Maury O., Ney B. 2006. Ara-Rhizotron: An effective culture system to study simultaneously root and shoot development of Arabidopsis. Plant Soil 280, 1/2, 253-266.

Drouet J.L., Pagès, L. 2003. GRAAL: a model of growth, architecture and carbon allocation during the vegetative phase of the whole maize plant - model description and parameterisation. Ecol. Modell. 165(2-3), 147–173.

Farrar, J. F. 1993. Sink strength: What is it and how do we measure it? Plant, Cell and Environ. 16(9), 1015–1016.

Filleur S, Dorbe MF, Cerezo M, Orsel M, Granier F, Gojon A and Daniel-Vedele F. 2001. An Arabidopsis T-DNA mutant affected in Nrt2 genes is impaired in nitrate uptake. FEBS Letters 489, 220-224.

Loudet O, Chaillou S, Merigout P, Talbotec J and Daniel-Vedele F. 2003. Quantitative trait loci analysis of nitrogen use efficiency in Arabidopsis. Plant Physiol. 131, 345-358.

Quillot B., Génard M., Kervella J., Lescourret F. 2004. Analysis of genotypic variation in fruit flesh total sugar content via an ecophysiological model applied to peach. Theor. Appl. Genet 109, 440-449.

Reymond M, Muller B, Tardieu F. 2004. Dealing with the genotype x environment interaction via a modelling approach : a comparison of QTLs of maize leaf length or width with QTLs of model parameters. J. Exp. Bot. 55, 2461-72.

Thaler P., Pagès L. 1998. Modelling the influence of assimilate availability on root growth and architecture. Plant Soil 201(2), 307–320.

Yin X, Chasalow S.D., Dourleijin C.J., Stam P., Kropff M.J. 2000. Coupling estimated effects of QTLs for physiological traits to a crop growth model: predicting yield variation among recombinant inbred lines in barley. Heredity 85 :539-549.

A model of nitrogen distribution and senescence in virtual wheat

Jessica Bertheloot[1], Bruno Andrieu[1], Christian Fournier[1], Pierre Martre[2]
[1] *INRA, UMR1091 Environnement et Grandes Cultures, AgroParisTech, F-78850 Thiverval – Grignon*
[2] *INRA, UR874 Agronomie, F-63100 Clermont-Ferrand*

Keywords: Nitrogen, light, senescence, lamina, grain, wheat, modelling.

Introduction

Modelling nitrogen dynamics is essential to model plant productivity. Indeed, foliar nitrogen is a major compound of the photosynthetic apparatus and is remobilized from the senescent leaves during grain filling. This remobilisation results in a decrease of leaf photosynthetic activity and finally leaf death (Masclaux, et al., 2001). It is a general observation that within a canopy, leaf nitrogen distributions are related to light gradients and that the most shaded leaves are also the first ones to die (*e.g.*, Ono et al., 2001). It results from nitrogen remobilisation from the oldest leaves to the new emerging ones. As a consequence, maximum photosynthetic capacity is found in the most lit leaves, as if the plant would adjust its nitrogen distribution for maximizing carbon gain. Authors used this optimization theory to model nitrogen distribution as function of light level (Hirose and Werger, 1987) and extended it to include prediction of leaf life span (Hikosaka, 2005). However, this idea was criticized since it is difficult to conceive that an optimization process can be a leading force in a plant. Chen et al. (1993) proposed a coordination theory to predict nitrogen distribution between leaves as the equilibrium between two rates limiting the photosynthetic processes, the rate of Rubisco carboxylation and the rate of electron transport. None of these two theories allowed closed simulation of the dynamics of vertical nitrogen distribution observed in the field. Moreover, these models are difficult to apply during the reproductive stage, where non leaf organs, such as stems and ears, represent a large fraction of plant nitrogen. Some models attempt to simulate nitrogen distribution based on a more explicit description of the processes (*e.g.*, Tabourel-Tayot and Gastal, 1998a,b; Thornley 1998, 2004). However, the processes in such models are significantly simplified, and need further evaluations against experimental data (Kull, 2002). Moreover, these models do not address the reproductive stage.

Here we present a simple "mechanistic" model aiming at predicting nitrogen and senescence distributions between leaves in a wheat shoot (*Triticum aestivum* L.) after flowering. The objective was to evaluate whether a simple mechanistic model could account for (i) the observed relationship between leaf nitrogen and light distribution within the canopy, and (ii) the acropetal sequence of leaf senescence. This work is based on a theoretical model described by Thornley (1998) for a single leaf. We extended this model to represent a wheat mainstem within a canopy, consisting of a series of leaves, a stem and a growing ear, and also to consider the sequential death of leaf tissues.

Model description and parameterization

The model described below focuses on nitrogen dynamics inside a wheat mainstem during the reproductive stage. In the current version of the model, carbon dynamics are not considered, thus no interaction was supposed to occur between carbon and nitrogen dynamics. Modelling is restricted to the grain filling period, which is after the completion of leaf growth.

The model starts at flowering and runs with a time step of 1 °Cday, with a base temperature of 0°C. Since the main objective is to predict nitrogen distribution between leaf laminae, individual modules are developed for each of them. Other vegetative organs (i.e., leaf sheaths, internodes, ear chaffs) are not considered individually and are pooled in a single module (termed stem), in order to give an appropriate context to the leaf laminae functioning. The grains are defined as one other module. Three nitrogen forms are considered: photosynthetic nitrogen, mobile nitrogen (representing amino acids and nitrate), and structural nitrogen that does not participate to the fluxes. Each lamina and the stem are characterized by their photosynthetic nitrogen content and their structural nitrogen. Mobile nitrogen is

treated as a common pool shared by all modules. In addition, each lamina is characterized by a quantity of green and dead tissues.

The main processes expressed in the lamina and grain modules are that:

(i) photosynthetic nitrogen is synthesized from the mobile nitrogen pool according to a Michaelis function depending on the concentration of mobile nitrogen, and on the irradiance intercepted by the lamina. This results in a flux of nitrogen from the mobile nitrogen pool to the lamina.

(ii) in green tissues, photosynthetic nitrogen is degraded at a constant rate. This results in a flux of nitrogen from the leaf to the mobile nitrogen pool, proportional to the amount of photosynthetic nitrogen in green tissues.

(iii) an additional degradation flux of photosynthetic nitrogen is induced if the quantity of photosynthetic nitrogen per unit area is lower than a given threshold. This nitrogen fluxes contributes to the mobile nitrogen pool and results in tissue death. The rate of photosynthetic nitrogen degradation is constant in thermal time.

(iv) grains take up nitrogen from the common pool. Potential rate of grain nitrogen accumulation follows an expolinear function, where the initial exponential phase correspond to the endosperm cell division period, and the linear phase correspond to the effective grain-filling period. The duration of each phase is constant in thermal time. At each time step, the actual rate is either equal to the potential rate, if sufficient nitrogen is available in the mobile pool, or is null.

Parameter values defining the photosynthetic apparatus turnover were taken from Thornley (1998). The other ones, specific to our model, were adjusted empirically: these are the threshold nitrogen concentration for tissue death, the maximum flux for the additional photosynthetic nitrogen degradation in dying tissues and the coefficients of the function for potential grain filling. Model was defined and evaluated with an experiment held on the bread wheat cultivar 'Apache' during the 2004-2005 growing season at Clermont-Ferrand, France, in condition of high nitrogen fertilisation. The dataset includes extensive description of the time course of biomass, total nitrogen and surface area of ear chaffs, internodes, leaf laminae (green and senescent parts) and sheaths, and grain biomass and total nitrogen. Irradiance distribution at various depths within the canopy was determined at weekly interval around noon from anthesis to total canopy senescence using a linear ceptometer. We used this dataset to (i) estimate model constants: these are structural biomass and structural nitrogen of each module, the number and the areas of the laminae containing green tissues at flowering and the light gradient, (ii) calculate the time course of forced variables, these are the time course of total shoot nitrogen and of stem nitrogen, and (iii) evaluate model predictions: these are time courses of each lamina nitrogen and tissue death, and of grain nitrogen.

The present version of the model is implemented in ModelMaker version 4.0 (Cherwell Scientific, UK), and it is currently being translated into L+C language (Karwowski and Prusinkiewicz, 2003), which will allow us to study the responses to changing plant density or architecture.

Results

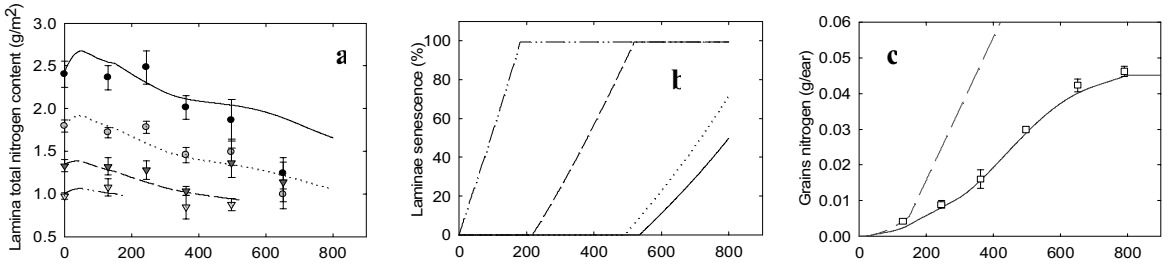

Fig 1. Time course of (a) lamina nitrogen content per unit area; (b) lamina senescence (% of tissue death); (c) Simulated potential (dashed line) and actual (solid line) grain nitrogen per ear, during the grain filling period for the bread wheat cultivar 'Apache' grown in the field under non-limiting nitrogen supply. Laminae 1 to 4 are represented respectively by solid, dash, long dash, and dotted lines (simulated) and by black circles, grey circles, black triangles, grey triangles (observed). Observed data are means $\pm$ 1 s.e. for $n = 3$.

At flowering, the fifth lamina (counted from the top of the canopy) was completely dead, thus four laminae were considered in the model. Simulation results showed that model behaviour was consistent with trends reported in the literature. In accordance with experimental data, simulated lamina nitrogen content decreased during the post-flowering period (Fig. 1a), due to nitrogen uptake by the grains, but the differences between leaves remains fairly stable. The model did reproduce the quasi linear relationship observed between the irradiance intercepted by the laminae and their area-based nitrogen content (not shown). The acropetal sequence of laminae senescence was also reasonably well simulated (Fig. 1b). However, in the simulation, the two upper leaves started senescing almost synchronously, and were not fully senesced at maturity when grain filling was completed. Insufficient experimental data were available to allow comparisons with simulations, but the simulated behaviour is reported to occur in some conditions, depending on cultivar and nitrogen fertilisation. Finally, the model predicted accurately the time course of grain filling (Fig. 1c). This, and the large difference between potential and actual grain filling, are strong indications that the time course of mobile nitrogen was also correctly simulated.

Discussion and conclusion

We have shown that a model based on some key nitrogen dynamics processes and with a restricted number of parameters (eight in the current version) is able to describe the main trends found in the literature in terms of nitrogen distribution among leaf laminae, leaf life span, and grain nitrogen accumulation. A virtue of the approach is that it does not rely on a predicted global behaviour, such as optimisation of canopy carbon assimilation, but rather show that this can be seen as an emerging property of simple local rules. This gives inherent plasticity and should make the model to cope with important perturbations, such as when new sinks of nitrogen are created by insects or diseases.

Several approximations were made in order to avoid the difficulties related to parameter estimations. The high nitrogen mobility and the existence of nitrogen exchange between phloem and xylem led us to approximate that all organs were connected to a single pool of mobile nitrogen. This avoids the problem of estimating resistance of the nitrogen transfer pathways between individual laminae and the common mobile nitrogen pool. Another main simplification deals with the restricted number of nitrogen forms. Only the most relevant ones in the process studied (here photosynthetic apparatus turnover) were taken into account.

The simple model presented here reproduces the behaviour of the shoot compartments reasonably well when shoot nitrogen absorption is forced to experimental data. The next step will be to include a feedback control on post-flowering absorption, involving nitrogen availability in the soil, the concentration in the mobile nitrogen pool and leaf photosynthesis. This will allow investigating responses in a wider range of experimental conditions. Inclusion of a photosynthesis model will allow to analysis carbon – nitrogen interactions.

References

Chen JL, Reynolds JF, Harley PC, Tenhunen JD. 1993. Coordination theory of leaf nitrogen distribution in a canopy. *Oecologia* 93: 63-69.

Hikosaka K. 2005. Leaf canopy as a dynamic system: ecophysiology and optimality in leaf turnover. *Annals of Botany* 95: 521-533.

Hirose T, Werger MJA. 1987. Maximising daily canopy photosynthesis with respect the leaf nitrogen allocation pattern in the canopy. *Oecologia*: 145-150.

Karwowski R, Prusinkiewicz P. 2003. Design and implementation of the L+C modeling language. Electronic Notes in Theoretical Computer Science 86: 1-19.

Kull O. 2002. Acclimation of photosynthesis in canopies: models and limitations. *Oecologia*: 267-279.

Ono K, Nishi Y, Watanabe A, Terashima I. 2001. Possible mechanisms of adaptive leaf senescence. *Plant Biology* 3: 234-243.

Masclaux C, Quillere I, Gallais A, Hirel B. 2001. The challenge of remobilisation in plant nitrogen economy. A survey of physio-agronomic and molecular approaches. Annals of Applied Biology 138: 69-81.

Tabourel-Tayot F, Gastal F. 1998a. MecaNiCAL, a supply-demand model of carbon and nitrogen partitioning applied to defoliated grass 1. Model description and analysis. *European Journal of Agronomy* 9: 223-241.

Tabourel-Tayot F, Gastal F. 1998b. MecaNiCAL, a supply-demand model of carbon and nitrogen partitioning applied to defoliated grass. 2. Parameter estimation and model evaluation. *Eur. J. of Agron.* 9: 243-258.

Thornley JHM. 1998. Dynamic model of leaf photosynthesis with acclimation to light and nitrogen. *Annals of Botany* 81: 421-430.

Thornley JHM. 2004. Acclimation of photosynthesis to light and canopy nitrogen distribution: an interpretation. *Annals of Botany* 93: 473-475.

A preliminary field evaluation of an automated vision-based plant geometry measurement system

Cheryl McCarthy, Nigel Hancock and Steven Raine
National Centre for Engineering in Agriculture and Cooperative Research Centre for Irrigation Futures, Faculty of Engineering and Surveying, University of Southern Queensland
Toowoomba, Queensland, Australia 4350
{mccarthc, hancockn, raine}@usq.edu.au

Keywords: internode length, data collection, image processing

Introduction

Machine vision is commonly reported for use in automated plant-based applications such as growth monitoring, stress detection, species identification and fruit harvesting. Geometric measurement of living plants using machine vision commonly requires depth perception, which typically entails establishing correspondence between multiple images. The complexity of such a task in an unstructured environment, such as foliage, often restricts automation of the process.

Automated measurement of the geometry of young plants has been reported using laser range finding and image processing (Kaminuma et al. 2004) or multiple camera views (Lin et al. 2001). Noordam et al. (2005) compared automated methods of locating the main stem of a rose plant using methods including stereo imaging, structured lighting and X-ray imaging, while Ivanov et al. (1995) reported using stereovision and a manually-operated 2D digitiser to model a maize canopy. However an automated vision system for measuring geometry of complex plants in the field is yet to be reported.

Plant geometry is a significant factor for irrigation purposes in cotton because the distance between main stem nodes indicates water stress in a growing cotton plant. However, manual measurement of internode length is a tedious task for even a small number of plants. An automated method for large scale measurement of plant geometry in the field would provide information about crop irrigation requirement as well as spatial and temporal variability in crop stress and growth.

This research aims to develop a real-time and automatic machine vision sensor for measuring structural parameters such as internode length for plants in a growing cotton crop.

Field measurement apparatus

A camera enclosure which continuously traverses the crop canopy was designed and constructed for field measurement of plant geometric parameters (Fig. 1a). A camcorder mounted within the enclosure was positioned such that the camera's image capture area corresponded to a transparent panel at the front of the enclosure. The camera enclosure makes use of the flexible upper main stem of the growing cotton plants to firstly contact the plant against the transparent panel, and then smoothly and non-destructively guide the plant under the curved bottom surface of the enclosure. When the plant's main stem contacts the transparent panel, the transparent panel becomes a fixed object plane from which reliable 2D geometric data can be derived. Fig. 1b contains a stylised sample image captured from the enclosure.

In the field the camera enclosure was suspended from a gantry above the cotton rows. Two different prototypes of camera enclosure conveyance gantry were used, featuring manual and automatic conveyance of the camera enclosure.

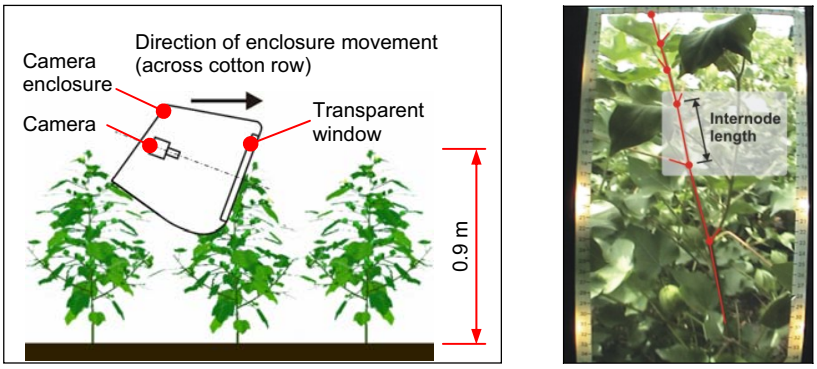

Fig. 1. (a) Image capture apparatus; and (b) stylised sample image from camera enclosure.

Collected datasets

Video sequences of cotton plants were collected throughout the 2005/2006 and 2006/2007 cotton growing seasons. Each video sequence consisted of a single pass of the camera enclosure over a target plant. In fifteen data collection sessions the following parameters were varied:

- time of day, i.e. morning, afternoon and night;
- cotton variety (six in total);
- plant growth stage;
- illumination scheme on camera enclosure (artificial or natural light);
- capture of near infrared/visible light images by use of narrowband optical filters and illumination;
- narrow or wide depth of field about the camera enclosure's transparent window;
- camera enclosure approach angle and orientation and movement down and across rows;
- speed of camera enclosure movement through crop canopy.

Each data collection session featured typically 13 to 16 plants. Manual measurements of plant height as well as internode distance and stem diameter were recorded for the top five nodes of each plant targeted by the vision system. Plant topological features significant for cotton growth and development (e.g. nodal positions of flowers and fruiting structures) were also measured.

Image processing

The initial image processing algorithm development focused on automated measurement of internode length. The internode length measurement algorithm featured two steps. In the first step, candidate nodes were identified from single frames, then in the second step, falsely identified nodes were eliminated by analysis of node trajectories throughout a sequence of frames. The basis for the two-step algorithm was that true nodes could be tracked throughout a video sequence whereas false positive nodes, which were transient in nature, could not be tracked. Typical results for candidate node identification are shown in Fig. 2. The image processing results yielded a correlation coefficient of 0.92 for fourteen measurements of internode length. Analysis of computational requirements indicates that the image processing algorithm could be executed in real-time.

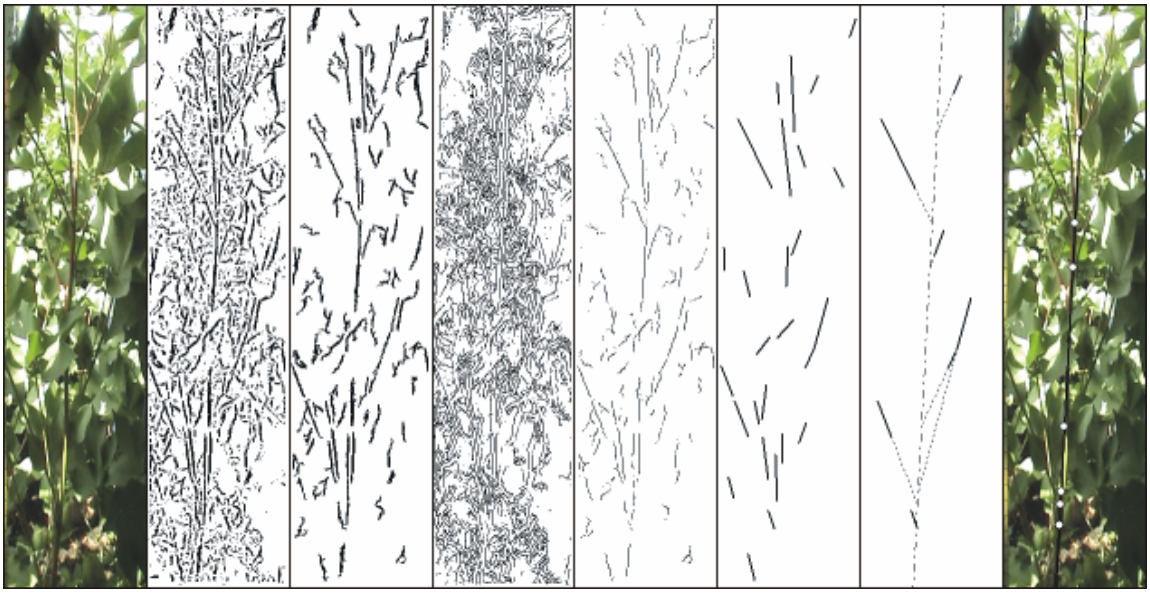

(a) (b) (c) (d) (e) (f) (g) (h)

Fig. 2. Automated image processing steps for single frame analysis: (a) region of interest in sample image; (b) likely line pixels; (c) likely branch pixels; (d) line centre points; (e) branch centre points; (f) lines fitted to *e*; (g) likely branches projected to main stem; and (h) identified candidate nodes represented by white discs.

Conclusions

The feasibility for real-time, automated measurement of cotton plant geometric parameters has been demonstrated. Extensive video footage datasets have been collected to enable evaluation of image processing algorithms under a variety of environmental conditions.

Acknowledgments

The authors are grateful to the Queensland cotton farms 'Macquarie Downs' and 'Adelong' for providing field trial sites and to our colleague Simon White for assistance in collecting field data. The senior author is grateful to the Australian Research Council and to the Cooperative Research Centre for Irrigation Futures <irrigationfutures.org.au> for funding support.

References

Ivanov, N., Boissard, P., Chapron, M. and Andrieu, B. 1995. Computer stereo plotting for 3-D reconstruction of a maize canopy. Agricultural and Forest Meteorology, vol. 75, pp. 85-102.

Kaminuma, E., Heida, N., Tsumoto, Y., Yamamoto, N., Goto, N., Okamoto, N., Konagaya, A., Matsui, M. and Toyoda, T. 2004. Automatic quantification of morphological traits via three-dimensional measurement of *Arabidopsis*. The Plant Journal, vol. 38, pp. 358-365.

Lin, T.T., Liao, W.C. and Chien, C.F. 2001. 3D graphical modeling of vegetable seedlings based on a stereo machine vision system. ASAE Meeting Paper No. 01-3137, Sacramento, California, ASAE.

Noordam, J.C., Hemming, J., van Heerde, C., Golbach, F., van Soest, R. and Wekking, E. 2005. Automated rose cutting in greenhouses with 3D vision and robotics: analysis of 3D vision techniques for stem detection. Acta Horticulturae, vol. 691, pp. 885-892.

Structural Tree Modelling of Aboveground and Belowground Poplar Tree using Direct and Indirect Measurements: Terrestrial Laser Scanning, WGROGRA, AMAPmod and JRC-3D Reconstructor ®.

Teobaldelli M.[1], Zenone T.[1-3], Puig D.[2], Matteucci M.[1], Seufert G.[1], Sequeira V.[2]

1. European Commission – DG Joint Research Centre, Institute for Environment and Sustainability, Climate Change Unit; corresponding author: maurizio.teobaldelli@jrc.it
2. European Commission – DG Joint Research Centre, Institute for the Protection and Security of the Citizen, Nuclear Safeguards Unit;
3. Department of Forest Environment and Resource University of Tuscia, Viterbo, Italy

Keywords:
Forest inventories, *Populus x canadensis*, tree architecture, root architecture, Zoller +Fröhlich LARA 53500

Introduction

The IES-Action GHG-AFOLU aimed to quantifying the effect of land use changes on the overall cycles of greenhouse gases. A major uncertainty for budget estimates is related to the amount of biomass accumulated in above and belowground parts of the forests. In order to made a reliable estimate of these factors it is necessary an enormous amount of manual labour for forest inventories and destructive measurements.
In this context, laser scanning seem to be promising and fast method for forest inventories (Holopainen and Kalliovirta, 2006). According to Thies and Spiecker (2004), terrestrial laser scanning system is not yet ready for practical forestry use. Even though, the advances in terrestrial laser-scanning of trees during the last few years resulted in a variety of tree structure reconstructions that are based on the evaluation of three-dimensional clouds of points (Fleck et al. 2004; Pfeifer and Winterhalder, 2004; Gärtner and Denier, 2006; Bucksch and Appel van Wageningen, 2006). Moreover cloud point images could be used to create geometric models simulating the three-dimensional architecture of a tree, useful for example to characterize interception of light by dense or sparse canopies or to model the competition for nutrient and water efficiency of root systems (Danjon et al. 1999).

The objectives of this research were:
- To investigate the suitability of advanced technologies like 3D-Laser scanning to acquire fair and sound information's on structural and architectural characteristics of poplar stand;
- To compare direct and indirect measurement;
- To validate geometric models of above- and belowground tree structures using the software's WGROGRA (Kurth, 1994), AMAPmod v.1.8 (Godin and Guédon, 2001) and JRC-3D-Reconstructor ® (patented by JRC, IPSC, Nuclear Safeguards Unit).

Material and method

The study area was an intensive poplar plantation located about 10 km north-west of the city of Pavia within the "Parco Regionale del Ticino", Italy.
The poplar site is part of the CarboEurope network with the flux tower situated in the middle of a 120 ha even-aged plantation (*Populus x canadensis* clone I-214); the turnover times of the poplar stand was 14 years. On March 2005, the diameter at breast eight (DBH) of around 200 trees were measured in a one ha rectangular plot, characterizing the Eddy covariance fetch.
The vertical and horizontal stand structure was measured in a smaller circular plot (2000 m^2) near the tower.
Overall, 3 representative trees were selected on the base of their DBH and crown morphology.
The indirect measurement of the stand was made in April 2005 using a spot Zoller +Fröhlich GmbH Laser Measurement System LARA 53500 (Fröhlich and Mettenleiter, 2004); scans were

made in the super high mode (time of acquisition 15 min/scan) with a linearity error less than 5 mm.
We selected three 14's years old poplar trees and measurements of above- and belowground tree structures were carried out.
- *Aboveground measurements*: reference points (square targets) were positioned before the measurements in the scene and scans were made in four different points around each tree.
- *Belowground measurements*: Each root system, completely excavated using an Air-spade ®-2000, was scanned from ten different points of view.
The direct measurement of the selected trees was made on June 2005; trees were felled and measured (main architectural characteristics of stem and branches). Root systems were dried and weighted and volume was determined by multiplying those values with wood density.
3-D tree modeling: Filtering and registration of terrestrial laser scanning were made using the software JRC-3D Reconstructor ® and a 3-D information system was created for the above- and belowground structures (fig.1a). Unfortunately, due to hardware limitations, the laser scans were processed with a reduced resolution (sub-sampling) that inevitably influenced the level of detail.
Geometric modeling's of above- and belowground structures (fig.2b) were created using the software's WGROGRA and AMAPmod; to test the goodness of our geometric models they were compared with the laser scans using the inspection tool, provided by the software JRC-3D Reconstructor ®.

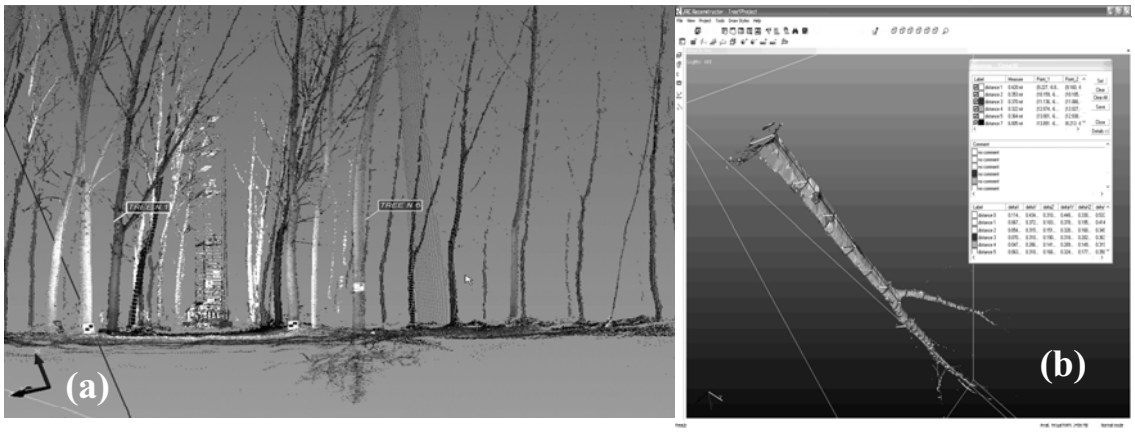

Fig. 1: Three-dimensional information system of aboveground and belowground structures (a) and analysis of stem and branches of a poplar tree (b)

Results

Considering the characteristics of the stand (plantation), the indirect measurement of aboveground structure was particularly simple and fast (half day, 12 scans) and there weren't problems due to the occlusion of laser beam from understory or dominated trees. The registration of the scans was accurate thanks to the square targets positioned in the scene before the measurements and to the possibility to translate and rotate manually each scan in a 3-D virtual space, using the software JRC-3D Reconstructor ®. Moreover the software tools permitted to extract geometric features of selected plants (topology) and to slice and export (*.dxf) the aboveground and belowground sections of the poplar trees. A good fitting ($r^2 \cong 0.8$) was found between direct and indirect measurements of stem sections. Indirect measurements of branches were less significant ($r^2 \cong 0.6$) because of (1) the scans sub-sampling, (2) the smaller diameter of the objects and (3) the distance of these from laser beam source.

The root systems (fig.1a, fig.2a) occupied a volume of soil ranging between 15 to 27 m^3; they were characterized by a central conical taproot and by several lateral branches. First-order plagiotropic branches (Intersection angles $\geq 70°$) are in the upper and middle parts of the taproot whilst geotropic (Intersection angles $\leq 30°$) are in the lower part. The taproot length

ranged between 1.3 to 1.5 m; probably, taproot length is related more to the 2-year-old unbranched seedlings, used during the plantation of the stand, than to the soil matrix.

WGROGRA and AMAPmod were used to create geometric models of selected trees, based on the structural information's collected during the direct and indirect measurements. In order to test the goodness of our geometric models, they were imported in the 3-D information system and a comparison was made with the cloud of point images using the inspection tool provided by the software JRC-3D Reconstructor ®.
The software reported an error of about 10 cm for the stem and from 10 to 40 cm for the branches. The information's were used in an iterative process to modify and ameliorate our geometric models.

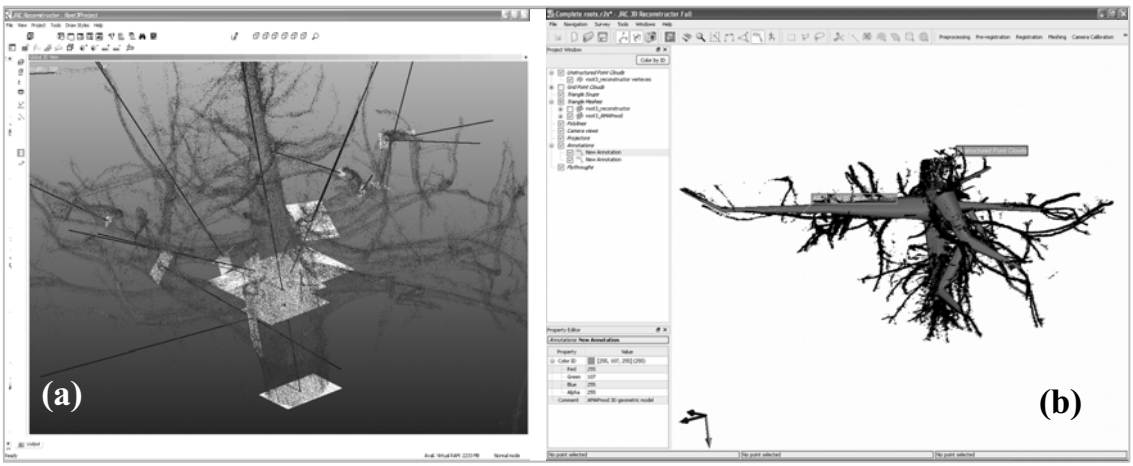

Fig. 2: (a)Topology of poplar root system extracted from point cloud image and (b) verification of a preliminary AMAPmod model (*.MTG) using a laser scan image and the JRC-3D Reconstructor®

Conclusion

We gathered high-resolution land cover information's of our test site using a terrestrial laser scan. The method was able to acquire fair and sound information's on structural and architectural characteristics of poplar trees. In fact, the three-dimensional information system of the poplar stand, created using the JRC-3D Reconstructor® software, has permitted to measure, from point cloud images, morphology of stems and branches, stand basal area, height of trees and to map topology of aboveground and belowground structures with an acceptable level of accuracy. Moreover it represented a source of information's that was used in combination with other software's (WGROGRA, AMAPmod) to validate geometric models of trees.
Although, the use of terrestrial laser scanning could be difficult in those stands, characterized by a complex horizontal and vertical structure, we believe that the use of this method on tree modelling activities or to detect forest volume and stand structure on large area at one time or in different decade should be more investigated.

Acknowledgements

This research was partly funded by the CarboEurope IP project (EU-Contract No. GOCE-CT-2003-505572) and by the JRC-IES-CCU-Action 24002 - Greenhouse Gases in Agriculture, Forestry and Other Land Uses - GHG-AFOLU. We would thank Marlene Dürr and the other colleagues of the Climate Change Units that helped us during the direct measurement. Beside we thank Frederic Danjon (INRA, France) and William Kurth (Brandenburgische Technische Universitat Cottbus; Germany) for suggest and help during the creation of routines respectively for the AMAPmod and WGROGRA software's.

References

Bucksch A., Appel van Wageningen H. 2006. Skeletonization and segmentation of point clouds using octrees and graph theory. In Proceedings of Commission V Symposium, Image Engineering and Vision Metrology. Dresden, Germany.

Danjon F., Sinoquet H., Godin C., Colin F., M. Drexhage M. 1999. Characterisation of structural tree root architecture using 3D digitizing and AMAPmod software. Plant and Soil 211: 241–258, 1999.

Fleck S., van der Zande D., Schmidt M., Coppin P. 2004. Reconstruction of Tree Structure from Laser-Scans and Their Use to Predict Physiological Properties and Processes in Canopies. In proceedings of the ISPRS, Session 4: Algorithm Development and Processing Methods for Analysis of Forests and Landscapes. Freiburg, Germany.

Fröhlich C., Mettenleiter M. 2004. Terrestrial Laser-Scanning - New Perspectives in 3D-Surveying. In proceedings of the ISPRS, Session 1: Techniques for Terrestrial and Airborne Laser-Scanning. Freiburg, Germany

Gärtner H., Denier C. 2006. Application of 3D laser scanning device to acquire the structure of whole root systems. A pilot study. In Heinrich I, Gärtner H, Monbaron M, Schleser G (eds) - TRACE – Tree Rings in Archaeology, Climatology and Ecology, Vol. 4, 288-294

Godin C., Guédon Y. 2001. AMAPmod, Introduction and Reference Manual version 1.8. CIRAD/INRA – UMR Melisation des Plantes, Eds. Marie-Hélène Lafond.

Holopainen M., Kalliovirta J. 2006. Modern data acquisition for forest inventories. In Kangas A. and Maltamo M. (eds.), Forest Inventory – Methodology and Applications, 343-362. ©, Springer. Printed in Netherlands

Kurth W. 1994. Growth Grammar Interpreter GROGRA 2.4. Berichte des Forschungszentrums Waldökosysteme Göttingen, Ser. B, Vol.38.

Pfeifer N., Winterhalder D. 2004. Modelling of tree cross sections from terrestrial laser scanning data with free-form curves. In proceedings of the ISPRS, Session 3: Processing Methods for Applied Analysis of Laser-Scanner Data. Freiburg, Germany

Thies M., Spiecker H. 2004. Evaluation and future prospects of terrestrial laser scanning for standardized forest inventory. In proceedings of the ISPRS Working group VIII/2. Laser-scanners for forest and landscape Assestment. Freiburg, Germany.

Use of Ground-Penetrating Radar (GPR) and Electrical Resistivity Tomography (ERT) to study tree roots volume in pine forest and poplar plantation

G.F. Morelli[1], T. Zenone[2-3], M. Teobaldelli[2], F. Fischanger[1], M. Matteucci[2] and G. Seufert

[1]Geostudi Astier. Livorno (Italy)
[2]European Commission. DG Joint Research Centre Institute for Environment and Sustainability
Climate Change Unit. Ispra (VA) Italy
[3]Department of Forest Environment and Resource University of Tuscia Viterbo.

Corresponding authors:
Gianfranco Morelli Phone +39 0586 864734 E-mail: gianfranco_morelli@fastwebnet.it

1. Introduction

The evaluation of tree root biomass is significant and difficult to survey accurately. Traditional approach used for roots biomass harvest (e.g., soil cores and trenches) provide reasonable accurate information but they are destructive in nature, labour intensive, and limited whit respect to soil volume and surface area that can be assessed. Data derived from traditional root extraction approaches are also generally limited to root biomass averages across plots or treatments rather than information on root distribution. Sampling needed to detect difference among treatments can be expensive as well as time consuming for technical personal. For the above reason test and develop new indirect tools for roots biomass survey appears of leading importance.

2. Objectives

In this study we have assessed the possibility to use Ground Penetrating Radar (GPR) and Electrical Resistivity Tomography (ERT) as a root volume indirect survey investigation.
Although previous studies have demonstrated the potentiality of these methodology to detect root systems (J. R Butnor et al 2001 J. Hruska et al 1999 L. Wielopolski, et al 2000) up to now few research (Stokes et al. 2002) has tried to compare the GPR and ERT response with direct observations of the entire root system.

3. Material and methods

3.1 Experimental site

Two experimental sites have been investigated in this study: a poplar plantation located in Zerbolo' (Pavia Italy) (45°12'03" N; 9°03'40" E) and a pinewood forest within the Regional park of San Rossore (Pisa Italy) (43°43'40" N; 10°17'04" E)
Both sites are part of the CarboEurope network, equipped with a eddy covariance flux tower.The poplar stand (*Populus* x *euramericana* clones I-214, spacing 6 x 6 m, density 270 plants ha^{-1}) was planted in a plain area of 120 ha, inside the Basin of Ticino River, characterized by alluvial soil (mostly clay, stone and lime). It was clearcutted in april 2005.
On the other hand, the pinewood forest (Pinus *pinaster,* Pinus *pinea,* Quercus *ilex*), is growing in a strip plantation, at 800 m distant from seashore. The area, characterized by the

presence of old coastal dunes with an elevation less than 4 m, is mostly formed by sand and slime. After a preliminary investigation of horizontal and vertical structures of the sites (basal area at breast height, n. of trees, total height), three trees were selected, in each stand, on the basis of their diameter at breast eight (DBH) for geophysical investigations.

3.2 *Ground penetrating radar*

The Ground penetrating radar (GPR) is an ultra-wideband imaging technique widely used for subsurface exploration and monitoring, in civil engineering, archaeology and forensic examinations, pipeline, cavity and tunnel detection. GPR is non-invasive, performed with hand-held portable units, and has the highest resolution of any subsurface imaging method. In this case we propose to perform a 3D GPR survey, where the density of survey lines is increased by acquiring data in different directions, resulting in 3D maps that can detect roots or other features regardless of their direction. The unsaturated sand and silt layers that characterize the top soil allow good radar penetration, even at the high frequencies needed to have the best detail, down to at least 1.5-2 meters.

3.3 *Electrical resistivity tomography*

The Electrical Resistivity Tomography (ERT) is a method that calculates the subsurface distribution of the volumetric resistance from a large number of measurements (current and potential) made from electrodes placed in an arbitrary geometric pattern. For geophysical applications ERT uses electrodes on the ground surface or in boreholes. By accurately calculating the soil resistivity it is possible to detect, water, clay layers, voids, but it also possible to reconstruct sections of the ground that can be used to choose and calibrate the parameters for GPR surveys. ERT surveys that employ large number electrodes arranged in grids or sets of lines, as in this case, can be used to reconstruct a 3D model of the subsurface, and allow the mapping of complex structures like root systems.

3.4 Direct measurements

The selected roots system were entirely excavated using AIR-SPADE® Series 2000; this system use a proprietary, synergistic combination of supersonic jets of air and high flow pneumatic vacuum transport. Supersonic air jets are extremely effective at penetrating most types of soil, but are harmless to all types of non-porous buried objects. This technique allow to dig out the entire roots system without damage it (E. T. Smiley 2001) After removal of shallow soil roots were pulled out using a digger. In order to acquire morphological information on root system to be compared with the GPR and ERT methods: poplar roots were scanned using a spot Zoller+Fröhlich GmbH Laser Measurement System LARA 53500. Ten different laser scans were made for each root; and after were elaborated using the software JRC–Reconstructor ®; orthogonal sections, with respect to the central axis of the taproot, were created and exported in dxf format (CAD).
Pine roots were completely excavated and several digital pictures were taken.

4. Selected Results

4.1 *Ground Penetrating Radar*

In test sections analyzed around the poplar trees (Fig 1) GPR with high frequency antennas showed to be able to detect roots with very small diameters and different angles, with the geometry of survey lines ruling the intensity of individual reflectors. A grid of parallel

lines in two directions was then acquired around each of the test trees, to try to achieve a sort of 3D reconstruction of the root system. The comparison with the Laser scan point-cloud of the extracted roots (Fig 2), has proven that the potential of high density 3-D GPR to map the entire system in unsaturated soil, with a strong preference for sandy and silty terrain, and problems arising when clay is predominant, and also when "clutter" produced by gravel and pebbles is mixed with the response of roots.
The Comparison between 3D rendering of Laser-scan point cloud and GPR sections. The red points, present in GPR section, represent the root position.

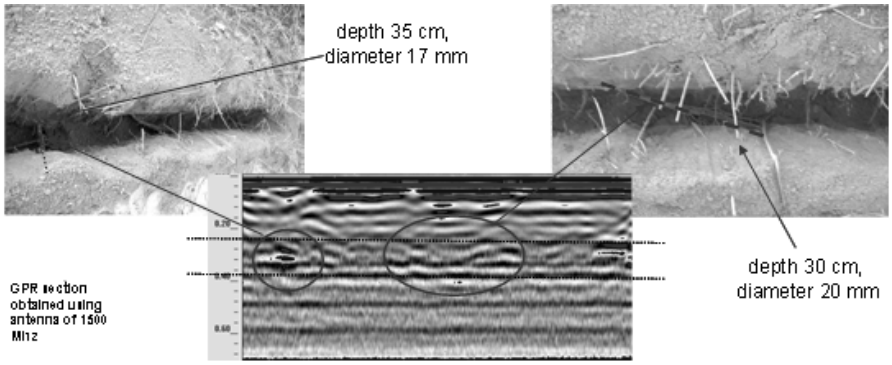

Fig 1.Comparison between root position and radar profile. Vertical scale is depth (m). The profile was excavated and the sources of radar reflection detected

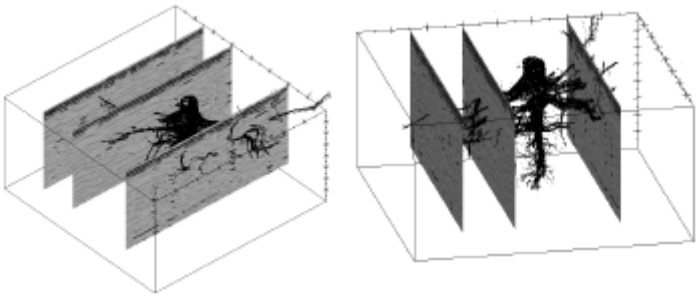

Fig2. Comparison between 3D rendering of Laser-scan point cloud and GPR sections. The red points, present in GPR section, represent the root position.

4.2 Electrical Resistivity Tomography

Three-dimensional reconstructions using grids of electrodes centered and evenly spaced around the tree have been used in all cases (poplar and pine), and repeated in different periods (April, June, September) to investigate the influence of water saturation in the results obtainable. While it was difficult to get much more than (detailed) stratigraphic information around poplar trees, the work performed on the pine trees shows clearly that the distribution of larger diameter roots has a strong correlation with the electrical resistivity 3-D models. Most of all (Fig 3) the use of difference images between successive sets of data revealed to be a powerful method, as the roots act like a "filter" for water thus causing a local increase of resistivity after a wetting period.

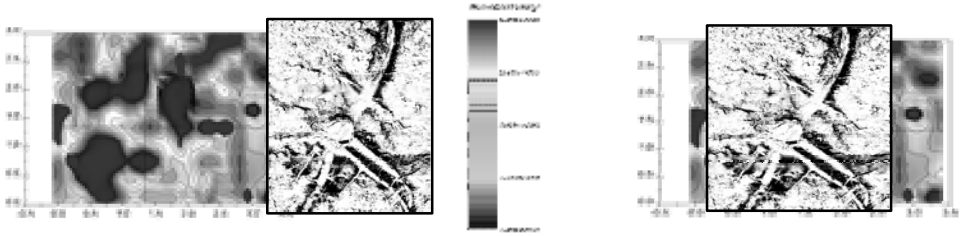

Fig. 3 Plan view slices of 3D resistivity percent increment (difference calculated between results obtained in dry and wet conditions) compared with view from top of unveiled roots system

5. Conclusions

Geophysical surveys can reveal a useful approach to roots investigation, both in describing the shape and behavior of the roots in the subsoil. To achieve the better results this paper underlines the need of integrating different techniques: GPR method is able of detecting with higher resolution the distribution of the tree roots in the subsoil. Three dimensional ERT can be useful in correlating the recovered resistivity distribution with root volumes. In particular the extraction of volumes of resistivity percent increment between dry and wet conditions in the subsoil around the trees seems a parameter that can be directly related to the volumes of roots. Further studies should focus on two directions: first, the improvement of a standard field-procedure to carry on the geophysical surveys; second, the development a statistical processing tool to relate root biomass to geophysical parameters.

Acknowledgements

This research was partly funded by the CarboEurope IP project (EU-Contract No. GOCE-CT-2003-505572) and by the JRC-IES-CCU-Action 24002 - Greenhouse Gases in Agriculture, Forestry and Other Land Uses - GHG-AFOLU. We would thank all colleagues of the Climate Change Units that helped us during the direct measurements.

References

- J. R. Butnor, J. A. Doolittle, L. Kress, S. Cohen and K. H. Johnsen (2001) Use of ground-penetrating radar to study tree roots in the southeastern United States Tree Physiology 21, 1269–1278

- Hruska J, Cermak J, Sustek S (1999) Mapping tree root systems with ground-penetrating radar. Tree Physiol. Feb;19(2):125-130

- L Wielopolski, G Hendrey, J Daniels, M McGuigan (2000) Imaging tree root systems in situ. D.A. Noon, G.F. Stickley, and D. Longstaff (ed.) Proceedings of the 8th International Conference on Ground-Penetrating radar, Gold Coast, Queensland, Australia, 23–26 May 2000. Proceedings of SPIE—the International Society of Optical Engineering, Bellingham, WA. 4084:642–646

- Stokes A. Fourcaud T. Hruska J. Cermak J. Nadyezhdin N. and Praus L. (2002) An evaluation of different methods to investigate root system architecture of urban trees in situ: I. Ground penetrating radar. Journal of Arboriculture 28(1): page 1-9

Functional –structural modelling using the generic tool PIAF-1 : a simulation example on young walnut

André Lacointe and Nicolas Donès
UMR (INRA - Université B. Pascal) PIAF, INRA, Site de Crouel,
234 avenue du Brézet, F-63039 Clermont-Ferrand Cedex 2, France
{lacointe|dones}@clermont.inra.fr

Keywords: simulation software, interactive modeling, modularity, carbon-based model

Introduction

The generic functional-structural tree modelling tool PIAF-1 was introduced in the previous FSPM workshop (Donès and Lacointe, 2004). Its modular structure allowed to choose (1) which process modules should be included within a simulation, and (2) the specific way to represent each process. Another feature of PIAF-1 was its ability to use time and space scales relevant to each process or tree element, making it possible, for example, to describe one branch at a very detailed temporal or spatial level while the rest of the tree, including other branches, was described at a courser scale. Such extended flexibility of the data structure is a major characteristic of PIAF-1 among other modelling tools of similar scope, e.g. LIGNUM (Perttunen et al., 2001) or GreenLab (Yan et al., 2004). However, that preliminary version was just a modelling tool, i.e. a data structure with a generic module pattern including data access procedures and a module chaining engine: no biological model was implemented yet; this has been done since. This presentation is aimed at showing the current development status of the project, with a simulation example on young walnut.

Data structure

In the original version, the description of tree structure was based solely on topology: an ordered, dual sequence of nodes and segments. The current version has been extended with more biological concepts like root types or stem growth units, considering them as extended, optional attributes of segments to keep the scaling flexibility (Fig. 1).

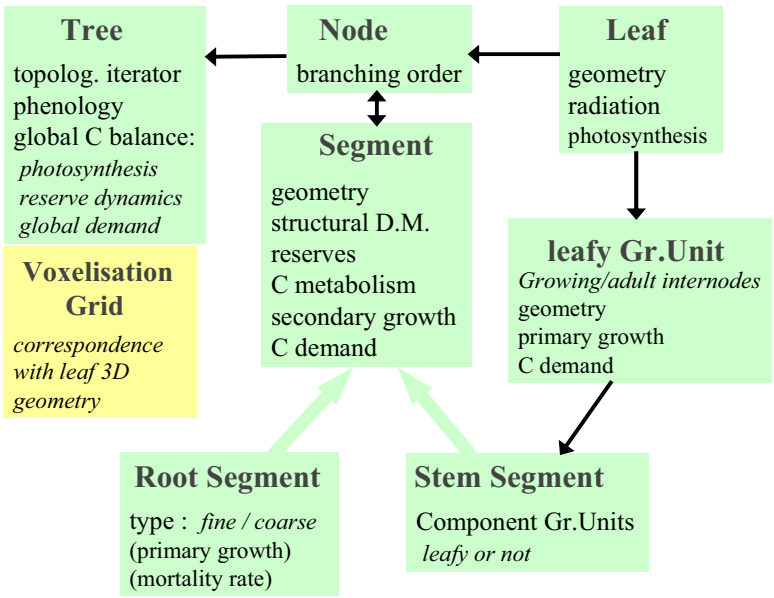

Fig. 1. Data structure of PIAF-1 (simplified) showing the major biological attributes attached to each class.

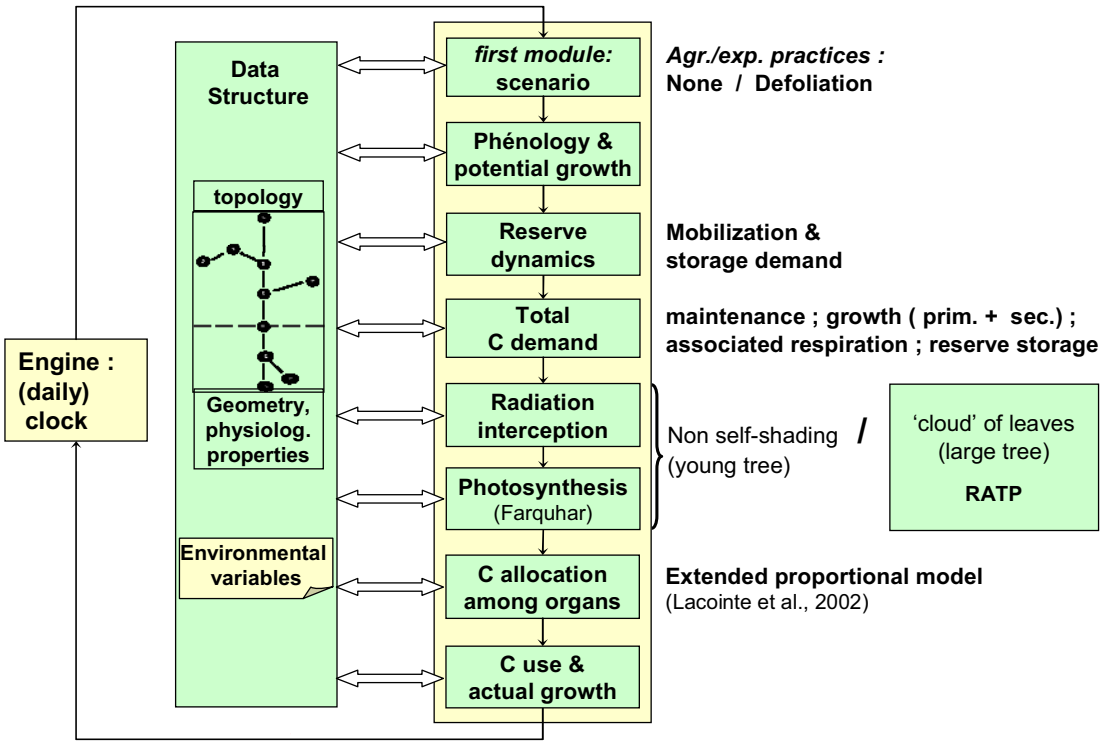

Fig. 2. Chaining of process modules currently implemented in PIAF-1.
When available, different versions for one process are indicated by the character ' / '

Process modules

Beside common processes that are usually included in FS plant models, like photosynthesis, carbon allocation or actual growth, some more specific processes have been implemented that are not so common in simulation models in spite of their increasingly acknowledged significance (Le Roux et al. 2001), *e.g.* reserve dynamics. Some of them, like radiation and photosynthesis, have been implemented in two versions, one of them more appropriate to small- and the other to large-sized trees. Specific agricultural practices or experimental protocols, *e.g.* harvesting, pruning or defoliation, can be easily included or discarded through a special 'scenario' module (fig 2).

User interface

The software provides a user-friendly graphic interface (Fig. 3) to specify the sequence of modules to include in the next simulation run; module-specific dialog boxes will be available for parameter editing, but these have not been designed yet. At runtime, real-time 3D visualization is available to follow the structural changes together with a log window for model output. Also available is automatic capture of the 3D image at every simulation time step to make video sequences.

A simulation example

This presentation will include a short demonstration of the software, simulating the carbon economy and growth of young walnut trees over one year. Two conditions are compared: control *vs.* periodic defoliation, as experimentally investigated in the PIAF laboratory, Clermont-Ferrand. Walnut-specific parameters were derived from the earlier model SimWal (Balandier et al., 2000) or

from more recent experiments (e.g. Lacointe et al., 2004). Beside a significant effect on growth, the impact on the reserve status is emphasized (Fig. 4), which is also found in current experiments. However, an extended parameterization/validation work still has to be done, including of course longer-term simulations.

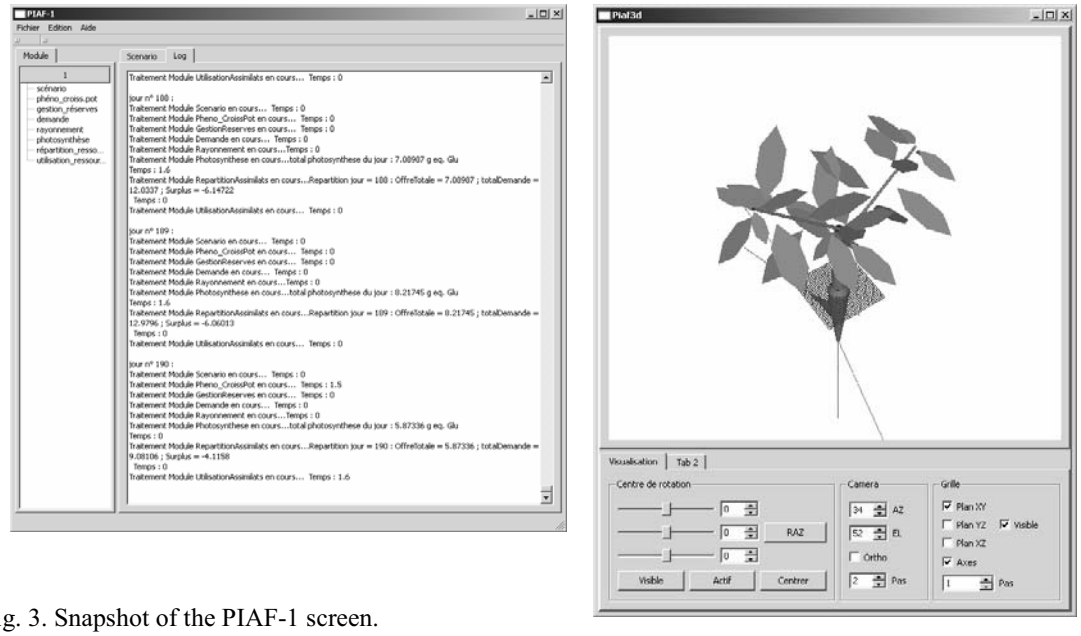

Fig. 3. Snapshot of the PIAF-1 screen.
The log window to the left displays output and error messages. The window to the right provides real-time 3D visualization, allowing to change the visualization angle.

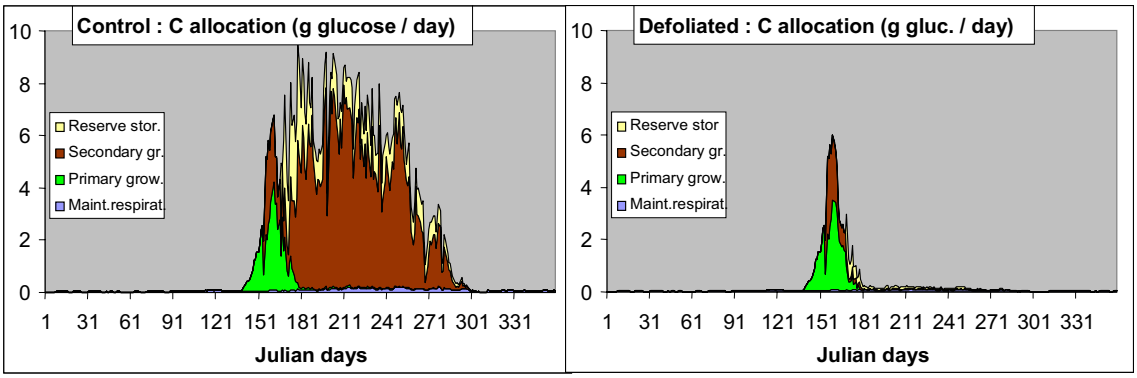

.Fig. 4. An example of simulation results on young walnut: whole-tree level daily C allocation in two situations : control *vs*. defoliated.

References

Balandier P., Lacointe A., Le Roux X., Sinoquet H., Cruiziat P., Le Dizès S., 2000. SIMWAL : a structural-functional model simulating single walnut tree growth in response to climate and pruning. Ann. For. Sci., 57, 571-585.

Donès N., Lacointe A., 2004. PIAF-1: a new topology-oriented, modular integrative modelling tool. *In*: C. Godin et al., eds, 4th International Workshop on Functional-Structural Plant Models, Montpellier (France), 7-11 June. 2004, .p. 277.

Lacointe A., Isebrands J.G., Host G.E., 2002. – A new way to account for the effect of source-sink spatial relationships in whole plant carbon allocation models. Can. J. For. Res 32, 1838-1848.

Lacointe A., Deléens E., Améglio T., Saint-Joanis B., Lelarge C., Vandame M., Song C.G., Daudet F.A., 2004. Testing the branch autonomy theory: a 13C /14C double labelling experiment on differentially shaded branches. Plant, Cell and Environm. 2, 1159-1168

Le Roux X., Lacointe A., Escobar-Gutiérrez A., Le Dizès S., 2001. Carbon-based models of individual tree growth : a critical appraisal. Ann. For. Sci., 58, 469-506.

Perttunen J., Nikinmaa E., Lechowicz M.J., Sievänen R., Messier C., 2001. Application of the functional-structural tree model LIGNUM to sugar maple seedlings (Acer saccharum Marsh) growing in forest gaps. Ann. Bot. 88, 471-481.

Sinoquet H, LeRoux X, Adam B., Ameglio T., Daudet F.A., 2001. RATP: a model for simulating the spatial distribution of radiation absorption, transpiration and photosynthesis within canopies: application to an isolated tree crown. Plant Cell and Env. 24, 395–406.

Yan H.P., Kang M.Z., de Reffye P., Dingkuhn M., 2004. A dynamic, architectural plant model simulating resource-dependent growth. Ann Bot. 93, 591-602.

The rule-based language XL and the modelling environment GroIMP, illustrated with simulated tree competition.

Ole Kniemeyer [1]
Gerhard Buck-Sorlin [1,2]
Reinhard Hemmerling [1,*]
Winfried Kurth [1]

[1] Brandenburg University of Technology at Cottbus
Chair for Practical Computer Science / Graphics Systems
P.O.Box 10 13 44, 03013 Cottbus, Germany
{okn|rhemmerl|wk}@informatik.tu-cottbus.de

[2] Wageningen UR
Crop and Weed Ecology Group
Haarweg 333, 6709 RZ Wageningen, The Netherlands
gerhard.buck-sorlin@wur.nl

[*] corresponding author

Keywords: L-systems, GroIMP, forest, spruce, beech, *Picea abies* (L.) Karst., *Fagus sylvatica* L., competition, radiation model

1 Introduction

Functional-structural plant modelling has to face three challenges, all dealing with complexity issues: the complexity of the modelled biological system itself, the complexity of integrating different sources of knowledge into one consistent modelling framework, and the complexity of implementation and simulation on a computer [1].

All three aspects can lead to long and obscure code when a standard programming language like C or Java is used, thus stimulating the wish for a model-specification formalism and language that is specifically adapted to the needs of plant modelling. The most well-known approach towards such a formalism are L-systems, introduced by Lindenmayer in 1968 and later applied to various aspects of plant architecture and growth, see [8, 7]. L-systems are rewriting systems operating on strings which can be interpreted as tree graphs.

However, as a formal tool for plant modelling L-systems still have some limitations [5]. Being based on strings of symbols, the only directly representable relation between symbols is the neighbourship of consecutive symbols, and geometry has to be created by an additional step (turtle interpretation). Modern data structures for 3D geometry like scene graphs do not need such an artificial segregation between structure and geometry, and graphs in general allow the representation of arbitrary relations. We thus have designed the formalism of Relational Growth Grammars (RGG) [4] which are rewriting systems to be applied in parallel to graphs. Nodes of these graphs are objects in the sense of object-oriented programming and can also represent geometrical entities, for example plant organs. This has the advantage that the complete model information including structure (specified by arbitrary relationships), geometry and internal state is always directly accessible within a single representation.

Based on RGGs, we have designed the programming language XL (eXtended L-system language) and the open-source modelling environment GroIMP [3]. XL extends the standard programming language Java and implements the formalism of RGGs. We will demonstrate some of the novel features of XL and the modelling environment GroIMP in the sequel.

2 The Rule-Based Language XL

Like L-systems, relational growth grammars are a formalism, not a concrete programming language. The concrete programming language XL is a complete extension of Java within which relational growth grammars can be specified. The common syntax of L-system rules is retained as in the simple rule

```
A(x) ==> F(x) [RU(30) A(x*0.5)] RH(180) A(x*0.9);
```

but also more complex rules making use of true graphs and arbitrary context can be specified. In fact, the definition of XL is quite general and covers not only relational growth grammars, but also allows a rule-based implementation of other graph rewriting formalisms like vertex-vertex algebras [9, 3] for the modelling of growth of surfaces.

Within XL, the current structure is represented as a graph whose nodes are Java objects and whose edges stand for specific relationships. Nodes generalize symbols of L-systems, edges generalize the adjacency of symbols in an L-system string. The software GroIMP provides a set of standard geometric node classes whose instances play the role of turtle commands of L-systems, but are now conceptually geometry nodes of a 3D scene graph. This true graph representation is advantageous for several reasons even if the structure is only tree-like so that it could easily be represented as a bracketed L-system string.

- Nodes are objects in the sense of object-oriented programming. Their classes can be equipped with methods and define an inheritance hierarchy of which one can take advantage in modelling.
- Nodes have an identity by which they can be addressed. This allows to reference them globally at any place in the model, regardless of a "cursor" in the structure like the current derivation position of an L-system interpreter. The following example makes use of this: A dormant bud is activated if the irradiance exceeds some threshold `T`. The irradiance is computed by a radiation model which receives the reference `b` to the bud in question.

  ```
  b:DormantBud, (radiationModel.getSensedIrradiance(b).integrate() > T) ==> Bud;
  ```

- Traversal within the structure is easy and efficient. There is no need to keep track of the special bracket symbols when moving forward or backward in the structure, because relationships are directly represented as edges. This simplifies the implementation of global interactions between specific parts of the structure.
- Nodes have named parameters, L-system symbols simply number their parameters. Being able to access parameters by name, a model only needs to deal with the relevant parameters. The unused parameters are set to default values implicitly. This is especially important for predefined node classes like turtle commands which have a lot of parameters: their default values are suitable for most models, but some models may want to tune them to fit their needs. A similar technique based on structured parameters is available for user-defined symbols within the L+C language [2].

As for L-systems, the rule application is in parallel. The advantage is that, within a single derivation step, one consistently operates on a single, fixed structure. Contrary to L-systems, nodes of the graph may not only be created or deleted like L-system symbols, but may also be kept and modified with respect to their parameters. To ensure the parallel mode also for such parameter modifications of kept nodes, XL provides special assignments of values to node parameters which are deferred and actually performed together with structural changes at the end of a step.

Rules of complex models typically require information not only about the nodes that are being modified, but also about their neighbours or an even wider context, say, the objects in geometric vicinity or all objects along the path from the root of a plant to the current node. XL's graph queries greatly simplify the specification of such models, allowing the search for nodes that fulfil certain conditions in an arbitrarily large context (namely, the whole graph). As a consequence, every node can have an influence on any other node within a single rewriting step, whereas L-systems restrict this influence to a finite local context (or, depending on direction of derivation, to symbols to either the left or right [2]). Thus, XL's queries can also be used to implement environmental interactions, or to analyze local and global properties of simulation results. The following growth rule is an example thereof which scans, for a node `n` of a meristem-like type `X` to be rewritten, the complete graph in order to allow growth only if there is no `F`-node within the 60° forward cone of `n` closer than a threshold `T`.

```
n:X, (empty((* f:F, (f in cone(n,true,60) && distance(n,f) < T) *))) ==> F [RU(a)X] X;
```

3 Tree and Competition Model

The modelled trees are young specimens of spruce (*Picea abies* (L.) Karst.) and beech (*Fagus sylvatica* L.) trees. Structural tree development is implemented by L-system-style rules which make use of XL's control statements like `if` or `for` governing the process of structure creation. The constructed graph is then subjected to functional rules, which preserve the structure but modify their geometric and internal state in order to model, e.g., the production and partitioning of assimilates or increment in girth. The production of assimilates depends on the locally available amount of radiation as computed by the radiation model (see next section), this leads to a competition for radiation between individuals.

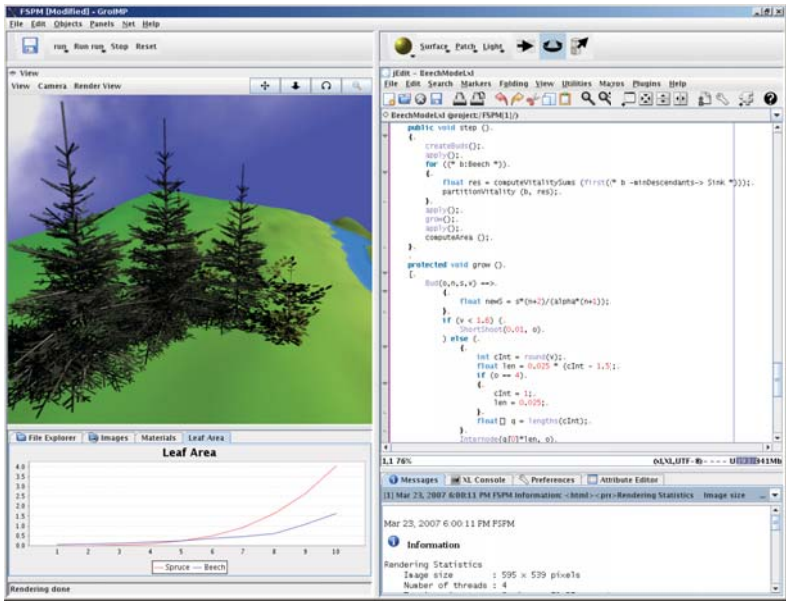

Figure 1: A screenshot of the GroIMP workbench showing a rendered image of the competition model, the source code, a rendering message, and a chart of leaf area development.

Within XL, one can enforce the end of the current derivation step. Furthermore, the rules to be applied can be organized in code blocks and invoked as part of methods and control structures such as `if` or `for`. Thus, time and order of rule application are completely under the control of the modeller. The model takes advantage of this feature by splitting up annual growth into several steps that are executed sequentially (e.g., flushing of the annual shoot, creation of buds for the next annual flush).

The architectural model of spruce is partially based on a previous GROGRA model [7]. The original model was based on measurements (mean and variance) to create a stochastic model of spruce. The new model adds light as limiting factor (values obtained from radiation model). In each iteration step, the amount of light received by the leaves of a branch is used to calculate how much that branch grows. Since only taking the light into account would result in exponential growth, the maximum value of the new model (light only) and the old model is used to obtain a value of how much a branch grows. The effect is that the old model now represents the limits given by other factors (like water, nutrients, etc.) except light.

The second tree model, representing beech, was designed with GroIMP from the beginning. It is based on observations of beech plants and on calibration using statistical analysis of model results and comparision with measured data (for details see [6]). The influence of light on growth is also represented in this model.

4 Radiation Model

The radiation model presented here uses a reversed path tracer algorithm based on [10]. Here, we give a brief description, details and full documentation will be available in [3]. The radiation model is invoked once per simulation step and applied to a scene created within the modelling environment GroIMP. The scene is a virtual world containing (amongst others) a number of light sources, visible objects, and light sensors. Essentially, the radiation model computes how much of the radiant power emitted by the light source(s) is absorbed by the objects in the scene, and how much radiant power is detected by the sensors. It has thus the functionality of a raytracer, only that the direction of traced rays is reversed.

The amount of radiation absorbed locally by an object or detected by a sensor may be queried at any point of simulation in order to be used in a model of, e.g., plant growth.

In GroIMP, several types of light sources are supported: Point lights, spot lights, directional lights, area lights, and a sky. A number of rays is generated by the light sources and traced along their paths across the scene. Each ray has three associated properties: origin, direction and spectral composition. One special case of spectral composition is RGB (Red, Green, Blue channel), but spectral compositions of any kind are possible.

When a ray hits a visible object, the intersection point with this object is calculated and a new ray is created. The direction and spectral composition of this new ray are determined by the material properties of the object that was hit. The origin of the new ray is set to the intersection point. The amount of radiation that was absorbed by the surface is calculated as the difference of the spectrum of the old and the new ray. This difference is added to the absorption spectrum of the object. For the new ray the whole process is repeated recursively. The recursion ends if a user-defined recursion depth is reached, if the contribution of the ray falls below a certain threshold or if no object was hit. Sensors are treated similarly, except that they do not modify the ray.

Usage of the radiation model is easy. First the model needs to be instantiated with the number of rays and recursion depth as parameter. Then the radiation contribution in the current scene is calculated by calling the function `compute()` on the instance of the radiation model. Now the amount of radiation received by every object can be queried by calling `getRadiantPowerFor(node)` on the radiation model instance, and the amount of irradiance sensed by a sensor is obtained by calling `getSensedIrradiance(node)`. No additional information needs to be provided, since the radiation model uses the current GroIMP graph as input, also taking into account material properties that were set for any node.

5 Results and Discussion

Figure 1 shows a screenshot of the GroIMP workbench with a simulation of tree competition in a mixed coniferous-deciduous stand of beech and spruce trees typically encountered in the montane layer of the German midland mountain forests. Several elements of the model can be viewed within GroIMP, e.g., the source code, some statistics of the rendering procedure in a message window (lower right), and a chart (lower left) showing the time course of simulated leaf area of spruce and beech. Our model is capable of a realistic dynamic reproduction of competition, thereby also demonstrating the relative ease of representing multiple scales (organ, individual, canopy, ...) within GroIMP/XL.

6 Acknowledgements

This research was funded in part by the Deutsche Forschungsgemeinschaft (DFG).

References

[1] C. Godin and H. Sinoquet. Functional-structural plant modelling. *New Phytologist*, 166:705–708, 2005.

[2] R. Karwowski. *Improving the Process of Plant Modeling: The L+C Modeling Language*. PhD thesis, University of Calgary, 2002.

[3] O. Kniemeyer. *Design and Implementation of a Graph Grammar Based Language for Functional-Structural Plant Modelling*. PhD thesis, BTU Cottbus, 2007. (forthcoming, see http://www.grogra.de).

[4] O. Kniemeyer, G. Buck-Sorlin, and W. Kurth. A graph-grammar approach to artificial life. *Artificial Life*, 10:413–431, 2004.

[5] O. Kniemeyer, G. Buck-Sorlin, and W. Kurth. GroIMP as a platform for functional-structural modelling of plants. In Jan Vos, Leo F. M. Marcelis, Peter H. B. de Visser, Paul C. Struik, and Jochem B. Evers, editors, *Functional-Structural Plant Modelling in Crop Production*, volume 22 of *Wageningen UR Frontis Series*, pages 43–52. Springer, 2007.

[6] O. Kniemeyer, J. Dérer, R. Hemmerling, G. Buck-Sorlin, and W. Kurth. Using the language XL for structural analysis. In *Proceedings of FSPM07 (this volume)*, 2007.

[7] W. Kurth. *Die Simulation der Baumarchitektur mit Wachstumsgrammatiken*. Wissenschaftlicher Verlag Berlin, 1999.

[8] P. Prusinkiewicz, M. Hammel, J. Hanan, and R. Měch. Visual models of plant development. In G. Rozenberg and A. Salomaa, editors, *Handbook of Formal Languages*, volume 3, pages 535–597. Springer, Berlin, 1997.

[9] C. Smith, P. Prusinkiewicz, and F. F. Samavati. Local specification of surface subdivision algorithms. In John L. Pfaltz, Manfred Nagl, and Boris Böhlen, editors, *AGTIVE 2003*, volume 3062 of *Lecture Notes in Computer Science*, pages 313–327. Springer, 2003.

[10] E. Veach. *Robust Monte Carlo Methods for Light Transport Simulation*. PhD thesis, Stanford University, 1998.

Manipulating virtual plants

Przemyslaw Prusinkiewicz[1], Brendan Lane[1], and Radomir Mech[2]
[1]Department of Computer Science, University of Calgary, Canada
[2]Adobe, San Jose, CA

Keywords: L-system, simulation, plant-modeling software design, virtual laboratory, L-studio, model specification and exploration, human-computer interaction

Summary: We propose programming constructs for interacting with virtual plants modeled using L-systems, and survey application areas that may benefit from interactive simulations.

Introduction and previous work

The first three-dimensional plant simulation models were implemented over 35 years ago [Honda 1971]. Since then, processor speed has been increasing exponentially (Moore's law), and powerful graphics cards have become ubiquitous. These technological advancements have had a significant impact on the methods for simulating and visualizing plants. The complexity of plant models has increased, and simulations that once could only be appreciated using single-frame animation (recording individual stages of the simulation, than playing them back as a movie) can now be viewed in real time, as the simulation progresses.

Fast simulations set the stage for interaction with plant models. First, graphically controlled sliders were introduced for manipulating model parameters in real time [Oppenheimer, 1986]. This concept was generalized into panels, which the user could configure and apply to control arbitrary model parameters. [Mercer et al 1990, Prusinkiewicz and Lindenmayer 1990]. Further extensions included graphically-defined functions, which made it possible to interactively specify and modify relations between parameter values [Lintermann and Deussen 1999, Prusinkiewicz 2004]. Plant models represented on the screen also lend themselves to direct manipulation [Shneiderman 1987], creating the impression of interacting with the plants themselves. Previous work in this area includes interactive bending and pruning of branches [Power et al. 1999, Boudon et al. 2003], and sketch-based techniques [Ijiri et al. 2005] for interactively specifying plant geometry.

Our work is focused on interactions with complex functional-structural plant models using visual techniques that resemble manipulations of real plants. For example, selected branches of a virtual tree trained for an espalier may be bent and attached to wires. This will affect the development and growth of further branches, which may be subject of manipulation at a later date. Creation of virtual plants capable of such interactions represents a methodologically challenging problem due to the contrasting demands of simulations and interactive control. On one hand, plant structure and behavior are defined by program execution; on the other, they are subject to user actions. Furthermore, the responses to user actions should themselves be programmable, to allow for easy changes and refinement during model development.

Implementation

We present a solution of this problem implemented in the L-system-based simulation program lpfg, a component of the L-studio and Virtual Laboratory modeling software [Prusinkiewicz

2004]. At the base of our implementation are two standard low-level operations of human-computer interface design: selection of a component, and location of a point on the screen [Foley et al. 1996]. In lpfg, the user distinguishes between these operations by pressing appropriate control keys on the keyboard. When a component of a virtual plant is *selected* with the mouse, a predefined module `MouseIns()` is inserted before the selected component's representation in the L-system string. When a point is *located* with the mouse, its coordinates are returned to the L-system-based model by calling the predefined function `GetMouseStatus()`. This function returns screen coordinates of the located point as well as object-space coordinates of the line traced from the located point into the screen. The automatic transformation of the traced line to the object-space coordinates makes it easy for the modeler to relate mouse position to the model using the coordinates in which the model is expressed.

The `MouseIns()` and `GetMouseStatus()` constructs are powerful building blocks for creating interactive virtual plants, and are well integrated into the L-system formalism. The module `MouseIns()` can appear on par with other L-system modules as a predecessor or context of productions. Thus, the designer of an L-system model can specify the reaction to module selection using the same formalism of L-system productions as that used to specify non-interactive aspects of the model behavior. Furthermore, in many applications the selection and location operations can be seamlessly combined, allowing for three-dimensional manipulations using a two-dimensional input device, a mouse. For example, a branch can be bent to a new position by selecting a branch component, then dragging it in the plane parallel to the screen with the mouse. Two coordinates of the new location are then calculated on the basis of the position of the mouse-controlled cursor, while the third coordinate, representing distance from the screen, is derived from the original depth of the selected component.

Applications

Although module selection has been available within the L-studio for some time, the recent addition of the location capability greatly enhances the spectrum of possible interaction modes. We are exploring the following application domains:

Horticultural plant manipulation. For example, a carbon-allocation model of a fruit tree may allow the user to pick selected fruits from a virtual tree, simulating thinning. A biomechanical tree model intended for designing topiary gardens, espaliers, or bonsai may allow the user to virtually prune branches, bend them, and tie them to wires. A plant model may also support virtual grafting operations.

Laboratory experiments and simulation of plant responses to stimuli. A virtual plant designed to study hormonal control of plant development may support interactive application of hormones to selected plant parts. The user may interactively deposit insects or pathogens on selected plant organs, inducing simulated defense mechanisms. The user may also "touch" the plant, inducing responses such as the collapse of Mimosa leaves, or the folding-up of the Venus flytrap [Simons 1992].

Interactive visualization. Examples include:

- Attachment of "probes", which dynamically monitor the state of selected modules of a model. The results may be presented in textual or graphical (histogram) form near the selected modules or in a separate window, and are useful both for monitoring simulated experiments and when debugging and testing plant models.

- Display of background reference information related to the selected modules or plant components. For example, selection of a flower in the model may create a new window which displays the corresponding image of the real flower, animation of its development, or references to the experimental data and literature used to construct the model.
- Modification of plant geometry, as needed to reveal hidden components. For example, leaves hiding the meristem from view can be removed (as is often done in microscopy), or internodes between rosette leaves can be made longer to expose lateral buds and the sequence of their development.
- Attachment of a virtual camera to specific parts of the plant. This can be used to focus on the development of a specific plant component, such as a leaf, flower, or shoot apex.

Conclusions

The augmentation of the L-system-based modeling language L+C with simple programming constructs for selecting modules and locating points on the screen has opened the door for constructing a wide range of interactive plant models. Control panels remain useful for specifying global parameters of the models, while direct manipulation makes it possible to interact with a virtual plant locally and in a more intuitive manner, resembling the manipulation of real plants. This is useful while experimenting with the models for research purposes, and has particular appeal in models designed for education and training.

The models outlined in this abstract represent only a small fraction of the wide range of possible interactive plant models. Construction of further models is an exciting area of research. As interactive models become more numerous and diverse, it will become increasingly important to inform the end-user of the operations that can be performed, and their meaning in the context of a specific model. What to select? Where to move? How to interpret the output? An instruction manual accompanying a model is a possible but unattractive solution. Self-documenting models, providing hints when needed, are a more appealing alternative. Concepts and programming constructs for creating such models are also an area of further research. Finally, on the more technical end of the spectrum of open problems is support for recording and "playing back" interactive simulations, so that the interwoven track of user manipulations and simulations can be easily reproduced.

Acknowledgments

The idea of accessing background information through the model was originally proposed by Andrew Bangham. The notion of probes was proposed by Mitch Allen. The initial implementation of module selection in the context of L-system was by Radoslaw Karwowski. Support of this research by the Natural Sciences and Engineering Research Council of Canada and Adobe is gratefully acknowledged.

References

F. Boudon, P. Prusinkiewicz, P. Federl, C. Godin and R. Karwowski [2003]. Interactive design of bonsai tree models. Proceedings of Eurographics 2003: *Computer Graphics Forum* 22 (3) (Proceedings of Eurographics 2003), pp. 591-599.

J. D. Foley, A. van Dam, S. K. Feiner and J. F. Hughes [1996]: *Computer Graphics. Principles and Practice*. Addison-Wesley, Reading.

H. Honda [1971]: Description of the form of trees by the parameters of the tree-like body: Effects of the branching angle and the branch length on the shape of the tree-like body. *Journal of Theoretiocal Biology* 31:331-338.

T. Ijiri, S. Owada, M. Okabe, and T. Igarashi [2005]: Floral diagrams and inflorescences: Interactive flower modeling using botanical structural constraints. *ACM Transactions on Graphics* 24 (3) (Proceedings of SIGGRAPH 2005), pp. 720-726.

B. Lintermann and O. Deussen [1999]: Interactive modeling of plants. *IEEE Computer Graphics and Applications* 19(1):56-65.

L. Mercer, P. Prusinkiewicz, J. Hanan [1990]: The concept and design of a virtual laboratory. Proceedings of Graphics Interface '90, pp. 149-155.

P. E. Oppenheimer [1986]: Real-time design and animation of fractal plants and trees. *Computer Graphics* 20 (4) (Proceedings of SIGGRAPH '86), pp. 55-64.

J. L. Power, A. J. Bernheim Brush, P. Prusinkeiwicz, and D. H. Salesin [1999]. Interactive arrangement of botanical L-system models. Proceedings of the 1999 Symposium on Interactive 3D Graphics, pp. 175-182 and 234.

P. Prusinkiewicz, A. Lindenmayer [1990]: *The Algorithmic Beauty of Plants*. Springer, New York. With J. S. Hanan, F. D. Fracchia, D. R. Fowler, M. J. M. de Boer and L. Mercer.

P. Prusinkiewicz, L. Mündermann, R. Karwowski, and B. Lane [2001]. The use of positional information in the modeling of plants. Proceedings of SIGGRAPH 2001, pp. 289-300.

P. Prusinkiewicz [2004]: Art and science for life: Designing and growing virtual plants with L−systems. *Acta Horticulturae* 630 (2004), pp. 15−28.

B. Shneiderman [1987]: *Designing the User Interface: Strategies for Effective Human-Computer Interaction*. Addison-Wesley, Reading.

P. Simons [1992]. *The Active Plant*. Blackwell, Oxford.

The architecture of OpenAlea: A visual programming and component based software for plant modeling

Christophe Pradal[1], Samuel Dufour-Kowalski[2], Frédéric Boudon[1], Nicolas Dones[3]
[1] CIRAD, Avenue Agropolis, 34398 Montpellier Cedex 5, France
[2] INRIA, 2004 route des lucioles BP 93, 06902 Sophia Antipolis, France
[3] INRA, Site de Crouël, 234 avenue du Brézet, 63100 Clermont-Ferrand, France

Keywords: plant modeling, software architecture, interactive modeling, dataflow

Introduction

The FSPM community develops models to understand the biological processes involved in the function and growth of plants. Researchers in botany, ecophysiology, forestry, horticulture, applied mathematics and computer science have developed several models and software tools. Due to the different constraints and background of the teams, the available models have been developed in different programming languages on different operating systems with the goal of answering specific biological questions at a given scale. They are often developed as "monolithic" programs which generally lack of interoperability. In this work, we present the software architecture of OpenAlea, a flexible component-based framework designed to facilitate the integration and interoperability of heterogeneous models and techniques from different scientific disciplines. OpenAlea is developed in Python, a high-level, object-oriented, interpreted language. The OpenAlea architecture consists of: (a) a set of tools to integrate heterogeneous models implemented in various languages and on different platforms; (b) a component framework that allows for the dynamic management and composition of software components; and (c) a graphical modeling environment for enhancing the use of complex models and for rapid prototyping. To illustrate the integration of a complex component and its use through the graphical modeling environment, the PlantGL library for 3D plant modeling and visualization is presented.

Related work

In the plant modeling community, the idea of using a modular platform with components can be traced in the Virtual Laboratory (Prusinkiewicz et al., 1990). This interactive environment consists of experimental units called objects that encompass data files, and programs that operate on these objects. An inheritance mechanism allows refining objects in an object-oriented file system. However, stand-alone programs have low interoperability and the shell language used in this case to combine them has limited expressivity that makes difficult specification of complex control flows.

Alternatively, XFrog, a computer graphics software (Lintermann et al., 1999), provides an intuitive visual environment to design plant models with predefined generative components. Unfortunately, the system has limited extensibility.

OpenAlea was also inspired from different visual programming environments developed for other scientific topics such as Vision (Sanner, 2002) in bioinformatics or Orange (Demsar et al., 2004) in data-mining. However, we introduce in our systems different architecture principles such as the separation between functionalities and graphical interfaces.

Language integration

OpenAlea is a Python-based framework for the integration and the interoperability of heterogeneous components. Python is used as a glue as well as a flexible language for interactive scripting and rapid development of applications.

In our "language-centric" approach, existing C, C++ or Fortran libraries are written as extension to the Python language. Standard wrapping tools, such as Boost.Python, Swig, and f2py, are used to

support the integration process of such heterogeneous components. One of the key objectives of OpenAlea is to be multi-platform. While Python components are platform independent, others have to be built and installed on the target platforms, which may be a rather complex task. To ease the integration process, we have developed various tools such as SConsX and DistX. SConsX is an extension package of SCons (Knight, 2005). It simplifies the building of complex platform dependent packages by supporting different types of compilers (i.e. gcc, MinGW, Visual C++), and the different steps involved in compiling for Windows and GNU/Linux. DistX extends the standard Distutils Python library to facilitate package installation in the OpenAlea framework. Windows and RPM installer as well as source distribution can be automatically created.

Integrating models in a common python framework enhance usability by providing a unique modeling language to heterogeneous software. It allows to extend, compare and reuse existing functionalities. To improve software quality and ease maintenance, the component framework follows separation of concerns (e.g. data, algorithms, data-structure, GUI), by having independent modules dedicated to shared data-structure, computational task, graphical representation, etc.

A component framework

The core of OpenAlea is a *component framework* that allows users to dynamically reuse and combine existing and independent pieces of software into customized work-flows according to their specific needs. This type of framework emphasizes decomposition of application into separated and independent functional subsystems. Communication between components is achieved through their explicit interfaces (Szyperski, 2002).

The OpenAlea framework proposes an implementation of these principles. The software architecture is organized according to several concepts: (a) a *node* represents a software unit and is also named logical component. It is a functor object (i.e. an operator or a function) which provides a certain type of service. It can exchange data through its input and output ports. (b) A *composite-node* is a node that encapsulates other nodes defining a hierarchy of components. Node composition allows creating extended and reusable subsystem. (c) A *dataflow* (Johnston et al., 2004) is a graph composed of nodes connected by edges representing the flow of data from one node to the next. It defines a high level functional process well suited for coarse grain computation and close to natural thinking.

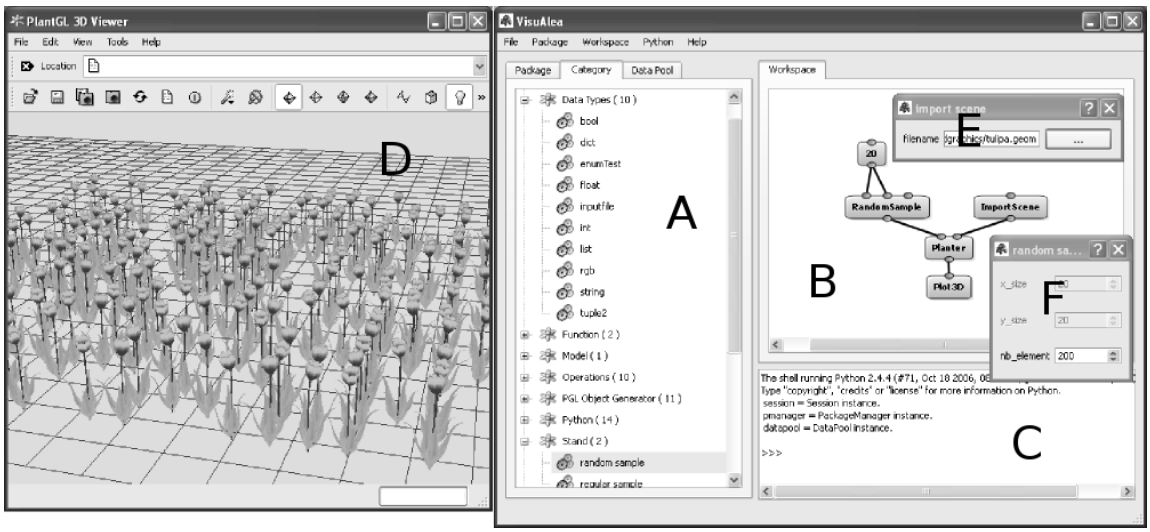

Figure 1. Snapshot of the OpenAlea visual modeling environment. (A) The package manager list packages and nodes found on the system. (B) The graphical programming interface enables users to build visual dataflow by interconnecting nodes. A 3D scene is built by associating a single geometry with a random distribution of points. (C) Low level interactions are done in the python interpreter. (D) PlantGL viewer is directly called by the Plot3D component. (E-F) Widgets specific to each component are automatically generated.

Others concepts are needed since the platform is developed in a distributed way. (d) A *package* is a deployment unit that contains a set of nodes, data as well as meta-information like authors, license, institutes, version, category, description and documentation. Finally, (e) the *package manager* allows for the dynamic discovery, introspection and loading of the available packages installed on the computer without requiring specific configuration. Thus, researchers can develop new functionalities that are added via the package manager at run-time without modification of the framework. Users can extend the framework by combining nodes into composite-nodes and share these macro nodes with other users. Dataflow containing nodes and composite-nodes can be saved as standalone application for end-user or as standard python script.

Data flowing through nodes are Python objects. An input and output port can be connected if their types are compatible, i.e. the output data can be implicitly cast to the type of the input port. Otherwise, an adapter has to be inserted between the two nodes to convert explicitly the data. A simple way to ensure input and output type compatibility between heterogeneous components is to use the standard data type available in python such as list, dictionary, etc. For more complex types such as graphs, some abstracts interfaces are provided in OpenAlea to standardize and ease communication.

Graphical environment

One of the key goals of OpenAlea is to enhance the use and the accessibility of plant modeling tools with a user-friendly interface. Particularly, the visual programming environment *Visualea* (see Figure 1.B) provides users the possibility to build graphically a dataflow by combining existing nodes and interactively edit them without having to learn a programming language. A graphical user interface (GUI) is associated with each computational node and enables the configuration and visualization of the node's data. Complex components will have specifically designed dialog boxes (see Figure 1.D). For others, a dialog box can be automatically generated according to the type of the input ports (see Figure 1.E-F). For that purpose, a widget catalog provides common widgets such as simple type editors (e.g. integer, float, string, color, filename, etc.), 2D and 3D data plotters, and sequence and graph editors. Thus, models that do not provide GUI can be easily integrated in the OpenAlea visual environment. Moreover, the catalog can be extended by packages to provide widgets for new data types. Finally, a Python shell has been integrated (see Figure 1.C) and provides a flexible way for programmers to interact procedurally with the components and to extend their behavior while taking advantage of the graphic representation of the data.

Integration of a component

PlantGL is a geometric library dedicated to plant modeling. It can be used as a versatile tool for functional structural plant modeling (Pradal et al., 2007). This library contains a hierarchy of geometric objects that can be assembled into a scene graph, a set of algorithms to manipulate the geometric objects and some visualization tools.

This module is written with 200k lines of C++ code that use various libraries such as Qt, OpenGL, qhull, *etc*. Relying on devoted tools such SConsX and DistX for compilation and installation makes the task easier since customization for a particular environment can be shared with other users of these tools.

Wrapping methods using Boost.Python have been implemented that make PlantGL accessible from python. Procedural composition of geometric objects can thus be quickly achieved with this language to build particular vegetal structures. Integration to *Visualea* enables graphical manipulation of the objects in the spirit of XFrog where visual programming is used for geometric plant modeling. Several levels of node abstraction have been implemented. The simplest one allows creating and editing the different geometric primitives of PlantGL (e.g. sphere, cylinder, NURBS surface, etc.). Basic primitives are graphically assembled in a scene graph and eventually passed on the visualization node. To simplify the construction of a complex model, more abstract nodes can

be defined with high level procedural geometric construction methods. In particular, some nodes that manifold a geometry and arrange the instances according to various biological patterns have been implemented. Figure 1.D shows for example a “planter” node that takes a random distribution of points on inputs and the geometry of an individual plant that can be used to create a natural scene by inferring a plant at each point. Additionally, nodes can easily be extended through the Python language to create new functionalities.

Several other components have been integrated in OpenAlea with similar techniques (Pradal et al., 2004). Some scenario, coupling different modules for plant architecture and ecophysiologial modeling will be presented during the poster session at the conference (Dufour-Kowalski et al., 2007).

Acknowledgments

This research has been supported by the developer community of OpenAlea and by grants from INRIA, CIRAD, and INRA (the Réseau Ecophysiologique de l’Arbre).

References

Prusinkiewicz, P. and Lindenmayer, A. 1990. The Algorithmic Beauty of Plants. Springer-Verlag New York, Inc.

Lintermann, B. and Deussen, O. 1999. Interactive Modeling of Plants. IEEE Comput. Graph. Appl. 19, 1, 56-65.

Fayad, M. and Schmidt, D. C. 1997. Object-Oriented Application Frameworks. Commun ACM 40, 10, 32-38

Johnston, Hanna, J., and Millar. 2004. Advances in dataflow programming languages. ACM Comp. Surv. 36, 1, 1-34

Pradal, Boudon, Donès, Durand, Fournier, Sinoquet, and Godin. 2006. OpenAlea: A platform for plant modelling, analysis and simulation, in: EuroPython 2006

Pradal C., Boudon F., Nouguier C., Chopard J., and Godin C. PlantGL : a Python-based software for 3D plant modelling at different scales. To be submitted.

Sanner M.F., Stoffler D. and Olson A.J. 2002. ViPEr, a visual Programming Environment for Python. In Proceedings of thre 10th International Python conference.

Szyperski, C. 2002. Component Software: Beyond Object-Oriented Programming. 2nd ed. Addison-Wesley Pro. Boston.

Demsar J, Zupan B, Leban G. 2004. Orange: From Experimental Machine Learning to Interactive Data Mining, White Paper (www.ailab.si/orange)

Knight, S. 2005. Building software with SCons. Computing in Science & Engineering 7, 1, 79-88

Pradal, Donès, Godin, Barbier de Reuille, Boudon, Adam, Sinoquet. 2004. ALEA: A software for integrating analysis and simulation tools for 3D architecture and ecophysiology, in FSPM04.

Dufour-Kowalski et al. 2007. OpenAlea: An open source platform for the integration of heterogeneous FSPM components, in FSPM07, Poster.

Modelling plant architecture to determine biocontrol strategies

Dave Skirvin and Irene Roberts
University of Warwick, Warwick HRI, Wellesbourne, Warwick, UK, CV35 9EF

Keywords: Biological control, natural enemy, movement, dispersal, virtual plants

Introduction

Due to pressure to reduce pesticide inputs, and the move to increasing the biodiversity of agroecosystems in the UK, there is greater interest in the use of biological control of pests. Biological control has been used successfully on protected edibles in the UK (Hussey, Parr & Gould 1965, Nachman 1981, Kropczynska and Tomczyk, 1996). There are however, difficulties in transferring this approach to both protected ornamental crops, which have a low tolerance to pest damage, and to outdoor crops, where environmental factors have a profound influence on biological control.

In order to understand how biological control can be effectively used within protected ornamental crops and outdoors, it is necessary to understand the searching behaviour of the predators within plant canopies. Previous modelling work has identified the movement of natural enemies as a crucial factor in determining the success of a prophylactic release programme for biological control in ornamental crops (Skirvin *et al.* 2002). Experimental work on movement of the predatory mite *Phytoseiulus persimilis* on *Choisya ternata* (Skirvin & Fenlon, 2003) has shown that the number of connections between plants has a significant impact on the dispersal of these natural enemies, which is in agreement with the work of Zemek and Nachman (1998, 1999).

Previous work with modelling biological control in virtual plant canopies (Skirvin, 2004) demonstrated the usefulness of using virtual plant canopies to model the movement of predators, but the modelling was very involved, and it was felt that a more parsimonious model could be created. The modelling approach needed to collapse the three dimensional problem to a one or two dimensional problem, but preserve the three dimensional information, in terms of the spatial relationships between parts of all; plants within the canopy.

This abstract describes ongoing work on the application of finite graph modelling to capture the 3D structure and connectedness of the plant canopy. The movement of insects within this structure will be simulated to aid the selection of introduction strategies for biological control.

Using a finite graph model for three dimensional plant canopies

The first step in creating the finite graph model of the canopy is to export the following information about the canopy from an L-system model:

- The types of canopy components
  (stem node & leaf node)
- The relative positions of the components
  (stored as e.g. plant 1, node 1, leaf 2 for the second leaf on the first node of plant 1)
- The spatial position of each component of the canopy
  (stored as x, y and z data)
- The connections between components
  (a list of the components that are connected to each other e.g. leaf 1 on plant 1 is connected to node 1 on plant 1 and leaf 3 on plant 4)

Once this information has been stored it can be used to generate the finite graph representation of the canopy. The finite graph is represented as a list of node objects that store the type, spatial

position and connectivity of the canopy components. From this class we can extract connectivity, distance and decision weighting (used for directed searching) matrices that act as a quick reference for the insects to look up information about the canopy.

The insects are simulated as a traversing object, which queries the matrices for information, which is then used to determine its movement within the plant canopy.

The simulation experiments

We aim to simulate two types of predators moving within the canopy that are described below.

Randomly searching predators

These predators represent the generalist predators, who generally do not use chemical cues to locate prey. Their decisions are made on a purely random basis, so that at any decision point in a network, each potential direction has an equal probability of being chosen.

Directed searching predators

These predators are representative of the specialist predators that are able to use volatile chemical cues emitted by plants to direct their movement within the canopy. To direct movement, we use a weighting matrix. The assumption is that a graph node containing a prey item emits a volatile cue, which can be detected by the predator. The strength of the cue is determined by the distance of a graph node from the emitting graph node (assuming equal distribution of cue in all directions) and the strength can either decrease monotonically or exponentially with distance to give different detection ranges. The weightings are calculated according to rate of change of signal strength along the direction between nodes, (effectively calculated as strength at destination node minus strength at current node divided by distance between the nodes) and stored in a weighting matrix. For a given node containing a predator, the probability of choosing a particular connection is calculated as the weighting for that connection divided by the sum of weightings for all connections (where a node has both positive and negative weightings, the negative weightings are ignored). Therefore, when a predator detects a cue, the decisions about which direction to take are biased by the weightings, increasing the likelihood of the predator moving in a direction towards the prey.

For example, using the finite graph example shown in Fig. 1: if we assume that the predator is on node 1 which has a signal strength of 70%, it has the choice of moving to node 2 (with a signal strength of 80% and a distance of 8 units) or to node 3 (with a signal strength of 85, but a distance of 15 units). Therefore the perceived rate of change of signal for the predator when moving to node 2 is 1.25, and to node 3 is 1.0, Therefore the probability of movement to node 2 is 1.25 / (1.25 + 1.0) which is 0.56, whilst the probability of moving to node 3 is 0.44.

When a predator cannot detect a cue, it follows a random search pattern, as described previously.

Simulating introduction strategies

Using the two types of predator searching, we are assessing a range of introduction strategies for the predators, based on a range of prey distributions within the canopy network. The model outputs the time taken to locate they prey items, and the minimum possible time that could be taken to locate the prey items. From this we can determine the efficiency of the different introduction strategies.

Future directions

This work is still in an early stage, and is providing baseline information about the efficacy of predator introduction strategies in plant canopies. Future work will focus on determining how predator introduction strategies will need to be adapted according to plant canopy structure and connectedness. From this information, and our work on lacunarity as a measure for distinguishing canopy structure types, we hope to be able to determine the most efficient

predator introduction strategies for particular canopy types. This would have a major benefit for improving the robustness of biological control within horticultural and agricultural crops.

Acknowledgments

The author would like to thank the UK Department for Environment, Food and Rural Affairs (DEFRA) for funding this work and Dr. Peter Room and Dr. Jim Hanan for their help with the development of the virtual plant work.

References

Hussey, N.W., Parr, W. J. & Gould, H. J. 1965; Observations on the control of *Tetranychus urticae* Koch on cucumbers by the predatory mite *Phytoseiulus regieli* Dosse. *Entomologia Experimentalis et Applicata*. 8: 285 –298.

Kropcynska, D. & Tomczyk, A. 1996; Development of *Tetranychus urticae* Koch and *Tetranychus cinnabarinus* Boisd. Populations on sweet pepper. *IOBC/WPRS Bulletin* 19(1): 71-74.

Nachman, G. 1981; Temporal and spatial dynamics of an acarine predator-prey system. *Journal of Animal Ecology* 50; 435-351.

Skirvin, D. J., De Courcy Williams, M. E., Fenlon, J. S. & Sunderland, K. D. 2002; Modelling the effects of plant species on biocontrol effectiveness in ornamental nursery crops. *Journal of Applied Ecology* **39:** 469-480.

Skirvin, D. & Fenlon, J. 2003. Of mites and movement: the effects of plant connectedness and temperature on movement of *Phytoseiulus persimilis*. *Biological Control* **27:** 242-250.

Skirvin, D. J. 2004; Virtual plant models of predatory mite movement in complex plant canopies. *Ecological Modelling* **171:** 301-313.

Zemek, R. and Nachman, G. 1998. Interactions in a tritrophic acarine predator-prey metapopulation system: effects of *Tetranychus urticae* on the dispersal rates of *Phytoseiulus persimilis* (Acarina: Tetranychidae, Phytoseiidae) *Experimental and Applied Acarology* 22: 259-278.

Zemek, R. and Nachman, G. 1999. Interactions in a tritrophic acarine predator-prey metapopulation system: prey location and distance moved by *Phytoseiulus persimilis* (Acari: Phytoseiidae) *Experimental and Applied Acarology* 23: 21-40.

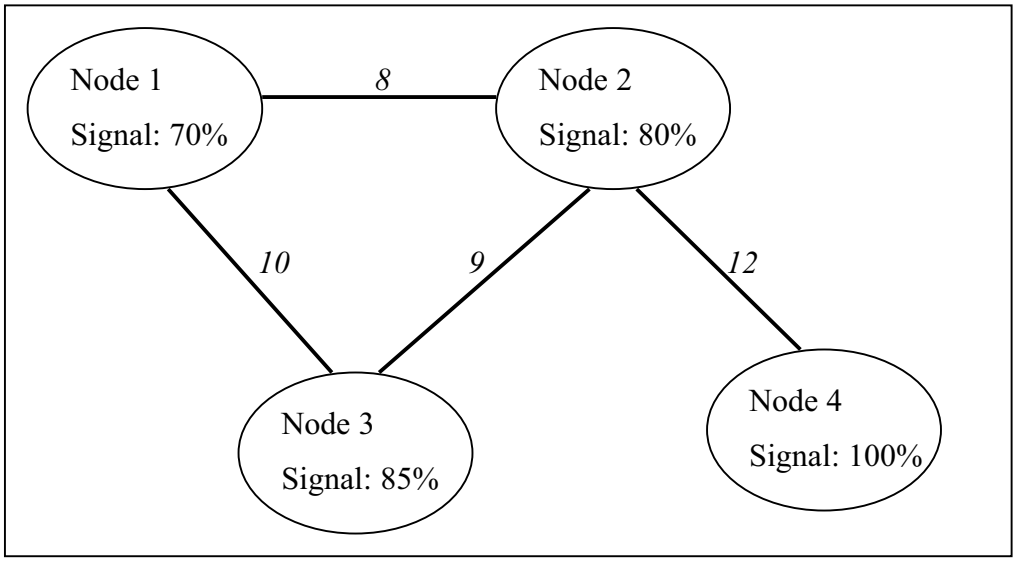

Fig. 1: Example finite graph network showing nodes and the strength of signal at each node based on distance from the emitting node (Node 4). Numbers in italics represent distances between nodes.

Coupling 3D virtual plant and foliar epidemic models: a new modelling approach to investigate plant-pathogen interactions linked to architecture

Corinne Robert, Christian Fournier, Bruno Andrieu, Bertrand Ney
UMR Environnement et Grandes Cultures, Institut National de la Recherche Agronomique
Thiverval Grignon, France 78850
E-mail corresponding authors: {robert or fournier}@grignon.inra.fr

Keywords: Plant pathogen interaction, epidemic model, L-system, *Septoria tritci*, virtual plant model

Introduction

Environmental pollution, quality problems and economic constraints require decreasing the use of pesticides in agriculture. To do so, integrated crop protection aims at developing new strategies that take into account the effects of the agricultural practices on the epidemics development. This requires predicting the development of the epidemics under particular crop practices. This, in turn, requires understanding the effects of the crop canopy on epidemics development.

The aim of our work is to better understand how canopy architecture interacts with the epidemics of foliar diseases. We focus on the case of a splashed-dispersed disease, *Septoria tritici,* which progresses from the base to the top of the plant during the crop growth. The dispersal by splashing induces a limitation on the distance at which spore can travel, while plant development tends to increase the distance between leaves. Differences in flag leaf height and in rate of stem extension could have epidemiological significance. Canopy growth and architecture may thus influence disease development (Royle, 1994). It has been suggested that such a process could be exploited in order to favor disease escape (i.e. to decrease the development of epidemics, Lovell et al., 1997). However, the complexity of the "architecture-pathogen" interactions has not been explored sufficiently to be able to quantify possibilities of disease escape.

Here, we couple a wheat architectural model to a *Septoria tritici* model. We show how this new modeling approach helps to understand and to quantify the effects of canopy architecture development on foliar disease epidemic development.

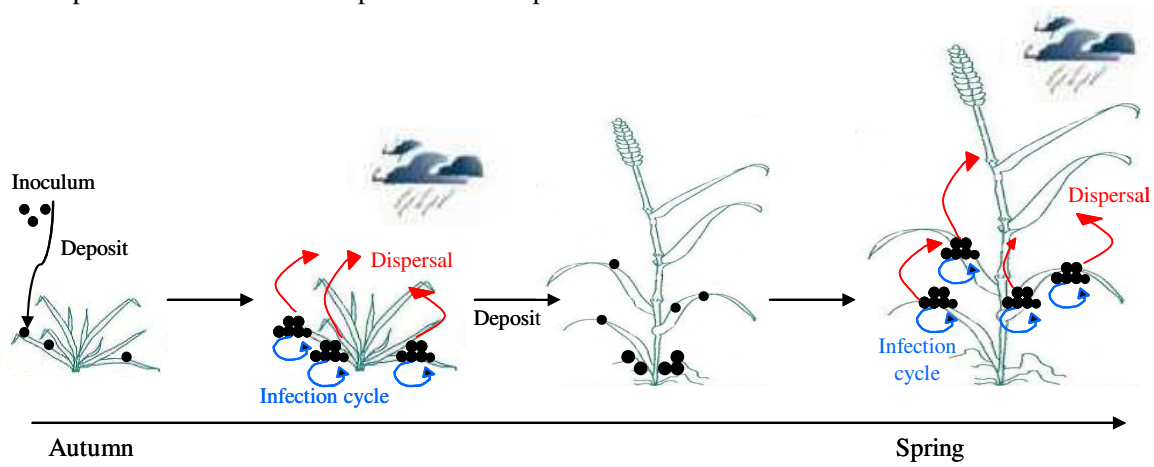

Fig. 1. Schematic of the development of a polycyclic foliar epidemic resulting from the succession of infection cycles (during which spores are produced) and spores dispersal (during which spores are dispersed through the canopy). During the season, as the plants develop, spores reach new green tissue and epidemics progress from the lower infected leaves to the upper leaves of the plants.

Description of the model

The model combines the dynamic architectural model ADEL (Fournier et al. 2003) with a dynamic foliar epidemic model based on Rapilly and Jolivet's model (1976). ADEL allows for simulating the architectural development of a population of wheat plants. To have a good description of green area dynamics, the model was completed with a parameterization of the progress of natural senescence and of tiller dynamics. *Septoria tritici* epidemics are polycyclic, i.e., they result from numerous infection cycles during which spores are produced, alternating with spores dispersal events (Fig.1). We use two sub-models to simulate these processes. The first one simulates the infection cycles, i.e. the development of a lesion from the spore's deposit on the leaf to the death of the lesion. The infection cycle results in spores production. The second one simulates pycnidiospores splash dispersal within and between leaves. We consider two kinds of processes: rain interception, and spores redistribution in the canopy. We compute phyloclimatic input variables for each sub-model.

In the model, plant development and the resulting canopy architecture influence epidemic development by three different effects. (i) They determine the distance between the sources of spores (lesions) and the receptors (green leaf tissues). (ii) They influence rain penetration and spores redistribution in the canopy. (iii) They determine, via the progression of green and senescent leaf tissues, the quantity of leaf area available for lesion development. Reciprocally, the development of lesions on the leaves decreases the green area resulting in a feedback loop in the coupled model.

Model implementation

The model is implemented with the L+C modeling language and runs under L-Studio which provides facilities for structuring the code, C/C++ extensibility and visual control of the simulation (Fig 2).

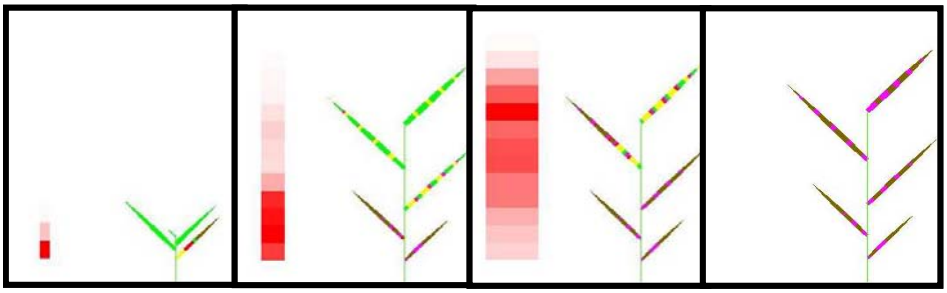

Fig. 2. Snapshots of one of the visual outputs of the model at 4 different time steps during a simulation. Only the main stem of one plant is drawn, as the model considers the canopy as a population of identical individuals. Color spots on the leaves allow to visualize the development of lesions on leaves (latent lesions, sporulating lesions, empty lesions and senescent tissues). The bar on the left is for the visualization of the quantity of spores intercepted by the leaves at different heights after splashing.

The model is developed as an extension of the L-System ADEL wheat model. For dealing with the pathogen, we develop a C-Library handling the functions involved in the dynamics of the infection cycle, and C++ objects for describing the structure of a population of lesions (cohorts of different ages). The coupling with ADEL is done by adding these new objects to leaf parameters. Productions dealing with pathogen development are grouped in a separate table to keep the complete model as modular as possible. The dispersal model is implemented as an environmental program interacting with the L-System using facilities of the communication library of L+C.

Simulations and results

To quantify the effects of the architectural development of the canopy on epidemics development, we vary some of the parameters of the canopy model while keeping the parameters for the infection cycle and spore dispersal constant. We vary phyllochron values, internodes length, the leaf area size and profile, and the angle of the leaves. These parameters modulate the dynamics of spacing between the healthy and the contaminated tissues and influence rain interception and spores interception. We use the classical integrated variable AUDPC (Area Under the Disease Progress Curve) to summarize the effects of canopy architecture on epidemic development. Simulations are done for several climatic scenarios and initial conditions.

Depending on the scenario and on the initial conditions the different canopy parameters have different effects on disease development, indicating the presence of interactions. In most of the simulations, there is almost no effect of changing the leaf area profile, while the biggest effect is observed for varying the value of the phyllochron. The amplitude of these effects also varies for the different leaves of the plants (flag leaf, second leaf etc.).

Discussion

Coupling an architectural model with an epidemic model allows us to perform an analysis of the impact of canopy architecture on the epidemic development, and unravel the numerous interactions existing between canopy structure and epidemics.

This approach may be important for *Septoria tritici*, one of the most damageable wheat foliar disease in Europe nowadays. There is no specific resistance known and pathogens have already evolved resistance to the recent fungicide strobilurine. Therefore, developing crop practices that induce disease escape would be useful. We hope continuation of this work could contribute to revealing traits of canopy architecture that promote disease escape.

A next step is to validate our model which requires specific field experiments. It could also be useful to incorporate the effects of *Septoria tritici* on leaf functioning which might influence disease development.

In a larger view, we think that Functional-Structural Plant Models are an attractive framework to study plant-disease interactions. They offer a practical framework to study effects of microclimate, of the localization and of the physiological status of the organs on disease development.

In conclusion, we hope that this modeling approach, by revealing interactions between canopy structure and disease development is of interest for evaluating the effects of agricultural practices on epidemic development and for designing ideotypes.

References

Fournier C., Andrieu B., Ljutovac S. & Saint-Jean S. 2003. ADEL-wheat: a 3D architectural model of wheat development. In: Plant Growth Modeling and Applications (eds B.-G. Hu & M. Jaeger), pp. 54-66. Tsinghua University Press and Springer, Beijing, China..

Lovell D.J., Parker S.R., Hunter T., Royle D.J., Coker R.R. 1997. Influence of crop growth and structure on the risk of epidemics by *Mycosphaerella graminicola (Septoria tritici)* in winter wheat. Plant Pathology, 46, 126-138.

Rapilly F., Jolivet E. 1974. Construction d'un modèle (episept) permettant la simulation d'une épidémie de Septoria nodorum BERK. sur blé. Revue de Statistique Appliquée. 3, 31-60.

Royle DJ. 1994. Understanding and predicting epidemics: a commentary based on selected pathosystems. Plant Pathlogly, 43, 777-789.

Spray deposition on plant surfaces: a modeling approach

Gary Dorr[1], Jim Hanan [2], Steve Adkins[3], Andrew Hewitt[1] and Barry Noller[1]
[1] Centre for Pesticide Application & Safety, University of Queensland, Gatton, Qld Australia, 4343
[2] ARC Centre for Complex Systems, ACMC, U Queensland, St Lucia, Australia 4072
[3] School of Land, Crop & Food Sciences, U Queensland, St Lucia, Australia 4072
g.dorr@uq.edu.au

Keywords: Spray, L-system, Model

Introduction

Pesticides are widely used in agriculture for the management of pests (weeds, insects or pathogens). They are generally applied as a spray to cover the target (e.g. an insect, leaf surfaces or part of a plant) with pesticide-laden droplets. Spray may, however, be lost to non-target areas within a crop through deposition on to the soil or on non-target plant surfaces. The plant architecture of the crop and weed species can influence the distribution of the spray droplets. The action of wind may also result in spray moving away from the spray area. By selecting and using spray equipment and techniques that maximise deposition of pesticides onto the target it is possible to both maximise the effectiveness of the pesticide application and reduce the amount of off-target deposition and damage.

Droplet movement (spray) models and plant architecture models are being combined using three-dimensional computer modeling techniques based on L-systems (Prusinkiewiez *et al.*, 2000) to develop a probabilistic model of turbulence-related spray transport around various plant architectures (Fig. 1). Measurements of pesticide droplet interactions with the crop canopy from wind tunnel and field studies are being used to refine and validate the combined spray and plant architecture model.

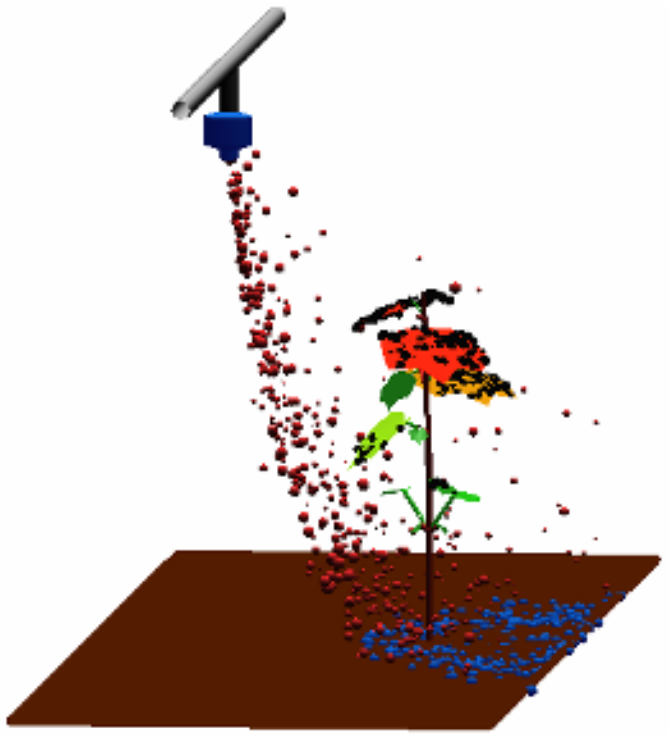

Fig. 1. Simulation of the movement of spray droplets and deposition on a cotton plant

Spray Model

Considerable research has been focused on understanding the movement of sprays from the release point and various computational models have been developed to simulate the spray application process. In general, spray application can be regarded as two-phase fluid flow where liquid droplets are released into an air (gas) flow. To adequately model this situation it is necessary to determine both the airflow in the system and spray movement in the prevailing airflow.

Models of droplet movement in the near nozzle region are often ballistic or particle trajectory models and are based around applying Newton's Second Law of Motion ($F=ma$). The two main forces acting on droplets during a typical spraying situation are gravity and drag. Velocity can be obtained by integrating the equations developed from Newton's Second Law of Motion and the position can be obtained by a further integration (Marchant, 1977). Since only empirical equations are available to describe the drag coefficient a numerical solution is required. A fifth-order variable step Runge-Kutta numerical integration technique has been used.

The trajectory of each droplet is followed as it moves through the atmosphere by dividing it into a large number of small discrete time steps during which the velocity components (u,v,w) of the particle are kept constant. A meaningful estimate of dispersal statistics can be obtained by following a large number of trajectories (Hashem and Parkin, 1991). The spray program (Dorr *et al.*, 2006) includes algorithms to account for droplet evaporation, entrained air and movement of air around the spray, droplet splash (Saint Jean *et al.*, 2004; Vander Wal *et al.*, 2006) and retention.

Plant Architectural Models

Existing functional-structural models of plants developed using cpfg, for example cotton (Room and Hanan, 1995) and sowthistle (Cici, 2007) have been sourced where possible. These have been inserted into the spray model as sub L-systems. An environment call (?E(leaf_id,area)) was added to the existing plant models before the code that generates the plant objects to be tested for interception with the spray droplets. The object is also given a unique identifying code and an extra module is added to enable the color of the object to change depending on the amount of spray impacting the object. The surface area of the object can be specified if it is known, otherwise it is calculated within the environmental program.

Dynamic plant models that show the development of the plant over time have been incorporated into the spray model. Since the time frame for plant growth is much greater than the time steps required for the spray model, the plant is allowed to develop for a predefined number of steps and then stopped before the spraying commences.

Environmental Program

The spray program is linked to an environmental program to determine if spray droplets will impact on plant components. If any plant object intersects a straight line between the start and finish position of the droplet for each time step the identity of the object and impact co-ordinates are returned from the environmental program to the spray program. The finish position of the droplet can be specified by the spray program or calculated within the environmental program. The C programming language used by the environmental program allows greater flexibility and capability than cpfg through the use of modules such as Runge-Kutta routines for calculation of the final droplet position and velocity.

An *Octree Space Partitioning* (OSP) data structure that automatically groups objects hierarchically while avoiding the representation of empty portions of the space is used to locate objects in a three-dimensional space (Yamaguchi *et al.*, 1984). Initially, the octree has only one cell representing the entire space it is modeling and this cell is called the root cell. The tree grows when the number of objects in a cell becomes greater than a pre-set maximum

value. When a cell contains too many objects, only that cell is expanded into 8 children (of equal size), and the objects in the original cell are distributed to its new children.

Using this type of data structure over a simpler one (e.g. a single array containing all objects) can give a dramatic improvement on performance, which becomes apparent when a large number of droplets are added to the system. If a single array was used to contain all objects, then each droplet would need to be checked against each object in the array for intersection in every step. When using an octree, the search can be narrowed down so that only objects in the cell containing the droplet are checked for intersection. Since the plant does not change in size or position during the spraying process a flag is used to keep the previous arrangement once the plant development ceases and prevent the octree being recreated each time step. This significantly reduces the running time of the program.

Comparison with Spray Deposition Measured in a Wind Tunnel

Sow thistle (*Sonchus oleraceus*) plants were grown in 150mm pots in a glasshouse until the advanced rosette stage (Fig. 2). Roundup CT (450g/L glyphosate) was applied to the sow thistle plants using an extended range nozzle (XR110015) and air induction nozzle (TDCFFC110015) at two application rates (57L/ha and 80 L/ha). A fluorescent tracer (pyranine) was added to the spray mix at a rate of 0.5g/L. An electronically controlled traversing mechanism was used within the tunnel to move the spray boom at a constant velocity along the length of the working section.

Fig 2. Example of sow thistle plants at the advanced rosette stage.

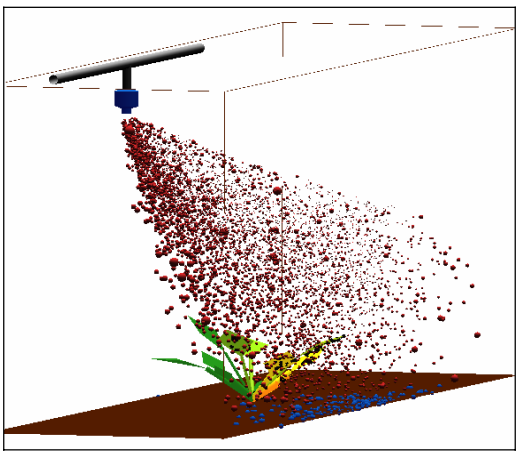

Fig 3. L-Studio simulation of sow thistle plant being sprayed in the wind tunnel.

After spraying all above ground parts of the sow thistle plant was placed in a plastic bag, 60mL of de-ionised water was added to the sample and the bag shaken. The concentration of dye was measured by a calibrated fluorometer (Turner-Sequia model 450). After the dye was removed from the sample the sow thistle leaves were removed, arranged flat on a stand, a photograph was taken and image analysis software (Image Pro v 5.0) was used to measure the surface area of the sample. The amount of dye per unit area was expressed as a percentage of the application rate to enable the two different rates to be compared. Fig. 3 shows an example of the simulation and Fig. 4 shows a comparison of measured spray deposition to modelled spray deposition. All treatments resulted in 100% control of the sow thistle plants.

Conclusion

By combining particle trajectory models with plant architectural models that enable the location of various plant components in 3-D space it is possible to effectively study the removal of spray droplets by various vegetative elements.

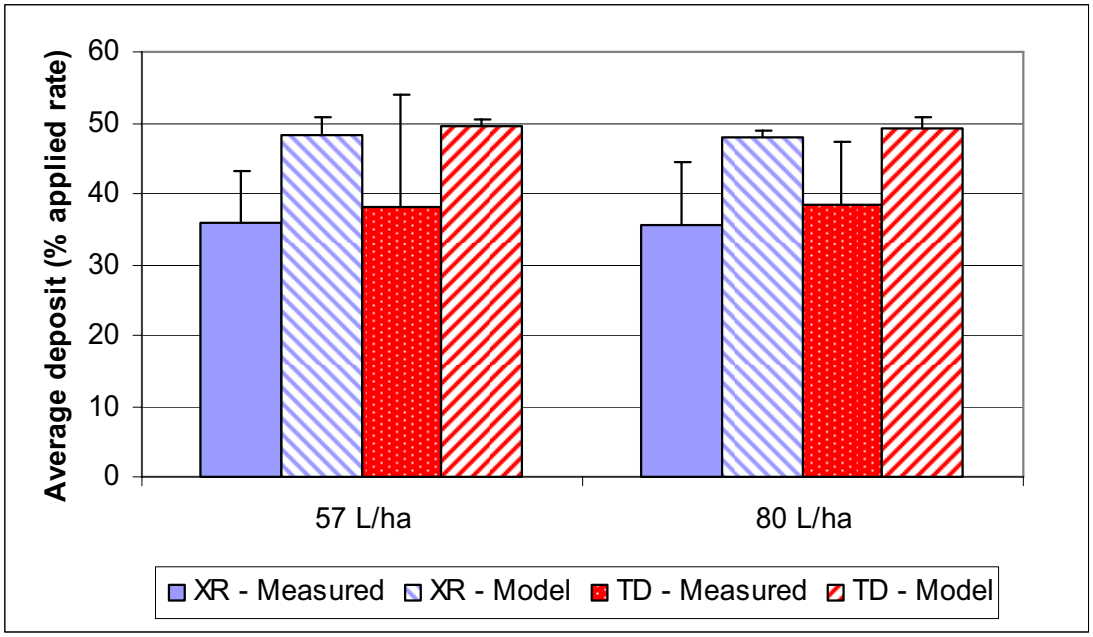

Fig 4. Comparison of measured and modeled spray deposition on sow thistle plants. Error bars show the standard deviation of the results.

Acknowledgments

This project is funded by an Australian Research Council (ARC) linkage project with assistance from Bayer CropScience, Syngenta Crop Protection, Nufarm Australia and Queensland Health Scientific Services.

References

Cici S.Z.H. 2007, Competitive ability of chickpea canopy with sowthistle: an architectural modeling study, Submitted PhD Thesis, University of Queensland.

Dorr G.J., Hanan J., Woods N., Kleinmeulman P., Adkins S. and Noller B. 2006, Simulating Spray Deposition on Plant Canopies Within a Wind Tunnel, *Aspects of Applied Biology*, vol. 77, pp. 395-403.

Hashem A. and Parkin C.S. 1991, A Simplified Heavy Particle Random-Walk Model for the Prediction of Drift from Agricultural Sprays, *Atmospheric Environment Part a-General Topics*, vol. 25, no. 8, pp. 1609-14.

Marchant J.A. 1977, Calculation of spray droplet trajectory in a moving airstream, *Journal of Agricultural Engineering Research*, vol. 22, pp. 93-6.

Prusinkiewiez P., Hanan J. and Mech R. 2000, An L-system-based plant modeling language, *Lecture Notes in Computer Science*, vol. 1779, pp. 395-410.

Room P.M. and Hanan J.S. 1995, Virtual cotton A new tool for research management and training, paper presented to Challenging the future proceedings of the world cotton research conference 1, Melbourne.

Saint Jean S., Chelle M. and Huber L. 2004, Modelling water transfer by rain-splash in a 3D canopy using Monte Carlo integration, *Agricultural and Forest Meteorology*, vol. 121, no. 3-4, pp. 183-96.

Vander Wal R.L., Berger G.M. and Mozes S.D. 2006, The splash/non-splash boundary upon a dry surface and thin fluid film, *Experiments in Fluids*, vol. 40, pp. 53-9.

Yamaguchi K., Kunii T.L. and Fujimura K. 1984, Octree-related data structures and algorithms, *IEE Computer Graphics and Applications*, vol 4, no 1, pp. 53-9

A software for the simulation of rainfall distribution on 3D plant architecture: PyDROP

Samuel Dufour-Kowalski, Céline Bassette and François Bussière
INRA, UR135 Agropédoclimatique de la zone caraïbe, F-97170 Petit-Bourg, Guadeloupe, France (Francois.Bussiere@antilles.inra.fr)

Keywords : rainfall interception, simulation software, triangulation

Introduction

Rainfall interception is highly dependent on plant architecture and affects key plant-environment relationships like plant water budget, soil hydrology and erosion, chemical leaching or disease propagation and development. Banana plantations in the tropics combines plant architectures with important funnelling properties, frequently high rainfall rates and sometimes important agrochemical use. In order to assess erosion and pollution hazards in banana plantations we developed a software simulating rainfall interception by 3D plant architecture.

The DROP model was created to simulate water flows on the plant and predict location of preferential pathways using geometrical and topological information obtained from 3-D digitising. (Bassette, 2005). We presented here new features, assembled in the PyDROP software, that were developed to build virtual plots combining plants of various ages and shapes and simulate rainfall interception on them. For this purpose we (i) account for elementary leaf surfaces water budget including primary and secondary rainfall interception, splashing and storage (ii) developed new algorithms for the triangulation of digitised data of complex leaf shapes (iii) developed a user-friendly computer interface for virtual banana plot construction, output visualisation, and possible use in a software platform (OpenAlea).

DROP model principles

The DROP (Distribution of Rainfall On Plant) model simulates water flows on plants. The DROP-TRI module provides the 3-D representation of the plant as a set of triangles from digitised data and the module DROP-INT simulates rainfall interception and water transfers on these triangles according to plant topology. (Bussière et al., 2002; Bassette and Bussière, 2005).

Rainfall interception simulation

Water retention and splashing from primary rainfall (rainfall) and secondary rainfall (drips from leaves above) were estimated in the DROP model according to surface position and inclination by empirical relationships (Bassette, 2005; Bassette and Bussiere, 2007).

Field data acquisition and triangulation

Virtual mock-up of banana plants up to 6m tall were built using plant coordinates collected with an electromagnetic digitiser (Fastrack Pholemus). For each leaf, points on each edge of the limb and on the midrib were recorded every 1 to 10 cm according to the geometry. Leaves of the top of the canopy, torn by wind, exhibited complicated shapes that cannot be classically simulated by Delaunay triangulation (Loch, 2004). The triangulation of a 3D polygon with potential overlapping is a NP-complete problem (Barequet et al., 1996) and we combined heuristic methods and adaptations of algorithms from Mündermann and Held to solve it (Mündermann et al., 2003; Held, 2001) Digitised points of leaves represented 3D polygons that were projected on planes maximising their surface and then were divided into smaller polygons according to the shortest diagonal between angles from the edge of the limb and the midrib. This process was applied recursively until each polygon was divided into triangles. When it fails, Held algorithm was applied (Fig. 1) (Dufour-Kowalski and Bussière, 2006). When compared to LICOR LI3100 planimeter measurements errors in total leaf area estimates did not exceeded 10% (Bassette and

Bussière 2005). Fifty plants were thus available in the database.

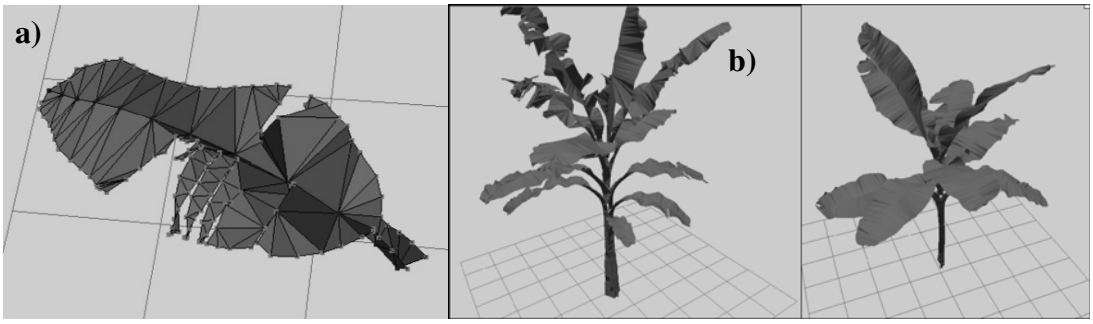

Fig. 1: Visualisation of mock-ups obtained from digitalised and triangulated plants. **a)** Torn leaf triangulation obtained from digitised points on the lamina edges and on the midrib. **b)** Plants of different ages and growth conditions.

PyDROP software:
Previous DROP modules and new features were integrated in a modular and multi-platform software written in Python language. This high level, interpreted and modular language allows either automation scripts for large data set treatments, or easy model improvements and future developments. The modular structure allow the use of modules independently and the further integration in the OpenAlea visual programming software (Pradal et al., 2004).

The main PyDROP modules are:

- The **plant manager** that must be used to build plots with banana plants from the database or imported digitised data files. (Fig. 2).
- The **mesh** module that creates sets of triangles from digitised data as presented above.
- The **rain interception** module that computes splash and storage of rain drops on elementary surfaces and then the transmission of water between surfaces or drippings.
- The **viewer** implemented with PyQt4 and OpenGL libraries that displays local or global plant architecture, visual simulation outputs like map of water flows at the soil surface (Fig. 2).

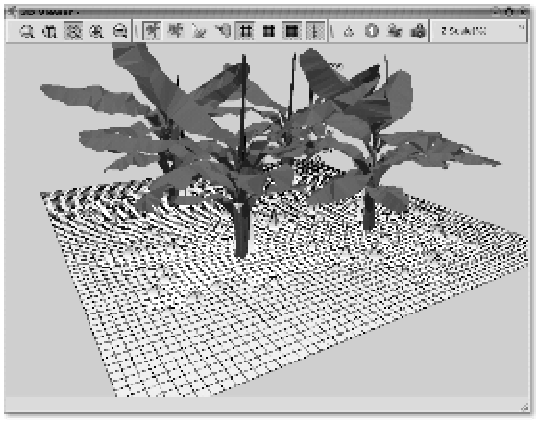

Fig. 2: Screen shot of the PyDROP viewer representing the map of transmitted rainfall below four young banana plants

Use of PyDROP for rainfall distribution assessment
PyDROP was used to compare two patterns of banana plantation for water flow management (Fig. 3). In the square plantation, the rows are evenly separated by a 2.35 m space while in the double row plantation rows are alternatively separated by 1.5 or 3 m. The amount of water stored and splashed on the four same plants were less for square plantation than for double row

plantation except for the stemflow of plant 2 and 4. The stemflow of the plant 2 was greatly reduced by double row plantations because of the increased plant overlapping.

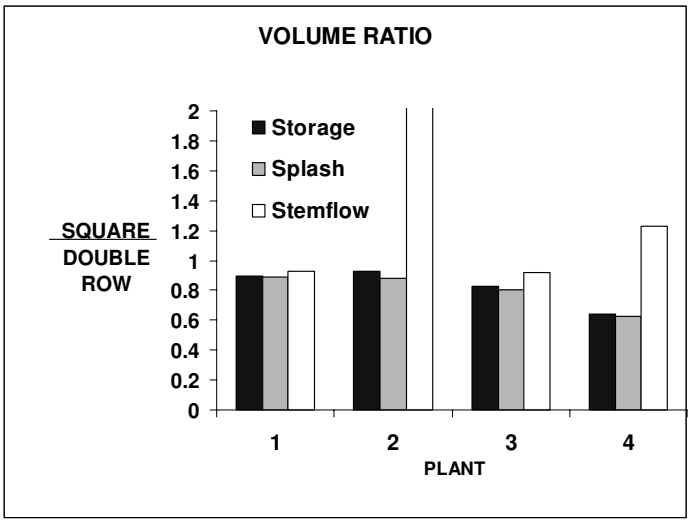

Fig. 3: Comparison of water amount in storage, splash and stemflow for four plants on a square or double rows patterns. Bar graphs represent for each plant, the volume ratio of the two patterns

Conclusion

We developed a new software for the simulation of rainfall interception and redistribution on plants. This software included a database of varied banana plants that can be used to design plant patterns for simulations. New triangulation algorithms were developed for the simulation of complicated banana leaf shapes. Simulation of rainfall interception account for water retention, splashing and funnelling on plant surfaces Outputs of the model were design for water flux assessment on and below the plants. The modular design of the PyDROP model facilitate further use of other geometrical data (i.e for other plant types), or the coupling with other models like radiative transfer models. The future implementation of new processes like energy budget will allow further estimate of surfaces wetness duration and hence the use of the PyDROP model for fungal disease investigation.

References

Barequet, G., Dickerson, M., and Eppstein, D. (1996). On triangulating three-dimensional polygons. In Symposium on Computational Geometry, pages 38–47.

Bassette, C. (2005). Modélisation 3D de l'interception de la pluie par le bananier : Effets des caractéristiques du couvert sur les flux d'eau et d'énergie cinétique transmis au sol. PhD thesis, Université des Antilles et de la Guyane.

Bassette, C. and Bussière, F. (2005). 3-d modelling of the banana architecture for simulation of rainfall interception parameters. Agricultural and Forest Meteorology, 129 :95–100.

Bassette, C. and Bussière, F. (2007). Partitioning of splash and storage during raindrop impacts on banana leaves. Accepted in Agricultural and Forest Meteorology

Bussière, F., Solmon, F., and Fouéré, A. (2002). Implementation and evaluation of drop, a model for the simulation of rainfall distribution below plants described in 3d. Agronomie, 22 :93–103.

Dufour-Kowalski, S. and Bussière, F. (2006). Measurement and computer representation of banana plants for environmental studies. In 15th Meeting of the Caribbean Academy of Sciences.

Held, M. (2001). FIST : Fast industrial-strength triangulation of polygons. Algorithmica, 30(4) :563–596.

Mündermann L., MacMurchy P., Pivovarov J., and Prusinkiewicz P.. (2003) Modeling lobed leaves. In Proceedings of CGI 2003, pp. 60-65.

Loch, B. (2004). Surface fitting for the modelling of plant leaves. PhD thesis, University of Queensland.

Pradal, C., Dones, N., Godin, C., de Reuille, P. B., Boudon, F., Adam, B., and Sinoquet, H. (2004). Alea : A software for integrating analysis and simulation tools for 3d architecture and ecophysiology. In Proceedings of the 4th International Workshop on Functionnal Structural Plant Models, pages 406–407.

A 3 dimensional physical model to predict temperature dynamics within fruits in response to environment changes

Saudreau Marc[1], Sinoquet Hervé[1], Marquier André[1], Adam Boris[1]
Santin Olivier[2] and Chelle Michaël[2]

[1] UMR547 PIAF, INRA, UNIV BLAISE PASCAL, 234 Avenue du Brézet, F-63100 CLERMONT FERRAND, France
[2] UMR1091, Environnement et grandes cultures, INRA, F-78850, Thiverval-Grignon, France

marc.saudreau@clermont.inra.fr

Keywords: Fruit, Temperature, Dynamics, Three-dimensional, Microclimate, Modeling

Introduction

Numerous biological processes involved in the development of fruits depend on temperature. Consequences on fruit quality such as size, taste, appearance are straightforward and well established (Tomes, 1963). Moreover, temperature gradients within fruits are of economic significance because of sunburn injury (Glenn & al, 2002), and of larval development (Kührt & al., 2005), with loss of yield. Fruit temperature is then a crucial parameter if one wants to investigate impacts of climate change or to develop strategies to control fruit or larval developments.
Models of organ temperatures have been already developed in the past but they do not predict both temporal and spatial temperature variations within fruits (Thorpe, 1974; Smart and Sinclair, 1976). Some models only estimate spatial average of organ temperature. However, in thick organs such as fruits, spatial distribution of temperature is not uniform and gradients of more than 10°C may occur in orchard. This raises the question of what the actual temperature of a fruit is. Other models give the thermal gradient within spherical fruits but they assume steady heat fluxes at fruit surface. The steady state assumption for boundary conditions leads to steady solutions but in orchard situation the microclimate fluctuates and a relevant model should take into account such temporal variations.
The model presented below is one solution to achieve this goal, namely to mimic temporal and spatial temperature dynamics within fruits in response to variations of atmospheric conditions.

Model description

Spatial and temporal variations of temperature in a fruit are governed by its heat budget. Considering an organ surrounded by moving air, factors involved in its heat budget are environmental factors as solar radiation, air temperature, air humidity, and wind intensity, as well as internal parameters as heat capacity, surface conductance to water vapour diffusion, metabolism activity, moisture content or heat transfer from the plant to the fruit.
This system is complex to model since numerous physical and physiological processes are coupled. Nevertheless, some *a priori* and fruit physiology based assumptions can be made to reduce this complexity. For example, the heat released from the metabolism activity within fruit and the energy exchange between fruit and plant are small enough in comparison to heat fluxes coming from the environment and were neglected. Also, fruits are known to exhibit diurnal diameter variations attributed to changes in hydration. However to simplify the system, the amount of water in fruit was, *a priori*, assumed to be constant in time. From these hypotheses the heat transport process within a fruit is only governed by heat conduction without any source term. Temperature dynamics were then modeled by Fourier's law (Eq. 1a):

$$\begin{cases} \dfrac{\partial}{\partial t}(\rho C_P.T) = \vec{\nabla}.(\vec{\vec{k}}\vec{\nabla}T) & \text{(1a)} \\ \left[-\vec{\vec{k}}\dfrac{\partial T}{\partial \vec{n}}\right]_{r\equiv R} = \Phi + \lambda_E + R & \text{(1b)} \end{cases}$$

where T (K) is the temperature, ρ (kg m^{-3}) is the density, C_p (J kg^{-1} K^{-1}) is the specific heat capacity and $\vec{\vec{k}}$ (W m^{-1} K^{-1}) is the thermal conductivity of the organ. $\vec{\vec{k}}$ was assumed to be nearly isotropic so the deviatoric part of $\vec{\vec{k}}$ was set to zero. Diagonal elements of $\vec{\vec{k}}$ can vary in space and over time to mimic moisture content variations or changes of tissue conductivity - the skin, the pit - within fruits.

Energy exchanges between the fruit and the surrounding air were modeled by specifying that the normal heat flux at any point of fruit surface was equal to the loss or gain of sensible energy by convection (Φ), the loss of energy by transpirational cooling (λ_E) and the energy exchange by radiation (R) (Eq. 1b). Beyond the modeling of Φ, λ_E and R, an important point is that these heat fluxes are function of space and time to mimic variations of the environment.

To solve the system composed from Eqs. 1a and 1b numerically, a finite volume formulation was chosen. Ellipsoidal fruits were divided into n_r radial elements, n_θ azimuthal elements and n_φ polar elements. From this mesh, spatial derivatives were evaluated following Patankar's previous work (Patankar, 1980), and time integration was based on an implicit formulation. The sparse linear system obtained was solved by a biconjugate gradient stabilized method (BICGSTAB, Van der Vorst, 1992). The resulting implicit scheme was first-order accurate in time and second-order accurate in space.

Model predictions

To assess the ability of the model to handle realistic fruit and microclimate conditions, experimental data collected during June 2005 on isolated fruits (3 apples cv. Golden, 3 apples cv. Redchief and 3 peaches cv. Alexis) were used. Inputs of the model were fruit properties measured or collected from literature, and microclimate variables measured such as air temperature, air humidity, wind velocity, solar and atmospheric radiation. The comparison between measured and simulated fruit temperature (at fruit surface and fruit core during one day) was very good (Figs. 1 and 2). Statistical analyses from all fruits, led to determination coefficients R^2 ranging from 0.971 to 0.977 and RMSE ranging from 0.7°C to 0.8°C (Fig. 1). Daily temperature dynamics at fruit surface and within fruits were very well captured by the model (Fig. 2).

Beyond temperature dynamics within fruits, the model can provide also useful information about heat transfer within fruits. At each point of fruit surface the heat balance dynamics can be computed. This is an important point since heat fluxes are related to the temperature at fruit surface which is not known. Therefore their values can not be calculated *a priori*. Heat flux simulation performed with our experimental conditions showed that the amount of heat released by evaporation was negligible. Thus, temperature dynamics only resulted from a balance between radiation and convection processes.

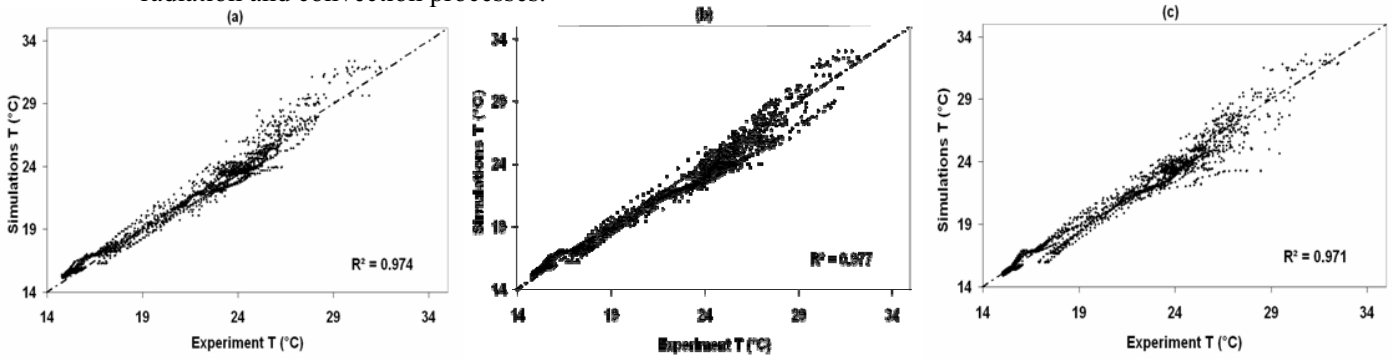

Figure 1: Measured *vs.* simulated temperature for apple cv. Golden (a), apple cv. Redchief (b) and peach (c). The long-dashed lines represent 1:1 relationships.

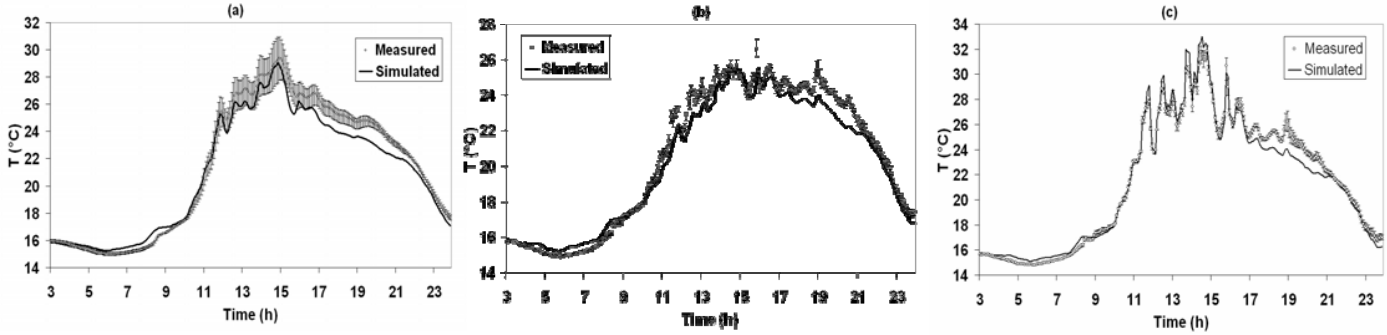

Figure 2: Daily variation of measured and simulated temperature of "Redchief" apple. At fruit center, (a). On the shaded face (bottom) (b). On the sunlit face (top) (c). Error bars represent the variations of measured temperature between 3 fruits.

From this study and from our point of view, the conduction process within fruits is not the main problem in modeling effects of microclimate on temperature of fruits. Finally, the proposed model enables a satisfying estimation of the within-fruit temperature distribution, if boundary conditions (surface irradiance, surrounding air temperature, humidity and speed) are known. Thus, using this model for attached fruits in orchard condition would require the characterization or modeling of the radiation transfer and air circulation within the tree canopy, which is a highly challenging task. Specialized models are now available to handle microclimate components within a tree canopy (Willaume & al, 2004, Finnigan, 2000). Therefore these models should be combined with our fruit temperature model in order to study temperature dynamics within fruits in orchards submitted to new training systems or global climate change scenarii.

Acknowledgments

This research has been supported by a grant from the Environment and Agronomy department of the French National Institute for Agricultural Research (INRA). Authors gratefully acknowledge Drs L. Guilioni and J.J. Longuenesse for their help during the field experiments.

References

Finnigan, J., 2000. Turbulence in plant canopies. Annual Review of Fluid Mechanics 32, 519–571.

Glenn, D. M., Prado, E., Amnon, E., McFerson, J., Puterka, G. J., 2002. A reflective, processed-kaolin particle film affects fruit temperature, radiation reflection, and solar injury in apple. Journal of the American Society for Horticultural Science 127 (2), 188–193.

Kührt, U., Samietz, J., Dorn, S., 2005. Thermoregulation behaviour in codling moth larvae. Physiological Entomology 30 (1), 54–61.

Patankar, S., 1980. Numerical Heat Transfer and Fluid Flow. Hemisphere Publishing Corporation, US.

Smart, R. E., Sinclair, T. R., 1976. Solar heating of grape berries and other spherical fruits. Agricultural Meteorology 17 (4), 241–259.

Thorpe, M., 1974. Radiant heating of apples. J. Appl. Ecol. 11, 755–760.

Tomes, M., 1963. Temperature inhibition of carotene synthesis in tomato. Botanical Gazette 11, 180–185.

Van der Vorst, H., 1992. Bicgstab: A fast and smoothly converging variant of bi-cg for the solution of nonsymmetric linear systems. SIAM J. Sci. Stat.Comput. 13, 631–644.

Willaume, M., Lauri, P. E., Sinoquet, H., 2004. Light interception in apple trees influenced by canopy architecture manipulation. Trees: Structure and Function 18 (6), 705–713.

Simulation of Apple Tree Development Using Mixed Statistical and Biomechanical Models

Colin Smith[1] Christophe Godin[2] Yann Guédon[2]
Przemyslaw Prusinkiewicz[3] Evelyne Costes[1]

[1] UMR DAP INRA/AgroM/CIRAD/UMII, Architecture et Fonctionnement des Espèces Fruitières (AFEF) Team, Montpellier, France (smithco@gmail.com, costes@supagro.inra.fr)
[2] UMR DAP INRA/AgroM/CIRAD, Virtual Plants Team, Montpellier, France (godin@sophia.inria.fr, guedon@cirad.fr)
[3] Department of Computer Science, University of Calgary, Canada (pwp@cpsc.ucalgary.ca)

Keywords: Tree simulation, L-systems, Biomechanics, Markov models, *Malus x domestica* Borkh.

1 Introduction

In the last twenty years, architectural studies in horticulture have led to a better understanding of fruit tree development and to improvements in tree and orchard management [7]. Tree architecture plays a key role in foliage distribution and consequently in light interception and carbon acquisition, which in turn strongly affect the reproductive growth of fruit trees. To integrate the acquired knowledge, we addressed the question of simulating the architecture of a developing tree over time. The objective of this project was to bring together the development of topology and geometry in a single simulation that characterises the architecture of an apple tree over time. As indicated previously [9, 3, 4], the simulation of shoot bending due to the weight of growing organs is particularly challenging because it is difficult to infer the mechanism of bending from direct measurements. To further the exploration of the bending dynamics in a developmental context, we have created an L-system simulation of a developing apple tree, called MAppleT (***M**arkov **Apple T**ree*), which is herein presented.

2 An Integrated Simulation

In MAppleT, a tree's architecture is determined by two types of information: the tree topology (*i.e.*, the connections between plant entities, such as the sequence of the growth units and the placement of the organs) and the temporal co-ordination of developmental events, which includes both morphogenesis and organ growth. From this information, a tree's geometry is determined by a biomechanical simulation.

2.1 Development of Tree Topology

As current mechanistic models do not represent branch distribution with sufficient precision, the topology of the trees was modelled using two types of Markovian models [10]. The first model captures the branching structure of the shoot and the second model captures the sequence of annual shoot types along the axes. The Markovian models used in MAppleT were originally devised to perform purely topological simulations of apple trees [16]. In these simulations, branching patterns were generated by hidden semi-Markov chains (HSMCs), with parameters depending on the shoot type (*i.e.*, long, medium, or short shoots). The elements of a sequence generated from one of these HSMCs describe the fate of the lateral buds in the following year. The type of the terminal shoot is determined between successive annual growth cycles using transition matrices of a simple Markov chain, which are selected according to the type of the current shoot and the age of the tree [8]. A distribution of shoot lengths, measured in the number of metamers, is attributed to each shoot type, whether in terminal or lateral position.

2.2 Chronological Control of Morphogenesis and Organ Dimensions

The parameters used in MAppleT originate from a number of studies performed by the AFEF team. The values are mostly from several independent datasets collected on the Fuji cultivar. Where data were unavailable from Fuji, values from other apple cultivars were used (*e.g.*, for the plastochron, diameter growth and wood properties). In each shoot category, new metamers are produced with a plastochron of three days [6], and each

metamer elongates over ten days. The final length of internodes depends on their position in the shoot, such that the internodes at the beginning and end of each shoot are shorter than those of the middle. Thus the lengths of the internodes depend on the zone along the shoot to which they belong. These values were estimated from data measured on Fuji trees.

The widths of the internodes are controlled with the pipe model [17]. The inputs to this model are the radii of leaf petioles and the radii of terminal apices. Since observations showed that the diameter at the shoot base increases after the cessation of primary growth [5], we augmented the pipe model with an additional hypothesis, which postulates that the diameter of the terminal apices increases over the season proportionally to the length of the shoot.

In Fuji trees, a leaf grows sigmoidally over twelve days, at which time it reaches maturity [14]. If a metamer supports an inflorescence, the flowers last for ten days and, if it becomes a fruit, the fruit lasts until harvest (approximately one hundred and fifty days). We assumed that each inflorescence develops into, at most, one fruit. The mass of a fruit increases according to the expolinear model [13], here calibrated to the fruit of Fuji.

2.3 Determination of Plant Geometry Using Biomechanics

The bending of each internode is calculated according to its biomechanics. The model used in MAppleT is derived from the work of Taylor-Hell [19], which, in turn, is based on Fournier's metaphor of bending beams applied to woody stems [9] and its initial implementation using L-systems [11]. Biomechanical simulations employ the fast information transfer construct in L-systems [12], and are divided into two phases [15]. First, bending moments acting on individual nodes are calculated in a backward scan of the L-system string (information is passed basipetally). Second, the shape of the branch is calculated in a forward (acropetal) scan of the string, taking these bending moments into account. As the modification of the branch shape changes the values of the bending moments, this computation of moments and shapes is carried out iteratively, until an equilibrium is found. The simulation takes into account negative geotropism, the elasticity of the wood, the amount of locally produced reaction wood, and the secondary branch growth, which results in a branch shape memory [2, 3].

3 Simulation Outputs

The architectural development of a typical tree produced by MAppleT is shown in Figure 1. To assess the model, the simulated trees were compared to two digitised Fuji apple trees [8], using a common set of descriptors. These two trees do not constitute an enterely independent dataset, because they were also used to estimate HSMC models and the value of the pipe model exponent (while others parameters came from independent datasets). However, the geometry, and consequently the set of descriptors used to perform the comparisons were considered independent between the digitised and simulated trees. The comparisons were performed at different scales of observation and for different values of input parameters. At small scales, descriptors of the shoots' morphology included, for example, the basal diameter and shoot length. At larger scales, envelopes encompassing a tree's crown and fruiting branches were calculated.

Figure 2 shows that, visually, the simulated trees are qualitatively close to the observed Fuji trees. An examination of the envelopes around the trees' crowns and branches revealed that the bending of the branches was slightly underestimated. A sensitivity analysis of the graphical and numerical outputs, as they vary over a range of parameters, led us to identify which parameters have large effects on a tree's form and which ones require further experimental data to improve the model. For example, the shoots' basal diameters were underestimated in the first and second order branches within the explored range of values of the pipe model exponent, while the same exponent value produces basal diameters close to those observed in higher-order branches (Figure 3). The simulated secondary growth dynamics, resulting from the augmented pipe model, is similar in character to those of observed axes: there is an initial rapid growth followed by a slower growth that continues after primary growth has ceased (Figure 4).

By integrating physical and architectural parameters calibrated to observed trees, MAppleT produces simulated trees that are subject to gravity and account for known growth dynamics. Presently, MAppleT still has a number of limitations that may be addressed in further research. Of particular note is the absence of gravimorphic responses to branch bending (*e.g.*, the preference of long shoots to grow from buds in dorsal positions). Nevertheless, the data obtained from the simulated trees produced by MAppleT complement those obtained with digitisation methods [18]. Simulated trees can be sampled continually, while digitisation is a time consuming process, typically done only once annually. Though MAppleT is currently used for synthesising existing data, it is also a platform appropriate for future *in silico* explorations, such as examining light interception or the interaction of architecture and physiology, as initiated in L-PEACH [1].

4 Acknowledgements

We thank Julia Taylor-Hell for kindly making her model of branch bending in poplar trees available, and likewise Michael Renton for his model of topological simulations of apple trees. We also thank Fredéric Boudon for his assistance on the Geom module from PlantGL, Jean-Jaques Kelner and Jean-Luc Regnard for allowing us to use their observations of apple trees, and Brendan Lane for his editorial assistance.

References

[1] M. Allen, P. Prusinkiewicz, and T. Dejong. Using L-systems for Modeling Source-Sink Interactions, Architecture and Physiology of Growing Trees: the L-PEACH Model. *New Phytologist*, 166(3):869–880, June 2005.

[2] T. Alméras. *Aquisition de la Forme des Axes Ligneux d'un An chez Trois Variétés d'Abricotier: Confrontation de Données Expérimentales à un Modèle Bioméchanique.* PhD thesis, École Nationale Supérieure Agronomique de Montpellier, April 2001.

[3] T. Alméras, J. Gril, and E. Costes. Bending of Apricot Tree Branches under the Weight of Axillary Growth: Test of a Mechanical model with Experimental Data. *Trees*, 16(1):5–15, January 2002.

[4] P. Ancelin, T. Fourcaud, and P. Lac. Modelling the Biomechanical Behaviour of Growing Trees at the Forest Stand Scale. Part I: Development of an Incremental Transfer Matrix Method and Application to Simplified Tree Structures. *Annals of Forest Science*, 61(3):263–275, 2004.

[5] S. Benzig. Patterns of Vegetative and Reproductive Growth in Apple (*Malus domestica* Borkh.) – Crop Load Effects in 'Golden Delicious' and the Self-Thinning INRA-Hybrid 'X 3274'. Master's thesis, Faculty of Wiesbaden Geisenhiem, 1999.

[6] E. Costes and P.-E. Lauri. *Processus de Croissance en Relation avec la Ramification Sylleptique et la Floraison chez le Pommier*, pages 41–50. INRA Editions, November 1993.

[7] E. Costes, P.-E. Lauri, and J.-L. Regnard. Tree Architecture and Production. *Horticultural Reviews*, 32:1–60, 2006.

[8] E. Costes, H. Sinoquet, J. Kelner, and C. Godin. Exploring Within-tree Architectural Development of Two Apple Tree Cultivars Over 6 Years. *Annals of Botany*, 91(1):91–104, January 2003.

[9] M. Fournier, B. Chanson, D. Guitard, and B. Thibaut. Mécanique de l'Arbre sur Pied : Modélisation d'une Structure en Croissance Soumise à des Changements Permanents et Évolutifs. 1. Analyse des Contraintes de Support. *Annales des Sciences Forestières*, 48(5):513–525, 1991.

[10] Y. Guédon, D. Barthélémy, Y. Caraglio, and E. Costes. Pattern Analysis in Branching and Axillary Flowering Sequences. *Journal of Theoretical Biology*, 212(4):481–520, October 2001.

[11] C. Jirasek, P. Prusinkiewicz, and B. Moulia. Integrating Biomechanics into Developmental Plant Models Expressed using L-systems. In H.-C. Spatz and T. Speck, editors, *Plant biomechanics 2000, Proceedings of the 3rd Plant Biomechanics Conference*, pages 615–624, Freiburg-Badenweiler, August 2000. Georg Thieme Verlag.

[12] R. Karwowski and P. Prusinkiewicz. Design and Implementation of the L+C Modeling Language. *Electronic Notes in Theoretical Computer Science*, 86(2):1–19, 2003.

[13] A. Lakso, Corelli L. Grappadelli, J. Barnard, and M. C. Goffinet. An expolinear Model of the Growth Pattern of the Apple Fruit. *Journal of Horticultural Science*, 70(4):389–394, 1995.

[14] C. Massonnet. *Variabilité Architecturale et Fonctionnelle du Système Aerien chez le Pommier (Malus domestica borkh.): Comparaison de Quatre Cultivars par une Approche de Modélisation Structure-Fonction.* PhD thesis, École Nationale Supérieure Agronomique de Montpellier, December 2004.

[15] P. Prusinkiewicz, R. Karwowski, and B. Lane. The L+C Modelling Language. In J. Vos, L. Marcelis, P. de Visser, P. Struik, and J. Evers, editors, *Proceedings of the Frontis Workshop on Functional-Structural Plant Modelling in Crop Production, Wageningen, The Netherlands, 5-8 March, 2006*, pages 27–42. Springer, Berlin, 2007.

[16] M. Renton, Y. Guédon, C. Godin, and E. Costes. Similarities and Gradients in Growth Unit Branching Patterns during Ontogeny in Fuji Apple Trees: a Stochastic Approach. *Journal of Experimental Botany*, 57(12):3131–3143, September 2006.

[17] K. Shinozaki, K. Yoda, K. Hozumi, and T. Kira. A Quantitative Analysis of Plant Form – The Pipe Model Theory I. Basic Analyses. *Japanese Journal of Ecology*, 14(3):97–105, June 1946.

[18] H. Sinoquet, P. Rivet, and C. Godin. Assessment of the Three-dimensional Architecture of Walnut Trees Using Digitising. *Silva Fennica*, 31(3):265–273, 1997.

[19] J. Taylor-Hell. Biomechanics in Botanical Trees. Master's thesis, University of Calgary, September 2005.

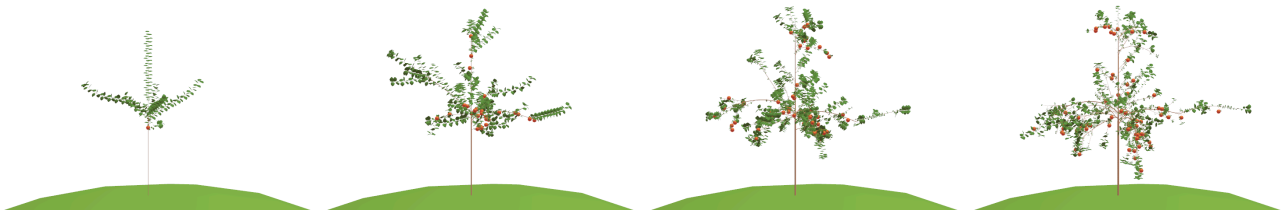

Figure 1: A simulated apple tree from the second through fifth year of growth

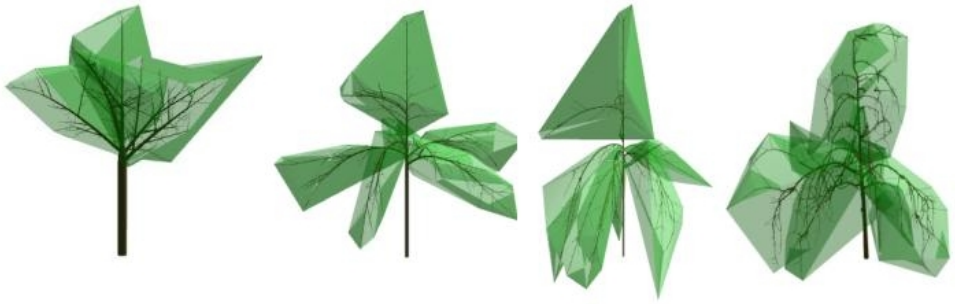

Figure 2: Fuji tree shapes in the fifth year of growth. From left to right, three trees simulated with different values of the pipe model exponent ($P = 2.0$, $P = 2.5$ & $P = 3.0$), and a digitised tree. The envelopes on the trees are calculated for branching systems originating in the second year of growth.

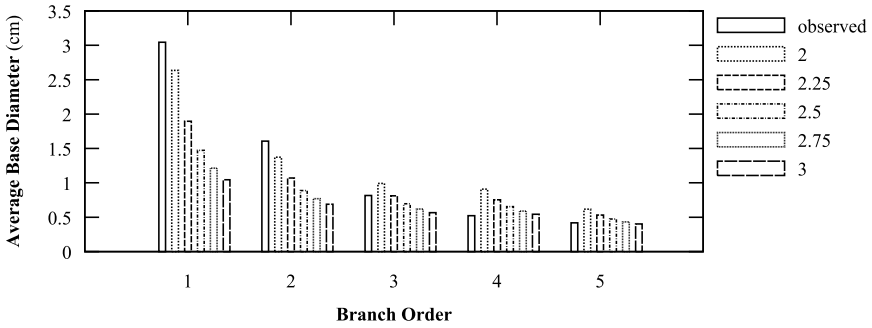

Figure 3: Variation of the average base diameter of the axes in different branching orders, with respect to P, the value of exponent in the pipe model

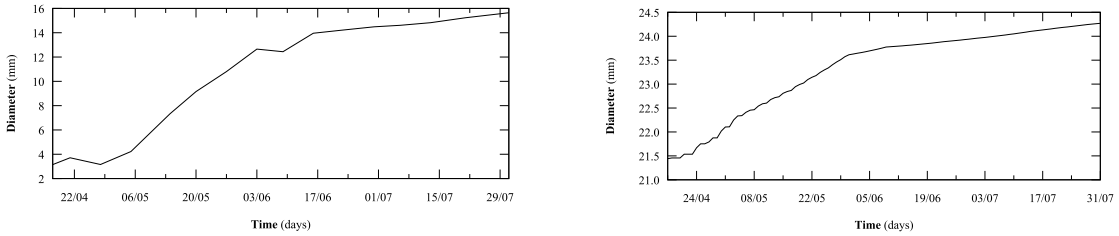

Figure 4: Comparison of the basal diameters of a first-order branch over a season from (Left) an observed tree and (Right) from a simulated tree

The role of structural and life-history tradeoffs in plant architecture: a model study of *Protea lepidocarpodendron* (Proteaceae)

Lawrence D. Harder[1], Brendan Lane[2], and Przemyslaw Prusinkiewicz[2]
[1]Department of Biological Sciences, University of Calgary, Calgary, Alberta, Canada T2N 1N4
[2]Department of Computer Science, University of Calgary, Calgary, Alberta, Canada T2N 1N4

Keywords: biomechanics, L-system, evolution, development, uncertainty

Summary: We present research in progress, aimed at explaining the tradeoffs between vegetative and reproductive structures in the architecture of Protea. The species of interest, *Protea lepido-carpodendron*, reproduces only after a fire that kills it. We aim at using a biomechanical developmental functional-structural model to demonstrate that *Protea lepidocarpodendron* is adapted to the statistical distribution of fires over time.

The bodies of most plants are comprised primarily of vegetative structures, with reproductive organs being comparatively ephemeral and involving relatively little investment. The greater investment in vegetative structures reflects their fundamental roles in resource capture and distribution, and in maintaining a plant's structural integrity. Nevertheless, from an evolutionary perspective, vegetative structures exist ultimately to support and nourish reproductive organs, which directly determine a plant's genetic contributions to subsequent generations. Thus, natural selection should favor plant architectures and mechanical characteristics that promote reproductive output within a specific environment. Conflicting demands for vegetative and reproductive functions may lead to vegetative characteristics that do not maximize photosynthetic capacity, resource deployment, and/or mechanical stability.

Many upright, shrubby *Protea* species of the Western Cape in South Africa (Midgley and Kruger 2000; see also Bond and Maze 1999) illustrate this conflict. These species produce orthotropic modules, which form sympodia with no distinct main stem (Fig. 1). Each module bears a terminal capitulum surrounded by showy involucral bracts. After flowering, a capitulum matures into a woody cone, which persists for several years, as long as the subtending stem maintains its evergreen, sclerophyllous leaves.

Figure 1. *Protea lepidocarpodendron*. Left, form of ~14-year old plant. Center, changes in branch width at a branching point. Right, a plant after fire reveals sympodial architecture and the distribution of cones.

In general, the species of interest occupy relatively open habitats that burn with an average frequency of 10–20 years. Seed dispersal occurs only when the heat of a fire opens the serotinous cones in a living canopy, releasing the seeds that can establish seedlings only in mineral soil exposed by fire. *Protea lepidocarpodendron* and similar species die during fire, so each individual reproduces once, when it dies, and its effective seed production depends on the number of cones in a shrub's canopy when it is burned. If fire does not occur for a long period, plants can become so large that they collapse during intense winds (Midgley and Kruger 2000). Such plants die without reproducing. We thus hypothesize that the vegetative structure of *Protea* is adapted to probability density distribution of inter-fire intervals: the plant does not invest in the creation of a long-lasting vegetative structure, but is built to maximize the number of reproductive structures at the time of its death by fire.

To test this hypothesis, we developed a biomechanical model of *Protea* trees (Fig. 2). The sympodial architecture of the trees is generated using an L-system implementation (Prusinkiewicz and Remphrey 2000) of a variant of Leeuwenberg's architectural model (Hallé et al. 1978). In Leeuwenberg's model, the growth of branches ends with the formation of terminal inflorescences; the thrust of the development then transfers to the lateral branches. In our model, a terminal bud may also initiate another annual growth increment or abort. According to observations of *Protea* in nature, continuation of a branch is a likely event in young trees, whereas production of an inflorescence is the usual event in older trees. The fate of buds (initiation or continuation of a branch, production of a terminal capitulum, or abortion) depends on the amount of photosynthate produced by the standing crop of leaves, which are allocated to specific buds using a stochastic process (Gillespie's [1976] algorithm). The distribution of shoot lengths is modeled stochastically according to measured data. The cost of growing a shoot includes its primary growth and the secondary growth of subtending branches, as needed to develop vasculature (pipe model, Shinozaki et al. 1964). On this basis, branch shape is modeled as the combined effect of gravity, reorientation of branch directions due to the production of reaction wood, average wind directions, and tropisms, using the biomechanical model of branch shape proposed by Fournier et al (1994) and adapted to L-systems by Jirasek et al. (2000) and Taylor-Hell (2005). A new element of the model is the combination of turtle geometry, which makes it possible to conveniently specify branching architecture of the tree (Prusinkiewicz and Lindenmayer 1990), and affine geometry, which is convenient in biomechanical simulations (Prusinkiewicz et al. 2007a).

Another novel element is the simulation of branch breaking, which occurs when bending moments exceed a threshold value. As an approximation, we assume that this threshold depends on the allocation of resources available to the tree: greater allocation to individual branches increases their resistance to breaking. This process creates a competitive situation, whereby a given pool of resources can be used to create either a more durable structure or one that ramifies more frequently. Competition is intertwined with developmental decisions: the plant may produce more capitula and cones at the expense of vegetative development, or invest in more extensive vegetative development with the prospect of supporting more capitula and cones in the future.

To our knowledge, the perspective that plant form represents an evolutionary compromise between vegetative and reproductive function has not been studied previously using simulation models. Early plant (tree) models addressing the question of the optimality of plant form focused on the influence of branching patterns on a plant's total leaf area (e.g., Horn 1971, Honda and Fisher 1978). Subsequent analyses accounted for the reduced energy-gathering efficiency that occurs when a plant's leaves shade each other (reviewed by Fisher 1992, see also Pearcy et al. 2005). In addition, more recent models have incorporated two mechanical properties of branched structures that impose functional limits on their size and form (e.g., Niklas 1986, Farnsworth and Niklas 1995). First, branches must be able to support themselves and the organs that they produce, with dissimilar branching patterns having different implications for structural integrity (King and Loucks 1978, Brüchert et al. 2003). Second, branching constricts the vessels that distribute water, nutrients, and products of photosynthesis and metabolism, thus

highly branched plants distribute these chemicals less efficiently (Zimmermann 1978). In contrast to this historical emphasis on vegetative function, our model aims at the exploration of tradeoffs associated with reproduction. The described model provides the foundation for this exploration, which is currently in progress.

Figure 2. A biomechanical model of a 5-year-old protea. Top: trees generated using (left to right) low, medium and high photosynthate allocation to secondary growth. The low-allocation structure exhibits highest branching and the most fruit, but is also subject to gravitational stress at the base of lower branches (shown in red in color figures), and so is more susceptible to breakage than the high-allocation structure. Bottom: the same trees, with the branches with the highest gravitational stress broken off. The low-allocation structure has suffered the most extensive damage, the high-allocation structure has experienced none, but the tree with medium allocation retains the most fruit and so would have highest fitness if fire now killed the trees and produced suitable conditions for seed germination.

References

Bond, W. J., and K. E. Maze. 1999. Survival costs and reproductive benefits of floral display in a sexually dimorphic dioecious shrub, *Leucadendron xanthoconus*. *Evolutionary Ecology* 13:1-18.

Brüchert, F., O. Speck and H.-C. Spatz. 2003. Oscillations of plants' stems and their damping: theory and experimentation. *Philosophical Transactions of the Royal Society, London, Series* B 358: 1487-1492.

Farnsworth, K. D. and K. J. Niklas. 1995. Theories of optimization, form and function in branching architecture in plants. *Functional Ecology* 9: 355-363.

Fisher, J. B. 1992. How predictive are computer simulations of tree architecture? *International Journal of Plant Sciences* 153(Supp.): S137-S146.

Fournier, M., H. Bailleres, and B. Chanson. 1994. Tree biomechanics: growth, cumulative prestresses, and reorientations. *Biomimetics* 2: 229-251.

Gillespie, D. T. 1976. A general method for numerically simulating the stochastic time evolution of coupled chemical reactions. *Journal of Computational Physics* 22: 403-434.

Hallé, F., R.A.A. Oldeman and P.B. Tomlinson. 1978. *Tropical Trees and Forests: An Architectural Analysis*. Springer, New York.

Honda, H., and J. B. Fisher. 1978. Tree branch angle: maximizing effective leaf area. *Science* 199: 888-890.

Horn, H. S. 1971. *The Adaptive Geometry of Trees*. Princeton University Press.

Jirasek, C., P. Prusinkiewicz and B. Moulia. 2000. Integrating biomechanics into developmental plant models expressed using L-systems. In: H.-Ch. Spatz and T. Speck (Eds): *Plant biomechanics 2000*, Georg Thieme Verlag, Stuttgart, pp. 615-624.

King, D., and O. L. Loucks. 1978. The theory of tree bole and branch form. *Radiation and Environmental Biophysics* 15: 141-165.

Midgley, J. J., and L. M. Kruger. 2000. Senescence in fire-adapted Cape Proteaceae. *Journal of Mediterranean Ecology* 1:181-185.

Niklas, K. J. 1986. Computer simulations of branching-patterns and their implications on the evolution of plants. *Lectures on Mathematics in the Life Sciences* 18: 1-50.

Pearcy, R.W., H. Muraoka and F. Valladares. 2005. Crown architecture in sun and shade environments: assessing function and trade-offs with a three-dimensional simulation model. *New Phytologist* 166: 791-800.

Prusinkiewicz, P., and A. Lindenmayer. 1990. *The Algorithmic Beauty of Plants*. Springer, New York.

Prusinkiewicz, P., and W. R. Remphrey. 2000. Characterization of architectural tree models using L-systems and Petri nets. In: M. Labrecque (Ed.): *L'arbre - The Tree 2000*. Institut de Recherche en Biologie Végétale, Montreal, pp 177-186.

Prusinkiewicz, P., R. Karwowski and B. Lane. 2007a. The L+C modelling language. In J. Vos, L.F.M. Marcelis, P.H.B de Visser, P.C. Struik and J.B. Evers (Eds), *Proceedings of the Frontis Workshop on Functional-Structural Plant Modelling in Crop Production*, Wageningen, The Netherlands, 5-8, March, 2006. Springer, Berlin, pp. 27-42.

Prusinkiewicz, P., Y. Erasmus, B. Lane, L.D. Harder and E. Coen. 2007b. Evolution and development of inflorescence architectures. *Science* 316: 1452-1456.

Shinozaki, K., K. Yoda, K. Hozumi and T. Kira. 1964. A quantitative analysis of plant form – the pipe model theory I: basic analyses. *Japanese Journal of Ecology* 14:97–105.

Taylor-Hell, J. *Biomechanics in Botanical Trees*. M.Sc. thesis, University of Calgary, September 2005.

Zimmermann, M. H. 1978. Structural requirements for optimal water conduction in tree stems. In: P.B. Tomlinson and M.H. Zimmermann (Eds), *Tropical Trees as Living Systems*, Cambridge University Press, pp. 517-532.

Numerical analysis of the influence of the aerial structure on tree dynamics

Damien Sellier[1,3], Thierry Fourcaud[2,3]

[1] ENSIS Wood Quality, Rotorua, New Zealand; [2] CIRAD UMR AMAP, Montpellier, France; [3] UMR LRBB, Bordeaux, France

Keywords: Tree wind-firmness, Tree architecture, Oscillation, Finite Element, Plant biomechanics, Wind loading.

Introduction

Wind is the primary physical agent of damage to harvested forests. The evaluation of tree stability to wind involves numerous, potentially coupled factors which are related to both the plant structure and its surrounding media. Over the past decades, the problem has been widely investigated by usually focusing on a particular component of the system such as the soil/root interface (Coutts 1986), the wind action (Oliver and Mayhead 1974) or the stem mechanics (Gardiner et al. 2000). The known, active turbulence of the air flow within forest canopies (Finnigan 2000) has led to model trees submitted to wind loads as dynamic structures since an early stage (Papesch 1974). Branches and especially their oscillations have been acknowledged to have a strong impact on dynamics of the whole aerial system (Scannell 1984, Sellier and Fourcaud 2005). As a consequence, recent models of a tree submitted to a dynamic load include branches as vibrating axes coupled to the stem (Fournier et al. 1993, Saunderson 1997, Moore 2005). This study presents a series of numerical experiments designed to investigate the tree mechanical response to a turbulent air flow as a function of the aerial system, its morphology and materials.

Material and Methods

Reference tree material

The study is done on a tree for which structural characteristics varied around a state of reference. Aerial morphology is provided by a numerical model of a 35-year old Maritime pine (*Pinus pinaster* Ait.) that was simulated with the AMAPsim software (AMAP CIRAD, Barczi *et al.* 2007). Growth parameters used in AMAPsim have been measured by Coudurier *et al.* (1993) in a Maritime pine stand site near Bordeaux, France (see also Heuret et al. 2006). As partially resulting from stochastic processes, the simulated tree corresponds to a possible and realistic one yet not to the mean tree of the stand. In an attempt to maintain practical computational time with the Finite Element analyses (cf. 2.5), all axes with a branching order greater than 3 have been removed from the topological structure. Properties used as reference for wood and foliage materials originate in the literature relevant to the studied species.

Test factors

Characteristics of the structure that have been included in the analysis fall into two different sets, each one independently tested. The first set relates to the geometry of the aerial system, including length and diameter of axes as well as the angle locally formed by the primary branches with the stem. The second set of factors encompasses physical – i.e. wood density, specific leaf area (SLA), linear leaf density – and mechanical – i.e. wood longitudinal modulus of elasticity and viscosity – characteristics of the structure. All factors vary separately for each branching order except for the insertion angle and SLA. Crown topology remains the same during the analyses. Altogether, influence of 20 independent factors on tree dynamics is assessed.

Experimental designs

Fractional experimental designs have been employed so as to minimize the number of simulations to be performed. For each set of factors, either geometrical or material, a design is done twice. The first run corresponds to the simulation of free sway. The analysis aims at identifying frequency and damping of the first bending mode of vibration. The second run corresponds to forced sway and allows calculating tree displacements and the bending moment as caused by wind loading. Each factor has 3 modalities: the reference state, -20% and +20% of the reference value. In this study, a Taguchi (1987) table is used to obtain 27 combinations of factor modalities instead of a full factorial design which would lead to 3^7 and 3^{11} modal combinations for the geometrical set of factors and the material one, respectively.

Theoretical wind velocity

The time series of streamwise wind velocity are representative of the turbulence that occurs within forest canopies. To a large extent, flow characteristics are generic among plant canopies provided that they are normalized by the mean canopy height and/or mean velocity at canopy height. Wind parameters have been chosen to obtain flow dynamics similar to the ones measured in Maritime pine forests near Bordeaux. The tree is submitted to 3 successive gusts, each with a time pattern as observed by Collineau and Brunet (1993).

Finite Element model

For each factorial combination, the mechanical analysis is performed with a Finite Element model relying on ABAQUS software (ABAQUS Inc., Providence RI, USA). A numerical routine generates a FE mesh from the tree originally described as a Multiscale Tree Graph (Godin and Caraglio 1998). Stem and branches are discretised into beam elements while foliage is aggregated on the branches. The equations of movement are solved iteratively by direct time integration (see Sellier *et al.* 2006) and are in the discrete form:

$$M\ddot{q} + D\dot{q} + Kq = G\left(+F\right) \qquad (1)$$

where *M*, *D* and *K* are mass, damping and stiffness matrices, respectively. $\ddot{q},\dot{q},q$ are the acceleration, velocity and displacement column vectors, respectively. G and F are the column vectors of gravitational and drag forces. In the case of wind-induced sway, F is applied to the structure and accounts for velocity of elements relatively to the flow:

$$F = \rho C_D A\left(U - \dot{q}\right)\left|U - \dot{q}\right| \qquad (2)$$

where ρ is air density, C_D the drag coefficient, A the exposed area and U the streamwise velocity of the flow, which depends on altitude in the canopy.

Results

Free sway

Among tested material factors, the most influential one on the frequency of tree natural sway is the modulus of elasticity (MOE) of the stem. The frequency scales up with MOE as expected in structural dynamics since frequency roughly depends on a stiffness over mass ratio. On the other hand, the MOE of branches has almost no effect of the sway frequency. Wood density has a negative influence which is stronger in the case of 2nd and 3rd order axes. Then, the increase in the density does not only contribute to increase the tree mass but also to displace the position of the mass centre upward, both aspects leading to a decrease in the sway frequency. The main factors having an effect on the damping ratio of the tree are the viscosity of the wood material and the specific area of the foliage, which are respectively related to material and aerodynamic damping. The remaining material factors have a very limited influence on motion damping.

Among geometrical factors, the diameter of the stem has the highest impact on the sway frequency. As the diameter increases, so does the frequency. This results from the stiffness of the axis scaling up with diameter as a 4th order power law whereas the volume hence the mass only depends on the square of diameter. The second most influential factor is the length of the stem. An increasing length has a negative influence on the sway frequency since it induces a linear decrease in the relative stiffness of the stem as well as an increase in the height of the centre of mass. Overall, variations of the damping ratio that are caused by geometrical factors are weak.

Wind loading

MOE of the stem is also found to be the most important factor regarding the maximal bending moment over time at the basis of the stem, BM_{max}. The more flexible the stem is, the more it can bend under wind action and then be submitted to lower wind speeds, i.e. lower drag forces. The same influence is observed for the primary branches although the influence is less pronounced. An increase in wood density of branches also causes BM_{max} to increase as a result of higher inertial effects in the crown. Factors that are effective on the damping of trees oscillation such as wood viscosity and foliage area also contribute to slightly reduce the magnitude of the bending moment as they increase.

All geometrical factors have a significant effect on BM_{max}. Of particular interest, the angle of insertion of the primary branches in the stem causes major variations. When the angle is small with the stem, branch extremities are submitted to high wind speeds and consequently important drag forces. On the contrary, when the angle is large, branches are submitted to relatively lower wind speeds. The influence of this factor is especially strong as the mean horizontal wind speed decays exponentially in plant canopies.

Conclusion

The study shows the predominance of the morphology of the aerial system over the characteristics of its constitutive materials as far as tree stability to wind is concerned. This aspect is likely to be even more pronounced in field conditions where geometrical variability of trees is much higher than what we accounted for. Additionally, results point out that tree oscillations are mainly driven by stem characteristics although crown elements are also found to have remarkable and significant effects on dynamics of the entire structure.

Acknowledgements

This study was funded by the VENFOR project (GIP-ECOFOR).

References

Barczi JF, Rey H, Caraglio Y, de Reffye P, Barthélémy D, Dong Q-X, Fourcaud T. 2007. *AmapSim: a structural whole plant simulator based on botanical knowledge and designed to host external functional models*. Annals of Botany, In press.

Collineau S, Brunet Y. 1993. *Detection of turbulent coherent motions in a forest canopy part II: Time-scales and conditional average*. Boundary-Layer Meteorology 66: 49-73.

Coudurier T, Barthelemy D, Chanson B, Courdie F, Loup C. 1993. *Premier resultats sur la modelisation du pin maritime Pinus pinaster ait. (pinecae)*. In Boucher J (ed) Architecture des arbres fruitiers et forestiers, pp 306-321. INRA editions, Paris, France.

Couts MP. 1986. *Components of tree stability in Sitka spruce on peaty gley soil*. Forestry 59(2):173-19.

Finnigan JJ. 2000. *Turbulence in plant canopies*. Annu. Rev. Fluid Mechanics 32:519-571.

Fournier M, Rogier P, Costes E, Jaeger M. 1993. *Modélisation mécanique des vibrations propres d'un arbre soumis aux vents, en fonction de sa morphologie*. Ann. Sci. For. 50:401-412.

Gardiner BA, Peltola H, Kellomaki S. 2000. *Comparison of two models for predicting the critical wind speeds required to damage coniferous trees*. Ecological modelling 129(1):1-23.

Godin C, Caraglio Y. 1998. *A multiscale model of plant topological structures*. J. of Theoretical Biology 191(1):1-46.

Heuret P, Meredieu C, Coudurier T, Courdier F, Barthelemy D. 2006. *Ontogenetic trends in the morphological features of main annual shoots of* Pinus pinaster *(pinacae)*. American Journal of Botany 93(11):1577-1587.

Moore JR, Maguire DA. 2005. *Natural sway frequencies and damping ratios of trees: influence of crown structure*. Trees – Structure and functions 19(4):363-373.

Oliver HR, Mayhead GJ. 1974. *Wind measurements in a pine forest during a destructive gale*. Forestry 2:185-194.

Papesch AJG. 1974. *A simplified theoretical analysis of the factors that influence windthrow of trees*. In: 5th Australasian conference on hydraulics and fluid dynamics, University of Canterbury, Christchurch, NZ, pp. 235-242.

Saunderson SET. 1997. *The aerodynamic behaviour of trees in high winds*. Ph. D. thesis, University of Nottingham.

Scannell B. 1984. *Quantification of the interactive motions of the atmospheric surface layer and a conifer canopy*. Ph.D. thesis, Cranfield Insitute of Technology, Bedford.

Sellier D, Fourcaud T. 2005, *Relationship between the oscillations of young pines (Pinus pinaster Aït.) and their aerial architecture.* Journal of Experimental Botany 56(416):1563-1573.

Sellier D, Fourcaud T, Lac P. 2006. *A Finite Element model to investigate the effects of aerial architecture on tree oscillations*. Tree Physiology 26:799-806

Taguchi G. 1987. *System of experimental design*. Quality resources. Translation of Jikken keikahuho, Maurzen Co., Tokyo, 1976.

A simple model simulating the construction of blade and sheath length in maize

Christian Fournier[1] and Bruno Andrieu[2]
1 INRA, UMR 759 LEPSE, 2 place Viala, 34060 Montpellier cedex 01, France
2 INRA, UMR Environnement et Grandes Cultures, Thiverval Grignon, France 78850
{Christian.Fournier|Bruno.Andrieu}@grignon.inra.fr

Keywords: regulation of architecture, simulation, ecophysiology, L-Systems.

Introduction

Thinking at plant architecture as emerging from a simple set of construction rules is a very appealing feature of L-Systems. In the context of crop modeling, it opens new ways to model the effects of environmental stresses on crop architecture, by pointing to regulation loops that are ignored in usual models (Fournier et al., 2007). As such, the triggering of leaf development by emergence events, which has been for long suggested to exist (Dobrynin 1960, Malvoisin 1984, Skinner and Nelson 1994), offers a simple and elegant frame for re-analysing the regulation by the environment of leaf area development (Durand et al., 1999, Fournier et al., 2005a). This would also explain the persistence of stable patterns in plant architecture, despite the variability of environmental conditions in which plants grow. Here we illustrate that point with a simple model simulating some of the regulation processes likely to be involved in the construction of maize shoot architecture.

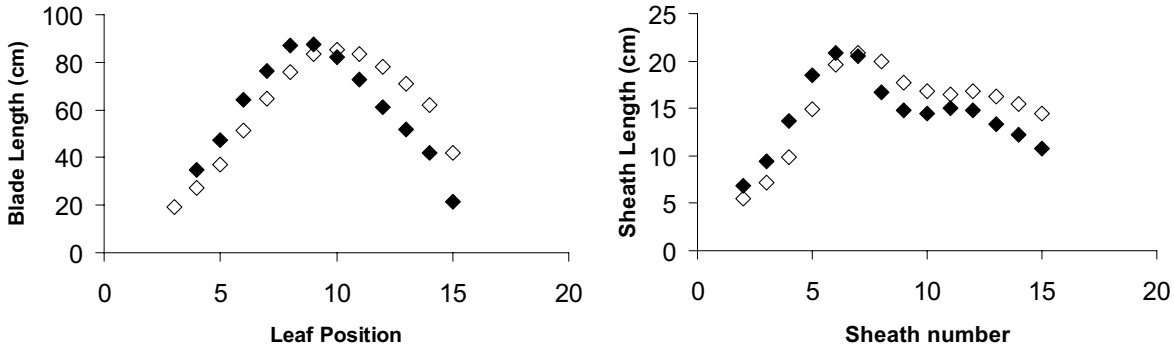

Fig. 1. Patterns of variation of blade (left) and sheath (right) length with leaf position in maize in two contrasted cases : open symbols are for maize grown at normal density, filled symbol are for maize grown at high density

Leaf ontogeny and patterns of leaf length variation in maize

The maize leaf is composed of a sheath, that encircles the stem, and a blade. The leaf appears at the shoot apical meristem as a small protuberance, that will become the blade. During a first stage, which corresponds to the set-up of the growing zone, growth occurs in all part of the blade/leaf. Afterwards, the extension only occurs in the basal zone of the leaf (the growing zone), that dynamically maintains its length, by producing new cells and pushing away mature tissues. At a given time, the leaf sheath boundary appears within the growing zone, defining the onset of sheath extension. This boundary is displaced within the growing zone, and defines, when it overcomes the growing zone, the end of blade extension. Finally, the growing zone collapses and leaf/sheath extension ends. The mature length of sheath and blade therefore reflects the timing of phase changes that occurred at the level of the growing zone during leaf extension. At the plant level, the

patterns relating leaf length and sheath length to leaf position (Fig 1) reflect the coordination of phase changes on successive leaves. The present work aim at explaining how these phase changes are regulated to produce these stable patterns.

Hypothesis

The model is based on the interpretation scheme discussed Andrieu et al. (2006), completed with hypothesis concerning the functioning of the growing zone presented in Fournier et al (2005a,b). It combines three main ideas. The first idea is that for the basal leaves of the plant, the emergence of leaf tips and leaf collars regulates both the transition from blade to sheath extension and the ontogeny of the growth zone, that is the phase changes of leaf extension. Tip emergence triggers the end of spatial extension of the division zone and of the elongation zone, and set-up sheath extension. The emergence of collars triggers the regression of the growing zone, and thus controls the duration of extension. The second idea is that for upper phytomers (those that elongates after floral transition) the dependence of leaf ontogeny to emergence events changes (Andrieu et al, 2006). For these leaves, the set-up of sheath extension occurs at a constant age after leaf initiation (when expressed in thermal time) and the timing of the installation of the growing zone is no longer related to tip emergence, but occurs at constant leaf length. Given the observed concurrent variation of the rate of extension during the installation of the growth zone, it is proposed that this corresponds to a stable number of division events since leaf initiation. Finally, the end of leaf extension remains correlated to collar emergence. The third idea is to use a model of the functioning of the growth zone to build correlations between variables and to predict the time-course of the elongation rate. Here, we consider the growth zone as composed of a division zone that produces a cell flux proportionally to its length, and an extension zone made of cells following an exponential cell extension pattern, whose duration correspond to a constant number of cell doubling periods (Fournier 2005b). As a result, in the model, the variation of the extension rate with leaf stage, leaf position or during stress is related to only two parameters : the length of the division zone and the relative extension rate of cells. Conversely, when, for example, the rate of cell extension is changed, it affects the growth rate of all phases of leaf extension in a coherent way. That model also allows to predict the time course of sheath extension, by simulating the trajectory of a transverse cell wall within the zone.

Model implementation and parameterisation

We implement the model in the L+C modeling language, which provides a good interactivity and a visualization of how the system is constructing the patterns. The computation of the plant according to its topology (from the base to the top) also offers a simple solution for the calculation of emergence events and the triggering of phase changes of young leaves by older leaves. We used the normal density sowing of the detailed dataset of Andrieu et al (2006) to parameterise our equations. We then modified a few parameters to simulate other scenarios and interpret the effects of stresses. In results presented here, we used simplified rules and a simplified model for the functioning of the growth zone. This allows to use directly the data of the original paper of Andrieu et al (2006), but produces some artifacts in the simulations. A re-parameterisation of the model is in progress, that relies on a more realistic description of the functioning of the growth zone. Currently, the model has 5 global parameters, and uses the relative extension rate of each leaf during the first stage (as calculated in Andrieu et al 2006) to calibrate the parameter of the growing zone. We also use exponential extension curves to have an estimation of internode extension, that is required to compute emergence events.

Frst results

Our first results indicate that the model is able to correctly simulate the kinetic of leaf extension (Fig 2), using a concise set of parameter and a common set of rules for triggering phase changes and the onset of sheath extension. The simulated variations of final length with leaf position are not completely realistic (Fig 2), but the model is able to reproduce the principal traits : leaf length is

increasing exponentially in a first stage, and then decreases with leaf position. To simulate the effects of density, we simply change the dimensions of the first three sheaths and reduce by 20% the relative extension rate of leaves that grow after floral transition (as proposed in Andrieu et al 2006). The resulting pattern reproduces qualitatively the observations, although it tends to amplify the effects of density (upper leaves are too much reduced) and produces some discontinuities. We think that these defaults are linked to the simplifications of the present model.

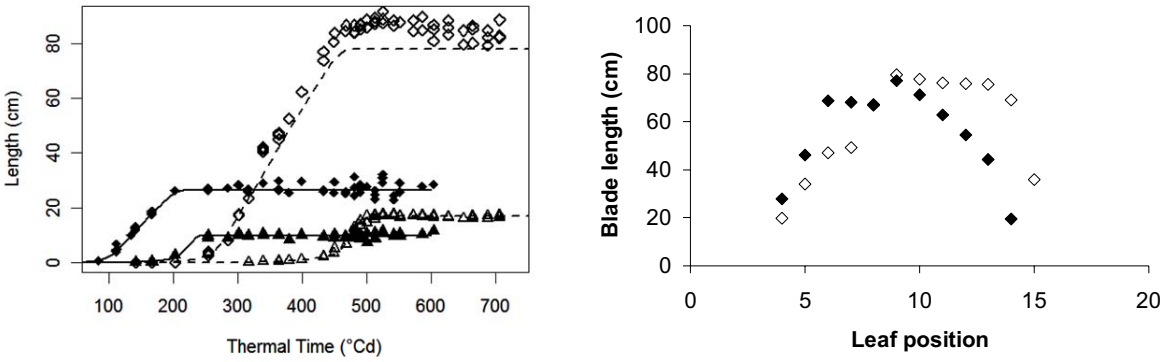

Fig2: Left : Thermal time courses of blade (diamonds) and sheath (triangles) length of leaf 4 (filled symbols) and 10 (open symbols), observed (symbols) and simulated (lines). Right : mature length of leaf blades as a function of leaf position, at normal (open symbols) and high density (filled symbols) with the model

Conclusion

Putting together, with simplifications, three type of ideas of how a maize plant constructs its shoot architecture allows us to reproduce important features of shoot plasticity with density. The role of the sheath tube in regulating plant architecture is confirmed, but this studies also points to the importance of the relative elongation rate of cells in that process. The model unifies three levels of description of shoot development used in ecophysiology : the functioning of the growing zone, the growth curve analysis of leaf extension and the analysis of pattern of mature dimension along the shoot. This open new opportunities to link and interpret the effect of stresses, for which we have details at several levels, but lack of an integrated view. In particular, the present model could help at predicting the consequences of a transient stress on subsequent leaves. This ability to reason phenotypic plasticity would greatly increase the range of application of FSPM in agronomy.

References

Andrieu B., Hillier J. & Birch C. (2006) Onset of Sheath Extension and Duration of Lamina Extension are Major Determinants of the Response of Maize Lamina Length to Plant Density. Annals of Botany, 98, 1005-1016.

Dobrynin G.M. (1960) Lois régissant la formation de la pousse chez certaines graminées. Doklady Akademii Nauk SSSR, 130, 223-226 (French translation, original in Russian).

Durand J.L., Schaufele R. & Gastal F. (1999) Grass leaf elongation rate as a function of developmental stage and temperature: Morphological analysis and modelling. Annals of Botany, 83, 577-588.

Fournier C., Durand J.L., Ljutovac S., Schaufele R., Gastal F. & Andrieu B. (2005a) A functional-structural model of elongation of the grass leaf and its relationships with the phyllochron. New Phytologist, 166, 881-894.

Fournier C., Muller B. & Tardieu F. (2005b) Which characteristics of the division and of the expansion of maize epidermal leaf cells are intrinsic to the genotype ? Paper presented at the XVII International Botanical Congress, 17 - 23 July, Vienna, Austria.

Fournier C, Andrieu B, Buck-Sorlin GH, Evers JB, Drouet J-L, Escobar-Gutierrez A, Vos J. 2007. Functionnal structural modelling of graminae. In: Vos J, Marcelis LFM, Visser PHBd, Struik PC, Evers JB, eds. Functional-Structural Plant Modelling in Crop Production. The Netherlands: Springer, 175-186.

Malvoisin P. (1984) Organogenèse et croissance du maître-brin du blé tendre (Triticum aestivum) du semis à la floraison.II.- Contrôle des relations entre la croissance et la vascularisation de la tige et des feuilles. Essai de modélisation. Agronomie, 4, 587-596.

Skinner R.H. & Nelson C.J. (1994) Epidermal cell division and the coordination of leaf and tiller development. Annals of Botany, 74, 9-15.

An L-system based model of a ryegrass heterogeneous population.

A. Verdenal, D. Combes, and A.J. Escobar-Gutiérrez
INRA, UR4 Unité d'Ecophysiologie des Plantes Fourragères,
BP 6, F-86600 Lusignan, France
abraham.escobar@lusignan.inra.fr

Keywords: perennial ryegrass, L-system-based model

Introduction

Grasslands, natural and cultivated, are one of the major sources of forage in European agricultural systems where they are exploited via grazing and mowing. In the European changing political context regarding environmental questions, social perception of grasslands has shifted. Grasslands are now seen as important due to two main functions: forage production (use value) and environmental roles (biodiversity preservation, carbon sequestration, soil conservation). They are well inserted in the multifunctional paradigm. In addition, compared with other crops, grasslands present some particularities that justify their specific study. For example, they are perennials populations repeatedly exploited via defoliation-regrowth cycles while growing under changing conditions. Grasslands also show high intra and inter specific variability.

Both the canopy structure and the genotypic composition of the population are the determinants of the grassland agricultural use value (quantity and quality of the harvested biomass) as well as of its environmental roles. Canopy structure and the genotypic composition of the population are emergent properties resulting from the behaviour of individual plants and their interactions during the grassland lifespan. Thus, the study of the morphogenesis of the individual is a relevant element to better understand the dynamics of the canopy structure and the population composition.

Several major environmental factors affect plant morphogenesis such as: light resource (trophic and photomorphogenetic signals), intensity and frequency of defoliation, nutrients supply, water availability and temperature dynamics. However, it is difficult to quantify the contribution of each of these factors to the phenotypic plasticity because of their multiple interactions.

Objectives

Our aim is to build up an individual-based Functional-Structural Model of a heterogeneous mini-population of perennial ryegrass, using L-systems. This model is built so that the morphogenesis of the individual is directly affected by its environment. It should allow us to better understand how the use-value of grasslands is modified by the behaviour of individuals under variable management regimes. Furthermore, the analysis of both i) the ryegrass genotypes responses and ii) the ability of genotype to compete under changing environments is a key-point that could help us to understand the genotypic changes in species mixture and opens perspectives towards ecological studies.

Material and method

The described model is based on the L-system formalism (Lindenmayer, 1968; Prusinkiewicz, 1999) using the L-Studio LPFG simulation platform (Karkowski, 2002). The model in itself will be constituted of a model of a sward canopy, along with a light environmental program.

Plant model

Structure and function

The plant model simulates the 3D development of the aerial parts of plants in the vegetative phase. Grasses have the particularity, in the vegetative phase, of not elongating their internodes so that the plant is mainly constituted of tillers, which are themselves made of leaves emitted at the basis of the plant by the apical meristems. Consequently, a realistic representation of the architecture can be obtained by a description of the topology of the plant and of the leaf dynamics (e.g. growth kinetic, lifespan, geometry) at different levels of organisation. The main criterions (not all comprehensive) that have been identified, at each organisation level, as essential to properly model the structure of a ryegrass canopy are listed in figure 1, along with the corresponding process that must be taken into account.

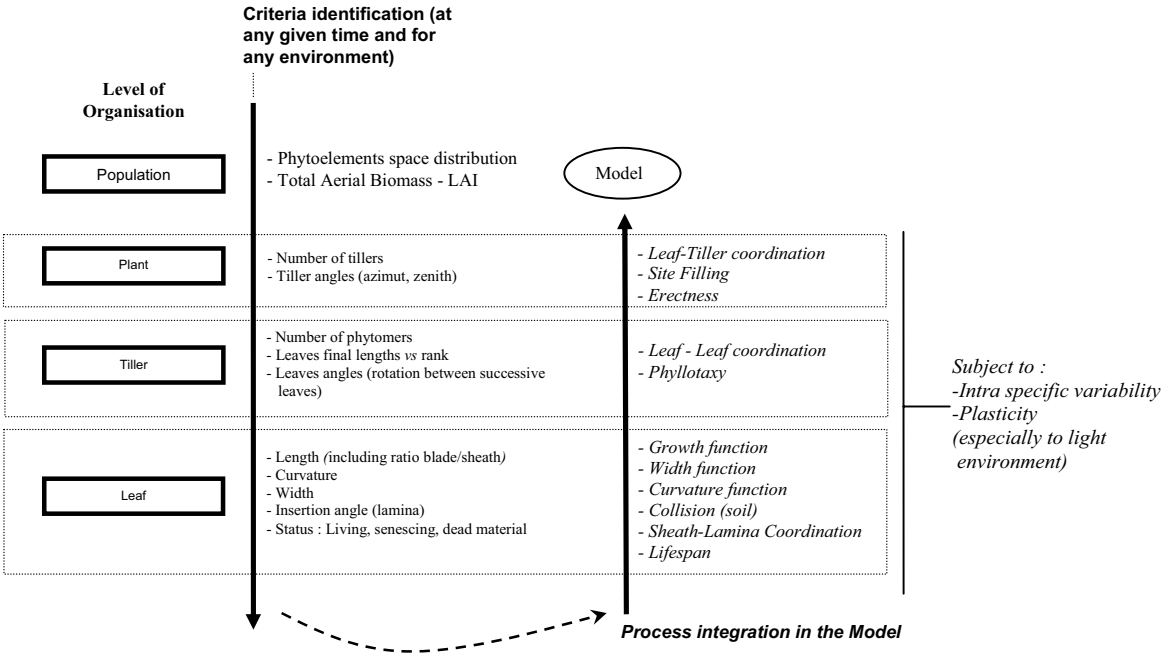

Fig. 1. Criteria identification and processes taken into account, each level of organisation, for building the population model. Basically, a realistic representation of the architecture relies on properly describing the number of leaves and tillers, space orientation and shape of the phyto-elements, at any given time and environment.

From a functional point of view, the processes controlling the triggering, coordination and kinetic of leaves and tillers growth are of utmost importance. The main static (e.g. final leaf length) and dynamic (growth rate, elongation duration) characteristics of the leaves can be described as a function of their phytomer relative number (Evers *et al*., 2005). They are input into the model to obtain realistic, but deterministic simulations of the gradients observed on a given axis. On the other hand, several author (e.g. Fournier *et al*., 2007) suggested that some events are controlled, in an indirect manner, by the pre-existing architecture. For example, the growth of a given leaf is triggered when the older leaf emerges out of the pseudostem cylinder. In our work, to test these hypotheses, we designed a model that is as "self-regulated" as possible, i.e. the only descriptive input is the general form of the growth function of the leaves. The values of the parameters of this function are modified by the current state of the plant. Furthermore, this approach actually allows simulating the impact of structural modifications, such as cutting, on the subsequent development of the plant architecture (Fig. 2). This is unavoidable to reach our objective.

Topology

In our model, the topological description of the plant relies on virtual phytomers that are created at the apices, as described by Fournier *et al*. (2007). The creation of a new phytomer is determined by the detection of a specific event: the emergence of a leaf out of the whorl formed by the sheaths of older leaves. When a phytomer is created, the elongation of its own leaf is triggered. Thus, the plant model does not emit organs according to a clock in order to obtain a given phyllochron, but creates its own phyllochron according to the kinetic of the growth of the leaves.

Leaf growth

The values of the parameters such as the elongation duration, the elongation rate and the final length are not given *a priori* as a function of the leaf rank on the axis, but are self-determined by the model according to the local growth conditions. For instance, the final leaf length is determined by the time that the leaf spends growing within the whorl. In other words, it is indirectly determined by the actual length of the sheath of the previous leaf.

Management methods: simulation of cutting regimes

As cited above, grasslands are grazed and/or mowed (cut). Cutting can be characterized by its intensity and its frequency. Combinations of these two factors affect mono-species grasslands productivity (Hernandez Garay *et al*., 1999) and could also modify the genotypic composition of heterogeneous populations (Hazard and Ghesquiere, 1995). Thus, we are aiming to simulate the modification of the canopy structure under different cutting regimes in order to better understand how the individual and the group of plants will react to the modification of their own structure and of their access to light, especially for shaded plants and organs.

Results

By dynamically adjusting the values of the various parameters, the model satisfactorily captures the evolution of the patterns and time kinetics of major architectural traits such as the final lengths and appearance rates of leaves (Fig. 2a, 2b). In its present state, the model also mimics the response of the plant to structural perturbations induced by differential cutting heights (Fig. 2c, 2d).

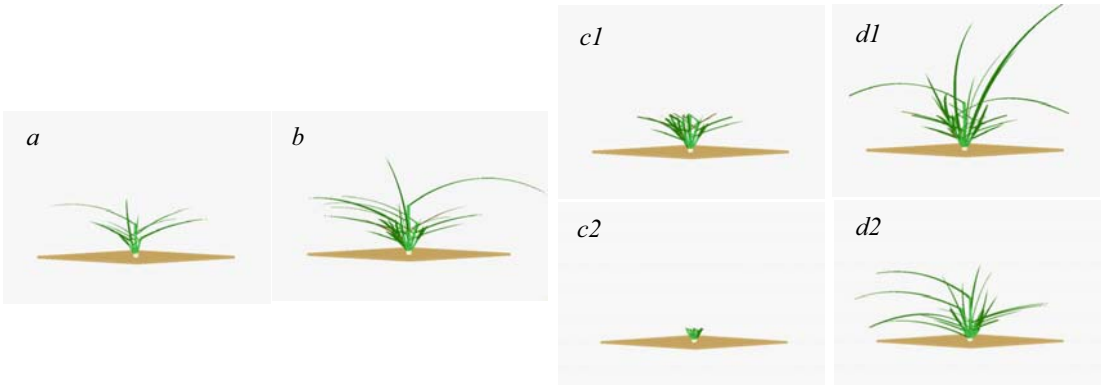

Fig. 2. Sequence illustrating the simulation of a plant at two developmental stage (a, b), defoliated (c1 and c2) and during regrowth after a cutting event at two different heights(d1 and d2).

Conclusion

Several hypotheses have been proposed to explain the dynamics of ryegrass population canopy structure and genotype composition (in the case of heterogeneous communities) under competition for light and different cutting regimes. However, we are lacking proper understanding of what are the utmost explanations: trophic responses, morphogenetic responses to signals, genotypic competing ability. Furthermore, we face difficulties when trying to design and conduct experiments allowing answering these questions. The FS approach could be a particularly well adapted tool to investigate these topics.

Perspectives

Some improvements of the model are needed, especially to properly simulate both the tillering and the behaviour of different genotypes.

Environmental programs. Site filling and other plant architectural traits are determined by the light environment. Thus, in a next stage, a radiation model will be coupled with the plant/population model, enabling us to simulate light micro-environment in the neighbourhood of each organ (Evers *et al*. 2005).

Genotypic heterogeneity. Another goal of our work is to characterize the behaviour of architectural traits of different genotypes under competition for light and under different management regimes. Populations constituted of two different simulated genotypes will be created, based on the characteristics of the short-leaved and long-leaved types selected by Hazard *et al*. (1996). Different mixtures will be artificially "sowed" and their evolution monitored, under the constraints cited above.

Acknowledgments

This research is supported by "La Région Poitou-Charentes", France.

References

Evers J.B., Vos J., Fournier C., Andrieu B., Chelle M., and Struik P.C. 2005. Towards a generic architectural model of tillering in Gramineae, as exemplified by spring wheat (*Triticum aestivum*). New Phytologist 166: 801-812.

Fournier C., Andrieu B., Buck-Sorlin G., Evers J.B., Drouet J.L., Escobar-Gutierrez A.J., and Vos J. 2007. Functional structural modeling of Gramineae. In: J. Vos, L.F.M. Marcelis, P.H.B. de Visser, P.C. Struik and J.B. Evers (eds.), Functional-Structural Plant Modelling in Crop Production. Springer. The Netherlands. pp 175-186.

Hazard L. and Ghesquiere, M. 1995. Evidence from the use of isozyme markers of competition in swards between short-leaved and long-leaved perennial ryegrass. Grass and Forage Science, 50, 241-248.

Hazard L., Ghesquiere M., and Barraux C.1996 Genetic variability for leaf development in perennial ryegrass populations. Canadian Journal of Plant Sciences 76: 113-118.

Hernandez Garay, A. Matthew, C. Hodgson, J. 1999. Tiller size/density compensation in perennial ryegrass miniature swards subject to differing defoliation heights and a proposed productivity index. Grass and Forage Science, 54, 347-356.

Karwowski, R. 2002. Improving the Process of Plant Modeling: The L+C Modeling Language. Ph.D. thesis, University of Calgary

Lindenmayer A., 1968, Mathematical models for cellular interaction in development, part I and II. Journal of Theoretical Biology 18: 280-315.

Prusinkiewicz P. 1999. A look at the visual modeling of plants using L-systems. Agronomie. 19:211-224.

Architectural Analysis and Modeling of Maize Growth and Development under Water Stress

Song Y[1], Birch CJ[1], Hanan J[2]
1. School of Land, Crop and Food Sciences, the University of Queensland, Gatton campus, Gatton, 4343, Australia
2. ARC Centre for Complex Systems, and Advanced Computational Modeling Centre, the University of Queensland, Brisbane, 4072, Australia
y.song@uq.edu.au; c.birch@uq.edu.au; jim@maths.uq.edu.au

Keywords: maize (*Zea mays*), plant architecture, water stress, modeling, extension

Introduction

Crop structural development influences canopy production, assimilate partitioning and final yield. Substantial progress of improving architectural modeling has been achieved in maize 3D development (Fournier and Andrieu, 1998), in developing an architectural model of maize (Fournier and Andrieu, 1999), and in quantifying internode and leaf kinetics (Fournier and Andrieu 2000, Birch et al, 2002, Birch et al, 2007a). The enhancement of architectural modeling facilitates the introduction of functionality at the level of individual organs and whole plants (Hanan and Hearn, 2003; Yan et al, 2004; Guo et al, 2006; Birch et al, 2007b). Maize cultivation is often subjected to water stress in the areas of water limitation. Water stress during vegetative stage limits cell division and expansion (Granier and Tardieu, 1999; Reymond et al, 2003), and thus reduces stem elongation and leaf area growth. The objectives of this research are (i) to examine plant architectural development at organ level under water stress, (ii) to revise an individual-based maize model (ADEL-Maize) based on data from Gatton, Southeastern Australia, and (iii) to implement the simulation of plant architectural development under water stress.

Materials and methods

Datasets from field trials carried out at Gatton, Australia in 2003-04 (Exp1) and 2006-07 (Exp2) are used in this study. Three water regimes were implemented in each trial: (i) RF, fully rainfed treatment, which completely depended on natural rainfall; (ii) IRF, irrigated followed by rainfed treatment, which was irrigated until anthesis, then irrigation was withheld; and (iii) FI, fully irrigated and used as the control. A pre-planting irrigation to supplement rainfall was used to ensure that the soil is fully wet to 1.8 m prior to sowing (the expected limit of root exploration). Maize (Pioneer 31H50) was planted at a density of 70,000 (in Exp1) and 60,000 (in Exp2) plants ha^{-1}. The seeds were chemically treated to prevent damage from insects and soil borne diseases. Sufficient fertilizer was applied to prevent nutrient stress. Ten plants in each treatment were selected at the four fully expanded leaf stage and tagged to monitor plant growth and development by non-destructive sampling. The leaves at position 5 and 10 on these plants were respectively tagged to avoid errors in leaf identification after senescence of lower leaves commenced. Crop growth and development was measured using destructive sampling at 2 or 3 day intervals by counting fully expanded and expanding leaf number on the 10 tagged plants in each treatment to obtain guidance to select representative plants (ie similar to the tagged plants) for destructive sampling. Data on ontogeny, length of lamina, sheath and internode, width of lamina was collected at each sampling. Daily environmental data was recorded by weather station near the field, and data on soil water content in RF and IRF was collected using Neutron Probe in Exp1 and T-Bug (SM2000,UK) in Exp2.

Data analysis

Rainfall during canopy growth in two experiments was shown in Fig.1. There was a 35d period without rain in Exp2, which happened during canopy rapid development, whereas the rainfall in Exp1 is relatively even. In Exp1, phenology was not significantly affected in RF treatment; leaf extension was unaffected until late in canopy expansion (ie only the top few leaf sheaths were affected); whereas internodes above position 12 which extended after water stress occurred were affected (Fig.2a). In

Exp2, a slight delay of 1-2d from emergence to tasseling, anthesis was observed only in RF treatment. The extension and final length of leaves and internodes was reduced by water stress (Fig.2bc). The reduction degree in both experiments varied with intensity and timing of water stress, lengths in RF treatment was consistently shorter than in the irrigated (control) treatment, and the values in IRF treatment basically fell between RF and FI treatment(last few internodes in Fig.2c was not calculated as lack of enough data). As four days significant rainfall happened to later canopy development in Exp2, the length of last few leaves was not significantly affected in IRF treatment; the reduction degree in RF treatment was also a bit decreased as water stress was relieved (Fig.2bc). By contrast, the high rainfall in Exp1 happened to organ almost fully expanded, thus water stress relief did not make much sense to internodes extension (Fig.2a). Leaf and internode extension under water regimes is being analyzed based on four-phase model (Fournier et al, 2000a; Birch et al, 2002), the analysis aims to find new algorithms for the mechanism of canopy expansion, which will then be used to model canopy production, final leaf area and plant height, but the detail is not shown here due to the limitation of abstract.

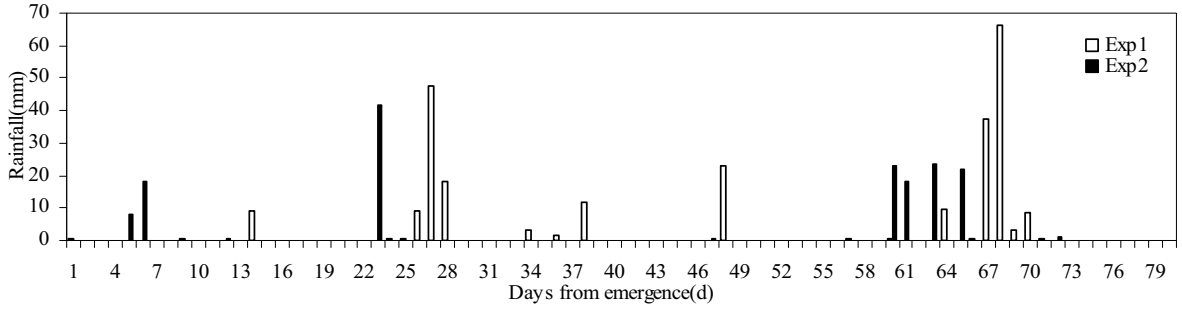

Fig.1. Rainfall during canopy development for two experiments

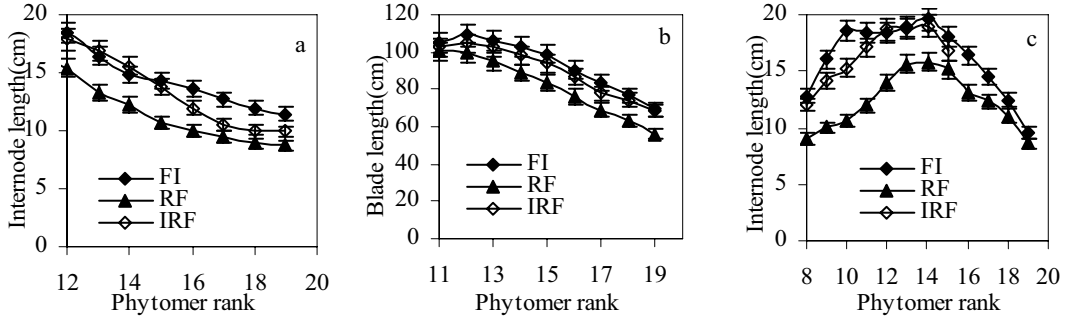

Fig.2. Final length of individual leaves, and internodes in 2003-04(a) and 2006-07(b and c) under three water regimes (vertical bars represent 95% confidence intervals).

Modeling analysis

The individual-based ADEL-Maize model was revised (Birch et al 2007b) to simulate maize crop growth under water stress. The revision required reexamining the model routines including phenology, organ development, leaf area growth and leaf senescence, which is sensitive to genotype or site-specific or water status. The revision was performed based on a subset of data of Exp1. Final plant height and leaf area in the Exp1 was fitted quite accurately with the revised model. However, the intermediate simulated values are lower than observed data (Birch et al, 2007b). The new dataset of Exp2 will be used to quantify the relationship of organ extension and soil water stress, and be incorporated in further incremental revision of the model to improve the simulation. This visualization of the crop canopy in Exp1 at completion of leaf expansion is realistic (Fig.3), it is now necessary to improve the estimation of earlier stages in the production of the canopy using the more intensive data from the experiment of Exp2. This will be achieved by better prediction of leaf area and plant height during canopy prediction.

Also, to further enhance the analysis and modeling, soil moisture extraction at different depths in two trials will be simulated by providing rainfall, irrigation and soil type using APSIM configured for maize (Keating et al, 2003). The analysis will supplement data on soil moisture collected in the trial

of Exp1 and Exp2. This additional work aims to expand the range of analysis and thus applicability of data from the experiments reported here using extensively tested and validated approaches to prediction of soil water status in maize crops (APSRU, 2003, Madhiyazhagan, 2005). These approaches will facilitate improving modeling the responses by the canopy to environmental influences.

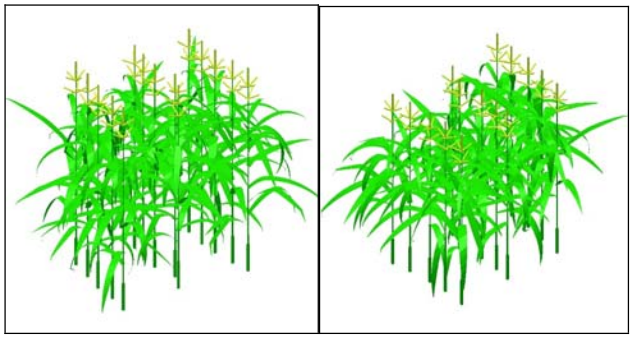

Fig. 3. Visualisation showing prediction of canopies for (a) left, fully irrigated and (b) right, rainfed maize crop grown at Gatton (Birch et al 2007b).

Acknowledgements

The financial support of the University of Queensland for the research and postdoctoral fellowship for the senior author is acknowledged.

References

1. APSRU 2003. The APSIM Maize Module. Online http:/www.apsim.info/apsim/Publish/apsimui/types.xml. Agricultural Production Systems Research Unit, Toowoomba, Australia.
2. Birch, C.J. Thornby, D. Adkins, S. Andrieu, B. and Hanan, J. 2007b. Architectural modelling of maize under water stress. Australian Journal of Experimental Agriculture. (in press)
3. Birch, C.J., Andrieu B., and Fournier, C. 2002. Dynamics of internode and stem elongation in three cultivars of maize. Agronomie 22: 511-524.
4. Birch, C.J., Andrieu B., Fournier, C. 2007a. Parameterization of processes of leaf extension in tropically adapted maize cultivars planted on two dates at Gatton. European Journal of Agronomy (in press).
5. Fournier C., Andrieu B., 1999. ADEL-maize: an L-system based model for the integration of growth processes from the organ to the canopy. Application to regulation of morphogenesis by light availability. Agronomie 19(3/4): 313-327.
6. Fournier, C. and Andrieu, B. 2000b. Dynamics of the elongation of internodes in maize (Zea mays L.): effects of a shade treatment on elongation patterns. Annals of Botany 86: 1127-1134.
7. Fournier, C. Andrieu, B. 2000a. Dynamics of the elongation of internodes in maize (Zea mays L.): analysis of phases of elongation and their relationships to phytomer development. Annals of Botany 86: 551-563.
8. Granier, C. and Tardieu, F. 1999. Water deficit and spatial pattern of leaf development. Variability in responses can be simulated using a simple model of leaf development. Plant Physiology, 119, 609-620
9. Guo, Y., Ma, Y.T., Zhan Z.G., LI, B.G., Dingkuhn, M. Luquet D, and de Reffye, P. 2006. Parameter Optimization and Field Validation of the Functional–Structural Model GREENLAB for Maize. Annals of Botany 97: 217-230
10. Hanan, J.S. Hearn, A.B. 2003. Linking physiological and architectural models of cotton. Agricultural Systems, 75(1): 47-77.
11. Keating BA, Carberry PS, Hammer GL, Probert ME, Robertson MJ, Holzworth D, Huth NI, Hargreaves JNG, Meinke H, Hochman Z, McLean G, Verburg K, Snow V, Dimes JP, Silburn M, Wang E, Brown S, Bristow KL, Asseng S, Chapman S, McCown RL, Freebairn DM, Smith CJ (2003) The Agricultural Production Systems Simulator (APSIM): its history and current capability. European Journal of Agronomy **18**,267-288.
12. Madhiyazhagan, R. 2005. Modelling approach to assess the impact of high temperature and water stress on dry land maize. PhD Thesis, The University of Queensland, Australia. February 2005.
13. Reymond, M. Muller, B. Leonardi, A. Charcosset, A. Tardieu, F. 2003. Combining quantitative trait loci analysis and an ecophysiological model to analyse the genetic variability of the responses of leaf growth to temperature and water deficit. Plant Physiology 131, 664-675.
14. Yan, H.P. Kang, M.Z. de Reffye, P. Dingkuhn, M. 2004. A dynamic architectural plant model simulating resource-dependent growth. Annals of Botany 93: 591–602.

Canopy Architecture Quantification and Spatial Direct Light Interception Modeling of Hybrid Rice

Bangyou Zheng[1], Lijuan Shi[2], Yuntao Ma[1], Qiyun Deng[2], Baoguo Li[1], Yan Guo[1*]
[1]Key Laboratory of Plant-Soil Interactions, Ministry of Education, College of Resources and Environment, China Agricultural University, Beijing, China, 100094; [2]China National Hybrid Rice R&D Center, Changsha, China, 410125.
*For correspondence. E-mail yan.guo@cau.edu.cn

Keywords: Hybrid rice, 3D digitizing, Plant architecture, Light distribution, model

Introduction

Rice is one of the most important crops in the world, and hybrid rice is planted broadly in China which accounts for half of China's rice acreage. Quantification of rice spatial architecture is useful for breeding high yield cultivars, and studies on morphogenesis and development of rice plant structure have been carried out (Watanabe *et al*., 2005). Three-dimensional (3D) digitizing has been a powerful method for the measurement of plant architecture (Sinoquet *et al*., 1998), and 3D light distribution model has been used for the evaluation of different plant architecture (Pearcy and Yang, 1996; Falster and Westoby, 2003; Sinoquet *et al.*, 2007). However, by far, few studies had been carried out on the simulation of spatial light interception of rice canopy grown in the field based on 3D digitized data. In this study, 3D canopies of two hybrid rice cultivars were computer reconstructed based on measurement data obtained with 3D digitizer. Then, characteristics of canopy architecture were analyzed and spatial direct solar radiation interceptions of these two cultivars were simulated with a 3D light distribution model (Wang *et al*., 2006).

Materials and Methods

Field experiment was conducted in 2006 at the experimental farm of China National Hybrid Rice R&D Center, Changsha, China (28˚11′59″N, 113˚04′35″E). Two cultivars of hybrid rice (*Oryza sativa* L.) were planted. One is 'Shanyou63' which has the largest planting area in China. Another is 'Peiai64S/E32' which rice breeders assumed to be a morphological model plant type of super high-yielding rice.

Nine plants (3 rows × 3 columns) were selected at grain filling stage (25 August) and a 3D digitizer (3Space Fastrak, Polhemus, USA) was used to collect the 3D coordinates of plant organs, including midrib of leaves, stems, and main axis of panicles. The length and maximum width of leaf blades, the diameters of stems and panicles were measured after digitizing using a ruler and a micrometer respectively. Then, 3D canopies of this two hybrid rice cultivars were computer reconstructed.

The surface of each leaf blade was divided into facets (Wang *et al*., 2006) which the maximum length of each side was 5 mm. The area of each facet and its inclination angle (zenith angle of the normal to the facet) was calculated according to facet 3D coordinates. The canopies were vertically divided into several layers with 30 cm interval. Then, the distribution of leaf area for each inclination angle with 10° interval at each canopy layer was computed. Leaf area distribution in vertical profile was characterized by leaf area density (LAD, leaf area per unit volume).

The stems and panicles were simplified into planes whose normal azimuths were the same with solar azimuth, and divided into facets like blades. Light interception of each facet in the canopy was computed on measurement date of digitizing (25 August) with a sun elevation increment 5° using a 3D model for direct solar radiation interception within the canopy, which based on parallel projection and Z-buffer algorithms (PPZB, Wang *et al.*, 2005). Light interception density (LID) was used to characterize the vertical profile of light distribution in the canopy which defined as the ratio

of direct photosynthetically active radiation (PAR) intercepted by facets per unit volume to the direct PAR at the top of canopy per unit area.

Results

There was a significant difference for the distribution of leaf inclination angle in the vertical profile for the two cultivars (Fig. 1). Peiai64S/E32 had more erect leaf area at the upper canopy with the angle between 70° and 90°. The maximum inclination angle decreased from the top to bottom, with a minimum of 30° to 50° at lower canopy. The inclination angle of Shanyou63 was relatively smaller with the value between 50° and 80° for the upper canopy and its distribution of inclination angle had a small variation in the vertical canopy profile.

The calculated LADs varied with plant height for both cultivars were shown in Fig. 2A. This clearly showed that the maximum value of LAD was at the middle of the canopy (about 65 cm), while LAD of Peiai64S/E32 distributed more evenly than Shanyou63 in the vertical canopy profile.

The simulated results using PPZB model showed that direct solar radiation can penetrate more deeply into the canopy with the sun elevation angle increasing (Fig. 2B). The sunlit area of the canopy can be divided into two parts: Shanyou63 intercepted more direct solar radiation at the upper of the canopy than Peiai64S/E32 with low sun elevation angles (< 32°, e.g. 10° and 30° in Fig. 2B), and this trend reversed at higher sun elevation angles (> 32°, e.g. 50° and 70°, in Fig. 2B).

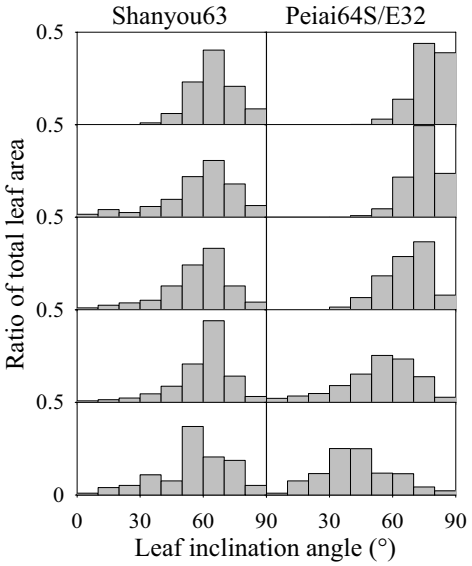

Fig. 1. The ratio of leaf area for each rank of inclination angle to the total leaf area per canopy height layer (30 cm) for Shanyou63 and Peiai64S/E32. Leaf inclination angle was computed as zenith angle of the normal to the facet.

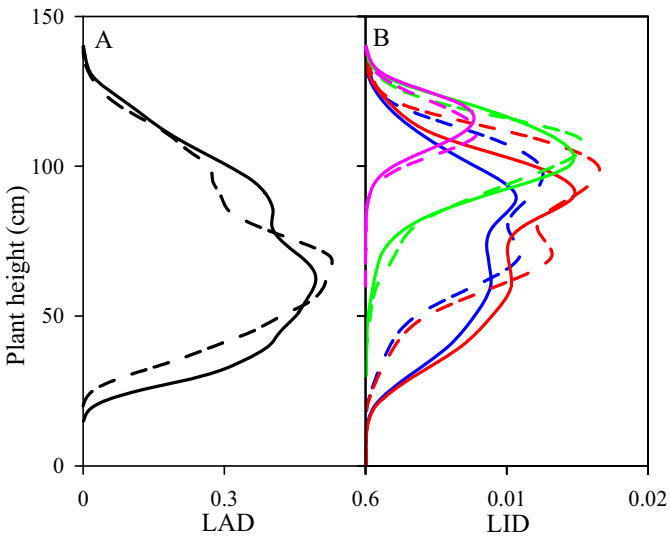

Fig. 2. Leaf area density (LAD, A) and light interception density (LID, B) as a function of plant height for Shanyou63 (dash line) and Peiai64S/E32 (solid line). LID was calculated when the sun elevation was at 10° (pink), 30° (green), 50° (blue) and 70° (red).

Fig. 3 showed the simulation results of the spatial distribution of solar radiation within the canopies for the two hybrid rice when the sun elevation angle was at the maximum sun elevation angle (73°). The canopy of Shanyou63 intercepted up to 92 % of direct solar radiation, which was more than Peiai64S/E32 (89 %). Leaves, panicles and stems contributed 85.8 %, 13.7 % and 0.5 % of light interception respectively for Shanyou63 and 81.9 %, 17.6 % and 0.5 % respectively for Peiai64S/E32. The sunlit leaf area was only 33.6 % and 36.1 % for Shanyou63 and Peiai64S/E32, respectively. The ratio of sunlit leaf area was even smaller with lower sun elevation angle.

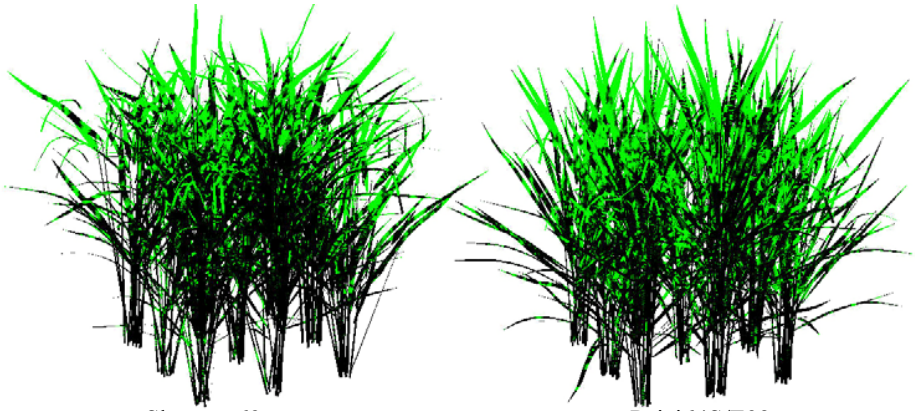

Fig. 3. The visualization of simulated spatial light distribution of Shanyou63 and Peiai64S/E32 canopies. The sun elevation angle was 73° (25 Aug, 12:30). The green color was for sunflecks, the black for shaded parts.

Conclusions

Leaf area and leaf inclination angle distribution in the vertical canopy profile for two hybrid rice cultivars were analyzed with reconstructed 3D architecture model based on the data collected with a 3D digitizer. The results showed that leaf inclination angle of Peiai64S/E32 was larger than Shanyou63, and leaf area distributed more evenly in the vertical canopy profile than the former one.

Spatial distribution of solar radiation within the canopies during the day of measurement was simulated by using PPZB model. The results showed that plant organs shaded each other dramatically with the sunlit leaf area less than 40 %. Shading effects of panicles in the grain filling stage should not be neglected. Generally speaking, rice cultivars with relatively evenly distributed leaf area in the vertical profile, and steeper leaf angle at the upper canopy and shallower at the lower canopy (e.g. Peiai64S/E32) can intercept more direct solar radiation at higher sun elevation angles, which is beneficial to lower leaves in the canopy for photosynthesis, thus increases crop yield.

Acknowledgements: This study was sponsored by "863" Hi-Tech Research & Development Program of China (2006AA10Z231), the Program for Changjiang Scholars and Innovative Research Team in University (IRT0412).

References

Falster, D. S. and Westoby, M. 2003. Leaf size and angle vary widely across species: What consequences for light interception? New Phytologist, 158: 509-525.

Pearcy, R. W. and Yang, W. M. 1996. A three-dimensional crown architecture model for assessment of light capture and carbon gain by understory plants. Oecologia, 108: 1-12.

Sinoquet, H., Thaniswanyangkura, S., Mabrouk, H. and Kasemsap, P. 1998. Characterization of the light environment in canopies using 3D digitising and image processing. Annals of Botany, 82: 203-212.

Sinoquet, H., Stephan, J., Sonohat, G., Lauri, P. E. and Monney, P. 2007. Simple equations to estimate light interception by isolated trees from canopy structure features: Assessment with three-dimensional digitized apple trees. New Phytologist, 175: 94-106.

Wang, X. P., Guo, Y., Li, B. G. and Ma, Y. T. 2005. Modelling the three dimensional distribution of direct solar radiation in maize canopy. Acta Ecologica Sinica, 25: 7-12. (in Chinese with English abstract)

Wang, X. P., Guo, Y., Li, B. G., Wang, X. Y. and Ma, Y. T. 2006. Evaluating a three dimensional model of diffuse photosynthetically active radiation in maize canopies. International Journal of Biometeorology, 50: 349-357.

Watanabe, T., Hanan, J. S., Room, P. M., Hasegawa, T., Nakagawa, H. and Takahashi, W. 2005. Rice morphogenesis and plant architecture: Measurement, specification and the reconstruction of structural development by 3D architectural modelling. Annals of Botany, 95: 1131-1143.

Identifying and characterizing the ontogenetic component in tree development

Yann Guédon[(1)], Yves Caraglio[(2)], Patrick Heuret[(2)], Emilie Lebarbier[(3)] and Céline Meredieu[(4)]

(1) *CIRAD, UMR DAP and INRIA, Virtual Plants*
TA A-96/02, 34398 Montpellier Cedex 5, France
E-mail: guedon@cirad.fr

(2) *UMR CIRAD/CNRS/INRA/IRD/Université Montpellier 2*
Botanique et Bioinformatique de l'Architecture des Plantes
TA A-51/PS2, 34398 Montpellier Cedex 5, France
E-mail: caraglio@cirad.fr, heuret@cirad.fr

(3) UMR *INA P-G/ENGREF/INRA MIA, 16 rue Claude Bernard*
75231 Paris Cedex 05, France
E-mail: lebarbie@inapg.fr

(4) *INRA, Unité EPHYSE - "Ecologie Fonctionnelle et Physique de l'Environnement"*
Site forêt-bois, 69 route d'Arcachon, 33 612 Cestas Cedex, France
E-mail: Celine.Meredieu@pierroton.inra.fr

Key words: hidden semi-Markov chain; morphogenetic gradient; multiple change-point detection; ontogeny; phase change.

Introduction

Observed growth, as given, for instance, by the length of successive annual shoots along the main axis of a plant, is mainly the result of two components: an ontogenetic component and an environmental component. We made the assumption of a decomposition model where the ontogenetic growth component and the environmental component (mainly of climatic origin) were combined in an additive manner. This relies on the fact that ontogeny generally has a longer term effect than time-varying environmental factors; see Barthélémy and Caraglio (2007).

A key question is whether the ontogenetic growth component along an axis (i.e. successive entities built by the same meristem) at the growth unit or annual shoot scale takes the form of a trend (i.e. a "long-term change in the mean level") or of a succession of roughly stationary phases. The main variable of interest is the length of the entity but additional variables may be useful such as the number of growth units for polycyclic annual shoots or the number of branches when the branches can be considered as morphologically similar.

Materials

Two types of retrospective observation protocol should be distinguished: (i) A single or a few mature trees are measured. The data thus provide an overall picture of tree life but sufficient information is only available in the case of long and well-defined stationary phases. (ii) Only the most recent entities are measured in a sample of tree trunks. Sufficient information is available whatever be the length of the phases but only a few (possibly censored) phases can be studied in this way. In order to extract the ontogenetic growth component on the basis of a sample of short sequences corresponding to the most recent entities, it is thus necessary to mix climatic years within a given ontogenetic phase. Hence, sub-samples of trees corresponding to different age classes and growing under similar conditions should be observed.

Example 1 - *Apical growth and branching in 70-year-old Corsican pines described at the annual shoot scale*

Six trunks of approximately 70-year-old Corsican pines (*Pinus nigra* Arn. ssp. *laricio* Poir., Pinaceae) planted in two forest stands in the "Centre" region (France) were described by annual shoot (approximately the first 2 years not measured). These 6 trees were taken from two stands

with contrasting densities and correspond for each stand to three different diameter classes. Two quantitative variables were recorded for each annual shoot, namely length (in cm) and number of branches per tier. Hence, information from both the parent entity (length of the annual shoot) and the offspring entities (number of branches per tier) were combined in the measurements.

Example 2 - *Apical growth and branching in young Corsican pines described at the annual shoot scale*

The data sample comprised four sub-samples of Corsican pine: 31 6-year-old trees, 29 12-year-old trees (first year not measured), 30 18-year-old trees (first year not measured) and 13 23-year-old trees (first 2 years not measured). Plantation density was 1800 stems/ha for the first sub-sample (6 year old) and 2200 stems/ha for the three other sub-samples. The observation protocol already described for the 70-year-old Corsican pines was applied to these young Corsican pines planted in the same forest.

Example 3 - *Apical growth in Dicorynia guianensis described at the internode scale*

A tree was described at the Paracou field station in a lowland tropical rain forest, near Sinnamary in French Guyana. This individual was selected according to its total main axis height and its apparent proper development (i.e. absence of damage) but no information was available concerning chronological age. The data consist of a sequence of 152 internode lengths taken from the base to the top of the main axis.

Methods for analyzing sequences

Various methods of analysis ranging from exploratory analysis (symmetric smoothing filters, sample autocorrelation functions) to statistical modeling (multiple change-point models and hidden semi-Markov chains) were applied to extract and characterize the ontogenetic growth component. Multiple change-point models (Guédon *et al.*, 2007) are used to delimit segments within sequences for which the data characteristics are homogeneous within each segment while differing markedly from one segment to another. Hidden semi-Markov chains (HSMCs) (Guédon, 2003) are particularly useful for analyzing homogeneous zones within sequences. Hidden semi-Markov chains generalize hidden Markov chains with the distinctive property of explicitly modeling the length of each zone. The structure of a hidden semi-Markov chain can be described as follows. The underlying semi-Markov chain represents both the succession of zones and the length of each zone while observation distributions attached to each state of the semi-Markov chain represent the values observed within a zone for each variable. It should be noted that both hidden semi-Markov chains and multiple change-point models with appropriate parameterizations can be applied to multivariate sequences build from variables of heterogeneous types.

Multiple change-point models and hidden semi-Markov chains share the same segmentation objective. However, the main difference between these two families of models is that, while in the case of change-point models, the change points are model parameters to be estimated, in the case of hidden semi-Markov chains, the change points are recovered from the most probable state sequence computed on the basis of the observed sequence using the estimated model. Another difference is that a multiple change-point model applies to a single sequence while a "left-right" hidden semi-Markov chain (i.e. composed of a succession of transient states and a final absorbing state) requires a sample of sequences to be estimated accurately. Contrarily to multiple change-point models for which methods have been proposed for the selection of the number of change points, there is no model selection method with a firm mathematical basis for the selection of the number of states of a non-ergodic hidden Markovian model and empirical methods should be used.

Results

Multiple change-point models and hidden semi-Markov chains were applied to identify growth phases on different samples of Corsican pine tree trunks described at the annual shoot scale and

on the main axis of a *Dicorynia guianensis* described at the internode scale (and on supplementary examples in Guédon *et al.* (2007)). A good agreement was noted between the segmentations obtained with multiple change-point models and hidden semi-Markov chain for the 70-year-old Corsican pines; see two individuals in Figure 1. Symmetric smoothing filters were also applied to extract trends in the 70-year-old Corsican pines. The results support the assumption of abrupt changes between roughly stationary phases rather than gradual changes; see Figures 1 and 2. It is important to note that phase identification accuracy is strongly related to phase length and to the magnitude of the change points that delimit the phase, the ideal situation being a long stationary phase delimited by two change points of high magnitude.

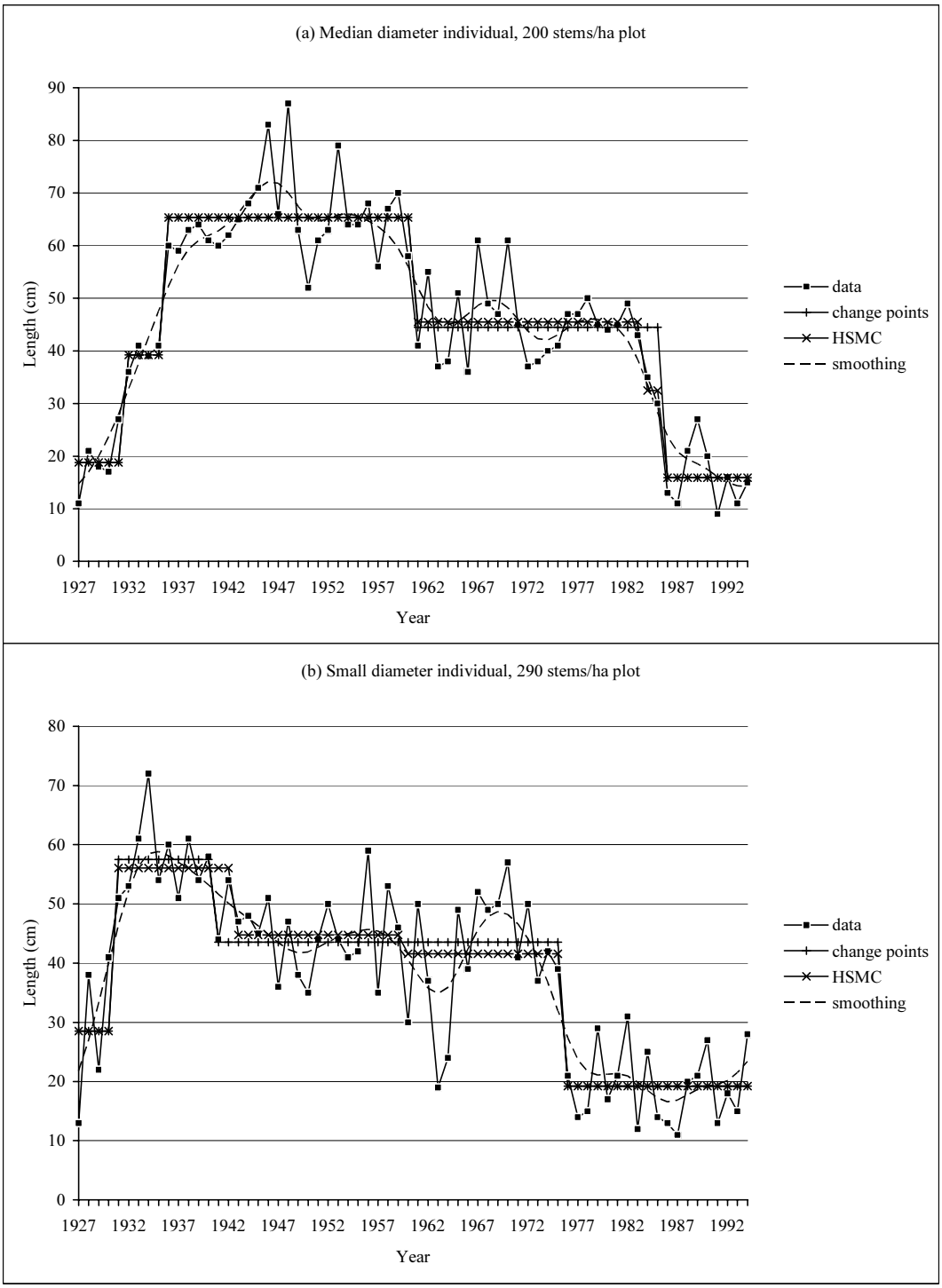

Figure 1. Seventy-year-old Corsican pines: segmentation of annual shoot length sequences.

According to the field observations, the first change point identified in the *Dicorynia guianensis* (Figure 2) corresponded approximately to the occurrence of the first offspring shoot while the second change point corresponded approximately to the beginning of a more intensive branching zone and these two change points corresponded most likely to an increase (by step of 2) in the number of leaflets. This latter point should be checked.

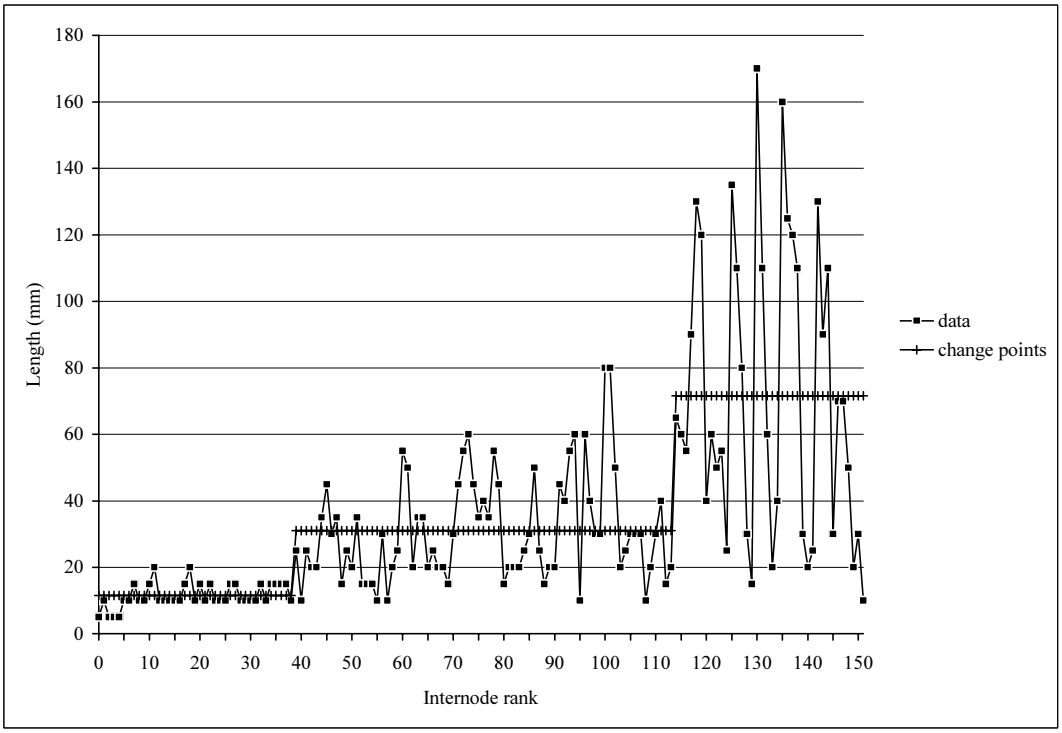

Figure 2. *Dicorynia guianensis*: segmentation of the internode length sequence.

While it is often admitted that root installation or stratum change (this latter factor is particularly relevant for the *Dicorynia guianensis* example) can induce an abrupt increase in the length of the entities, the ageing process is often viewed as a gradual decrease (called "drift") in the length of the entities. Hence, identifying phase changes of high magnitude in 70-year-old Corsican pines when growth globally decreases is an unexpected result. We checked that the residual sequences, obtained by subtracting from each original sequence the step function deduced from the estimated multiple change-point model (Lavielle, 1998), were stationary and close to white noise sequences. We also checked that the change points corresponding to the decrease in shoot length of highest magnitude were not synchronized (see Figure 1), thus eliminating a purely climatic origin for these abrupt changes. We thus suspect that these phase changes are expressions of endogenous equilibriums. These results support the general botanical notion of "morphogenetic gradient" but also highlight thresholds in plant architecture development (threshold of differentiation, see Barthélémy and Caraglio, 2007).

Perspectives

In the proposed approach, the climatic component was globally characterized as a roughly random stationary component but it may be interesting to study in detail the plant's response to changing climatic conditions. Markov switching linear mixed models, i.e. models that combine linear mixed models in a Markovian manner, were introduced in Véra *et al.* (2004). These models belong to the family of hidden Markovian models. The underlying Markov chain represents the succession of growth phases while the linear mixed models attached to each state of the Markov

chain represent both the influence of explanatory variables (mainly climatic variables which are time-varying explanatory variables) and inter-individual heterogeneity due to unobserved factors such as plant pathogen infestation within a given growth phase. New developments and results of Markov switching linear mixed models are presented in Chaubert *et al.* (2007).

In the case where climatic data are not available, the climatic component could be modeled as synchronous fluctuations between individuals incorporating a random time effect in multiple change-point models or Markov switching models.

References

Chaubert, F., Caraglio, Y., Lavergne, C., Trottier, C. and Guédon, Y. (2007). A statistical model for analyzing jointly growth phases, the influence of environmental factors and inter-individual heterogeneity: Application to forest trees. In: 5*th International Workshop on Functional-Structural Plant Models (FSPM07).*

Barthélémy, D. and Caraglio, Y. (2007). Plant morphology and architecture: a dynamic, multilevel and comprehensive approach of plant form and ontogeny. *Annals of Botany* 99(3), 375-407.

Guédon, Y. (2003). Estimating hidden semi-Markov chains from discrete sequences. *Journal of Computational and Graphical Statistics*, 12(3), 604-639.

Guédon, Y., Caraglio, Y., Heuret, P., Lebarbier, E. and Meredieu, C. (2007). Analyzing growth components in trees. To be published in *Journal of Theoretical Biology.*

Lavielle, M. (1998). Optimal segmentation of random processes. *IEEE Transactions on Signal Processing*, 46(5), 1365-1373.

Véra, C., Guédon, Y., Lavergne, C. and Caraglio, Y. (2004). Analysis of longitudinal data applied to plant architecture study In: 4*th International Workshop on Functional-Structural Plant Models*, Montpellier, 65-69.

Linking Carbon Economy and Architectural Development of Peach Trees by Integrating Markovian Models into L-PEACH

Evelyne Costes[1], Colin Smith[1,3], Romeo Favreau[3], Yann Guédon[2] and Theodore DeJong[3]
[1] UMR DAP CIRAD/INRA/SupAgro/IRD
Architecture et Fonctionnement des Espèces Fruitières Team, Montpellier, France
costes@supagro.inra.fr, smithco@gmail.com
[2] UMR DAP CIRAD/INRA/SupAgro/IRD Virtual Plants INRIA Team, Montpellier, France
guedon@cirad.fr
[3] Department of Plant Sciences University of California Davis, CA 95616 USA
rrfavreau@ucdavis.edu, tmdejong@ucdavis.edu

Keywords: carbohydrate partitioning, L-systems, functional structural plant modeling, plant growth simulation, branching patterns.

Introduction

Linking tree architectural development and carbon partitioning during a growing season has been identified as a weak point in functional-structural plant models (LeRoux *et al.*, 2001). In the L-PEACH model (Allen *et al.*, 2005), carbon partitioning was used to drive organ growth, but the organs and shoot types were not accurately distributed within the tree. Our goal was to propose a solution for linking statistically-based models of architectural development with a physiologically-based model of carbohydrate partitioning in peach trees. The approach was to integrate Markovian models representing the tree's topology, that is, the connectivity of the tree's entities (Guédon *et al.*, 2001 and Renton *et al.*, 2006), into the L-PEACH model.

Simulating Peach Tree Topology with Markovian Models

In peach trees, each node can lack a bud (blind node) or can have a central bud that can be blind, floral or vegetative. Vegetative central buds can have zero, one or two lateral floral buds (Costes *et al.*, 1999). Axillary buds are organized along a shoot into successive zones. Within each zone the bud fates are homogeneous and between zones they strongly differ. For example, in one zone there may be dormant vegetative buds mixed with short lateral shoots, while in another zone, axillary flowers mixed with sylleptic shoots. To represent these branching patterns, bivariate hidden semi-Markov chains (HSMCs) were parameterized from observations (Costes *et al.*, 1999). The first variable represented the central bud fate and the second variable represented the number of additional floral buds. Models were developed for different shoot types. Three shoot types with decreasing vigor were considered: very vigorous (or water sprouts), vigorous (or mixed shoots) and moderate. Short shoots (spurs of low vigor) were assumed not to branch. HSMCs corresponding to the categories of branched shoots mainly differed by the number of zones: basal and distal zones were common to all shoot types while the median zones disappeared when moving from the most to the least vigorous shoot types.

Linking Carbon Availability and Growth

In the L-system simulation, the tree was started in the first spring with a very vigorous shoot. Then, a shoot category was attributed to each bud depending on its position within the tree. Each attributed category was assumed to represent the maximum growth that can develop from each bud. Axillary bud fates were determined by HSMCs. Terminal bud categories had decreasing length potentials as the tree developed, based on observations of tree ontogeny that have been carried out on different species (Gatsuk *et al.*, 1980 and Nozeran *et al.*, 1984). As previously done in an apple tree model (Smith *et al.*, 2007), the changes in shoot category with years were modeled with transition probability matrices of simple Markov chains.

To link tree growth to carbon economy, we first assumed that a given amount of carbon is required to build up each new metamer. If the tree has a sufficient amount of carbon the shoots grow to their full size; but, if there is a carbon deficit, the shoots are reduced in length. When the rate of growth is significantly slower than a target rate of growth, buds produced by the metamer are downgraded. For example, a central vegetative bud with two lateral floral buds may have the floral buds removed. Since the rate of growth only slows when there is a carbon deficit, this ties the local shoot architecture to carbon availability. If the rate of growth remains slow for several consecutive metamers in a zone, the remaining metamers in that zone are skipped. A limit is also placed on the potential length of shoots based on how late in the growing season the shoot starts growing. A shoot that begins growth at spring bud break may reach its full size; but, a shoot that begins growth later in the season, as may happen with sylleptic shoots or in response to summer pruning, will have its size limited. This is imposed by reducing the bounds of the Markovian sequences (*e.g.*, a medium shoot at bud break may be 16–35 metamers, but later in the season it will only be 12–25 metamers). If the bounds are reduced by a large amount, the shoot category may be downgraded (e.g., a moderately vigorous shoot may be downgraded to a low vigor shoot).

Simulation Results and Interpretation

Using HSMCs for determining axillary bud fates and Markov chains for terminal bud fates, we simulated a series of trees which displayed different lateral branching along the one-year-old trunks (Figure 1).

Fig. 1. Two stochastic simulations of growth and lateral branching on trunks of peach trees. Colors represent the successive branching zones along the shoots. The simulated time span is 1.5 years.

The dependence between the current charge of the last internode developed and the potential of the shoot to develop new organs, allowed linkage of tree organogenetic potential to carbon availability. Thus the length of a developed shoot depended on both its initial category and the carbon available during its growth period. One of the most obvious results obtained concerned the median zones (particularly, the zones of sylleptic and floral axillary shoots) which varied greatly depending on the carbon threshold of the growing zones along the shoot (Figure 2). A higher carbon threshold for continuing into some zones led to a progressive reduction in the organogenetic activity in both the main shoot growth and in lateral shoots. Both the number of internodes along the main shoots and the number of lateral shoots decreased as the thresholds increased. The most extreme case resulted in such a decrease in the main shoot growth that branching did not occur (Figure 2, right). The reduction of the current shoot length due to carbon limitation also impacted the subsequent year of growth.

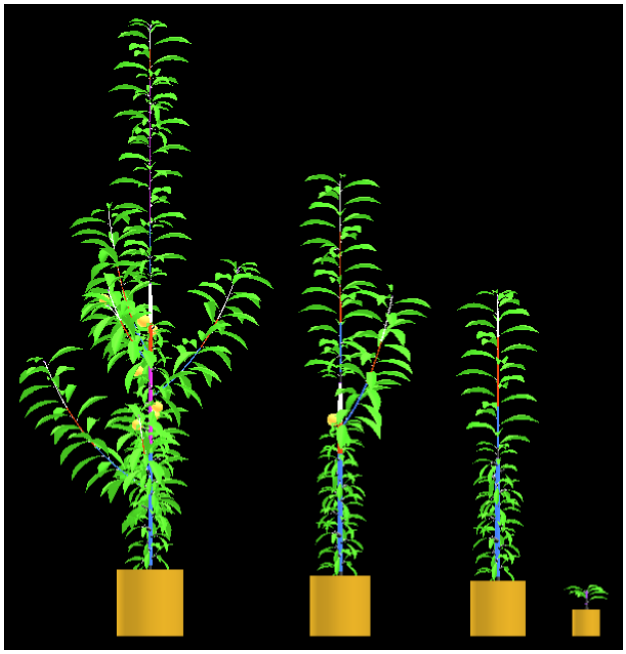

Fig. 2. Reduction in growth and lateral branching along a peach tree trunk depending on the carbon threshold required to build successive zones. The tree on the left is the normal case (all zones are developed). In the right most tree, the carbon thresholds for each zone were twice those of tree on the left. The simulated time span is for 1.5 years.

Conclusion

The integration of Markovian models for representing the tree topology in terms of shoot categories provides a new version of L-PEACH with the capability to tune the architectural development of whole trees according to carbon economy. This constitutes a step forward the integration of interactions between the bud organogenetic potential and carbon partitioning since the previous version of L-PEACH only tuned the organ development. Moreover, this model provides a new tool to further investigate the interactions between tree ontogenetic gradients and growing conditions. However, as was noted, the mechanism of skipping branching zones when carbon is in short supply is hypothetical; the values chosen for the thresholds are thus speculative. Further research must be done to establish experimental support for this mechanism and quantify the carbon thresholds.

References

Allen M., Prusinkiewicz P. and DeJong T. 2005. Using L-systems for modeling source-sink interactions, architecture and physiology of growing trees: the L-PEACH model. New Phytologist 166, pp. 869-80.

Costes E., Guédon, Y. and Fournier D. 1999. Analysis and modelling of fruit tree axillary shoot and flowering distribution. Fruits, 54, pp. 431-440.

Gatsuk L., Smirnova O., Vorontzova L., Zaugolnova L. and Zhukova L. 1980. Age states of plants of various growth forms: a review. Journal of Ecology 68, pp. 675-96.

Guédon Y., Barthélémy D., Caraglio Y. and Costes E., 2001. Pattern Analysis in Branching and Axillary Flowering Sequences. Journal of Theoretical Biology 212(4), pp. 481-520.

LeRoux X., Lacointe A., Escobar-Gutiérrez A., LeDizès S. 2001. Carbon-based models of individual tree growth: a critical appraisal. Annals of Forest Science 58, pp. 469-506.

Nozeran R. 1984. Integration of organismal development. In Positional controls in plant development. P.W. Barlow and D.J. Carr (Editors), pp. 375-401.

Renton M., Guédon Y., Godin C. and Costes E. 2006. Similarities and Gradients in Growth Unit Branching Patterns during Tree Ontogeny based on a stochastic approach in 'Fuji' Apple Trees. Journal of Experimental Botany 57(12), pp. 3131-3143.

Smith C., Godin C., Guédon Y., Prusinkiewicz P. and Costes E. On the simulation of apple tree development using mixed statistical and biomechanical models. Accepted to FSPM 2007.

Parameter Identification of a Functional-Structural Tree Growth Model and Application to Beech Trees (*Fagus sylvatica*, Fagaceae)

Véronique Letort[1], Paul-Henry Cournède[1], Amélie Mathieu[1], Philippe de Reffye[3, 4], Thiéry Constant[2]
[1] MAS, Ecole Centrale de Paris, France; {letort|cournede}@mas.ecp.fr
[2] INRA Nancy, Lerfob, France ; constant@inra.nancy.fr
[3] INRIA Futurs, DigiPlante, France
[4] Cirad, Montpellier, France ; philippe.de_reffye@cirad.fr

Keywords: Substructure factorization, FSM calibration, *Fagus sylvatica.*

Introduction

Classical process-based forestry models usually rely on a very coarse description of tree architecture and thus are not sufficient to study specific processes in which plant geometry plays a key role. It has lead to the emergence of functional-structural models, simulating interactively the architectural development of trees and their physiological functioning (Sievanen *et al.* 2000, Prusinkiewicz 2004). However, due to the complexity of tree architecture, validation of such models remains a critical point. Indeed, although several models can provide a very fine description of the tree at organ scale, such a level of details is not easily available on real data: only global, aggregated or sampled measurements are reasonable to expect. Consequently, the model parameterization generally relies on the independent parameterization of the physiological processes involved (e.g. Perttunen *et al*., 2001). The model validation is often restricted to comparison of the model behaviour to general observation on real trees. Besides the problem of data collection, another obstacle limiting the calibration of complex topological structures is the speed of simulation. Any model inversion procedure relies on a large number of direct model simulations so a time-consuming simulation algorithm is not suitable for an efficient calibration. In this context, this paper presents and discusses a method to estimate the parameters of the functional-structural model GreenLab (Yan *et al*., 2004) dedicated to the special case of trees, or more generally to plants with a complex topological structure. The major idea is to adapt the model to a level of simplification in adequacy with the level of experimental data aggregation.

Materials and Methods

The GreenLab model simulates the architectural development and the dynamic allocation of biomass at organ level. Both processes are driven in parallel by a ratio of biomass supply (Q) and demand (D). For a detailed presentation, we refer to Yan *et al.* (2004) and Cournede *et al*., (2006). The topology of the plant is described using botanical observations, namely hierarchic organization and repetition phenomena in tree architecture (Barthélémy and Caraglio, 2007). The botanical concept of physiological age (PA) allows the structural factorization of the plant (*i.e.* the multi-scale decomposition of the plant into structural units that are computed only once and assembled to form the tree architecture). Thus, owing to a compact writing of the dynamical development equations (see Cournède *et al*., 2006), the computational time is reduced from exponential to quadratic time-dependence. At each growth cycle (one year for trees of temperate regions without polycyclism), the biomass produced by the leaves is allocated to buds and rings, according to their respective demands. The ring compartment is assumed to play a buffer role (not detailed here) so

that the simulated tree invests more in secondary growth if the conditions are favorable. Biomass allocation to the annual ring is computed for each internode according to the foliage surface above its position in the tree architecture, from an equation generalizing the often-limited Pressler law (Deleuze and Houllier, 2002). Bud demand depends on the tree architecture and on its potential ability to set up new metamers. Tree architectural plasticity is modeled by a feedback influence of photosynthesis on organogenesis. The number of metamers forming a new shoot depends on the biomass allocated to the bud, which is determined according to its potential demand and to the trophic competition state of the tree at the previous growth cycle. It can be modeled as a function of the ratio of available biomass to plant demand Q/D (Mathieu *et al*, 2004). For example, the number of new metamers from a bud of PA *i* and potentially bearing axillary buds of PA *k* is given by Equation (1):

$$M_{ik}(t) = \left\lfloor M_{ik}^{1} + M_{ik}^{2} \cdot \frac{Q}{D}(t) \right\rfloor \quad (1)$$

where $\lfloor x \rfloor$ represents the integer part of x and M_{ik}^{1}, M_{ik}^{2} are parameters of the model. They can be estimated from sampled observations or estimated at any structure level by model inversion. As a consequence, it is possible to incorporate some species-specific general laws for the branching patterns, such as maximal branching order, maximal physiological age of axillary buds or the general structure of branching hierarchy. The remaining parameters are fitted to create an average structure with the same global demand at each growth cycle as the real one.

To test this method, three beech trees (*Fagus sylvatica*) were measured in May 2006 from a natural stand near Nancy (north-eastern France). The goal of the calibration was to find back the evolution of the main biomass compartments in the tree throughout its growth, with a particular focus on the main stem whose quality contributes to the determination of the yield. For each growth unit of the main stem, fresh mass, mean diameter and length were measured. At regular intervals, ring rays were recorded in 4 directions. For each branch of order 2, its length, basal diameter and total fresh weight were measured. They were classified into three categories of PA: short axes (short internodes, no branches) for PA 4, mean branches (bearing mainly axes of PA 4) for PA 3 and large complex branches for PA 2. The ratio of blade mass over wood mass and the specific leaf weight were estimated by sampling. The sink values (relative to blade sink of PA1 that is set to 1) were calculated from the ratio of new blade mass over new internode mass and averaged. These data were fitted with GreenLab using the non linear least square method, the simulated annealing algorithm and the particle swarm optimization implemented in the DigiPlant software (Ecole Centrale Paris).

Results and Discussion

For these first fitting results, one 21-year-old tree was considered. Four functional parameters and 15 topological parameters (driving the metamer and axis numbers for each PA-based category) remained to be fitted (results not shown). The parameter value found for biomass repartition to rings was similar to the one predicted by the Pressler law. The comparison between measured and fitted data is represented for compartment biomass on PA 2 branches (Fig. 1A). The hierarchical organization was set up following the simple rule that a growth unit of given PA can bear only branches of higher PA (e.g. each growth unit on the main stem consists of metamers possibly bearing either no branch and/or PA 4, PA 3 and/or PA 2 branches). The topological structure of the fitted tree is shown in Fig 1B. The numbers of axes are not the same than in the target tree but their demand is similar enough to reproduce the biomass allocation to each compartment and to each growth unit of the stem. The basal effect that can be observed on each substructure (the numbers of metamers and axes progressively increase) is dynamically generated by the model.

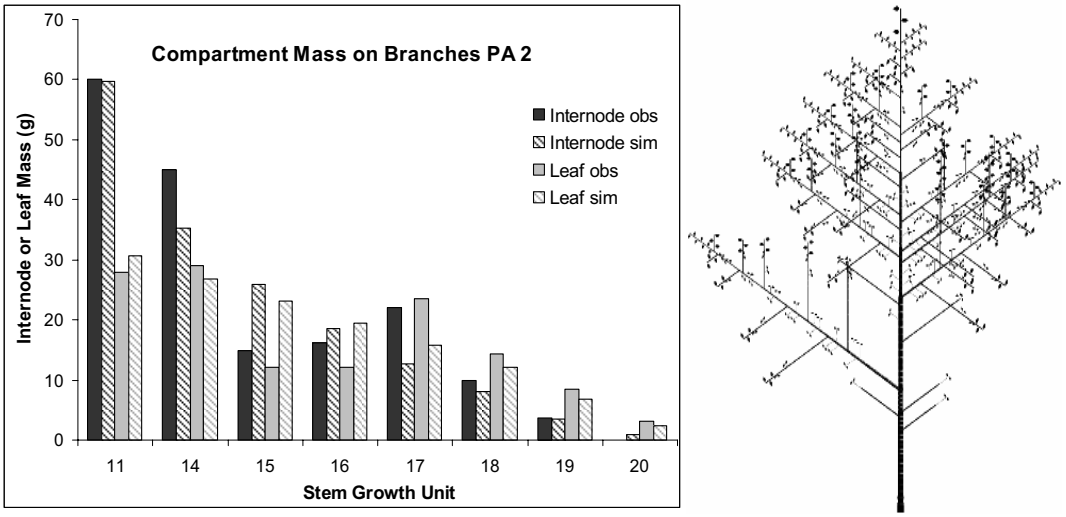

Fig. 1. Some fitting results : (A) graph of compartment biomass (leaf and internode) for substructures of PA 2 branched on the main stem ; (B) fitted tree topology (one grey scale for each PA). The number of branches and the number of metamers per growth unit are driven by the ratio of biomass supply over demand (Q/D).

The substructure factorization results in a natural simplification of the topology: it is no longer based on a detailed description of each branch growth, which would entail facing an inextricable variability. An exhaustive description of an individual tree is not useful if the objective is to determine general results about the interaction between a species and its environment, and transpose results to other individuals. For this reason, the GreenLab model focuses more on the average behavior of the plant and tries to define global rules from botanical observations. Although further study is needed, these first fitting results show that a tree with a simplified structure can reproduce the architectural and functional plasticity of a target tree growth when the branching structure is controlled by a dynamic feedback of its trophic state on its organogenesis processes.

References

Barthélémy D and Caraglio Y. 2007. Plant architecture: a dynamic, multilevel and comprehensive approach to plant form, structure and ontogeny. Annals of Botany 99: 375 - 407.

Cournède P-H, Kang M, Mathieu A, Yan H, Hu B, Reffye (de) P. 2006. Structural factorization of plants to compute their functional and architectural growth. Simulation. 82(7): 427–438.

Deleuze C and Houllier F. "A flexible radial increment taper equation derived from a process-based carbon partitioning model". Annals of Forest Science. 2002, 59: 141-154.

Mathieu A, Cournède P-H, Reffye (de) P. 2004. A dynamical model of plant growth with full retroaction between organogenesis and photosynthesis. ARIMA Journal. 4 : 101-107.

Perttunen J, Nikinmaa E, Lechowicz MJ, Sievänen R, Messier C. 2001. Application of the functional-structural tree model LIGNUM to Sugar Maple Sapling (*Acer saccharum* Marsh) growing in forest gaps. Annals of Botany 88: 471-481

Prusinkiewicz P. 2004. Modeling plant growth and development, Current Opinion in Plant Biology 7(1): 79-83.

Sievänen R, Nikinmaa E, Nygren P, Ozier-Lafontaine H, Perttunen J, Hakula H. 2000. Components of functional–structural tree models. Ann Sci 57:399-412.

Yan H-P, Kang M Z, Reffye (de) P, Dingkuhn M. 2004. A dynamic, architectural plant model simulating resource-dependent growth. Annals of Botany 93: 591–602.

Does the response of leaf stomata to light and vapour pressure follow from limitations in long distance transport?

Eero Nikinmaa*, Teemu Hölttä', Martti Perämäki*, Risto Sievänen[§] and Timo Vesala'
*University of Helsinki, Department of Forest Ecology
'University of Helsinki, Department of Physical Sciences
[§]The Finnish Forest Research Institute

The Water transport capacity of the soil-plant - atmosphere- continuum restricts leaf gas-exchange. The quantity of transpired water cannot exceed that transported from soil to leaves on sustained bases. The plant properties that influence the transport rate are permeability and path length of the conducting tissue and the area of conducting and uptaking tissue relative to the area of the transpiring surface. When trees transpire excessively relative to the supply capacity the tension in the water column rises and air is drawn into the conducting tissue leading to embolism. If the transpiration remains high, this may lead to a so called runaway embolism resulting into permanent dysfunction of xylem. To avoid these negative impacts, plants seem to regulate stomatal opening before a threshold tension, or minimum leaf water potential, is reached (Sperry et al. 2002). As tree height increases, the minimum leaf water potential is reached with lower transpiration rate as the maintenance of same transpiration rate with increasing length requires larger pressure difference, i.e. lower water potential at the leaf (Ryan and Yoder 1997). The hydraulic limitation may thus decrease the productivity of large trees (Ryan and Yoder 1997).

Less attention has been paid to the implications of phloem transport to stomatal regulation and tree productivity although sink limitation has been suggested to be one important restriction for photosynthetic production. Continuous phloem transport requires that the sugar loading to phloem is able to draw water osmotically from the surrounding cells at the source tissue (i.e. leaves) while it is lost to surrounding tissue at sinks as response to sugar unloading. If this was not the case, the phloem sieve tubes would lose the turgor pressure gradient and sugar translocation form the leaves would stop. In practise this means that phloem transport is competing with transpiration for water in leaves. In principle, the sugar loading rate could compensate any transpiration rate. However, very high sugar concentration in phloem sap would make too viscous preventing the transpiration. Like runaway embolism also the latter phenomena has very strong positive feedback resulting into very abrupt stop in the phloem transport (Hölttä et al. 2005).

We studied how stomata should regulate leaf gas exchange to maintain as high assimilate tranport in phloem as possible in a coupled tree xylem - phloem transport model (Hölttä et al. 2005). From the point of view of trees this means maximizing the available assimilates at the sites of carbon utilisation (i.e. sinks). We kept the stomata as open as possible while maintaining the xylem and phloem fluxes and kept phloem turgor positive throughout the phloem and observed how variation in the main driving variables of photosynthesis, intercepted radiation and air vapour pressure deficit influenced stomatal opening. For the sake of simplicity, we assumed a simple Michaelis-Menten light response and linear response to leaf internal CO_2 for photosynthetic rate. The sugar loading at the source was considered directly proportional to photosynthetic rate and unloading at the sink was assumed proportional to phloem sugar concentration.We also assumed increased xylem embolism with increasing water tension in the stem according to the air-seeding hypothesis.

Figure 1 shows the variation of stomatal conductance as a function of light and vapour pressure deficit. The form of the response is very close to observed variation of stomatal conductance to variation of these variables. In low light the stomata are kept closed due to low photosynthetic rate that allows only very low osmotic pressure to develop in the phloem tissue. If stomata would be

opened more, transpiration would start to draw water also from the phloem leading to loss of turgor there. At high light, excessive sugar loading would make the viscosity of the phloem sap so high that it would prevent transport of sugars, leading to so called feed-forward response of the stomata.

The above model is applied to realistic tree structures using the model LIGNUM (shading and transport pathway) to study how variation in leaf position as regards to light and transport pathway should influence the stomatal behaviour relative to the top of the tree.

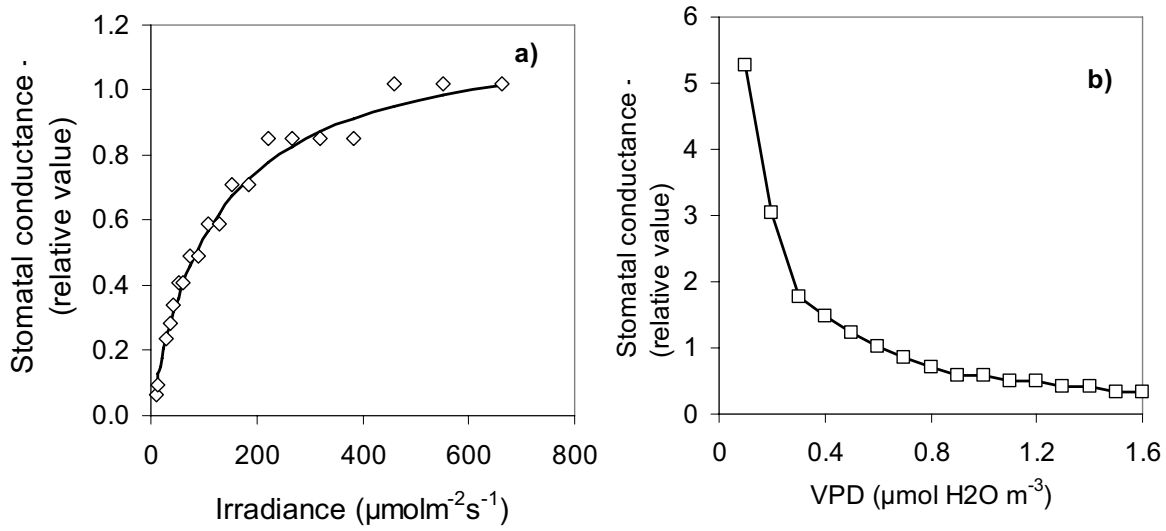

Figure 1. a) Simulated response of stomatal conductance to irradiance on the leaf surface and b) Simulated response of stomatal conductance to leaf vapour pressure deficit when leaf absorbed irradiance was kept at 400 µmolm^{-2}s^{-1} . The stepwise increase in the stomatal conductance in figure a) is due to used numerical method. The used trend line is fitted using Michaelis-menten type function.

References

Hölttä, T., Vesala, T., Sevanto, S., Perämäki, M. and E. Nikinmaa. 2006. Modeling xylem and phloem water flows in trees according to cohesion theory and Münch hypothesis. Trees 20(1):67-78

Ryan, M.G. and Yoder B.J. 1997. Hydraulic limits to tree height and growth. Bioscience 47(4):235-242.

Sperry, J.S., Hacke, U.G., Oren, R., Comstock, J.P. 2002. Water deficits and hydraulic limits to leaf water supply, Plant, Cell Environ. 25, 251-263.

Modeling leaf phototropism in a cucumber canopy

Katrin Kahlen, Dirk Wiechers and Hartmut Stützel
Institute of Biological Production Systems, Leibniz Universität Hannover
Herrenhäuser Straße 2, 30419 Hannover, Germany
kahlen@gem.uni-hannover.de

Keywords: L-system, tropism, *Cucumis sativus* L., light

Introduction

In many species, it can be observed that plants actively adjust the exposition of their leaves into the direction of the incoming radiation, a phenomenon termed phototropism. This results in increased light utilization and higher plant productivity. Shade avoidance responses may be highly adaptive in a natural setting to help plants out-compete neighboring vegetation, but for many crop species a reallocation of resources can reduce crop yield. In maize, where in recent years yield gains have largely come through the breeding of varieties with reduced shading responses, at least some reactions to light gradients can be beneficial to crop performance (Maddonni et al. 2002). Cucumber hypocotyls respond to light signals with a high developmental plasticity (e.g., Shinkle et al. 2005) and wild-type cucumber plants preferentially project leaf area into light gaps and avoid poorly illuminated sites (Ballaré et al. 1995). Based on the data of an experiment conducted in spring 2006, we want to conceptualize and parameterize an extension of the cucumber L-system (Kahlen 2006) that takes into account the plant response to green shading.

Model

The presented model is an extension of the original L-system for cucumber (Kahlen 2006), designed to predict photomorphogenic responses of canopy elements induced by gradients in the local light environment. The model uses the absorbed photosynthetically active radiation (PAR) of the two leaf halves to detect a gradient in PAR between the sunlit parts on the left and right leaf half, LPAR and RPAR. This gradient acts as the driving force for the differential growth response of the corresponding petiole. The response to this gradient leads to tropic movement of the lamina.

For the simplicity of the model, incoming PAR is perpendicular to the ground with a constant intensity of 500 µmol m^{-2} s^{-1}. This corresponds to the mean PAR inside a greenhouse on a sunny summer's day in Germany. Each time step phyllochron is increased by 1. A leaf is visualized by a set of contiguous triangles with a predefined area distribution. It is assumed to reflect 6 % and transmit 7 % of the incident PAR. Each triangle perceives PAR via its corresponding communication module. On leaf level, PAR is assumed to be the mean triangle PAR weighted by the triangle areas. The leaf PAR per phyllochron is converted to the increase in leaf dry weight per phyllochron assuming a day length of 14 h, a phyllochron of 1.3 days, a light use efficiency of 3.4 g MJ^{-1} and an energy equivalent of $0.235 \cdot 10^6$ J per mol of photons. In addition, the model assumes a threshold temperature sum of 136 °Cd for leaf expansion. When reaching this value, a leaf stops expanding. In contrast to the model of Kahlen (2006), maximum leaf area is not an input variable anymore. Leaf area results from leaf dry weight calculated as the ratio of leaf dry weight over specific leaf area, SLA. SLA is assumed to be constant, e.g., 300 cm^2 g^{-1} in the case of two plants per m^2 in row distribution (Kahlen and Stützel 2007). An allometric relationship derived from Kahlen and Stützel (2007) is used to calculate petiole length from lamina dry weight. A linear relationship between leaf area and leaf length is used to calculate leaf length. All lengths used to construct the lamina triangulation are proportional to leaf length. The deviation angle from the initial azimuth orientation of a leaf due to leaf tropism is termed tropism angle. The tropism angle is calculated in relation to the LPAR:RPAR ratio and the petiole age. The maximum angle resulting from differential growth is assumed to be 30°

per phyllochron. If the thermal age of the petiole exceeds 153 °Cd, differential growth stops. The leaf moves to its left side, if the LPAR:RPAR ratio is greater than 1. Else, it moves to its right side. The zone of differential growth of a petiole is located in close vicinity to the intersection of petiole and stem. The bending of up to 90° occurs on a length of a few centimeters. In the model, the tropism angle results in a bending of the basal part of the petiole.

Simulation

The L-system production rules are interpreted by the program CPFG implemented in the software L-studio 4.0.54 (e.g., Měch 2004). The distribution of light in the canopy is simulated using the classical radiosity model integrated in the interface CARIBU 4.4. Only direct lighting on a finite view reduced by reflection and transmission is used. Four scenarios were considered: One and two plants per m^2 grown in rows with and without the option for leaf tropism. Each virtual canopy consisted of five plants in a row. Thus, two plants were border plants. The plant in the center of these small canopies is termed 'center plant'. Simulations were done for 15 phyllochrons.

Evaluation of the model

Simulated leaf tropism in the case of the dense canopy led to a realistic restructuring of the whole canopy (Fig 1). The leaves moved away from the poorly illuminated to the sunlit gaps in the canopy. This means, a leaf did not maintain its orientation when it was in line with the main row axis. Leaves growing perpendicularly to the main row axis did not move at all as were already in their 'optimum' light environment.

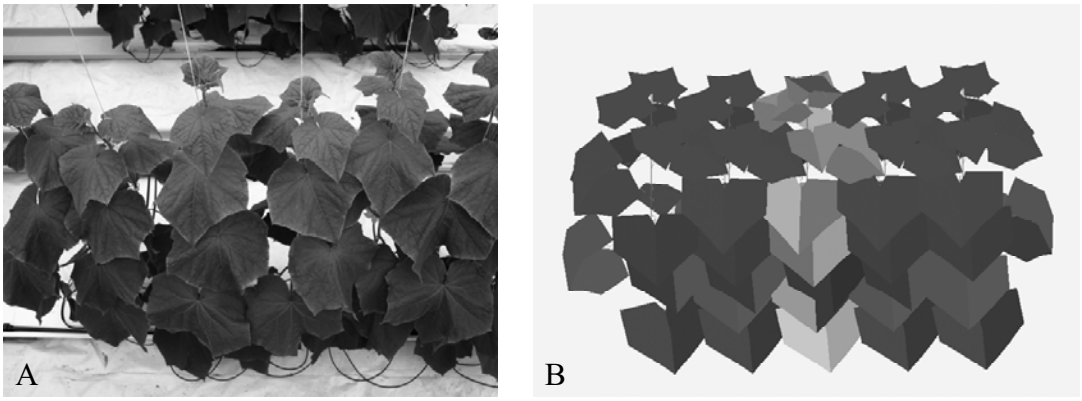

Fig. 1. A) Photograph of a cucumber canopy with two plants per m^2 in row distribution. Plants were vertically trained by clips which do not disturb the reallocation of the leaves. B) Simulation of a cucumber canopy in the same distribution at phyllochron 15. Left and right leaf halves are colored differently. The center plant is colored individually, because it represents a typical canopy plant.

In all simulations, the initial azimuth orientation of a leaf was not affected by the plant distribution. But, we observed in the simulation of the dense canopy both: two consecutive leaves may move either to opposite or to the same side of the row (Fig 1). In contrast, allowing leaf tropism in the wide canopy did not affect single leaf orientation (picture not shown). All effects were observed in the experiment, too. One consequence of the simulated leaf tropism in the dense canopy is that all leaves reaching an age of ca. eight days can increase (e.g., leaf 3 in Fig 2A) or maintain (e.g., leaf 6 in Fig 2A) the mean leaf PAR in comparison to the mean leaf PAR in the simulation without leaf tropism. This might be of particular importance for a plant, because a lamina of this age reaches its maximum net photosynthetic rate (Wiechers, pers. comm.). The simulation also shows that, leaf tropism is beneficial for PAR absorption on plant level, too. In comparison to the normalized PAR of the dense stand, mean PAR of the wide stand is higher (Fig. 2B).

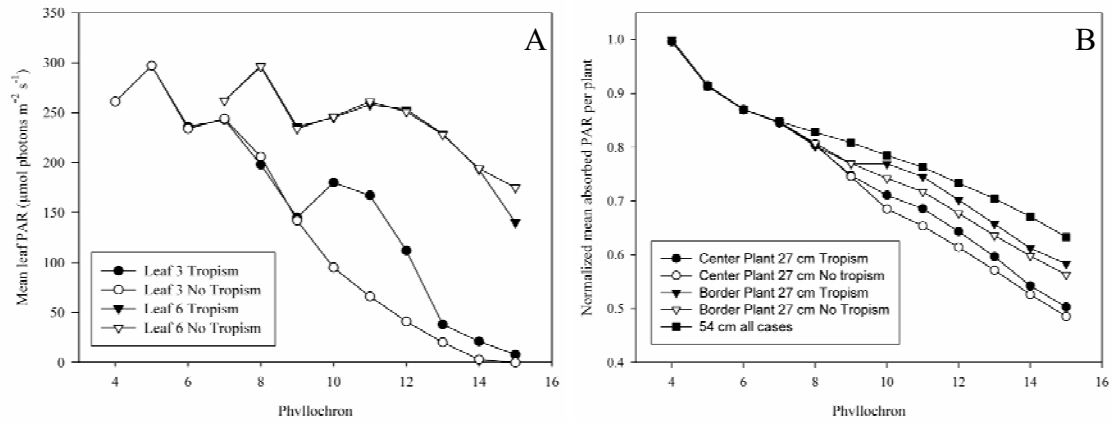

Fig. 2. A) Simulated mean absorbed direct PAR of leaf 3 and 6 in relation to phyllochrons. The leaves are parts of the center plant grown in a virtual canopy with 2 plants m^{-2} and row distribution with a distance between neighboring plants within the row of 27 cm. 'No tropism' means that plants were not allowed to reorient their leaves due to mutual shading. B) Simulated normalized mean absorbed direct PAR per plant in relation to phyllochrons.

Conclusions

The software L-studio and the interface CARIBU established the basis for the presented functional-structural model of cucumber. Even in its preliminary form, it can be used to simulate photomorphogenic canopy responses induced by gradients in the local light environment of the individual leaf. The model advances the state of the art in canopy modeling by considering leaf reorientation as triggered by a stimulus and the plant's response in terms of petiole bending. In future, some model features will have to be improved, e.g., the petiole bending by differential growth and the model time step to keep track of the sun position, because our eventual goal is to use a model to identify improved greenhouse cucumber production systems.

Acknowledgments

We thank Michael Chelle and Pieter de Visser for the support of the CARIBU interface. This project has been supported in part by the German Research Foundation (DFG).

References

Ballaré, C.L., Scopel, A.L., Roush, M.L., and Radosevich, S.R. 1995. How plants find light in patchy canopies. A comparison between wild-type and phytochrome-B-deficient mutant plants of cucumber. Functional Ecology 9:859-868.

Kahlen, K. and Stützel, H. 2007. Estimation of geometric attributes and masses of individual cucumber organs using 3d digitizing and allometric relationships. JASHS (in press).

Kahlen, K. 2006. 3D Architectural modeling of greenhouse cucumber (*Cucumis sativus* L.) using L-systems. Acta Horticulturae 718:51-59.

Maddonni, G.A., Otegui, M.E., Chelle, M., and Casal, J.J. 2002. Maize leaves turn away from neighbors. Plant Physiology 130:1181-1189.

Měch, R., 2004. CPFG Version 4.0 User's Manual.
Available: [http://algorithmicbotany.org/lstudio/CPFGman.pdf] (14. March 2007).

Shinkle, J.R., Derickson, D.L., and Barnes, P.W. 2005. Comparative photobiology of growth responses to two UV-B wavebands and UV-C in dim-red-light- and white-light-grown cucumber (*Cucumis sativus*) seedlings: Physiological evidence for photoreactivation. Photochemistry and Photobiology 81:1069-1074.

3D Modelling of growth and ornamental quality of chrysanthemum at different plant densities

Pieter de Visser, Gerie van der Heijden and Ep Heuvelink
Wageningen University and Research Centre
Wageningen, The Netherlands
pieter.devisser@wur.nl

Keywords: L-system, radiosity model, light interception, FSPM

Introduction

Adaptation of plant form, growth and ornamental quality to local climatic conditions has been reported frequently. In commercial practice, such conditions are continuously manipulated, by e.g. change of plant density, level of assimilation light and temperature regime. The question how the plants react on these changes is of scientific and, ultimately, economic importance. Model simulation of the effects of different cultivation strategies may help growers in their decision making. Local climate conditions can best be described by 3D models that quantify interactions between local microclimate and local plant organs.

For chrysanthemum, both FSPM (Functional Structural Plant Model), dealing with growth and shape at the organ scale (De Visser et al., 2006), and mechanistic models, operating at the crop level (Lee and Heuvelink, 2003; Larsen and Gertsson, 1992), have been developed. To what extent do FSPM render better results in explaining effects of horticultural measures? Crop level models necessarily require some assumptions with regards to effects of light on morphogenesis, which could be tackled by 3D models explicitly. For example, leaf thickness (Acock et al., 1979) and indentation (Spaargaren, 1996) will be affected by the local light level during its growth. A 3D plant model should incorporate carbohydrate dynamics and temperature driven organ developmental processes to account for such effects, i.e. a coupling of function and structure. Our FSPM of chrysanthemum (De Visser et al., 2006) is able to simulate such processes.

In this paper the outcomes of the 3D model are compared to the greenhouse observations and to conventional, 1-D calculations of light interception. Since chrysanthemum plantings are more or less homogeneous in the horizontal, effects of simplifications of the 3D light model to a typical Lambert-Beer approach on the simulation results were tested. The use of properties in the 3D model that were determined at the crop level and not at the organ scale, like observed specific leaf area (SLA) and scattering coefficients, are evaluated. For this, crop properties and plant growth at two different planting densities and two temperature regimes were used. The tests can indicate at which scale specific properties are required to give acceptable model results. The reported model functionality will be most useful to understand and predict response of chrysanthemum plants to a number of cultivation measures commonly used in commercial practice.

Model description

The FSPM of Chrysanthemum consists of three modules:

1. An architectural module, describing the spatial properties and development of the plant-organs in terms of symbols, according to the L-alphabet (*e.g.* Lindenmayer and Prusinkiewicz , 1990).

2. A light-interception module, which takes as input the 3D-scene, including the position and intensity of photosynthetic active radiation (PAR) of the light sources. The nested radiosity model, developed by Chelle and Andrieu (1998), is used to calculate the absorbed PAR at every leaf.

3. A carbon module, which consists of two sub-modules:

- an assimilation module according to the biochemical model of Farquhar (Farquhar et al., 1980), which calculates the hourly produced amount of assimilates per leaf.

- a sink/source module, which takes into account the maintenance respiration and the assimilate distribution over the various plant organs according to a relative sink strength model (Marcelis, 1996). The hourly assimilation per leaf is aggregated to plant level each day and distributed over the plant.

For further model details we refer to De Visser et al. (2006).

Experiment

A greenhouse experiment was carried out with cuttings of chrysanthemum, cultivar Reagan Improved, that were planted at two densities (32 and 64 plants per m^2), each density grown at temperature set points of 16 and 20°C respectively. All four treatments were duplicated. Growth started 4th November 2004 and ended between 24th January and 14th February depending on the treatment. Assimilation light was provided for 18 and 8 hours in long day (LD) and short day (SD) period respectively at 44 µmol PAR m^{-2} s^{-1}. Light extinction at diffuse light conditions was measured (n=6) 10 times during crop development.

The model, calibrated for a growth chamber trial (see De Visser et al., 2006), was validated on the greenhouse data set. At three moments during crop development, when the plants carried 8, 14 and 33 leaves respectively, plant structure in the L-system was fixed and light extinction simulation by the radiosity model was calibrated by adjusting its reflection and transmission coefficients. For this, diffuse light was assumed to originate from 12 light sources, distributed along the hemisphere following Goudriaan and Van Laar (1994). Direct light followed the solar track, and assimilation light originated from the azimuth only.

Results

Light extinction of PAR strongly increased during growth to values above 95% of incoming light at harvest, as illustrated for the high plant density in Fig. 1. A Lambert-Beer relationship with a 0.8 extinction coefficient could be fitted from the data of this density. Similarly, the radiosity model

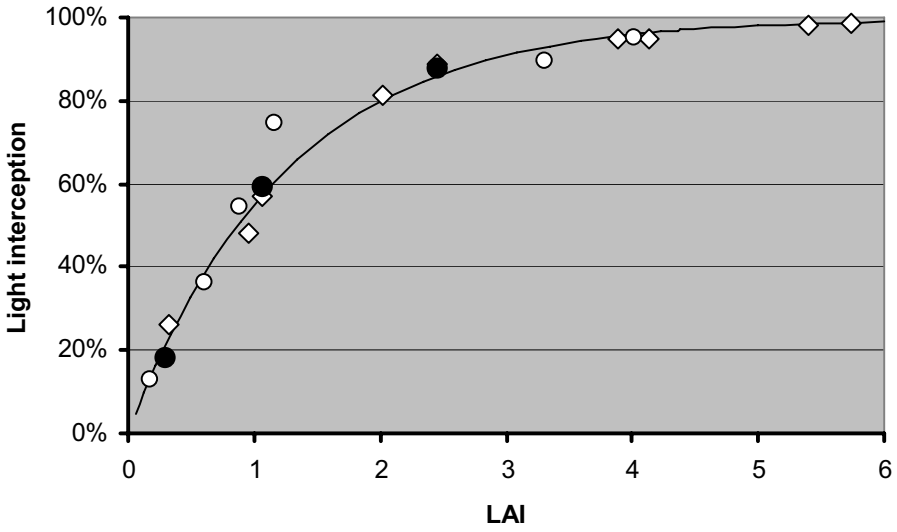

Fig. 1. Light interception in relation to LAI in the low (open circles) and high (diamonds) plant density treatment. Filled circles, radiosity model; Line, fitted Lambert-Beer relationship

simulated light extinction correctly with calibrated reflection of 15% and transmission of 20% (Fig.1). This relationship was valid for both plant density treatments, although at LAI of ca. 1 in the low plant density treatment a slightly higher extinction was observed, which might be attributed to formation of side shoots. On basis of the values for photosynthesis, allometry and respiratory losses, as determined in an earlier study (De Visser et al., 2006), for most of the greenhouse treatments simulated plant growth was comparable to the observations (Table 1).

Table 1. Total simulated plant biomass (g DM) for 4 treatments at harvest. Observed : between brackets.

	16°C	**20°C**
32 pl m^{-2}	11.2 (10.0)	7.6 (8.1)
64 pl m^{-2}	8.8 (6.2)	5.1 (5.0)

In the 20°C treatment SLA was ca. 7% higher at the highest plant density, and combined with the higher number of plants resulted in an LAI of 5.4. At the low plant density LAI was 4.0, caused by heavy leaves and enhanced side shoot formation. The 3D plant model simulated a higher number of side shoots at the lower density, because the model relates this number to the plant biomass during the time frame of bud break (see De Visser et al., 2006). The increase of side shoots and, thus, area for light interception, caused an increase in biomass relative to the higher density plants. The slight change of SLA at the high density was not incorporated in the model: leaf area was directly proportional to leaf weight. Ornamental quality was increased at the lower plant density due to an increase in flower number and, less pronounced, an increase in flower weight. A more detailed comparison of simulation results and greenhouse data will be presented extensively in a full paper.

References

Acock, B., Charles-Edwards, D.A. and Sawyer, S. 1979. Growth response of a *Chrysanthemum* crop to the environment. III, Effects of radiation and temperature on dry matter partitioning and photosynthesis. Ann.Bot. 44: 289-300.

Chelle M. and Andrieu, B. 1998. The nested radiosity model for the distribution of light within plant canopies. Ecol. Modelling 111: 75-91.

De Visser, P.H.B., Van der Heijden, G.W.A.M., Heuvelink, E., S. Carvalho, S. 2006. Functional-structural modeling of chrysanthemum. In: J.A. Vos and L.F.M. Marcelis (eds.), Functional-structural Plant Modelling in Crop Production. Kluwer Acadamic Publishers, The Netherlands.

Farquhar, G.D., Von Caemmerer, S. and Berry, J.A. 1980. A biochemical model of photosynthetic CO_2 assimilation in leaves of C3 species. Planta 149: 78-90.

Goudriaan, J. and Van Laar, H.H.1994. Modelling potential crop growth processes: textbook with exercises. Current issues in production ecology 2. Dordrecht: Kluwer Academic Publishers, 238pp.

Larsen, R. and Gertsson, U. 1992. Model analysis of shoot elongation in *Chrysanthemum x morifolium*. Sci. Hort. 49: 277-289.

Lee J.H. and Heuvelink E. 2003. Simulation of leaf area development based on dry matter partitioning and specific leaf area for cut chrysanthemum. Ann. Bot. 91 (3): 319-327.

Lindenmayer, A. and Prusinkiewicz, P. 1990. The algorithmic beauty of plants. New York, Springer-Verlag.

Marcelis, L.F.M. 1996. Sink strength as a determinant of dry matter partitioning in the whole plant. J. Exp. Bot. 47: 1281-1291.

Spaargaren, J.J. 1996. The year round production of Chrysanthemum (in Dutch). Applied Plant Research, Aalsmeer.

Long-term crown expansion of *Quercus crispula* in Hokkaido, northern Japan: observation and modeling

Kiyoshi Umeki, Kentaro Tada, En-Mi Lin, and Tsuyoshi Honjo

Graduate School of Horticulture, Chiba University
Matsudo, Chiba 271-8510, Japan
umeki@faculty.chiba-u.jp

Keywords: crown expansion, light availability, thinning, tree architecture

Introduction

Canopy structure is one of the most important factors influencing ecological processes in forest ecosystems. For example, it determines light interception and photosynthesis, transpiration, rain interception, litter production, the modification of environmental conditions under the canopy, and the creation of habitats for various organisms (e.g., Montgomery and Chazdon, 2001; Mariscal et al., 2004). Therefore, a better knowledge of canopy structure and its dynamics is indispensable for clarifying the functions of forest ecosystems and managing forests appropriately.

To understand the structure and dynamics of a forest canopy, elucidating the developmental processes of individual crowns is important because a canopy consists of crowns. We analyzed the crown expansion in an oak forest in Hokkaido, northern Japan, and modeled the crown expansion rate in relation to light availability at the crown surface and individual size based on long-term *in situ* observation of crown dimensions. We used the ray-tracing method to estimate light availability at the crown surface and a linear mixed-effects model to relate crown expansion rate with factors influencing it.

Methods

We placed two plots (25 × 50 m) in a secondary hardwood forest stand in Nishiokoppe, Hokkaido, northern Japan, in 1992. The forest stand was dominated by *Quercus crispula.* One of the plots was heavily thinned in 1994, whereas the other remained intact.

For all trees >5 cm in diameter at breast height (*D*), we measured tree height (*H*), height of the live crown base (*Hb*), and the horizontal distance from trunk base to crown edge (*W*) in four directions (north, east, south, and west) in 1995, 1999, and 2003 (Fig. 1a). We recorded the coordinates of the trunk base of trees using a two-dimensional coordinate system on slopes where the plots were located and converted them to three-dimensional coordinates using topological data for the slopes.

To express trees in a modeled stand, an individual tree was divided into a crown and a trunk. A crown was modeled by an ellipsoid and a trunk was modeled by a cone whose tip was at the center of the crown ellipsoid (Fig. 1b). Although this representation of trees is rather simple, we used this because it is directly related to the tree measurement. Using this tree model, we visualized the thinned plot as in Fig. 2.

To evaluate horizontal crown expansion, we calculated the change in the horizontal distance from trunk base to crown edge (*W*) in four directions (changes in the north, east, south, and west

directions are denoted as ΔW_N, ΔW_E, ΔW_S, and ΔW_W, respectively) for the intervals 1995–1999 and 1999–2003. In the analysis, ΔW_N, ΔW_E, ΔW_S, and ΔW_W were pooled and denoted as ΔW. To evaluate vertical crown growth, we calculated the change in crown length (ΔL) whereby crown length (L) is tree height (H) minus the height of the live crown base (Hb).

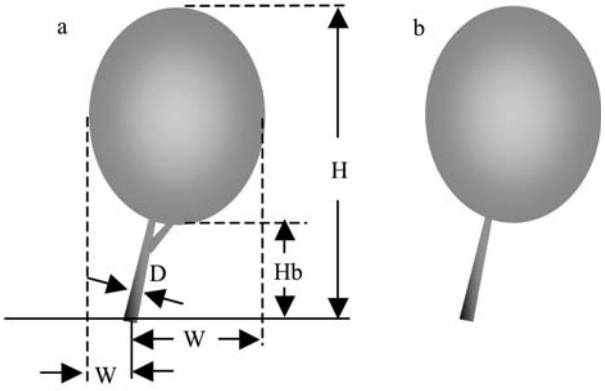

Fig. 1. Schematic diagram of a tree. (a) Measured dimensions of a tree; (b) modeled tree.

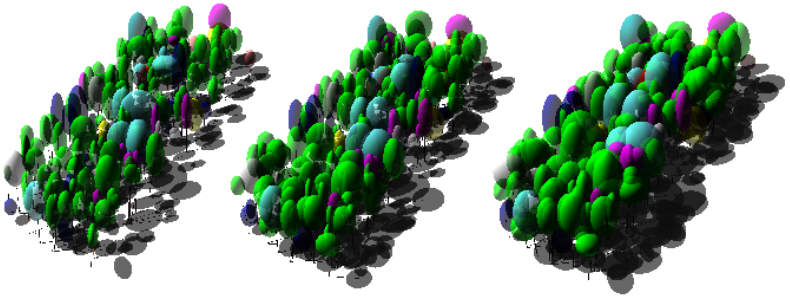

Fig. 2. Three-dimensional visualization of a modeled forest stand for the thinned plot in Nishiokoppe, Hokkaido, northern Japan, in 1995 (left), 1999 (center), and 2003 (right).

Using a ray-tracing method (Sievänen et al., 2000), we calculated canopy openness at 13 points (light sensors) on the surface of the modeled crown as a surrogate of light availability at the points. One light sensor was located at the top of crown. The other light sensors were located on the side surfaces of the crown. Their vertical heights were located at the heights where the distance from the crown base was 1/2, 2/3, and 5/6 of the crown length. At each height, four light sensors were located corresponding to four directions (north, east, south, and west; Fig. 3a). At each light sensor, canopy openness was calculated using 32,768 light beams (128 zenith and azimuth 256 angles); we judged whether each light beam hit crowns or trunks, and evaluated canopy openness as the ratio of the number of light beams that did not hit any objects to the total number of light beams (Fig. 3b).

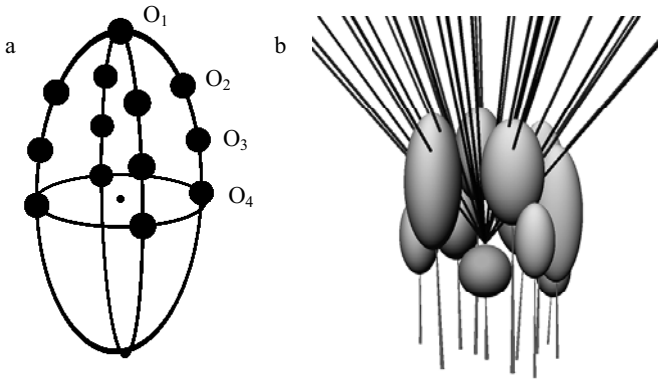

Fig. 3. Method for calculating canopy openness of modeled trees. (a) Positions of light censors on the crown surface of a tree; (b) light beams from a light sensor.

We used a linear mixed-effects model (Pinheiro and Bates, 2000) to construct the relationship between horizontal crown expansion (ΔW) and the explanatory variables of canopy openness at the crown surface for four height levels (O_1–O_4; Fig. 3a), tree height (H), diameter at breast height (D), horizontal distance from the trunk base to the crown edge (W), a qualitative variable representing the effect of different aspects (A; north, east, south, or west), and a binary variable representing the effect of different measurement intervals (I; 1995–1999 or 1999–2003). We considered random variation associated with individual trees and incorporated a random effect (t) into the model. Therefore, the full model was

$$\Delta W = a_0 + a_1O_1 + a_2O_2 + a_3O_3 + a_4O_4 + a_5H + a_6D + a_7W + A + I + t.$$

Four values of ΔW were measured for each individual. For ΔW in a particular direction, we used data for O_2–O_4, W, and A in the corresponding direction (e.g., for ΔW_N measured on the north side of a crown, we used O_2 calculated on the north side). In fitting the model, we pooled data from the thinned and intact plots.

We selected models for the model that best expressed the patterns in the data using the Akaike information criterion (AIC). The candidate models were the full model and its reduced models in which the explanatory variables were a subset of those for the full model.

We analyzed ΔL using a similar method. The full model for ΔL was

$$\Delta L = b_0 + b_1O_1 + b_2Mo_2 + b_3Mo_3 + b_4Mo_4 + b_5D + b_6L + b_7Mw + I + t,$$

where Mo_2, Mo_3, Mo_4, and Mw are the averages of four values of O_2, O_3, O_4, and W, respectively. The best model was selected using the AIC.

Results

The best model for ΔW contained O_1, O_4, H, D, W, A, and I. The best model for ΔL contained O_1, D, L, Mw, and I. The light availability on the side surface of the crown was important in determining horizontal crown expansion, whereas the light availability on the top of the crown determined vertical crown growth. The parameters for O_1 and O_4 (i.e., b_1, a_3, and a_4, respectively) were all positive, indicating that crowns expanded more rapidly as light availability increased.

Discussion

Because crown development determines important ecological processes within forests, numerous observations have been made on crown development using certain crown dimensions (e.g., Osada, 2006; Remphrey and Pearn, 2006; Takahashi and Rustandi, 2006). We observed crown development for 8 years and succeeded in modeling crown development in relation to the localized light environment. The models obtained can be used to predict crown development for forest management purposes.

The results demonstrated that crown development is autonomous to some extent. The selected model for ΔW showed that horizontal crown expansion in a certain direction is dependent on the light availability on the side surface of crown in that direction. The selected model for ΔL indicated that vertical crown growth is dependent on the light availability at the top of the crown. The autonomous response of crowns to the heterogeneous light conditions around them causes an asymmetric crown shape (Sorrensen-Cothern et al., 1993; Takanaka, 1994). Plants can capture more light via plastic adjustment of their foliage distribution to match the heterogeneous light availability (Umeki, 1995). At the stand or forest level, the morphological plasticity in crown shape increases light interception and biomass production (Umeki, 1997).

Future research on the crown expansion should address: 1) can more realistic calculation of the amount of intercepted light that takes sun tracks into consideration explain crown expansion better?, 2) can more realistic representation of crown shape improve the model fitting?, and 3) if we divide the growth process into two parts: matter production and growth allocation, can it explain crown expansion better?

References

Mariscal, M.J., Martens, S.N., Ustin, S.L., Chen, J., Weiss, S.B., and Roberts, D.A. 2004. Light-transmission profiles in an old-growth forest canopy: simulations of photosynthetically active radiation by using spatially explicit radiative transfer models. Ecosystems 7:454-467.

Montgomery, R.A. and Chazdon, R.L. 2001. Forest structure, canopy architecture, and light transmittance in tropical wet forests. Ecology 82:2707-2718.

Osada, N. 2006. Crown development in a pioneer tree, Rhus trichocarpa, in relation to the structure and growth of individual branches. New Phytologist 172:667-678.

Pinheiro, J.C. and Bates, D.M. 2000. Mixed-effects modes in S and S-PLUS. Springer Verlag, Neww York.

Remphrey, W.R. and Pearn, L.P. 2006. Crown architecture development in Salix 'Prairie Cascade', a pendulous willow. Canadian Journal of Botany 84:1531-1541.

Sieväen, R., Nikinmaa, E., Nygren, P., Ozier-Lafontaine, H., Perttunen, J., Hakula, H. 2000. Components of functional–structural tree models. Annals of Forest Science 57:399–412

Sorrensen-Cothern, K.A., Ford, E.D., and Sprugel, D.G. 1993. A model of competition incorporating plasticity through modular foliage and crown development. Ecological Monographs 63: 277-304.

Takahashi, K. and Rustandi, A. 2006. Responses of crown development to canopy openings by saplings of eight tropical submontane forest tree species in indonesia: a comparison with cool-temperate trees. Annals of Botany 97:559-569.

Takenaka, A. 1994. A simulation model of tree architecture development based on growth response to local light environment. Journal of Plant Research 107: 321-330.

Umeki, K. 1995. Importance of crown position and morphological plasticity in competitive interactions in a population of *Xanthium canadense*. Annals of Botany 75: 259–265.

Umeki, K. 1997. Effect of crown asymmetry on size-structure dynamics of plant populations. Annals of Botany 79: 631–641.

Extension of a single tree functional-structural model to stand level

Risto Sievänen, Jari Perttunen
Finnish Forest Research Institute, PB 18, 01301 Vantaa, Finland
Eero Nikinmaa
Department of Forest Ecology, University of Helsinki, 00014 University of Helsinki, Finland
risto.sievanen@metla.fi

Keywords: Functional-structural model, forest stand, Scots pine

Background

The functional-structural tree model LIGNUM (Perttunen et al., 1996; Perttunen and Sievänen, 2005) has been originally constructed to be applied to single trees. The above ground part of the coniferous and the deciduous trees is modeled with structural units. They are tree segment, branching point and bud. So far the root system is represented with a single variable denoting its mass. LIGNUM combines in one modeling framework a process based model and the architectural development of three-dimensional tree crown. The architectural development is accomplished with the aid of Lindenmayer systems. The time step is one year.

The metabolic processes in a tree are explicitly related to the modeling units in which they are taking place. The main functioning unit is the tree segment. The intercepted solar radiation can be computed for each segment with the aid geometrical and optical properties of conifer segments (shoots) or leaves. Photosynthesis is directly proportional to intercepted radiation. The net (carbon) production of the tree is obtained by subtracting respiration losses of the tree compartments and the root system from the whole tree production. The allocation of the net photosynthates in a tree is used to primary growth based on the growth vigor of the terminal buds scattered in the tree, to the secondary growth by defining pipe model relationships invariant in any branching point, and to the renewal of the root system.

The original formulation of LIGNUM employs about 15 parameters and a few functions. In the single tree applications this parameterization has worked satisfactorily. However, there are ample evidence that many of the parameters of LIGNUM change within the crown and during tree development. We report here an exercise where we have extended LIGNUM to a stand (group of trees). It has required taking into consideration the variability of parameter values and functions, and using the voxel space method to assess the radiation conditions.

LIGNUM forest

We have realized LIGNUM forest as consisting of a group of Scots pine trees on a plot 20 m by 20 m. The locations of trees are random with minimun distance between trees of 0.5 m. We have evaluated the radiation conditions (photosyntheically active radiation, reflection ignored) in the stand using a method based on voxel space (or 3D discretization of the space) approach which nevertheless enables us to calculate radiation conditions of single shoots based on their optical properties as described in Perttunen et al. (1998). Unlike in the normal voxel space methods (e.g. Knyazikhin et al. (1997)) we do not evaluate the mean condition in a voxel but rather use it to store information of shoot locations to speed up calculations. The method is described in detail in contribution Perttunen et al. (2007) of the present meeting.

As the calculation of radiation is computationally demanding, we have simplified the stand simulation by growing one tree in the middle of the plot and assuming all the other trees to be identical to the subject tree. In this way we have saved LIGNUM from calculating radiation conditions of all trees that would have been too complex to determine computationally. These stand simulations thus pertain to an even-aged, single species stand. We did not simulate tree mortality but specified stand density as a function of average tree diameter. The initial density was 9400 trees/ha and declined to 2200 trees/ha when diameter is 15 cm at ages beyond 20 years.

We made an analysis on the basis of studies made at the Department of Forest Ecology, University of Helsinki (e.g. Palmroth (2000); Vanninen (2003)) and literature about how the parameters (pertaining to individual tree segments) of LIGNUM vary with local conditions inside the crown and during tree development. The following main parameters are changing within the tree:

Parameter	Depends on
Foliage-wood relationship in shoot	Light conditions
Needle angle	Light conditions
Effect of branching order on segment length	Light conditions
Density of wood	Branching order, age of segment
Light use efficiency	Shading foliage area
Specific needle area	Shading foliage area
Number of buds	Foliage mass of mother segment, light conditions
Length of new segment	Light conditions, branching order
Pipe model coefficient	Branching order

Results

We have compared simulated tree height and diameter to measured ones and they agree reasonably well with an average Scots pine tree growing in a dense stand (Fig. 1). Figure 2 shows two trees grown with different strategy of foliage expansion (otherwise the parameter values have been the same). This indicates how important the flexible response of foliage and branching habit to local conditions is for tree and forest growth. We will present further results on the effect of local flexibility of organ properties on forest growth.

We will also study how this application of LIGNUM to an even-aged single species stand can be extended to a mixed, inhomogeneous forest without losing details or ending up with computational problems.

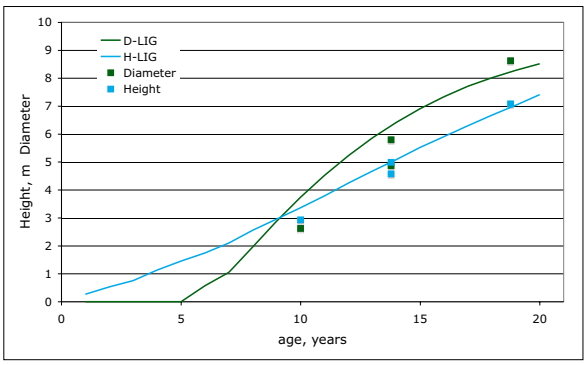

Figure 1: Comparison of simulated (solid line) diameter at breast height (green) and tree height (blue) with measured values (squares).

Figure 2: Effect of distribution of new growth between apical and lateral shoots. Two 20 year old trees; the left one (11.3 m high) has been grown with promotion of apical shoots, in the right one growth has been divided more evenly between apical and lateral shoots.

References

Knyazikhin, Y., Mießen, G., Panfyorov, O., Gravenhorst, G., 1997. Small-scale study of three-dimensional distribution of photosynthetically active radiation in a forest. Agricultural and Forest Meteorology 88, 215 – 239.

Palmroth, S., 2000. Photosynthetic production and resource use efficiency of scots pine: an analysis along environmental gradients. Ph.D. thesis, University of Helsinki Department of Forest Ecology, Publications no. 23.

Perttunen, J., Sievänen, R., 2005. Incorporating lindenmayer systems for architectural development in a functional-structural tree model. Ecological Modelling 181 (4), 479 – 491.

Perttunen, J., Sievänen, R., Nikinmaa, E., 1998. LIGNUM: A model combining the structure and the functioning of trees. Ecological Modelling 108 (1–3), 189–198.

Perttunen, J., Sievänen, R., Nikinmaa, E., 2007. Assessing the light environment for scots pine in the functional-structural tree model LIGNUM. Oral presentation at 5th International Workshop on Functional-Structural Plant Models.

Perttunen, J., Sievänen, R., Nikinmaa, E., Salminen, H., Saarenmaa, H., Väkevä, J., 1996. LIGNUM: A tree model based on simple structural units. Annals of Botany 77 (1), 87–98.

Vanninen, P., 2003. Development of the production and biomass structure of scots pine: effects of competition, tree age and site fertility. Ph.D. thesis, University of Helsinki Department of Forest Ecology, Publications no. 28.

Leaves to landscapes: using high performance computing to assess patch-scale forest response to regional temperature and trace gas gradients

George E. Host[1], Harlan W. Stech[2], Kathryn E. Lenz[2],
Kyle Roskoski[1], Richard Mather[2] and Michael Donahue[2]

[1]Natural Resources Research Institute, University of Minnesota Duluth, Duluth MN USA
[2] Department of Mathematics and Statistics University of Minnesota Duluth, Duluth MN USA
ghost@nrri.umn.edu

Keywords: Photosynthesis, process model, ozone, patch model

Introduction

ECOPHYS is one of the early FSTM's that integrated plant physiological and tree architectural models to assess the relative importance of genetic traits in tree growth, and explore the growth response to interacting environmental stresses (Host et al 1999, Isebrands et al 1999, Martin et al 2001). This paper will describe extensions of the ECOPHYS individual tree model to the scale of tree patches distributed across a regional landscape. The complexity of quantifying hourly light interception within the patch canopy has required the use of various high-performance computing platforms. Additional extensions include advances in photosynthesis modeling, strategies for simulating photosynthetic response to increased atmospheric ozone, and validation of tree growth characteristics with experimental data on *Populus tremuloides* from the Aspen FACE experiment (Rhinelander, WI, USA; Karnosky et al 2003). These advances have led to the ability to use the patch model to simulating changes in forest productivity under 20 and 40 year ozone forecasts across the north central United States.

Parallel Computing

We have implemented a parallel modeling strategy to run simultaneous individual tree models across an N x N patch of trees. The patch consists of "core" trees, which are individually-simulated instances of trees with varied physiological and phenological characteristics, surrounded by rings of "neighbor trees", with canopies created as translates of the core trees. The patch thus represents a 'closed canopy' in which interactions among trees with different attributes and environmental sensitivities, and resulting patch-level responses, can be assessed.

The parallel routines use the standard Message Passing Interface (MPI) Library, and run on 1 to *n* number of computer processors. In the current implementation, a cluster of computer processors collaborates on each simulation, with individual computer processors exchanging canopy information daily. Direct and diffuse radiation are derived from measured weather traces in conjunction with hourly temperature, relative humidity, and atmospheric CO_2 and O_3 concentrations to predict individual leaf photosynthate production and respiratory loss. At the end of each day, photosynthates are distributed via a carbon allocation model (Martin et al 2001, Laconite et al 2002) and used for growth of leaves and branches. Updated canopy information from each processor is then distributed to other processors in the cluster, and the process is repeated for the duration of the simulation.

The code has been tested on patches with core sizes up to 6 x 6, and with simulation lengths of up to 6 years. Code testing has been performed on a small "Beowulf" class cluster located at the University of Minnesota Duluth Visualization and Digital Imaging Laboratory. The model is numerically tractable even on "clusters" consisting of a single Linux computer possessing only two processors. Simulations have also been performed on the high-performance facilities of the Minnesota Supercomputer Institute (MSI), as well as a heterogeneous cluster of networked Linux workstations. Simulating a 6x6 core patch (36 individual trees; 324 trees in full canopy) for three years takes approximately six minutes on our cluster of networked Linux workstations, and one minute using the BladeCenter supercomputing cluster at MSI. A 6x6 patch run for five years at MSI requires approximately eight minutes. The diversity of tree architectures resulting from different clonal attributes and inter-tree interactions are shown in Figure 1.

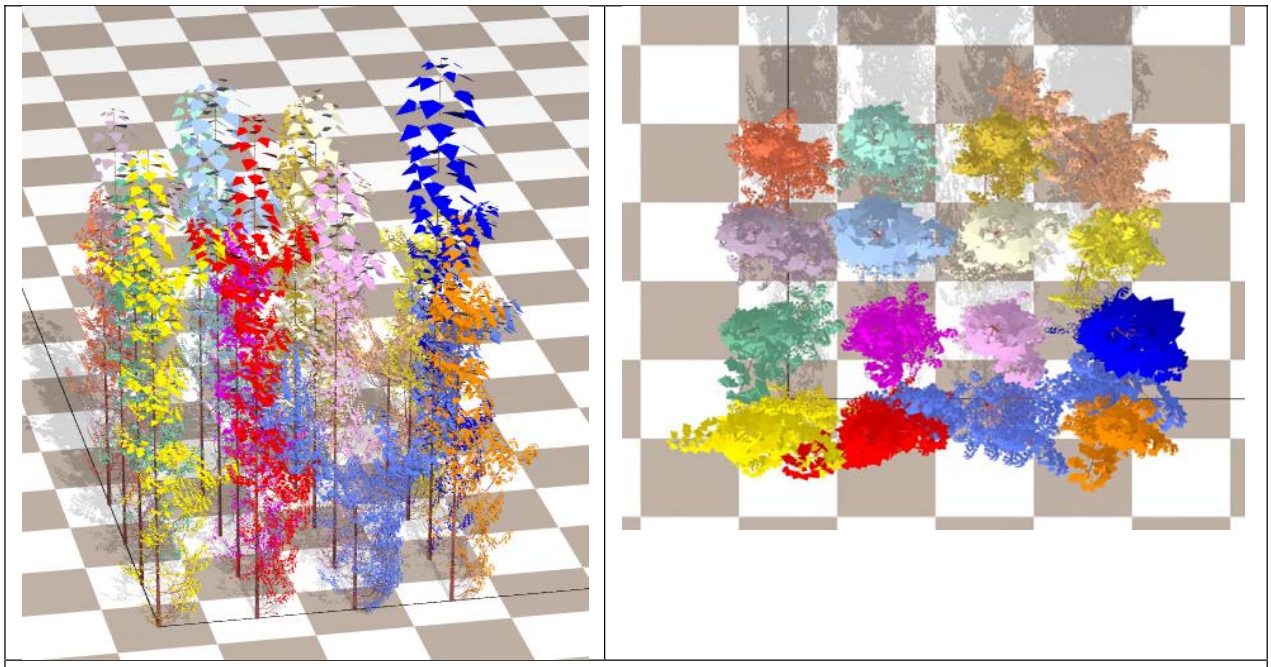

Figure 1. Side and top views of the canopies of a 4x4 patch during the third season of growth. Images are rendered using POV-RAY, a public domain visualization and animation package.

The ability to simulate multiple trees provides the opportunity to assess the sensitivity of the model to key tree and patch scale attributes. Patch attributes include tree spacing patterns, the size of the core patch, and the number of shade rings. These attributes were evaluated under different environmental conditions and with different species characteristics to quantify the relative importance of individual variables and identify interactions among variables; we have employed a fractional factorial design to identify the most sensitive combinations of patch, environmental and tree variables. Tree spacing, parameters of the random leaf drop algorithm and weather year were among the most influential factors; the size of the core patch did not strongly impact growth response variables.

Ozone Modeling

We have developed a model of ozone damage that adds new elements to the model of Martin et. al. (2001); the model views leaf photosynthetic health as an aggregate, dynamic quantity that is reduced by the presence of ozone-produced reactive oxygen species (ROS), but may improve due to various leaf repair mechanisms. The revised model allows for scavenging of ROS as well as

repair or recovery of photosynthetic tissues. The resulting ozone damage/leaf recovery model was integrated with a photosynthesis production model. The augmented system couples stomatal conductance, internal CO_2 concentration, the rate of CO_2 fixation, leaf photosynthetic mechanism "health" and leaf (aggregate) ROS concentration. The system has been shown to be numerically solvable using the mathematical package *Mathematica,* and has been validated by comparing model simulations to a variety of chamber studies taken from the literature – it is currently being calibrated with leaf gas exchange data from *Populus tremuloides* published by Noormets et. al. (2001).

Landscape-scale modeling

The patch model has been applied to regional ozone concentrations projected to 2020 and 2040, under warm/dry (1999) and cool/wet (2001) seasonal weather traces (Fast and Heilman 2005). Ozone concentrations were projected over a 12 x 12 km grid, which was resampled to approximately 40 x 40 km cells, resulting in ~1500 data points distributed across the north central United States. The underlying photosynthesis model in ECOPHYS was modified to simulate water stress effects, following Wang et al. (2001). Water stress (fw) is derived from soil moisture content (θs) relative to the wilting point (θmin), and the field capacity (θmax). Soil moisture content values were obtained from the US National Data Climate Center; we used a linear interpolation between monthly points to determine a value for soil moisture content each day. The fw value reduces photosynthate produced by scaling the Vcmax and the Jmax values within the photosynthesis model. A series of approximately 1500 patch runs across a three-state region of the northern United States showed significant variation related to weather gradients, soil moisture characteristics and regional seasonal trends in ozone exposure (Figure 2).

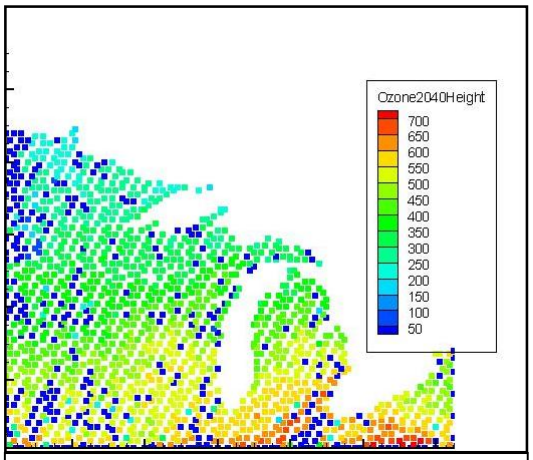

Figure 2. Average height (cm) of a *P. tremuloides* patch under a projected ozone scenario for Yr 2040. Region extends from Minnesota to Ohio, USA.

Acknowledgements

This work was funded in part by the Northern Global Change Program of the USDA Forest Service Award# 05-CA-11242343-036 and the USDA Forest Service North Central Research Station Integrated Program, Agreement 03-JV-11231300-086.

Literature Cited

Fast, J. D and W. Heilman. 2005. Simulated sensitivity of seasonal ozone exposure in the Great Lakes region to changes in anthropogenic emissions in the presence of interannual variability. Atmospheric Environment 39:5291-5306.

Host, G. E., G. W. Theseira, C. Heim, J. G. Isebrands and R. Graham. 1999. EPIC-ECOPHYS: A linkage of empirical and process models for simulating poplar plantation growth. In: (A.

Amaro and M. Tome Eds.) Empirical and Process Models for Forest Tree and Stand Growth Simulation. Edicos Salamandra pp. 419-429.

Isebrands, J. G., G. E. Host, K. McTavish and K. E. Lenz. 1999. Modeling short-rotation forest plantations using hierarchical, parallel computing: A developmental history of ECOPHYS. In: (A. Amaro and M. Tome Eds.) Empirical and Process Models for Forest Tree and Stand Growth Simulation. Edicos Salamandra pp. 537-51.

Karnosky, D.F., D.R. Zak, K.S. Pregitzer, C.S. Awmack, J.G. Bockheim, R.E. Dickson, G.R. Hendrey, G. E. Host, W.S. Jones, J.S. King, B.J. Kopper, E.L. Kruger, M.E. Kubiske, R.L. Lindroth, W.J. Mattson, E.P. McDonald, A. Noormets, E. Oksanen, W.F.J. Parsons, K.E. Percy, G.K. Podila, D.E. Riemenschneider, P. Sharma, A. Sober, J. Sober, S. Anttonen, E. Vapaavuori, and J.G. Isebrands. 2003. Tropospheric O_3 moderates responses of temperate hardwood forests to elevated CO_2: A synthesis of molecular to ecosystem results from the Aspen FACE project. Functional Ecology 17:289-304.

Laconite, A., J. G. Isebrands, and G. E. Host. 2002. A new way to account for the effect of source-sink spatial relationships in whole plant carbon allocation models. Canadian Journal of Forest Research 32:1838-1848.

Martin, M. J., G. E. Host, K. E. Lenz, and J. G. Isebrands. 2001. Simulating the growth response of aspen to elevated ozone: a mechanistic approach to scaling a leaf-level model of ozone effects on photosynthesis to a complex canopy architecture. Environmental Pollution 115: 425-436.

Noormets, A., A. Sober, E.J. Pell, R.E. Dickson, G.K. Podila, J. Sober, J.G. Isebrands, and D.F. Karnosky, 2001. Stomatal and non-stomatal limitation to photosynthesis in two trembling aspen (*Populus tremuloides Michx*.) clones exposed to elevated CO_2 and/or O_3. Plant, Cell and Environment 24:327-336.

Wang, Y.P., R. Leuning, H.A. Cleugh, and P.A. Coppin. 2001. Parameter estimation in surface exchange models using non-linear inversion: how many parameters can we estimate and which measurements are most useful? Global Change Biology 7: 495-510.

Plant architecture comparison methods: A review of existing algorithms and examples of application

Aïda Ouangraoua[a], Vincent Segura[b], Evelyne Costes[b] and Pascal Ferraro[a]

[a]LaBRI – Université Bordeaux 1 - Talence, France {ouangrao|ferraro}@labri.fr
[b]INRA – UMR DAP - AFEF Team INRA, Montpellier, France {segura|costes}@supagro.inra.fr

Keywords: Plant comparison, edit distances, local similarities

Introduction

Among a number of generic tools that have been developed in the last decade to measure, explore, analyze, model and visualize plant architecture in 3-dimensions, this paper focuses on methods dedicated to the comparison between plant architectures. After a first step that has been reached with the comparison of branching sequences along axes (Guédon *et al.*, 2003), Ferraro and Godin (2000) have extended comparison methods to the whole branching systems. Their method was applied to the comparison of plants formalized as tree-graphs (Godin and Caraglio, 1998). In the last two years, new algorithms were explored and implemented in order to compare plant architectures with different relationships between components of the plant structure taken into account in the corresponding formal representations. The present paper provides a brief review of the comparison techniques now available to compare plant architectures depending on their formal representation. Their relative advantages / disadvantages are presented through an example of application on the comparison of two-year-old apple F1 hybrids.

Formal representation of plants

Plant architecture can be formally described as tree-graphs (Godin and Caraglio, 1998) by defining a set of vertices V that represents the plant components, and a list E of vertex pairs that describes the adjacency of these components. Modeling a plant topology by an *unordered tree-graph* (*ie.* no ordering is considered on the set of siblings of any vertex) corresponds to a general representation of plant architectures (Ferraro and Godin, 2000). However, in plants that give rise to one branch on each node, the set of plant components is totally ordered and the topological structure of the plant can be represented by an *ordered tree-graph* (Fig. 1a). For plants bearing more than one branch on each node, only a semi-order between siblings of a node can be defined. This phenomenon is observed for instance in whorl plants, or can result from sampling procedure when a large number of plants have to be described (Segura *et al.*, 2006). In this case, the plant topology is represented by a *semi-ordered tree-graph* (Fig. 1b) (Ouangraoua and Ferraro, 2007b).

Furthermore, to take into account the multiscale nature of plant structures, plants can also be represented by quotiented tree-graphs (Godin and Caraglio, 1998). A *quotiented tree-graph* is a tree-graph with an equivalence relation defined on the set of vertices such that the resulting quotient graph is also a tree-graph. So far, a plant can be represented by a tree-graph quotiented or not, and ordered, semi-ordered or unordered. Thus, the comparison of plant architectures consists in comparing tree-graphs of one of these six data structures types.

Plant comparison methods

The Tree-to-Tree Editing Problem (Selkow, 1977) consists in computing a distance between two tree-graphs as the minimum cost of a *sequence of elementary operations* that converts one tree-graph into the other. Three elementary operations called *edit operations* on tree-graphs are currently used: vertex *insertion*, vertex *deletion* and *substitution* of vertices. The core structure of the

algorithms computing an edit distance between tree-graphs is based on the dynamic programming principle and determines an optimal *mapping* between tree-graphs. Intuitively, a mapping between two tree-graphs is a description of which operation in a sequence of edit operations was applied to each vertex of both tree-graphs. Definitions of mappings between tree-graphs and algorithms determining the corresponding optimal mapping have been first proposed by Zhang and Shasha (1989) and Zhang (1996) for respectively ordered and unordered tree-graphs. To deal with other plant architecture representations, we recently introduced new constraints on the definition of mappings (and then new algorithms) adapted to semi-ordered (Ouangraoua and Ferraro, 2007a), quotiented unordered (Ferraro and Godin, 2003), quotiented ordered and quotiented semi-ordered (Ouangraoua and Ferraro, 2007b) tree-graphs.

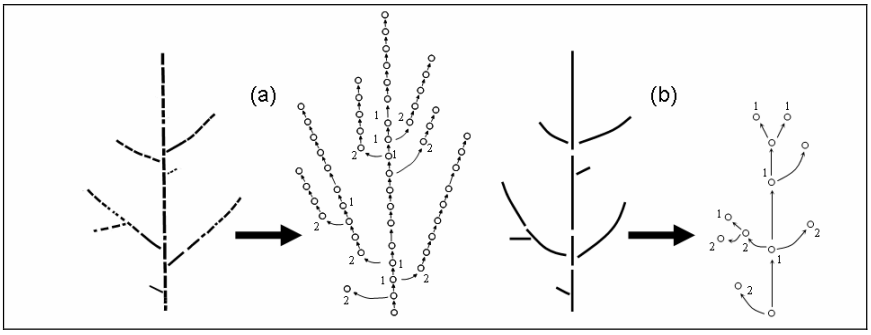

Fig. 1**: Schematic representations of a plant architecture (left) and corresponding tree-graph (right); (a) Ordered tree-graph representation: each node bears no more than two branches; (b) Same tree without information at node level and the corresponding semi-ordered tree-graph. The order relationship between children is indicated only when there is more than one child.**

Furthermore, in many cases plants share only a limited region of similarity. This may be a common domain or simply a short region of recognizable similarity. The *local similarity problem* (Smith and Waterman, 1981) aims at identifying the best pair of regions, one from each plant, such that the similarity of these two regions is the highest possible. In order to deal with this problem, we used two variants of the global edit distance algorithms to locally compare tree-graph representations of plant architecture: namely local similarity algorithm (Ouangraoua *et al.*, 2007) and *end-space free alignment* (Gusfield, 1997). The end-space-free alignment between two trees T_1 and T_2 is similar to the global edition. In this variant, any indel operations at the end or at the beginning of T_2 contribute to a weight zero. Since the indel operations have different cost depending if there are applied in one or the other tree, the corresponding dissimilarity measure $d(T_1,T_2)$ is not symmetric. The symmetry was reached by taking the minimum between $d(T_1,T_2)$ and the end-space-free alignment between T_2 and T_1 (ie. $d(T_2,T_1)$) : $D(T_1,T_2) = \min \{d(T_1,T_2), d(T_2,T_1)\}$. By contrast, the local similarity algorithm tends to maximize the similarity score between the compared plants and the resulting score is directly symmetric.

For each algorithm a distance matrix containing the distances between topological structure tree-graph representations of all pairs of plants in the database can be computed. Plants can thus be classified on the basis of the distance matrix, by classic clustering algorithms such as Ward's method (Gordon, 1999). However, in end-space-free comparison the relative dissimilarities are not conserved within the set of trees, and the triangular inequality is not preserved. This didn't allow us to biologically interpret the clustering method which was thus not applied in that particular case. By contrast, in the local similarity, the triangular inequality is preserved and allowed us to interpret the clustering which was performed after transformation of the scores into dissimilarities.

In all cases, 3D representations of the plants, obtained with PlantGL viewer (Boudon, 2001), provides a useful tool to interpret the results. Within-tree local similarities are then analyzed by identifying mapped entities on pairwise tree-graphs.

Example of applications to two-year-old apple hybrids

Global comparison algorithms presented in the previous section were performed to evaluate topological similarity of plants on a database of hybrids of apple trees (Segura *et al*., 2006). The results show that ordered, semi-ordered and unordered edit distance methods allow us to globally compare plant architectures (Segura *et al.*, 2007). Plants were grouped in three clusters according to their small, medium or large number of topological components (Fig. 2). However, the clustering remained unchanged when geometrical features or the class of entities were taken into account in the comparisons. An effect of the entity rank along ordered axes (mainly the trunk) was detected in the semi-ordered comparison, but only in the deepest steps of the clustering. When quotiented comparisons were performed, the results were still strongly correlated to the plant size, even though the dispersion of matching components was avoid by merging the conserved areas.

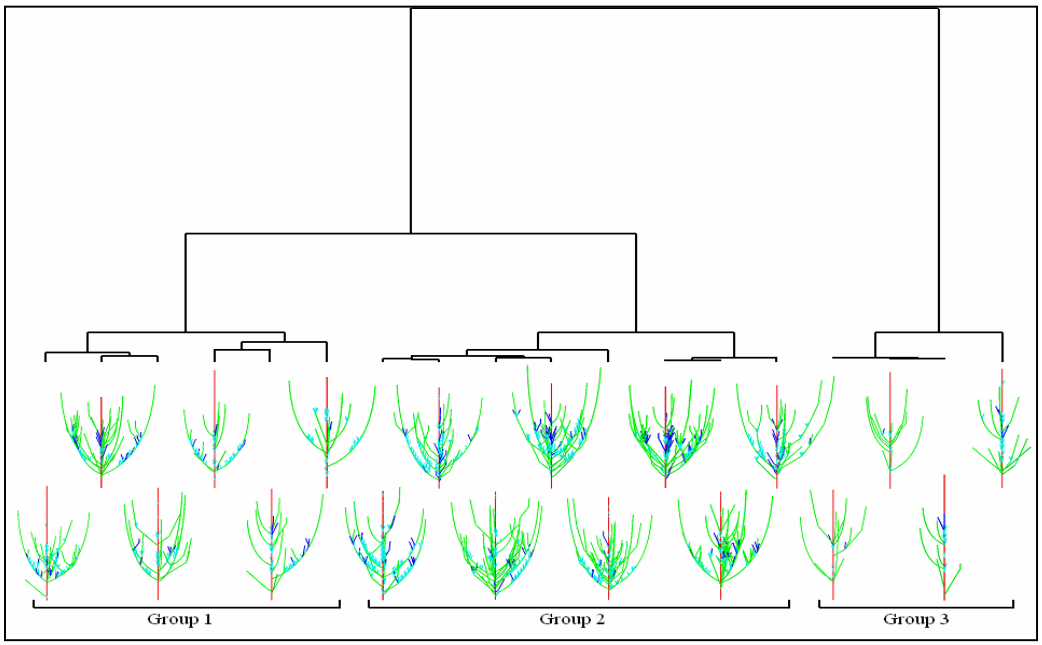

Fig. 2: **Cluster dendrogram from the distance matrix resulting from the unordered comparison of a sub-sample of 18 apple hybrids. Groups resulting from the selected separating level and used in the analysis are indicated.**

Local and end-space free comparisons were also applied to the database. Clustering methods show that the local comparison led to similar results as global comparison since the plants are still grouped according to their topological size. By contrast, different results were obtained with end-space free comparisons mainly because the non-matched extremities of trees were not taken into account during the distance computation. As previously mentioned, end-space free comparisons could not be interpreted by clustering techniques, and rather 3-D representations were used for interpretation purpose (Fig. 3). The distance between plants decreased spectacularly when compared plants had very different topological sizes. In fact, relatively small plants defined sub-parts that aligned in larger plants. By contrast, when plants with a close topological size were compared, the distance did not vary with the comparison method.

Conclusion

Finally, a set of edit distance algorithms is currently available to compare plants with different topological representations. For a given formal representation, both global and local comparison methods can be applied depending on the biological context and goal. However, each method is more or less appropriate depending on (*i*) the heterogeneity of the topological size of the compared

plants; (*ii*) the traits that must be taken into account. From a theoretical point of view, this analysis opens new perspectives to improve and extend the plant architecture comparison methods, especially the local comparisons or for dealing with more than two scales in the formal representation. Moreover, some general aspects concerning plant architecture, such as clustering problems, automatic labeling of plant structure and the evaluation of simulated plants arose from the definition of a distance between plants and will need further discussion.

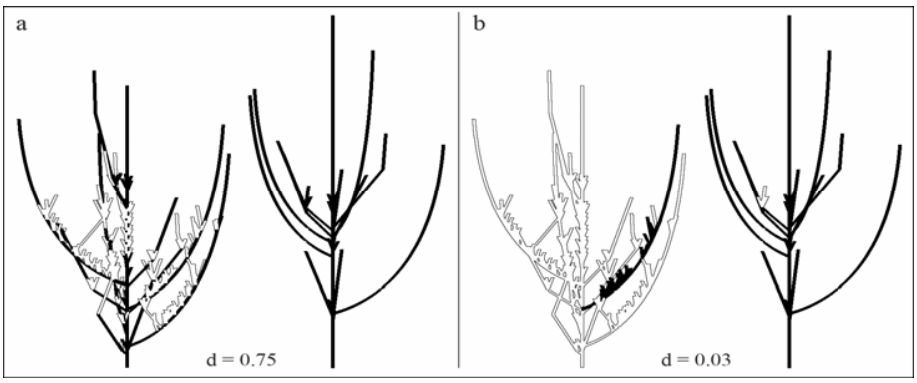

Fig. 3: **3-D Representation of the topological (a) and end-space free (b) comparisons between a pair of semi-ordered trees. Axes were colored depending on the comparison. Unmatched axes, resulting from insertion and deletion, were colored in white, while matched axes were colored in black. Distances between plants compared are indicated by the letter d.**

References

Boudon, F., Nouguier and C., Godin, C., GEOM module manual user guide, CIRAD, **2001**.

Ferraro, P. and Godin, C., A distance measure between plant architectures, *Annals of Forest Science*, **2000**, 57, 445-461.

Ferraro, P. and Godin, C., An edit distance between quotiented graphs, *Algorithmica*, **2003**, 36, 1-39.

Godin, C. and Caraglio, Y., A multiscale model of plant topological structures, *Journal of Theoretical Biology*, **1998**, 191, 1-46.

Gordon, A. D., Classification. 2nd edition. London: Chapman & Hall, **1999**.

Guédon, Y., Heuret, P. and Costes, E., Comparison methods for branching and axillary flowering sequences, *Journal of Theoretical Biology*, **2003**, 225, 301-325.

Gusfield, D., Algorithms on strings, trees and sequences - Computer Science and Computational Biology Cambridge University Press, **1997**.

Ouangraoua, A. and Ferraro, P., A new constrained edit distance between quotiented ordered trees, *submitted to Journal of Discrete algorithms*, **2007a**.

Ouangraoua, A. and Ferraro, P., An edit distance between partially ordered trees to evaluate similarity between plants, *submitted to Information Processing Letters*, **2007b**.

Ouangraoua, A., Ferraro, P., Dulucq, S. and Tichit, L., Local similarity between quotiented ordered trees, *Journal of Discrete Algorithms*, **2007**, 5, 23-35.

Segura, V., Cilas, C., Laurens, F. and Costes, E., Phenotyping progenies for complex architectural traits: a strategy for 1-year-old apple trees (Malus x domestica Borkh.),*Tree Genetics and Genomes*, **2006**, 2, 140-151.

Segura, V., Ouangraoua, A., Ferraro, P. and Costes E., Comparison of tree architecture using tree edit distances: application to two-year-old apple hybrids, *Euphytica*, **2007, doi:** 10.1007/s10681-007-9430-6.

Selkow, S. M., The tree-to-tree editing problem, *Information processing letters*, **1977**, *6*, 184-186.

Smith, T. and Waterman, M., Identification of common molecular subsequences, *Journal of Molecular Biology*, **1981**, 147, 195-197.

Zhang, K., A constrained edit distance between unordered labeled trees, *Algorithmica*, **1996**, 15, 205-222.

Zhang, K. and Shasha, D., Simple fast algorithms for the editing distance between trees and related problems, *SIAM Journal on Computing*, **1989**, 18, 1245-1262.

Self-similar analysis of plant architecture reveals hierachical classes of meristem states

Christophe Godin[1] and Pascal Ferraro[2]
[1] INRIA, Equipe Virtual Plants, UMR DAP, Montpellier, France
[2] LABRI, Université de Bordeaux I, France
(on leave of absence at the University of Calgary)

Keywords: plant architecture, self-similarity ; meristem; differentiation; physiological age; tree reduction; inverse problem;

Introduction

Apical meristems are small embryogenic regions, located at the tip of plant axes, that build up plant organs by cellular division. The production of the meristems depends on their internal physical, physiological and genetic state and is controled by contextual factors (like micro-environment, availability of nutrients, *etc.*). In principle, the number of variables that may be used to define the state of a meristem, taking account the nature and the concentrations of molecules in each cell, their position, the physical stresses at each point, the geometry of cells, their genetic contents, *etc.*, is infinitely large. Due to this intrinsic complexity, and to the current lack of hindsight on processes at such small scales, the connection between a meristem state, its micro-environment and what it produces at varying time scales seems until now largely out of reach.

However, the remarkable organization of plants at macroscopic scales makes the situation not so hopeless. The fact that plants are made up of the repetition of many similar components, at different scales e.g. (Arber, 1950; Hallé et al., 1978; Gatsuk et al., 1980; Harper et al., 1986; Barthélémy et al., 1997; Godin and Caraglio, 1998), provides macroscopic evidence for regularities and similarities in processes that drive meristem activity at microscopic scales.

In this paper, we propose to formalize this connection between macroscopic observations and microscopic, mostly invisible, processes. To achieve this connection, we formulate the following simplifying, though fundamental, scaling hypothesis during growth :

Scaling hypothesis: *If two branching structures in a plant are similar, they were (probably) produced by meristems with similar states and contexts.*

In other terms, if we consider the function that associates each branching structure of a plant with the state of the meristem that produced it, this scaling hypothesis states that this function is continuous. Note that this implicitly requires that metrics are defined on both the branching system space and the meristem state space. In this presentation, we shall show that it is possible to use this idealized - but useful - hypothesis to organize the multitude of meristem states and contexts by classes of equivalence with respect to the similarity of what they produce.

In this first approach, the similarity between branching systems is considered to be purely structural (no geometry is taken into account for instance). Due to the nested nature of these structures, we show that the study of similarities between all parts of a plant boils down to studying the self-similar nature of the plant structure. Based on previous attempts to quantify self-similarity in plants (Prusinkiewicz, 2004; Ferraro et al., 2005), we introduce a new method that enables us to define the degree of self-similarity of any plant as a departure coefficient from pure self-similarity. As a by-product, the method enables us to identify hierarchies of classes of meristem states.

From biology to mathematical formalization: modelling plant architecture self-similarity

Different strategies can be used to define an equivalence relationship between branching systems. They can be equivalent because they have the same root diameter, because they have the same size or because they bear the same number of flowers. Here we consider structural equivalence. Formally, this comes down to defining a notion of isomorphism between branching systems. In (Ferraro et al., 2005), we defined isomorphism between axial branching systems (i.e. branching systems for which a trunk is defined). Here we consider a less restrictive class of isomorphim between branching systems which holds for any type of tree structure. In the following, any graph G is represented by a pair (V, E) where V is the set of vertices of G and E its set of edges (i.e. a set of oriented pairs of vertices). A tree-graph is a graph for which a particular vertex, called the root, is identified and such that any vertex different from the root is linked to the root by a unique oriented path in the graph (see (Godin and Caraglio, 1998) for detailed definitions).

Definition 1 (tree isomorphism). *Let $T_1 = (V_1, E_1)$ and $T_2 = (V_2, E_2)$ be two rooted trees. A bijection ϕ from V_1 to V_2 is a tree isomorphism if for each edge $(x, y) \in E_1$, $(\phi(x), \phi(y)) \in E_2$. We note $T_1 \equiv T_2$.*

To compute whether two branching structures T_1 and T_2 are isomorphic, we use a notion of edit-distance between trees (Zhang, 1996; Ferraro and Godin, 2000). The distance between T_1 and T_2, $D(T_1, T_2)$, is defined as the minimal number of elementary edit operations (insert, delete or match vertices) that is necessary to transform T_1 into T_2. This distance has the following property: $D(T_1, T_2) = 0 \Leftrightarrow T_1 \equiv T_2$.

Definition 2 (Reduction of a tree). *Let T be a tree, we denote by $\mathcal{R}(T)$ the graph obtained by quotienting T by the equivalence relation $\equiv$. We call this graph the* reduction of T.

This definition relies on the construction of a graph corresponding to the reduction of the initial tree, when all the structural redundancy has been removed. It can be shown that this graph is a directed acyclic graph (DAG) and that there exists an algorithm that can compute this DAG in time $O(|T|^2 ln|T|)$ (Godin and Ferraro, 2007). Let us call *linear* a DAG for which there exists a path going through all its vertices. Then, by definition, we say that a tree T is *self-similar* if $\mathcal{R}(T)$ is linear.

Under the scaling hypothesis, the nodes of $\mathcal{R}(T)$ can be interpreted as meristem states, and the edge between two states would denote the occurence of a meristem differentiation (from the initial to the final state). Paths in $\mathcal{R}(T)$ therefore denote all possible meristem differentiation sequences. In self-similar plants, there is thus a unique differentiation sequence for all the meristems of the plant.

Among all the self-similar trees, let us denote $\mathcal{S}(T)$ the subset of self-similar trees that contain T. Then, we consider trees T^* in this set that minimize the distance to T.

Definition 3 (Smallest Self-similar Tree, SST). *Let T be a tree and $\mathcal{S}(T)$ be the set of all the self-similar trees that contain T. Then, we define the set of smallest self-similar trees containing T by:* $SST(T) = \{T^* | T^* = \underset{T' \in \mathcal{S}(T)}{\operatorname{argmin}} D(T, T')\}$

We show that, for any tree T, it is possible to find an element $T^* \in \mathrm{SST}(T)$ in polynomial time[3] $O(h \times w \times \ln(w))$, and give the corresponding algorithm (Godin and Ferraro, 2007). In addition, the algorithm returns the mapping from T^* to T that corresponds to the minimal distance $D(T, T^*)$. Under the scaling hypothesis, this makes it possible to associate with each tree T a single sequence of states. This sequence may be interpreted as the template differentiation sequence of the plant meristems. Thanks to the mapping from T^* to T, each branching system of the original plant may then be associated with one of these computed, hypothetical, meristem states, representing the state of the meristem that produced this branching system.

Hierarchical organization of meristem states in Rice

The above approach was tested on different plant architectures. We present here results corresponding to the analysis of a rice panicle (Fig. 1.a), already described in (Ferraro et al., 2005). The topological structure of the panicle T is depicted in Fig. 1.b.

We first computed the reduction tree $\mathcal{R}(T)$, (Fig. 1.c). This graph, from which the original tree can be reconstructed (Godin and Ferraro, 2007), is not linear and shows a number of different meristem differentiation sequences. By computing an element T^* of $\mathrm{SST}(T)$ (Fig. 1.d), it is possible to find a single sequence of meristem state differentiation that best corresponds to the original plant. The states of this sequence can be subsequently projected onto the original topological structure using the resulting mapping from T^* to T, thus providing an interpretation of the entire structure in terms of meristem differentiation (Fig. 1.e).

Perspectives: from mathematical formalism back to biology

The above approach makes it possible to formally retreive the sequences of meristem state differentiation corresponding to each axis of a given plant. Based on the scaling hypothesis and its variants, this opens up the perspective to use such an analysis on various plant species as a guiding principle to further investigate the notion of meristem state and differentiation at a bio-molecular and genetic levels, in the spirit of the pioneering work described in (Prusinkiewicz et al., 2007).

References

Arber, A. (1950). *Natural philosophy of plant form.* University Press, Cambridge.

Barthélémy, D., Caraglio, Y., and Costes, E. (1997). Architecture, gradients morphogénétiques et âge physiologique chez les végétaux. In Bouchon, J., Reffye, P. d., and Barthélémy, D., editors, *Modélisation et Simulation de l'Architecture des Végétaux*, Science Update, pages 89–136. INRA Editions, Paris, France.

Ferraro, P. and Godin, C. (2000). A distance measure between plant architectures. *Annals of Forest Science*, 57:445–461.

Ferraro, P., Godin, C., and Prusinkiewicz, P. (2005). Toward a quantification of self-similarity in plants. *Fractals*, 13(2):91–109.

Gatsuk, L. E., Smirnova, O. V., Vorontzova, L. I., Zaugolnova, L. B., and Zhukova., L. A. (1980). Age states of plants of various growth forms : a review. *J. Ecol.*, 68:675–696.

[3] h and w represents respectively the height (*i.e.* the length of the minimum path between the initial node and any leaf) and the width of $\mathcal{R}(T)$ (*i.e.* the maximum number of nodes at a given height in $\mathcal{R}(T)$)

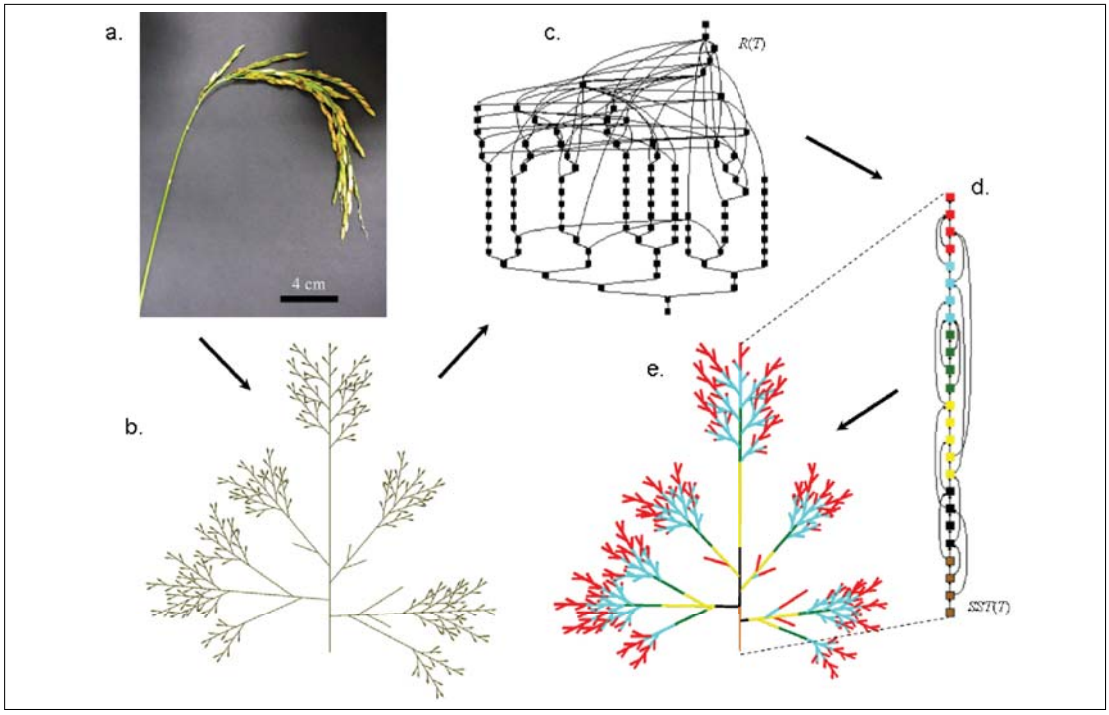

Figure 1. a. A rice panicle photograph and b. its topological structure (courtesy of C. Paul-Victor, Y. Caraglio). c. Its reduction as a DAG, d. the corresponding DAG of its smallest self-similar tree and e. the projection of meristem states onto its topological structure.

Godin, C. and Caraglio, Y. (1998). A multiscale model of plant topological structures. *Journal of Theoretical Biology*, 191:1–46.

Godin, C. and Ferraro, P. (2007). A general method for quantifying the structural self-similarity of trees. Technical report, INRIA.

Hallé, F., Oldeman, R. A. A., and Tomlinson, P. B. (1978). *Tropical trees and forests. An architectural analysis*. Springer-Verlag, New-York.

Harper, J. L., Rosen, B. R., and White, J. (1986). *The growth and form of modular organisms*. The Royal Society, London, UK.

Prusinkiewicz, P. (2004). Selfsimilarity in plants : integrating mathematical and biological perspectives. In Novak, M. M., editor, *Thinking in Patterns: Fractals and Related Phenomena in Nature*, pages 103–118. World Scientific, Singapore.

Prusinkiewicz, P., Erasmus, Y., Lane, B., Harder, L. D., and Coen, E. (2007). Evolution and development of inflorescence architectures. *Science*, 316(5830):1452–1456.

Zhang, K. (1996). A constrained edit distance between unordered labeled trees. *Algorithmica*, 15(3):205–222.

Non-incremental inference of 0L-systems with positive sample

Farah Ben-Naoum and Mustapha Mechab
EEDIS, UDL, Computer Science Department. Sidi Bel-Abbes Algeria bp 89 22000

Keywords: grammatical inference, non incremental Inference, positive sample, 0L-system, rules generalization, self-similarity, heuristic training algorithm, method SAR.

Introduction

Many algorithms of grammatical inference were developed for several types of grammars (Adriaans, Fernau and Van Zaanen, 2002). The inference problem consists of finding, from a set of strings, a grammar that produces all the strings of this set (Miclet and Cornuéjols, 2002). We are interested here by the inference of a particular class of L-systems, noted the 0L-systems (Yokomori, 1992). We present a *heuristic algorithm*, which only uses positive sample corresponding to either independent or developmental biological structures. The *positive sample* noted I_+ is the set of all strings that the inferred 0L-system must produce. It is a *non-incremental algorithm* in the sense that the positive sample becomes unchanged (new strings cannot be added progressively) (Miclet and Cornuéjols, 2002).

Biological motivation

Developmental biology and inference: The problem of inductive inference has in recent years been extensively investigated. It has particular significance for developmental languages in which the description of the developmental stages of an organism is formally defined as a series of strings of symbols. The problem is to devise developmental rules which transform the strings of symbols in a way consistent with observations for a particular species. In this sense, there is an overlap between model building in developmental biology and the *grammatical inference* problem. This problem enters the realm of developmental biology in the following way. The biologist interested in a particular plant is confronted with a large number of experimental observations. His task is to explain on the basis of such experimental results the way in which the particular plant develops (Feliciangeli, Gabor and Herman, 1973).

Studying self-similarities in plant structures: In the growth processes of many living organisms, especially plants, regularly repeated appearances of closely related biological structures are readily noticeable. This phenomenon of *self-similarity* has been tentatively captured by several botanical notions (Prusinkiewicz 2004), (Ferraro, Godin, and Prusinkiewicz, 2005). Our main objective is to use the *grammatical inference* in the detection of this *self-similarity* from a symbolic representation of a tree structure in development, or from several tree structures corresponding to different varieties in the aim to compare them.

Complementary arguments for such a biological motivation, as well as some similar problems, are discussed in (Herman and Walker, 1972).

Specificities of the proposed method

Inference of L-systems was recently studied using genetic programming (Jacob, 1998). By proposing this new heuristic method we avoid some of the drawbacks of the genetic algorithms, i.e.: uncertainty on the algorithm convergence, unknown time of convergence, the great spatial complexity dependent on the size of the population ... (Koza, 1993). On the other hand, the advantages of this algorithm, regarding to the other heuristic algorithms already proposed (Doucet, 1974; Feliciangeli, Gabor and Herman, 1973; Herman and Walker, 1972; Nevill-Manning and Witten, 1997), are its ability to:

- work on tree structures while previous works were limited to simple sequences like red algae,
- perform on any kind of sequence (containing ordered or unordered strings of I_+, independent or developmental, structures), the others performs only on ordered sequences in development,

- generalize the rules by studying the possible existing recursivities. The generalization consists on the creation of a grammar that generates the language containing the positive sample. By comparison, let us consider the method of Nevill-Manning and Witten (1997) in which they proposed an algorithm that forms a grammar from a sequence based on repeated phrases in that sequence. Each repetition gives rise to a rule in the grammar, and the repeated subsequence is replaced by a non-terminal symbol. In this case the grammar is inferred from a positive sample containing only one sequence, and it can only generate this sequence without generalization (only non-recursive grammar are inferred by this method). This process cannot represent the biological development of a plant structure in which repeated modules as well as modules generated by a regular developmental model, called self-similar modules, can be found. The detection of self-similar modules and their representation by recursive rules avoids doing the generalization of the resulting L-system. This represents the specificity of our new method.

Description of the SAR method

The particularity of L-systems is their ability to models the development of higher plants and complex branching structures, described as configurations of modules in space; the term module denotes any discrete constructional unit that is repeated as the plant develops (Prusinkiewicz, Hammel, Mech, and Hanan, 1995).

The main idea in the inference of 0L-system generating a sequence of strings associated with the sequence of structures of plants is to explore all sub-strings of the sequence strings and to select those representing modules that correspond to two cases: In the first one, the selected module can be decomposed into other nested modules; the nesting must be done in a regular manner which leads to the creation of a recursive rule. In this case, the modules are called self-similar in the sense that they are composed of a succession of possibly nested identical sub-modules. In the second case, the selected module is only repeated in the sequence of the developmental structure, and then the rule inferred simply associates one symbol with this module. These two cases are considered respectively in the first and the second loop *repeat* of the SAR algorithm mentioned in the annex.

The selection of modules must take into account the vocabulary used to represent the branching structure in the 0L-systems using the turtle interpretation (Prusinkiewicz, Hammel, Mech, and Hanan, 1995). Each module corresponds to a valid plant structure if and only if the associated string (containing brackets to represent branches) is well-parenthesed.

The proposed ***Method SAR***: (search of self-similarities and redundancies) builds a 0L-system starting from a positive sample $I_+=\{x_i, i=1..|I_+|\}$ by making a partition of each string x_i into repeated or recursive sub-strings being able to be produced in the same step of derivation (to deal with the parallelism in the derivation in the L-systems). This partition includes well-parenthesed sub-strings lengths varying from n to 2 with n=len(x_i). The recursive application of this principle to unit I_+ enables us to reconstitute all the successive steps for the generation of all strings of I_+.

The method SAR identifies in the limit the 0L-system generating I_+ , since it makes it possible to reduce successively all the strings of I_+ after N steps (Gold, 1967), the algorithm then converges towards a solution, starting from a finite N, i.e.$H^{N-1}(I_+)= H^N(I_+)$. Where N is at most equal to the number of productions created by the algorithm plus 1.

The method SAR was developed in python which requires about 550 lines for the algorithm. The temporal complexity of SAR is $O(r.m.n)$, where $n=|x_i|$ and x_i is the longest string in the positive sample, m is the size of the positive sample I_+. In the worst case the algorithm creates 1 production at each step of the two loops *Repeat* doing the detection of nested modules and the detection of repeated modules in the SAR algorithm given in the annex, then the algorithm performs this creation of productions r times, with r=max(number of recursive versus non-recursive symbols).

Examples

1) **Positive sample I_+ containing strings associated to independent plants**. The first one correspond to the step 3 of development of the plant of figure2(a) generated by the L-system

L_1(Axiom: F productions: F→FF-[Fc-F+F+F]d+[Fc+F-F-F]d c→c, d→d; homomorphism c→, d→;), the second correspond to the step 2 of development of the plant of figure2(b) generated by the L-system L_2(axiom: F productions: F→FF+\[,+F-&Fc[-F+F+F+F]d-F]-\[,-&Fc[-F+F+F+F]d+F] c→c, d→d; homomorphism c→, d→;). The resulting inferred L-system must be the union of L_1 and L_2.

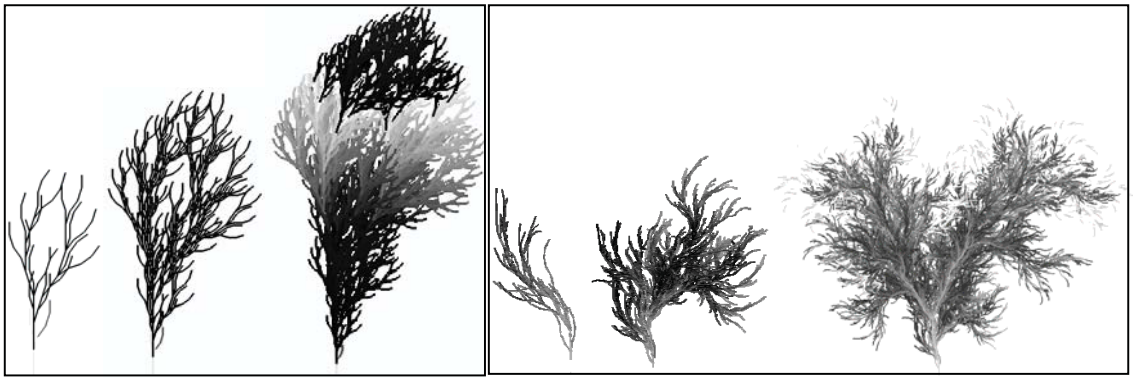

(a) (b)

Figure 2: (a) Steps 2, 3 and 4 of the plant generated by L_1,
(b) Steps 2, 3 and 4 of the plant generated by L_2, using the L-studio v.4.0.5 beta

Result of the SAR algorithm: axiom: h

productions:	homomorphism:
h -> b h -> a	b -> F
b->bb+\[,+bgbc[-b+b+b+b]d-b]-\[,gbc[-b+b+b+b]d+b]	a -> F
a -> aa-[ac-a+a+a]d+[ac+a-a-a]d	g -> -&
c -> c,	c -> ,
d -> d;	d -> ;

The resulting L-system is the union of L_1 and L_2. The development of trees associated to L_1 and L_2 correspond respectively to the recursive symbols a and b in the inferred L-system; representing the self-similarity in the development of the tow structures of figures 2(a) and 2(b). They also have common sequences of successive ‘,’ and ‘;’ represented respectively by the recursive symbols c and d. Then we find in the inferred L-system common rules corresponding to c and d.

2) **Positive sample I_+ containing a sequence of strings associated with different stages of development of the plant** (stages 2 and 3 of figure1).

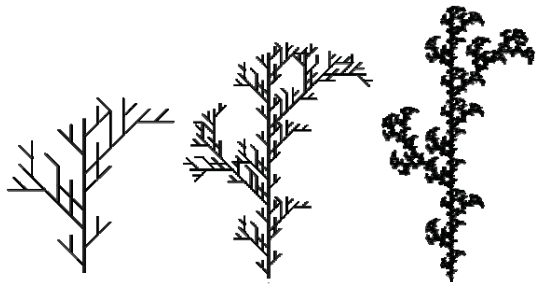

Figure1: Steps 2,3,5 of the plant generated by the L-system L_1(Axiom: A, A→A[+BA]A[-CA]A, B→BF[-FD], C→CF[+FD], homomorphism A→F, B→F[-FD], C→F[+FD], D→[F+F]) using L-studio v.4.0.5 beta

The resulting L-system L_2 must be equivalent to the one used to create the positive sample. Result of the SAR algorithm:

axiom: c

productions:	homomorphism:
c -> c[+bc]c[-ac]c	c -> F
b -> bF[-e]	b -> F[-e]
a -> aF[+e]	a -> F[+e]
	e -> F[F+F]

The symbols c, a, b are recursive and then represent self-similar parts in the tree of figure1.

To study the equivalence between this resulting L-system L_2 and the one used to generate I_+ (noted L_1), we verify whether they are isomorphic by an adequate change of the names of the generated symbols. The SAR algorithm detects the repetition of F[F+F] represented by the production

e→F[F+F] in L_2, we also remark the repetition of FD in L_1 with D→[F+F]. Then the symbol e is equivalent to FD. By replacing e by FD, and e→F[F+F] by D→[F+F] in L_2, and after replacing the axiom c (in L_2) by A (used in L_1), and the symbols b and a (in L_2) by respectively B and C (used in L_1), we obtain: (axiom: A, productions: D->[F+F], A->A[+BA]A[-CA]A, A->F, B->BF[-FD], B->F[-FD], C->CF[+FD], C->F[+FD]). We thus obtain a transformed L-system identical to that used to generate I_+.

3) **Positive sample I_+ containing seven strings associated with an abstract language**:

I_+={[aaaa[ccccccc]aaaadt]b[aaaa[cc]aaaadt]b[aaaa[ccccccc]aaaadt]b, dtcfcfcfdt[aaaaaa[ccccccc]aaaaaadt]b [aaaaaa[ccccccc]aaaaaadt]bdt, dgrtmmmAmAmmmAmAmmmmmAmAmmmAmAmmm, dthgjdt, [dt][dt][dt], [aaaaaa[ccccccccccc]aaaaaadt]b[aaaaaa[ccccccccccc]aaaaaadt]b, dtdthgdthgdtdtdthgdthgdtdt }

Result of the SAR algorithm: axiom: u

production	u -> dgrtA	p ->	A -> mAmAm	homomorp	o -> s
s:	u -> qkqpq	p[i[e]iq]b	k -> kcf	hism:	n -> [q]
u -> o	p ->	o -> qoqoq	i -> ia	u -> qsjq	k -> cf
u -> p	[i[e]iq]b	n -> n[q]	e -> ec	s -> hg	i -> a
u -> n				q -> dt	e -> c

This abstract example finally shows how the SAR approach may be used to infer rules from more complex structures.

Conclusion

This paper addressed the problem of inferring a 0L-system from a sequence of tree structures. To this end, we introduced the notion of self-similarity detected from symbolic representation of trees. In practice, the proposed SAR method proved its efficiency for the inference of abstract languages as well as for the languages which, associated with the turtle interpretation, expresses structures of trees and their development.

The class of 0L-systems inferred by this method concern parenthesized languages generating tree structures, to infer more realistic structures we must first study the learn-ability of each class of L-systems (Fernau and De la Higuera, 2004; Yokomori, 1992) and next try to find the appropriate extension of our method. For example, in the future, we attempt to combine our inference method to an adaptation of some methods of learning stochastic grammars in the aim to generate stochastic L-systems. We also aim to perform the algorithm to work incrementally, and include negative samples (strings that the inferred 0L-system must refuse). This method can be considered as a theoretical step towards more practical results in the future. In this aim, we intend to compare the SAR method with the method described in (Godin and Ferraro, 2007) for quantifying self-similarity in plants.

Acknowledgments: I would like to thank Christophe Godin and Pascal Ferraro for the interactive feedback that helped creating the SAR-method.

References

Adriaans, P. , Fernau, H., Van Zaanen, M., (2002). *Grammatical Inference: Algorithms and Applications; 6th International Colloquium, ICGI 2002*, volume 2484 of *LNCS/LNAI*. Springer.

Cornuéjols, A., Miclet, L., (2002). *Apprentisage artificiel : concepts et algorithmes*. Eyrolles.

Doucet, P. G., (1974). *The syntactic inference problem for D0L-sequences*, lecture notes in Computer Science 15.

Feliciangeli, H., Gabor, Herman, T., (1973). *Algorithms for producing grammars from sample derivations: a common problem of formal language theory and developmental biology*, journal of computer and system sciences 7, 97-118.

Fernau, H., De la Higuera, C., (2004). *Grammar Induction:An Invitation for Formal Language Theorists,* Grammars **,** volume 7, 45–55.

Ferraro, P., Godin, C., Prusinkiewicz, P., (2005). *Toward a Quantification of Self-similarity in Plants*, in Fractals, Vol. 13, No. 2, 91-109.

Godin, C. and Ferraro, P. (2007). *A general method for quantifying the structural self-similarity of trees*. Technical report, INRIA.

Gold, E.M., (1967). *Language Identification in the limit*, Information and control, Vol.10, No.5, pp, 447-474.
Herman, G.T., Walker, A. D., (1972). *The syntactic inference problem applied to biological systems*, in "Machine Intelligence 7" (Michie, Ed.), Edinburgh University Press, Edinburgh.
Jacob, C., (1998). *Genetic L-system programming*, Chair of programming Languages, Department of computer Science, University of Erlangen-Nurnberg, Germany.
Koza, J. R., (1993). *Genetic programming, On the programming of computers by means of natural selection*, MIT Press, London.
Nevill-Manning, Craig G., Witten, Ian H., (1997). *Identifying Hierarchical Structure in Sequences: A linear-time algorithm*. Journal of Artificial Intelligence Research 7, 67–82
Prusinkiewicz, P., (2004). *Self-similarity in plants: integrating mathematical and biological perspectives*. In: M.M. Novak (Ed.) Thinking in Patterns. Singapore: World Scientific.
Prusinkiewicz, P., Hammel, M., Mech, R., Hanan, J., (1995). *The Artificial Life of Plants*. From artificial life for graphics, animation, and virtual reality, volume 7 of SIGGRAPH'95. ACM Press.
Yokomori, T.,(1992). *Inductive inference of 0L languages*, in: G. Rozenberg and A. Salomaa (eds.), Lindenmayer Systems: Impacts on Theoretical Computer Science, Computer Graphics, and Developmental Biology, Springer, 115-- 132.

Annex: Pseudo code of the SAR algorithm:

Repeat for all strings of $I_+=\{x_i, i=1..|I_+|\}$ *#detection of nested modules*
  For all sub-strings y_j of x_i with $2\leq len(y_j)\leq len(x_i)$ and y_j is well-parenthesed:
    If **is_recursive1**(y_j)=true then
      Create a recursive rule of the form $A\rightarrow c_1Ac_2\ Ac_3\ \ldots c_{d-1}\ Ac_d$ and $A\rightarrow\beta$
      Replace the module y_j in x_i by the symbol A.
      Add sub-modules $c_1,c_2,c_3\ \ldots c_{d-1},c_d,\beta$ to I_+ in the aim to be also considered later.
    else if **is_recursive2**(y_j)= true then
      Create the productions $A\rightarrow Aa$, $A\rightarrow a$
      Replace occurrences of y_j in x_i by the symbol A.
      Add the sub-module a to I_+ in the aim to be also considered later.
Until stabilization of I_+
Repeat for all strings of $I_+=\{x_i, i=1..|I_+|\}$ *#detection of repeated modules like in (Nevill-*
  For all sub-strings y_j of x_i with $2\leq len(y_j)\leq len(x_i)$ and y_j is well-parenthesed: *# Manning and Witten, 1997)*
    If y_j is quite simply a repetition in I_+ (i.e. if the number of occurrences of y_j in strings of I_+ is >1) then
      Create the production $A\rightarrow y_j$
      Replace all occurrences of y_j by the symbol A
      Add the sub-module y_j to I_+ in the aim to be also considered later.
Until stabilization of I_+.

Function **is_recursive1**(y_j) *# this function verifies whether y_j correspond to a module that can be regularly*
  begin *decomposed into other nested modules (if y_j is self-similar)*
  $A_0=y_j$ *#max-len-red try to find the longest repeated sub-string of y_j that are also*
  A_1=max-len-red(A_0) *well-parenthesed*
  While max-len-red(A_k)≠'' and are isomorphic to all the precedent created $A_1..A_{k-1}$
    A_{k+1}= max-len-red(A_k)
    Replace occurrences of max-len-red(A_k) in A_k by A_{k+1}
    k=k+1
  if k≥2 then **is_recursive1**(y_j)=true
    return the list $(c_1,c_2,\ldots,c_d,\beta)$ with $y_j= c_1A_0c_2\ A_0c_3\ \ldots c_{d-1}\ A_0c_d$ and $A_k=\beta$
    else **is_recursive1**(y_j)=false
  end

Function **is_recursive2**(y_j) detects the existence of the smallest sub-module "a" in y_j so that y_j is composed of a succession of this module (y_j="aa...a"), if this module exists this function takes the value of true and returns "a".

Example explaining the steps of function **is_recursive1(y_j):**

Let y_j= "aaaβbβcbaβbβccbaaβbβcbaβbβccc", Thus we have:

A_1=max-len-red(y_j)= "aaβbβcbaβbβcc"	⇒	y_j="aA_1bA_1c"
A_2=max-len-red(A_1)="aβbβc"	⇒	A_1="aA_2bA_2c"
A_3=max-len-red(A_2)="β"	⇒	A_2="aA_3bA_3c"
max-len-red(A_3)=""	⇒	end of the loop while

Remark that all modules y_j, A_1, A_2 are isomorphic (they have the same structure up to the indexing of of A_k). We find here a suite in the development of the module y_j that can be generalized by the rules $A\rightarrow aAbAc$, $A\rightarrow\beta$. A is called recursive symbol.

Logistic-based growth under resource limitation: equations, analytical solutions and applications

Alla N Seleznyova

The Horticulture and Food Research Institute of New Zealand Limited
Palmerston North Research Centre, Tennent Drive, Private Bag 11030
Palmerston North, 4474, NZ
aseleznyova@hortresearch.co.nz

Keywords: Logistic, model, growth, resource limitation, analytical solution, θ-logistic,

Introduction

Some recent functional-structural plant models (FSPMs) combine an explicit representation of plant architecture with a mechanistic approach to carbohydrate (C) allocation [1]. In this context, a plant is represented by a set of connected semi-autonomous modules and the C flow into the growing modules is determined by the intrinsic properties of the modules, environmental conditions and the sink/source interactions within the whole system [2]. While numerical methods for calculation of C flow within the plant are now available [3], there are no direct methods for dynamical modelling of resource limited growth of plant modules such as leaves and internodes.
A logistic function [4]

$$a(t) = A(1 + \exp((t_0 - t)/\tau))^{-1}, \quad (1)$$

where t is time, A is an asymptote (final size of an organ/population), t_0 is an inflection point, and τ is a duration of rapid expansion phase, is often used for retrospective representation of the growth data and can be used in empirical modelling of growth. A differential equation (DE)

$$\frac{da(t)}{dt} = \frac{1}{\tau} a(t)\left(1 - \frac{a(t)}{A}\right), \quad (2)$$

often associated with logistic growth [5], is not suitable for use in mechanistic modelling, where the final size A is a result of the system dynamics and cannot be stated a priori. Thornley & France [6, 7] suggested modification of (2) for modelling limited growth

$$\frac{da_f(t)}{dt} = f_1 \cdot r \cdot a_f(t)\left(1 - \frac{a_f(t)}{A_f(t)}\right), \quad (3a)$$

where r is a parameter, $0 \le f_1 \le 1$ represents a degree of limitation on growth and $A_f(t)$ is a projected final size - a new state variable that can decrease depending on the growth limitation, according to the equation

$$\begin{cases} \dfrac{dA_f(t)}{dt} = -f_2 \cdot D\left(A_f(t) - a_f(t)\right) \\ A_f(0) = A \end{cases} \quad (3b)$$

where D is a parameter and $0 \le f_2 \le 1$ is interpreted as a degree of limitation of development and a maximum rate of development, respectively [7].

In the current paper I propose an alternative approach that is based on a single linear DE and does not include the notion of final size. I derive analytical solutions for growth responses to constant and pulse-like growth limiting conditions and show that this approach, although being simpler, is equivalent to the formulation of Thornley & France (3).

Linear equation for logistic growth

Derivation of equation (2), given in Thornley & Johnson [5], is based on three assumptions: 1) the growth machinery is proportional to current size $a(t)$, 2) the growth machinery works at a rate proportional to the amount of substrate $S(t)$, 3) there is no net gain or loss from the system, so that the current amount of substrate $S(t) = A - a(t)$, where A is an initial amount of the substrate. As a result, the growth is limited by the initial amount of substrate. The third assumption of this derivation does not hold for leaves and internodes of a growing shoot. These organs are connected to a common C pool; hence the amount of C available to each organ depends on the amount on photosynthesis and on competition with other organs. In addition, even when C is not limited, it does not result in indefinite growth of leaves and internodes; their growth curves can still be well approximated by the logistic function (1) [8]. According to experimental data on kiwifruit shoots, the parameter τ, which controls duration of expansion in these organs, depends mostly on temperature but not on C limitation [8]. Studies of leaf growth in wild-type and mutant of *Arabidopsis thaliana* under different light environments demonstrated a significant and robust negative correlation between the duration of expansion and the initial relative expansion rate [9]. Similar correlation, robust with respect to temperature, is established for kiwifruit growth under constant temperatures [8]. These results suggest the existence of an intrinsic growth pattern that originates within the organ and unfolds according to environmental conditions. This hypothesis is strongly supported by a controlled environment experiment on kiwifruit leaf growth under a set of step-wise changing temperature regimes (12/28/20 ^{o}C, 20/28/12 ^{o}C, etc.) [10]. The growth curves of leaves in this experiment plotted against time were not logistic and showed distinct changes in growth rates, corresponding to the step-wise temperature changes. However, when the measured leaf area data were plotted against a new variable

$$\varphi(t) = \int_0^t \frac{dz}{\tau(T(z))}, \tag{4}$$

where $T(t)$ is a time course of temperature, each growth curve was well fitted ($r^2 \cong 0.999$) by a logistic function $a(\varphi) = A(1+\exp(\varphi - \varphi_0))^{-1}$, where $\varphi_0 = \varphi(t_0)$ is an inflection point. Apart from the final size, the growth curves for leaves grown under different temperature sequences differed only by the values of the inflection point φ_0, which was determined by the time of leaf appearance.

Based on these results, I propose to represent the intrinsic growth pattern corresponding to logistic growth by a relative growth rate expressed as a function of organ developmental age, measured with respect to the inflection point, $(\alpha = \varphi - \varphi_0)$. It follows from (4) that

$$\alpha = (t - t_0)/\tau \quad \text{for} \quad T(t) = const. \tag{5}$$

For simplicity and for ease of comparison with existing results, in the following derivations I assume that $T(t) = const$ and use time rather than φ as an independent variable in equations. However these derivations can be generalised for the case of variable temperature using φ as an independent variable. From (1) relative growth rate can be expressed in a form that depends on α but not on the final size parameter *A,* leading to a linear DE for $a(t)$. Namely,

$$\frac{da(t)}{dt} = g(t)a(t), \tag{6a}$$

where

$$g(t) \equiv \frac{1}{\tau(1+\exp((t-t_0)/\tau))} \tag{6b}$$

is a relative growth rate determined by the organ age (5). The solution of (6) with an initial condition $a(t_a)$, where t_a is a time of organ appearance, can be presented in the form

$$a(t) = a(t_a)G(t_a,t)\,, \tag{7a}$$

where

$$G(t_1,t_2) = \exp\left(\int_{t_1}^{t_2} g(s)ds\right) = (1+\exp((t_0 - t_1/\tau))(1-\tau\cdot g(t_2))\,, \tag{7b}$$

is a function that propagates the solution from t_1 to t_2. Formulation (6) corresponds to the case when the C is not limited and the growth is limited by an intrinsic growth rate depending on the organ age. Resource limitation on growth is modelled by introducing a multiplier $0 < f \le 1$ into the right-hand side of (6a), namely

$$\frac{da_f(t)}{dt} = f\cdot a_f(t)g(t)\,. \tag{8}$$

In the context of transport-resistance sink-source allocation models, f is interpreted as a sink response to C limitation and is usually represented by a non-linear function of C concentration in the vicinity of the sink [2, 3].

Analytical solutions and applications

Constant C limitation For $f = const$ (8) can be solved analytically using a substitution

$$a_f(t) = (y(t))^f \tag{9}$$

and noting that $y(t)$ satisfies (6a). This gives

$$a_f(t) = a(t_a)(G(t_a,t))^f = a(t)(G(t_a,t))^{f-1}\,. \tag{10}$$

The upper asymptote of this solution (the final size) $A_f = a(t_a)(G(t_a,\infty))^f$ can be expressed in terms of the final size $A = a(t_a)G(t_a,\infty)$ for unlimited growth, namely

$$A_f = (a(t_a))^{(1-f)}A^f\,. \tag{11}$$

This solution coincides with a particular case of the well-known Richards function [11] or θ-logistic [7]. Note that in the current formulation the final size is a function of the initial size, initial developmental age and the growing conditions. Hence the potential to reach a certain size is included via the initial conditions.

Fig. 1 shows the effects of growth limitation on the characteristics of the solution (10), time interval between appearance and inflection $(\mu_f = t_{0f} - t_a)$, duration of growth defined as a time interval d_f between the organ appearance and reaching a fraction δ of final size (e.g. δ=0.95), $\rho_f = d_f - \mu_f$ and final A_f. In the vicinity of $f = 1$, the final size A_f is very sensitive to the value of f (Fig. 1b), while the effects on time characteristics are relatively small (Fig. 1a). The current analysis is in agreement with a recent study of leaf growth in kiwifruit [8] and explains that, even when leaf size was the most reduced by fruit presence, no deviation from logistic growth pattern was detected in the growth data. Indeed, the shape of the solution (10) is extremely robust in the vicinity of $f = 1$, e.g., for $f = 0.8$ the final size is considerably reduced, while the theoretical growth curve is practically undistinguishable from the fitted logistic (Fig. 1a).

Pulse-like C limitation. Note first that function G satisfies the following relationship,

$$G(t_1,t_2)\cdot G(t_2,t_3) = G(t_1,t_3) \tag{12}$$

graphically illustrated in Fig. 2a. A graphical solution of (8) for a pulse-like perturbation, where resources are limited $f < 1$ for a period of time (t_1,t_2), is shown in Figs. 2b,c and gives

$$a_f(t) = (G(t_1,t_2))^{f-1}a(t) \tag{13}$$

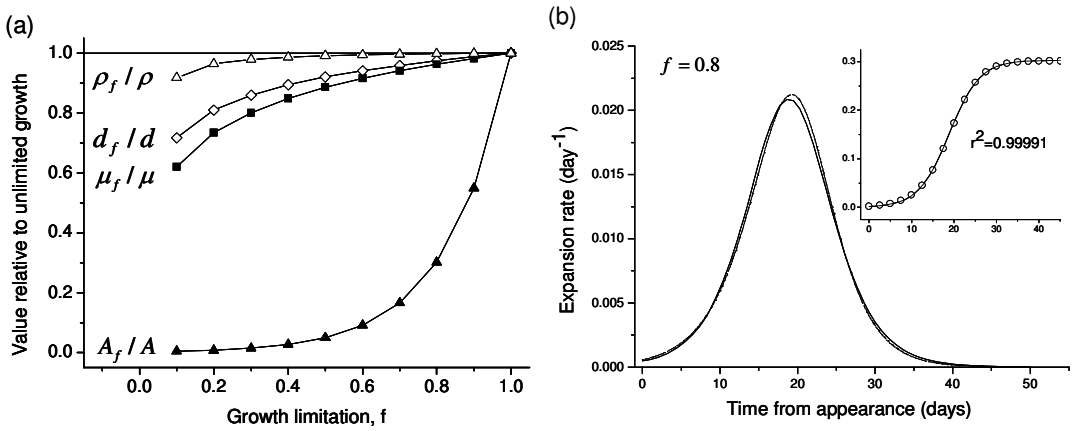

Figure 1. Properties of resource-limited growth (a) Effect of f on growth characteristics A_f, μ_f, d_f, and ρ_f (relative values of these variables with respect to values for unlimited growth A, μ, d, and ρ are shown) (b) Growth curve (open circles) and its derivative (dotted line) for $f = 0.8$, solid lines are the fitted logistic (1) (insert graph) and its derivative (main graph).

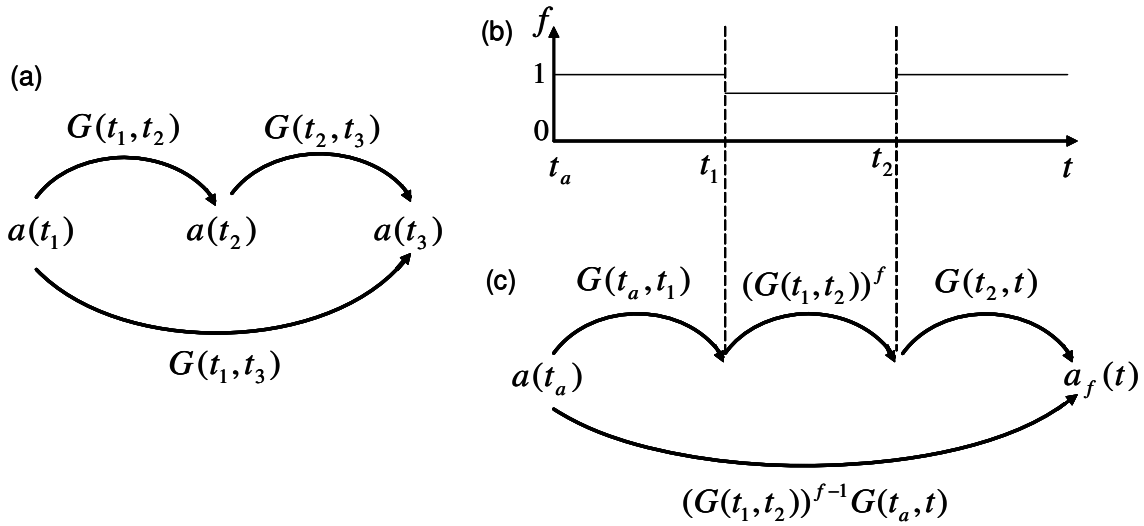

Figure 2. Growth under pulse-like perturbation of C supply (a) Schematic of the equation (12) (b) Pulse-like perturbation of C with $f < 1$ for $t_1 < t < t_2$ (c) Solution of (8) for this case.

Comparison with the approach by Thornley & France. Within the current approach, the projected final size variable $A_f(t)$, introduced by Thornley & France [6, 7], can be interpreted as an asymptote of the solution for the case where C limitation applies from the moment of appearance to the moment t, namely

$$A_f(t) = (G(t_a,t))^{f-1} A . \tag{14}$$

Substitution of $A_f(t)$ and $a_f(t)$ (10) into the system (3) and some rearrangements, show that these functions satisfy system (3) if and only if

$$f = \frac{f_1 \cdot r}{f_1 \cdot r + f_2 \cdot D} \quad \text{and} \quad \tau = \frac{1}{f_1 \cdot r + f_2 \cdot D} . \tag{15}$$

Although the approach by Thornley & France has four parameters, there are only two degrees of freedom in the parameter space, because the parameters enter equations (3) in the form of two products $(f_2 \cdot D)$ and $(f_1 \cdot r)$. For any given values of τ and f, the corresponding values of these products can be calculated from (15). Hence, the system (3) is equivalent to a single liner DE (8) with two parameters: τ - representing effects of environment (temperature) and f - representing effects of resource limitation.

Further extensions. Using variable φ (4), equation (8) can be generalised for the case of variable temperature. Taking advantage of linearity of this equation, analytical solution can be obtained for time-dependent $f = f(t)$. The present approach can be extended to the Boltzmann function that is also used in plant modelling [8] using a substitution $y(t) = a(t) - B$, where B is a lower asymptote of the Boltzmann function.

Conclusions

The simple linear DE proposed here allows intrinsic patterns of leaf and internode growth, temperature effects and C limitation to be taken into account. In the context of mechanistic modelling, C availability within the vicinity of each module is a result of the system dynamics, hence the equations describing the growth of individual modules are solved simultaneously and C distribution within the system is determined as a part of the solution process [2, 3]. Numerical solutions for such systems are not always easy to interpret. Analytical solutions provide an additional insight into the problem. They are more transparent and allow analysis of relationships between the system variables as well as comparisons with other systems. The linear DE proposed here is equivalent to a non-linear system (3) proposed previously by Thornley & France [6]. This DE can be also used as a linear DE corresponding to the Richards function [11], also known as θ-logistic or a "power-law logistic" [6, 7], allowing a mechanistic interpretation of these functions.

Acknowledgements

This study was supported by New Zealand Foundation for Science Research and Technology, contract C06X0202.

References

[1] Godin C, Sinoquet H 2005. Functional-structural plant modelling. *New Phytologist* 166: 705-708.

[2] Allen MT, Prusinkiewicz P, DeJong TM 2005. Using L-systems for modeling source-sink interactions, architecture and physiology of growing trees: the L-PEACH model. New Phytologist 166(3): 869-880.

[3] Prusinkiewicz P, Allen MT, Escobar-Gutiérrez A, DeJong TM 2007. Numerical methods for transport-resistance sink-source allocation models. In: Vos J, Marcelis LFM, de Visser PHB, Struik PC, Evers JB ed. *Functional-structural plant modelling in crop production.* Berlin, Springer. Pp. 123-137.

[4] Causton DR, Venus JR 1981. The Biometry of Plant Growth. London, Arnold

[5] Thornley JHM, Johnson IR 1990. *Plant and crop modelling: a mathematical approach to plant and crop physiology*. Oxford, UK, Clarendon Press.

[6] Thornley JHM and France J 2005. An open-ended logistic-based growth function. *Ecological Modelling* 184(2-4): 257-261.

[7] Thornley JHM, Shepherd J, France J 2007. An open-ended logistic-based growth function: analytical solutions and the power-law logistic model. *Ecological Modelling*. 204 (3): 531-534.

[8] Seleznyova AN, Greer DH 2007. Integrating developmental variables into process based modelling. Submitted for publication.

[9] Cookson SJ, Lijsebettens MV, Granier C 2005. Correlation between leaf growth variables suggest intrinsic and early controls of leaf size in Arabidopsis thaliana. *Plant, Cell and Environment* 28(11): 1355-1366

[10] Seleznyova AN, Halligan EA 2006. Modelling effect of temperature on area expansion at the leaf, the shoot and whole plant level. *Acta Horticulturae* 707: 167-174.

[11] Richards FJ 1959. A flexible growth function for empirical use. *Journal of Experimental Botany* 10: 290-300.

Creating Complex Patterns from Simple Developmental Rules

Scott Hotton and Jacques Dumais

Department of Organismic and Evolutionary Biology
Harvard University, Cambridge MA, USA

Keywords: plant development, dynamical systems, cell division, Errera's Rule, Sachs' Rule.

Iterative developmental processes as discrete dynamical systems

Many developmental processes in plants involve the iteration of simple geometrical rules. Examples of such processes are the initiation of lateral organs at the shoot apical meristem and the division of cells during tissue growth. A powerful way to study these iterative developmental processes is to recast them as discrete dynamical systems. In this context, development is fully determined by specifying the initial state of the system and the set of geometrical rules to be applied to evolve the system in time. L-systems are also dynamical systems that typically involve rewriting rules applied to strings of characters instead of geometrical rules applied in space. *The foremost motive to formulate developmental processes as L-systems or geometrical dynamical systems is to allow one to study systematically the morphogenetic potential of a specific set of developmental rules*. Although similar in their approach, geometrical dynamical systems offer one important advantage over L-systems – they operate directly on 2-D or 3-D space. This feature allows greater flexibility to capture complex developmental processes. We illustrate our approach with an analysis of cell division patterns in plant tissues.

Cell geometry in growing tissue layers

The development of the wide array of cell patterns in plants has attracted a lot of attention from biologists (e.g. Lück et al. 1988; Nakielski 1999; Barlow and Lück 2004). Historically, two main rules have been recognized for the division of plant cells. Sachs' Rule stipulates that cells divide such that the two daughter cells are of equal size. Errera's Rule of cell division stipulates that new cell walls behave like soap films (Errera 1888). A consequence is that new walls take the configuration of least possible area subject to some constraints. These constraints are that new walls have constant curvature and meet older walls at right angle.

These two simple geometrical rules were used to explain rather complex division patterns (Thompson 1942). Figure 1A shows the cellular pattern of the glandular trichomes located on the adaxial leaf surface of the Venus flytrap (*Dionaea muscipula*). The trichomes are made of a single cell layer atop a short stalk. The cell pattern is definitely intricate but offers, upon inspection, a few suggestive symmetries. We owe to D'Arcy Thompson the first detailed explanation for the development of this pattern. His argument is based on Sachs' and Errera's rules which, together, lead to a characteristic sequence of divisions (Fig. 1B-F). An initial circular cell is first divided along one of its diameter (Fig. 1C) and then at right angle from the first plane of division (Fig. 1D). These two rounds of radial division fulfill the division rules stated above and lead to the

four nearly equivalent quadrants seen in Fig. 1A. The third round of cell division is the most revealing since there are more than one division plane that seem plausible. The most natural inclination would be to divide the cell along the bisecting radial line as in the previous two rounds of division (Fig. 1G, upper right quadrant). This new wall, however, would not meet at 90˚ with older walls. Alternatively, the cell could divide periclinally (Fig. 1G, lower right quadrant). This division seems promising but it is not the shortest wall compatible with both Sachs and Errera's Rules. The shortest possible division plane is anticlinal and culminates in the formation of asymmetric daughters cells (Fig. 1E). It is this division that is observed most frequently in glandular trichomes (Fig. 1A).

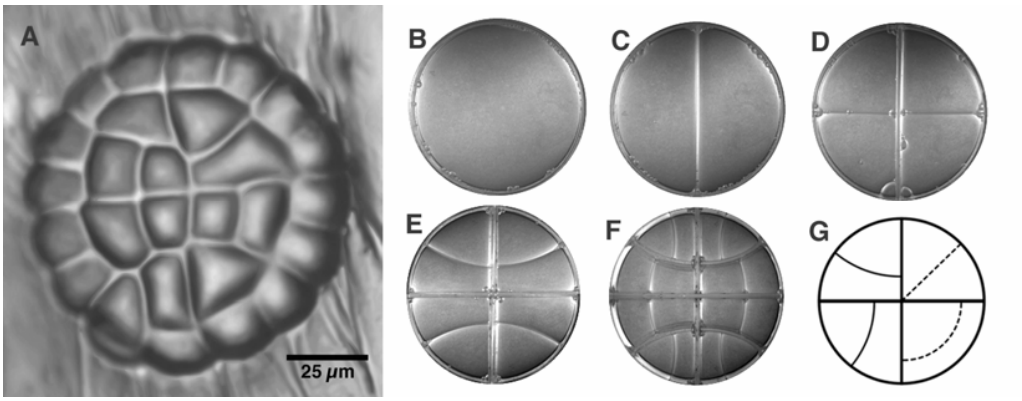

Figure 1: Cell patterning in glandular trichomes. A) Fully developed glandular trichome from the adaxial leaf face of the Venus flytrap. B) - F) Sequential subdivision of a circular dish with soap bubbles. New walls are assumed to rigidify after formation and serve as a fixed template for the next division. G) Possible wall positions for the third round of cell division. The dashed lines indicate divisions that are not compatible with Sachs and Errera's Rules while the solid lines represents the two geometries that fulfill the two rules and are observed in Nature. (From Dumais 2007)

The ability of these geometrical rules to predict several rounds of cell division indicates that they capture a fundamental aspect of the mechanism of cell division in these structures. Patterns akin to the one just described were first studied by Berthold (1886) who reported them from various algal species. Errera's rule was also verified in fern protonemata (Miller 1980, Cooke and Paolillo 1980). The rules, therefore, may be quite general.

Although the predictions made with the geometrical rules can be quite robust, we have also found some exceptions. For example, our observations of glandular trichomes reveal that approximately 15% of the divisions in the third round are of the periclinal type instead of the anticlinal type predicted by the application of Sachs and Errera's Rules. This result has led us to reformulate Errera's Rule such that all walls of constant curvature and right-angle contact are considered. It is then possible, with a simple geometrical argument, to predict what proportion of each division types should be observed. We have found that the 85:15 ratio of anticlinal versus periclinal walls can be predicted by assuming a random selection of the plane of division followed by

minimization of the wall area to conform, locally, to Errera's Rule. The simple modification has increased tremendously the predictive power of the geometrical model.

Acknowledgements
The authors thank Kajetan Zwieniecki for help with the experiments. Part of this work was supported by NSF grant #0540662 to JD.

References

Barlow PW, J Lück. 2004. Deterministic cellular descendance and its relationship to the branching of plant organ axes. Protoplasma 224: 129-143.

Berthold G. 1886. *Studien über Protoplasmamechanik.* Leipzig: Arthur Felix Verlag.

Cooke TJ, Paolillo DJ. 1980. The control of the orientation of cell divisions in fern gametophytes. *Amer J Bot* 67:1320-1333.

Dumais J. 2007. Can mechanics control pattern formation in plants? *Curr Opin Plant Biol* 10: 58-62.

Errera L. 1888. Über Zellformen und Seifenblasen. *Botanische Centralblatt* 34:395-398.

Green PB, RS Poethig. 1982. Biophysics of the extension and initiation of plant organs. In *Developmental Order: Its Origin and Regulation.* Edited by Subtelny S, Green PB. Alan R. Liss.

Lück J, A Lindenmayer, HB Lück. 1988. Models of cell tetrads and clones in meristematic cell layers. *Bot Gazette* 149: 127-141.

Miller JH. 1980. Orientation of the plane of cell division in fern gametophytes: the roles of cell shape and stress. *Amer J Bot* 67:534-542.

Nakielski J. 1999. Tensorial model for growth and cell division in the shoot apex. In *Pattern Formation in Biology, Vision, and Dynamics*. Edited by A. Carbone, M. Gromov, and P. Prusinkiewicz. World Scientific.

Thompson DW. 1942. *On Growth and Form*. Cambridge: Cambridge University Press. (Dover republication, 1992).

Using mechanics in the modelling of meristem morphogenesis

Szymon Stoma[1,†], Jérôme Chopard[1,†], Christophe Godin[1,†], Jan Traas[3,‡]

[1] INRIA, 2004 route des lucioles BP 93, 06902 Sophia Antipolis, France
[3] INRA, 147 rue de l'Université, 75338 Paris Cedex 07, France
[†] Virtual Plants, UMR Développement et Amélioration des Plantes, TA A-96/02, 34398 Montpellier Cedex 5, France
[‡] Laboratoire de Reproduction et Développement des plantes, UMR INRA/CNRS/ENS, 46 allée d'Italie, 69364 Lyon Cedex 7, France

Keywords : shape development ; mass-spring ; tensor mechanics ; wall loosening

Introduction

Shoot apical meristems are small groups of rapidly dividing, undifferentiated cells, which generate all aerial parts of the plants. Recently, spectacul ar advances in molecular biology and genetics have provided a wealth of information on meristem functioning. However, the amount of available information is now such, that an integrated view is no longer possible. As a result, researchers have been led to develop computational models in the form of *virtual meristems* to analyse this complexity *in silico* and to test different hypotheses. Only very recently three such models have been described [10, 1, 5]. All three are able to integrate various cell-based processes and show different emerging behaviours (e.g. meristem maintenance, phyllotaxis). This pioneering work has demonstrated that the *in silico* analysis of plant development can be an extremely useful complement to classical experimentation.

Previous models have focused their interrogations on physiological processes in the meristem for a given, predefined, tissue shape. However, in nature, the shape itself is the result of a continuous feedback loop between physiological information and growth. As suggested by [4, 2], the mechanical components of the cells could provide such a link. In this work, we consider the problem of integrating such a feedback loop in meristem development.

The role of mechanics

As physical objects, cells obey mechanical laws. In plants, a major factor controlling cell shape is the cell wall, which resists to the internal turgor pressure and guarantees the final shape of the cell [9]. Turgor (Π_0) induces mechanical constraints ($\underline{\underline{\sigma}}$) into the walls :

$$\mathrm{div}\underline{\underline{\sigma}} = \Pi_0 \tag{1}$$

Being elastic, walls deform and elongate to adjust to this stress. This deformation ($\underline{\underline{\varepsilon}}$) depends on mechanical properties of each wall which is caracterized by set of parameters (called tensor of elasticity, $\underline{\underline{\underline{\underline{K}}}}$):

$$\underline{\underline{\sigma}} = \underline{\underline{\underline{\underline{K}}}}(\underline{\underline{\varepsilon}} - \underline{\underline{\varepsilon^0}}) \tag{2}$$

The equations of mechanics (1 and 2) allow us to compute the elongation ($\underline{\underline{\varepsilon}} - \underline{\underline{\varepsilon^0}}$) of each wall (and thus each cell) for a given state (turgor pressure). However, to obtain a given shape, elastic deformations are not sufficient and plants must add material into the walls to achieve some plastic deformation. One biochemical hypothesis [3] is that cells add material to fill the void between cellulose microfibrils in the wall. The more the wall is stretched, the more gaps are being created between fibrils, the more material must be added to the wall. This modifies the reference state ($\underline{\underline{\varepsilon^0}}$) of the wall and thus growth is increased in the direction for which ($\underline{\underline{\varepsilon}} - \underline{\underline{\varepsilon^0}}$) reaches maximum. By synthesising expansins (e.g. auxin) that change cell walls' elasticity ($\underline{\underline{\underline{\underline{K}}}}$ and then $\underline{\underline{\varepsilon}}$) or wall *repair* rate (parameter G in equation 3), meristem shape can emerge fom cell physiological properties.

Mechanical model of meristem surface

In *Arabidopsis*, the external cell layer (called L1) plays a crucial role in meristem functioning [6]. To build up a mechanical model of this surface, we projected the L1 cells on the external surface of the meristem to obtain a polygonal mesh. Each polygonal cell is surrounded by the edges that stand for the projection of

its anticlinal walls, assuming an infinitely small thickness of the walls. A junction between edges is called a vertex. The behaviour of all inner cells of the meristem is summarized by an overall turgor pressure that perpendiculary pushes the surface and prevents the L1 layer from collapsing (as expressed in (d) on figure 1).

To describe the mechanical properties of a meristem the representation described above is expressed (as in [7]) in terms of a mass-spring system (MSS). Each edge e_i has an associated spring while masses are attached to the vertices. The mechanical behaviour of each spring is characterised by two parameters: a stiffness K_i and a rest length l_i^0. Growth is expressed as a change of spring rest length l^0 depending on the current spring tension :

$$\frac{\partial l_i^0}{\partial t} = \begin{cases} 0 & \text{if} \quad [l_i(t) - l_i^0] < \text{threshold} \\ G[l_i(t) - l_i^0] & \text{else} \end{cases} \tag{3}$$

where G is a growth rate. This change, in turn, induces a new mechanical state. A solver for particle systems [11] was designed to trace the shape evolution of the mesh.

This model was used to reproduce *in silico* the change of shape of the *Arabidopsis pin1* mutant depicted by Reinhardt [8]. This paper describes the emergence of a young primordium near the position of an applied patch of auxin. Cells with high auxin concentration grow faster, possibly due to the change in the mechanical properties of their walls. We simulate this behaviour by changing the mechanical parameters K of the springs associated with edges of the cells with high auxin concentration. In our model this resulted in faster, local growth in the *auxin-positive* region (in red on figure 1 (a)). The *bump* shaped structure, that appears, reproduces the appearance of a young primordium (simulation output presented in figure 1 (a)).

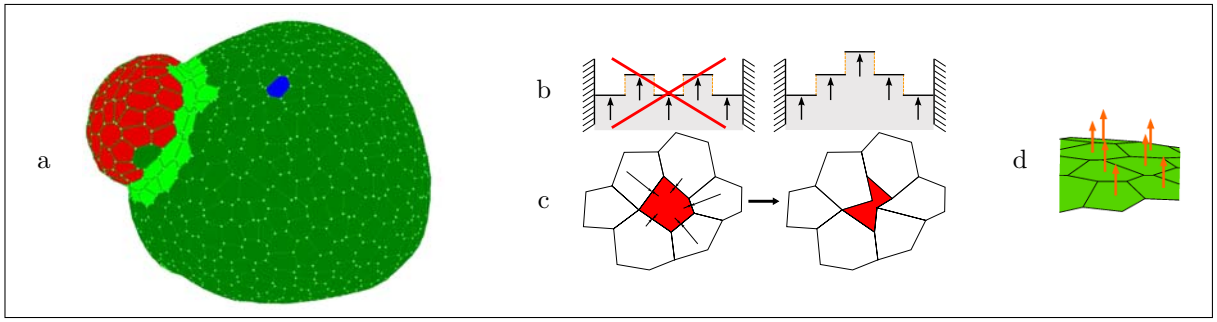

Figure 1: Model of meristem surface

This figure shows in (a) the modelling of *primordium* induction by an auxin patch applied in the red region. On (b), solid bars (horizontal segments, in black) are linked by elastic springs (vertical segments, in yellow). Extremities of the system are fixed. A pressure applied from bottom on the system will push all the bars to top. Crest formation is thus impossible. The red cell in (c) collapses due to the load of its neighbors. The explicit L1 layer representation (green poligons) with implicit inner cells (represented as pressure force – orange arrows) in (d).

Modelling only surface cells with 1D walls as springs is an efficient way to address meristem shape modelling. It allows fast computation of meristem shapes when testing different parameters of this complex system. In addition, the use of springs seems to be compatible with what is known on the biological system. In particular the concept of growing springs yielding to an inner force is clearly coherent with the idea of cell wall synthesis permitting the cells to yield to inner pressure. However, the implicit representation of the inner cells as a generalised pressure makes it impossible to generate more complex shapes (see figure 1 (b)). To model a crest instead of a bump, for instance, we need to explicitely represent the interior of the meristem. In addition, the use of MSS is suitable for small shape deformations but becomes less straight forward when dealing with more complex deformations. Because the link between two springs has no rotational constraint, cells under external load tend to collapse (see figure 1 (c)).

Mechanical model of meristem volume

To address complex shape changes, we need to model explicitly the interior of the meristem. The simplest conceptual way to do it consists of implementing a full 3D model of a tissue. In this model, all cells are

represented as polyhedra as shown on figure 2 (a). We assume that the wall between two cells remains planar and can thus be represented as a polygon in space. Wall mechanical properties are summarized by the two principal directions of the elasticity tensor in this plane. This assumption allows us to use the shell theory to compute strains and constraints in the meristem with a finite elements method. As in the previous model, growth is computed as a function of the amount of strain of the mesh standing for the meristem, parameterized by the physiological state of each individual cell.

The young carpels formed by the young Arabidopsis flower, arise together as a cylindrical shape on the top of the floral meristem. They provide a typical example of complex structure (see figure 2 (b)) previously described on figure 1 (b). The model makes it possible to simulate the result of a differentiation of a ringlike domain cells around the meristem center. These cells grow out more quickly than their neighbours, which is caracterized by a more rapid extension of the cell walls in the model. A 3D representation of this meristem shows the formation of the cylindrical *style tube* (see figure 2 (c))

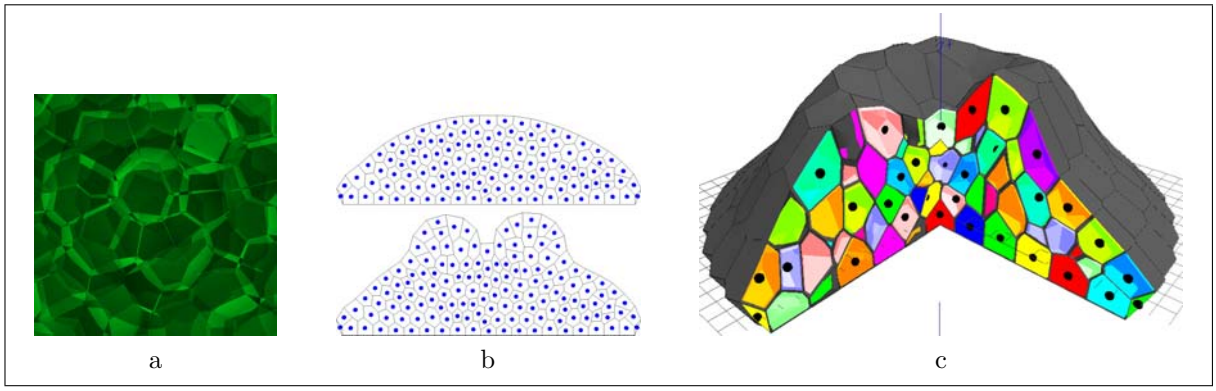

Figure 2: Carpel formation

(a) 3D meristem representation where cells appear as polyhedra. (b) Simulation of carpel development. From an initial state (on top) with a bump shaped meristem, the simulation runs to a crest shaped tissue (on bottom). (c) 3D representation of the final state of the simulation depicted in (b) that shows the formation of the *style tube*.

Conclusion

In the talk, we shall present the application of mechanical models to the integrated simulation of primordia generation and carpel development. We shall discuss how these models relate physiological information to meristem morphogenesis. By closing the feedback loop, they provide, a useful complement to previous models that mainly concentrated on physiological processes.

References

[1] Pierre Barbier de Reuille, Isabelle Bohn-Courseau, Karin Ljung, Halima Morin, Nicola Carraro, Christophe Godin, and Jan Traas. Computer simulations reveal properties of the cell-cell signaling network at the shoot apex in arabidopsis. *PNAS*, 103(5):1627–1632, 2006.

[2] Enrico Coen, Anne-Gaëlle Rolland-Lagan, Mark Matthews, J. Andrew Bangham, and Przemyslaw Prusinkiewicz. The genetics of geometry. *PNAS*, 101(14):4728–4735, 2004.

[3] Daniel J. Cosgrove. Growth of the plant cell wall. *Nature reviews*, 6:850–861, 2005.

[4] Jacques Dumais and Charles R. Steele. New evidence for the role of mechanical forces in the shoot apical meristem. *Journal of Plant Growth Regulation*, 19:7–18, 2000.

[5] Henrik Jönsson, MArcus G. Hesler, Bruce E. Shapiro, Elliot M. Meyerowitz, and Eric Mjolsness. An auxin-driven polarized transport model for phyllotaxis. *PNAS*, 103(5):1633–1638, 2006.

[6] Sharon Kessler, Brad Townsley, and Neelima Sinha. L1 division and differentiation patterns influence shoot apical meristem maintenance. *Plant Physiology*, 141:1349–1362, 2006.

[7] Przemyslaw Prusinkiewicz and Aristid Lindenmayer. *The algorithmic Beauty of Plants*. New-York, 1996.

[8] Didier Reinhardt, Therese Mandel, and Cris Kuhlemeier. Auxin regulates the initiation and radial position of plant lateral organs. *The Plant Cell*, 12:507–518, 2000.

[9] Peter Schopfer. Biomechanics of plant growth. *American Journal of Botany*, 93(10):1415–1425, 2006.

[10] Richard S. Smith, Soazig Guyomarc'h, Therese Mandel, Didier Reinhardt, Cris Kuhlemeier, and Przemyslaw Prusinkiewicz. A plausible model of phyllotaxis. *PNAS*, 103(5):1301–1306, 2006.

[11] Andrew Witkin. Physically based modeling. Technical report, Pixar AnimationStudio, 2001.

Growth dynamics of the shoot apical meristem: global, cellular and sub-cellular approach

Anne-Lise Routier-Kierzkowska[1] and Dorota Kwiatkowska[2]
[1]Institute of Plant Biology, Wroclaw University
Kanonia 6/8, 50-328 Wroclaw, Poland, annelise.routier@gmail.com
[2]Department of Biophysics and Cell Biology, University of Silesia
Jagiellonska 28, 40-032 Katowice, Poland

Keywords: meristem growth, stereoscopic reconstruction, cell growth, cell division orientation, cell wall growth

The shoot apical meristem (SAM) is responsible for the whole shoot morphogenesis (stem and lateral organ formation). Different SAM zones contribute to organ initiation and its self-perpetuation. They exhibit various cytohistological traits, as well as growth rate and anisotropy, which dynamically evolve during SAM ontogeny. These zones are believed to be linked with the gene expression patterns through differential mechanical properties of the meristem tissue (Green, 1999), among which the outmost cell layer seems to play a crucial role.

The recent years have seen a growing interest in the modeling of SAM morphogenesis, in link with the genetic regulation and mechanical aspects. In order to make realistic hypothesis for these models and test them, there is a need for empirical data at different levels: (1) at the whole SAM level; (2) at the individual cell level; and (3) at the cell wall level. Here, we present a method, which has proven to be useful in obtaining information on the growth at the whole SAM level and which with further improvements can provide us with data on the cellular and cell wall levels. The analysis using this method is performed for shoot apices of *Arabidopsis thaliana* and *Anagallis arvensis*, two small dicot herbs. Computations are performed with the aid of original codes written in Matlab (The Mathworks, Natick, MA, USA).

The sequential replica method and existing protocols for growth and geometry assessment

The sequential replica method is a non invasive method allowing one to follow the shape and growth of an individual SAM surface for several days. Briefly, replicas (molds) are taken from the surface of an individual shoot apex at 12-24 h intervals for up to several days (Williams and Green, 1988).The molds are then filled with epoxy resin in order to prepare casts, which are observed in a scanning electron microscope, providing an indirect observation of the meristem surface at different instants. To reconstruct the 3-D shape of the surface, two images (a stereopair) are taken for every cast, one from a top view and the other tilted by 10º in the microscope chamber. Vertices, i.e. contacts of three anticlinal walls of neighboring cells, are used as marker points to reconstruct the 3-D shape of the apex surface. Their position is digitized on the first image and then semi-automatically recognized on the second. Differences in relative vertex positions on the two images are used to compute the third coordinate. Based on the comparison of successive replicas the same cells and vertices can be recognized on the individual apex surface at consecutive instants. This enables computation of growth parameters for each vertex based on the deformation of the triangle formed by its three nearest neighbors. Next, the parameters are computed for each cell as the average for its vertices (Goodall and Green, 1986; Dumais and Kwiatkowska, 2002). Growth is described by the principal directions of growth, growth rates along these directions, growth anisotropy and areal cell growth. For each 3-D reconstruction, shape of the SAM surface can be also quantified by means of curvature directions and Gaussian curvature.

The method has been successfully used to describe zones of different growth on the wild type *Arabidopsis* and *Anagallis* apices, showing that different growth patterns occur in inflorescence and vegetative

meristems (e.g. Kwiatkowska, 2006) and zones of different growth evolve in time, rather than being a steady field of growth. The existing computation method is thus sufficient to analyze growth and geometry on the whole SAM level. However, the stereoscopic reconstruction technique had several drawbacks which lead to imprecision in the reconstruction, and the growth computation protocols are based on averaging for SAM portions composed of more than a single cell. Therefore, we need to improve the computational part of the protocols in order to use the replica method at smaller scale (cell, cell wall).

Improvement of the stereoscopic reconstruction technique

Imprecision in the existing reconstruction technique is due to errors in the placement of each vertex on the two images of the stereopair, perspective deformation of scanning electron microscope images, and lens deformation of the microscope. The first step of the improved reconstruction technique involves an automatic robust matching of the features of the two images in order to recover the epipolar geometry. This is followed by an auto-calibration stage to correct the perspective deformation through recovering focal length for both images (Zhang 1998), dense matching of the paired images (Zitnick and Kanade, 2000) and, finally, triangulation leading to a dense high resolution reconstruction of the SAM surface (Hartley and Zisserman, 2000) (fig.1). This dense reconstruction can be afterwards approximated by a continuous surface, allowing a much more precise quantification of the SAM geometry, good enough for studies at the cell wall level.

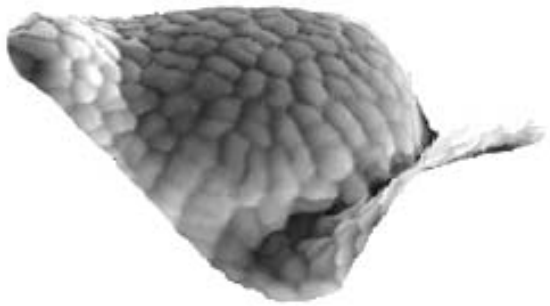

fig. 1. A dense reconstruction of the meristem surface

New questions to be answered and new empirical data to come from the improved protocols

The whole SAM level:

Previous studies show that morphogenesis at the SAM involves rather dramatic changes in both geometry and growth. We therefore speculate that some regions at the SAM surface are especially affected by tensile, compressive and shear stress. In order to identify such SAM regions we have to combine the local growth and shape analysis with an analysis of the vertex displacement field with respect to an arbitrarily chosen fixed region of the meristem. This is achieved through the superposition of landmarks (vertices) on the consecutive reconstructions with the aid of the procrustes algorithm (Eggert et al., 1997).With a good choice of the reference region and a careful analysis, non radial displacements can be interpreted, for example, as a consequence of shear occurring on the meristem surface.

The cellular level:

New models of meristem growth preferentially incorporate a realistic cell behavior, where cell shapes are preserved during the growth through a good choice of parameters of cell growth and divisions (e.g. Smith et al. 2006, Nakielski and Barlow 1995). Several rules have been proposed to link cell growth, shape and division planes, however, few experimental observations had been provided for their falsification.

The first rules have been proposed long ago by the plant biologists Hofmeister (1863), Sachs (1878) and Errera (1888). Hofmeister's rule states that if an organ grows in different directions, cell division planes are perpendicular to the direction of the fastest growth. According to the Errera's rule, new walls follow the shortest path that will halve the parental cell. The Sachs' rule states that the new cell wall meets parental walls at a right angle. A more general rule formulated by Hejnowicz and Romberger (1984) states that the cell division plane is always perpendicular to one of the cell principal growth directions. Using the improved protocols to compute growth for individual cells we aim to perform a statistical analysis of the presumable link between principal growth directions, cell shape and the orientation of division plane. We will also check whether the cell behavior is the same in the different zones of the SAM.

A preliminary analysis of the relation between maximal cell growth and the new cell wall orientation was already made. A Monte-Carlo method was used in order to exclude from the analysis the cells for which the direction of maximal growth cannot be robustly determined (due to cell growth being nearly isotropic, too small growth rates in comparison to the noise, or special cell shape). Then we computed the angle between the direction of maximal growth and the normal to the new cell wall.

One difficulty in our data interpretation comes from the fact that the growth rates we compute are averaged value for the time lapse between two replicas. A cell division wall visible on a replica (at time T2) could appear just before the replica was made, or just after the preceding replica (made at T1). As a result the growth computed between T1 and T2 is the sum of growth before *and* after cell division, in unknown proportions. We thus need to compute also the direction of maximal growth between times T0 and T1, and to compare its orientation with that of the new cell wall.

Preliminary results show that, for *Anagallis* cells, the direction of maximal growth computed for the timelapse T1-T2 is clearly correlated with the new cell wall orientation, PDG max being most often in the direction normal to the new cell wall (fig 2). On the contrary there is no clear relation between the direction of maximal growth between T0 and T1 and orientation of the new cell wall in T2. However, a comparison between growth in two successive time intervals suggests that some cells switch their growth orientation upon cell division. More data are needed to draw clear conclusions, and other factors (cell shape, curvature, position on the meristem) have to be taken into account in the analysis.

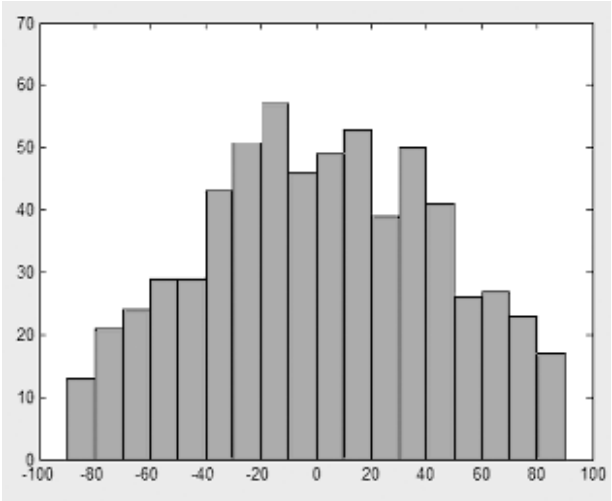

fig. 2. Angle (in degrees) between normal to the new cell wall and direction of maximal growth

The cell wall level:

Just after division, the daughter cells do not have the typical shape of older cells, which are most often pentagons or hexagons with the cell walls meeting at approximately 120°. Since the new cell walls, as stated by Sachs' rule, are supposed to appear always at right angles with respect to the old ones, the angle between walls has to change in time. This change of cell shape is possible only if there is a difference in growth rates between the different walls of the same cell. Two antagonistic models have been proposed. D'Arcy Thompson (1942) speculates that the new formed cell wall gradually stiffens so that its tension progressively approaches the older walls tension, while Korn (1980) supposes that the young cell wall is not able to grow for a few cell cycles. Both these models can explain theoretically the changes in angles between cell walls (Lloyd 1991). We aim to test them by following actual changes in cell wall growth and angles between walls, thus providing both important data for SAM modeling and a clue on the development of cell wall properties after its formation.

Acknowledgments

This work is supported by a Marie Curie Action Grant MRTN-CT-2004-005336
"SYSTEMS BIOLOGY OF STEM CELL FUNCTION IN ARABIDOPSIS THALIANA" (SY-STEM)

References

D'Arcy Thompson W, 1942. On growth and form. Cambridge University Press, Cambridge.

Dumais J, Kwiatkowska D. 2002. Analysis of surface growth in shoot apices. Plant Journal 31, 229-241.

Eggert DW, Lorusso A, Fisher RB. Estimating 3-D rigid body transformations: a comparison of four major algorithms. Machine Vision and Applications 9, 272-290.

Goodall CR, Green PB. 1986. Quantitative analysis of surface growth. Botanical Gazette 147, 1-15.

Green PB. 1999. Expression of pattern in plants: combining molecular and calculus-based biophysical paradigms. American Journal of Botany 86(8): 1059-1076.

Hartley R, Zisserman A, 2000. Multiple view geometry in computer vision. Cambridge University Press.

Hejnowicz Z, Romberger JA. 1984. Growth tensor of plant organs. Journal of Theoretical Biology 110, 93-114.

Korn RW, 1980. The changing shape of plant cell: transformations during cell proliferation. Annals of Botany 46, 649-666.

Kwiatkowska D, 2006. Flower primordium formation at the Arabidopsis shoot apex: quantitative analysis of surface geometry and growth. Journal of Experimental Botany 57(3), 571-580.

Lloyd CW, 1991. How does the cytoskeleton reads the laws of geometry in aligning the division plane of plant cells? Development Supplement 1, 55-56.

Nakielski J, Barlow PW, 1995. Principal directions of growth and the generation of cell patterns in wild-type and gib-1 mutant roots of tomato (Lycopersicon esculentum Mill.) grown in vitro. Planta 196(1), 30-39.

Smith RS, Guyomarc'h S, Mandel T, Reinhardt D, Kuhlemeier C, Prusinkiewicz P. 2006. A plausible model of phyllotaxis. PNAS 103(5) , 1301-1306.

Williams MH, Green PB. 1988. Sequential scanning electron microscopy of a growing plant meristem. Protoplasma 147, 77-79.

Z. Zhang, 1998. Determining the epipolar geometry and its uncertainty : a review. IJCV 27(2), 161-198.

L. Zitnick, T. Kanade, 2000. A cooperative algorithm for stereo matching and occlusion detection. IEEE Transactions on Pattern Analysis and Machine Intelligence 22 (7), 675-684.

Trichome patterning on growing tissue

Pierre Barbier de Reuille [*†] Adam Runions[*] Richard Smith[*] Enrico Coen[†]
Przemyslaw Prusinkiewicz[*]

Keywords: trichome, reaction-diffusion, genetic regulatory network, growth

Introduction

Leaves of *Arabidopsis thaliana* bear trichomes, or hairs, which are spaced in an approximately regular pattern on their adaxial side. Trichome cells differentiate in the fast-growing basal part of the leaf and do not divide. The regular spacing of trichomes is controlled by cell-to-cell interactions (Larkin et al., 1997). We created simulation models of these interactions to gain a better understanding of the patterning process. The models operate on a growing virtual leaf with dividing and differentiating cells. We show that, within the previously proposed class of reaction-diffusion processes (Hülskamp, 2004), trichome patterning is more readily generated by activator-inhibitor than activator-substrate models (Meinhardt and Gierer, 1974). We then report on current work, in which an activator-inhibitor model is being refined by taking into account present understanding of the genetic regulatory network that controls trichome differentiation in Arabidopsis.

Reaction-diffusion models

Growing leaf surface was specified by interpolating between a sequence of keyframe B-spline surfaces (Foley et al., 1996) that represented selected stages of leaf growth. These surfaces were defined interactively using a graphical editor according to the current qualitative understanding of the dynamics of early leaf growth. Specifically, the zone of maximum growth was first located at the tip of the leaf, then progressively displaced toward the leaf base. The leaf surface supported a layer of cells growing symplastically and dividing upon reaching a threshold size (Nakielski, 2000; Smith et al., 2006). An exception was made for the trichome cells, which stopped growing upon reaching a maximum size (their vertices have then "slided" with respect to the supporting surface). The entire model was implemented within the vv modeling environment (Smith and Prusinkiewicz, 2004).

We used the equations for activator-inhibitor model as given by Meinhardt and Gierer (1974):

$$\frac{\partial a}{\partial t} = c\frac{a^2}{1+jh^2} + \rho_a - a\mu_a + D_a\nabla^2 a \qquad \frac{\partial h}{\partial t} = ca^2 + \rho_h - \mu_h h + D_h\nabla^2 h$$

where a is the activator concentration, h the inhibitor concentration, c the autocatalysis constant of the activator, j the efficiency of the inhibition, ρ_a and ρ_h the production constants, μ_a and μ_h the degradation constants, and D_a and D_h are the diffusion constants.

It is known that, on a regular grid, activator-inhibitor models can produce a pattern of regularly spaced activation peaks when the diffusion rate of the inhibitor is much greater than the diffusion rate of the activator (Meinhardt and Gierer, 1974). We observed that the same conditions apply in models of cellular tissues. Moreover, as existing activated cells move apart due to the tissue growth, in-between cells may switch to the activated state. The resulting pattern closely resembles the pattern of trichome differentiation observed in nature (Fig. 1a-c).

The activator-substrate model was implemented using a slightly modified version of the equations proposed by Meinhardt (1982, chap. 5):

$$\frac{\partial a}{\partial t} = ca^2 s - \mu_a a + D_a\nabla^2 a \qquad \frac{\partial s}{\partial t} = \rho_s - ca^2 s - \mu_s s + D_s\nabla^2 s$$

where the same notation as for the activator-inhibitor model is used. On a regular grid and in a non-growing tissue the activator-substrate model can produce a pattern of activation peaks similar to that obtained with the activator-inhibitor model, although their spacing is less regular. When a tissue grows, however, the peaks spread over neighboring cells, forming clusters that move with the cellular structure, and eventually split (Fig. 1d). This behavior is consistent with Meinhardt's (1982, Chapter 5) observations of activator-substrate model operating on a growing linear array of cells, but is inconsistent with the dynamics of trichome patterning of nature. Thus, if trichome patterning is governed by a reaction-diffusion process, it is an activator-inhibitor rather than an activator-substrate process.

Biology of trichome patterning

Larkin et al. (1997) proposed a simple genetic network for trichome patterning involving three genes: Glabra1

[*]Department of Computer Science, University of Calgary, 2500 University Drive NW, Calgary, AB, Canada T2N 1N4
[†]Department of Cell and Developmental Biology, John Innes Centre, Colney Lane, Norwich NR4 7UH, United Kingdom

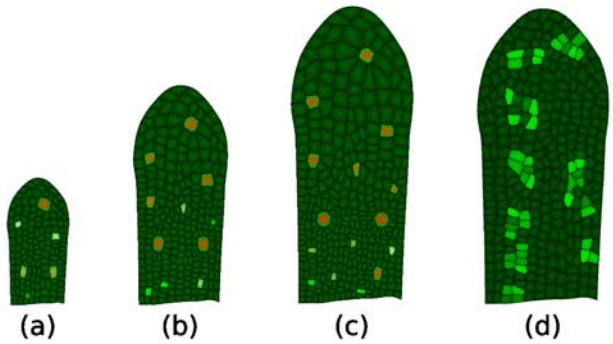

Fig. 1: **(a-c)** Activator-inhibitor model on a growing surface. The model includes three cell types in addition to the reaction-diffusion. In the basal part, there are immature cells and trichomes; in the distal part there are mature cells and trichomes. Mature cells do not divide. Trichomes grow up to a maximum size, and tend to be circular, as observed in nature. The concentration of activator is indicated in green (bright = high concentration). The trichomes have a different color in their center, scaling from white for young trichomes to red for old ones. Note approximately uniform distribution of trichomes on the leaf surface. **(d)** Activator-substrate model on the same growing surface. Note that activated cells are clustered, and clusters are not uniformly distributed.

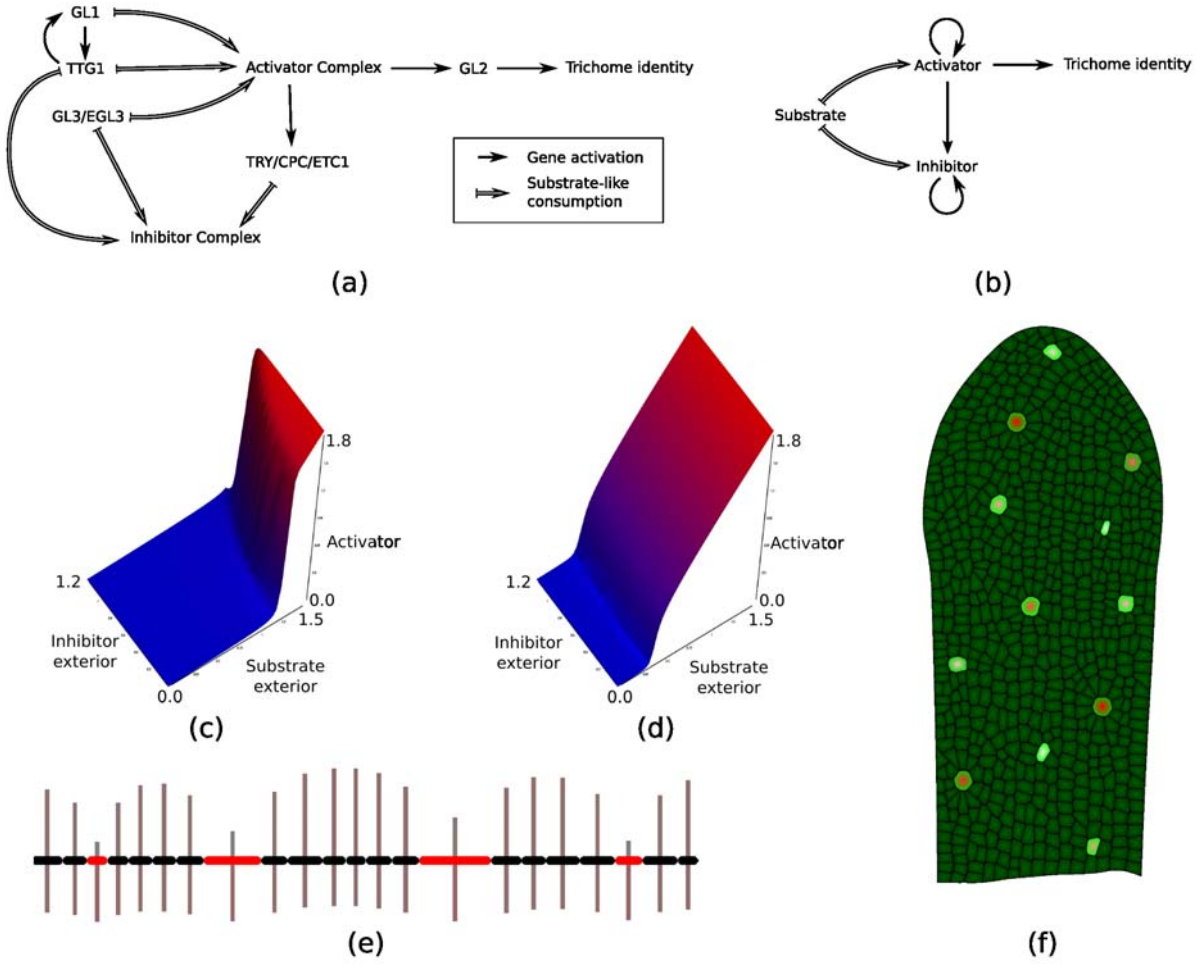

Fig. 2: **(a)** Genetic network for trichome positioning as described by Hülskamp (2004). **(b)** Substrate-activator-inhibitor (SAI) model. **(c,d)** Sample studies of the behavior of a single cell. The three-dimensional plots show the concentration of the activator as a function of the concentrations of the inhibitor and substrate, external to the cell, and the initial concentration of the activator, which is low for (c) and high for (d). The difference between plots c and d reflects different cell histories (hysteresis), and represents an essential component of cell differentiation. **(e)** Simulation of trichome differentiation in a filament. Trichome cells are shown in red. The upper and lower bars indicate concentrations of the substrate and the inhibitor, respectively. **(f)** Cell tissue simulation result with parameter values $\rho_a = 0.01, \rho_s = 1, \rho_h = 0, D_a = 0, D_h = 10, D_s = 5, \alpha = 1.6, \beta = 0.6, \lambda = 4.0, \mu_a = 0.2, \mu_h = 1.0, \mu_s = 0.3$. The color scheme is as described in Fig. 1. Note regular spacing of trichomes generated by this model.

(GL1), Transparent Testa Glabra (TTG) and Tryptychon (TRY). The first two genes form an autocatalytic activator of the trichome identity while the third one is an inhibitor of this identity. The model proposed by Larkin et al. can thus be viewed as an elaboration of the mechanism of activation-inhibition.

Since 1997, the understanding of the genetic network behind trichome patterning has evolved to include more genes and a more precise view of gene-proteins interactions. According to Hülskamp (2004), the patterning involves seven genes. Three of the resulting proteins (TTG1, GL3 and Enhancer of GL3 (EGL3)) form a complex that can further bind to either GL1 or TRY, Caprice (CPC) and Enhancer of TRY and Caprice 1 (ETC1). The complex with GL1 activates the trichome identity of a cell. The binding of TRY, CPC and ETC1 proteins to this complex prevents GL1 from binding to it, and thus indirectly inhibits trichome identity. We can describe the resulting mechanism as a competition between GL1 on one hand, and TRY, CPC and ETC1 on the other hand, for binding to the complex of TTG1, GL3 and EGL3. In addition, the complex including GL1 promotes the expression of the genes TRY, CPC and ETC1 (Fig. 2a). Of all the proteins, only CPC is known to diffuse (Hülskamp, 2004).

Substrate-Activator-Inhibitor (SAI) model

We modeled the network of gene and protein interactions, described above, as competition for a substrate s (representing TTG1, GL3 and EGL3) between a slowly diffusing activator a (representing the complex with GL1), and highly diffusive inhibitor h (representing the complex with TRY, CPC and ETC1, Fig. 2b). The concentration of the three morphogens in each cell is governed by the following system of ordinary differential equations:

$$\frac{\partial a}{\partial t} = \alpha a^2 s + \rho_a s - \mu_a a + D_a \nabla^2 a \qquad \frac{\partial h}{\partial t} = \beta h^2 s + \lambda a - \mu_h h + D_h \nabla^2 h$$

$$\frac{\partial s}{\partial t} = -\alpha a^2 s - \beta h^2 s - \lambda a + \rho_s - \mu_s s + D_s \nabla^2 s$$

where α and β are the autocatalytic constants for the activator and inhibitor, λ characterizes the upregulation of the inhibitor production by the activator, ρ_s, ρ_a, ρ_h are the production constants, μ_s, μ_a, μ_h are the degradation constants and D_s, D_a, D_h the diffusion constants.

We have developed three software tools to study this system. The first tool is a simulator of individual cells, implemented using NumPy (Oliphant, 2006), a scientific computing library for Python, and VTK (Schroeder et al., 2006), a 3D visualization toolkit. It allows for the exploration of the parameter space, considering a large number of individual cells simulated with different parameter values (Fig. 2c,d). The second tool is a simulator of a filament of cells, written using L+C (Karwowski and Prusinkiewicz, 2003). We use it to study the interaction between cells in an idealized, one-dimensional setting (Fig. 2e), which is simpler than a two-dimensional layer of growing and interacting cells. The third tool is the full simulator of the leaf, obtained by extending the activator-inhibitor model described earlier (Fig. 2f).

With this model, we were able to show that a reaction-diffusion based on competition over substrate can produce regularly spaced peaks. According to present knowledge, this is the most likely mechanism used by the plant to position the trichomes.

References

James D. Foley, Andries van Dam, Steven K. Feiner, and John F. Hughes. *Computer graphics - Principles and practice*. Addison Wesley, 2nd edition, 1996.

Martin Hülskamp. Plant trichomes: a model for cell differentiation. *Nature Reviews: Molecular Cell Biology*, 5(6):471–480, June 2004. doi: 10.1038/nrm1404.

Radoslaw Karwowski and Przemyslaw Prusinkiewicz. Design and implementation of the L+C modeling language. *Electronic Notes in Theoretical Computer Science*, 86(2):1–19, September 2003. doi: 10.1016/S1571-0661(04)80680-7.

John C. Larkin, M. David Marks, Jim Nadeau, and Fred Sack. Epidermal cell fate and patterning in leaves. *Plant Cell*, 9(7): 1109–1120, July 1997. doi: 10.1105/tpc.9.7.1109.

Hans Meinhardt. *Models of biological pattern formation*. Academic Press, London, 1982.

Hans Meinhardt and A. Gierer. Applications of a theory of biological pattern formation based on lateral inhibition. *Journal of Cell Science*, 15(2):321–346, July 1974. URL `http://jcs.biologists.org/cgi/reprint/15/2/321`.

Jerzy Nakielski. *Pattern formation in biology, vision and dynamics*, chapter Tensorial model for growth and cell division in the shoot apex, pages 252–286. World Scientific, 2000.

Travis E. Oliphant. *Guide to NumPy*. Trelgol Publishing, December 2006.

Will Schroeder, Ken Martin, and Bill Lorensen. *Visualization toolkit: an object-oriented approach to 3D graphics*. Kitware, Inc., 4 edition, 2006.

Colin Smith and Przemyslaw Prusinkiewicz. Simulation modeling of growing tissues. In *Proceedings of the 4th International Workshop on Functional-Structural Plant Models*, pages 365–370, 2004.

Richard S Smith, Soazig Guyomarc'h, Therese Mandel, Didier Reinhardt, Cris Kuhlemeier, and Przemyslaw Prusinkiewicz. A plausible model of phyllotaxis. *Proceedings of the National Academy of Science of the USA*, 103(5):1301–1306, January 2006. doi: 10.1073/pnas.0510457103.

Simulating the red:far-red ratio of individual plant organs, a key issue for phytochrome-driven processes.

M. Chelle[1], J. B. Evers[2], C. Fournier[1], D. Combes[3], J. Vos[2], B. Andrieu[1]

[1]INRA, UMR1091 Environnement et Grandes Cultures, F-78850 Thiverval-Grignon, France
[2]Crop and Weed Ecology, Plant Sciences Group, Wageningen University, Haarweg 333, 6709 RZ Wageningen, the Netherlands
[3]INRA, UR4 Écophysiologie des Plantes Fourragères, F-86600 Lusignan, France

chelle@grignon.inra.fr

Keywords: L-system, light model, radiosity, wheat, red:far-red

Introduction

The red:far-red ratio (R:FR) is a key variable in many biological processes from basic ones such as the response of phytochrome to more integrated ones, such as tillering or weed competition. Accurate estimation of the red:far-red ratio of plant organs in field condition is an important issue to be able to integrate the increasing knowledge on phytochrome-driven processes from cell and organ scale to canopy scale. In this paper, we interfaced an architectural plant model (ADEL-wheat) with a 3D light model (nested radiosity) to simulate the red:far-red signal actually perceived by plant organs in crop canopies.

A coupled model

ADEL-wheat (Evers et al., 2005; Fournier et al., 2003) is an architectural model of wheat, implemented with the L-studio software. It uses the open L-system principles (Mech and Prusinkiewicz, 1996) that enable data exchange with an environmental program. From a given initial planting pattern of seeds, the model calculates growth and development, size, shape and orientation in space of each organ in relation to thermal time. Leaf blade curvature and orientation in space are stochastic elements based on distributions derived from experiments (Fig. 2).

The nested radiosity model (NR) was adapted from the radiosity method to calculate light transfer between plant organs within explicitly described canopies (Chelle et al., 1998). This model requires (i) a 3D description of a canopy pattern by a set of triangles, (ii) a set of light sources described as infinitely far collimated light sources, and (iii) the optical properties (reflectance and transmittance) of soil and phytoelements. To avoid border effects, the model infinitely repeats the canopy pattern (Chelle et al., 1998). From these parameters, the irradiance and absorbed energy of each triangle describing the canopy can be calculated. The NR model is coupled with the ADEL-wheat model using the Caribu interface (Chelle et al., 2004) to manage the data exchanges and programs synchronization.

Experiment and simulations

An experiment using two contrasting wheat canopies (low and high plant population density) was performed in Wageningen (NL) during spring 2004. Downward and sideward R:FR ratios were measured using a Skye SKR100/116 sensor at soil level near midday at six dates during the vegetative cycle. Plant measurements, described in Evers et al. (2006; 2007) were used to fit ADEL-wheat so that the time course of simulated plant architecture matched the measured one.

Light simulations were performed for six dates (Julian days 111, 118, 125, 132, 139, and 146), which corresponded to a large range (0.1-10) of leaf area index (LAI). Four types of sky condition were used: three sun courses respectively corresponding to 6-8 UT hour (Universal Time), 11-13 UT hour and the whole day, an overcast sky (SOC; CIE, 1994). To enable the comparison with measurements, virtual flat square sensors with an area of 13 cm^2 were randomly located at 24 positions in the canopy, at a height of approximately 8 cm above soil surface. Calculations were performed for five orientations of each sensor (horizontal facing zenith and vertical facing North, East, South and West) and three

different fields of view (FOV) (hemispherical, 40°, and 80°, the latter corresponding to the Skye SKR100/116 sensor).

A variable very sensitive to measurement conditions

Downward and sideward R:FR at soil level calculated by the ADEL-wheat x NR model at the six dates for two plant population densities agreed well with measurements. Simulations were also consistent with previously published results, showing a decrease of R:FR with LAI (Sattin et al., 1994; Sparkes et al., 2006), this decrease being sharper for sideward radiation than for downward one. Simulated R:FR also decreased at low sun elevation, as previously measured by Battla et al (2000).
More specifically, the simulations showed an important effect of the measurement conditions on the relationship between LAI and R:FR. (sensor orientation and FOV, duration, sky type). Figure 1a illustrates that, under overcast condition, the decrease of sideward R:FR with LAI was highly depending on sensor FOV, due to the contribution of direct sky light in the measured signal. Figure 1b compares the sideward R:FR measured by a North looking sensor to that obtained by the average of North- East-, South-, and West- looking sensors. As expected, measurements compared well in the case of an overcast sky, but large difference occurred under clear sky conditions, whatever the time of measurement. Such results showed that extreme care should be taken when comparing experimental results obtained by following different measurement protocols.

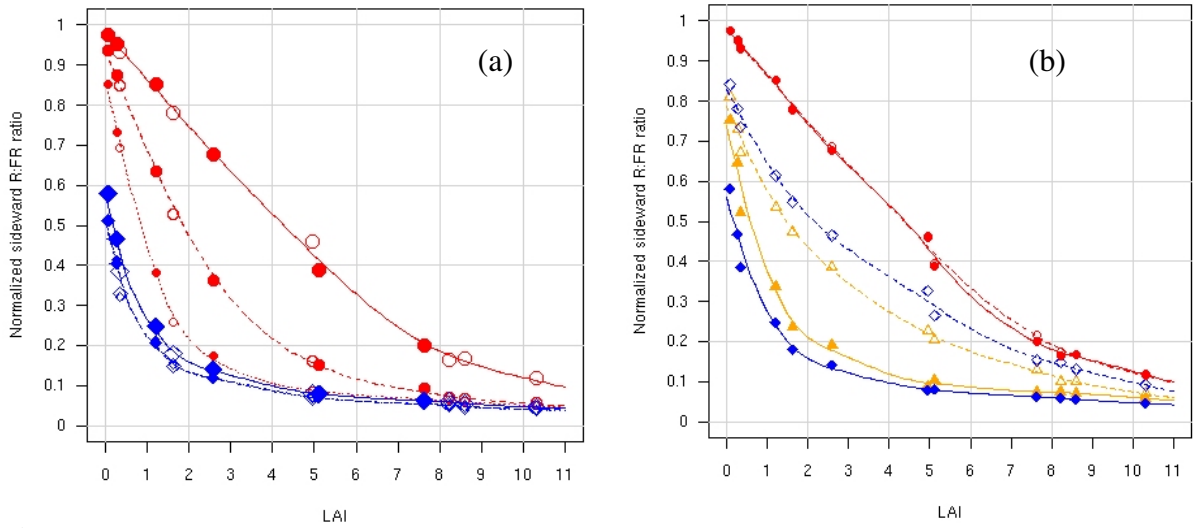

Fig. 1 Interactions between sensor field of view and illumination conditions on the relationship between LAI and R:FR at soil level (a) North-coming sideward fluxes simulated with various FOV (180° - solid line; 80° - long-dashed line; 40° - short-dashed line), (b) North-coming (solid symbols) and North-, East-, South-, West- coming (open symbol) sideward fluxes simulated with 180° FOV. Sky conditions were overcast sky (●) , noon clear sky (◆), and morning clear sky (▲). R:FR ratio were normalized with the R:FR ratio at top of the canopy.

Estimating the R:FR of target organs within crop canopies

This high variability of R:FR to changing environment and to the orientation of the receptor also underlines the necessity of a direct estimation of the red:far-red ratio at the organs of interest (e.g., internodes) in order to calculate the response to R:FR and to integrate such responses over the plant geometry/structure. The proposed coupled model enables the calculation of the R:FR of plant organs (or even part of organ) within crop canopies (Fig. 2). Level and variability of R:FR from organ to canopy scale may be calculated from the wheat simulations and discussed in relation to the response functions proposed in the literature to model phytochrome-driven processes.

The ability to estimate the R:FR distribution on individual plant organs makes this coupled model a powerful frame to test hypotheses on photomorphogenetic processes from organ to plant to canopy scale. Also, it would provide a way to link the vast body of results obtained at smaller scales from genomic and physiological studies to canopy behavior. Moreover, due to recent progresses in plant architecture modeling, the proposed tool would be suitable for other crop species studied, such as rice, maize, and faba bean.

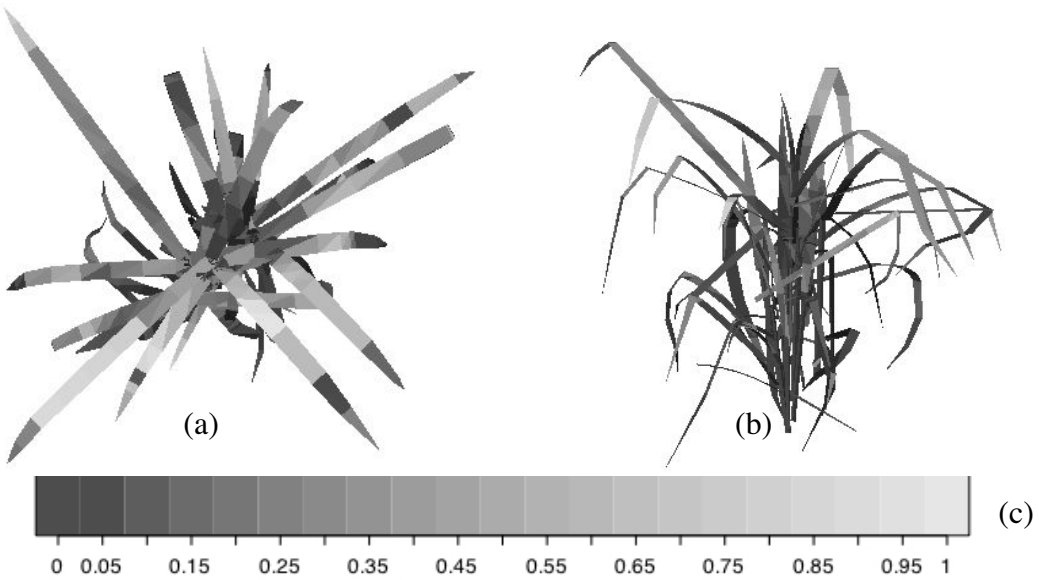

Fig. 2 Simulated normalized R:FR of plant organs within a low-density wheat canopy at Julian day 132 near midday under clear sky: (a) top view of a single plant, (b) side view of the same plant, (c) grey scale of R:FR.

Acknowledgments

The authors thank Sreten Jutovac for his contribution on ADEL-wheat as well as several WUR staff members for their contributions in the experiment. INRA, the C.T. de Wit Graduate School for PE&RC, and the Netherlands Organisation for Scientific Research (NWO) provided financial support.

References

Ballaré C, Scopel A, Radosevich S, Kendrick R. 1992. Phytochrome-MediatedPhototropism in De-Etiolated Seedlings; Occurrence and Ecological Significance. Plant Physiology 100:170-177.

Batlla D, Kruk B, Benech-Arnold R. 2000. Very early detection of canopy presence by seeds through perception of subtle modifications in red:far red signals Functional Ecology 14: 195-202

seedlings: occurrence and ecological significance. Plant Physiol. 100: 170-177

Chelle M, Andrieu B, Bouatouch K. 1998. Nested radiosity for plant canopies. The Visual Computer 14:109-125

Chelle M., Hanan J., Autret H. 2004. Lighting virtual crops : the CARIBU solution for open L-systems. In: 4th International Workshop on Functional-Structural Plant Models, Montpellier.

Commission Internationale de l'Eclairage. 1994. Spatial distribution of daylight - luminance distribution of various reference sky. CIE Publication 1105

Evers JB, Vos J, Andrieu B, Struik P. 2006. Cessation of tillering in spring wheat in relation to light interception and red:far-red ratio. Annals of Botany 97: 649-658

Evers JB, Vos J, Fournier C, Andrieu B, Chelle M, Struik P. 2005. Towards a generic architectural model of tillering in Gramineae, as exemplified by spring wheat (Triticum aestivum). New Phytologist 166: 801-812

Evers JB, Vos J, Fournier C, Andrieu B, Chelle M, Struik P. 2007. An architectural model of spring wheat: evaluation of the effects of population density and shading on model parameterization and performance. Ecological Modelling 200: 308-320

Fournier C, Andrieu B, Ljutovac S, Saint-Jean S. 2003. ADEL-wheat: a 3D architectural model of wheat development. In: Hu B & Jaeger M, eds. International Symposium on Plant Growth Modeling, Simulation, Visualization, and their Applications, Beijing, China: Tsinghua University Press / Springer, 54-63

Mech, R. and Prusinkiewicz, P. 1996. Visual models of plants interacting with their environment. Proceedings of SIGGRAPH 1996. New Orleans, LA, pp. 397-410.

Sattin M, Zuin M, Sartorato I. 1994. Light quality beneath field-grown maize, soybean and wheat canopies-red:far red variations. Physiologia Plantarum 91: 322-328

Sparkes D, Holme S, Gaju O. 2006. Does light quality initiate tiller death in wheat? European Journal of Agronomy 24: 212-217

Quasi-Monte Carlo Simulation of the Light Environment of Virtual Plants

Mikolaj Cieslak[1], Christiane Lemieux[2], and Przemyslaw Prusinkiewicz[3]
[1]Department of Mathematics, University of Queensland, QLD 4072, Australia
[2]Department of Statistics and Actuarial Science, University of Waterloo, ON, Canada N2L 3G1
[3]Department of Computer Science, University of Calgary, AB, Canada T2N 1N4
[1]cieslak@maths.uq.edu.au, [2]clemieux@math.uwaterloo.ca, [3]pwp@cpsc.ucalgary.ca

Keywords: virtual plant modelling, path tracing, quasi-Monte Carlo sampling, variance reduction, red/far red ratio, open L-systems.

Introduction

The distribution of light in the canopy is a major factor regulating the growth and development of a plant. Consequently, simulation of light environment is an important component of functional-structural plant modelling. The main variables of interest are the quantity of photosynthetically active radiation (PAR) reaching different elements of the plant canopy, and the quality (spectral composition) of light reaching those elements, which is a signal for photomorphogenesis.

Light environment models estimate the irradiance reaching a plant from direct light sources (e.g., sun and sky), and often include indirect sources (e.g., light reflected from/transmitted through plant organs). These estimates rely on the description of the plant canopy, which may be approximated as a turbid-medium or specified explicitly as a geometric structure (virtual plant). Models of light environment at the plant structure level are usually based either on the Monte Carlo path tracing method or the radiosity method (Chelle and Andrieu, 2007). In the past, attention was given to improve the efficiency of the radiosity method (Chelle and Andrieu, 1998; Soler *et al.*, 2003), with Monte Carlo path tracing used as a benchmark for comparison. Here, we focus on improving the accuracy and efficiency of path tracing.

Monte Carlo path tracing is derived from standard ray tracing. Both methods approximate the solution to the rendering equation, which describes the transfer of light energy between one point on a surface to another (Kajiya, 1986). Path tracing differs from ray tracing by following many single light paths from a surface point instead of recursively following a single reflecting and refracting ray. Thus, path tracing captures some optical phenomena, such as diffuse light reflection and transmission, which ray-tracing does not.

A ray is traced through the plant canopy until all of its radiant energy is absorbed by the plant's organs. When the ray intersects an organ, a local light model is applied to calculate how much light is reflected, transmitted, or absorbed by that organ. In Monte Carlo path tracing (Kajiya, 1986), a reflected or transmitted ray is then generated stochastically. The direction and energy of these rays depends on the bidirectional reflectance distribution function (BRDF) or bidirectional transmittance distribution function (BTDF) of the organ's surface.

From a computational perspective, a light ray may originate from a light source and be traced towards the plant canopy, or from a plant organ and be traced backward towards a light source. When the canopy is dense, the former method is advantageous, because many rays originating at plant organs would never reach a light source. In contrast, when organs are small relative to the whole plant and are highly dispersed, the latter method is advantageous, because rays traced from a light source would often miss organs.

A light environment model based on Monte Carlo path tracing was developed by Měch (1997), and can be conveniently interfaced with virtual plants expressed using the open L-system formalism (Měch and Prusinkiewicz, 1996). Měch applied two variance-reduction techniques to calculate light distribution efficiently. First, rays are generated not with a uniform distribution, but

preferentially in the direction from which (or towards which) most energy goes (importance sampling). Second, individual rays may carry information regarding several wavelengths simultaneously. This technique reduces variance of the ratios of energy associated with different light wavelengths, which is important in estimating the spectrum of light reaching plant organs (Měch, 1997; Gautier *et al.*, 2000).

To further improve the efficiency of the light distribution calculations provided by Měch's model, we have implemented an alternative method for generating reflected or transmitted rays, called the quasi-Monte Carlo method (surveyed in the context of computer graphics by Owen, 2003). While Monte Carlo (MC) path tracing relies on random sampling of the space of reflected or transmitted rays, and results in a set of independent paths, quasi-Monte Carlo (QMC) is based on a highly regular sampling that produces a set of correlated paths. As shown by Keller *et al.* (1996) and Veach (1997), this reduces the number of rays required for path-tracing virtual 3D scenes within given error bounds. Several algorithms for generating sets or sequences of regularly spaced sampling points have been proposed for use in QMC computations; the most commonly used in practice are by Korobov (1959), and Sobol' (1967), Halton (1960) and Faure (1982). We chose Korobov's algorithm because it can generate sampling points dynamically, as the tracing proceeds, without knowing in advance how many ray-surface intersections will occur in each path, and thus how many sampling points will be needed to trace it.

In principle, QMC methods are deterministic, but they can be randomized in a way that preserves highly regular distribution of the sampling points. This can be used to estimate error/variance of the computation (QMC paths are not independent, so simple error estimation as in MC is not possible otherwise). *Randomized quasi-Monte Carlo* methods can thus be seen as a general variance reduction technique that can be coupled with more problem-specific methods, such as importance sampling, to improve upon MC. These methods are used in our simulation program for approximating the error in computation.

The QuasiMC program for simulating light distribution in a canopy

The L-system-based plant model and the light environment model are executed as two separate processes that communicate using the open L-system formalism (Měch and Prusinkiewicz, 1996). The plant simulator, *cpfg/lpfg*, sends information about the location, size and orientation of the virtual plant's organs to the light environment, and the light environment simulator, *QuasiMC*, returns the lighting distribution among those organs. Figure 1 shows the two programs, *lpfg* and *QuasiMC*, from the user's perspective.

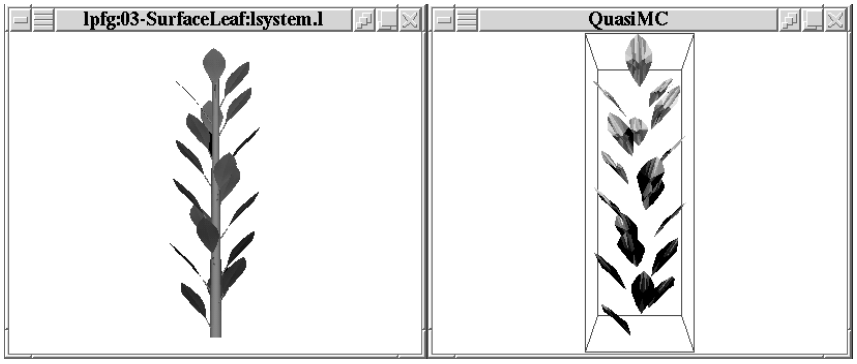

Figure 1: The plant-light simulation software from the user's perspective: on the left, the plant simulator *lpfg*, and on the right, the light environment simulator *QuasiMC*. The *QuasiMC* program shows the plant organs which are included in the light distribution simulation.

The *QuasiMC* program supports two types of light sources: directional light sources, with all rays having the same initial direction, and a hemispherical approximation of the sky based on the CIE standard clear sky model and overcast sky model (CIE 110, 1994). The user can specify parameters of either light source type, for example the radiant energy of each directional light source or the time of day for the sky model. The user can also specify which tracing method (from the light sources to the canopy or from the canopy to the sources) should be employed in the computations.

A plant organ is represented as a triangle, a parallelogram, or a Bezier surface. Each organ is associated with a set of user-specifiable parameters that characterize its optical properties according to the *Blinn-Phong* local illumination model (Měch, 1997, page 283). This model is not based on measured phytoelement data from a device such as a spectrogoniometer, but Chelle has shown the suitability of a similar model for simulating light absorption in plants (Chelle, 2006).

Similarly to Měch's *MonteCarlo* program, *QuasiMC* uses uniform spatial subdivision to speed-up computation. The benefit comes from the reduced time needed to find intersections between a light path and a plant organ. Where a basic method would test each organ for a possible intersection with a ray, the spatial subdivision method only tests those organs that are close to the ray.

Results and Discussion

We compared QMC and MC methods by performing numerical experiments on a virtual canopy of randomly distributed leaves. These experiments were similar to those by Chelle and Andrieu (1998, page 81). The canopy model consisted of 500 triangles uniformly distributed and oriented within a cube (Figure 2). Each triangle was set to behave as a Lambertian surface with 10% of the radiant energy reflecting from the surface and 10% transmitting through it. The scene was illuminated from above, using a directional light source. Each experiment involved the same number of light paths, 65,536. To estimate error in the results, the experiments were repeated 10 times for both the MC and QMC methods using the *QuasiMC* program (it is possible to use Monte Carlo sampling with this program). The results are shown in Figure 3.

The mean values of the irradiance reaching each leaf over the 10 simulations for the MC and QMC methods are similar (compare Fig. 2a with Fig. 2b), but the QMC method produced significantly smaller variance (compare Fig. 2c with Fig. 2d). Fitted curves are shown in all four graphs to highlight the overall trends. The mean variance over all 500 leaves in the MC sample is 75.46×10^{-5} with standard deviation 99.79×10^{-5}, while in the QMC sample it is 9.37×10^{-5} with standard deviation 10.78×10^{-5}. The computation time was about 4 seconds in both cases on a PC 3.0GHz computer, but even when the number of leaves was increased to 10,000, the computation time was only about a minute. The ultimate benefit of using QMC method is that fewer light paths must be computed to achieve the same level of accuracy as the Monte Carlo method. For example, in our experiment, four times fewer light paths needed to be traced by the QMC method compared to the Monte Carlo method (16,384 instead of 65,536) to calculate light distribution with approximately the same variance (for the QMC method with 16,384 rays, the mean variance was 67.39×10^{-5} with standard deviation 72.33×10^{-5}).

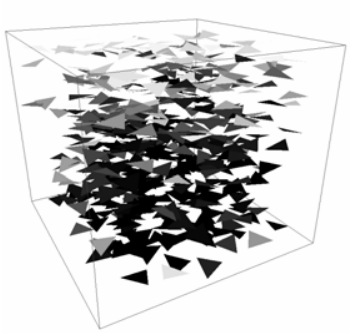

Figure 2: 3D canopy mock-up of 500 triangles uniformly distributed within a cube. Each triangle is shaded according to the amount of light reaching it, with lighter shades representing high irradiance and darker shades representing low irradiance.

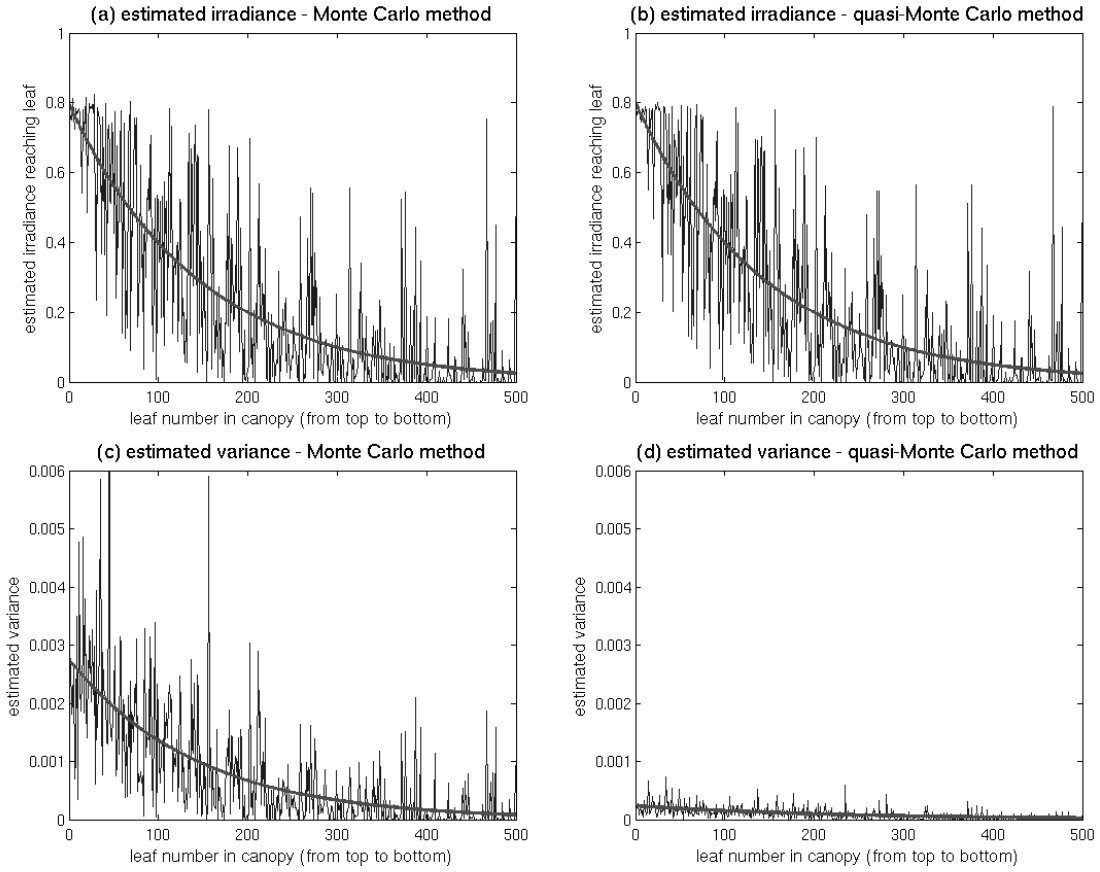

Figure 3: Comparison of estimated irradiances, reaching individual uniformly distributed leaves in a plant canopy model. The fitted curves are described by equations of the form $y = Ae^{-\lambda x}$. Parameters A and λ were estimated by minimizing the sum-of-squares error for $\sum_i Ae^{-\lambda x_i} - y_i$, where i is the leaf number. (a) Monte Carlo estimate of irradiance, (b) (randomized) quasi-Monte Carlo estimate of irradiance, (c) estimated variance in Monte Carlo calculation, and (d) estimated variance in (randomized) quasi-Monte Carlo calculation.

References

Chelle, M. 2006. Could plant leaves be treated as Lambertian surfaces in dense crop canopies to estimate light absorption? *Ecological Modelling* 198:219-228.

Chelle, M. and Andrieu, B. 1998. The nested radiosity model for the distribution of light within plant canopies. *Ecological Modelling*, 111:75-91.

Chelle, M. and Andrieu, B. 2007. Modelling the light environment of virtual crop canopies. In J. Vos, L. Marcelis, P. de Visser, P. Struik, and J. Evers, editors, *Functional-Structural Plant Modelling in Crop Production*, pages 75-89. Springer.

CIE 110. 1994. Spatial distribution of daylight – luminance distributions of various reference skies. *CIE Publication 110*. Vienna, Austria: Commission Internationale de l'Eclairage.

Faure, H. 1982. Discrépance des suites associées à un système de numération. *Acta Arithmetica*, 61:337-351.

Gautier, H., Měch, R., Prusinkiewicz, P. and Varlet-Grancher, C. 2000. 3D Architectural modelling of aerial photomorphogenesis in White Clover (*Trifolium repens L.*) using L-systems. Annals of Botany, 85: 359-370.

Halton, J.H. 1960. On the efficiency of certain quasi-random sequences of points in evaluating multi-dimensional integrals. *Numerische Mathematik*, 2:84-90.

Kajiya, J.T. 1986. The rendering equation. *Computer Graphics (SIGGRAPH '86 Conference Proceedings)*, 20(4):143-150.

Keller, A. 1996. Quasi-monte carlo methods in computer graphics: the global illumination problem. *Lectures in Applied Mathematics*, 32:455-469.

Korobov, N.M. 1959. The approximate computation of multiple integrals. *Dokl. Akad. Nauk SSSR*, 124:1207-1210. In Russian.

Měch, R. 1997. *Modeling and Simulation of the Interaction of Plants with the Environment using L-systems and their Extensions*. Ph.D. thesis, University of Calgary.

Měch, R. and Prusinkiewicz, P. 1996. Visual models of plants interacting with their environment. Proceedings of SIGGRAPH 1996. New Orleans, LA, pages 397-410.

Owen, A.B. 2003. Quasi-Monte Carlo sampling. In Jensen, H.W., editor, *Monte Carlo Ray Tracing: Siggraph 2003 Course 44*, pages 69-88. SIGGRAPH.

Sobol', I.M. 1967. The distribution of points in a cube and the approximate evaluation of integrals. *U.S.S.R. Comput. Math. and Math. Phys.*, 7:86-112.

Solar, C., Sillion, F., Blaise, F. and Dereffye, P. 2003. An efficient instantiation algorithm for simulating radiant energy transfer in plant models. *ACM Transactions on Graphics*, 22(2).

Veach, E. 1997. *Robust Monte Carlo methods for light transport simulation*. PhD thesis, Stanford University.

Modeling light phylloclimate within growth chambers.

Michaël Chelle[1], Christophe Renaud[2], Samuel Delepoulle[2], Didier Combes[3]

[1] INRA, UMR1091 Environnement et Grandes cultures, F-78850 Thiverval-Grignon , France
[2] Laboratoire d'Informatique du Littoral (LIL), BP 719, F-62228 Calais, France
[3] INRA, UR4 Écophysiologie des Plantes Fourragères, BP6, F-86600 Lusignan, France
chelle@grignon.inra.fr

Keywords: light model, ray tracing, growth chamber

Introduction

Functional-structural plant modeling (FSPM) requires accurate data on plant growth. These data are often obtained by experiments in growth chambers. Most genomic studies also use plants grown in controlled conditions. For such studies, a well-controlled and spatially homogeneous climate is necessary to be able to strictly compare results from different treatments or genotypes (and not phenotypes).

A large variety of growth chambers with differing geometry, materials, lighting and control system exist. Each growth chamber should be considered as a unique radiative system, characterized by a specific spatial light distribution. Moreover, although it has been designed to minimize the spatial heterogeneity of climate, measurements have shown that plants may experience different microclimate conditions depending on their location within the same chamber (Measures et al., 1973; Boonen et al., 2002a ; Chelle et al., 2004). The effect of the light variability on the plant population heterogeneity would be higher for small plants (small specie (*Arabidopsis thaliana*); seedling) than for tall plants. However, for tall plants, the light variability would perturb studies at organ scale (Fig. 1). By-passing the "growth chamber" effect for light in ecophysiology could be done by estimating the light phylloclimate (Chelle, 2005).

Measurement of light phylloclimate could not automatically be done during growth chamber experiments, because the required number of sensors would perturb the plant growth (Chelle, 2005). Cavazonni et al. (2002) and Boonen et al. (2002b) independently proposed a light model dedicated to growth chamber. However, their model relies on the turbid medium approximation, which does not enable the estimation of the irradiance of individual plants or organs. Modeling light phylloclimate implies that the 3D structure of individual plants and the directionality of radiation are taken into account. Chenu et al. (2005) proposed a two-step method consisting on the measurement of above-plant radiances using a 6-face turtle PAR sensor (Den Dulk, 1989) and the "projection" of this incident radiance distribution on a 3D plant using the Archimed model (Dauzat & Elroy, 1997). The method was used to estimate the PAR irradiance of *Arabidopsis thaliana* plants. However, the extension to other spectral band and to the case of tall plants (Fig. 1) has to be assessed. In this paper, we propose a full-modeling approach based on a 3D description of the growth chamber, its lighting system, and plants, as proposed by Chelle et al. (2004).

SEC2, a photon tracing dedicated to growth chamber

In a previous study (Chelle et al., 2004), measurements and Radiance simulations (Ward, 1994) in an empty growth chamber were analyzed, mainly regarding the relative contribution of first, second and higher order of scattering. A deeper analysis of these results led us to propose general specifications for light models dedicated to growth chamber phylloclimate:

- Taking into account the 3D geometry of the growth chamber, its lighting system, and plants;
- Taking into account multiple light sources, which may be punctual or surfacic and have anistropic emission;
- Taking into account diffuse, specular, and translucent materials;
- Estimating the irradiance of several plant organs and of virtual light sensors;
- Easy implementation, maintenance, and use;

- Reasonable simulation time.

From these specifications, we developed a lighting simulator (SEC2) dedicated to growth chambers. It is based on models and algorithms currently in use in Computer Graphics (CG) research area. Indeed, CG researchers have developed efficient methods for computing global illumination in any environment with arbitrary materials and light sources. These methods provide both photorealistic images and physically accurate results (Sillion et al., 1994; Shirley et al., 1996).

The core of SEC2 is based on the photon tracing approach (Arvo, 1986; Jensen 2001), which consists in tracing photons from their emission point on light sources to their absorption location after several bounces onto the 3D models surfaces. Contrary to CG where measurements are mainly performed through each pixel of the computed image, SEC2 requires making measurements at specific locations in the chamber. Thus, SEC2 enables the inclusion of different kinds of sensors into the scene, these sensors being either virtual (recording irradiances without affecting the light propagation) or real (in the same way as light sensors are used in an actual growth chamber). Moreover, SEC2 enables the estimation of the irradiance and the light absorption of plant organs. Optionally, SEC2 is able to provide views of the simulated environment using different CG rendering methods (Fig. 2b).
SEC2 was developed in C++ following an Object Oriented approach, which provides both efficiency and easy software maintenance capabilities.

First results

A virtual growth chamber was built from the measurement of a Strader growth chamber (Angers, France), whose features are a complex lighting system (1) (2 rows of discharge lamps surrounded by three glossy reflectors), a white working table (2), 4 vertical grey walls (3), and two specular panels (4) to mimic canopy boundary conditions (Fig. 2a).

The ability to reproduce a virtual growth chamber as well as the correctness of SEC2 were assessed by comparing measured and simulated transversal profiles of PAR irradiance at two elevations in an empty room (Fig .3). The angular and spatial distribution of radiance appeared satisfyingly simulated; the pseudo-homogeneity at 1.0m height as well as the pattern due to the anisotropy of light sources observed at 1.8m height. Figure 4 shows how highly variable was the simulated PAR irradiance of horizontal sensors within the virtual Strader chamber. This result confirmed the interest in a full-modeling approach to estimate light phylloclimate, as conceptually established in Figure 1.
Moreover, the SEC2 model enables the simulation of the light distribution within the growth chamber, that is table and walls, with plants included, that is of primary interest for the FSPM community. Figure 2b presents such a simulation in the case of a heterogeneous canopy containing three various types of virtual plants (2 young maize (Drouet, 2003); 16 young and 4 adults and true myrtle (Beaujard et al., 2001); 40 *Arabidopsis thaliana* (Chenu et al., 2005)).

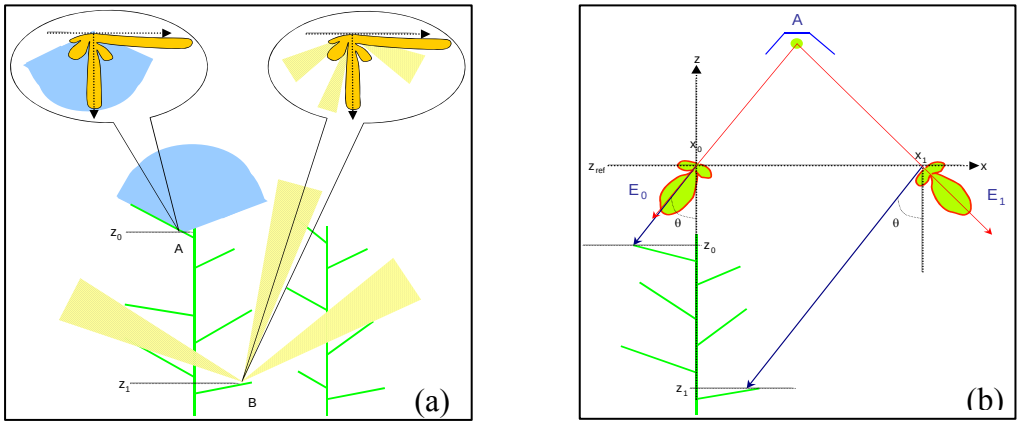

Figure 1: Scheme illustrating the difference in the directional sampling (a) and in the angular distribution (b) of the incident light field between leaves located in the top (A) and the bottom (B) of a canopy.

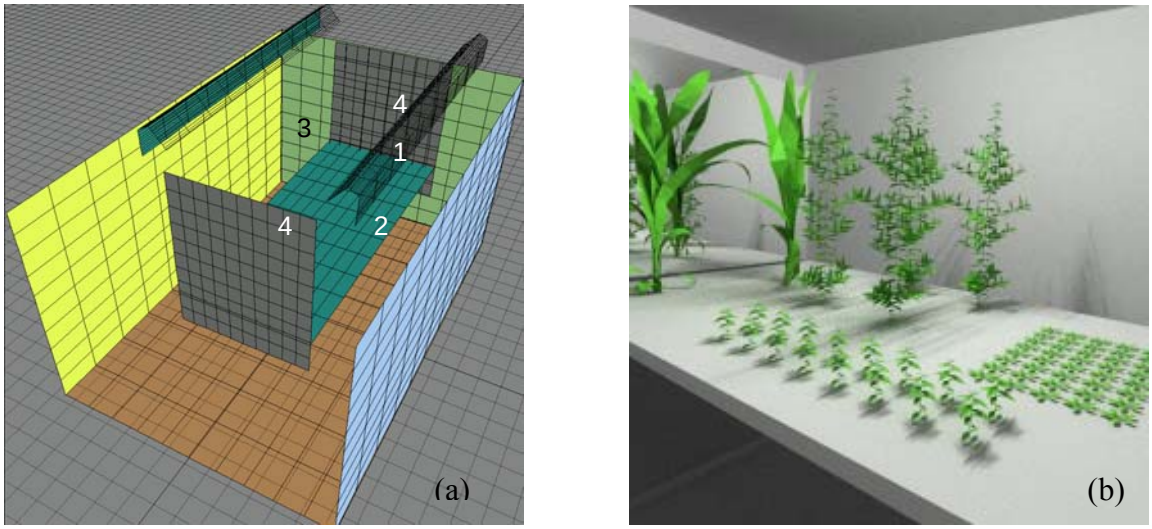

Figure 2 The virtual Strader growth chamber (a) and its simulated light distribution when filled by a heterogeneous canopy (maize, true myrtle, arabidopsis) (b).

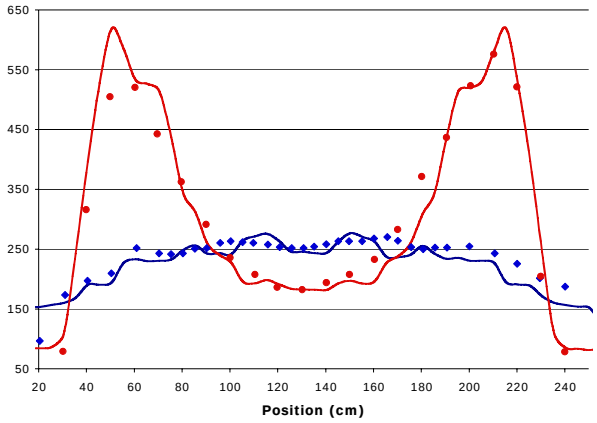

Figure 3 Measured (symbols) and simulated (solid lines) transversal profile of PAR irradiance within the empty Strader growth chamber at two elevations (1m (blue), 1.8m (red) height).

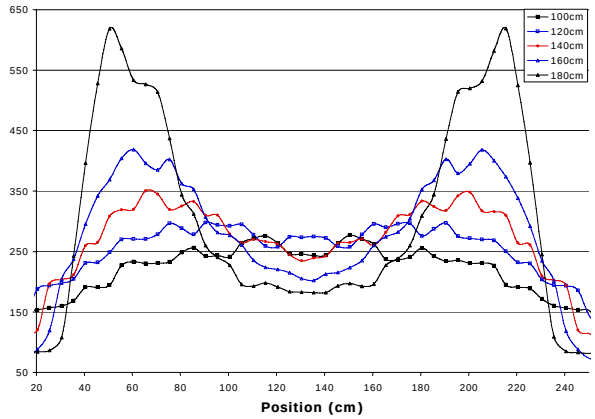

Figure 4 Simulated transversal profiles of PAR irradiance within the Strader growth chamber at 5 elevations (1, 1.2, 1.4, 1.6, 1.8 m height).

In conclusion, SEC2 would be an useful tool to estimate the light phylloclimate of plants grown in controlled conditions, which is required to by-passed the intra- and inter-growth chamber light variability. Next simulation steps will focus on the inter-plant and intra-plant variability of light and be discussed regarding ecophysiological processes. Finally, it could be used to design new types of growth chamber providing a low heterogeneity of light phylloclimate.

References

J. Arvo. 1986 Backward Ray Tracing. *In: Developments in Ray Tracing*, SIGGRAPH `86 Course Notes.

F. Beaujard, D. Pithon, M. Chelle. 2001. Ramifications rythmiques et absorption par simulation dans le PAR chez Myrtus communis L. (Myrtacées) *in:* L'Arbre 2000 The Tree. Isabelle Quentin, Montreal, Canada

C. Boonen, R. Samson, K. Janssens, H. Pien, R. Lemeur, D. Berckmans, 2002. Scaling the spatial distribution of photosynthesis from leaf to canopy in a plant growth chamber, Ecol. Modell, 156:201-212.

J. Cavazzoni, T. Volk, F. Tubiello, O. Monje, 2002. Modelling the effect of diffuse light on canopy photosynthesis in controlled environments, Acta Horticulturae.

M. Chelle, M. Demirel, C. Renaud, 2004 Towards a 3D light model for growth chambers using an experiment-assisted design *In*: 4th International Workshop on Functional-Structural Plant Models, Montpellier

M. Chelle. 2005. Phylloclimate or the climate perceived by individual plant organs: What is it? How to model it? What for?, New Phytologist 166 :781-790

K. Chenu, N. Franck, J. Dauzat,, J.F. Barczi, H. Rey, J. Lecoeur. 2005 Integrated responses of rosette organogenesis, morphogenesis and architecture to reduced incident light in *Arabidopsis thaliana* results in higher efficiency of light interception. Functional Plant Biology 32 (12) :1123-1134

J., Dauzat, M.N., Eroy. 1997 Simulating light regime and intercrop yields in coconut based farming systems". European Journal of Agronomy, 7: 63-74.

J.A. Den Dulk. 1989 The interpretation of remote sensing, a feasibility study. Thesis, Wageningen, N.L.

T.. Dougher, B. Bugbee, 2001 Differences in the response of wheat, soybean and lettuce to reduced blue radiation, Photochemistry and Photobiology, 73:199-207.

J.-L. Drouet. 2003 MODICA and MODANCA: modelling the three-dimensional shoot structure of graminaceous crops from two methods of plant description. Field Crops Research 83 (2): 215-222

H. Jensen 2001. Realistic Image Synthesis Using Photon Mapping. A.K. Peters LTD, Natick, Massachussets,

M. Measures, P. Weinberger, H. Baer. 1973 Variability of plant growth within controlled-environment chambers as related to temperature and light distribution," Canadian Journal of Plant Science, 53

P. Shirley, C. Wang, K. Zimmerman.1996 Monte Carlo techniques for direct lighting calculations. ACM Transactions on Graphics, 15:1-36,

F.X. Sillion, C. Puech. 1994 Radiosity and Global Illumination. Morgan Kaufmann Publishers Inc.

G. Ward. 1994 The RADIANCE lighting simulation and rendering system. *in: SIGGRAPH'94*: 459-472

Modeling of light transmission under heterogeneous forest canopy: model description and validation

David Da SILVA[‡], Philippe BALANDIER[1,†], Frédéric BOUDON[2,‡], André MARQUIER[3,†], Christophe PRADAL[2,‡], Christophe GODIN[4,‡], Hervé SINOQUET[3,†]

[1] CEMAGREF, Domaine des Barres, 45290 Nogent-sur-Vernisson, France
[2] CIRAD, Avenue Agropolis, 34398 Montpellier Cedex 5, France
[3] INRA, Site de Crouël, 234 avenue du Brézet, 63100 Clermont-Ferrand, France
[4] INRIA, 2004 route des lucioles BP 93, 06902 Sophia Antipolis, France
[‡] Virtual Plants, UMR DAP, TA A-96/02, 34398 Montpellier Cedex 5, France
[†] UMR PIAF, Site de Crouël, 234 avenue du Brézet, 63100 Clermont-Ferrand, France

Keywords : light transmission, heterogeneous canopy, foliage distribution, 3D reconstruction

Introduction

Growth and survival of regeneration saplings and understorey vegetation development is closely related to light available below the forest trees. Manipulating the forest structure by thinning adult trees is a major tool to control light transmission to the understorey. The transmission is related to the attenuation of light which is usually estimated with the Beer-Lambert law assuming homogeneous foliage within the canopy. However forest canopies are far from homogeneous, which requires models that can take into account the effect of clumping between and within trees. In this work we present a model that can be readily used with both coarse or detailed parameterization to generate any type of stand and compute the distribution of light transmitted below the canopy. To evaluate the accuracy of the model, we compared model results with field measurement from several stands of *Pinus sylvestris L.* in the French Massif Central.

Material

The pine stands are located in the Chaîne des Puys, a mid-elevation volcanic mountain range (45°42' N, 2°58'E) at a place named Fontfreyde. The elevation is 900 m a.s.l., mean annual rainfall is about 820 mm, and mean annual temperature is about 7°C. The soil is a volcanic brown soil at pH 6.0 with no mineral deficiency. The pines were 30-year-old at time of measurement, with a density ranging from 500 to 4000 stem ha^{-1}. All trees in an area of 30 by 30 m were located by their x,y coordinates, and measured for their total height (14.1 ± 2 m mean $\pm$ SD) and DBH (16.3 ± 5 cm mean $\pm$ SD). Crown height was also measured. Crown extents was assessed by visually projecting to the soil its characteristic points (i.e. the points that better describe the crown irregularities) in, at least, four directions. The azimuth and distance of those points from trunk were then measured (see Figure 1).

Methods

Envelope reconstruction

To reconstruct the 3D envelopes of the trees from the field measurements, we used the PlantGL library [Boudon et al., 2001]. This library contains several geometric models, including different types of envelopes and algorithm to reconstruct the geometry of plants at different scales. For this particular case, we used the *skinned surface* implemented in PlantGL which is a generalization of surface of revolution with varying profiles being interpolated. This surface is thus built from any number of profiles with associated direction. The profiles we defined were inspired by *Cescatti* work [Cescatti, 1997]. A profile is supposed to pass through top and bottom points and an intermediate point at maximum radius. Two shape factors, C_T and C_B, are used to describe the shape of the profiles above and below the maximum width. Mathematically, two quarters of super-ellipse of degree C_T and C_B are used to define the top and bottom part of the profiles. Isopoints of the profiles are interpolated with B-Spline curves of given degree. Note that our envelopes can be viewed as extension of *Cescatti*'s asymmetric hull with profiles in any direction instead of restricted directions (cardinal directions). Flexibility of our model enables us to measure the most adequate profiles in case of irregular crowns.

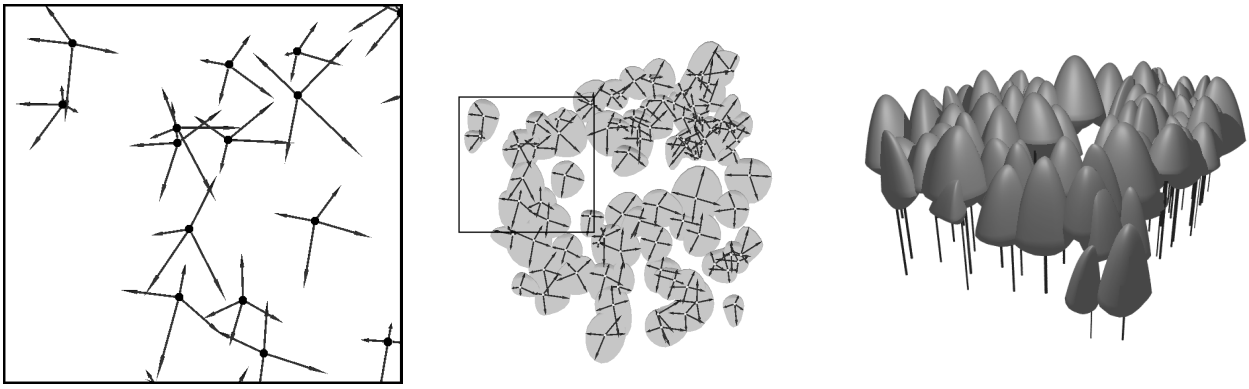

Figure 1: From left to right : Field data sample. Each circle locates a tree and each connected arrow defines a specific azimuth and distance from the tree trunk. Field data along with their matching projected crown. 3D reconstruction using *skinned surface hulls* from PlantGL library with maximum radius at the quarter of crown height and $C_T = C_B = 2$.

Light Transmission Model

The presented model derives from Oker-Blom's model [Oker-Blom et al., 1989] where crowns are considered as porous envelopes but extends it to the more complex ones described above (p.1). Light interception by a crown $\mathcal{C}$ is related to the crown projection area, $S_\Omega(\mathcal{C})$, in the sun direction Ω [Nilson, 1999]. In the case of an isolated tree, let $\mathcal{E}(\mathcal{C})$ be a convex hull of $\mathcal{C}$, we will use the projected area of $\mathcal{E}(\mathcal{C})$ as the area of interest. Hence, the fraction of light intercepted by $\mathcal{C}$, $p_\Omega(\mathcal{C})$, can be expressed as the ratio between $S_\Omega(\mathcal{C})$ and the area of interest, $S_\Omega(\mathcal{E}(\mathcal{C}))$

$$S_\Omega(\mathcal{C}) = S_\Omega(\mathcal{E}(\mathcal{C}))p_\Omega(\mathcal{C}) \tag{1}$$

$p_\Omega(\mathcal{C})$ acting as an opacity factor for the envelope of $\mathcal{C}$. In a crown, leaves can either be uniformly distributed or assigned to specific spatial positions. In the case of uniform distribution the light attenuation is a function of the distance the solar beam travels within the crown. In the other case, the attenuation depends on the relative position of the beam and the leaf. Hence we discretize the volume $\mathcal{E}(\mathcal{C})$ using a set $\mathcal{B}$ of β parallelepipedic voxels of direction Ω representing light beams. The set of beams is large enough so that the discretization does not change volume or projected area. Let $p^b_\Omega(\mathcal{C})$ be the probability for the beam b to be intercepted by $\mathcal{C}$ (i.e. the opacity of $\mathcal{C}$ for the beam b), therefore the probability that b is not intercepted by $\mathcal{C}$, $1 - p^b_\Omega(\mathcal{C})$, is a function of the number of leaves in $\mathcal{C}$ and can be expressed using Beer-Lambert law or a binomial law if leaf size is to be taken into account :

$$p^b_\Omega(\mathcal{C}) = 1 - \prod_{\ell \in \mathcal{L}(\mathcal{C})} \left[1 - p^b_\Omega(\ell)\right] \tag{2}$$

where ℓ is a leaf, $\mathcal{L}(\mathcal{C})$ the set of leaves of $\mathcal{C}$. The probability, $p^b_\Omega(\ell)$, for b to be intercepted by the leaf ℓ is known when spatial positions of leaves are taken into account; in the uniform distribution case, it can be shown that $p^b_\Omega(\mathcal{C})$ can be expressed as a function of projected leaf area, $S_\Omega(\ell)$, volume of crown, $\mathcal{V}(\mathcal{C})$, and the distance b travels within the crown, $l^b(\mathcal{C})$ [Sinoquet et al., 2005]:

$$p^b_\Omega(\mathcal{C}) = 1 - \prod_{\ell \in \mathcal{L}(\mathcal{C})} \left[1 - \frac{S_\Omega(\ell) l^b(\mathcal{C})}{\mathcal{V}(\mathcal{C})}\right] \tag{3}$$

Hence we can compute the light transmission for each beam in both cases, when position of leaves is known and when we assume an homogeneous distribution, finally global opacity for $\mathcal{C}$ is simply the mean of beam opacity.
Since Eq.(2) and (3) do not depend on scale, leaf scale is not mandatory and there is no restriction concerning the number of scales being used. This forest stand application illustrates the multi-scale approach with two scales, the finest one being the tree crown scale, and also illustrates how to take into account the finite size of a stand. Therefore, in this specific case and using above notations, $\mathcal{L}(\mathcal{C})$ is

the set of tree crowns in $\mathcal{C}$ and $p^b_\Omega(\ell)$ is the opacity of the crown ℓ for the beam b that can be either computed using Eq.(2) or (3) recursively if informations on finner scale is available or set with empirical or measured value.

Results

Using this model, we computed the light attenuation for each cast beam and therefore generated a shadow map for different directions Ω; in this study we use the 46 directions sky discretization proposed in [Den Dulk, 1989]. Computations were done for the stand reconstruction (Fig.1), uniform foliage distribution hypothesis, and random positioning of reconstructed crowns in forest space. The results (Fig.2)

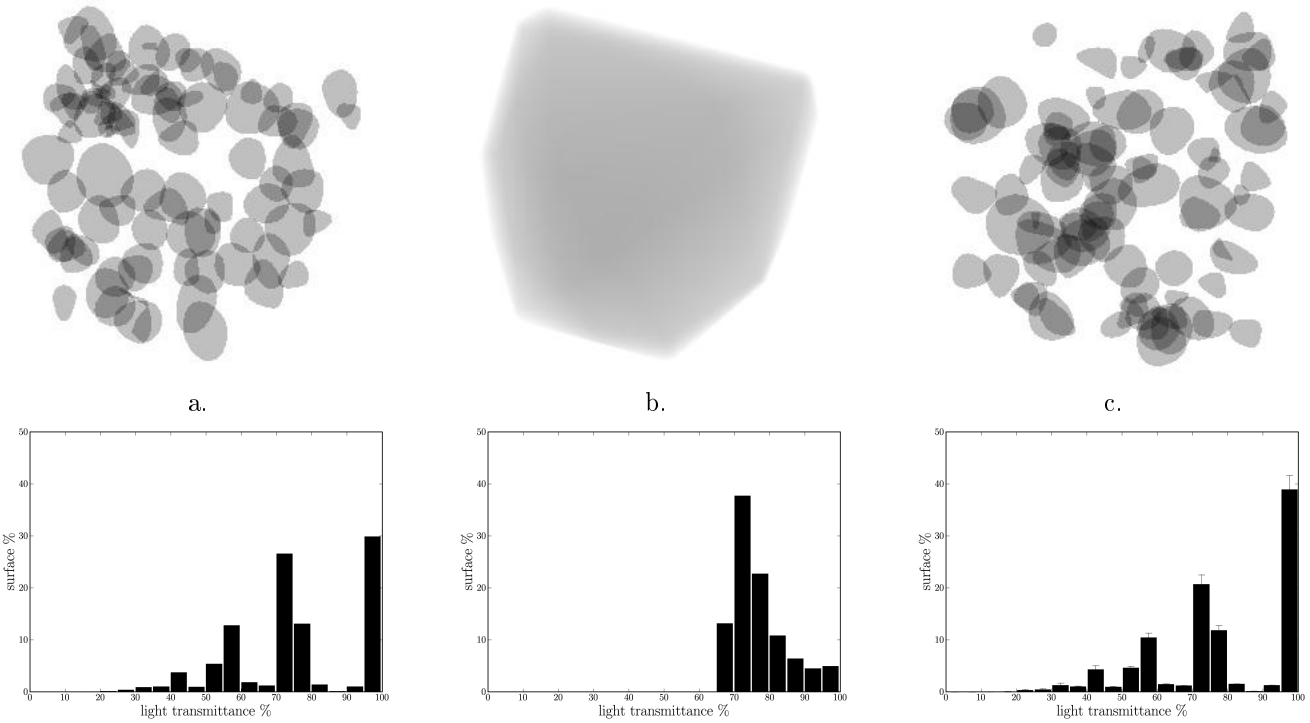

Figure 2: Top view shadow maps with associated grey level histogram of: a. stand reconstruction, b. uniform foliage hypothesis and c. one example of random distribution of reconstructed crowns, in this case the histogram shows the mean light transmitance over a set of 20 random distributions. Azimuth is 180° and elevation is 90° for all views. Each tree crown has an overall direction opacity of 0.25.

clearly show that if we are interested in light distribution in transmission classes, the hypothesis of uniform foliage distribution does not hold and thus cannot be used to model stands (Fig.2 b.). The distribution of light transmitted by stands generated using a random spatial ditribution of the reconstructed crowns (Fig.2 c.) was much closer to the distribution found with the real stand (fig.2 a.). However, the higher gap frequency in the random stand (see transmission class of 100 %) suggests that the tree distribution in real stands is slightly more regular than random. Further investigations on spatial distribution characterisation are being done in order to obtain more simple way of recreating stands with better light interception properties.

Concluding remarks and perspectives

The integration of all those directional maps onto a ground projection yields a global shadow map that will allow us to study light intensity distribution over different time period and quantify the impact of clumping between and within trees. A light mesurement campaign is being done in order to obtain data for validation purpose. This better characterization and understanding of light transmission will hopefully lead us toward simplified and efficient models.

References

[Boudon et al., 2001] Boudon, F., Pradal, C., Nouguier, C., and Godin, C. (2001). Geom module manual: I user guide. Technical Report 3.

[Cescatti, 1997] Cescatti, A. (1997). Modelling the radiative transfer in discontinuous canopies of asymmetric crowns. ii. model testing and application in a norway spruce stand. *Ecological Modelling*, 101(2):275–284.

[Den Dulk, 1989] Den Dulk, J. A. (1989). *The interpretation of Remote Sensing, a feasibility study.* PhD thesis, Wageningen university.

[Nilson, 1999] Nilson, T. (1999). Inversion of gap frequency data in forest stands. *Agricultural and Forest Meteorology*, 98-99:437–448.

[Oker-Blom et al., 1989] Oker-Blom, P., Pukkala, T., and Kuuluvainen, T. (1989). Relationship between radiation interception and photosynthesis in forest canopies: Effects of stand structure and latitude. *Ecological Modelling*, 9(1-2):73–87.

[Sinoquet et al., 2005] Sinoquet, H., Sonohat, G., Phattaralerphong, J., and Godin, C. (2005). Foliage randomness and light interception in 3-d digitized trees: an analysis from multiscale discretization of the canopy. *Plant, Cell & Environment*, 28(9):1158–1170.

Assessing the light environment for Scots pine in the functional-structural tree model LIGNUM

Jari Perttunen[1], Risto Sievänen[1] and Eero Nikinmaa[2]
1. Finnish Forest Research Institute, Vantaa Research Unit
P.O. Box 18, FI-01301 Vantaa, Finland
2. Department of Forest Ecology, University of Helsinki
P.O. Box 27, FI-00014 Helsinki, Finland
jari.perttunen@metla.fi

Keywords: Scots pine, radiation regime, carbon balance

Introduction

The functional-structural tree model LIGNUM (Perttunen et. al., 1996) represents coniferous and deciduous trees with simple structural units called tree segment, bud, branching point and axis that have close resemblance to real tree parts. These units model both the functioning of the tree and the dimensional architecture of a tree crown.

We present the work which aims at solving the computational problems related to the assessment of the radiation regime of the tree crown enabling us to calculate the self shading of fully developed Scots pine trees and extend our approach from a single tree to forest stands.

Light models approximate radiative fluxes received by a plant. This requires the description of radiative interactions between light and plant parts and integration of the local phenomena to whole plant structure. The complexity of the descriptions for light absorption and scattering depends on the level of detail in the structural description of the plant.

The turbid medium approaches (e.g. Sinoquet et. al., 2001) consider the transmission of light through a continuous medium. To model the spatial heterogeneousness of the foliage the canopy is divided into volume elements and the properties of the foliage contained in a volume element is described in an aggregated manner. The volume element can be for example a horizontal layer of foliage or a cubic cell also known as voxel.

The surface based approaches (Chelle and Andrieu, 2007) describe the three dimensional structure of canopy explicitly with suitable geometric elements for plant parts and foliage. The advantage is that the size, position and orientation of each plant part can be taken into consideration. The disadvantage is the computational complexity when calculating radiative fluxes on each plant part.

We have developed three alternative approaches to calculate light climate of the forest canopy in the model LIGNUM. The first two are based on turbid medium approach and the third is surface based. In addition, we simplify the approximation of radiative fluxes by considering photosynthetically active radiation (PAR) only, i.e. we assume no reflection of light from foliage but the light is absorbed and transmitted. The objective is to study consequences of using different light models for the development of tree stand when a common growth allocation method is used.

Material and Methods

Here we describe the assessment of the light environment for coniferous trees in three different ways to overcome the computational complexity for the calculation of the canopy light climate due to multiple directions of light sources and large number of shading elements causing a need for exploding number of pairwise comparison of tree segments when the number of segments becomes large (several thousands). The time step for simulations is 1 year.

Common to all methods, a model sky has been implemented where the hemisphere is divided into sectors of approximately solid angles. The incoming radiation originates from the midpoint of each sector applying the standard overcast sky radiation (SOC) distribution (Ross, 1981).

We have implemented the division of the growth space of a tree or forest stand into equal size cubic volume elements and the fast voxel traversal algorithm (Amanatides and Woo, 1987) that finds the entry and exit points of the light ray between adjacent voxels before crossing the voxel boundaries.

Method 1

The first method follows our previous work (Perttunen et. al., 2005) and ignores the geometry of the shading and shaded segments and uses the mean characteristics of foliage instead. First, the voxels each shading segment belongs to is determined by the user defined equally spaced points on the segment cylinder and the proportions of the foliage areas of the shading segments is assigned into their respective voxels. The woody parts of the segments are ignored. Secondly, incoming and absorbed radiation is assessed to the center point of each voxel using the fast voxel traversal algorithm to follow the routes of the light rays (Amanatides and Woo, 1987).

First, define the transmission $h1$, proportion of radiation going through one voxel as:

$$h1 = \mathrm{e}^{0.14 L \frac{A_f}{V_{box}}} \qquad \text{(Eq. 1)}$$

where L is the path length of the ray in the voxel, A_f the foliage area of the segments in the voxel, V_{box} the volume of the voxel and 0.14 is assumed to be the mean shoot silhouette to total area ratio or $\overline{STAR}$ (Oker-Blom and Smolander, 1988). The proportion of radiant energy, H, through N shading voxels reaching the target voxel is the production of transmissions $h1_j$ in each shading voxel:

$$H = \prod_N h1_j \qquad \text{(Eq. 2)}$$

The incoming radiant energy, I_{c_i}, reaching the target voxel from the ith sky sector is:

$$I_{c_i} = HI_0 \qquad \text{(Eq. 3)}$$

where I_0 represents the irradiance (both direct and diffuse) from the ith sky sector. The total radiant energy, I_{TOT}, reaching the voxel is the sum of the irradiances from every sector of the model sky:

$$I_{TOT} = \sum I_{c_i} \quad \text{(Eq. 4)}$$

Finally, the total absorbed radiation, I_a^{TOT}, on one segment depends on the $\overline{STAR}$ and on the foliage area of the segment:

$$I_a^{TOT} = 0.14 A_f I_{TOT} \quad \text{(Eq. 5)}$$

Method 2

The second method recovers the geometry of the shaded segment as in Perttunen et. al., 1998. The fast voxel traversal algorithm (Amanatides and Woo, 1987) starts from the center of the shaded segment and assesses the incoming radiation as in the first method (Eq. 1 – Eq. 3).

The amount of radiation, I_a^i, the shaded segments absorbs from the *i*th sector is then given by Perttunen et. al., 1998:

$$I_a^i = (1 - e^{-K(\phi)A_f / A_C}) A_c I_0 \quad \text{(Eq. 6)}$$

where A_f is the foliage area of the shaded segment, $K(\phi)$ defines the light beam extinction as a function of the angle ϕ between the direction (axis) of shaded segment and the direction of the light beam (Oker-Blom and Smolander, 1988). The A_C is the projection area of the segment cylinder in the direction of the light beam:

$$A_C = 2LR\cos(\phi) + \pi R^2 \sin(\phi) \quad \text{(Eq. 7)}$$

where *L* and *R* are the segment length and radius including foliage respectively.

The total radiant energy absorbed by the shaded segment is the sum of absorbed radiation from all sectors of the sky:

$$I_a^{TOT} = \sum I_a^i \quad \text{(Eq. 8)}$$

Method 3

The third method recovers the geometry of the shading segments (Perttunen et. al., 1998). This is achieved by caching the geometric information of the tree segments into voxels where they belong. This allows us to compute the distance light beam traverses through segment foliage along the route in the voxel space defined by the fast voxel traversal algorithm (Amanatides and Woo, 1987). The transmission *h*3 of the light beam through one segment is (Perttunen et. al., 1998):

$$h3 = e^{-K(\phi)(A_f / V_f) l} \quad \text{(Eq. 9)}$$

where V_f is the volume occupied by the foliage in the segment and *l* the length the light beam traverses in the foliage of the segment defined by the entry and exit points of the beam on the surface of the foliage cylinder. If the light beam hits the woody part of the shading segment the

transmission is 0 from that sector of the sky. The proportion of radiant energy, H, through N shading segments on the path of one light beam is:

$$H = \prod_{N} h3_j \quad \text{(Eq. 10)}$$

and the radiant energy reaching the shaded segment from the ith sector is then:

$$I_{c_i} = HI_0 \quad \text{(Eq. 11)}$$

The total incoming radiation is the sum of the irradiances from all sectors of the model sky (Method 1, Eq. 4). The absorbed radiation for the shaded segment is as in the Method 2 (Eq. 6 – Eq. 8).

Allocation of photosynthates: carbon balance

The metabolism of the tree follows our previous work, assuming that photosynthesis in a segment is assumed to be proportional to absorbed radiation and respiration is proportional to biomass and tissue activity (Perttunen et. al., 1998). New growth in the tree is possible if the production of the photosynthates in the tree, P, exceeds the respiration costs of the tree, M. We assume that all net production is allocated: $P - M = iWn + iWd + iWr$, where iWn is the needle and shoot growth, iWd the secondary wood growth and iWr the root growth.

Results

We compare all three methods and assess their applicability for use in forest simulations. We present simulations of a Scots pine stand using these three methods to assess light environment. For this a 20 m X 20 m X 20 m voxel grid with 0.16 m X 0.16 m X 0.16 m sized voxels. The total amount of unshaded incoming radiant energy of PAR was 1200 MJ/m2 per year including both diffuse and direct radiation corresponding to the conditions in Southern Finland. The physiological parameters for the Scots pine are from our previous work.

To represent the forest stand 87 seven tree locations were randomly created to model initial density of 2100 trees/ha. The tree was initially 30 cm long and it was set to grow at the center of the forest in the opening with 1.0 m radius. Each growth step the tree was copied to the random locations, i.e. the forest consisted of identical trees. When the diameter at breast height (D1.3) of the subject tree exceeded 16 cm the density of the forest was reduced to 800 trees/ha. The tree (forest stand) after simulation was 30 years old.

To study the results we examined in the first instance the appearance and the general shape of the tree representing all trees in the forest stand. Secondly, we collected photosynthesis, P, and the foliage mass, W_f, and the ratio of the two to initially study the model behavior in more detail (Fig. 1).

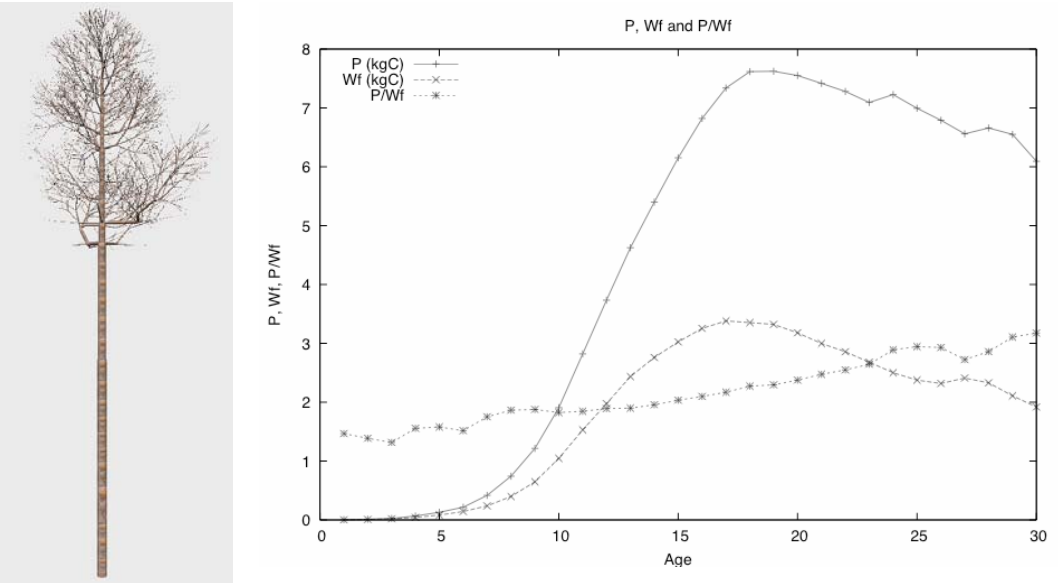

Fig 1. Left: A 30 year old simulated Scots pine with Method 3: Height = 9.4 m, D1.3 = 18 cm. Right: P, W_f and P/W_f.

The overall shape and dimensions of the tree are acceptable. It is also capable to produce the crown rise during the canopy close. The values for P and W_f are realistic. There is a slight increase in P/W_f ratio when the foliage mass in the tree starts to decrease but that too is within acceptable values.

Our work will concentrate in comparing the three methods to assess light climate in a forest stand. We will compare our results with empirical stand models and analyze the results the different light models produce. We aim in the future to develop light calculations in LIGNUM so that it can simulate within computationally reasonable time (e.g., a twenty-four-hour period) a small forest stand representing for example a research plot consisting of different trees and tree species.

References

Amanatides, J. and Woo, A. 1987. A fast voxel traversal algorithm for ray tracing. Proc. Euro-graphics '87, pp. 1–10.

Chelle, M. and Andrieu, B. 2007. Modelling the light environment of virtual crop canopies. In: Vos, J., Marcelis L.F.M., de Visser, P.H.B., Struik, P.C. and Evers, J.B. (eds.). Functional-Structural Plant Modelling in Crop Production. Springer, Netherlands, pp. 75-89.

Oker-Blom, P. and Smolander, H. 1988. The ratio of shoo silhouette area to total needle area in Scots pine. For. Sci., 34(4):894–906.

Perttunen, J., Sievänen, R., Nikinmaa, E., Salminen, H., Saarenmaa, H. and Väkevä, J. 1996. LIGNUM: A tree model based on simple structural units. Annals of Botany, 77(1):87–98.

Perttunen, J., Sievänen, R. and Nikinmaa, E. 1998. LIGNUM: A model combining the structure and the functioning of trees. Ecological Modelling, 108(1–3):189–198.

Perttunen, J., Sievänen, R., Nikinmaa, E., and Mäkelä, A. 2005. Extrapolation of a detailed tree model to stand level. In: Innes, J., Edwards, I., and Wilfors, D., editors, Forestsi n the Balance: Linking Tradition and Technology. XXII IUFRO World Congress, 8-13 August 2005, Brisbane, Australia. Abstracts, volume 7(5), p. 25. The International Forestry Review, August 2005.

Ross. J. 1981. The Radiation Regime and Architecture of Plant Stands. W. Junk, The Hague-Boston-London.

Sinoquet, H., Le Roux, X., Adam, B., Ameglio, T. and Daudet, F.A. 2001. RATP: a model for simulating the spatial distribution of radiation absorption, transpiration and photosynthesis within canopies: application to an isolated tree crown. Plant, Cell and Environment, 24:395-406.

Posters

3D virtual plants to phenotype differences among genotypes: Taking into account plant-environment interactions to better understand genetic variability in leaf development response to light

Karine Chenu[1] and Jérémie Lecoeur[2]
[1] INRA, UMR 759 LEPSE, 2 place Viala, 34060 Montpellier, France
[2] SupAgro, UMR 759 LEPSE, 2 place Viala, 34060 Montpellier, France
chenu@supagro.inra.fr - lecoeur@supagro.inra.fr

Keywords: *Arabidopsis*, leaf development, absorbed radiation, light intensity, 3D virtual plant, genotypic variability.

Incident light affects orgnaogenesis and morphogenesis processes involved in leaf development through the amount of radiation absorbed by the plant (Chenu *et al*., 2005). The genetic variability of these responses was investigated on *Arabidopsis thaliana* ecotypes (Col, Di-m, Ler, Ws) and mutants (*se-1*, *rot3-1*, *ron2-2*, *p70S-KOR*) displaying contrasted architectures and radiation use efficiencies (Fig. 1).

Plants were grown under various levels of incident light, with a stable light quality. The local plant-environment interactions were estimated for each genotype, from plant emergence to the end of rosette expansion, using an architectural model (Barczi *et al*., 1997) coupled with a radiative model (Dauzat and Eroy, 1997). Leaf development was assessed in terms of the date of leaf initiation, the relative leaf expansion rate and the duration of leaf expansion.

A reduction in light intensity affected with different extents the final leaf area of the genotypes, through modifications in the leaf development processes. For each genotype, stable relationships were found for (i) leaf initiation and (ii) initial leaf expansion rate with the amount of absorbed radiation, and for (iii) the duration of leaf expansion with the level of radiation intensity. Genotypes displayed different sensitivities in their responses of leaf initiation rate (Fig. 2) and duration of leaf expansion, whereas they all had a similar response in terms of initial relative expansion rate.

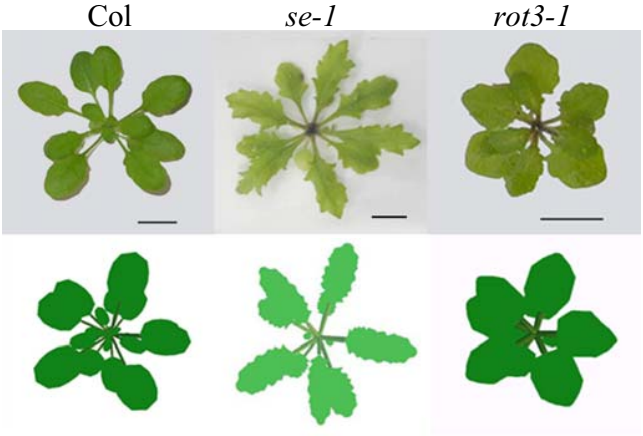

Fig. 1. Photographs of a sampled plant for the ecotype Col and its mutants *se-1* and *rot3-1* (first row) and three-dimensional virtual plants corresponding to the mean representation of the observed plants (second row). Scale bar = 1 cm.

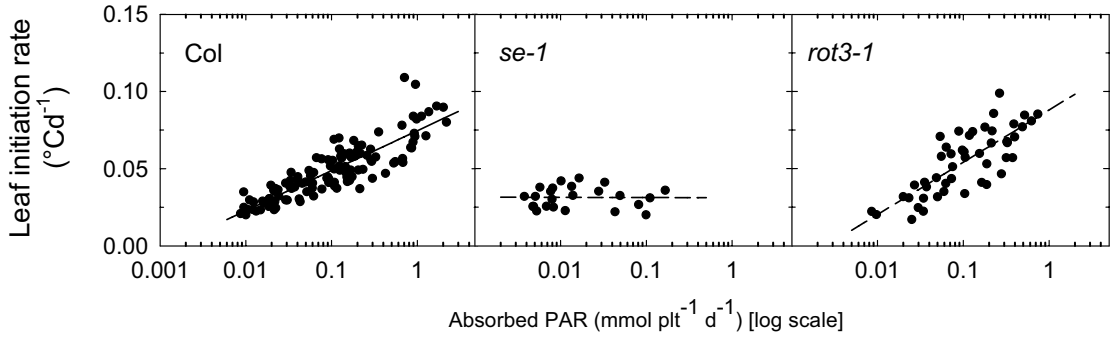

Fig. 2. Leaf initiation rate related to the amount of radiation absorbed by the plant for the ecotype Col and its mutants *se-1* and *rot3-1*.

Using a 3D virtual plant approach allowed us to take into account the genotype-environment interactions through the estimation of the amount of light absorption, and thus to better understand the genotypic differences in physiological responses to light. For example, an unexpected phenotype was revealed in the *se-1* mutant. The SERRATE gene (SE) recently shown to determine early leaf development via leaf organogenesis and morphogenesis patterning (Grigg *et al*., 2005) was demonstrated here to also affect late leaf development and their responses to incident light (Chenu *et al*., 2007). Furthermore, contrary to its wild-type (Col) and the other studied genotypes, the *se-1* mutant displayed a leaf initiation that was totally insensitive to the amount of absorbed radiation (Fig. 1) suggestion a role of carbon metabolism in SE functioning.

The consistent relationships found between plant and light variables had genotype-specific parameters that were independent from the environment. Such parameters can therefore be considered as genotypic characteristics and could be used to identify associated QTL (Reymond *et al*., 2003).

The method developed in this study comprises a new phenotypic tool that allows genotype characterisation for leaf development response to light, for a wide range of radiative environments. This approach was sufficiently precise to characterise the effect of monogenetic mutations and could be applied on a wider range of genotypes to focus on genes and pathways involved in leaf expansion responses to light. The presented results could also be used to integrate the knowledge collected among genotypes in order to predict their behaviour in various light environments.

References

Barczi, J.F., de Reffye, P., Caraglio, Y. 1997. Essai sur l'identification et la mise en oeuvre des paramètres nécessaires à la simulation d'une architecture végétale. In: Modélisation et simulation de l'architecture des végétaux. Science Update. INRA éditions, Paris, France, pp. 205-254.

Chenu, K., Franck, N., Dauzat, J., Barczi, J.F., Rey, H., Lecoeur, J. 2005. Integrated responses of rosette organogenesis, morphogenesis and architecture to reduced incident light in *Arabidopsis thaliana* results in higher efficiency of light interception. Functional Plant Biology 32: 1123-1134.

Chenu, K., Franck, N., Lecoeur, J. 2007. Simulations of virtual plants reveal a role for SERRATE in the response of leaf development to light in *Arabidopsis thaliana*. New Phytologist. in press.

Dauzat, J., Rapidel, B., Berger, A. 2001. Simulation of leaf transpiration and sap flow in virtual plants: model description and application to a coffee plantation in Costa Rica. Agricultural and forest meteorology 109: 143-160.

Grigg, S.P., Canales, C., Hay, A., Miltos, T. 2005. *SERRATE* coordinates shoot meristem function and leaf axial patterning in *Arabidopsis*. Nature 437: 1022-1026.

Reymond, M., Muller, B., Leonardi, A, Charcosset, A, Tardieu, F. 2003. Combining quantitative trait loci analysis and an ecophysiological model to analyze the genetic variability of the responses of maize leaf growth to temperature and water deficit. Plant Physiology 131: 664-675.

The Application of a Functional-Structural Plant Model to Validate a Mechanistic Model of Ozone-Induced Photosynthetic Rate Reduction in *Populus tremuloides.*

Michael A. Donahue**, George E. Host*, Kathryn E. Lenz**, Kyle Roskoski*,
and Harlan W. Stech**
*Natural Resources Research Institute
**Department of Mathematics and Statistics
University of Minnesota Duluth, Duluth MN, USA 55812
Corresponding Author: Harlan W. Stech (hstech@d.umn.edu)

Keywords: Ozone damage model, calibration, *Populus tremuloides*, ECOPHYS, FACE.

Abstract:

The problem of predicting ozone-induced reduction of leaf photosynthetic rates in the context of elevated CO_2 poses significant modeling challenges. Biologically realistic damage models must reflect the complex inter-relationships between stomatal conductance, photosynthetic rate and intercellular CO_2 concentration. Recognizing the apparent high level of variability between plant species, such models should allow for ozone scavenging mechanisms, as well as leaf damage and repair capabilities, all of which may be dependent on leaf photosynthetic rate and leaf age. Moreover, if such models are to be useful for predicting tree and stand level ozone effects, these models must be calibrated in a light environment that is representative of real forest canopies.

The authors will report on the development of a process-based model of ozone-induced photosynthetic rate reduction in the presence of ambient (~360ppm) and elevated (~560ppm) concentrations of carbon dioxide gas. The model extends the earlier work of [4] in that it attempts to explicitly model leaf damage and repair mechanisms. It differs conceptually from [4] in that the photosynthetic rate parameters Vcmax and Jmax are assumed to depend on the (effective) fraction of healthy chloroplasts within the leaf. The rate change of this indicator of leaf health is modeled as the difference between the damage rate attributed to unscavenged "reactive oxygen species", which are created by the reaction of ozone within the leaf, and a hypothesized leaf repair rate.

Chamber studies from the literature have been used for the initial validation/calibration of the model in the context of highly controlled light, temperature, relative humidity and ozone treatment levels. In order to test the performance of the model under more realistic environmental conditions, the model has been installed in the functional-structural plant model ECOPHYS [2], [3]. ECOPHYS has been developed to simulate the growth of aspen clones raised under conditions measured at the Aspen Free-air CO_2 and O_3 Enrichment (FACE) Project (USDA Forest Service, North Central Research Station, Rhinelander, Wisconsin, USA) [1]. Leaf-level gas-exchange data [5] collected at the FACTS Experiment has been used to calibrate the ozone damage/repair model for a specific clone of *Populus tremuloides*.

References:

[1] Dickson, R.E., K.F. Lewin, J.G. Isebrands, M.D. Coleman, W.E. Heilman, D.E. Riemenschneider, J. Sober, G.E. Host, D.R. Zak, G.R. Hendrey, K.S. Pregitzer, and D.F. Karnosky. 2000. *Forest Atmosphere Carbon Transfer and Storage (FACTS-II): The Aspen Free-Air CO2 and O3 Enrichment (FACE) Project: An Overview*. USDA Forest Service NCRS, St. Paul, Minnesota, USA.

[2] Host, G. E., K.E. Lenz, and H. W. Stech. 2004. Mechanistically-based functional-structural tree models for simulating forest patch response to interacting environmental stresses. In: (C. Gin et al. eds.) Proceedings of the 4th International Workshop on Functional-Structural Plant Models, Publication UMR AMAP/2004, pp. 150-153.

[3] Isebrands, J. G., G. E. Host, and K. E. Lenz. 1999. Individual-based models of tree plantations using hierarchical and parallel approaches. In: *Empirical and Process Models for Forest Tree and Stand Growth Simulation.* (A. Amaro and M. Tome Eds.) Edicos Salamandra pp. 537-51.

[4] Martin, M. J., G. E. Host, K.E. Lenz, and J. Isebrands. 2001. Simulating the growth response of aspen to elevated ozone: a mechanistic approach to scaling a leaf-level model of ozone effects on photosynthesis to a complex canopy architecture. *Environmental Pollution* 115, pp. 425-436.
[5] Noormets A., McDonald E. P., Dickson R. E., Kruger E. L., Sôber A., Isebrands J. G., Karnosky D. F., 2001. The effect of elevated CO2 and O3 on leaf and branch level photosynthesis and potential plant level carbon gain in aspen. *Trees* 15: 262-270.

An Architectural Modelling Study of Chickpea-Sowthistle Interactions

S-Zahra-Hosseini Cici[146], Steve Adkins[34], Brian Sindel[45] and Jim Hanan[12]

[1]Advanced Computational Modelling Centre, [2]ARC for Integrative Legume Research, [3]School of Land and Food Sciences, University of Queensland, [4]CRC for Australian Weed Management, [5]University of New England, [6]Shiraz University, Iran jim@maths.uq.edu.au

Keywords: L-systems, Plant architecture Informatics, Integrated weed management, Legume, Chickpea, Sowthistle

It is now widely accepted that integrated weed management (IWM) approaches, making use of the competitive ability of the crop canopy and the application of other cultural practices, will ultimately reduce the level of dependence on herbicide use (Swanton and Murphy, 1996). To help understand the complexity of the different IWM choices available, computational models could be used by the agronomist, plant breeder or agricultural practitioner to simulate, visualise and evaluate different ways of enhancing crop competitiveness with its common weeds. In this study, the effect of chickpea (*Cicer arietinum* L.) canopy on sowthistle (*Sonchus oleraceus* L.) performance is evaluated using an architectural modelling (Prusinkiewicz *et al.*, 1997) approach. In order to determine the potential for canopy manipulation to improve chickpea competitive ability (an important legume in sustainable agriculture) with sowthistle (a common weed in chickpea), an experiment was conducted in which sowthistle plants were grown under two densities of chickpea and in full sunlight (Cici *et al.*, 2006).

To capture the 3D architecture of the chickpea and sowthistle, plants were grown separately in a sandy, well watered and fertilized soil and a sonic digitizer system was used to follow a number of aspects of morphology, topology, and geometry in a non-destructive way over time. The resulting data sets were analysed and used to develop a realistic, dynamic architectural model for each species using L-systems (Lindenmayer, 1968).

A quasi-Monte Carlo light environment model (Lemieux *et al.*, 2004) was used to connect the model of chickpea canopy (Cici *et al.*, 2005) with a virtual sowthistle calibrated to respond to light availability (Cici *et al.*, 2006). This chickpea-light environment-sowthistle (CLES) model (Fig 1) captured the hypothesis underlying this research study: the architecture of virtual chickpea changed the light environment inside the canopy, which influenced the morphogenesis of virtual sowthistle that in turn determined the sowthistle responses to different canopy management strategies. The model was validated against data from glasshouse experiments and the literature. Both the simulated and observed data showed that the most significant canopy features of chickpea for enhancing its competitive ability with sowthistle are increasing its leaf production rate (phyllochron) and leaflet size or decreasing the branching delay.

The potential power of the CLES model becomes more obvious when it is used for choice of cultivar, row spacing and seeding rate. As part of an IWM program, this work provides a basis for a computer model to help choose more competitive cultivars to ensure better weed suppression, thus reducing the need for herbicide application.

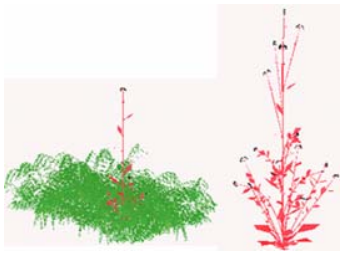

Fig 1. The CLES model showing a side view of a virtual field of chickpea with a sowthistle growing in the middle (left) and a sowthistle in full light (right image) when plants were 75 days old

Acknowledgment

The first author wishes to thank the invaluable volunteer help of Mr. Farri during 3 years of conducting extensive glasshouse experiments for this study. Thanks are also extended to Mick Cieslak and Time Rouger for the light model.

References

Cici SZH, Hanan J, Sindel BM and Adkins S (2006). Phenotypic plasticity of sowthistle and its offspring in response to light availability. In Proceedings of the Fifteenth Australian Weeds Conference, Adelaide, Eds. Preston C, Watts JH and Crossman ND. 172-175. Weed Management Society of South Australia.

Cici SZH, Sindel B, Adkins S and Hanan J (2005). Using L-systems to simulate chickpea cultivars and their shading abilities. In Proceedings of the Fifth International Congress on Modelling and Simulation, Melbourne, Australia, Eds. Zerger A and Argent R. 1230-1236. Modelling and Simulation Society of Australia and New Zealand.

Lemieux C, Cieslak M and Luttmer K (2004). RandQMC User's Guide. pp. 62. University of Calgary, Calgary, Canada.

Lindenmayer A (1968). Mathematical models for cellular interactions in development. *Journal of Theoretical Biology*. 18: 280-315.

Prusinkiewicz P, Hammel M, Hanan J and Mech R (1997). Visual models of plant development. In Handbook of Formal Languages. Eds. Rozenberg G and Salomaa A. 535-597. Berlin, Germany.

Swanton CJ and Murphy SD (1996). Weed science beyond the weeds: the role of integrated weed management (IWM) in agroecosystem health. *Weed Science*. 44: 437-445.

Asynchronous cell division model for morphogenesis of plant leaves

Toshiya Kazama and Satoshi Murata
Interdisciplinary Graduate School of Science and Engineering,
Tokyo Institute of Technology
4259, Nagatsuta, Midori, Yokohama, Kanagawa, 226-8502, Japan
{kazama|murata}@mrt.dis.titech.ac.jp

Keywords: leaf morphogenesis, asynchronous cell division, cell/physical rules, mechanical interaction, simulation model

Introduction

In order to describe the developmental process of plants, we have to consider various factors (Taiz and Zeiger, 2002). Many models of morphogenesis have been proposed so far, and each of them shed a light on a certain aspect of the complicated phenomena.

Map L-system extends the concept of the L-system on the planar network (Prusinkiewicz and Lindenmayer, 1990). This model is based on a symbol dynamics driven by a set of rewriting rules similar to its original system (Lindenmayer, 1968). It successfully describes the developmental process of fern gametophytes etc., however, the argument for each rule is a segment of cell wall, and therefore even a simple developmental process requires an artificial set of rules. Also, it deals with only the topological connectivity and neglects the mechanical interaction among cells.

The context-sensitive cell system is a model in which rules operate on cells, not on cell walls (Fracchia, 1996). The orientation of the division plane is determined by concentration gradient of the morphogen calculated by the reaction-diffusion equation. Both the above two models are synchronous.

Some asynchronous models have been proposed to capture the development of phyllotaxis (Smith, et al., 2006)(Jönsson, et al., 2006). In these models, asynchrony is realized by the following mechanism. Cells are assumed to expand at constant speed. A cell divides when its size reaches the constant threshold. If they divide unequally, the length of time before the next division will be different. The orientation of division plane is determined by geometry of the cell polygon (Smith, et al., 2006) or determined at random (Jönsson, et al., 2006).

In this paper, we propose a new model to give a general framework to describe varieties of developmental processes of plant leaves. Our model possesses the following three features: asynchronous cell division, explicitly described determination rules for the cell division plane, and inter-cellular mechanical interactions. Although cell division is synchronous in early stage of embryogenesis, it must be described as asynchronous process in later development. The determination rules are given as functions of the cell type (internal state of the cell) and the types of the neighboring cells. This is important because vegetable cells are usually surrounded by rigid cell walls that prevent cell migration, thus the local connectivity is almost determined at the time of cell division. The inter-cellular mechanical interactions distort the network among cells whenever the cells divide or expand, eventually leading to the reconfiguration of the network. In the asynchronous cell division model, the rearrangement may cause instability, e.g. the resultant morphology may become sensitive to the order of activation. Therefore we think it is essential to study the mechanism of development of multi-cellular organisms.

Model

In this model, cells are represented as nodes with discrete internal states. Each cell is connected to neighbors via "link"s. Linked cells can refer to each other's state.

There are two sets of rules that interact each other: cellular rules and physical rules.

The cellular rules represent state transition or cell division. Updated state and direction of cell division is defined by current states of itself and linked cells (Fig. 2). State transition and division are executed asynchronously. These rules are described in a uniform manner, thus it is easy to build modular and hierarchical rule set for complex morphology.

The physical rules rearrange the connectivity network among cells. Each cell has the same mass, and its position is defined on two-dimensional space. Linked cells are connected by springs and dampers. If the distance between neighboring cells becomes shorter than a constant threshold value, they are connected by a new link. Links can be disengaged or locally rearranged (by Delaunay flip (de Berg, et al., 2000)) when the distortions of the spring-mass-damper networks exceeds a threshold (Fig. 3).

Fig. 4 shows the morphogenesis of fern leaves generated by our model. The venation pattern of the leaf was obtained mainly by the cellular rules. Cells that compose the segments of the vein are produced by division at the tip. The length of each segment is determined by counting the number of cell divisions, and at the predefined interval, branches are generated. At the same time, additional cells grow around the vein segments. Interaction between the cellular rules and the physical rules make the vein structure stable under the asynchronous activation of rules. We have conducted several simulations from different random seeds and obtained slightly different patterns (Fig. 4 c)).

```
Set initial network
Put all the cell IDs in queue Q in random order
While Q is not empty do {
   Pick a cell C from Q
   Apply cellular rules to cell C
   Relaxation of spring-mass-damper network
   Apply physical rules to all cells
}
```

Fig. 1. Simulation procedure of proposed model. For asynchronous update, we introduce a random cell cycle. The cellular rules are applied just once in a cycle in random order. When a cellular rule applied, the physical rules are immediately applied to all cells.

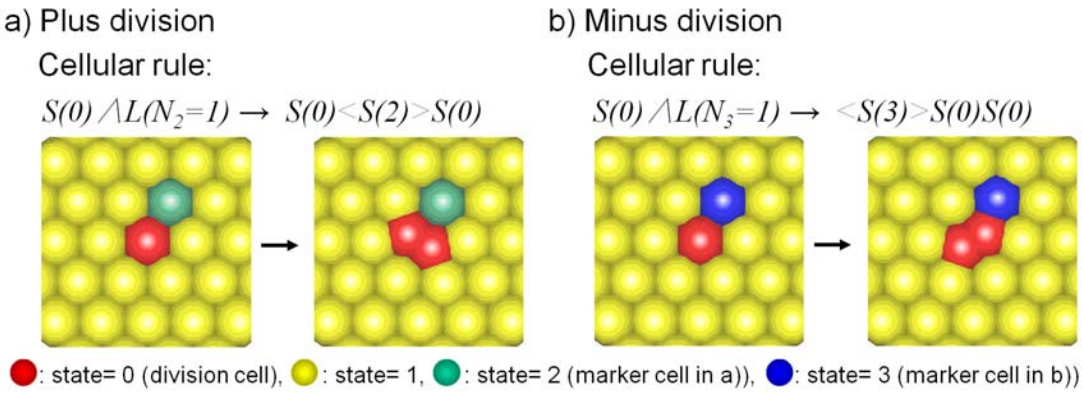

Fig. 2. Determination of the division direction by the cellular rule. The division procedure is as follows: (1) Select a "marker" cell from the linked cells according to the left-hand side of the rule. (2) Divide the cell according to the right-hand side of the rule. (a) Plus division: Both of the new cells connect to the marker cell. (b) Minus division: one of the new cells connects to the marker cell.

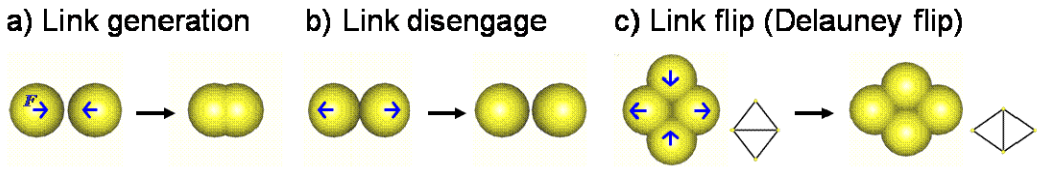

Fig. 3. Physical rules. A) Link generation: If the distance between neighboring cells becomes shorter than a constant threshold, they are connected by a new link. B) Link disengage: If the distance between neighboring cells becomes longer than a constant threshold, they are disengaged. C) Link flip: Links are rearranged by Delaunay flip to release the distortion energy in the network.

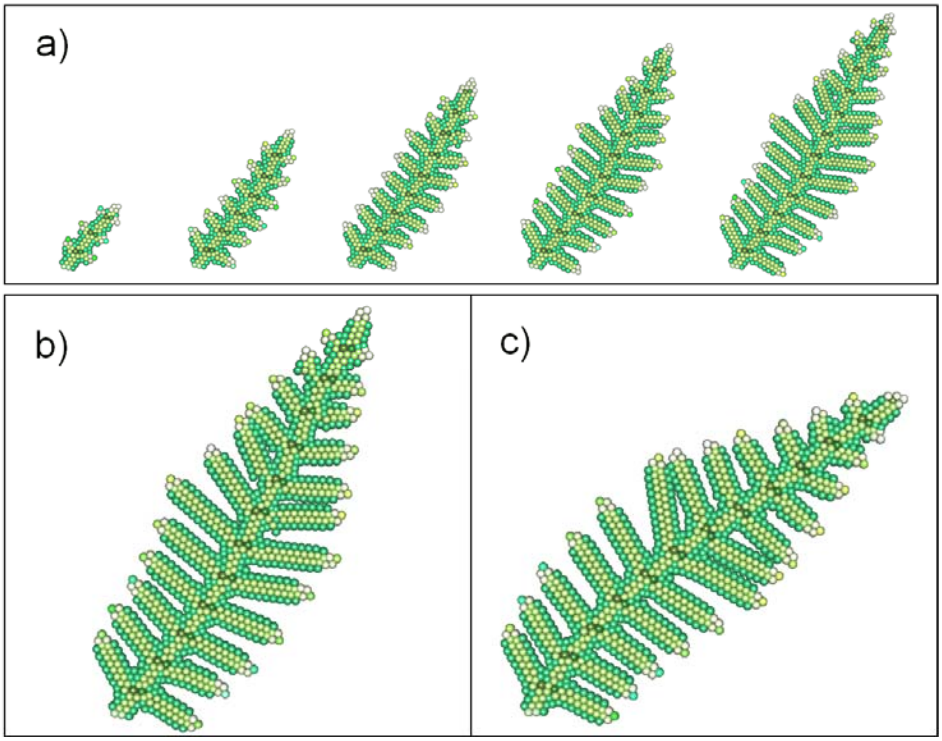

Fig. 4 The morphogenesis of fern leaves generated by the model. a) Snapshots from the simulated growth process (100, 300, 500, 700 and 900 cells). b) A close-up of a pattern when the number of cells reaches 1000. c) A close-up of a pattern by different random seed. Colors represent the internal states.

References

de Berg, M., van Kreveld, M., Overmars, M., Schwarzkopf, O. 2000. Computational Geometry: Algorithms and Applications. Springer.

Fracchia, F. D. 1996. Integrating lineage and interaction for the visualization of cellular structures. In J. Cuny, H. Ehrig, G. Engels, and G. Rozenberg (Eds.): Graph Gramars and Their Application to Computer Science, 5th International Workshop, Selected Papers. Lecture Notes in Computer Science 1073, Springer, pp. 521-535.

Jönsson, H., Heisler, M. G., Shapiro, B. E., Meyerowitz, E. M., Mjolsness, E. 2006. An auxin-driven polarized transport model for phyllotaxis. Proc. Natl. Acad. Sci. USA 103, pp. 1633-1638.

Lindenmayer, A. 1968. Mathematical models for cellular interaction in development, Parts I and II. Journal of Theoretical Biology 18, pp. 280-315.

Prusinkiewicz, P., Lindenmayer, A. 1990. The Algorhithmic Beauty of Plants, Springer-Verlag.

Smith, R. S., Guyomarc'h, S., Mandel, T., Reinhardt, D., Kuhlemeier, C., Prusinkiewicz, P. 2006. A plausible model of phyllotaxis, Proc. Natl. Acad. Sci. USA 103, pp. 1301–1306.

Taiz, L., Zeiger, E. 2002. Plant Physiology (3rd ed.), Sinauer associates, Inc.

Automated procedures for estimating LAI of Australian woodland ecosystems using digital imagery, Matlab programming and LAI / MODIS LAI relationship

Sigfredo Fuentes[1], Anthony R. Palmer[1], Daniel Taylor[1], Chris Hunt[2] Derek Eamus[1],

[1]*Institute for Water and Environmental Resource Management (IWERM), University of Technology, Sydney, NSW 2007. Australia.*
[2]*AgResearch Grasslands, Private Bag 11008, Palmerston North, New Zealand*

Corresponding author: sigfredo.fuentes@uts.edu.au.

Abstract

Leaf area index (LAI) is one of the most important variables required for modelling growth and water use of forests. The implementation an approach to estimate LAI from digital pictures (LAI_D) has recently been advanced in Australia using digital image capture and gap analysis, which employs a novel methodology (Macfarlane et al 2006). This technique uses upward-looking wide-angle digital photographs to capture canopy LAI_D and analyses these images using gap fraction analysis at a single zenith angle (0^o – 57^o), using commercial image processing software. After implementing this technique in Australian evergreen *Eucalyptus* woodland, we have improved the picture analysis method from a time consuming manual technique to an automated procedure. Furthermore, in this paper, we compare MODIS LAI values with digital image LAI values for a range of woodlands in Australia.

We used Matlab 7.4 (The Mathworks, Inc), to batch process numerous upward-looking digital images (at least 50 per site) to estimate LAI (LAI_M) from different woodland sites within New South Wales, Australia. The blue band (450 – 495 nm) of each image was extracted and explored to identify a threshold between foliage and sky. In the procedure, the selection of a suitable luminance value from the blue band histograms can be fully automated for numerous images or manually generated for each image. After assigning a suitable blue layer threshold, the image is transformed into a binary image for gap analysis.

The gap analysis is performed by automatically dividing each binary image into nine sub-images. From each sub-image, the program counts the total of pixels corresponding to sky (S) and leaves (L). A big gap is considered when the ratio $S/L \geq$

0.75 is met for each sub-image. In this case, the pixel count for sky (S) is added to the big gap count for that particular image. If this ratio is not met for a specific sub-image, the pixel count contribution to the total big gap count of that particular image is equal to zero.

The fractions of foliage projective cover **(f_f)**, crown cover **(f_c)** and crown porosity **(Φ)** are calculated from Mcfarlane et al (2006) as:

$$\mathbf{f_c\ (\%)} = 100 * (1 - \text{large gap pixels} / \text{total pixels}) \quad \textbf{[1]}$$

$$\mathbf{f_f\ (\%)} = 100 * (1 - \text{total gap pixels} / \text{total pixels}) \quad \textbf{[2]}$$

$$\mathbf{\Phi} = 1 - f_f/f_c \quad \textbf{[3]}$$

LAI_M is calculated from Beer's Law, assuming an extinction co-efficient (k) of 0.5 as follows:

$$\mathbf{LAI_M} = -f_c \ln\Phi / k \quad \textbf{[4]}$$

and the clumping index at the zenith, **$\Omega(0)$**, is calculated as follows:

$$\mathbf{\Omega(0)} = (1-\Phi) \quad \ln(1- f_f) / \ln(\Phi) / f_f \quad \textbf{[5]}$$

The same equations [1 – 5] are used to calculate LAI_D using Adobe PhotoShop® 7.0 and the methodology described in Macfarlane et al (2006). The automated maximum threshold value using Matlab resulted in a good average LAI_M compared to the averaged LAI_D for five sites (Figure 1a) ($y = 1.01LAI_D$; $R^2 = 0.95$, using four sites). When patchy clouds are present in the pictures, the manually generated threshold was more appropriate to obtain accurate individual LAI_D from single pictures when compared to LAI_D ($y = 0.951LAI_D$; $R^2 = 0.98$, from 50 pictures; Hornsby site only, data not shown). A Matlab code was also developed to acquire images using a high resolution web cam attached to a laptop for in-field real-time digital image acquisition and analysis.

Following the capture of digital images and determination of LAI_D in eight examples of *Eucalyptus* woodland, we assessed the relationship between LAI_D and MODIS LAI products for each of the ground measurements. We extracted the 8-day 1 km MODIS LAI (collection 4) data for New South Wales from the MODIS distributed archive and imported these into a GIS. Ground sampling sites were established along a precipitation gradient (450 – 1400 mm) in New South Wales, Australia. 8-day LAI values for ground sampling stations (of approximately 1 ha) were extracted using a data-drill. At each ground sampling station, canopy LAI (LAI_D) was calculated from at least 50

randomly collected images from the 1 ha stations within the 1 km MODIS pixel. Individual modeled MODIS LAI values for each sampling occasion were selected from the 8-day image closest to the date of the LAI_D sampling event. Although seasonal variations in MODIS LAI was apparent at each sampling site (e.g range from LAI 1 to 4 in wet sites), the ground sampling events coincided with periods when MODIS LAI closely approximated LAI_D. The ground sampling excluded the contribution of understorey LAI, and was conducted during the dry season when the contribution of the understorey would have been at its minimum. The regression LAI_D = 0.8822 MODIS LAI + 0.0701(R^2 = 0.85) describes the relationship between LAI_D and MODIS LAI for eight sites.

We concluded that digital image acquisition; coupled with Matlab data analysis capacities, provide a rapid, robust, cheap and simple method for determining the LAI of tree canopies. Furthermore, we conclude that for evergreen woodland, where seasonal understorey growth is limited due to drought, the MODIS LAI product provides a useful surrogate for LAI_D. This is probably not true when understorey LAI makes a large contribution to the MODIS LAI.

Keywords: Eucalyptus forest; Leaf area index; Digital photography; Matlab; Remote sensing; MODIS LAI

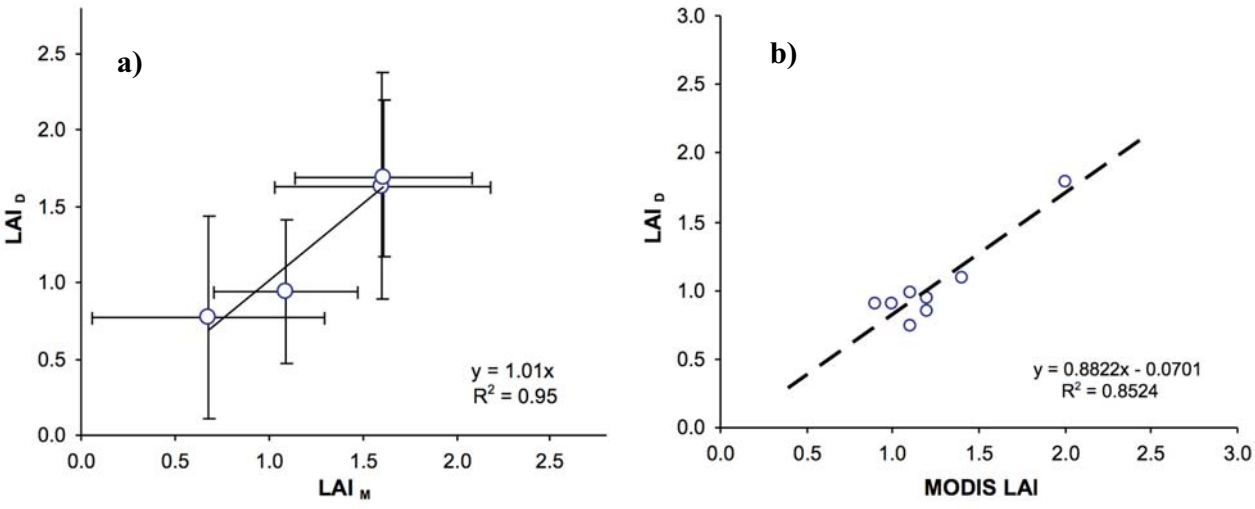

Figure 1: a) Relationship between LAI_M and LAI_D for four NSW sites. **b)** Relationship between LAI_D and MODIS LAI for eight NSW sites.

Automatic instantiation of a structural leaf model from 3D scanner data: application to light interception computation

Jean-Christophe Chambelland, Boris Adam, Nicolas Donès, Philippe Balandier, André Marquier, Mathieu Dassot,Gabriela Sonohat, Marc Saudreau, Hervé Sinoquet
UMR547 PIAF INRA-UBP, 234 Av. du Brézet, F-63100 Clermont-Ferrand, France
sinoquet@clermont.inra.fr

Keywords: structural leaf model, laser scan non-contact digitizer, light interception rate

Three-dimensional (3D) plant modelling has become a promising tool for simulating plant functional-structural processes (Godin & Sinoquet 2005), especially those related to the 3D plant organization. An emerging approach for constructing virtual plants is based on non-contact 3D measurement devices which offer a fast and accurate way to capture the plant hull into a dense set of 3D coloured points. Except for very simple cases, making a relevant description of 3D whole plant features from this type of punctual data remains a difficult task and it is often suitable to design the whole plant architecture from different sub-models representing the geometry of each organ (Dornbuch & al. 2007). For leafy tree reconstruction, the definition of a suitable leaf model and its assignment from data points remain a critical task which directly conditions the accuracy of further functional-structural simulations and the amount of computing time.

In this poster, a new parametric structural leaf model and its automatic instantiation from 3D digitized (Hanan & al. 2004, Loch & al. 2005) data are exposed. From a limited number of meaningful real-valued parameters controlling the main morphological leaf features (curvature, openness angle, border oscillations …), the proposed model allows representing a large spectrum of leaf shapes. Using a set of suitable geometrical hypothesis and a devoted curve fitting technique, we show how to automatically extract the model parameters from dense digitized data provided by a non-contact digitizer Konica Minolta vi-910. A quantitative assessment, based on an inversion algorithm allowing building a triangulated leaf model from a prescribed set of parameters, demonstrates both the reliability of the proposed model and the efficiency of the related instantiation process. Using the software VegeSTAR (Adam & al. 2002), an application to light interception computation is presented with virtual *Fagus sylvatica* trees. The related results exhibit the impact of the 3D leaf features on the light interception rate.

References

Adam, B., Donès, N., Sinoquet, H., 2002. VegeSTAR-software to compute light interception and canopy photosynthesis from images of 3D digitized plants. V3.0. UMR PIAF INRA-UBP, Clermont-Ferrand, France.

Dornbuch, T., Wernecke, P., Diepenbrock, W., 2007. A method to extract morphological traits of plant organs from 3D point clouds as a database for an architectural plant model. Eco. Modelling 200, pp 119-129.

Godin, C., Sinoquet, H., 2005. Functional–structural plant modelling. New Phytologist 166, pp 705–708.

Hanan, J.S., Loch, B., McAleer, T., Processing laser scanner data to extract structural information. In: Godin, C., Hanan, J., Kurth, W., Lacointe, A., Takenaka, A., Prusinkiewicz, P., DeJong, T., Beveridge, C., Andrieu, B. (Eds.), *Proceedings of the 4th International Workshop on Functional-Structural Plant Models*. Proceedings-FSPM04, pp 9-12, Montpellier.

Loch, B. I., Belward, J. A., Hanan, J. S, 2005. Application of surface fitting techniques for the representation of leaf surfaces. In: Zerger, Andre and Argent, Robert M., (Eds.). *MODSIM 2005 International Congress on Modelling and Simulation*, 12-15 Dec 2005, Melbourne, Australia.

Contribution of Leaf Orientation and Leaf Physiology to the Maximization of Plant Carbon Gain

Juan M. Posada[1], Risto Sievanen[2], Jari Perttunen[2], Christian Messier[3] and Eero Nikinmaa[4],

(1) Center for Forest Research (CFR), Biology Department, Université du Québec à Montréal, Montreal, QC, Canada, posada.juan@courrier.uqam.ca (2) The Finnish Forest Research Institute, Vantaa Research Unit, Vantaa Unit, PL 18, FI-01301, Vantaa, Finland, (3) Sciences Biologiques, Université du Québec à Montréal, 141 Président Kennedy, C.P. 8888, Montréal, QC H3C3P8, Canada,(4) Department of Forest Ecology, University of Helsinki, Latokartanonkaari 7, (P.O. BOX 27), FIN-00014 University of Helsinki, Helsinki, Finland

Keywords: Optimal resource allocation; leaf nitrogen; leaf Amax; leaf angle; leaf functional traits, canopy photosynthesis, scaling-up

Research area: Applications of FSPM to fundamental biology

Introduction

Optimal nitrogen allocation theory predicts that plant photosynthesis will be maximized if the photosynthetic capacity of individual leaves (A_{max}) in a canopy scales proportionally to the availability of light in the vicinity of a leaf (Field 1983, Farquhar 1989, Field 1991). However, many plants do not follow the expected distribution (e.g., Hirose and Werger 1987, Evans 1993, Hollinger 1996). This discrepancy has generally been interpreted as being the results of physiological constraints and ecological trade-offs that impede plants to reach the predicted "true" optimal A_{max} distribution. Yet, optimal allocation resource allocation theory does not take into consideration the potentially important role of leaf orientation as a modulator of the light environment of individual leaves. Moreover, it is not yet clear that the predicted optimal A_{max} distribution does in fact maximize plant photosynthesis. The objective of our study was to find the distribution of leaf functional traits that maximized plant carbon gain when both leaf A_{max} and leaf orientation were allowed to vary with the light gradients in the canopy.

LIGNUM Simulations

We did three-dimensional simulations of trees using the functional-structural plant model LIGNUM. We grew realistic 1-4 m tall trees of *Acer saccharum* and *Populus deltoids* and used them as plant architectural "templates" to search for distributions of leaf traits that maximized plant photosynthesis. Light above the trees was distributed assuming standard overcast conditions. Self-shading between leaves generated a gradient of photosynthetic photon flux density (PPFD) within the canopy and LIGNUM calculated PPFD incident at the point of emergence of each individual leaf bud. The function relating leaf A_{max} to PPFD incident on buds varied hyperbolically while leaf inclination changed linearly with PPFD. We used quasi-Newton and simulated annealing methods to

find combinations of parameter that maximized whole tree carbon gain. A_{max} defined the photosynthetic light response of each individual leaf assuming a linear relationship between A_{max} and dark respiration (R_d) while apparent quantum yield (ϕ) and curvature (θ) were kept constant.

Results and Discussion

One-dimensional optimizations showed that plants that gradually increased the inclination of leaves with PPFD had higher carbon gain than leaves with either horizontal or vertical leaves. When individual leaf A_{max} changed linearly with PPFD plant photosynthesis was higher than if all leaves had the same A_{max}, supporting the initial predictions of optimal allocation theory. However, when leaf A_{max} changed as a hyperbolic function of PPFD plant carbon gain was enhanced further contradicting the above predictions. Furthermore, the hyperbolic A_{max} functions were qualitatively similar to distributions observed in natural conditions. Maximum plant carbon gain was obtained when both leaf inclination and leaf A_{max} changed with PPFD availability in the canopy. Our simulations show that plant photosynthesis was maximized when the leaf array in the canopy attained maximum average photosynthetic light use efficiency. Thus, these results suggest that natural selection should favor a distribution of A_{max} that maximizes photosynthetic efficiency of all individual leaves.

Cited References

Evans, J. R. 1993. Photosynthetic acclimation and nitrogen partitioning within a Lucerne Canopy. II* Stability through time and comparison with a theoretical optimum. Australian Journal of Plant Physiology **20**:69-82.

Farquhar, G. D. 1989. Models of integrated photosynthesis of cells and leaves. Philosophical Transactions of the Royal Society of London, Series B **323**:357-367.

Field, C. 1983. Allocating leaf nitrogen for the maximization of carbon gain: leaf age as a control on the allocation program. Oecologia **56**:341-347.

Field, C. B. 1991. Ecological scaling of carbon gain to stress and resource availability. Pages 35-65 *in* H. A. Mooney, W. E. Winner, and E. J. Pell, editors. Integrated responses of plants to stress. Academic Press, London.

Hirose, T., and M. J. A. Werger. 1987. Maximizing daily canopy photosynthesis with respect to the leaf nitrogen allocation pattern in the canopy. Oecologia **72**:520-526.

Hollinger, D. Y. 1996. Optimality and nitrogen allocation in a tree canopy. Tree Physiology **16**:627-634.

Describing hierarchical canopy structure and within-canopy multiple scattering with spectral invariants for remote sensing purposes

Sampo Smolander
Department of Geography, University College London
Gowet St., WC1E 6BT, London, UK
sampo.smolander@helsinki.fi

Keywords: canopy structure, radiative transfer, remote sensing, recollision probability, specral invariant

In the study of physical modelling of reflective properties of vegetation canopies, there has recently been interest in the concept of spectral invariants (Huang et al. 2007). The spectral invariant approach aims at separating radiative transfer inside canopy to terms that depend only on canopy structure, and to terms that depend only on wavelength. The wavelength dependent part being leaf optical properties (leaf reflectance and transmittance in different wavelengths). The spectral invariants are wavelength independent and describe canopy geometrical structure. Current studies show a good prospect of there being only a small set of parameters that well describe the effect of canopy structure on the multiple scattering of radiation inside the canopy. The most essential canopy spectral invariant is the recollision probability. The idea is a simple one: the recollision probability gives the chance that a photon, after being scattered from a phytoelement, again hits an element of the canopy. To be precise, the recollision probability should vary according to the orders of scattering, and according to the position inside the canopy. In practice, the simulation studies have shown that there is a robust single effective value. Thus, the recollision probability is a pure geometric concept and, together with leaf optical properties, it relates the canopy structure to the amount of absorbed multiply scattered radiation. The amount of absorbed direct (non-scattered) radiation is of course easily obtained from leaf optical properties and canopy direct transmission. To date, the recollision probability has been successfully used to describe shoot structure (Smolander and Stenberg 2005) and leaf internal structure (Lewis and Disney 2007) in canopies with homogeneous higher level structure, and crown structure when the within-crown structure is homogeneous (Huang et al. 2007, Mõttus et al. 2007). In the poster I will present results from applying the recollision probability for canopies with several levels of hierarchical structure (shoots, branches, tree crowns) and discuss the usefulness of the concept for relating models of canopy structure to models of canopy radiative transfer and reflectance.

References

Huang, D., Knyazikhin, Y., Dickinson, R.E., Rautiainen, M., Stenberg, P., Disney, M., Lewis, P., Cescatti, A., Tian, Y., Verhoef, W., Martonchik, J.V. and Myneni, R.B. 2007. Canopy spectral invariants for remote sensing and model applications. Remote Sensing of Environment 106(1): 106-122.

Lewis, P. and Disney, M. 2007. Spectral invariants and scattering across multiple scales from within-leaf to canopy. Remote Sensing of Environment 109(2): 196-206.

Mõttus M., Stenberg, P., and Rautiainen, M. 2007. Photon recollision probability in heterogeneous forest canopies: Compatibility with a hybrid GO model. Journal of Geophysical Research 112: D03104 doi:10.1029/2006JD007445.

Smolander S. and Stenberg P. 2005. Simple parameterizations of the radiation budget of uniform broadleaved and coniferous canopies. Remote Sensing of Environment 94(3): 355-363.

A dynamic model system to couple the organ length and mass dynamics specified for spring barley (*Hordeum vulgare* L.)

Peter Wernecke, Tino Dornbusch and Johannes Müller
Institute of Agricultural and Nutritional Science, Martin-Luther-University Halle-Wittenberg
06108 Halle / Saale, Germany
{peter.wernecke|tino.dornbusch}@landw.uni-halle.de

Keywords: modeling, mass length dynamics, spring barley

Introduction

An important goal in developing functional-structural plant models (FSPMs) is a reliable and adequate description of the inherent interactions between processes controlling plant growth and formation of plant architecture. Several architectural models have been introduced for specific crops using temperature-driven descriptive models based on the phyllochron / plastochron philosophy (Dornbusch et al., 2007; Drouet, 2003; Evers et al., 2005; Fournier et al., 2003; Prévot et al., 1991; Watanabe et al., 2005). In order to couple those architectural models to process models, which lastly compute the amount of mass assimilated by the photosynthetically active organs, an interface between mass dynamics and the formation and growth of new organs needs to be developed. Fournier et al. (2005) introduced a model to describe the length dynamics of leaf blades and leaf sheaths of wheat (*Triticum aestivum* L.). Here we propose an extension of this model to describe the length dynamics coupled with the corresponding mass dynamics of barley (*Hordeum vulgare* L.) organs (blades, sheaths and internodes) based on experimental data. The proposed model includes a set of coupled ordinary differential equations (ODEs). The model performance is demonstrated by simulation studies.

Model description

Fournier et al. (2005) describe the organ length dynamics of blades and sheaths using cell fluxes between three cell pools: i) the cell pool in the division zone (D), ii) the cell pool in the elongation-only zone (E) and iii) the cell pool in the mature zone (M). Here we introduce a different notation for the state variables in the model by Fournier et al. (2005):

$$\frac{dZ_D}{d\tau} = R_{Z,D} - F_{Z,D\to E}\,, \qquad R_{Z,D} = K_1 \cdot Z_D\,, \tag{1}$$

$$\frac{dZ_E}{d\tau} = R_{Z,E} + F_{Z,D\to E} - F_{Z,E\to M}\,, \qquad R_{Z,E} = K_2 \cdot Z_E\,, \tag{(2)}$$

$$\frac{dZ_M}{d\tau} = \qquad\qquad + F_{Z,E\to M}\,, \tag{3}$$

with the initial conditions:

$$Z_D(\tau = 0) = Z_{D0}\,, \quad Z_E(\tau = 0) = 0\,, \quad Z_M(\tau = 0) = 0\,, \tag{4}$$

where τ = phyllochronic time. The state variables Z_D, Z_E and Z_M are vectors and define the length Z of the zones D, E, and M of blades, sheaths and internodes. The total organ length equals to $Z_T = Z_D + Z_E + Z_M$. The vector R is the increase in length in the respective zone and F the length fluxes between them. K_1 and K_2 are defined in Eq. (6) and (7). To couple the mass and length dynamics of each organ, we introduce a function *CF,* which controls the availability of assimilates required for building up the structure of an organ. Using the assimilated carbon $m_{C,ass}$ and the dry mass m_{tiller} of a tiller and introducing the concentration C defined as $C = m_{C,ass} / m_{tiller}$ we formulate the control function CF as:

$$CF(\tau, C) = \frac{C}{K_C + C} \cdot (\tau > \tau_0), \quad CF(\tau \le \tau_0) = 0, \quad 0 \le CF \le 1. \tag{5}$$

The parameter K_C is a model parameter stating a critical concentration of available carbon, below which no organ growth is initiated, and τ_0 is the phyllochronic time where fluxes into a respective organ are initiated. Using the model parameters k_1 and k_2 (cf. Fournier et al. 2005) the functions K_1 and K_2 are defined as:

$$K_1(\tau) = k_1 \cdot CF, \tag{6}$$

$$K_2(\tau) = k_2 \cdot CF. \tag{7}$$

The production terms $R_{Z,D}$ and $R_{Z,E}$ characterize cell division and cell elongation rates (cf. Eq. (1) and (2)). The cell exchange fluxes $F_{Z,D\to E}$ and $F_{Z,E\to M}$ between two cell pools are defined as:

$$\begin{aligned} F^{BL}_{Z,D\to E} &= K_1 \cdot a(\tau) \cdot (Z^{BL}_D + Z^{SH}_D) \cdot Z^{BL}_D \quad \text{for} \quad (Z^{BL}_D > 0), \\ F^{SH}_{Z,D\to E} &= K_1 \cdot a(\tau) \cdot (Z^{BL}_D + Z^{SH}_D) \cdot Z^{BL}_D \quad \text{for} \quad (Z^{BL}_D \le 0), \end{aligned} \tag{8}$$

$$\begin{aligned} F^{BL}_{Z,E\to M} &= K_2 \cdot b(\tau) \cdot (Z^{BL}_E + Z^{SH}_E) \cdot Z^{BL}_E \quad \text{for} \quad (Z^{BL}_E > 0), \\ F^{SH}_{Z,E\to M} &= K_2 \cdot b(\tau) \cdot (Z^{BL}_E + Z^{SH}_E) \cdot Z^{BL}_E \quad \text{for} \quad (Z^{BL}_E \le 0), \end{aligned} \tag{9}$$

$$a(\tau) = \max(0, p_{a1} \cdot (\tau - \tau_a)), \quad b(\tau) = \max(0, p_{b1} \cdot (\tau - \tau_b)), \tag{10}$$

with the time functions $a(\tau)$ and $b(\tau)$, the model parameters p_{a1} and p_{a2}, and the characteristic times τ_a, τ_b. We propose a flux of carbon mass $F_{m,E->M}$ into the organ proportional to the cell flux $F_{Z,E->M}$ as:

$$F_{m,E\to M} \approx p_m \cdot F_{Z,E\to M}. \tag{11}$$

The proportional factor p_m defines the need of carbon mass per unit length of new organ tissues. The carbon mass flux $F_{m,E->M}$ is sink and source limited. On the one hand, if the sink organ cannot be sufficiently supplied with assimilates produced by the source organ (the carbon concentration in the source organ decreases), the control function CF in Eq. (5) approaches zero and, thus, one gets a source limitation. On the other hand, the number of cells (organ length in the elongation zone) determines the sink limitation.

Organ senescence causes some outflow of carbon F_{sens}. We set this flux proportional (factor p) to the carbon mass of the organ as a function of phyllochronic time $f(\tau)$ (cf. Eq. (15)):

$$F_{sens} = p \cdot f(\tau) \cdot m_C \,. \tag{12}$$

The balance equation for the carbon masses m_C of organs is given by:

$$\frac{dm_C^{BL}}{d\tau} = F_{m,E\to M}^{BL} - F_{sens}^{BL}, \quad F_{m,E\to M}^{BL} = p_1^{BL} \cdot F_{Z,E\to M}^{BL} + p_2^{BL} \cdot F_{Z,E\to M}^{SH}, \tag{13}$$
$$F_{sens}^{BL} = p_3^{BL} \cdot f(\tau) \cdot m_C^{BL},$$

$$\frac{dm_C^{SH}}{d\tau} = F_{m,E\to M}^{SH} - F_{sens}^{SH}, \ldots F_{m,E\to M}^{SH} = p_1^{SH} \cdot F_{Z,E\to M}^{SH}, \quad F_{sens}^{SH} = p_3^{SH} \cdot f(\tau) \cdot m_C^{SH}, \tag{14}$$

$$f(\tau) = \max(0, \min(p_4 - \tau, \tau)), \tag{15}$$

where only carbon mass of leaf blades m_C^{BL} and leaf sheaths m_C^{SH} are presented here. The first term on the right side of the ODEs (Eq. (13) and (14)) describes the contribution of organ growth proportional to the cell fluxes from blade and sheath organ. The senescence flux F_{sens}^{BL} and F_{sens}^{SH} in (Eq. (13) and (14)) is proportional to the organ carbon mass and its magnitude is determined by the time function $f(\tau)$ (Eq. (12)). The parameter p_4 determines the phyllochronic time of the onset of organ senescence. Knowing the carbon masses by solving the ODE system, then the dry mass m_T can be computed as:

$$m_T = k_{C2M} \cdot m_C, \tag{16}$$

with k_{C2M} being the unit dry mass per unit carbon mass.

Results and discussion

Based on experimental data for organ length and masses of spring barley organs, values for the parameters in the ODEs were estimated. Using the parameterized ODEs, it was possible to describe the organ dynamics (blades, sheaths, internodes) from the day of planting until ripeness of organs.

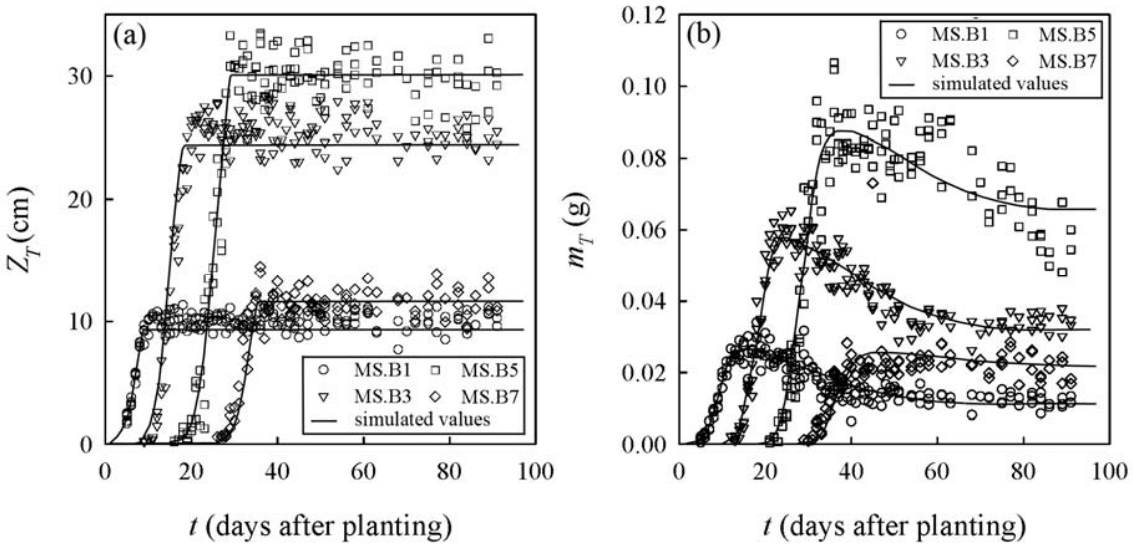

Figure 1: a) Measured values of leaf blade length (Z_T) on the main stem (MS) vs. time (t); some leaf ranks (B2, B4 and B6) were left out for clarity; b) measured values for of leaf blade dry mass (m_T) on the main stem vs. time (t); the solid lines represent the approximation of Z_T and m_T with the proposed model.

To demonstrate the performance of the model we present two examples. First, the length dynamics of leaf blades on the main stem are presented in Fig. 1a. All model parameters (values not shown) are estimated based on experimental data. Second, we tested the new approach to describe the mass dynamics of the same organs based on the formulated balance equations, fluxes and senescence rates (Fig. 1b). Results indicate that the model is capable to simulate the organ mass dynamics on the main tiller as a result of cell division, cell elongation, and mass transport to and from each plant organ.
The simulated dynamics depends on ontogenetic events. If an organ state switches from the cell division state to the state of cell elongation, a new sink creates mass fluxes towards this new organ proportional to the corresponding cell fluxes. The following questions need to be addressed in future work. How robust is the length and mass dynamics of an organ depending on the carbon supply (as e.g. influenced by the radiation conditions inside the canopy)? Which key processes can be incorporated into the model to synchronize the architecture and mass dynamics not only on the basis of characteristic times (e.g. parameters τ_a, τ_b), but on the basis of characteristic concentrations of key substrates?

Acknowledgments

The present study was funded by the DFG under grant DI 294/23 in the framework of the research unit 'Virtual Crops'. The support of the state of Saxony-Anhalt is highly appreciated.

References

Dornbusch, T., Wernecke, P., Diepenbrock, W., 2007. A method to extract morphological traits of plant organs from 3D point clouds as a data base for an architectural plant model. Ecological Modelling 200, 119-129.

Drouet, J.L. 2003. MODICA and MODANCA: modelling the three-dimensional shoot structure of graminaceous crops from two methods of plant description. Field Crops Research 83, 215-222.

Evers, J.B., Vos, J., Fournier, C., Andrieu, B., Chelle, M., Struik, P.C., 2005. Towards a generic architectural model of tillering in *Gramineae*, as exemplified by spring wheat (*Triticum aestivum*). New Phyt 166, 801-812.

Fournier, C., Andrieu, B., Ljutovac, S., Saint-Jean, S., 2003. ADEL-wheat: a 3d architectural model of wheat development. In: B.G. Hu and M. Jaeger (Ed.), 2003' International Symposium on Plant Growth Modeling, Simulation, Visualization, and their Applications. 2003' International Symposium on Plant Growth Modeling, Simulation, Visualization, and their Applications, Bejing, China PR, 54-63

Fournier, C., Durand, J.L., Ljutovac, S., Schaufele, R., Gastal, F., Andrieu, B., 2005. A functional-structural model of elongation of the grass leaf and its relationships with the phyllochron. New Phyt 166, 881-894.

Prévot, L., Aries, F., Monestiez, P., 1991. A model of maize plant morphology. Agronomie 11, 491-503.

Watanabe, T., Hanan, J.S., Room, P.M., Hasegawa, T., Nakagawa, H., Takahashi, W., 2005. Rice morphogenesis and plant architecture: measurement, specification and the reconstruction of structural development by 3D architectural modelling. Annals of Botany 95, 1131-1143.

Dynamical models for plant pattern formation

Scott Hotton and Jacques Dumais
Department of Organismic and Evolutionary Biology, Harvard University,
Biological Laboratories 1103, 16 Divinity Ave., Cambridge MA 02138
shotton@fas.harvard.edu jdumais@oeb.harvard.edu

Keywords: dynamical system, morphogenesis, pattern formation, phyllotaxis

In recent years computer models have become increasingly important in providing insights into the developmental process of plants. The study of phyllotactic patterns provides a good example of this. Despite the huge diversity of plant forms there are only a few ways in which plant organs such as leaves, florets, scales, *etc.* are arranged along a plant stem. The prevalence of a small number of phyllotactic patterns is the result of a regularly occurring process in the shoot apical meristem (SAM). Plant organs begin in the SAM as primordia which form in succession with the position of the newest primordia determined by the existing primordia. Processes such as this are well suited to being modeled with discrete dynamical systems.

This poster will present the results of a family of discrete dynamical systems [1,2] based on developmental rules proposed by Hofmeister [3] and the Snows [4]. These developmental rules are compatible [5,6,7] with recent discoveries on auxin efflux transporters in meristematic tissue [8].

These models have been analyzed both mathematically and with computer simulations. We will show that the structure of the bifurcation diagram for the fixed points of these discrete dynamical systems consists of a collection of curves inside the space of spiral lattices. The longest curves correspond to the spiral lattices whose parastichy numbers are consecutive Fibonacci numbers. Other bifurcation curves correspond to spiral lattices whose parastichy numbers are consecutive Lucas. Such patterns have also been observed in plants. We will discuss the role patterns in the early stages of plant development have in selecting which curve of fixed points are exhibited by plants thereby accounting for the prevalence of Fibonacci numbers as well as less commonly observed phyllotactic patterns.

References:

[1] Atela P., Golé C., and Hotton S., A Dynamical System for Plant Pattern Formation: A Rigorous Analys**is ,** J. Nonlinear Sci., **12** pp. 641-676 (2002)

[2] Hotton S., Johnson V., Wilbarger J., Zwieniecki K., Atela P., Gole C., Dumais J., The Possible and the Actual in Phyllotaxis: Bridging the Gap between Empirical Observations and Iterative Models, J. Plant Growth Regul. **25** pp. 313-323 (2006)

[3] Hofmeister, W., Allgemeine Morphologie der Gewachse, in Handbuch der Physiologischen Botanik, 1, Engelmann, Leipzig, pp. 405-664 (1868)

[4] Snow M, Snow R., Experiments on phyllotaxis. II--the effect of displacing a primordium. Phil Trans R Soc Lond, **222** pp. 353-400 (1932)

[5] **J**önsson, H., Heisler, M. G., Shapiro, B. E., Meyerowitz, E. M., and Mjolsness, E., An auxin-driven polarized transport model for phyllotaxis, Proc. Nat. Acad. Sci. **103** (5) pp. 1633-1638 (2006)

[6] de Reuille, P. B., Bohn-Courseau, I., Ljung, K., Morin H., Carraro, N., Godin, C., Computer simulations reveal properties of the cell-cell signaling network at the shoot apex in *Arabidopsis*, Proc. Nat. Acad. Sci. **103** (5) pp. 1627-1632 (2006)

[7] Smith, R. S., Guyomarch, S., Mandel, T., Reinhardt, D., Kuhlemeier, C., and Prusinkiewicz P., A plausible model of phyllotaxis, Proc. Nat. Acad. Sci. **103** (5) pp. 1301-1306 (2006)

[8] Reinhardt, D., Pesce, E., Stieger, P., Mandel, T., Baltensperger, K., Bennett, M., Traas, J., Friml, J., and Kuhlemeier, C., Regulation of phyllotaxis by polar auxin transport, Nature **426** pp. 255-260 (2003)

The effect of branching on cotton plant growth and development

Dong Li, Yan Guo, Zhigang Zhan
College of Resources and Environment, China Agricultural University
Beijing, China, 100094
{lidong | yan.guo | zhigang.zhan}@cau.edu.cn

Keywords: Plant development, biomass partitioning, specific leaf weight, leaf blade area

Introduction

Cotton plant development is usually predicted through a function of thermal time either at a daily step (Hanan and Hearn, 2003) or at a growth cycle (de Reffye *et al*., 1999). The GREENLAB model fits well to the architecture of some simple structured plants, e.g. pruned cotton (de Reffye *et al*., 1999) and maize (Guo *et al*., 2006). In the model, it is assumed a constant developmental rate and also stable specific leaf weight (SLW) throughout all the plant developmental stages. We are interested to see whether and how the existence of branches will influence cotton growth and development in terms of metamer production rate, SLW, and blade area profiles.

Materials and methods

The cotton (*Gossypium hirsutum* L.) cultivar DP99B was used in the field experiments under non-limiting conditions in 2006. Three treatments were conducted: (1) the control cotton plants whose branches were removed immediately after initiation; (2) two-branch cotton that remains only two vegetative branches; (3) unpruned cotton plants. Plants were weekly measured on fresh weight and area for leaf blades, the fresh weight, length and diameter for internodes.

Results and discussion

Compared with the control plants, the two vegetative branches had little effect on the main stem development, while for the unpruned cotton the developmental rate of the main stem was slowed at later stage. The presence of branching caused distinct biomass partitioning patterns in terms of compartmental partitioning coefficients. The variation of SLW between and within treatments indicates that SLWs must be treated as developmental and leaf-specific variables. The maximum area of the fully expanded leaves was smaller for branched plants. All the results are being considered in the construction and validation of a new functional structural cotton model.

Acknowledgments: This research has been supported by the Hi-Tech Research and Development (863) Program of China (2006AA10Z229).

References

de Reffye, P., Blaise, F., Chemouny, S., Jaffuel, S., Fourcaud, T., and Houllier, F., 1999. Calibration of a hydraulic architecture-based growth model of cotton plants. Agronomie. 19, pp. 265–280.

Hanan, J.S, Hearn, A.B., 2003. Linking physiological and architectural models of cotton. Agricultural Systems. 75, pp. 47–77.

Guo, Y., Ma, Y.T., Zhan, Z.G., Li, B.G., Dingkuhn, M., Luquet, D., and de Reffye, P., 2006. Parameter optimization and field validation of the functional–structural model GREENLAB for maize. Annals of Botany. 97, pp. 217–230.

Effect of the plants azimuth on light phylloclimate within a virtual maize canopy

Michaël Chelle[1] , Paul Toulouse[1]

[1] *INRA, UMR1091 Environnement et Grandes cultures, F-78850 Thiverval-Grignon – France*
chelle@grignon.inra.fr

Keywords: light phylloclimate, nested radiosity, canopy structure, maize, plant azimuth

FSPMs have mainly focused on the growth and development of a single plant, even if its parameters were measured on plants sampled in a canopy. Usually, this virtual plant was duplicated and simply translated to simulate a canopy. Improved duplication processes have introduced the inter-plant variability by randomly sampling in-field measurements. Thus, the resulting inter-plant geometry may be far from reality. For example, an actual leaf never goes through another one, when a virtual leaf can do it. However, simulating an actual inter-plant geometry would require simulating how neighbor plants "interact" to colonize free space with their respective organs, thus modeling complex processes and interactions resulting from photomorphogenesis (Ballaré et al., 1997) and thigmorphogenesis (Jaffe and Forbes, 1993). Thus, the question of the effective need of an accurate inter-plant geometry raises. This effectiveness would partly be the ability to accurately simulate physical transfer within virtual canopies, and thus satisfyingly estimate phylloclimate (Chelle, 2005) and dispersion, *e.g.,* of pathogen spores and pollen grains. Among the numerous variables characterizing the inter-plant geometry, the presented study focused on the relative azimuth of maize plants. Indeed, the distribution of leaf azimuth for a given plant results from light-driven leaf reorientation (Girardin and Tollenaar, 1992; Maddonni et al., 2002). The effect of this leaf reorientation on light interception at canopy scale was found weak and significant by Drouet et al. (1999) and Maddonni et al. (2001), respectively. These contradictory results motivated this study, which consists in assessing the importance of taking into account actual plants azimuths in virtual maize canopies to correctly simulate the light interception at canopy but also at leaf scale, the FSPMs one.

The architecture of maize miniplot (3 x 8 plants) and associated light interception profiles were measured within a maize field at various development stages in 2002 at Grignon (France). Virtual plots were built from measurement following Drouet (2003). Artificial plots were generated from the actual ones by rotating plants 2, 5, 10, 20, 30, 45, 65, 90°. Light interception on this set of real and virtual plots was calculated using the nested radiosity model (Chelle et al., 1998). Three light sources were used: a daily suncourse, a standard overcast sky, and a parallel zenith one. Results showed that taking not into account inter-plant azimuth in maize FSPMs is acceptable regarding the light interception of a whole canopy and a leaf layer, but less regarding the one of an individual plant (maximum error of 15%). Moreover, errors on inter-plant azimuth led to erratic and significative errors on the light interception of individual leaves. Another result was that the high variability of the light interception by individual leaves, *e.g.,* the coefficient of variation for leaf 10 was around 60%. These preliminary results raise two questions: how reliable are FSPMs using leaf irradiance but taking not into account inter-plant geometry and how validates the canopy architecture component of FSPMs regarding leaf irradiance estimation, knowing that integrated light variables such as soil irradiance or ground cover, are not well suited?

Ballaré C., Scopel A., Sanchez R. 1997. Foraging for light: photosensory ecology and agricultural implications. Plant, Cell & Environment, 20: 820-825

Chelle M., Andrieu B., Bouatouch K. 1998. Nested radiosity for plant canopies. The Visual Computer, 14:109-125

Chelle M.. 2005 Phylloclimate or the climate perceived by individual plant organs: What is it? How to model it? What for?, New Phytologist 166 :781-790

Drouet J. L., Moulia B., Bonhomme R. Do changes in the azimuthal distribution of maize leaves over time affect canopy light absorption? Agronomie 19: 281-294 1999

Drouet J.-L. 2003 MODICA and MODANCA: modelling the three-dimensional shoot structure of graminaceous crops from two methods of plant description. Field Crops Research 83: 215-222

Girardin P., Tollenaar M. 1992 Leaf azimuth in maize: origin and effects on canopy patterns. Eur J Agron 1:227-233

Jaffe M. J.; Forbes S. 1993. Thigmomorphogenesis: the effect of mechanical perturbation on plants. Plant Growth Regulation 12:313-324

Maddonni G., Chelle M., Drouet J.-L., Andrieu B. 2001 Light interception of contrasting azimuth canopies under square and rectangular plant spatial distributions: simulations and crop measurements. Field Crops Research 70:1-13

Maddonni G, Otegui M., Andrieu B., Chelle M., Casal J. 2002 Maize Leaves Turn Away from Neighbors. Plant Physiol. 130:1181-1189

Enhancing the simulation of a hydraulic tree-soil system by an interface between the hydraulic models HYDRA for Quercus petraea (Matt.) Liebl. and the hydraulic soil model SilVlow

Dzierzon H.[1], Schulte M., Blendinger Ch., Sloboda B., and Kurth W.

1 Corresponding author: NZ School of Forestry, Private Bag 4800, Christchurch, New Zealand
email: helge.dzierzon@canterbury.ac.nz

March 21, 2007

Hydraulic processes within trees have long been subject of research activities. Thereby, many empirical research activities base on the assumption of Darcy's law about hydraulic potentials and conductance including the soil space (e.g. Clausnitzer and Hopmans (1994)). These basic principles let Früh and Kurth (1999) create a model about the hydraulic structure within a tree including the relation between hydraulic properties and the architecture of a tree. They implemented the model in form of a simulation software they called 'HYDRA'. HYDRA numerically simulates the water potential structure within a tree and is parametrised for conifers, in particular Pinus sylvestris L. HYDRA simulates the hydraulical structure of the tree over time (usually a single day). The hydraulical structure, thereby, depends also on a conductance model which gives as a result the transpiration rate. The conductance model relies on empirical obtained micro climate information. The numerical simulation of water potentials considering the architecture causes severe numerical problems which are taken care of by a moderate restructuring of tree architecture prior to simulation. HYDRA is a very sophisticated model for the description of the hydraulic situation within a tree crown but does lack a connection to the soil-root layer. In the contrary, the initial potential which is represented at the very bottom of the tree is given by a single parameter and has to be set artificially by the user. The aim of this work was to replace this parameter by an interface to a soil-root simulation system. Here, the model HYDRA was used in a greater project which aimed at the reparameterisation of HYDRA for the tree species Quercus petraea (Matt.) Liebl. Intensive measurements were conducted to get a sufficient amount of information for parameterisation as well as for validation purposes. Hydraulic conductance and potentials are concepts well known in the area of soil sciences. In literature many models exist which describe the concepts of water flow within the soil layer. One approach is that of Blendinger (1995). He describes the hydraulic conditions in the soil layer using the finite element approach well known from physics. Blendinger (1995) created a two dimensional finite element space where the hydraulic potentials are attributed to the finite elements. Furthermore, the model allows to define root elements within these finite elements which then create a sink of hydraulic potential caused by differences of potential at the soil-root boundary. Using these root elements allows studying the impact roots have on the water flow conditions in the soil layer. Having only a two dimensional space available causes the necessity to average the hydraulic states and root information over the third dimension.
In this particular work, an interface between both above mentioned models was implemented to enhance the soil-root-tree connection in HYDRA. The aim was to improve the model in two ways: On one hand this opens the way to work with realistic initial potentials instead of an artificial single parameter, and on the other hand HYDRA gets a dynamic input at the tree-root-soil boundary. The similar concepts of both models allowed such an interface which, furthermore, allowed to study HYDRA regarding changing hydraulic soil conditions caused, e.g., by varying precipitation rates. The preliminary results show that a higher degree of realism of the simulation can be obtained. Furthermore, the pattern of the potentials within a tree has become sensitive to the hydraulic conditions in the soil and beyond that to precipitation. Thus, by introducing the interface the model HYDRA has also obtained a further interface to the environment of the tree, additional to that provided by evapotranspiration.

References

C. Blendinger. silVlow – Ein Programm zur Berechung gesättigt-ungesättigter Strömung im zweidimensionalen porösen Medium. Projektbericht 13, SFB 350 / Institut für Angewandte Mathematik, Universität Bonn, August 1995.Th.
Clausnitzer V., Hopmans J.W. (1994), "Simultaneous Modeling of Transient 3-Dimensional Root-Growth and Soil-Water Flow". Plant and Soil 164:299-314.
Früh and W. Kurth and refs. therein. The hydraulic system of trees: Theoretical framework and numerical simulation. Journal of Theoretical Biology, 201:251–270, 1999.
B. Sloboda, C. Leuschner. Numerische Simulation des hydraulischen Systems Baum-Boden bei der Traubeneiche (Quercus petraea (Matt.) Liebl.). Final Report of DFG project SL 11/8-3, http://www.uni-forst.gwdg.de/~wkurth/ber_l_schulte.pdf, 2002.

Estimation of the amount of light intercepted by a plant in natural and artificial environments: Contribution of 3D virtual plants in sunflower and *Arabidopsis thaliana*

Karine Chenu[1], Hervé Rey[2], Jean Dauzat[2] and Jérémie Lecoeur[3]
[1] INRA, UMR 759 LEPSE, 2 place Viala, 34060 Montpellier, France
[2] CIRAD, UMR AMAP, Bd de la Lironde, 34398 Montpellier, France[3] SupAgro, UMR 759 LEPSE, 2 place Viala, 34060 Montpellier, France
chenu@supagro.inra.fr - lecoeur@supagro.inra.fr

Keywords: light interception, 3D virtual plant, radiative balance model, sunflower, *Arabidospsis*.

Light interception is a major contributor to biomass accumulation of crops. Beer's law has been extensively used to estimate the amount of light intercepted by a plant at canopy level. This method, based on the use of the leaf area index (LAI), is designed for well-developed crops where the canopy is assumed to be a turbid medium (Jones, 1992). However this assumption is seldom verified and in most situations canopies are strongly heterogeneous, as for example in perennial crops such as vineyards and orchards (*e.g.* Louarn *et al.*, 2007) or in row crops during the first developmental stages or when leaf senescence occurs. We propose here to test a method based on 3D modelling to quantify the local light environment of plants in different situations, including artificial conditions.

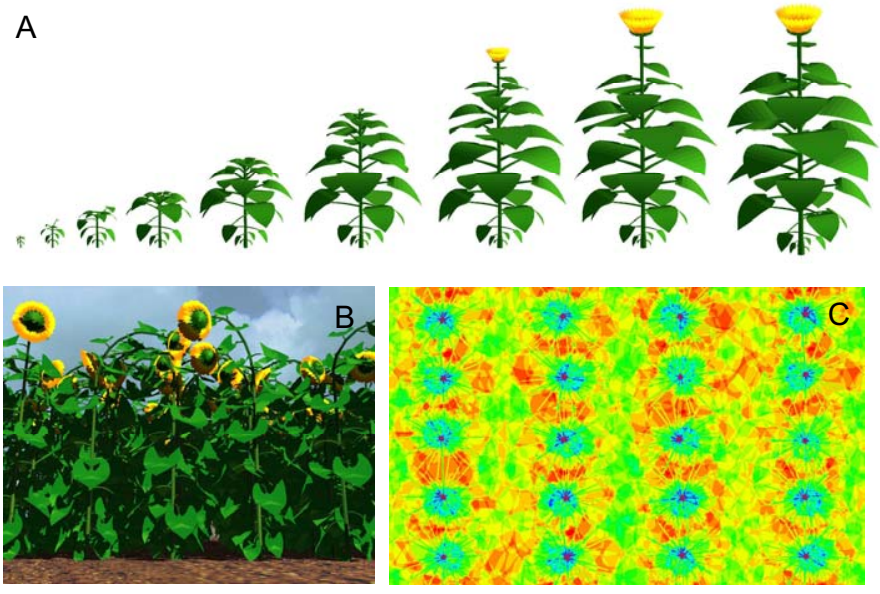

Fig. 1. (A) Change in virtual sunflower plants over time (100°Cd time step). (B) Representation of a virtual canopy of sunflower at flowering. (C) Map of intercepted light in a virtual canopy of sunflower (top view of the canopy).

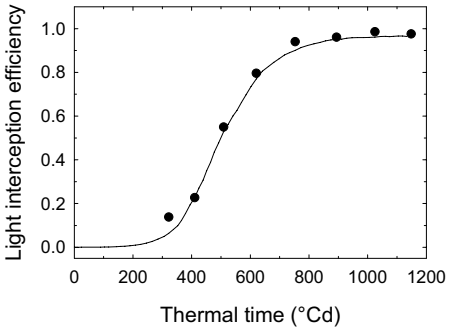

Fig. 2. Change with thermal time of observed (dots) and simulated (line) light interception efficiency for a sunflower canopy in a field experiment.

3D virtual plants built from architectural measurements (Barczi JF *et al*., 1997) were used with a radiative balance model (Dauzat and Eroy, 1997) to characterise plant-environment interactions. A multi-directional approach was chosen to take into account direct and diffuse photosynthetically active radiations (PAR) which have a major influence on the plant radiative balance. Under natural conditions, when there was no obstacle to light, the direct-diffuse PAR ratio was derived from a single measurement of solar radiation above the canopy. In artificial conditions such as growth chambers or greenhouses, because of the presence of various occulting and reflecting materials and artificial light supplies, this ratio is more difficult to estimate. PAR sensors were specifically designed to measure the directional radiations received by plants in such environments. The effective radiation climate was mimicked by different virtual light sources whose characteristics were estimated from the directional measurements.

The method was tested in sunflower and in the rosette of *Arabidopsis thaliana*, in canopy or isolated plants, from plant germination to the end of the vegetative period (Fig. 1). Experiments were carried out in natural (field), semi-controlled (greenhouse) and totally artificial (growth chamber) light environments. Various light levels were imposed and different genotypes were used to test the model relevance to environmental and genetic variations in the plant architecture.

This approach was evaluated using measurements on light interception efficiency (Fig. 2) and it was compared to classical approaches (Beer's law for sunflower; leaf area x incident PAR for *Arabidopsis*) in the different situations. The model was particularly relevant to quantify light interception for crops in early growth stages, isolated plants or artificial environments. It was also able to characterise the local environment of different genotypes and to quantify the impact of architectural modifications on light interception. This 3D virtual plant approach is proposed as a tool to analyse the genotype-environment interactions and identify new selection criteria to improve light interception which is directly related to biomass production and yield.

References

Barczi, J.F., de Reffye, P., Caraglio, Y. 1997. Essai sur l'identification et la mise en oeuvre des paramètres nécessaires à la simulation d'une architecture végétale. In. Modélisation et simulation de l'architecture des végétaux. Science Update. INRA éditions, Paris, France, pp. 205-254.

Dauzat, J., Rapidel, B., Berger, A. 2001. Simulation of leaf transpiration and sap flow in virtual plants: model description and application to a coffee plantation in Costa Rica. Agricultural and forest meteorology 109: 143-160.

Jones, H.G. 1992. Plants and microclimate. A quantitative approach to environmental plant physiology. Cambridge University pres, Cambride, UK.

Louarn, G., Guédon, Y., Lecoeur, J., and Lebon, E. 2007. Quantitative analysis of the phenotypic variability of shoot architecture in two grapevine cultivars (*Vitis vinifera* L.). Annals of Botany 99: 425-437.

Evaluating a Three-Dimensional Model of Incident Radiation in Maize Canopy

Xiping Wang[1], Yan Guo[2], Xiyong Wang[3], Baoguo Li [2*]

1. College of Resources and Environmental Sciences, Hebei Normal University, Shijiazhuang, 050016, China. 2. Key Laboratory of Plant-Soil Interaction, Ministry of Education, College of Resources and Environment, China Agricultural University, Beijing, 100094, China. 3. Department of Computer and Information Science and Engineering, University of Florida, Gainesville, FL 32611, USA.
(* Corresponding author: libg@cau.edu.cn)

Keywords: Three-dimensional model, maize canopy, photosynthetically active radiation

Introduction

The knowledge of three-dimensional (3D) radiation distribution in crop canopy is pivotal for understanding and modeling of plant eco-physiological processes (Chelle & Andrieu 1999; Sinoquet *et al*. 2000; Dauzat *et al*. 2006). A 3D model for simulating the distribution of incident radiation (3DIRM) in crop canopy is evaluated in this paper.

The modelling scheme

The static virtual canopy was reconstructed by representing organ surfaces as little triangular facets positioned according to the 3D digitized data by Fastrak digitizer (Polhemus, USA). Parallel projection and Z-buffer algorithms (Chelle & Andrieu 1999; Espana *et al*. 1999; Maddonni *et al*. 2000) were utilized to simulate the sunfleck area ratio and the intensity of solar beam radiation to every facet in canopy. A sub-model, named as DSHP (Dividing Sky Hemisphere with Projecting), was set up for computing the incident diffuse radiation in crop canopy (Wang *et al*., 2006). The total incident radiation in canopy could be calculated by just summing up the solar beam and incident diffuse radiation to each canopy facet.

Evaluating the model with field experiment

A mast was built for supporting an AccuPAR ceptometer (Decagon Devices Inc. USA) to measure the 3D PAR distribution in maize canopy and an additional point PAR sensor, LI-190SA, to simultaneously measure the incoming PAR above canopy. The field measurements were carried out in maize canopies in the early filling stage near Beijing in 2002 (Wang *et al*., 2006).

Based on the assumption that the intensity of beam PPFD (Photosynthetically photon flux density) was much higher than sky diffuse PPFD under sunshine conditions, when an AccuPAR sensor registered PPFD in canopy more than beam PPFD that had been estimated from the global PPFD measured by the LI-190SA above canopy, then this sensor point was considered to be sunfleck. Sunfleck area ratio was set to be the ratio of the number of sunfleck sensors and the total sensor number for each height. The sensors with PPFD lower than beam PPFD was set to be umbrage. The

average total and diffuse PPFD was calculated by averaging the PPFD values among all the AccuPAR sensors and only the umbrage sensors at each height.

In model evaluation, the simulated incident diffuse PPFD was slightly lower than the measured diffuse PPFD that included incident diffuse PPFD and secondary scattering PPFD by canopy elements, with a mean error of ME (Mean Error) =20.78 μmol m^{-2} s^{-1} (Refer to Wang *et al*. 2006) for detailed information). The simulated total incident PPFD ($PPFD_{sim}$) and sunfleck area ratio (FR_{sim}) were consistently close to the measured results ($PPFD_{obs}$ and FR_{obs} respectively) with correlation equations of $PPFD_{sim}$=1.026$PPFD_{obs}$ (μmol m^{-2} s^{-1}) with R^2=0.95 (n=74), and FR_{sim}=0.810FR_{obs}+4.10 (μmol m^{-2} s^{-1}) with R^2=0.96 (n=74).

Discussion

The 3DIRMS model achieved incident PAR (Photosynthetically active radiation) and sunfleck area estimation very close to the measurement. DSHP sub-model generated obvious errors with neglecting secondary scattering in canopy in diffuse PAR estimation. Nevertheless diffuse PAR only occupied a small proportion of total PAR in crop canopy during sunny daytime, thus DSHP sub-model can be an usful tool for incident diffuse radiation simulation in crop canopy.

It is difficult to carry out a 3D radiation measurement *in situ* in a real crop canopy. We hope the methodology of 3D measurement of PAR in maize canopy for evaluating a 3D radiation model introduced in this paper is referential to related studies.

Acknowledgements

This study was sponsored by "863" Hi-Tech Research & Development Program of China (2006AA10Z229), the Program for Changjiang Scholars and Innovative Research Team in University (IRT0412) and Research Foundation of Hebei Normal University (L2004B13). Dr. Yuntao Ma, Mr. Zhicai Zhang and Meiping Wen gave a lot help in field measurements and data treatments.

References:

Chelle, M., Andrieu, B., 1999. Radiative models for architectural modeling. Agronomie. 19, pp. 225-240.

Dauzat, J., Franck, N., Rapidel, B., Luquet, D., Vaast, P. 2006. Simulation of ecophysiological processes on 3D virtual stands with the Archimed simulation platform. PMA06: The Second International Symposium on Plant Growth Modeling, Simulation, Visualization and Applications. November 13-17, 2006, Beijing, P.R. China.

Espana, M., Baret, F., Aries, F., Andrieu, B., Chelle, M. 1999. Radiative transfer. sensitivity to the accuracy of canopy structure description. The case of a maize canopy. Agronomie 19, pp. 241-254.

Maddonni, G. A., Chelle, M., Drouet, J. L., Andrieu, B. Light interception of contrasting azimuth canopies under square and rectangular plant spatial distribution: simulations and crop measurements. Field Crop Res. 2001, 70: 1-13.

Sinoquet, H., Rakocevic, M., Varlet-Grancher, C. 2000. Comparison of models for daily light partitioning in multispecies canopies. Agric. For. Meteorol. 101, pp. 251-263.

Wang, X. P., Guo, Y., Li, B. G., Wang, X. Y., Ma, Y. T., 2006. Evaluating a three dimensional model of diffuse photosynthetically active radiation in maize canopies. Int. J. Biometeorol. 50, 349-357.

Evaluation of a turbid medium model to simulate light interception by plant canopies at three spatial scales

D. COMBES[(1)], M. CHELLE[(2)], H. SINOQUET[(3)] , A.J. ESCOBAR-GUTIERREZ[(1)], C. VARLET-GRANCHER[(1)]

(1) INRA, UR4 Unité d'Ecophysiologie des Plantes Fourragères, BP 6, F-86600 Lusignan, France
(2) INRA, UMR1091 Environnement et Grandes cultures, F-78850 Thiverval-Grignon – France
(3) UMR547 PIAF, INRA, Université Blaise Pascal, F-63100 Clermont Ferrand, France
didier.combes@lusignan.inra.fr

Keywords: Radiative Transfer, Turbid Medium, Computer Model

Light is one of the most important environmental factors to be included in functional-structural models of plants and plant communities to simulate key biophysical processes involved in plant growth and development, such as photosynthesis, evapotranspiration, and photomorphogenesis. Such inclusion would require the simulation of light interception at organ scale. To achieve this goal, two approaches are possible.
The first way is to consider the plant canopy as a turbid medium in which radiation attenuation is described by the Beer-Lambert law (NILSON, 1971; ROSS, 1981). The second way is based on virtual representation of plants where light interception is computed from the projection of vegetation components in a given direction (Chelle et al, 1998) (i.e. without light scattering).
Only few studies have shown the comparison between turbid medium and computer simulation models (CHEN *et al.*, 1997; PINTY *et al.*, 2000; SINOQUET et al., 2005).
In this study, we assessed the hypothesis of leaf random dispersion in the Beer-Lambert law at three scales (the whole canopy, horizontal layers and local scale). We compared two calculation methods of radiation interception: one using the Beer-Lambert law (with three dimensional turbid medium model; RIRI, SINOQUET and BONHOMME, 1992) and the other based on simulation models (CANESTRA, Chelle et al, 1998); multiple scattering having not been taken into account in this study. The two models were compared by applying the calculations to two walnut trees and two sorghum canopies which present contrasted structure characteristics. The structures of these canopies were measured in three dimensions in order to take into account the arrangement and orientation features of the plant elements. Main results were that interception computations were satisfying at the whole canopy and layer scale whatever the canopy considered. However, at locale scale, discrepancies turbid medium showed high difficulty in estimating light interception.

References

CHELLE M., ANDRIEU B., BOUATOUCH K. 1998 Nested radiosity for plant canopies. The Visual Computer, 14:109-125
CHEN, J. M., BLANKEN, P. D., BLACK, T. A., GUILBEAULT, M. and CHEN, S. (1997). "Radiation regime and canopy architecture in a boreal aspen forest." Agricultural and Forest Meteorology **86**: 107-125.

NILSON, T. (1971). "A theoretical analysis of the frequency of gaps in plant stands." Agricultural and Forest Meteorology **8**: 25-38.

PINTY, B., GODRON, N., WIDLOWSKI, J.-L., BACOUR, C., GASCON, F., et al. (2000). "The RAdiation transfer Model Intercomparison (RAMI) Exercise." Journal of Geophysical Research **in press**.

ROSS, J. (1981). The Radiation regime and architecture of plant stands. The Hague, Dr Junk Publishers.

SINOQUET, H. and BONHOMME, R. (1992). "Modeling radiative transfer in mixed and row intercropping systems." Agric. For. Meteorol. **62**: 219-240.

SINOQUET, H., SONOHAT, G., PHATTARALERPHONG, J., GODIN, C. (2005). Foliage randomness and light interception in 3D digitised trees: an analysis from multiscale discretisation of the canopy. Plant Cell and Environment, 28, 1158-1170.

Examining the influences of canopy structure on the light distribution and canopy productivity of cucumber using a 3D structural plant model approach

Dirk Wiechers, Katrin Kahlen and Hartmut Stützel
Institute of Biological Production Systems, Leibniz Universiät Hannover
Herrenhäuser Straße 2, 30419 Hannover, Germany
wiechers@gem.uni-hannover.de

Keywords: light interception, radiation transfer, 3D canopy architecture, *Cucumis sativus* L., crop modelling

Introduction

Greenhouse cucumber production systems are usually intensively managed close to the optimum with light as a major limiting growth factor. To understand the effects of light distribution on productivity in terms of photosynthesis, a spatial examination of this driving force of productivity is required. Cucumber is usually grown in a distinct row structure, resulting in an uneven distribution of leaf area and light. This makes it a well suited crop for examining the effects of heterogeneous canopies on light distribution and productivity.

Material and Methods

To test plant and environment interactions, four canopy architectures with two different plant densities and spatial structures were analyzed (Wiechers et al., 2006). The experimental setup included measurements of plant architecture by 3D-digitizing, leaf level measurements of photosynthetic active radiation (PAR) in the greenhouses and leaf gas exchange measurements of photosynthesis in the growth chamber. Plants were digitized weekly to build a static model of plant architecture accompanied by PAR measurements.

To obtain parameters for the light interception virtual images of the plants (www.povray.org) were rendered in a vertical direction (zenith angle 0°) to the ground plane (Sinoquet et al., 1998). Sunlit and shaded leaf area were distinguished using a projection algorithm to get a measure for the fraction of sunlit leaf area. The intensity of direct light on the sunlit leaf area was calculated by the incoming PAR intensity depending on the angle between irradiance vector and area normal derived from the static model. The radiation transfer on the shaded leaf parts (diffuse light) was calculated based on data measured on single leaves within the canopy. Intensities of the sunlit and shaded leaf areas were used to calculate the corresponding rates of photosynthesis based on a Farquhar-Model (Farquhar et al., 1980; Kim and Lieth, 2003) parameterized for greenhouse cucumber. Calculating these rates from a single leaf over leaf cluster of five leaves up to plants or a whole canopy allows us to identify the effects of canopy architecture on productivity.

Preliminary results and prospect

First results show that for a precise modeling of the assimilation of a heterogonous crop it is necessary to consider the spatial and dynamical differences in light distribution and photosynthesis. For the first productive weeks of the canopy an increase up to 6% in the rate of photosynthetic assimilation per m² ground can be simulated for the same plant density only due to a change of the canopy structure from a row crop to an isometric stand.

Future prospects will be to couple a radiation transfer model with modules of photosynthesis and assimilate allocation to one functional-structural model.

Acknowledgments
This research has been supported by grants from the German Research Foundation (DFG).

References

Farquhar, G. D., Caemmerer, S. and Berry, J. A. (1980). A biochemical model of photosynthetic CO_2 assimilation in leaves of C_3 species. *Planta* 149, 78-90.

Kim, S. H. and Lieth, J. H. (2003). A coupled model of photosynthesis, stomatal conductance and transpiration for a rose leaf (*Rosa hybrida* L.). *Annals of Botany* 91, 771-781.

Sinoquet, H., Thanisawanyangkura, S., Mabrouk, H. and Kasemsap, P. (1998). Characterization of the light environment in canopies using 3D digitising and image processing. *Annals of Botany* 82, 203-212.

Wiechers, D., Kahlen, K. and Stützel, H. (2006). A method to analyse the radiation transfer within a greenhouse cucumber canopy (Cucumis sativus L.). *Acta Horticulturae* 718, 75-80.

Experimental and model evidence for complementary resource use in mixed-species rainforest tree plantations

Anna E. Richards[A], Susanne Schmidt[B] and Jim Hanan[C]

[A]Department of Biological Sciences, Macquarie University, Australia (arichards@bio.mq.edu.au)
[B]School of Integrative Biology, University of Queensland, Australia
[C]ARC Centre for Complex Systems and Advanced Computational Modelling Centre, University of Queensland, Australia

There is a growing scientific interest in tree plantations of high-value native rainforest timbers, planted as mixtures, in subtropical and tropical Australia. These plantations can provide ecological benefits, such as improved nutrient cycling and restoration of biodiversity, which cannot be provided by monoculture plantations. In addition, there is evidence that mixed-species plantations are more productive than monocultures if species interact in a complementary fashion. Most designs of rainforest tree mixtures are based on the concept that pairings of fast growing and light demanding species are less productive than pairings of species with different shade tolerances, although there is minimal data to support this assumption. We examined the dominant paradigm that mixtures of two fast growing species (*Grevillea robusta* and *Elaeocarpus angustifolius*) compete for site resources, while mixtures of shade tolerant (*Castanospermum australe*) and shade intolerant (*G. robusta* or *E. angustifolius*) species are complementary. Ecophysiological characteristics of young trees grown in a mixed-species plantation in subtropical Queensland were studied to determine interactions between species for nutrients. Plant characteristics were also entered into a physiologically based canopy model (MAESTRA, an updated version of MAESTRO[1,2]) to test hypotheses of interactions between species for light. MAESTRA uses plant functional attributes (such as leaf biochemistry) and structural variables to simulate radiation absorption and photosynthesis by individual plants in a stand. Essentially, a forest is represented as a three-dimensional array of tree crowns with a defined canopy shape and leaf distribution. Each crown is given an *x* and *y* co-ordinate, height, trunk space, canopy radius and one-sided leaf area. Radiation interception, photosynthesis and stomatal conductance are calculated for a target crown which is divided into 72 subvolumes (6 horizontal layers separated into 12 gridpoints). Interception of both beam and diffuse radiation for each subvolume is calculated and used to drive leaf models of photosynthesis[3] and stomatal conductance[4].

Contrary to predictions, there was experimental evidence for complementary interactions between the fast-growing species in terms of nutrient uptake, nutrient use efficiency and nutrient cycling. *E. angustifolius* had maximum demand for soil nutrients (79 g nitrogen (N) and 7 g phosphorus (P) tree^{-1}) during summer, efficient internal recycling of N (56% resorption from senescing leaves), produced a large amount of nutrient rich litter and had low P use efficiency at the leaf (70 μmol CO_2 (g P)$^{-1}$ s^{-1}) and whole plant level (3118 g biomass (g leaf P)$^{-1}$ y^{-1}). In contrast, *G. robusta* had high nutrient use efficiency for both N (7 μmol CO_2 (g N)$^{-1}$ s^{-1} and 198 g biomass (g leaf N)$^{-1}$ y^{-1}) and P (194 μmol CO_2 (g P)$^{-1}$ s^{-1} and 5600 g biomass (g leaf P)$^{-1}$ y^{-1}), maximum demand for soil nutrients (239 g N tree^{-1} and 9 g P tree^{-1}) in spring and produced litter low in nutrients.

MAESTRA simulations were performed for each species planted as a monoculture and results re-interpreted for a mixed species scenario. *E. angustifolius* monoculture

simulations reduced rates of canopy photosynthesis by 70% compared to a single tree scenario. *G. robusta* maintained the highest rates of gross and net photosynthesis (5.4 mol CO_2 $tree^{-1}$ d^{-1}) of the three species, while *C. australe* suffered comparatively little reduction in photosynthetic rates (19%), in a monoculture design compared to isolated trees. Initial model simulations tend to support the original hypothesis that mixtures of two light-demanding species (*E. angustifolius* and *G. robusta*) may not be as productive as combinations of shade tolerant (*C. australe*) and shade intolerant species.

However, in its present form, the MAESTRA model results have limited applicability for mixed-species plantations because they only simulate a single species stand scenario. Currently, the MAESTRA model is being modified to allow neighbouring trees to have a different canopy architecture and foliage distribution compared to the target tree. The combination of computer models and empirical data offer a new approach for analyzing stand dynamics in mixed-species plantations as well as establishing testable hypotheses that could be applied to a large-scale experimental system of replicated mixture and monoculture plots.

[1]Wang, Y. P., Jarvis, P. G. (1990) Description and validation of an array model – MAESTRO. *Agricultural and Forest Meteorology*, 51: 257-280.
[2]Medlyn, B. E. (2004) A MAESTRO retrospective. In *Forests at the Land-Atmosphere Interface*. Eds. M. Mencuccini, J. Grace, J. Moncrieff and K. G. McNaughton. CAB International, Wallingford, pp 105-121.
[3]Farquhar, G. D., von Caemmerer, S., Berry, J. A. (1980) A biochemical model of photosynthetic CO_2 assimilation in leaves of C3 species. *Planta,* 149: 78-90.
[4]Ball, J. T., Woodrow, I. E., Berry, J. A. (1987) A model predicting stomatal conductance and its contribution to the control of photosynthesis under different environmental conditions. In *Progress in Photosynthesis Research vol 5, proceedings of the VII International Photosynthesis Congress*. Ed. I Biggins. Martinus Nijhoff, Dordrecht, pp. 221-224.

Exploring morphogenetical gradient variability using hidden Markov tree models in young individuals of the tropical species *Symphonia globulifera* (Clusiaceae).

Patrick Heuret[(1)], Jean-Baptiste Durand[(2)], Eric Nicolini[(3)],
Sabrina Coste[(4)], Yves Caraglio[(3)]

(1) INRA, (3) CIRAD, UMR Botanique et Bioinformatique de l'Architecture des Plantes (AMAP)
TA A-51/PS2, 34398 Montpellier Cedex 5, France
{heuret|nicolini|caraglio}@cirad.fr
(2) Laboratoire Jean Kuntzmann – INRIA *Virtual Plants* – Grenoble Universités
51 rue des Mathématiques, BP 53, 38041 Grenoble Cedex 9, France
jean-baptiste.durand@imag.fr
(4) INRA, UMR Ecologie des Forêts de Guyane (ECOFOG)
BP 709, 97387 Kourou Cedex, Guyane Française
coste_s@kourou.cirad.fr

Keywords: *Symphonia globulifera*, physiological age, hidden Markov tree, morphogenetical gradients, growth strategy

In uneven-aged tropical rainforests, mechanisms of recruitment, *i.e.* the sustainable appearance of new individuals, rests on many mechanisms such as the phenology of flowering and dissemination, the survival of seedlings and their waiting capacities in the understorey (Oldeman, 1974). To understand how long young trees can survive in the understorey before reaching the canopy and with which morphological adaptations, a precise study of their morphology and their architecture is capital. Objectives of such descriptive approaches are (i) to identify the rules of plant construction; (ii) to apprehend their phenotypical plasticity in light stress conditions and their waiting capacities; (iii) to determine morphological markers that can inform about the development potential of the considered individual; and finally (iv) to provide information on the plant environment and its life-history directly integrated in the perennial structure of the tree.

The aim of this work is to characterize the phenotypical plasticity of young individuals of *Symphonia globulifera* L. f. (Clusiaceae), a species of South America and Africa tropical forests. A first set of data concerns 30 two-year-old individuals raised in a nursery in French Guyana under three different light treatments (5%, 10% and 20% of incident light). The morphological changes of the growth units (GUs) were explored using a hidden Markov tree model (HMT) that permits to identify homogeneous structures and their succession in a tree structure (Durand et al., 2005). For each GU, three variables were taken into account: the number of cataphylls, the number of leaves and the length. The estimated model permits us to identify seven well differentiated types of GUs. The HMT parameters allow these types to be interpreted as follows: the first one corresponds to the GU issued from germination; the second and third types characterize GUs issued from the branching process with a lower number of cataphylls; the 4 other types express a gradient of vigor characterized by an increasing length of the GUs and of their number of leaves. Considering transitions between these different GU types, we highlight various trajectories of tree development in relation to light environment. A second data set concerns 25 individuals of natural French Guyana forest growing up to 2m50 without knowledge about the age or the past growth of the trees. The structure of the trees was described and modelled according to the same protocol as the nursery trees. Comparison with the trees of the nursery enables us to make strong assumptions about the waiting capacities in understorey of this species and on the growth dynamics during time of the measured individuals.

In restricted light availability conditions, trees desynchronize and develop more GUs on the branches than on the trunk, thus forming a plate. The growth on the trunk occurs by elongation of very short GUs only, which are made up of one pair of cataphylls, a pair of leaves and one ultimate pair of cataphylls. Trees showing equivalent height and diameter can be constituted by a very different number of Gus, thus indicating a potentially very high difference in age, and consequently a great waiting potentiality in the understorey for this species.

References :

Durand, J.-B., Guédon, Y., Caraglio, Y., Costes, E., 2005. Analysis of the plant architecture via tree-structured statistical models: the hidden Markov tree models. *New Phytologist,* 166 (3) : 813-825.

Oldeman, R. A. A., 1974. L'architecture de la forêt guyanaise. Mém. ORSTOM, 73 : 204 p

Fast Forest Visualization on Hierarchical Images and Visibility

Qingqiong DENG[1,2], Xiaopeng ZHANG[1,2], Xiangdong LEI[3], Marc JAEGER[4]

[1]Sino-French Laboratory LIAMA, CAS Institute of Automation, Beijing, China
[2]National Laboratory of Pattern Recognition, CAS Institute of Automation, Beijing, China
[3]CAF Institute of Forest Resource Information Techniques, Beijing, China
[4]INRIA-Rocquencourt, Project DigiPlante, CIRAD AMAP, Montpellier, France
{qqdeng, xpzhang}@nlpr.ia.ac.cn, xdlei@caf.ac.cn, jaeger@cirad.fr

Keywords: plant, forest, visualization, level of detail, multi-resolution, billboard, visibility

Introduction

Fast visualization of plant functional and structural information facilitates the understanding of the natural disturbance of trees in a forest. It is an important work in forest management on forest growth, species composition, forest structure and dynamic changes at different scales. Plant growth modeling has been widely researched, and many successful methodologies have been developed, such as L-system (Prusinkiewicz et al, 1990) and GreenLab (Yan et al, 2004). Using such approaches, plant modeling is efficient with high realism. However, the geometric complexity of representing a forest with thousands of plants usually far exceeds the processing and rendering capabilities of current computer hardware. Thus, specific software techniques should be developed for fast forest visualization.

One efficient rendering technique is the image-based rendering. Complex geometry of trees is represented by a few texture-mapped polygons (Meyer et al, 2001), so that the rendering is drastically accelerated. Unfortunately, classical image-based methods usually produce weak parallax effects due weak geometry. Billboard clouds (Behrendt et al, 2005) show a better balance between plant geometry and parallax with a static set of free oriented billboards. However, this method consumes immense memory for textures, and foliage occlusion is not considered.

We propose an improved approach with billboard clouds for interactive visualization of functional structural plant models. A billboard hierarchy is generated corresponding to the plant topology in preprocessing. And a view-dependent billboard level is chosen from the hierarchy to represent the geometry on both distance and visibility of the plant in rendering. Besides, The plant self-similarity (Ferraro et al, 2005) is applied to reduce the memory cost for textures.

Hierarchical Structure of Billboards for Foliage

The hierarchical structure of a plant is use here, where the side branch of the trunk is called as level-1 branch, and their children branches are called as level-2 branch, etc. We define a sub-tree structure for each branch as a set of all its successor branches, their associated leaves and the branch itself. Then a billboard is generated corresponding to each sub-tree level. The form and the number of all billboards in a sub-tree are calculated through the approach of Behrendt (Behrendt et al, 2005) according to the size of the bounding box of the sub-tree. For each billboard, a texture is created for each side by an orthogonal projection of all included geometry onto the billboard. The resolution of all textures is independent of the bounding box size, but it is defined by the user.

One optimal case to represent a sub-tree with a billboard happens when the projected size of the sub-tree equals to the size of the billboard. For each sub-tree, a distance, called optimal distance, is calculated so that the optimal projection will happen. After obtaining optimal distances for all sub-trees, the billboards are organized into a hierarchical data structure according to the levels of their corresponding branches. The optimal distance of each billboard is recorded also.

In rendering, the hierarchical structure is traversed until reaching proper nodes, whose optimal distances are not larger than the current distance between the rendered tree and the viewer. In this way, an appropriate LOD model is obtained. In order to alleviate popping artifacts between different levels, neighboring LOD level of textures are alpha blended.

Visibility Algorithm

The positions of branches give a strong hint about the occlusion of organs: leaves held by "rear branches" are more often occluded by other leaves and branches than those held by "front branches". Based on this observation, Deng et al. propose a simple visibility algorithm (Deng et al. 2007) of some leaves on the dot product of the viewing direction and direction of the level-1 branch, which holds the leaves. If the product is positive, all leaves held by this branch are as more or less occluded. But this algorithm does not guarantee a precise visibility. As shown in Fig.1(a), if level-1 branches distribute sparsely around the trunk, the rear branches and leaves (in blue) will not be occluded by the front ones (in green).

In order to overcome the above drawback, the density of level-1 branch is considered as another visibility parameter for each level-1 branch in this new approach. This density is defined as the number of sibling branches falling in the neighborhood of the considered branch (see Fig.1(b)). Then, if a branch is located in a space with low density, the branch and its leaves should be considered as visible, even its corresponding dot product is positive.

Therefore, the density-adapted visibility is used as a scaling factor on the distance in rendering, so that when traversing the hierarchical structure, the optimal distances of occluded sub-trees will be compared with scaled distances. In this way, invisible regions of a tree are rendered with less detail than the visible, so that fewer billboards are rendered while visual quality is maintained.

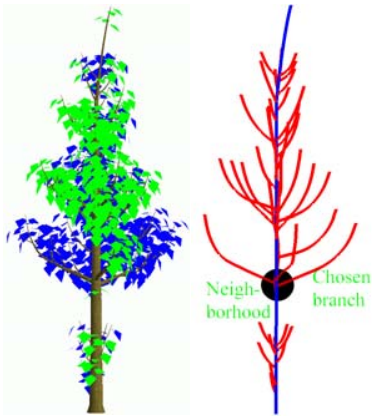

(a) Front view (b) Density definition

Fig. 1: Visibility calculation

Memory Strategy

However, like other image-based approaches, the memory cost for the texture images of all sub-trees is still a bottleneck in our algorithm. Fortunately, trees show self-similarities: leaves of a tree look like each other, and a branch may be similar to several others. Even one whole tree looks like another tree with the same species and a similar age. So a tree can be represented by a small number of representative sub-trees. Two sub-trees are represented by a common instance if they have the same levels and similar number of leaves, as well as similar number of child branches. Only representative texture images are saved, and one representative is assigned to a sub-tree of the plant. As a result, the memory cost is dramatically reduced.

Application to Forest Management

With this technique, a visualization tool is constructed for tree crown health monitoring (such as color and the number of leaves) and silviculture decision (for example, thinning and selective logging). Structural information was combined with individual empirical growth models here for tree growth projection (Lei et al., 2006). Visualization techniques developed in our study, in conjunction with GIS, were applied to demonstrate the application of realistic visualizations to depict the dynamic change of forest resource at the stand level and the landscape level. Fig. 2 shows an example of larch-dominant mixed forest with spruce, fir, ash and birch etc. in Northeast China. 4992 tree samples are included in this forestry. The shadow is generated through stencil buffer and

the projective mapping of billboards on a planar ground. The rendering speed is 2 to 12 frames per second for shading and shadows on the ground.

Fig. 2 Interactive visualization of a larch-dominant mixed stand

Conclusion

We propose a view-dependent image-based rendering method in this paper to construct multi-resolution models for trees and plants. Rendering of both single plant (or stand) and forest (or landscape) are supported. Compared with other image-based methods, the main advantages of our method consist in multi-resolution representations, view-dependency, lower memory costs, and higher efficiency in pre-processing leading to higher data compression. Therefore, a proper frame rate is realized in rendering, and it can thus be used for the applications in forestry visualization.

This approach can only be used to static trees and static plants, so it cannot be directly used for rendering a developing forest. Popping artifacts is still obvious, so that a more continuous method should be developed in the future. Furthermore, at present, only the occlusion within a tree is considered. A more promising aspect, the occlusion among different trees should be taken into account in our future work for further decrease of the geometric complexity.

Acknowledgments

This work is supported in part by National Natural Science Foundation of China projects No. 60073007, 60473110, 30371157; in part by National High-Tech Research and in part Development 863 Plan of China project No. 2006AA01Z301; part by the French National Research Agency within project NATSIM ANR-05-MMSA-45; and by LIAMA funding with the project GreenLab.

References

Behrendt, S., Colditz, C., Franzke, O., Kopf, J., Deussen, O. 2005. Realistic Real-time Rendering of Landscapes Using Billboard Clouds. Proceedings of Eurographics 2005, 24(3), pp.507-516.

Deng, Q. Q., Zhang, X. P., and Jaeger, M. 2007. View-dependent Hierarchical Foliage Simplification. Proceedings of The 2nd International Conference of E-Learning and Games, Lecture Notes in Computer Science, pp 44-55.

Ferraro, P., Godin, C. and Prusinkiewicz, P. 2005. Toward a quantification of self-similarity in plants. Fractals, 13, 91-109.

Lei X., Zhang Z., Chen X. 2006. Crown-width prediction models for several tree species including Larix olgensis in northeastern China, In Chinese, Journal of Beijing Forestry University, 28(6), pp.75-79.

Meyer A., Neyret F., Poulin P. 2001. Interactive rendering of trees with shading and shadows. In Eurographics Workshop on Rendering Techniques, pp. 183-196.

Prusinkiewicz, P. and Lindenmayer, A. 1990. The Algorithmic Beauty of Plants, Springer-Verlag, New York.

Yan, H. P., Kang, M.Z., de Reffye, P. and Dingkuhn, M. 2004. A dynamic, Architectural Plant Model Simulation Resource-dependent Growth, Annals of Botany, 93, pp.591-602.

From ALife Plant Models toward Evolutionary FSPM

Stefan Bornhofen and Claude Lattaud
LIAP5, Université de Paris 5, 45 rue des Saints-Pères, 75006 Paris, France
{stefan.bornhofen|claude.lattaud}@math-info.univ-paris5.fr

Keywords: artificial evolution, artificial life, plant communities, population dynamics

The Plant Model

The complexity of current functional-structural plant models (FSPM) most often involves a computational cost per individual which renders simulations of large plant communities difficult to realize. Moreover, such models are typically designed or customized for scenarios of specific natural species without genetic change. Complementarily, an amount of studies on plants have been carried out within the research field of Artificial Life. Their primary objective is the application of bottom-up design, especially evolutionary algorithms, in the context of plant development. In such models, plants are typically represented as structures based on a set of morphological growth rules with no or only minimal physiology and interactions with their environment. Priority is given to simplification, and the emerging results are qualitatively compared to observations on natural plants.
To bridge the gap between these two approaches, a plant model of intermediate complexity has been developed and implemented as a simulation platform. Based on Artificial Life concepts, the virtual plants combine a physiological transport-resistance model [5] with a morphological model using the L-system formalism [4] and grow in a 3D artificial ecosystem which provides light and soil nutrients. The plant development is ruled by a set of genetic information which describes parameters concerning morphological as well as physiological processes. To reproduce, the virtual plants are able to grow flowers and seeds which hold, depending on the study, either an exact (population level) or a mutated (evolutionary level) copy of the mother plant genotype.

Simulations and Results

To illustrate the possibility of using the model as an investigation tool at population level, a series of simulations on intra- and interspecific competition for resources were conducted and subsequently compared to the corresponding Lotka-Volterra differential equations [3]. Despite its simplicity, the plant model was able to not only qualitatively reproduce the dynamics of the aggregate model, but also to assess the influence of various biotic and abiotic parameters such as the range of seed dispersal or the soil diffusion rate whose impact on population dynamics is difficult to describe in concise mathematical formulas.
The major advantage of the presented model is its potential to study evolution in plant communities. Two previous papers already discussed the evolutionary adaptation of some morphological and life history traits and compared the results to growth patterns of natural plants. In [2], the conducted simulations allowed to reveal developmental constraints on the placement of flowers within a plant architecture, and to observe morphological responses to different resource dispositions in the environment. The simulations in [1] addressed the trade-off between resource allocation to vegetative and reproductive structures. It was shown that the introduction of an age at maturity enhances both life history traits. Furthermore, depending on the competitive pressure plants evolved more investment of resources into growth than into reproduction.
As the results at both population and evolutionary levels corroborate some assertions and hypotheses of theoretical biology, the presented model may be a promising approach to capture important dynamics within plant communities and notably to broaden the scope of FSPM to evolution.

References

[1] Bornhofen S., Lattaud C. (2006) Life History Evolution of Virtual Plants : Trading off between Growth and Reproduction. Lecture Notes in Computer Science 4193, Springer-Verlag, 808-817
[2] Bornhofen S., Lattaud C. (2007) Evolution of Virtual Plants interacting with their Environment, in Proceedings of the 9th International Conference on Virtual Reality (VRIC'07), 172-176
[3] Lotka A.J. (1924). Elements of physical biology. Williams and Wilkins, Baltimore, Maryland, USA
[4] Prusinkiewicz P., Lindenmayer A. (1990) The Algorithmic Beauty of Plants, Springer-Verlag, Berlin
[5] Thornley J.H.M. (1998) Modelling shoot:root relations:the only way forward?, Ann.of Bot. 81,165-171

A functional-structural model of rice (*Oryza sativa* L.) linking morphogenesis with quantitative trait loci

Lifeng Xu[1], Ole Kniemeyer[2], Jun Zhu[1] and Gerhard Buck-Sorlin[3,*]
[1]Institute of Bioinformatics, Zhejiang University, Hangzhou, P.R. China, 310029
[2]Dept. of Computer Science, Chair for Practical Computer Science / Graphics Systems, Brandenburg Technical University Cottbus, Ewald-Haase-Str. 12/13, D-03044 Cottbus, Germany
[3]Crop and Weed Ecology Dept., Wageningen University and Research Centre, Haarweg 333, 6709 RZ Wageningen, The Netherlands; gerhard.buck-sorlin@wur.nl; *corresponding author

Keywords: Rice, *Oryza sativa* L., Quantitative Trait Loci (QTL), L-system, GroIMP

Rice (*Oryza sativa* L.) is the most important staple food in East and Southeast Asia. Possessing the shortest genome of the Gramineae crops, it is furthermore a model plant of crop plant genetics, with a fully sequenced genome and many studies on quantitative inheritance of agronomical and morphological traits on offer for modelling (e.g., Zhang et al. 2006).
Previous architectural modelling approaches dealing with rice have been largely descriptive and based on morphometric datasets (Watanabe et al. 2005). Buck-Sorlin and Bachmann (2000) introduced a simple method to link virtual genes (Mendelian and quantitative) with morphogenetical rules, the latter implemented as L-system production rules, at the example of barley. Buck-Sorlin et al. (2005) showed how a virtual genotype could be connected to a biosynthesis network and rules simulating architectural development, using relational growth grammars which are an extension of the L-system formalism.
We have created a conceptual model of rice architectural development to reproduce different morphological phenotypes from a genotype consisting of a set of virtual QTLs for spikelet and tiller number as well as other agronomical traits considered as yield components (Wu et al. 1999, Kato 2004, Zhang et al. 2006). The relational growth grammar of the model will be implemented in XL within the modelling platform GroIMP. (Kniemeyer 2004). Using this example, we show how mechanisms of quantitative inheritance could be generalised for use in ecophysiological FSPMs, by implementing a generic description of QTL x environment interactions (Yang & Zhu, 2005) into a virtual rice model. The implications for "virtual breeding" will be discussed, where the latter means the design of rice ideotypes using FSP modelling.

References

Buck-Sorlin, G.H. and Bachmann, K. 2000. Simulating the morphology of barley spike phenotypes using genotype information. *Agronomie: Plant Genetics and Breeding* **20**, 691-702.

Buck-Sorlin, G., Kniemeyer, O. and Kurth, W. 2005. Barley morphology, genetics and hormonal regulation of internode elongation modelled by a Relational Growth Grammar. *New Phytologist* **166**, 859-867.

Kato, T. 2004. Quantitative trait loci controlling the number of spikelets and component traits in rice: their main effects and interaction with years. *Breeding Science* **54**, 125-132.

Kniemeyer, O. 2004. Rule-based modelling with the XL/GroIMP software. In: Harald Schaub, Frank Detje, Ulrike Brüggemann (eds.), The Logic of Artificial Life. Proceedings of 6th GWAL, Bamberg April 14-16, 2004, AKA Akademische Verlagsgesellschaft Berlin (2004), 56-65.

Watanabe, T., Hanan, J.S., Room, P.M., Hasegawa, T., Nakagawa, H. and Takahashi, W. 2005. Rice morphogenesis and plant architecture: measurement, specification and the reconstruction of structural development by 3D architectural modelling. *Annals of Botany* **95**, 1131-1143.

Wu, W.-R. 1999. Time-related mapping of quantitative trait loci underlying tiller number in rice. *Genetics* **151**, 297-303.

Yang, J. and Zhu, J. 2005. Methods for predicting superior genotypes under multiple environments based on QTL effects. *Theoretical and Applied Genetics* **110**: 1268-1274

Zhang, Y., Luo, L., Xu, C., Zhang, Q. and Xing, Y. 2006. Quantitative trait loci for panicle size, heading date and plant height co-segregating in trait-performance derived near-isogenic lines of rice (*Oryza sativa*). *Theoretical and Applied Genetics* **113,** 361-368

GRAAL-CN: a model of GRowth, Architecture and ALlocation for Carbon and Nitrogen dynamics within whole plants formalized at the organ level

Jean-Louis Drouet[1] and Loïc Pagès[2]
[1] Unité INRA/AgroParisTech Environnement et Grandes Cultures, BP 1, 78850 Thiverval-Grignon, France
[2] Unité INRA Plantes et Systèmes de culture Horticoles, Domaine Saint-Paul, Site Agroparc, 84914 Avignon cedex 9, France
Jean-Louis.Drouet@grignon.inra.fr, Loic.Pages@avignon.inra.fr

Keywords: virtual plant, carbon and nitrogen allocation dynamics, functional-structural model, organ development, organ to whole plant integration, shoot and root systems, source-sink balance

The functional-structural plant model GRAAL-CN has been developed to analyze the dynamics between morphogenetic processes and assimilate (carbon and nitrogen) management processes, the dynamics between carbon and nitrogen metabolism (acquisition and allocation) as well as the regulation of those processes during the vegetative development of individual plants. GRAAL-CN follows up and generalizes the work of Drouet and Pagès (2003), which considered carbon assimilates alone. It associates models of plant morphogenesis and models simulating the growth of plant compartments as related to assimilate availability. Using object-oriented modeling methods, knowledge is formalized at the organ level (local rules of development and resource management), and the behavior of the plant arises from interactions between those organs and the integration of the processes into the whole plant. Shoot and root organs are initiated as a function of temperature. Using the source-sink concept, organ growth is calculated from its individual potential growth and assimilate availability within the plant. Both assimilates, carbon and nitrogen, interact symmetrically and regulate both resource acquisition and developmental processes. Simulations using maize illustrate the capacity of the model to mimic the main features of plants in relation to development and resource allocation (e.g., dynamics of root:shoot ratio for carbon and nitrogen, changes in priority between organs as well as plant plasticity to assimilate availability). GRAAL-CN has been designed to be coupled with three-dimensional (3D) models of the shoot (Drouet, 2003) and root (Pagès et al., 1989) systems. Then, this coupled model can be associated with a model of light transfer and a model of nitrogen transfer within the soil to investigate the exchanges between plant and environment at the organ level. Conceptually, the model constitutes a generic framework with concepts and structure transposable to various species. It is a highly suitable tool for testing and sorting out hypotheses on growth and allocation processes involved in plant development. In the fields of systems biology and ecology, it can contribute to current work aimed at analyzing the interactions between genotypic and environmental characteristics affecting plant behavior.

Drouet J.-L., 2003. MODICA and MODANCA: modelling the three-dimensional shoot structure of graminaceous crops from two methods of plant description. Field Crops Research, 83: 215-222.

Drouet J.-L., Pagès L., 2003. GRAAL: a model of GRowth, Architecture and carbon ALlocation during the vegetative phase of the whole maize plant. Model description and parameterisation. Ecological Modelling, 165: 147-173.

Pagès L., Jordan M.O., Picard, D., 1989. A simulation model of the three-dimensional architecture of the maize root system. Plant and Soil, 119: 147-154.

GREENLAB as a tool to solve source-sink relationships in tomato – Application to the quantification of specific leaf area and fruit set dependences to the level of competition for assimilates

Gaëtan Louarn[1], Yang Lili[1], Dong Qiaoxue[1], Phillipe De Reffye[2].

[1] China Agricultural University (CAU), College of Information and Electrical Ingeneering, Box 63, 100083 Beijing, China.
[2] INRIA Roquencourt, Equipe Digiplante, F78153, Le Chesnay, France

Abstract –

The definition of relevant indicators to quantify the satisfaction of organ demands is of practical importance in crop models. In the case of greenhouse tomato for instance, environmental conditions change drastically around the year, leading in winter to significant reductions of specific leaf area (controlling leaf area expansion and ultimately light interception and crop productivity) and fruit set proportion (partly controlling yield through the number of fruits initiated) that can be related to fluctuations in the competition for assimilates. The supply-demand ratio (S/D) defined in process-based models to account for this phenomenon presents the main drawback of using a rather arbitrary and non-functional potential demand function. This function is valid only for a limited range of growing conditions and management practices. Its use is particularly questionable in studies implying a strong modification of the productivity potential through manipulation of plant and/or stand architecture (e.g. pruning, planting density…).

The mathematical model GREENLAB on the contrary seeks to estimate actual organ sink strengths by optimisation procedures against biomass measurements performed regularly in the course of plant development. It rests on a simple mathematical formalism applied to all plant organs of a given type and can be used in any growing condition. However, in spite of several numerical case studies, S/D estimated using this method have never been compared with measurements on real plants.

The present study aims at evaluating the possibility of using GREENLAB as a solver of source-sink relationships and as a potential supplier of ecophysiological variable characterising the competition for assimilates among organs. To do so, we tried to link overall plant S/D computed with the recently validated GREENLAB-tomato, with observed fluctuations of fruit set and specific leaf area (SLA). Plants grown at four planting densities (1, 2.8, 6.1, 11.2 plant.m^{-2}) and for two sowing dates (spring: 15/03/06; autumn: 15/08/06) were used to generate a gradient of assimilate availability.

Model fitting were accurate from organ to whole plant scales in all the studied situations. This result confirmed that both net production (S) and net demand (D) were dynamically estimated with a satisfying range of precision. S/D evolution displayed a characteristic shape for all the treatments (minimal a few days after seed reserve extinction; maximal around fruit set on the first truss; stabilisation after fruit set on the 5th truss) that was consistent with our knowledge of sink-source relationships in indeterminate tomato cultivars. A sigmoidal relationship between average S/D during the week following flowering and fruit set was found. A clear relationship between average S/D during leaf expansion and SLA was also identified. However this last relationship differed between experiments in spring and autumn indicating that other environmental variables were involved in SLA determinism.

To conclude, this study showed how interesting mathematical structure-function models can be from an analytical point of view for plant physiologists. In our particular case, it helped to build a generalised variable synthesising all together resource availability, plant growth and plant development to explain a targeted process (e.g fruit set). Focusing on modelling outlook, it also demonstrated how this kind of model, proceeding from a bottom-up integration of physiological knowledge, can be used as a research framework for its own complication. Response curve have now been established and could be included in a more sophisticated version of the model linking functionally organogenesis and growth.

Growth and architecture modeling of yerba-mate cultivated in contrasting light environments using AMAPmod

Miroslava Rakocevic [1], Adriano Franzoni Otavian [1], Sílvio Evangelista [1], Érica Vitória Picarelli [1,2], Eduardo Delgado Assad [1]

[1] Embrapa Informática Agropecuária, Av. André Tosello 209, P.B. 6041, 13083-886 Campinas, SP, Brazil
[2] UNICAMP – IMECC, Rua Sergio Buarque de Holanda, 651, 13083-859 Campinas, SP, Brazil
mima/adriano/silvio/erica/assad@cnptia.embrapa.br

Keywords: branching, internodes, metamers, plant architecture, shoot growth

Yerba-mate is a dioecious, subtropical tree. Industrially processed leaves of this species are used to prepare a South-American tea. Two growth pauses regularly appear each year in yerba-mate grown in natural conditions, one in summer (total or partial), and second (total) in winter (Bazzo and Rakocevic, 2005). This species shows a combination of monopodial and pseudo-sympodial branching and extension. The few branches grouped around the dead apex, together with some extremely short internodes, mark the separation of each annual shoot into two successive growth units (Rakocevic *et al*., 2006).

This work, still in execution, aimed at understanding the growth patterns of primary shoots and branching in yerba-mate. Two independent experiments were conduced. In the first one, fifteen adult plants cultivated in each of two contrasted light environments (monoculture - MO and forest understorey - FUS) were marked. Metamer emission, leaflet-area expansion and internode elongation were observed during two years (period between two successive prunings) on three branches of each plant. The data set from a second experiment, conduced on one-year-old plants (Bazzo and Rakocevic, 2005), analyzed a branching pattern of yerba-mate.

Internode distribution and leaf survival are being studied on a growth unit level. The data are being analyzed using V-Plants software, successor of AMAPmod, freely available at http://www-sop.inria.fr/virtualplants/wiki/doku.php?id=software. To define the branching pattern on young yerba-mate by testing appropriate models in STAT module is being tried, while the existence of differences in growth patterns of primary shoots of adult plants grown in two light environments are being tested by histogram distribution. The structure constructed during a biennial period in two contrasted light environments also tended to explore the yerba-mate photomorphogenetic reactions and sex dimorphism (Rakocevic *et al*., 2006b).

Previous results indicated that growth flushes and pauses in the annual growing cycle of yerba-mate are controlled endogenously and modified by environmental factors (Rakocevic *et al*., 2006a), and it is expected that the actual architectural analysis throws a light on those controlling processes.

References:

Bazzo, K. C. de and Rakocevic, M. 2005. Periodicidade no crescimento vegetativo de *Ilex paraguariensis* (St. Hil) Aquifoliaceae. Série Documentos da Embrapa Florestas 117, CD-ROM.

Rakocevic, M., Medrado, M. J. S., Lucambio, F. and Valduga, T. A. 2006a. Shoot growing characterization in yerba-mate (*Ilex paraguariensis* St. Hil.) cultivated in two contrasting light environments. Proceedings of 4th South - American Congress in Yerba-Mate, November, 5th - 8th, 2006, Pousadas, Argentina, pp. 244-249.

Rakocevic, M., Medrado, M. J. S., Lucambio, F. and Valduga, T. A. 2006b. Ritmicidade de emissão e de queda de folhas e as suas conseqüências no manejo da erva-mate. Proceedings of 4th South - American Congress in Yerba-Mate, November, 5th - 8th, 2006, Pousadas, Argentina, pp. 250-256.

Growth unit dimorphism in mango. Consequences for structure-function modelling

Frédéric Normand[1], Abdoul Kowir Pambo Bello[1] and Pierre-Eric Lauri[2]

[1]: CIRAD-PERSYST, UPR Production Fruitière Intégrée, Station de Bassin-Plat, BP 180, F-97455 Saint-Pierre cedex, Réunion Island, France normand@cirad.fr
[2]: UMR DAP, INRA-SUPAGRO-CIRAD-UM II, Equipe 'Architecture et Fonctionnement des Espèces fruitières', 2 place Viala, F-34060, Montpellier, Cedex 1, France

Keywords: *Mangifera indica*, branching, flowering, fruiting, growth unit position

Introduction

Mango tree is characterised by rhythmic growth and terminal flowering. Thus, flowering depends on, and in turn influences, vegetative growth. Close relationships between reproductive and vegetative developments are consequently suspected and should be integrated in a structural-functional model of mango tree. Our objective was then to identify and organize into a hierarchy some key parameters related to tree and shoot architecture. In relation with this objective, we investigated on four mango cultivars (namely Cogshall, Irwin, José and Kensington Pride) the effect of growth unit architectural position on its morphological characteristics and its functioning (branching pattern, flowering and fruiting probabilities).

Materials and Methods

The effect of growth unit position on its morphology was investigated on 10 to 15 current-year shoots sampled randomly on each cultivar in 2004 and in 2006. Several variables were recorded at the growth unit level: stem length and dry mass, stem dry matter content, number of leaves, total leaf area and dry mass, individual leaf area and dry mass, leaf dry matter content and leaf mass per area. The effect of growth unit position on branching pattern, flowering and fruiting was investigated with a dataset resulting from an exhaustive description of growth units, flowering and fruiting of 5 trees per cultivar during two phenological cycles from June 2003 to February 2006. Morphological data were analysed with analysis of variance. Branching pattern, flowering and fruiting were analysed for each year with generalised linear models.

Results and discussion

The main and original result of this study was that growth unit position had a conspicuous influence on its morphology and functioning in mango. Apical growth units were generally larger and had a 2 to 3 times greater leaf area than lateral growth units. They branched more and had higher flowering and fruiting probabilities. These results were common to the four cultivars, with however cultivar-specific effect. These results are being integrated in a structure-function model which considers mango tree as a meta-population of apical and lateral growth units with their own morphological and functional attributes. Their relative proportion determines the leaf area at the periphery of the tree, and the branching, flowering and fruiting potential of the tree. The relative proportions of apical and lateral growth units vary at each growth or flowering event as a result of their specific branching and flowering behaviour. This modelling approach therefore accounts for the reciprocal relationships between vegetative and reproductive development on a mango tree. Further investigations are nevertheless necessary to identify other relevant factors (e.g., fruit load) affecting shoot morphology and/or functioning and to integrate their effects in the model.

A hybrid method to estimate light phylloclimate within growth chambers

D. COMBES [(1)], B. ADAM [(2)], A. CHRISTOPHE [(3)], M. CHELLE [(4)]

(1) INRA, UR4 Unité d'Ecophysiologie des Plantes Fourragères, BP 6, F-86600 Lusignan, France
(2) UMR547 PIAF, INRA, Université Blaise Pascal, F-63100 Clermont Ferrand, France
(3) UMR759 LEPSE, F-34060 Montpellier, France
(4) INRA, UMR1091 Environnement et Grandes cultures, F-78850 Thiverval-Grignon – France
didier.combes@lusignan.inra.fr

Keywords: Controlled environment, Radiative Transfer

In most functional-structural plant models, light is only considered as a consumable resource and plants are usually assumed to be blind to light signals (FSPM04). However, the perception of these signals by the plant is now well documented (e.g. Smith, 1997) and light quality is considered to play a key role in the changes of plant's architecture and the dynamics of vegetation (e.g. Ballaré et al, 1997). In order to introduce the photomorphogenesis process in FSPM, it is necessary to determine how the perception of the light signal occurs on the whole plant. This determination of the perception requires the estimation of light received locally under global controlled environment i.e. in growth chambers.
One way to locally estimate the light is the use of a radiative transfer model based on a virtual plant approach. Such model has to take into account different components such as the light sources characteristics, plant structure and optical properties of the chamber's matters (chelle et al, 2004) .
In our study, we present an alternative approach that corresponds to couple measurements with modeling based on the projective method. This approach was first proposed on PAR using a six-face sensor (Chenu et al, 2005). The proposed method improves it by using a home-developped automatic apparatus to characterize not only the spatial variation of light in growth chambers but also its directional (1293 directions) and spectral (300-1100 nm) variation. The used model was VegeStar (Adam et al, 2002).
Results show that the light within a growth chamber varied spatially but also directionally.. The directional variation in the PAR showed higher values of variation coefficient (until 43%) in a field of view of 60° than for grazing directions. Moreover, the contribution of vertical component radiation to hemispherical radiation varied between 31 % close to the wall and 47 % in the center. Using these results, the effect on plant and organ interception estimation in the PAR was analyzed using Vegestar. Assuming a vertical component lead to an underestimation of plant interception compared with the same calculation using the 1293 directions whatever the position in the growth chamber. At an organ scale, as expected, the variability of light interception is higher than at plant scale.
This original approach enables not only to quantify the light spatial, directional and spectral variability but also to bring out the effect of this variability on plant and organ light interception.

B, Adam, N. Donès, H. Sinoquet, VegeSTAR - software to compute light interception and canopy photosynthesis from images of 3D digitised plants. UMR PIAF INRA-UBP, Clermont- Ferrand, 2002.

C.L. Ballaré, 1994. Light gaps: sensing the light opportunities under highly dynamic canopy environments. In "Exploitation of environmental heterogeneity by plants" M.M. Caldwell and R.W. Pearcy Eds, Academic Press, 73-110.

M. Chelle, M. Demirel, C. Renaud, 2004 Towards a 3D light model for growth chambers using an experiment-assisted design In: 4th International Workshop on Functional-Structural Plant Models, Montpellier

K. Chenu, N. Franck, J. Dauzat,, J.F. Barczi, H. Rey, J. Lecoeur. 2005 Integrated responses of rosette organogenesis, morphogenesis and architecture to reduced incident light in Arabidopsis thaliana results in higher efficiency of light interception. Functional Plant Biology 32 (12) :1123-1134

H. Smith, 1997. Photomorphogenesis. Special Issue. Plant, Cell and Environment, 20, Issue 2: i-iii.

Including the effect of biological processes in the allometric scaling relationships

Pekka Kaitaniemi[1] and Anna Vehanen[2]
[1]Hyytiälä Forestry Field Station, University of Helsinki
Hyytiäläntie 124, FI-35500 Korkeakoski, Finland
Pekka.J.Kaitaniemi@helsinki.fi
[2]Department of Forest Ecology, University of Helsinki
P.O. BOX 27, FI-00014 University of Helsinki, Finland
Anna.Vehanen@helsinki.fi

Keywords: allometry, interactions between plants, plant structure, scaling

Introduction

Allometric scaling relationships of the form $Y = aX^b$ are widely utilized in many types of biological models. In the functional-structural plant models, for example, they can be used for estimating unmeasured plant traits based on some easily measurable traits such as the length or diameter of structures. Allometric scaling relationships are, however, usually viewed as static relationships where both the scaling exponent (b) and the normalization constant (a) are fixed according to their empirical values. This may have unpredictable effects in dynamic models where the structure of a plant, its physiological processes, and its growth environment are under a constant change. The value of the scaling exponent has been under intense theoretical and empirical investigation, but the allometric equations can incorporate also additional biologically relevant information.

Normalization constant reflects the effect of dynamic processes

We show that by using a thoretically predicted fixed value for the exponent b, instead of an empirical value determined by regression, it is possible to make the normalization constant suitable for biological interpretation in terms of dynamically changing environment, along with improving the overall model fit.

Measurements on silver birch (*Betula pendula* Roth.) were used to establish allometric scaling equations relating the radius (r) of a branch to either the length (l) or the shoot number of the branch (n). It was assumed that the relationship between r and l can be modeled as $l = ar^{2/3}$, and the relationship between r and n as $n = ar^2$. The value of a was then predicted with a sample set of explanatory variables reflecting the dynamically changing structural traits of the study trees (tree age, breast diameter, crown length, tree height) and the characteristics of the stand surrounding the trees (two competition indices, neighbor species, relative availability of photosynthetic radiation). This procedure eliminated a significant proportion of variation from a, and improved the overall fit of the allometric models by up to 11%. The increased number of parameters did not explain the improvement.

Accordingly, there is potential for using the value of the normalization constant to depict biologically important information in a manner that improves the accuracy of model predictions.

The influence of branching pattern on the performance of tree species

Sandra Mueller, Ernst-Detlef Schulze
Max-Planck-Institute for Biogeochemistry
Hans-Knoell-Str. 10, 07745 Jena, Germany
smueller@bgc-jena.mpg.de

Keywords: branching pattern, carbon allocation, functional groups, functional structural plant models

Abstract

The dynamic development and the formation of a tree crown is based on species specific branching patterns. At the same time the architectural structure of a tree is directly linked to and interacts with its physiological processes. In order to understand a species' performance within a community it is essential to understand how structural and physiological processes interact. The shape of a tree is the result from of the genetic constitution and environmental influences. Light is probably the prime environmental factor influencing the crown shape of a tree. Each tree has to find the balance between optimal light interception and transpiration, carbon allocation for structural support, assimilation organs and nutrient supplying organs (Cannel and Dewar 1994).

To investigate which crown traits are beneficial under given light conditions, eight tree species with different ecological traits (e.g. *Populus tremula, Fagus sylvatica, Picea abies*) were subjected to varying light conditions in a field experiment. Trees were planted on two sites which have a size of 23ha and 11ha between 2003 and 2004. The two experimental sites are part of the BIOTREE-Project and located in Thuringia/ Germany.

During the summer 2007, the eight tree species were shaded in five different treatments: 1. No shading, 2. 70% reduced light over the whole tree crown, 3. 50% reduced light over the whole tree crown, 4. 70% reduced light over half the crown, 5. Shading of buds only. Each treatment is repeated ten times. In the course of the study the effect of shading on branching pattern, carbon allocation and storage will be measured. Using the modeling platform GroIMP (Growth Grammar-related Interactive Modeling Platform) I want to analyze the interaction between architecture and physiological processes like carbon gain and resource allocation. Integrated within GroIMP is the modeling language XL (eXtended L-System language), "which combines the rule based-programming paradigm of graph grammars and L-systems with the imperative and object orientated programming paradigm of Java" (Kniemeyer 2004).

In this presentation I will demonstrate the experimental setup. Furthermore I will show preliminary results on the generic architectural traits that species from similar functional groups (e.g. all light demanding species) have in common. These are based on my own field observations and an intensive literature survey. Finally I will give examples on how the architecture of a tree can be displayed in GroIMP.

References

Cannel, M.G.R. and R.C. Dewar 1994. Carbon allocation in trees – a review of concepts for modelling. . Advances in Ecological Research. 25:59-104.

Kniemeyer, O. 2004. Rule-based modelling with XL/ GroIMP software. *In* The logic of artificial life. Proceedings of 6th GWAL Eds. H. Schaub, F. Detje and U. Brüggemann. AKA Berlin, Bamberg, pp. 56-65.

Is Lacunarity a valuable measure of plant canopy structure?

I. J. Roberts,[1] R. A. Roemer,[2] D. Skirvin[1]

[1,] *Warwick HRI, University of Warwick, Wellesbourne, Warwick, CV35 9EF, UK*
[2] *Physical Sciences, University of Warwick, Coventry, CV4 7AL, UK*

Keywords Lacunarity, canopy structure, voxelisation, biodiversity.

Introduction

In the UK, a greater emphasis is being placed on increasing the biodiversity of agricultural land. There is a particular emphasis on increasing functional biodiversity for biological control. The structure of a plant canopy is crucial in determining the micro-environment within a habitat and hence the biodiversity that that habitat will support. Our aim in this work is to develop a method for comparing canopies to allow assessment of the impact of canopy structure on biodiversity.

Novel use of Lacunarity measures

3-Dimensional Lacunarity analysis is a recently developed scale-dependent measure from the 2-Dimensional gliding box approach that provides a useful indication of spatial arrangement or texture of plant structures in a given canopy volume using voxels. Lacunarity effectively describes the 'gaps' in a volume (Chmiela and Slota 2006; Cheng, 1997; Plotnick and Gardner, 1993, 1996; Allain and Cloitre, 1991).

To measure the lacunarity of a canopy, we create a virtual canopy from digitised plant data . We then voxelise the canopy using Euclidean co-ordinates of x, y, and z within a virtual volume of 1000000units^3. Occupied voxels are given an index of 1 for and un-occupied voxels 0. For our purposes, Lacunarity is calculated in a 2-dimensional X-Z plane for each Y pixel. A gliding box algorithm (Cheng, 1999; Plotnick, et al. 1993; Plotnick and Gardner, 1996) is used to calculate the lacunarity for the plane. This creates a spectrum of lacunarity values through the canopy.

The spectrums generated can then be used to compare canopies and related to biodiversity measures to determine the influence of canopy architecture on biodiversity. Through this approach we hope to be able to determine the canopy structure with the greatest biodiversity benefits for agricultural land.

Acknowledgements

This research is part of a PhD project conducted at the University of Warwick Physical Sciences department, Centre for Scientific Computing, and Warwick Horticulture Research International (IPM Biocontrol) financially supported by BBSRC funds. Many thanks are also due to Desmond Roberts who contributed essential computer programming codes and graphical interpretations for the concept model.

Literature

Allain, C. and Cloitre., M. (1991). Characterizing the lacunarity of random and deterministic fractal sets. *Physical Review* A **44**(6): 3552.

Cheng, Q. (1997). Multifractal Modeling and Lacunarity Analysis. *Mathematical Geology* **29**(7): 919-932.

Cheng, Q. (1999). The gliding box method for multifractal modeling. *Computers & Geosciences* **25**(9): 1073Â±1079.

Chmiela, J., Slota, D. (2006). Analysis of emptiness (lacunarity) as a measure of the degree of space filling and of the internal structure of a set. *Materials Characterization* **56**(4-5): 421-428.

Plotnick, R. E., Gardner, R. H. (1996). Lacunarity analysis: A general technique for the analysis of spatial patterns. *Physical Review* E **53**(5): 5461.

Plotnick, R. E., Gardner, R. H. and O'Neill, R. V. (1993). Lacunarity indices as measures of landscape texture. *Landscape Ecology* **8**(3): 201-211.

A model for sporophyte development in the filamentous brown alga *Ectocarpus siliculosus*

Bernard Billoud[1], Aude Le Bail[2], Bénédicte Charrier[2]

(1) Université Pierre et Marie Curie - Paris 6, Atelier de BioInformatique, 12, rue Cuvier 75005 Paris, France.
(2) UMR7139, Station Biologique, CNRS, Université Pierre et Marie Curie, Place Georges Teissier, 29 682 Roscoff cedex, France.

Keywords: filamentous algae, cellular automaton, development, morphology

Background and biological model

Brown algae are marine multicellular plant organisms evolutionary very distant from land plants (Baldauf, 2003). *Ectocarpus siliculosus* (Dillw.) is a small brown alga, growing throughout the world in temperate areas (Müller, 1979). Its body architecture is filamentous (Ravanko, 1970). Molecular phylogeny showed that, despite its simple architecture, *Ectocarpus* belongs to the most evolved brown algae, with Laminariales ("giant kelps") and Fucales, both developing 3-D vegetative structures (parenchyma) (Draisma *et al*., 2003). Moreover, plasmodesmata differentiate, resulting in symplastic communications between adjacent cells (de Reviers, 2003) potentially involved in the establishment of integrated developmental mechanisms.

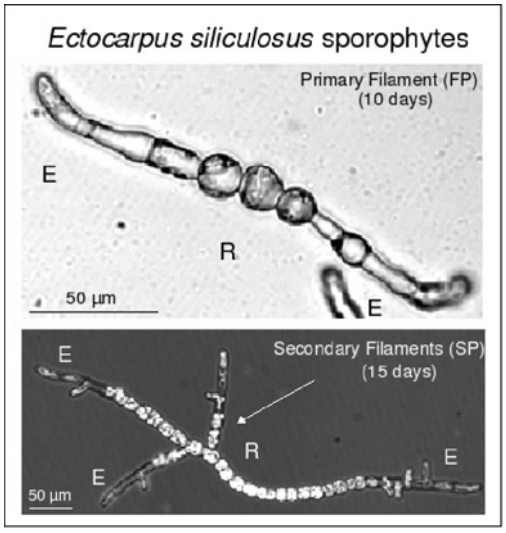

Sporophytes develop from an initial cell (spore, unfertilised gamete or zygote), which divides sequentially and uni-directionally to produce a uniseriate filament ("Primary Filament", PF) composed of two types of cells with different shapes and location: round cells (R), grouped by the centre of the PF, and elongated cells (E), found at the extremities. After a few more mitoses, changes in cell polarisation make cell division produce branches ("Secondary Filaments", SF), eventually leading to the formation of a basal and vegetative filamentous network. All basal filaments display the same general architecture. Growth is not apical, but intercalary and diffuse.

Results

Morphometric analyses carried out on the early stages of the sporophyte development (Le Bail *et al*., in prep) showed that the position of the SFs is neither precisely scheduled, nor a uniform random process. It appears to be linked with the distribution of the two kinds of cells. This distribution is for instance not canonical in ecotypes or mutants characterized by their unusual branching structure. The R/E-shaped cell pattern is also the primary target of the phytohormone auxin which leads to a change in the R/E ratio and to perturbations in the SF distribution. This pattern is thus a key feature for the subsequent branching structure development.

We studied the establishment of the R/E cell pattern as the result of two local processes: cell division and cell differentiation. Using an asynchronous cellular automaton, we modelled the development of a PF, starting from a unique, round cell, up to a 10-cell filament. The parameters (*ie* relative frequencies of division and differentiation events) were adjusted by a maximum-likelihood approach, in order to fit with the patterns actually observed during the first steps of PF growth, and their respective prevalence. This allowed us to predict which intermediary steps and transformations are the most likely to occur during the sporophyte development.

Conclusion and perspectives

Using morphometry and growth simulation, we described and quantified the cell-level processes involved in the whole individual morphology construction. Because of its growth in liquid medium, algal development might recruit different processes from land plant. These studies also aim at identifying which mechanistic process is modified in response to phytohormones and in morphological mutants.

References

Baldauf, S. L. The deep roots of eukaryotes. *Science* 13;300(5626):1703-6, 2003.

Draisma, S. G. A., Peters, A. F. and Fletcher, R.L. Evolution and taxonomy in the Phaeophyceae: effects of the molecular age on brown algal systematics. In: *Out of the Pas*t. Ed. T.A. Norton. *British Phycological Society*, pp. 87-102, 2003.

Müller, D. G. Genetic affinity of *Ectocarpus siliculosus* (Dillw.) Lyngbye from the Mediterranean, North Atlantic and Australia. *Phycologia* 18: 312-318, 1979.

Ravanko, O. Morphological, developmental and taxonomic studies in the *Ectocarpus* complex (Phaeophyceae). *Nova Hedwigia* 20:179-252, 1970.

Reviers, B. de. *Biologie et phylogénie des algues*. Tome 2. Paris : Belin, 255 p. ISBN 2-7011-3512-5, 2003.

Modeling tree crown photosynthesis in elevated atmospheric CO_2

David Ellsworth
Centre for Plant and Food Science
University of Western Sydney
Richmond, NSW 2753 AUSTRALIA

Marion Liberloo
Dept. of Biology, Antwerp University and
Centre for Plant and Food Science, University of Western Sydney
Richmond, NSW 2753 AUSTRALIA

While much effort has been devoted toward measuring and modeling the leaf-level response of trees to elevated atmospheric CO_2, far less effort has been dedicated to modeling whole-tree photosynthesis in elevated CO_2. We link a leaf photosynthesis model and a tree architecture model (using Y-PLANT; Pearcy and Yang 2006) to predict the effects of elevated atmospheric CO_2 concentration on crown-level carbon assimilation of two *Eucalyptus* species. The two species are characteristic of fast-growing plantations and stress-tolerant Eucalypt woodlands, respectively. Crown attributes of these species were measured by recording 3-dimensional point locations of leaves and stems for small saplings. Although the species differed by about 1/3 in their leaf-level maximum photosynthetic rates, modeled crown-level carbon assimilation normalised by plant size was similar for the two species at the sapling stage. For the fast-growing *Eucalyptus saligna*, crown carbon assimilation estimated by the YPLANT model in both ambient and elevated CO_2 was strongly determined by leaf area ratio, and leaf angle, both of which controlled the effective leaf area displayed. Elevated CO_2 enhanced leaf area ratio, which combined with enhanced leaf CO_2 assimilation to stimulate crown carbon assimilation. The results indicate that photosynthetic performance is strongly dependent on whole-plant architecture. Future refinements of the model will incorporate plant hydraulic considerations. The results suggest that elevated [CO_2] may affect the balance of competition between a fast-growing and slow-growing species of Eucalyptus, and suggest that plant form and architecture should be considered in the choice of appropriate species in schemes involving using trees for carbon offsets.

Modelling the time course of senescence in winter wheat at the individual leaf and whole plant level

Jonathan Hillier[1], Jillian Watt[2], Jessica Bertheloot[3], Phillip Lewis[2], Christian Fournier[3], Bruno Andrieu[3].

1. Aberdeen University, School of Biological Sciences, Cruickshank Building, St Machar Drive, Aberdeen, AB24 3UU, UK. j.hillier@abdn.ac.uk
2. University College London, Department of Geography, Gower Street, London WC1E 6BT, UK
3. UMR1091 Environnement et Grandes Cultures, INRA, AgroParisTech, F-78850 Thiverval-Grignon, France. Bruno.Andrieu@grignon.inra.fr

Keywords: Winter wheat, ADEL-wheat, dynamic structural model, senescence

Abstract

ADEL-wheat (Fournier *et al*, 2003) is a 3D architectural model developed for winter wheat, which exploits observed stable patterns regarding the timing of organ production, final organ size profile, and geometry. In order to accurately model the 3D-structure it is also important to similarly describe the time course of senescence both at the whole plant level and at that of the individual organs. This is particularly so for applications such as, for example, remote sensing in which the remote signal is known to be sensitive to LAI and leaf distribution, both of which require the evolution and the vertical profile of senescence to be well represented.

Field experiments were conducted in 2004 and 2006 on a total of 9 varieties. We then constructed a leaf senescence index for each shoot (SSI), and analysed its thermal time course. It has previously been observed that, in terms of leaf appearance, tiller development mimics that of the main stem, except that each tiller is delayed by a constant amount with respect to the main stem, and also that the profiles of the final sizes of organs on all axes are similar once the concept of a "phytomer shift" (e.g. Evers *et al*, 2005) is introduced. From the point of view of leaf senescence an analogous observation can be made - that once the developmental delay is accounted for the advancement of senescence on all axes is similar. These observations together mean that (once a certain point in the development has been reached) the instantaneous leaf area and vertical profile per shoot are conservative across all axes. At the individual leaf level senescence progresses more-or-less sequentially during the vegetative growth phase – with the senescence of a given leaf commencing as that of its predecessor finishes. This behaviour differs for the later leaves, which senesce simultaneously, albeit at varying rates, which also differ somewhat between genotypes. Finally, these observations permit a parsimonious parameterisation of the thermal time course of senescence which enables an improved modelling of 3D structure with relatively little increase in the size of the model's parameter set.

Acknowledgements

This research was carried out under the UK's Natural Environment Research Council project NER/Z/S/2002/00908. We gratefully acknowledge their support.

References

1. Fournier C, Andrieu B, Ljutovac S, Saint-Jean S. 2003. ADEL-wheat: A 3D architectural model of wheat development. In Plant Growth Modeling and Applications, Proceedings of 2003 International Symposium, ed. B-G Hu, M Jaeger, pp. 54-63. Beijing, CHN Tsinghua University Press - Springer Verlag

2. Evers JB, Vos J, Fournier C, Andrieu B, Chelle M, Struik PC. 2005. Towards a generic architectural model of tillering in Gramineae, as exemplified by spring wheat (Triticum aestivum). New Phytologist 166: 801-12

Modelling wheat behaviour under different population densities using the stochastic GreenLab model

MengZhen Kang[1], Jochem B. Evers[2], Véronique Letort[3], Jan Vos[2], Philippe de Reffye[1,4,5]

[1]LIAMA, Institute of Automation, CAS, 100080, BeiJing, China
[2]Crop and Weed Ecology, Plant Sciences Group, Wageningen University, Haarweg 333, 6709 RZ, Wageningen, The Netherlands
[3]MAS, Ecole Centrale de Paris, France
[4]Projet DigiPlante, INRIA Rocquencourt, France
[5]CIRAD, Montpellier, Cedex 5, France

Keywords: Stochastic FSPM, GreenLab, bud probability, model calibration, validation

Introduction

Plant architecture is determined by both the genetic basis of the plant (e.g. Wang and Li, 2006) and the effects of environmental factors (e.g. Evers et al., 2006). It can be described in terms of the dynamics of buds, with the fate of buds depending on their relative positions in space and time (Buck-Sorlin and Bell, 2000). The variation in architecture is obvious in wheat plants (*Triticum aestivum* L.), especially regarding the degree of tillering and consequently yield per plant (Darwinkel, 1978). Deterministic functional-structural plant models (FSPMs) are limited in the simulation of plasticity in development in terms of bud behaviour.

In the current study, the difference and statistical similarity of individual wheat architectures are taken into account in the context of the function-structural model GreenLab. The aim of this paper is to simulate the stochastic development and mean production of wheat plants grown with different population densities, based on calibration of a stochastic GreenLab model. The results are validated with independent data.

Experiment setup and data collection

Two successive experiments have been conducted in the same growth chamber with identical climate conditions in Wageningen, the Netherlands. Spring wheat plants (cv. Minaret) were grown in containers. Seeds were sown at population densities of 100 plants m^{-2} in experiment 1, and 100, 262 and 508 plants m^{-2} in experiment 2. In both experiments, six plants per population density per sampling occasion (four sampling occasions in total) were dissected destructively. Measured data included the dimensions and/or weights of leaf blades, sheaths, internodes, ears and roots. The harvest criteria of the two experiments were similar. Leaf state (appearance, growing, full-grown, dead) was monitored two or three times per week for main stem as well as primary tillers (Exp. 1) or of all orders (Exp. 2), on six plants per population density.

Stochastic GreenLab model

GreenLab (Yan et al. 2004) is a functional-structural model that has been calibrated for different crops. The stochastic GreenLab model (GL2) extends the potential of model applications by introducing bud probabilities (see below) (de Reffye et al. 1988) into its architectural part. Despite its complexity, the analytical output of this stochastic functional-structural model (mean and variance of organ number, as well as mean product of plant) has been computed (Kang et al., 2007a).

Compared to the deterministic GreenLab model for wheat (Kang et al., 2007b), in GL2, the *bud breakout probability* (P_b) describes the chance that a bud develops into a tiller. The *tiller survival probability* (P_f) describes the chance that a tiller survives and ultimately bears an ear. The probabilities can be different for main stem and tillers of different order. The third probability is *phytomer growth probability* (P_g). It is introduced as tillers often contain less and variable phytomers compared to the potential pattern (Bos and Neuteboom, 1998) which is the upper boundary of the topological structure.

Model calibration

The parameters to be calibrated consist of two parts: (I) the bud probabilities and (II) the parameters describing sink and source functions. For (I), the fitting targets are (a) the mean and variance of the total number of phytomers from the emergence to the appearance of the flag leaf; these data were obtained from the record on leaf state on six plants; (b) the mean and variance of number of ears at grain-filling stage. For (II), the fitting targets are the mean weight of organs at each phytomer rank for main stem and tillers, obtained from the destructive measurement at the four sampling stages.

A non-linear least square method is used to minimize the root mean square error between the fitting targets and the model output, the latter being functions of model parameters. To compute the numerical output for a stochastic model with Monte-Carlo simulation is time-consuming. In contrast, the analytical results of the stochastic GreenLab model (Kang et al., 2007a) provide a fast and precise way to do the computations with recurrent equations.

Preliminary results

The analytical mean and variance of number of organs computed with methods described in Kang et al. (2007a), are close to the measured data from Exp. 1 (densities 100 plants m^{-2}), see Figs. 1 and 2. The fitting process resulted in a set of bud probabilities (Table 1) for each population density. Using mean organ number, the model computed the mean value of organ weight along the phytomer position at each plant age (in growth cycles). This output fitted well to the measured data (figures and parameters shown in later communications). The stochastic GreenLab model is a promising tool to simulate wheat samples of which the architecture and product vary with population density.

Acknowledgements

This work is supported by NSFC (60073007), Chinese 863 plan (2006AA10Z229), and C.T. de Wit Graduate School for (PE&RC). Help from staff members of Crop and Weed Ecology and of the experimental facilities UNIFARM of Wageningen University in the setup of the experiment and data collection is acknowledged.

References

Bos HJ and Neuteboom JH. 1998. Morphological analysis of leaf and tiller number dynamics of wheat (Triticum aestivum l.): responses to temperature and light intensity. *Annals of Botany* 81: 131–139.

Buck-Sorlin GH and Bell A. 2000. Models of crown architecture in Quercus petraea and Q. robur: shoot lengths and bud numbers. *Forestry* 73:1-19.

Darwinkel A. 1978. Patterns of tillering and grain production of winter wheat at a wide range of plant densities. *Netherlands Journal of Agricultural Science* 26: 383-398.

Evers JB, Vos J, Andrieu B, Struik PC. 2006. Cessation of tillering in spring wheat in relation to light interception and red : far-red ratio. *Annals of Botany* 97: 649-658.

Kang MZ, Cournrède P, de Reffye P, Auclair D, and Hu BG. 2007a. Analytical study of a stochastic plant growth model: application to the GreenLab model. *Mathematics and Computers in Simulation*, in press.

Kang MZ, Evers JB, Vos J, de Reffye P. 2007b. The derivation of sink functions of wheat organs using the GreenLab model. *Annals of Botany*, in press.

de Reffye P, Edelin C, Francon J, Jaeger M, and Puech C. 1988. Plant models faithful to botanical structure and development. *Computer Graphics* 22(4): 151-158.

Yan HP, Kang MZ, de Reffye P, and Dingkuhn M. 2004. A dynamic, architectural plant model simulating resource-dependent growth. *Annals of Botany* 93: 591–602.

Wang Y, Li J. 2006. Genes controlling plant architecture. *Current Opinion in Biotechnology* 17: 123-129.

Table 1. Estimated bud probabilities for each population density in Exp. 2, of the main stem (PA 1), primary tillers (PA 2) and secondary tillers (PA 3). The tiller bud break probability for PA 1 is the seed emergence probability.

Density (plants m^{-2})	Bud break probability P_b			Phytomer growth probability P_a			Tiller survival probability P_f		
	PA 1	PA 2	PA 3	PA 1	PA 2	PA 3	PA 1	PA 2	PA 3
100	0.85	0.95	0.97	0.78	0.91	0.91	0.92	0.79	0.47
262	0.76	0.89	1.00	0.69	0.61	0.61	1.00	0.52	0.08
508	0.79	0.45	0.97	0.80	0.42	0.42	1.00	0.34	0.00

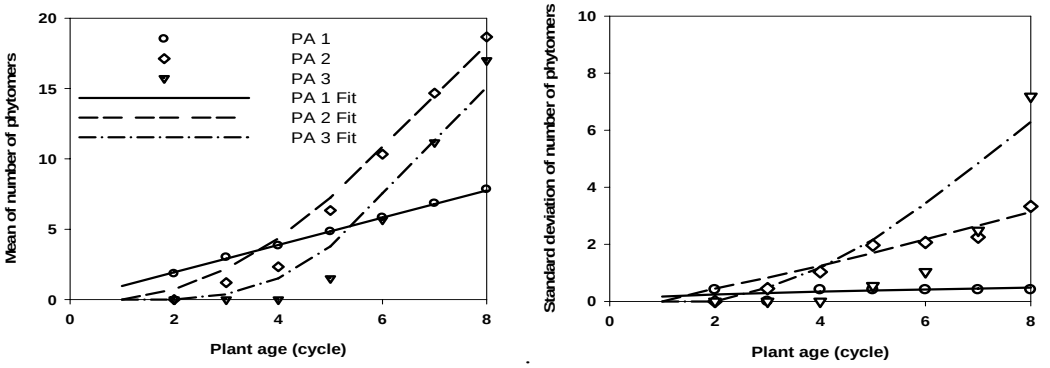

(a) (b)

Fig.1. The mean (a) and standard deviation (b) of the number of phytomers in main stem (PA 1), primary tillers (PA 2), secondary tillers (PA 3) of a wheat plant at each plant age (in growth cycles), at a population density of 100 plants m^{-2}, from observation (symbols) and model output (lines).

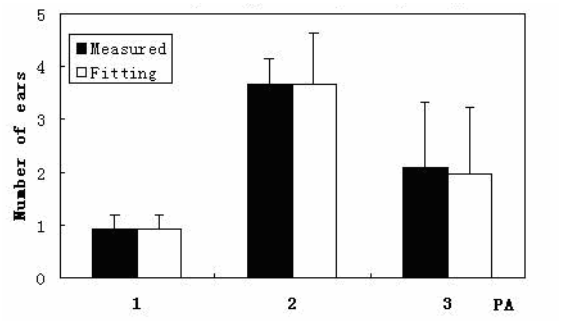

Fig.2. The mean and standard deviation of the number of final ears in main stem (PA 1), primary tillers (PA 2), secondary tillers (PA 3).

On the implementation of the functional-structural tree model LIGNUM

Jari Perttunen[1], Risto Sievänen[1], Jouni Hartikainen[1] and Eero Nikinmaa[2]
1. Finnish Forest Research Institute, Vantaa Research Unit
P.O. Box 18, FI-01301 Vantaa, Finland
2. Department of Forest Ecology, University of Helsinki
P.O. Box 27, FI-00014 Helsinki, Finland
jari.perttunen@metla.fi

Keywords: Simulation software, Lindenmayer system, generic programming,

The simulation program implementing the model LIGNUM

The functional-structural tree model LIGNUM represents the tree crown for coniferous and deciduous trees with four structural units. The units are tree segment, branching point, bud and axis. LIGNUM is intended as a generic modeling tool for woody perennial plants (Perttunen et. al., 1996, Perttunen et. al., 2001) and shrubs (Salemaa et. al., 2003). The growth of different species is simulated by changing model parameters, descriptions of metabolism and structural dynamics (birth, growth and senescence of the structural units) and the tree architecture is represented with Lindenmayer systems (Perttunen and Sievänen, 2005). Photosynthetic production depends on the photosynthetically active solar radiation in the tree crown.

The model LIGNUM is being developed with C++ language and STL library using generic programming. We do not emphasize polymorphism or inheritance (i.e. object oriented paradigm) in program design but instead implement the structural units of the model as abstract classes using C++ template mechanism. The template mechanism allows specifications how one data type is generated given another type as an argument. This modelling paradigm implements a tree as an abstract data type. It has the important advantage that we can implement generic algorithms to work for this common framework of a tree reducing the work to implement different tree species.

We will present the general program architecture and the new features such as the graphical user interface and the use of XML allowing the persistence of simulated trees, i.e. they can be saved into a file for later analysis. These features are implemented with Qt 4 library (see www.trolltech.com) that enables the use of LIGNUM in leading operating systems including Windows, Linux and Mac OS X. We will also present some modelling work done with LIGNUM.

References

Perttunen, J., Sievänen, R., Nikinmaa, E., Salminen, H., Saarenmaa, H. and Väkevä, J. 1996. LIGNUM: A tree model based on simple structural units. Annals of Botany, 77(1):87–98.

Perttunen, J., Nikinmaa, E., Lechowicz, M.J., Sievänen, R. and Messier, C. 2001. Application of the functional- structural tree model LIGNUM to sugar maple saplings (Acer saccharum Marsh) growing in forest gaps. Annals of Botany, 88(3):471–481.

Perttunen, J. and Sievänen, R. 2005. Incorporating Lindenmayer systems for architectural development in a functional-structural tree model. Ecological Model ling, 181(4):479–491.

Salemaa, M., Sievänen, R. and Perttunen, J. 2003. Branching architecture of Arctostaphylos uva-ursi in two contrasting environments. In A. Tolvanen, A. Siikamäki, P. Mutikainen, J. Tuomi, and C. Nuortia, editors, 7th Clonal Plant Workshop. Reproductive Strategies, biotic interactions and metapopulation dynamics. 1st-5th August 2003, Kuusamo Finland, p. 68.

OpenAlea: An open-source platform for the integration of heterogeneous FSPM components

S. Dufour-Kowalski[1], C. Pradal[2], N. Dones[3], P. Barbier de Reuille[1], F. Boudon[2], J. Chopard[1], D. DaSilva[4], J.-B. Durand[7], P. Ferraro[6], C. Fournier[5], Y. Guédon[2], A. Ouangraoua[6], C. Smith[8], S. Stoma[1], F. Théveny[2], H. Sinoquet[3] and C. Godin[1]

[1] INRIA, 2004 route des lucioles BP 93, 06902 Sophia Antipolis, France
[2] CIRAD, Avenue Agropolis, 34398 Montpellier cedex 5, France
[3] INRA, Site de Crouël, 234 avenue du Brézet, 63100 Clermont-Ferrand, France
[4] Université Montpellier 2, place Eugène Bataillon,34095 Montpellier, France
[5] INRA, Centre de Grignon, BP 01, 78850 Thiverval Grignon, France
[6] Université Bordeaux 1, LaBRI, 351 cours de la Libération, F-33405 Talence Cedex, France
[7] INPG, LJK/IMAG, BP 53, 38041 Grenoble cedex 9, France
[8] INRA, 2 place Viala, 34060 Montpellier cedex 1, France

Keywords: open source, component framework, plant modeling

Introduction

The open source OpenAlea project's goal is to share and reuse heterogeneous models from the FSPM community. In this poster, we present our development strategy to create an open source research platform as well as some of the main components of OpenAlea.

A collaborative approach for sharing a software framework

The open source development model provides a framework to efficiently develop a software platform in a scientific context. It improves: (a) scientific validation by providing access to the source code for the entire community; (b) scientific collaboration by providing free access to published scientific models; (c) synergy by enhancing the collaboration between multidisciplinary research teams; (d) economies of scale by sharing development, distribution and maintenance cost; and (e) software quality by enforcing common rules and best practices. The OpenAlea platform is based on this principle. Documentation, source code, forum, bug tracking and binary distributions are freely available in a collaborative web space (http://openalea.gforge.inria.fr). Developers and modelers start collaboration and work together in pairs on a common objective during coding and modeling sprint sessions, encouraging communication, feedback and exchanges. The OpenAlea platform is distributed under a free license (GNU LGPL) allowing external components to choose their own license (including proprietary). Each modeler is responsible for the development of its modules but takes advantage of the facilities provided by the framework.

Available OpenAlea functionalities

Heterogeneous components are integrated in OpenAlea: (a) simulation models of ecophysiological processes (e.g. RATP, PyCaribu, PyDrop, etc.); (b) topological and geometrical analysis of plant architecture (e.g. V-Plants, formerly AMAPmod); (c) geometric representation, and visualization of plants at different scales (e.g. PlantGL); (d) common data structures (e.g. sequence, tree, graph, MTG, grid, etc.); and (e) simulation models and reconstruction of meristem (e.g. Merrysim, TissueMeca, etc.). Using OpenAlea and standard Python scientific libraries, users can combine components into customized data flows according to their specific needs. A demonstration of the OpenAlea platform and the requirements to integrate a module will be carried out at the conference.

Reference

Pradal C., Dufour-Kowalski S., Boudon F. and Dones N. 2007. The architecture of OpenAlea: A visual programming and component-based software for plant modeling. FSPM07.

Pradal C., Boudon F., Donès N., Durand J.-B., Fournier C., Sinoquet H., Godin C. 2006. OpenAlea - A platform for plant modelling, analysis and simulation, in: EuroPython 2006.

Pradal C., Boudon F., Nouguier C., Chopard J., and Godin C. PlantGL : a Python-based software for 3D plant modelling at different scales. To be submitted.

Godin C., Guédon Y. and Costes E. 1999. Exploration of plant architecture databases with the AMAPmod software illustrated on an apple-tree hybrid family. Agronomie 19.

Sinoquet H., Le Roux X., Adam B., Ameglio T. and Daudet F.A. 2001. RATP : a model for simulating the spatial distribution of radiation absorption, transpiration and photosynthesis within canopies : application to an isolated tree crown. Plant cell environ 24.

Bussière F., Dufour-Kowalski S. and Bassette C. 2007. A software for the simulation of rainfall distribution on 3D plant architecture: PyDROP. FSPM07.

Relative contribution of foliage display and leaf functions to branch physiological capacities in two apple cultivars: a functional-structural modeling approach

Catherine MASSONNET[(1)], Jean-Luc REGNARD[(1)], Pierre-Eric LAURI[(1)], Hervé SINOQUET[(2)] and Evelyne COSTES[(1)]
[(1)] UMR DAP – Equipe Architecture et Fonctionnement des Espèces Fruitières, INRA – SupAgro ; 2 Place Pierre Viala - 34060 Montpellier Cedex 1 – France, costes@supagro.inra.fr
[(2)] UMR547 PIAF, INRA, UNIV BLAISE PASCAL, F-63100 CLERMONT FERRAND, France

Keywords : gas exchange, LAD, RATP model, STAR, 3-D virtual plants

Introduction

The vegetative and reproductive growth of fruit trees depends on assimilate production which is controlled by tree canopy structure and leaf functions, both modulated by their interactions with the environment (Lakso 1994). Understanding more precisely how these factors influence the variation of growth and yield is a major issue for fruit growers. Functional-structural plant models (FSPMs) offer promising perspectives to understand these complex interactions at different spatial and temporal scales (Godin and Sinoquet 2005). In this context, the aim of the present study was to unravel in apple the relative contribution of foliage display and leaf functions (leaf stomatal and photosynthetic properties) on light interception, transpiration and photosynthetic capacities of branching systems.

Material and methods

Two apple (*Malus* x *domestica* Borkh.) cultivars with contrasted architectures, 'Fuji' and 'Braeburn' were studied at the INRA experimental station of Melgueil (near Montpellier, France). Three eight-year-old trees per cultivar, grafted on M9 rootstock, were digitized to obtain 3-D representations of foliage geometry. Branch light interception was estimated by STAR (Silhouette to Total leaf Area Ratio) values on the tree mock-ups. Branch transpiration was measured in field by sap flux and net photosynthetic rate by branch bags. A set of parameters previously established in both cultivars (Massonnet et al, submitted) was used to run RATP model (Radiation Absorption, Transpiration and Photosynthesis, Sinoquet et al., 2001). The RATP outputs were evaluated by comparison against measurements. The model was then used to evaluate the impact of virtual scenarii switching foliage display and/or leaf functions on light interception, transpiration and photosynthetic capacities at branch scale in both cultivars.

Results and discussion

'Fuji' branches presented lower leaf area density (LAD) values than Braeburn. Consequently, this resulted in higher STAR values, transpiration and photosynthetic rates in 'Fuji' than in 'Braeburn' branches. The analysis of the virtual scenarii revealed that the variations in foliage display and leaf functions had additive effects on the reduced transpiration and photosynthetic rates of 'Braeburn' branches compared to 'Fuji'. Leaf display and leaf functions had equivalent impacts on branch transpiration rates while the former had a predominant impact on branch photosynthetic rates. This can be interpreted as a consequence of the difference in leaf stomatal conductance between the cultivars whereas their leaf photosynthetic capacity was similar.

Conclusion

This study demonstrated the relevance of FSPM to disentangle physiological differences between cultivars through an *in silico* approach. We showed here the large impact of foliage display on the branching system functions. This study could be further investigated through additional studies of the complex interactions between plant structure, leaf physiology and environment at different time scales, making use of recent dynamic simulations of apple tree development (Smith et al., submitted).

References

Massonnet C. et al. Photosynthesis and Stomatal Regulation in Apple Leaves: Evidence for Different Water Use Strategies between two Cultivars. Submitted to Annals of Botany.

Sinoquet H. et al. 2001. RATP: a model for simulating the spatial distribution of radiation absorption, transpiration and photosynthesis within canopies: application to an isolated tree crown. Plant Cell Environ. 24:395-406.

Godin C. and H. Sinoquet. 2005. Functional-structural plant modelling. New Phytol. 166:705-708.

Lakso, A.N. 1994. Apple. *In* Handbook of environmental physiology of fruit crops. Eds. B. Schaffer and P.C. Andersen. CRC Press Inc., University of Florida, pp 3-35.

Smith C. et al. 2006 On the simulation of apple tree development using statistical and biomechanical models. Submitted to the 5th FSMP workshop

Scaling up to whole-plant and crop levels short-term responses of leaf growth to water deficit

Karine Chenu[1], Scott C. Chapman[2], Graeme L. Hammer[3], Greg McLean[4], Christian Fournier[1], François Tardieu[1]
[1] INRA, UMR 759 LEPSE, 2 Place Viala, 34060 Montpellier cedex 01, France
[2] CSIRO Plant Industry, St. Lucia, Qld 4072, Australia
[3] APSRU, University of Queensland, Brisbane, Qld 4072, Australia
[4] APSRU, Climate and Systems Technologies, DPI, Toowoomba, Qld 4350, Australia
chenu@supagro.inra.fr

Keywords: maize, leaf elongation, leaf development, water deficit, crop model.

Introduction

One challenge of FSPM in ecophysiology is to bridge the gap between physiological and genetic studies that focus on short-term mechanisms, and whole-plant models designed to predict biomass accumulation, transpiration and yield in field conditions. We developed here a model of leaf growth and development in maize and interfaced it with the crop model APSIM for simulation at canopy level.

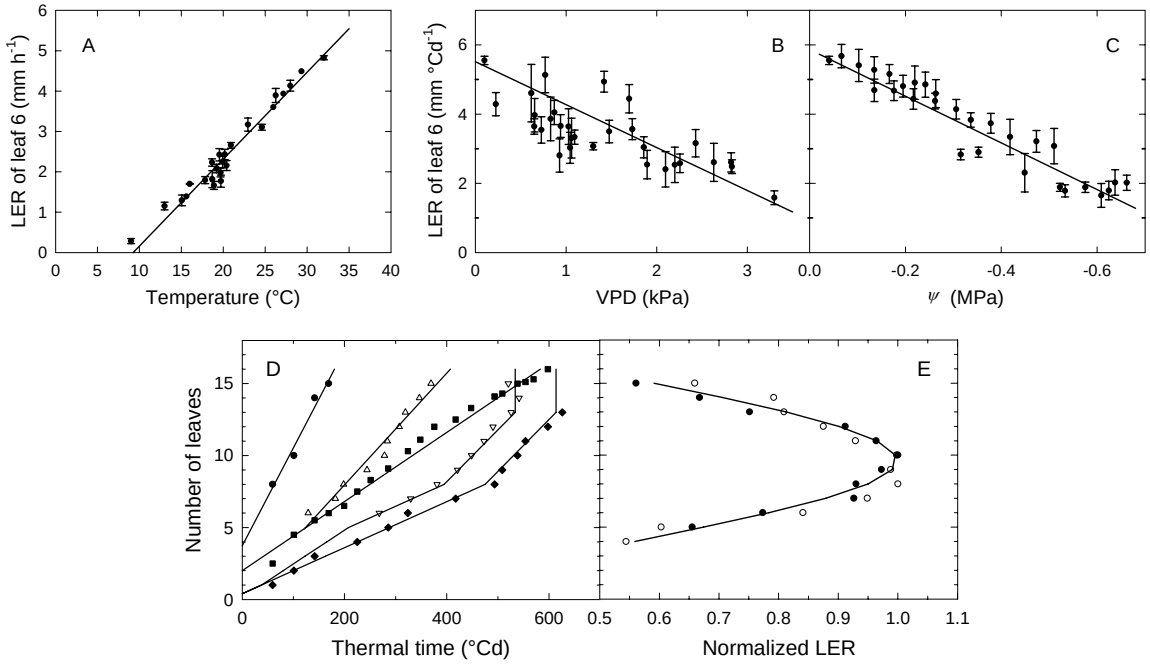

Fig. 1. Models used for predicting individual leaf extension and their responses to water deficit in soil and air. (A-E) Responses of leaf elongation rate (LER) of leaf 6 to temperature, vapour pressure difference between meristem and air (VPD), and predawn leaf water potential (ψ). (D) Timing of leaf development expressed in thermal time for individual leaves (●, leaf initiation; △, beginning of linear expansion; ■, tip appearance; ▽, end of linear expansion). (E) Normalized leaf extension rate as a function of leaf position. Data from greenhouse and growth chamber experiments (A-C) and one field experiment (D-E).

The model

The model of leaf growth and development combined (i) the model of leaf extension proposed by Reymond *et al*. (2003) to predict effects of QTLs on leaf expansion rate under short-term environmental variations (Fig. 1 A-C) with (ii) a model coordinating the development of the

individual leaves of a plant (Fig. 1 D-E). The latter was based on results of three experiments where all leaves were measured every second day from their initiation. The resulting whole-plant model was incorporated as a replacement module for canopy development in the APSIM platform (Wang *et al.*, 2002; Keating *et al.*, 2003). In addition, a new micrometeorological module was added to APSIM to provide environmental inputs at an hourly time-step to the leaf extension module.

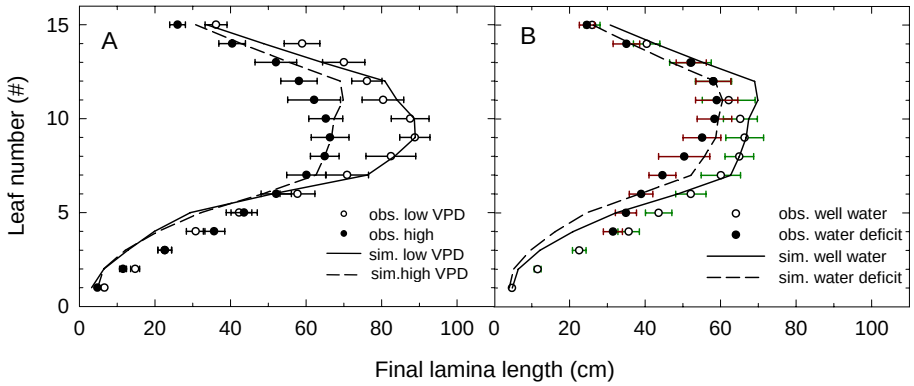

Fig. 2. Observed and simulated length of fully expanded leaves, for plant grown in field with contrasting vapour pressure deficits (A) and soil water status (B).

Results

Twelve field situations with contrasting temperatures, evaporative demands and soil water status were used to test the model. The model showed strong effects of high evaporative demand and water deficit in reduced leaf area at the whole-plant level (Fig. 2). Short water deficits affected only leaves developing during the stress, either visible or still hidden in the whorl, independently of other leaves. The model adequately simulated whole-plant profiles of leaf area with a single set of parameters which applied to the same genotype in all experiments. It was also suitable to predict biomass accumulation and yield of a similar hybrid in different field conditions.

Conclusion

This model extends existing physiological knowledge of leaf elongation responses to environmental conditions. It can be applied to determine how the genetic controls of these responses translate into yield differences for large ranges of climatic scenarios.

References

Keating B.A., Carberry P.S., Hammer G.L., Probert M.E., Robertson M.J., Holzworth D., Huth N.I., Hargreaves J.N.G., Meinke H., Hochman Z., McLean G., Verburg K., Snow V., Dimes J.P., Silburn M., Wang E., Brown S., Bristow K.L., Asseng S., Chapman S., McCown R.L., Freebairn D.M., Smith C.J. 2003. An overview of APSIM, a model designed for farming systems simulation. European Journal of Agronomy 18: 267-288.

Reymond M., Muller B., Leonardi A., Charcosset A., Tardieu F. 2003. Combining quantitative trait loci analysis and an ecophysiological model to analyze the genetic variability of the responses of maize leaf growth to temperature and water deficit. Plant Physiology 131: 664-675.

Wang E., Robertson M., Hammer G.L., Carberry P., Holzworth D., Meinke H., Chapman S.C., Hargreaves J., Huth N., Campbell G.S. 2002. Development of a generic crop model template in the cropping system model APSIM. Euopean Journal of Agronomy 18: 121-140.

Segmentation-based approaches for characterising plant architecture and assessing its plasticity at different scales

Jean-Baptiste Durand[(1)], Yves Caraglio[(2)], Patrick Heuret[(3)], Eric Nicolini[(2)]

(1) Laboratoire Jean Kuntzmann – INRIA *Virtual Plants* – Grenoble Universités
51 rue des Mathématiques, BP 53, 38041 Grenoble Cedex 9, France
jean-baptiste.durand@imag.fr

(2) CIRAD, (3) INRA, UMR Botanique et Bioinformatique de l'Architecture des Plantes
TA A-51/PS2, 34398 Montpellier Cedex 5, France
{caraglio|nicolini|heuret}@cirad.fr

Keywords: hidden Markov tree model, categories of entities within tree structures, Symphonia globulifera, Fagus sylvatica

Introduction

Plants are modular organisms that develop by the repetition of elementary botanical entities or constructional units through the three main and fundamental morphogenetic processes of growth, branching and reiteration (Barthélémy and Caraglio, 2007). Repetition of these entities induces gradual or abrupt changes in their characteristics. These characteristics are quantified through several variables, called the entity attributes. On the one hand, differences between entities reflect different stages of differentiation in the meristems (Nicolini and Chanson, 1999), which are ordered in time and correspond to the notion of physiological age of meristems (Barthélémy and Caraglio, 2007). The changes of one attribute through the plant structure are referred to as morphogenetic gradient. On the other hand, part of the entity differences can be imputed to environmental factors.

Based on this botanical model of plant functioning, our approach jointly relies on categories of entities with similar characteristics, a description of those within-category characteristics and the category topological organisation within the plant. This constitutes a useful summary of the plant architecture, which is the basis for 1) highlighting hidden regularities in plant structures, for a better understanding of the gradients and organisation rules; 2) proposing and validating ecophysiological hypotheses, and new sampling protocols; 3) adopting a powerful paradigm for modelling plant development.

In this work, the entity categories are identified using a hidden Markov tree (HMT) model, in which local dependencies only (*i.e.* interactions between connected entities) are accounted for. This is not sufficient to accurately describe the topological distribution of the entities within the plant, and the changes of the plant topology. This is why various complementary methods and models (among which edit distance algorithms and sequence analysis using Markovian models), performed at different scales, are used in our approach to provide a more detailed description of the architecture, and to assess how various controlled factors affect architecture plasticity.

Segmentation of plant entities using hidden Markov tree models

Measurements collected on plants are coded as Multiscale Tree Graphs (MTGs), considered at a single given scale. The root vertex corresponds to the first entity at the basis of the tree trunk; thus the tree is oriented from the topological root vertex to the terminal (or "leaf") vertices. The HMT model is used to perform entity segmentation and to represent the state transitions within tree-structures (see Durand *et al.,* 2005). HMT models are statistical models that assign a hidden state to each observed vertex. As a first step, the model parameters are estimated. Model parameters provide information about the state dynamics through the tree structure. The second step corresponds to a segmentation using the observed characteristics and the parameter values; this results into assigning a state value to each entity, taking into account connections between entities. This state is expected to reflect the stages of differentiation of the meristems, and can be

used as a summary of the entity attributes if the states are well separated. Those algorithms are implemented in the OpenAlea software (Pradal *et al.*, 2007).

The HMT model with conditionally independent children states, given the parent state, captures some local (parent-child) dependencies between tree entities. However, the HMT model is unable to account for direct dependencies between several ancestor vertices, or for changes, concerning state definition or dynamics, caused by individual variability (or other variability sources). On the basis of experiences with hidden Markov models for sequences, we expect the segmentation to be robust to these model limitations. This is related to certain robustness when estimating the distributions of the observed characteristics given the states, even if the dynamics of the states are poorly modelled. Such robustness can be interpreted as well-differentiated stages, in terms of entity characteristics.

Analysing the architecture of Symphonia and beech trees

This section presents a methodology based on entity segmentation for analysing the architecture of young *Symphonia globulifera* L. f. (Clusiaceae) and branching systems of beech trees (*Fagus sylvatica L*, Fagaceae). Firstly, categories of tree entities were obtained using an HMT model, which revealed the attribute distribution within each state and the probabilistic succession of the states within each individual. The states can be interpreted as stages of differentiation of the meristems.

Then the state frequencies were computed at the individual scale. Thus each tree was characterised by a vector of frequencies, which was used to perform a clustering of the individuals. The trees within one tree-cluster are expected to have comparable degrees of architectural development. The variability of the state frequencies according to controlled factors was also assessed.

At the scale of branching systems, the identification of borne complexes of similar importance was achieved by computing the edit distance between trees proposed by Ferraro and Godin (2000). This distance was computed using a local distance based on state labelling only, as opposed to the attributes. This corresponds to a denoising step where the attribute variability (for example due to variations in environmental conditions) is eliminated. Segmentation also avoids undesired interactions between local and global metrics. The question of synchronous growth of the trunk entities with those of the branching systems, or synchronous growth of several branching systems, was handled by extracting alignments provided by the edit distance computation.

Symphonia

30 young *Symphonia globulifera* individuals are considered. They were grown for 2 years in a greenhouse nursery in semi-controlled conditions under 3 light treatments of 5%, 10% and 20% of incident light. The aim of this study is to describe how *S. globulifera* individuals develop, and how their architecture is related to light environment (see Heuret *et al*., in this workshop).

The HMT analysis was performed at the growth unit (GU) scale. The considered attributes are GU length, number of pairs of cataphylls and number of pairs of leaves. The model identification stage led to a seven-state model, where the states can be interpreted as levels of vigour, or basal position in borne branched systems.

The GU segmentation highlights some heterogeneity concerning the state frequencies, discriminating individuals with greater vigour and branching intensity than average (characterised by a high frequency of GUs in states of highest vigour) from those with less advanced development (low frequencies of those states). Moreover, the state frequencies were computed for each light treatment. As a result, low-vigour GUs have a markedly higher frequency for the 5% light treatment than for the other treatments, whereas GUs related to branching have lower frequencies.

Beech trees

A first set of 16 30-year-old beech trees is considered. This set is divided into 2 subsets of 8 individuals grown in different places. This is completed with a second set consisting of the last 25 years of growth of tree tops of 43 100-year-old individuals. The aim of this study is to highlight ordered stages in the differentiation

sequence of the meristems, and to assess the effect of population diversity (age and conditions of growth) on the number, the nature and the dynamics of the stages.

The HMT analysis was performed at the annual shoot (AS) scale. The considered attributes were AS length, number of cycles of extension and presence/absence of flowers. HMT models were identified separately on each dataset, and joined into a third model estimated using both datasets. This led to a twelve-state model.
On the basis of the AS segmentation, four clusters of individuals were visually identified in the first dataset: strong growth, moderate growth, slow growth and flowers. The state frequencies were compared between both growth places. This shows a clear separation between individuals with highest or lowest frequencies of the medium, short and flowering AS (corresponding to three given states). To validate the interpretation of the states as a quantification of physiological age, their stability (number and the nature) was assessed when extending the population diversity (age and conditions of growth). The distribution of the states along the trunk was also computed and compared with their global distribution, which highlights a higher frequency of long bicyclic AS than on the branches.
Moreover, the analysis performed on the second dataset emphasised complex patterns in the state succession leading to flowering, which could be characterised using variable-order Markov chains applied to selected paths within the trees. Synchronous nature of the AS on the trunk and branches was also emphasised by the states, which could be quantified through sequence alignments between the trunk and the borne axis.
We intend to carry other approaches to validate this methodology, by assessing how increasing the population diversity (for example diverse social status), or selecting different sets of attributes to build the HMT model, affects the state number or dynamics. The model ability to predict future flowering can also be investigated, by removing flowering AS from the data and identify some patterns characterising near apparition of flowers.

Importance of entity segmentation for assessing architecture variability at branching system or individual scales

Entity segmentation has a polyvalent status in the above studies: firstly, this provides a synthetic overview of the gradients, represented in the model through attribute distributions within each state, and the transition probabilities between states. Adding the state as a new synthetic variable in the data, allow complementary approaches for benefiting from a reduction of complexity (dimensionality), and some denoising. Secondly, the state-based approach reinforces the botanical notion of physiological age, since the state number remains very low, given the large complexity of measured trees, the number of individuals and of entities (hence the entity diversity). However, our model is not appropriate to model patterns, to relate the states with the topological growth, nor to resume the characteristics of whole branched systems. This is why HMT-based segmentation has to be combined with those complementary approaches, to precise and characterise states of architectural development.

Acknowledgments

The authors are thankful to Sabrina Coste for providing the plant material, and to Pascal Ferraro, Aïda Ouangraoua, Jean Bérard and Anne Perrut concerning the use of various tools for data analysis.

References

Barthélémy D. and Caraglio Y. 2007. Plant architecture: a dynamic, multilevel and comprehensive approach to plant form, structure and ontogeny. Annals of Botany, 99, pp. 375-407.

Durand J.-B., Guédon Y., Caraglio Y. and Costes E. 2005. Analysis of the Plant Architecture via Tree-structured Statistical Models: the Hidden Markov Tree Models. New Phytologist, 166(3), pp. 813-825.

Ferraro P. and Godin C. 2000. A distance measure between plant architectures. Annals of Forest Sciences, 57, pp. 445-461.

Nicolini E. and Chanson B. 1999. La pousse courte feuillée, un indicateur du degré de différenciation chez le Hêtre (*Fagus sylvatica* L.). Canadian Journal of Botany, 77(11), pp. 1539-1550.

Pradal C., Dufour-Kowalski S., Boudon F. and Dones N. 2007. The architecture of OpenAlea: A visual programming and component-based software for plant modeling. Submitted to FSPM07.

Shedding Morphogenetically Active Radiation on Functional Structural Plant Models

Combes D., Escobar-Gutiérrez A.J., Varlet-Grancher C.

INRA, UR4 Unité d'Ecophysiologie des Plantes Fourragères, BP 6, F-86600 Lusignan, France
didier.combes@lusignan.inra.fr

Keywords: Light Quality, Photoequilibrium, Red:Far-Red Ratio

Although light quality plays a key role in the dynamics of vegetation, in most FSPM, light is viewed simply as a consumable resource and plants are assumed to be blind to light signals. However, prior to any effort for modelling photomorphogenetic mechanisms, it is necessary to characterise the spatial distribution of light quality over and within plant canopies.

The measurement of local light quality and its modelling approach are rather complex and not currently applied. Nevertheless, measurements of local photosynthetic photon flux density (PPFD) and broadband irradiance (Es) are easy to carry out by using small sensors. Thus, the local spectral photon distribution within a canopy can be estimated whenever the functional relationships between these measurements and photon flux within any spectral band, as well as the photoequilibrium and red:far-red ratio, are known.

The objective of this work was to determine these functional relationships from the light spectra received above and within a canopy. Measurements were made at various positions around a target plant within a population of growing fibre sorghum. The places and the orientations of the sensor were chose to be representative of the main likely perceptive organs in gramineous.

The photomorphogenetic variables considered in this work, are related either to photon flux densities in various wavebands between 330 and 950nm or to the ratio between two photon flux densities. A part of the photon fluxes variables are strictly included in the photosynthetically active radiation band and might be estimated from PPFD measurements using a linear relationship. The other variables are related to both PPFD and Es within a multiple linear relationship. The photoequilibrium and red:far-red ratio were related to the relative transmitted PPFD and to the ratio PPFD/Es within the canopy using a nonlinear model.

Simulating perennial ryegrass cutting

A. Verdenal, D. Combes and A. Escobar-Gutiérrez
INRA, UR4 Unité d'Ecophysiologie des Plantes Fourragères,
BP 6, F-86600 Lusignan, France
alban.verdenal@lusignan.inra.fr

Keywords: grassland, perennial ryegrass, cutting, L-system-based model

Perennial ryegrass is one of the most commonly cultivated forage species in Europe, where grazing and mowing (cutting) are used to manage this resource. Cutting can be characterized by its intensity (height) and its frequency. Combinations of these two factors affect mono-species grasslands productivity and could also modify the genotypic composition of heterogeneous populations. Indeed, the hierarchy of genotypes in a mixture is affected by cutting regimes in terms, for instance, of tillers relative frequency in the sward (Hazard and Ghesquiere, 1995).

It has been suggested that these observations could be explained by the modification of the structure and function of the individual plant induced by the removal of a part of the leaves, and by the subsequent modification of the light resource accessibility for shaded plants/organs. However, it is difficult to assess whether, and to what extent, these phenomena are due to reactions of the plant to the defoliation *per se* (e.g. reduction of the leaf area) or to the changes that occur in the physical environment in which the plant is growing.

The aim of our work is to better understand how cutting regimes affect the productivity and the genotypic composition of grasslands, and thus their use-value, via the modification of the canopy structure. To this end, an individual-based FS model enabling to simulate a mini-sward canopy and its cutting seems to be an appropriate and valuable tool. To our knowledge, the L-system-based approach has still not been used in the case of cutting/mowing. Indeed, when testing "alternative canopy structures" (Vos *et al.*, 2007) for plants with FS models, attention has rather focused on pruning.

Pruning often consists in the selective removal of entire phytomers (including lateral buds and the terminal apex) in order to modify the shape or the functioning of the plant. On the other hand, in the case of mowing, apex are not removed as they are situated at the bottom of the leaves, close to the ground, and cutting itself only consists in the removal of every tissues situated above a given height (Fig.1), independently of their age, physiological role or any other property.

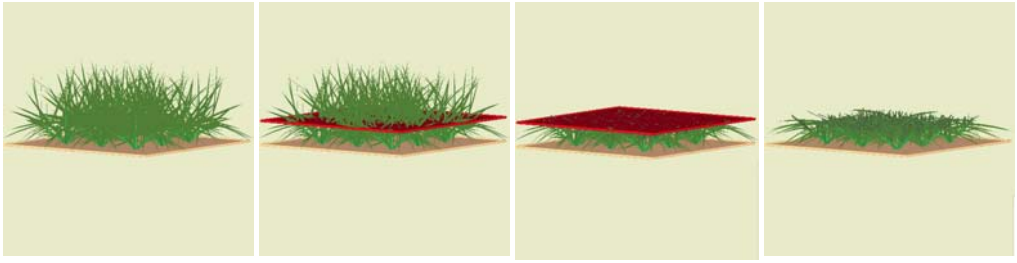

Fig. 1. Sequence of 4 images illustrating a simulated defoliation of a rye-grass mini-sward.

Ultimately, cutting could be compared with hedge-pruning (Prusinkiewicz *et al.*, 1994) which is also based on a purely spatial criterion. However, in our particular case, it is not possible to simulate the truncation by simply removing unwanted modules as they are dedicated to the representation of

whole leaves. Consequently, it is necessary to develop the algorithms allowing to determine, for each leaf, the length of the remnant after a cutting event (Fig. 1.).

We explored several algorithmic options for L-system-based models. For example: i) the use of query modules in order to make the leaves "remember" their length when they first cross the defined cutting plane, ii) decomposition/reconstruction of the plant using LPFG's feature enabling to create several groups of production, and iii) vector-based calculations. We will present and discuss them in relation with the structure of the plant.

References

Hazard, L. and Ghesquiere, M. 1995. Evidence from the use of isozyme markers of competition in swards between short-leaved and long-leaved perennial ryegrass. Grass and Forage Science, 50, 241-248.

Prusinkiewicz, P., James, M., Mech, R. 1994. Synthetic Topiary. In Computer Graphics Proceedings, Annual Conference Series, ACM SIGRAPH, 351-358.

Vos, J., Marcelis, L.F.M., Evers, J.B. 2007. J.Vos, L.F.M. Marcelis, P.H.B. de Visser, P.C. Struik and J.B. Evers (eds), Functional Structural Plant Modelling in Crop Production, 1-12. Springer.

Simulation of fertility behavior of natural populations of rice at two environments using L-system

Lakshmi P. Subedi[1] and Tara N. Subedi[2]
[1]Department of Plant Breeding, Institute of Agriculture and Animal Science(IAAS), [2]Center for Information Technology, Institute of Engineering (IOE),
Tribhuvan University, Nepal

Keywords: spikelet fertility, L-system, simulation, rice genetics

Introduction

In two populations of rice in Nepal: a bold grain variety, Taichung , and a long grain variety, P. Masino, the partial sterile panicles were collected from two different places in Bhaktapur, a hilly district. Parental or most prevalent genotype had 81.3% (with pink apiculus type hybrid swarm, Taichung type) and 82.9% (with brown apiculus type hybrid swarm, P. masino type) spikelet fertility. The partial sterile panicles were of two types: I →7.7-8.9% fertility and II→30% fertility. The relative frequencies of the sterile types varied from 1-2% per plot(≅100sq m) to even 50% per plot among different farmers' fields. A view of partial sterility is given below:

The distribution of spikelet fertility was trimodal. These data will be simulated considering 3 loci: A. B and C affecting fertility. Let α be frequency of fertile spikelets, N be the total number of spikelets, π_i be the effect of each loci and h_i be the out-crossing rate The expression can be written as $\alpha=\Theta(N,\pi,$ and h) based on Matsubara et. al.(2003) .

Simulation programs

Plant growth and development of rice field will be simulated through cpfg modified from Watanabe et. al. (2005), a visual output is provided below:

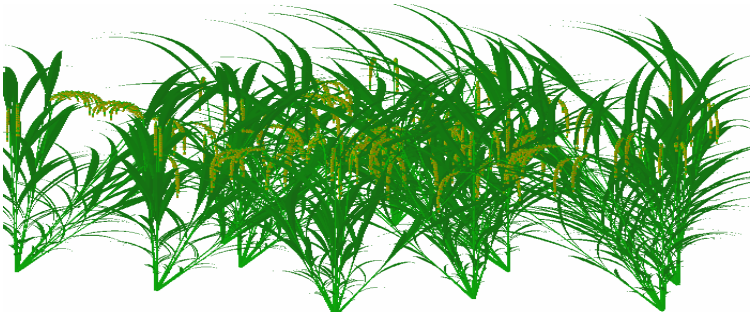

Similarly, flowering as affected by temperature and day length will be simulated. Pollination or pollen flow will also be simulated as given below:

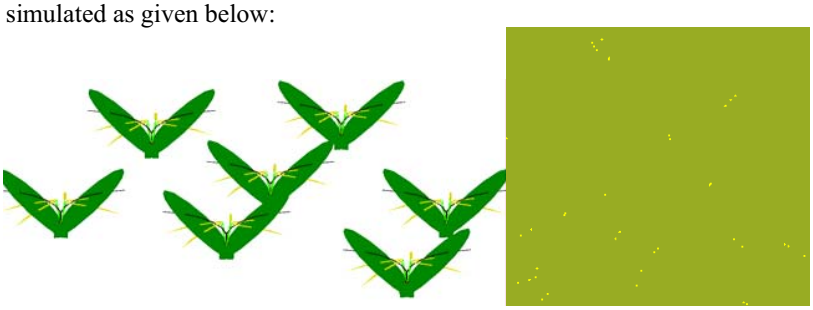

Then the spikelet fertility as described previously will be simulated.

References:

K. Matsubara, Khin-Thidar and Y. Sano.2003. A gene block causing cross-incompatibility hidden in wild and cultivated rice. Genetics 165: 343–352

T. Watanabe, J.S. Hanan, P. M. Room, T. Hasegawa, H. Nakagawa and W. Takahashi. 2005. Rice morphogenesis and plant architecture: measurement, specification and the reconstruction of structural development by 3D architectural modelling. Annals of Botany 95: 1131–1143

A statistical model for analyzing jointly growth phases, the influence of environmental factors and inter-individual heterogeneity. Applications to forest trees.

Florence Chaubert[1], Yves Caraglio[2], Christian Lavergne[3], Catherine Trottier[3] & Yann Guédon[1]

[1] *CIRAD, UMR Développement et Amélioration des Plantes*
INRIA, Equipe de recherche Virtual Plants
Avenue Agropolis, TA A-96/02, 34398 Montpellier Cedex 5, France
E-mail: chaubert@cirad.fr, guedon@cirad.fr

[2] *CIRAD, UMR botAnique et bioinforMatique de l'Architecture des Plantes*
TA A-51/PS2, 34398 Montpellier Cedex 5, France
E-mail: caraglio@cirad.fr

[3] *UMR Institut de Mathématiques et de Modélisation de Montpellier,*
Place Eugène Bataillon, 34095 Montpellier Cedex 5, France
E-mail: trottier@math.univ-montp2.fr, Christian.Lavergne@math.univ-montp2.fr

Keywords: Markov switching model, linear mixed model, growth phases, ontogeny.

Introduction

Observed growth, as given for instance by the length of successive annual shoots along a tree trunk, is mainly the result of two components: an ontogenetic component and an environmental component. The ontogenetic component is assumed to be structured as a succession of roughly stationary phases, asynchronous between individuals, while the time-varying environmental component (mainly of climatic origin) is assumed to take the form of local fluctuations, synchronous between individuals. Guédon *et al.* (2007) proposed a set of methods for analyzing these components. In their approach, the environmental component was simply characterized globally but it may be interesting to study in detail the plant's response to changing climatic conditions. Here, we propose a statistical modeling approach that enables to differentiate the role of environmental explanatory variables and the part of inter-individual heterogeneity between the growth phases.

First results for a sample of 18-year-old Corsican pines and another sample of 15-year-old sessile oaks were reported in Vera *et al.* (2004). We propose to extend these analyses to data samples grouping for each species (Corsican pine and sessile oak) several sub-samples corresponding to different age classes, all the trees having grown during a common range of years. In this way, different climatic years are mixed for a given ontogenetic phase.

Markov switching linear mixed model

Vera *et al.* (2004) introduced Markov switching linear mixed models, i.e. models that combine linear mixed models (Verbeke and Molenberghs, 2000) in a markovian manner. These models belong to the family of hidden Markovian models (Ephraim and Merhav, 2002). The underlying Markov chain represents the succession of growth phases while the linear mixed models attached to each state of the Markov chain represent both the influence of time-varying climatic explanatory variables and inter-individual heterogeneity due to unobserved factors such as plant pathogen infestation within a given growth phase. The influence of climatic explanatory variables is modeled as a fixed effect and the inter-individual heterogeneity as a random effect (Verbeke and Molenberghs, 2000). Thus, the introduction of random effects makes it possible to decompose the total variability into two parts: variability due to inter-individual heterogeneity and residual variability.

In temperate regions, rainfall can have a one-year-delayed effect (on the number of elements) or an immediate effect (on shoot elongation) depending on whether it occurs during the organogenesis or the elongation. We therefore chose to use rainfall cumulated during a selected period

of the previous year (organogenesis) and rainfall cumulated during a selected period of the current year (elongation) as climatic explanatory variables. These explanatory variables may be considered quite rough compared to explanatory variables computed on the basis of sophisticated ecophysiological models.

We propose two nested families of Markov switching linear mixed models which differ in the assumptions made concerning inter-individual heterogeneity:

- model 1: The individual tree status within the population (tree growing either quickly or slowly than the average tree) is common to all the growth phases;
- model 2: The individual tree status is different in each growth phase.

Markov switching linear mixed models were estimated using a Stochastic or Monte-Carlo Expectation Maximization (SEM or MCEM) algorithm (McLachlan and Krishnan, 1997) whose elementary iteration decomposes into three steps: sampling of state sequences, random effect prediction and maximization.

We are interested both by the quantification of the inter-individual heterogeneity of the tree population and by the behavior of each individual within the population.

Applications to forest trees

Sessile oaks

The data sample comprised two sub-samples: 46 15-year-old trees (from 1983 to 1997) and 20 29-year-old trees (24 last years measured from 1974 to 1997). These trees originating from natural regenerations were observed in a private forest near Louppy-le-château (north-east France). It should be noted that the silvicultural practices favored synchronous germinations in the years following mass fruiting . Stand density was 2000 stems/ha. Tree trunks were described by annual shoot where the length (in cm) was recorded for each annual shoot.

Length of annual shoots

"Left-right" two-state Markov switching linear mixed models composed of a transient state followed by a final absorbing state were estimated on the basis of the two sub-samples of sessile oaks. The inter-individual heterogeneity is greater at the beginning of the plant life (first growth phase) while the influence of climatic explanatory variables is roughly proportional to growth level. For the two models, the part of variability due to inter-individual heterogeneity is less than 8% in the second phase (of strongest growth). Moreover, the more general assumption of model 2 (a random effect attached to each state) seems more realistic. For example, a tree can grow more slowly in the first phase than the average tree and then more quickly in the second phase. The small part of variability due to inter-individual heterogeneity can be explained by the fact that the individuals were selected among the dominant or codominant trees, by the thinning and by the synchronous natural regeneration for each sub-sample.

Corsican pines

The data set comprised four sub-samples of Corsican pines planted in a forest stand in the "Centre" region (France): 31 6-year-old trees, 29 12-year-old trees (first year not measured), 30 18-year-old trees (first year not measured) and 13 23-year-old trees (two first years not measured). Plantation density was 1800 stems/ha for the first sub-sample (6 year old) and 2200 stems/ha for the three other sub-samples. Tree trunks were described by annual shoot where two quantitative variables were recorded for each annual shoot, namely length (in cm) and number of branches per tier. These trees were not subject to any silvicultural interventions.

Length of annual shoots

"Left-right" three-state Markov switching linear mixed models composed of two successive transient states followed by a final absorbing state were estimated. As for the sessile oaks, model 2 seems more realistic although the behaviors on the last two phases (of strongest growths) are generally similar. On the first two growth phases, climatic explanatory variables have a moderate influence on the length of annual shoots. On the phase of strongest growth, the annual shoots

length is markedly influenced by the current year rainfall (elongation) and a little less by the previous year rainfall (organogenesis). As for sessile oaks, the inter-individual heterogeneity is greater at the beginning of the plant life (cf Table 1). The important heterogeneity can be explained by the time spent in nursery, the lack of thinning and the sampling strategy (trees chosen in order to cover the whole range of behaviors).

	Intercept	Current year rainfall (Elongation)	Previous year rainfall (Organogenesis)	Part of inter-individual heterogeneity	Residual variability
Growth phase 1	4.69	6.62×10^{-3}	-4.43×10^{-3}	64.81%	10.16
Growth phase 2	22.4	2.89×10^{-3}	2.54×10^{-3}	65.98%	95.13
Growth phase 3	33.04	$\mathbf{25.31} \times 10^{-3}$	$\mathbf{10.32} \times 10^{-3}$	49.62%	166.19

Table 1: Corsican pines, Model 2 - linear mixed model estimated on each growth phase.

Number of branches per tier

It should be noted that the number of branches per tier is strongly correlated with the annual shoot length ($r = 0.66$). Hence, when introducing the annual shoot length as an explanatory variable, it is no more necessary to model explicitly the phases for the "number of branches per tier" response variable. A simple linear mixed model was thus estimated where both the annual shoot length, the previous year rainfall (annual shoot organogenesis) and the current year rainfall (annual shoot elongation and branch organogenesis) were taken into account as explanatory variables (and their influences modeled as fixed effects). The influence of the previous year rainfall and the current year rainfall is not significant while as expected, the influence of the annual shoot length is strong. Since most of the inter-individual heterogeneity is already reflected in the "length of the annual shoot" explanatory variable, the part of variability due to the supplementary inter-individual heterogeneity is less than 14%.

Discussion

We note the same behavior for these species: the inter-individual heterogeneity is greater at the beginning of the plant life (first growth phases) while the influence of climatic explanatory variables is roughly proportional to growth level. However, the tree origin, the silvicultural interventions and the sampling strategy seems to influence the inter-individual heterogeneity part. To understand which among these three factors have the greatest influence is a challenging problem. It would be very useful to study the part of inter-individual heterogeneity for various species in similar conditions or for a given species in various conditions.

Another approach to take into account the influence of the environment on plant growth would be to introduce a year random effect common to all the individuals to model the synchronous part of the inter-annual fluctuations. The total variability would decompose into three parts: variability due to the environment (year random effect), variability due to the inter-individual heterogeneity (individual random effect) and residual variability.

References

Ephraim, Y. and Merhav, N. (2002). Hidden Markov processes. *IEEE Transactions on Information Theory*, 48(6), 1518-1569.

Guédon, Y., Caraglio, Y., Heuret P., Lebarbier, E., and Meredieu, C. (2007). Analyzing growth components in tree. To be published in *Journal of Theoretical Biology*.

McLachlan, G.J. and Krishnan, T. (1997) *The EM algorithm and extensions*, New York: Wiley.

Véra, C., Guédon, Y., Lavergne, C. and Caraglio, Y. (2004). Analysis of longitudinal data applied to plant architecture study In: *4th International Workshop on Functional-Structural Plant Models*, Montpellier, 65-69.

Verbeke, G. and Molenberghs, G. (2000). *Linear Mixed Models for Longitudinal Data*. New York: Springer.

Using the Language XL for Structural Analysis

Ole Kniemeyer [1,*] Jan-Anton Dérer [1] Reinhard Hemmerling [1]
Gerhard Buck-Sorlin [2] Winfried Kurth [1]

[1] BTU Cottbus, Department of Computer Science, Chair for Practical Computer Science / Graphics Systems, P.O.Box 10 13 44, 03013 Cottbus, Germany
[2] Wageningen UR, Crop and Weed Ecology Group
Haarweg 333, 6709 RZ Wageningen, The Netherlands
[*] corresponding author, okn@informatik.tu-cottbus.de

Keywords: Structure analysis, plant modelling, querying language, L-systems, GroIMP

The analysis of plant structures is an important issue in functional-structural plant modelling, especially in the context of parameterization and validation. This holds equally for structures resulting from measurements of real plants and for modelled structures, i.e., the outcome of virtual plant simulations. Such an analysis has to consider both the topology of the structure and the values of parameters of its constitutive entities (e.g., geometry-related parameters, internal state). For example, one may be interested in the number of internodes of growth units as a function of their age (a purely topological property) or in the length ratio of consecutive growth units, which also includes geometric information.

The AMAPmod software [1] is an example of a sophisticated program which has been specifically designed for plant structure analysis. Existing structures (results of measurements or virtual plant simulations) are read in, the user then extracts the desired information using the querying language AML, and results can be visualized as a 3D-model or via several types of plots.

We present another analysis technique based on the programming language XL within the open-source modelling environment GroIMP [2]. Although XL has been designed as an extension of L-systems, i.e., for the implementation of functional-structural plant models, it turns out to be equally suitable for the analysis of plant structures by virtue of its graph query facilities. These queries allow the search for occurrences of patterns in the current structure which is represented as a graph. The advantage of this approach is that the same language can be used to model a virtual plant, to analyze the results, and to compare it with measured data. The analysis can be invoked interactively within GroIMP's XL console, or it can be part of the source code of the model itself for automatization purposes. As an example, the statement

```
plot(int age => double count((* g:GU, (g.age == age) *)), 0:10);
```

draws a plot of the total number of growth units `GU` as a function of their age, and

```
statistics(((* g:GU h:GU, (g.order == 0) *), h.len/g.len));
```

computes mean value, standard deviation and skewness of the ratio of lengths of consecutive growth units of branching order 0. The examples make use of XL's graph queries of the form `(*...*)` and aggregate methods like `count`, `statistics` and `plot`. We will give a concrete demonstration of its usage using a model of a young beech tree, where measured tree data is analyzed in order to parameterize the model, which in turn is analyzed for validation.

References

[1] C. Godin, Y. Guédon, E. Costes, and Y. Caraglio. Measuring and analysing plants with the AMAPmod software. In M. Michalewicz, editor, *Plants to Ecosystems: Advances in Computational Life Sciences*, pages 53–84. CSIRO Publishing, Australia, 1997.

[2] O. Kniemeyer. *Design and Implementation of a Graph Grammar Based Language for Functional-Structural Plant Modelling*. PhD thesis, BTU Cottbus, 2007. (forthcoming, see http://www.grogra.de).

Variation of leaf blade optical properties with the time cut from plant

Cailian Lao[1], Jinhe Hu[2], Yuntao Ma[2], Baoguo Li[2], Yan Guo[2]*
[1] College of Information and Electrical Engineering, China Agricultural University, Beijing, China, 100083; [2] College of Resources and Environment, China Agricultural University, Beijing, China, 100094. (*Corresponding author: yan.guo@cau.edu.cn)

Keywords: optical properties, measurement, light distribution, leaf, maize

Introduction

Quantification of the behavior of light scattering from leaves is critical to investigate the interaction of radiation with plants. Methods for measuring light distribution scattering from plant leaf have been developed from 2-dimensional plane to 3-dimensinal space. Most of these measurements were taken in lab and the samples of leaves were cut from plants. Does leaf optical properties keep stable while it is under tests? A experiment was carried out to answer this question.

Materials and Methods

Maize (*Zea mays* L. variety 'PingYu 5') leaf blades were taken as test samples in the early grain filling stage. On illumination of 650 nm and 780 nm with incidence azimuth angle of 60^o and zenith angle of 0^o , angular reflectance of maize leaves were recorded at viewing azimuth angle of 60^o and zenith angles of -50^o, -40^o, -30^o, -10^o, 0^o, 10^o, 30^o, and 50^o respectively within 4 h at an interval of 5 s, with first record started 1 min after the sample cut from the plant.

Results and Conclusion

Angular reflectance increased slowly with the cut time at wavelength of 780 nm. With illumination of 650 nm, the variation of reflectance was relatively small in the first 50 min, and it had a sharply increase in the following 40 min and then it had a smoothly increase with the cut time. It is recommended to finish the angular reflectance measurement in 50 min after leaf sample cut from plant if the measurement *in situ* is not possible. Further work is expected to explain the variation of leaf optical properties with the time cut from plant.

Acknowledgements

This study was sponsored by "863" program of China (2006AA10Z231).

References

Bousquet L, Lach′erade S, Jacquemoud S, Moya I. 2005. Leaf BRDF measurements and model for specular and diffuse components differentiation. *Remote Sensing of Environment* 98: 201-211.

Brakke TW, Smith JA, Harnden JM. 1989. Bidirectional scattering of light from tree leaves. *Remote Sensing of Environment* 29: 175-183.

Grant L. 1987. Diffuse and specular characteristics of leaf reflectance. *Remote Sensing of Environment* 22: 309-322.

Grant L, Daughtry CST, Vanderbilt VC. 1993. Polarized and specular reflectance variation with leaf surface features. *Plant Physiology* 88: 1-9.

Virtual Kiwifruit: Modelling Annual Growth Cycle and Light Distribution

Mikolaj Cieslak[1], Alla N. Seleznyova[2], and Jim Hanan[1]
[1]ARC Centre for Complex Systems & Advanced Computational Modelling Centre
Department of Mathematics, University of Queensland, Brisbane, QLD 4072, Australia
[2]HortResearch, Private Bag 11 030, Palmerston North, New Zealand
{cieslak|jim}@maths.uq.edu.au or aseleznyova@hortresearch.co.nz

Keywords: Kiwifruit (*Actinidia*), plant architecture, branching, plant modelling, L-systems

Introduction. The aims of our research are to develop hypotheses related to the processes underlying branching pattern of the kiwifruit vine, and to study the effects of horticultural manipulation (winter pruning and rootstock) on the light distribution within the vine's canopy.

Kiwifruit (*Actinidia deliciosa*) is a perennial vine of horticultural importance. The pattern of growth cessation of annual shoots creates three distinct shoot types (short, medium, and long), and is influenced by genotype, environmental conditions, and rootstock (Foster *et al*., 2007). These shoot types are not evenly distributed along the parent shoot, but form branching zones (Seleznyova *et al*., 2002).

We base our modelling approach on the assumption that branching pattern emerges from the overall vigour of shoots and the likelihood of shoot tip abortion at the preformed and neoformed stages of primordia outgrowth. This approach differs from that of Seleznyova *et al*. (2002) for kiwifruit because we do not represent branching patterns as a succession of branching zones, but instead model axillary shoot development as a stochastic process. Similarly, it differs from the approach of Louran *et al*. (2007) for modelling shoot architecture of grapevine cultivars, because we do not represent final metamer (phytomer) number as sequences in segmented zones, but instead model shoot growth cessation. This allows us to compute distributions of final node number and of different axillary shoots types along the parent shoot.

Hypotheses.

H_1. Axillary shoot vigour depends on its position along the parent cane. Kiwifruit conforms to Champagnat's architectural model (Hallé *et al*., 1978), so that relay axes (vigorous shoots) develop in the region of the maximum curvature of the parent axis.

H_2. There is intrinsic variation in shoot vigour emerging during budbreak (Foster *et al*., 2007).

H_3. Growth cessation occurs with different probabilities during any of three developmental stages: opening of the initial cluster of leaves, expansion of the preformed metamers, and production and expansion of the neoformed metamers (Seleznyova *et al*., 2002; Foster *et al*., 2007).

Model. We use L-systems (Karwowski and Prusinkiewicz, 2003) to create a 3-D virtual plant representation (Room *et al*., 1996) of the annual growth cycle of a managed mature kiwifruit vine. In the beginning of each cycle, the structure consists of the main trunk, two leaders, and a specified number of canes trained on a T-bar structure. We focus on the development of axillary bud outgrowth from these canes. Axillary shoot growth is modelled as a discrete-time non-stationary Markov chain (Taylor and Karlin, 1998), with three states: dormant, growing and aborted. The transition probabilities are defined over one phyllochron, and are modulated by a function of position (H_1), initial shoot vigour (H_2) and stage of shoot development (H_3). The distribution of the initial cluster size is based on data from Seleznyova *et al*. (2002).

This approach differs from that of Godin *et al*. (1997), which may be used to model branching patterns with Markov processes, because we represent the temporal structure of the data rather than

the spatial structure. That is, the states in our model correspond to the physical states of the shoot apical meristem instead of the branching zones as would be the case in Godin *et al*.'s approach.

Our architectural model simulates distributions of different shoot types along the parent canes and node number distributions for axillary shoots (Fig. 1). These are compared with the existing experimental data from Seleznyova *et al*. (2002) (not shown).

To study the effects of canopy structure on light distribution, we interface our virtual kiwifruit vine with a light environment model using the open L-system formalism. The light environment model estimates the irradiance reaching the canopy leaves using a quasi-Monte Carlo path tracing algorithm (Cieslak *et al*., 2007). We manipulate the canopy structure by changing parameters related to the position and number of canes along the leaders, and quantify the effect of canopy structure on light interception.

Conclusion. The presented architectural model forms a basis for further modelling of the vine's growth and of the interactions between plant architecture, resource allocation and environment. The model will be used to explore the complexity of the vine's architecture, and to predict its behaviour under the influence of various management practices and environmental parameters (e.g., temperature and light).

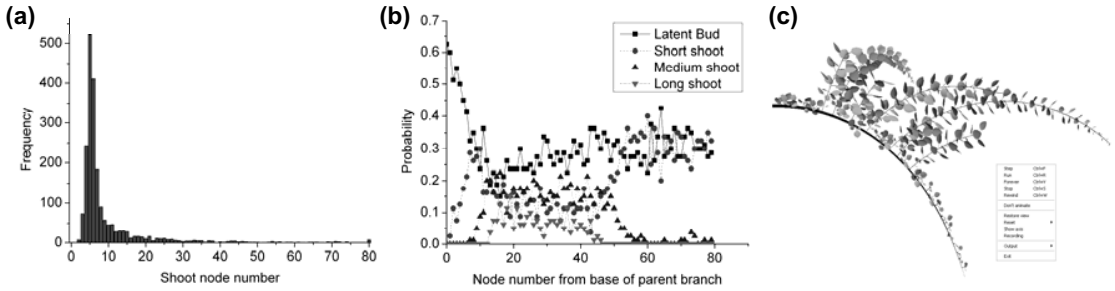

Figure 1: Output from the virtual kiwifruit model: (a) final node number distribution, (b) probability distributions of different axillary shoot types for long parent shoots, and (c) 3-D representation of an individual cane.

References

Cieslak, M., Lemieux, C. and Prusinkiewicz, P. 2007. Quasi-Monte Carlo simulation of the light environment of virtual plants. In *Proceedings of the 5th International Workshop on Functional-Structural Plant Models*.

Foster, T.M., Seleznyova, A.N. and Barnett, A.M. 2007. Independent control of organogenesis and shoot tip abortion are key factors to developmental plasticity in kiwifruit (*Actinidia*). *Annals of Botany*, doi: 10.1093/aob/mcm140.

Godin, C., Guedon, Y., Costes, E., and Caraglio, Y. 1997. Measuring and analysing plants with AMAPmod software. In: Michalewicz MT, ed. *Plants to ecosystems. Advances in computational life sciences*. Melbourne: CSIRO Publishing, 45-52.

Hallé, F., Oldeman, R.A., and Tomlinson, P.B. 1978. *Tropical trees and forests: an architectural analysis*. Berlin, New York: Springer-Verlag.

Karwowski, R. and Prusinkiewicz, P. 2003. Design and implementation of the L+C modeling language. *Electronic Notes in Theoretical Computer Science*, 86(2):19 pp.

Louran, G., Guedon, Y. Lecoeur, J. and Lebon, E. 2007. Quantitative analysis of the Phenotypic variability of shoot architecture in two grapevine (*Vitis vinifera*) cultivars. *Annals of Botany*, 89:1-13.

Room, P., Hanan, J. and Prusinkiewicz, P. 1996. Virtual plants: new perspective for ecologists, pathologists and agricultural scientists. *Trends in Plant Science*, 1:33-38.

Seleznyova, A.N., Thorp, T.G., Barnett, A.M., and Costes, E. 2002. Quantitative analysis of shoot development and branching patterns in *Actinidia*. *Annals of Botany*, 89:471-482.

Taylor, H.M., and Karlin, S. 1998. *An introduction to stochastic modeling*. San Diego: Academic Press.

Virtual phyllotaxis and real plant model cases

Beata Zagórska-Marek and Marcin Szpak
Institute of Plant Biology, Wroclaw University, 50-328 Wrocław, Kanonia Str. 6/8, Poland
beata@biol.uni.wroc.pl

Keywords: phyllotaxis, pattern formation, ontogenetic transitions, *Magnolia*, *Verbena*

Introduction

Phyllotaxis is the distribution of lateral organs in plants. The organ primordia are initiated reiteratively (Hofmeister 1868) on the organogenic surface of the shoot apical meristem (SAM). The regularity of phyllotactic patterns has always puzzled scientists. Today there is still no exaggeration in quoting Darwin's famous statement and saying, that both phyllotactic diversity and, especially, ontogenetic transitions of phyllotaxis remain an "abominable mystery" in plant biology. The **phylogenetic** aspect of the diversity is that phyllotactic patterns can be species specific. Having the status of a diagnostic feature in plant taxonomy, they fall into two major categories: of whorled - achiral patterns and of helical - chiral patterns. The **ontogenetic** aspect is that the pattern often changes together with the developmental phase of plant's growth. From the biological point of view it is the ontogenetic, qualitative changes of phyllotaxis, which occur for no apparent reason and are not associated with the developmental switch of plant organ identity, that are truly challenging. The mechanism positioning the primordia of leaves, flowers or flower parts on the organogenic surface of SAM is unknown. It is undoubtedly genetically controlled (phylogenetic aspect) but also flexible enough to assure the plant's phenotypic plasticity (ontogenetic transitions).

The latest developments in plant biology point out the role of auxin, transported in the superficial cellular layer of SAM. Each primordium acts as a sink, competing for the hormone with others and inhibiting the formation of similar structures in its close vicinity. The efficiency of a sink can be measured by the size of the inhibition field, within which the auxin concentration is below the level required for the formation of a new sink. New elements emerge in the first available space between already existing neighboring primordia (Snow & Snow 1931, 1952). This space is created by the constant and continuous addition of new cells as a result of SAM's apical growth. Based on these concepts two new models of phyllotaxis have recently been introduced (Jönsson et al. 2006, Smith et al 2006a). It is still uncertain to what degree the SAM is autonomous in positioning organ primordia and what role the signals, which flow acropetally from differentiated tissues (Banasiak, Zagórska-Marek 2006), play in this process.

This study was undertaken in hope of finding, in a computer simulation, the causes of phyllotactic transitions known from plant model cases. The principles affecting the direction of phyllotactic transition and thus the quality of the emerging pattern were of particular interest.

The model

The physiological size of primordia may have nothing to do with their real geometric size. However, in the models of phyllotactic pattern formation and the pattern's subsequent transformation, it is convenient to have the primordia represented by circles tightly packed on a cylindrical surface representing the organogenic, lateral surface of the growing SAM.

In order to understand the emergence of various patterns and their ontogenetic transitions, we have simulated SAM's growth using a special computer program. In our model we assumed:

- an infinite cylinder of a constant width as simulation space
- primordia as circles of a changing radius
- primordia emerging in the first available space

The "first available space" rule is ambiguous

The assumption that the size of primordia is subject to ontogenetic change appeared to be particularly fruitful. The model, in testing, produced an almost infinite number of transitions, with many resulting patterns of primordia spacing, more or less regular. The changes applied were abrupt or continuous, quick or slow, with the radius decreasing or increasing. The results of the simulations showed, however, that the quality of the emerging pattern did not solely depend upon the way the primordia size was controlled. The position of a newly initiated primordium, appearing in the first available space between two, already initiated laterals, **sometimes had to be selected from two equivalent positions**. The choice, once made, affected the developing pattern of primordia spacing, even though all other parameters of the simulation were the same (Fig. 1). This shed a new light on the possible causes of transitions known to occur in plants.

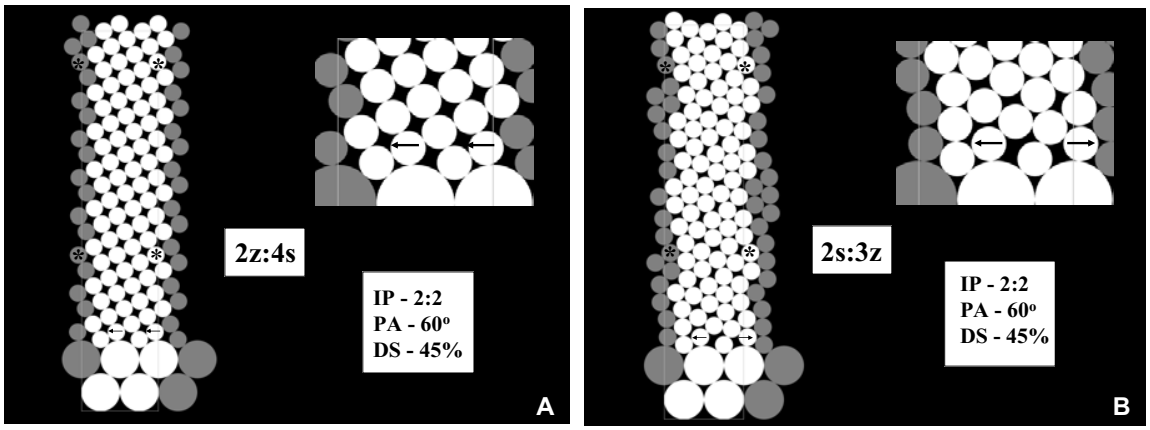

Fig. 1. The simulation of abrupt change in the size of circular primordia, added to the working space according to the principle of Snow & Snow. Only one of two equivalent positions: to the left or to the right (arrows) has to be selected by each of two newly initiated, small primordia. When the choice for both is the same – the developing pattern is bijugy (A), when it is different – the main Fibonacci emerges (B). The initial pattern (IP) is decussate. Primordia decrease in size (DS) by 45%. The same primordium is shown on the opposite sides of organogenic frame (as either grey or white), selected pairs are marked with asterisks. The numbers of the conspicuous parastichy pair identifying the emergent phyllotactic pattern are supplemented with **S** and **Z** indexes of parastichy orientation. They allow the recognition of pattern chirality.

The confrontation of simulation results with real cases showed that the quality of natural changes in phyllotaxis may indeed be affected:

- by the change in the size of a pattern element assuming new identity in the course of development (case study *Magnolia*)
- by the way the initiation site is selected from two equivalent positions in the first available space (case study *Verbena*)

Case study *Magnolia*

The outstanding diversity of phyllotactic patterns present in magnolia flowers (Zagórska-Marek 1994) is most probably an outcome of the double change in the size of floral primordia (Zagórska-Marek, Stoma 2005). The computer simulation of this case is very sensitive to even small changes in the values of parameters used. The initial pattern of the largest perianth primordia is tricussate (achiral), which explains the frequent appearance of trijugy in the later helical arrangement of the smaller stamen primordia and slightly larger carpel primordia. Together with the small size of generative elements in relation to the width of organogenic space, the double change can be held responsible for the rich spectrum of final phyllotactic solutions.

Still, some unexplained problems remain:

- qualitative changes in phyllotaxis sometimes occur within the zone of primordia of the same identity
- the spectrum of final patterns is species or genet specific (phyllotactic fingerprint) despite the general rule of a double change. More detailed quantitative studies are needed to resolve this dilemma.

Case study *Verbena*

The decussate (achiral) vegetative phyllotaxis of *Verbena* changes within inflorescence into the helical (chiral) pattern. It is mostly the main Fibonacci pattern. In the simulation it emerges from the decussate pattern when the two smaller, "generative", primordia choose their initiation site oppositely in two equivalent positions (Fig. 2B). The above transition should be the most frequent among plants, which **quickly** develop helical phyllotaxis from the initial pattern of opposite cotyledones or prophylls. Sometimes the developing helical pattern is bijugy implying the situation already shown in Fig. 2A. The unresolved problem is that on the axis of inflorescence further sequential changes of phyllotaxis often take place even though the identity of primordia remains the same. The transitions involve helical patterns (Lucas, second accessory) as well as whorled (tricussate).

Conclusion

Simulation results quite well coincide with the real organographic changes in the systems of phyllotaxis exemplified by *Magnolia* and *Verbena* shoots. Similar coincidence has been observed by other authors for other plants (Couder 1998, Smith et al 2006b). The new development in our model application is that, sometimes, there is more than one initiation site available for an emerging primordium. **Its selection, together with other factors such as the varying extent and rate of change in primordia size, affects the quality of the resulting pattern and ontogenetic transition**.

Our future specific goals in exploring the potentials of the model are to:

- systematically explain and predict all, including the less common patterns
- explain the direction of other pattern transitions i.e. why the pattern may be transformed in many different ways
- elucidate why the spectrum of patterns can be species or genet specific

References:

Banasiak A., Zagórska-Marek B. 2006. Signals flowing from mature tissues to SAM determine the phyllotactic continuity in successive annual increments of the conifer shoot. Acta Soc.Bot Pol. 75 (2): 113-121.

Hofmeister W. 1868. Allgemeine Morphologie der Gewächse. Engelmann, Leipzig.

Couder Y. 1998. Initial transitions, order and disorder in phyllotactic patterns: the ontogeny of *Helianthus annuus*. A case study. Acta Soc. Bot. Pol. 67:129-150

Jönsson H., Heisler M.G., Shapiro B.E., Meyerowitz E.M., Mjolsness E. 2006. An auxin-driven polarized transport model for phyllotaxis. Proceedings of the National Academy of Sciences USA. 103 (5): 1633-1638

Smith R.S., Guyomarch S., Mandel T., Reinhardt D., Kuhlemeier C., Prusinkiewicz P. 2006a. A plausible model of phyllotaxis. Proceedings of the National Academy of Sciences USA. 103 (5): 1301-1306

Smith R.S., Kuhlemeier C., Prusinkiewicz P. 2006b. Inhibition fields for phyllotactic pattern formation: a simulation study. Can. J. Bot. 84: 1635 – 1649.

Snow M., Snow R. 1931. Experiments on phyllotaxis. I. The effect of isolating a primordium. Philosophical Transactions of the Royal Society London 221B: 1–43.

Snow M., Snow R. 1952. Minimum areas and leaf determination. Proceedings of the Royal Society 139B: 545 – 566.

Zagórska-Marek B. 1994. Phyllotaxic diversity in *Magnolia* flowers. Act. Soc. Bot. Po.l. 63: 117-137.

Zagórska-Marek B., Stoma S. 2005. What makes floral phyllotaxis in *Magnolia* diverse – a lesson from virtual garden. Proceedings of XVII International Botanical Congress.Vienna. p. 308.

Zagórska-Marek B., Szpak M. 2006. Model of changing phyllotaxis in plants. International FNP Conference "Mathematical modeling of biological processes". Poznań.

Virtual rose: a new tool to optimize plant architecture in glasshouse rose production systems

G.H. Buck-Sorlin, B.S. Burema, J.B. Evers, G.W.A.M. van der Heijden, E. Heuvelink, L.F.M. Marcelis, P.C. Struik, P.H.B. de Visser, T.H.J. Damen and J. Vos

Plant Sciences Group, Wageningen University and Research Centre, P.O. Box 430, 6700 AK Wageningen, The Netherlands
jan.vos@wur.nl

Keywords: flower production, functional-structural plant model, plant architecture, plant manipulation

Cut roses (*Rosa hybrida*) represent a high input and high-value ornamental glasshouse crop. Many factors affect number and quality of flowers, among them most prominently the manipulation strategy exercised by the grower, which aims at (i) maintaining a sufficient number of leaves exposed to light in order to sustain growth and (ii) to stimulate 'bud break', i.e. the emergence of new shoots from bud positions that yield high quality flowers. Basically, current plant manipulation strategies were developed empirically in practice. A more objective tool to guide growers in their decisions on plant manipulation is required. The objectives of the project include (i) to study bud break in relation to plant architecture and environment, and (ii) to use that knowledge to create a model that calculates flower production over time in relation to plant architecture, plant manipulation and glasshouse environment and that thus goes beyond existing process-based rose models (e.g. Lieth & Pasian, 1991), which fail to predict this spatial crop dynamics.

A preliminary version of a cut rose model written in XL using the modeling environment GroIMP (Kniemeyer 2004) will be shown. In a next step, this essentially morphological model will be turned into a functional-structural plant model by linking it with various submodels simulating external environmental (light, temperature) and internal processes (transport of nutrients, signal transduction). GroIMP's potential for user interaction and global context sensitivity will be explored in the context of management practices and their effects on crop physiology at different scales: shoot bending to increase source strength, pruning, and rose cutting for harvest.

So far, a conceptual model for the rose FSPM as well as two morphological models have been devised (see figure above). The model concept is based on knowledge about the topology of rose organs, whereas the morphological models are the first results of detailed morphometric and developmental studies of the primary shoot and the flower, respectively. Further modeling tasks include: development and growth over time (kinetics); assimilation and carbon partitioning; experiments to quantify the behaviour of axillary buds, as a function of interference with plant architecture: (pruning, harvesting, flower bud removal), light microclimate, source-sink balance.

Acknowledgement

Funding: Technology Foundation STW (www.stw.nl); project number WLW.7435

References

Kniemeyer, O. (2004). Rule-based modelling with the XL/GroIMP software. In: Harald Schaub, Frank Detje, Ulrike Brüggemann (eds.), The Logic of Artificial Life. Proceedings of 6th GWAL, Bamberg April 14-16, 2004, AKA Akademische Verlagsgesellschaft Berlin, pp. 56-65.

Lieth J.H., Pasian C.C. (1991): A simulation model for the growth and development of flowering rose shoots. *Scientia Horticulturae* 46, 109-128.

Visualizing reaction of chrysanthemum to temperature and light: model calibration and validation

MengZhen Kang[1], Ep Heuvelink[2], Véronique Letort[3], Paul-Henry Counède[3], Susana M.P. Carvalho[2] and Philippe de Reffye[1,4,5]

[1] LIAMA, Institute of Automation, CAS, 100080 BeiJing, China; mzkang@liama.ia.ac.cn
[2] Horticultural Production Chains, Wageningen University, 6709 PG Wageningen, The Netherlands; ep.heuvelink@wur.nl
[3] MAS, Ecole Centrale de Paris, France; {letort|cournede}@mas.ecp.fr
[4]Projet DigiPlante, INRIA Rocquencourt, France
[5]Cirad, Montpellier, Cedex 5, France; philippe.de_reffye@cirad.fr

Keywords: sink-source regulation, functional-structural plant model, GreenLab feedback model

Introduction

The external quality of chrysanthemum includes morphology (number and size) of stem, leaf and flower (Carvalho and Heuvelink, 2001). Each character is influenced by several growth conditions interacting with each other. Higher temperature increases internode elongation rate and number of flowers per plant, and reduces individual flower size (Carvalho et al., 2005); light intensity increases assimilate availability, and consequently the weight of the plant and number of flowers, whereas the size of the flowers is hardly influenced (Carvalho and Heuvelink, 2003).

Descriptive models for chrysanthemum have been developed for some quality aspects. However, several important quality aspects like flower characteristics and leaf size are absent, and the mentioned characteristics were never integrated in a single model. Functional-structural plant models (FSPMs) aim at modelling plant development and growth and their interactions. It is potentially a suitable tool for evaluating the external quality of ornamental crops. For chrysanthemum FSPMs have been developed based on L-systems (de Visser et al., 2006) and GreenLab methodology (Kang et al., 2006, Fig. 1). In the latter study, all the external quality aspects mentioned above, were computed by the model based on sink-source relations.

Fig.1. Virtual chrysanthemum (Kang et al., 2006)

The aim of the current study is modelling of the external quality of chrysanthemum in reaction to different combinations of temperature and light with the GreenLab model. The new feature is the feedback of plant production on plant development in order to simulate the architecture plasticity of chrysanthemum.

Material and Methods

Experiment setup and data collection

The experiment was conducted in growth chambers using block–rooted cuttings of Chrysanthemum 'Reagan Splendid'. 16 treatments were achieved, being combinations of four temperature (15°C, 18°C, 21°C, 24°C) and four light levels obtained with shading screens (100%; 297 μmol m^{-2} s^{-1}), (65%; 194 μmol m^{-2} s^{-1}), (51%; 152 μmol m^{-2} s^{-1}) and (40%; 118 μmol m^{-2} s^{-1}). Plants were1 placed at a density of 69 plants m^{-2}. CO_2 concentration was maintained at ambient level.

The first destructive measurement was carried out at planting and was followed by eight destructive measurements (every 7-10 days) on five plants per treatment, starting at the beginning of the short day (SD) period (15 days after planting). For each plant collected data (at plant level) includes the number of leaves on the main stem (MS), the length of MS, the area and weight of leaves on MS and side shoots (SS) respectively, the weight of MS and SS respectively, the number and weight of flowers and flower buds. In four extreme treatments (combinations of temperature 15°C and 24°C with light level 40% and 100%), detailed measurements were conducted on individual organs (leaf blades, petioles, internodes, flowers) at three plants per treatment three weeks after visible bud stage and at final harvest.

GreenLab model with interaction between plant production and development

GreenLab model has been described in previous publications (de Reffye et al, 2003; Yan et al., 2004). In previous applications of GreenLab (Guo et al., 2006, Kang et al., 2006), the plant development follows a predefined pattern without being influenced by the assimilate availability. It is suitable mostly for a fixed environment. In current study, not only the size and weight of organs, but also the plant development change with climate condition. Thus GreenLab model with feedback of plant production on the plant topological structure (Mattieu, 2006) is used in this study. With this new feature, the varying branching order and number of flowers along the stem according to environment can be simulated through parameters (*a* and *b*) linked to assimilate demand and supply, as shown in Eqn. (1).

$$v_B = a + b \cdot \frac{Q}{D}(n) \quad (1)$$

v_B is a coefficient describing speed of top-down flowering as described in (Kang et al., 2006). Q and D are assimilate supply and demand at plant age (in cycles) n.

The model is first calibrated using data from the four extreme treatments and four intermediate treatments. The calibrated model is to be validated with independent data set from other eight intermediate treatments. The model output can be visualized with 3D virtual chrysanthemum, showing the effect of climate conditions on chrysanthemum external quality.

Outlook

The experimental results show that the branching order, number of flowers, as well as organ weight changes with the different combinations. It is promising to predict such behaviour with a model with feedback. As the current work is still ongoing, the full results are to be presented in coming article.

Acknowledgements

This work is supported by LIAMA, Natural Science Foundation of China (60073007), Chinese 863 plan (2006AA10Z229), and C.T. de Wit Graduate School for Production Ecology and Resource Conservation (PE&RC). Master student Eshetu Janka (Wageningen University), is acknowledged for experiment organisation and data collection.

References

Carvalho SMP, Abi-Tarabay H, Heuvelink E. 2005. Temperature affects *Chrysanthemum* flower characteristics differently during three phases of the cultivation period. *Journal of Horticultural Science and Biotechnology* 80: 209-216.

Carvalho SMP, Heuvelink E. 2003. Effect of assimilate availability on flower characteristics and plant height of cut chrysanthemum: an integrated study. *Journal of Horticultural Science and Biotechnology* 78: 711-720.

Kang MZ, Heuvelink E, and De Reffye P. 2006. Building virtual chrysanthemum based on sink-source relationships: Preliminary results. *Acta Horticulturae* 718: 129–136.

Guo Y, Ma YT, Zhan ZG, Li BG, Dingkuhn M, Luque D and de Reffye P. 2006. Parameter optimization and field validation of the functional-structural model GREENLAB for maize. *Annals of Botany* 97: 217-230.

Mathieu, A. 2006. Essai sur la modélisation des interactions entre la croissance et le développement d'une plante: cas du modèle GreenLab. PhD Thesis. Ecole Centrale de Paris.

de Reffye P. and Hu BG. Relevant qualitative and quantitative choices for building an efficient dynamic plant growth model: GreenLab Case. PMA03 proceedings, Beijing, Oct 13-16, 2003, pp. 87-107

de Visser PHB, Van der Heijden GWAM, Marcelis LFM, Carvalho SMP, Heuvelink E. 2006. A functional-structural model of chrysanthemum for prediction of ornamental quality. *Acta Horticulturae* 718: 59-66.

Yan HP, Kang MZ, De Reffye P, and Dingkuhn M. 2004. A dynamic, architectural plant model simulating resource-dependent growth. *Annals of Botany* 93: 591–602.

Woody stem itself senses light environment and phototropically bends by asymmetrical xylem formation

Jun Matsuzaki *, Masaya Masumori, and Takeshi Tange

Graduate School of Agricultural and Life Sciences, the University of Tokyo, Tokyo 113-8657, Japan
*Present address: Faculty of Science, Hokkaido University, Hokkaido 060-0810, Japan
jmatsuzaki@07.alumni.u-tokyo.ac.jp

Keywords: phototropism, posture control, light environment, tension wood, tree

Introduction

Plants control posture of stems, so that they optimize photosynthesis of leaves and dispersal of pollen and seeds under mechanical restrictions. For elongating stems, phototropism, gravitropism, and autostraightening have been known. However, it is only gravitropism and autostraightening that have been recognized and existence of phototropism had not been documented for non-elongating and radially growing stems (hereafter, woody stems) characteristic of woody plants. Woody stems of angiosperm species gravitropically bend by asymmetrical formation of tension wood and normal wood and thus asymmetrical generation of longitudinal tensile stresses during maturation of the xylem toward one side of the stems. Recently, we have found out that woody stems do reveal phototropism and that it is implemented by the asymmetrical xylem formation (Matsuzaki *et al.* 2007), as such occurs for gravitropism of woody stems. Preliminary experiments suggested that woody stem itself rather than leaves is a photoreceptive site in the phototropic bending of woody stems. In this study, we examined role of woody stem as a photoreceptive site and longitudinal signal transmission of information on light gradient.

Experimental settings and results

We inclined one-year-old potted seedlings of a deciduous oak *Quercus crispula* Blume 45º from the vertical and grew them under overhead fluorescent illumination. We defined the stem portion that had elongated within a given growth flush as a growth unit (GU). Among three GUs consisting inclined one-year-old main stems, the middle GU was laterally illuminated with an array of blue light emitting diodes (LEDs). Significant bending and asymmetrical tension wood formation toward the flank illuminated with blue LEDs at the middle GUs was observed compared with the middle GUs of non-treated seedlings. GUs basal and apical to the middle ones, which were not illuminated laterally with the blue LEDs, showed neither lateral bending nor lateral asymmetry in xylem formation.

Conclusions

It is shown that gradient in light environment is perceived by woody stem itself and that the gradient locally induces asymmetrical xylem formation and resulting bending. Acropetal and basipetal transmission of information on the light gradient is not apparent. Integrating phototropism of woody stems into functional-structural plant models may improve prediction of tree architecture and photosynthesis under spatially heterogeneous light environment.

References

Matsuzaki, J., Masumori, M., and Tange, T. (2007) Phototropic bending of non-elongating and radially growing woody stems results from asymmetrical xylem formation. *Plant, Cell and Environment* **30,** 646-653.

Index of Authors

S

T